BIOBASED REACTIVE COMPOUNDS IN NOVEL & SUSTAINABLE ADHESIVE SYSTEMS

Inaugural dissertation

To obtain the academic degree
Doctor rerum naturalium (Dr. rer. nat.)
of the Faculty of Mathematics and Natural Sciences

of the Heinrich-Heine University Düsseldorf

in cooperation with Henkel AG & Co. KGaA

submitted by

Marlo Kropff

born in Hattingen

The work presented in this thesis was accomplished between 15.05.2020 and 15.05.2023 in cooperation of the Bio-Renewables Scouting department at Henkel AG & Co. KGaA under the supervision of Dr. Adrian Brandt and Prof. Dr. Laura Hartmann from the Institute of Organic Chemistry and Macromolecular Chemistry at the Heinrich-Heine University Düsseldorf.

Printed with the permission of the

Faculty of Mathematics and Natural Sciences of the

Heinrich-Heine University Düsseldorf

1st reviewer: Prof. Dr. Laura Hartmann

2nd reviewer: PD Dr. Klaus Schaper

Date of the oral examination: 26.03.2024

Declaration of authorship

I hereby declare that the thesis submitted is my own work without making use of impermissible aids, considering the “Rules on the Principles for Safeguarding Good Scientific Practice at Heinrich Heine University Düsseldorf”. All direct or indirect sources used are acknowledged in the bibliography as references. I further declare that I have not submitted this nor a similar thesis to any other examination board in order to obtain a degree.

M. Kropff 28.05.2024

Marlo Kropff Date

Acknowledgements

Mein erster Dank gilt **Prof. Dr. Laura Hartmann** für die Ermöglichung dieser Promotion und vorallem für ihre fachliche wie administrative Unterstützung dieser Arbeit. Weiterhin möchte ich mich bei **Dr. Klaus Schaper** bedanken, der als Mentor dieser Promotion fungiert hat.

Mein besonderer Dank gilt **Dr. Adrian Brandt** für seinen stetigen Einsatz und sehr hilfreiche fachliche Unterstützung während dieser Arbeit. Außerdem möchte ich mich bei **Dr. Hendrik Lützen** und **Dr. Brian Spiegelberg** bedanken, die mich immer wieder mit wichtigem Input weitergebracht haben.

Großer Dank gebührt meinem Zellengenossen **Martin Diekmann** für seinen Input in unseren konstruktiven und professionellen Diskussionen, ebenso wie seinen Beiträgen im von uns geleiteten Forum. Ohne seinen Beistand im Arbeitsumfeld wie im Privaten wäre diese Arbeit so nicht zustandegekommen.

I owe great thanks to **Kamela Myrtollari** for her strong support in- and outside of the lab. And natürliχ for making work much more enjoyable with her imperturbable ability to spread good mood and optimism.

Außerdem bedanke ich mich herzlichst bei **Alexander Kux**, **Alissa Besler** und **Astrid Angenvoort**, die mir immer mit Rat und Tat zur Seite standen und mir dabei immer die Stange gehalten haben. Besonderer Dank gilt an dieser Stelle **Andrea Hoffmann** für ihre harte Arbeit und die fruchtbare Zusammenarbeit im Labor sowie in Meetings. Ich möchte ebenfalls **Kerstin Schröder, Jannis Reinartz**, **Johannes Reiter** und **Philip Ezau** für Ihre Unterstützung danken.

Weiterhin möchte ich mich bei **Philipp Ernst**, **Frank Göthel** und **Dr. Kang-Wei Chou** für die konstruktive sowie unterhaltsame Zusammenarbeit bedanken.

Für ihre Unterstützung von der analytischen Seite dieser Arbeit möchte ich mich besonders bei **Verena Schön** und **Dr. Oliver Seiler** bedanken, die mir stets geholfen haben egal wie absurd meine Anliegen waren. An dieser Stelle danke ich ebenfalls **Kenan Kenaar** und **Martin Altrock** für ihre Hilfe. Moreover, I want to thank **Dr. Qi Wu** and **Dr. Anthony Romanelli** for their support.

Großer Dank gebührt ebenfalls **Benjamin Orgis** und **Bernhard Putz** für ihre Unterstützung besonders beim Säulen. Außerdem möchte ich mich bei **Moritz Arnold** und **Kausar Mohammed** für unsere Zusammenarbeit bedanken.

I also want to thank **Zahra Mazloomi** and **Sarah Kirchhecker** for our cooperation and especially for the first syntheses of styrene sulfate.

Zuletzt möchte ich mich bei der Fachagentur Nachwachsende Rohstoffe e.V. für die Finanzierung dieser Dissertation im Zusammenhang mit dem BIOVIN Projekt bedanken.

Vielen Dank, Thank You and Ευχαριστώ!

Table of content

Index of abbreviations

Abbreviation	Unit	Description
PS		photosensitizer
ΔG	J	Free Gibbs energy
F	C/mol	Faraday constant
$E_{\frac{1}{2}}^{\mathrm{ox}}$	V	Oxidation potential
$E_{\frac{1}{2}}^{\mathrm{red}}$	V	Reduction potential
4-MeOS		4-methoxy styrene
4-HS		4-hydroxystyrene
4VP		4-vinylphenol
T_g	°C	Glass transition temperature
ECD		Electrochemical debonding
EDL		Electrochemical delamination
IL		Ionic liquid
PIL		Polymerizable ionic liquid
PI 440		Bis(4-methylphenyl)iodonium hexafluorophosphate
PI 7MS		(7-methoxy-4-methylcoumarin-3-yl)phenyl iodonium hexafluoroantimonate
PS 1331		9,10-Dibutoxyanthracene
DSC		Differential scanning calorimetry
G'	Pa	Storage modulus
G''	Pa	Loss modulus
tan δ		Dissipation factor
HBVE		4-hydroxybutyl vinyl ether
CDVE		1,4-cyclohexanedimethanol divinyl ether
DEGDVE		di(ethylene glycol) divinyl ether
TEGDVE		tri(ethylene glycol) divinyl ether
CVE		cylcohexyl vinyl ether
BDVE		1,4-butanediol divinyl ether
C10DVE		1,10-decanediol divinyl ether
PrDVE		1,3-propanediol divinyl ether
THFDVE		2,5-bis((vinyloxy)methyl)tetrahydrofuran
1,4-PDVE		1,4-pentanediol divinylether
IBVE		Isobutyl vinyl ether
FFAVE		2-((vinyloxy)methyl)furan
PU-2		Difunctional urethane-based vinyl ether prepolymer

PU-3		Trifunctional urethane-based vinyl ether crosslinker
PU-3a		Trifunctional urethane-based vinyl ether crosslinker with 67 % free isocyanate groups
4,4’-MDI		4,4’-methylene diphenyl diiscocyanate
F-U		Urethane-based vinyl ether adhesive formulation
F-Ua		Urethane-based vinyl ether adhesive formulation with additional moisture cure step
σ_{max}	MPa	Maximum stress
$\varepsilon_{\mathrm{max}}$	%	Strain at break
M_n	Da	Number-average molecular weight
M_w	Da	Weight-average molecular weight
PD		Polydispersity
ΔH_l	J/g	Reaction enthalpy of unreacted formulation
ΔH_s	J/g	Reaction enthalpy of irradiated formulation
DOC	%	Degree of cure
X		Conversion
RH	%	Relative humidity
GPC		Gel permeation chromatography
DMA		Dynamic mechanical analysis
NMR		Nuclear magnetic resonance
FTIR		Fourier-transform infrared
PP		Polypropylene
PA		Polyamide
ABS		Acrylonitrile butadiene styrene
PC		Polycarbonate
PMMA		Poly(methyl methacrylate)
δ	MPa	Lap shear strength
n	mol	Amount of substance
T	°C	Temperature
c	mol/L	Concentration
w	wt%	Mass fraction
TMPMP		1,1,1-tris-(hydroxymethayl) propan-tris-(3-mercaptopropionat)
PETMP		Pentaerythrit-tetrakis-(3-mercapto propionate)
TEMPIC		Tris [2-(3-mercaptopropionyloxy) ethyl] isocyanurate
MTMO		3-mercaptopropyl trimethoxysilane

V-65	2,2’-azobis(2,4-dimethylvaleronitrile
PHAE-2	Difunctional hemiacetal ester-based vinyl ether prepolymer
PHAE-4	Hemiacetal ester-based crosslinker with four vinyl ether moieties
F-T1	Adhesive thiol-vinyl ether formulation with radical curing
F-T2	Adhesive thiol-vinyl ether formulation with cationic curing
F-T2a	Adhesive thiol-vinyl ether formulation with cationic curing and vinyl ether excess
HAE-1	1-(4-(vinyloxy)butoxy)ethyl cyclohexanecarboxylate
HAE-2	bis(1-(4-vinlyoxy)butoxy)ethyl) isophthalate
U-1	4-(vinyloxy)butyl cyclohexylcarbamate
U-2	bis(4-vinyloxy)butyl) (4-methyl-1,3-phenylene)dicarbamate
PI 184	1-hydroxy cyclohexyl phenyl ketone
PI BMS	4-(4-methylphenylthio)benzophenone
PI ITX	2-isopropyl thioxanthone
TTMSS	tris(trimethylsilyl)silane
F-HAE	Adhesive hemiacetal ester-based vinyl ether formulation
F-HAEa	Adhesive hemiacetal ester-based vinyl ether formulation with silane-mediated curing mechanism
F-HAEb	Adhesive hemiacetal ester-based vinyl ether formulation with silane-mediated curing mechanism and without PHAE-4
F-HAEc	Adhesive hemiacetal ester-based vinyl ether formulation with 4-MeOS (final prototype)
SSS	Sodium p-styrene sulfate
DMF	Dimethyl formamide
DCM	Dichloromethane
RT	Room temperature
DMSO	Dimethyl sulfoxide
TBASS	Tetrabutyl ammonium styrene sulfate
PIL-1	1-hexyl-3-methylimidazolium styrene sulfonate
PIL-2	1-vinyl-3-methylimidazolium bistriflimide
IL-1	1-butyl-3-methylimidazolium bistriflimide
IL-2	1-ethyl-3-methyldimidazolium triflate
F-PIL-1	Acrylate-based reactive adhesive formulation with two polymerizable ionic liquids for EDL (reference)
F-PIL-2	Acrylate-based reactive adhesive formulation with two polymerizable ionic liquids for EDL. PIL-1 was replaced by TBASS

F-IL-1	Acrylate-based reactive adhesive formulation with an inert ionic liquid for EDL (reference)
F-IL-2	Acrylate-based reactive adhesive formulation for EDL (reference). IL-1 was replaced by TBASS.

Abstract

Currently, the chemical and materials industry adapts processes towards a more circular economy due to challenges posed by climate change. Potential strategies for the adhesives industry deal with the incorporation of sustainable materials by using circular feedstocks to become independent from fossil fuels which enables the exploitation of novel molecules for new and exciting systems with unique properties. Furthermore, the development of long-lasting products has gained much attention by enabling recycling and repair solutions via debonding mechanisms. During recent years, academic and industrial research focuses more and more on evaluating advantages and drawbacks of novel adhesive systems with high renewable carbon content and debonding features. In this context, this thesis aims at the evaluation of vinyl ethers and 4-vinylphenol derivatives in adhesive systems. Both compound classes are already available from biobased resources to a certain extent.

Vinyl ethers possess a unique combination of properties that make them an attractive alternative for use in many industries, particularly those that are concerned with sustainability or environmentally friendly practices. One reason is the potential production from biobased sources from a variety of routes. Another is their extraordinarily high reactivity in living cationic polymerizations. A major objective of this thesis is to understand and subsequently control exothermic vinyl ether polymerization and therefore develop a pathway for their extended commercial use in industry. Cationic photopolymerization of small monomers results in intense heat generation and consequently a degradation of mechanical properties from deterioration on a molecular level. In this work, control of these drawbacks from exothermic behavior is demonstrated by the utilization of self-synthesized urethane-based prepolymers with vinyl ether functionality and by the subsequent addition of various filler materials. Moreover, the scope of vinyl ether curing was expanded by adding a moisture-driven post-curing step and by the utilization of thiols in thiol-ene polyaddition reactions. To investigate possible debonding-by-hydrolysis features in vinyl ether systems, hemiacetal ester prepolymers were synthesized and implemented. The impact on mechanical properties and the potentials and limitations of the resulting debonding capabilities were analyzed. In addition, comparative kinetic experiments were conducted to evaluate cationic polymerization of hemiacetal ester and urethane prepolymers. Finally, a prototype was developed by incorporating a 4-vinylphenol derivative, 4-methoxy styrene, with considerable adhesive performance and debonding features.

In literature, polymerizable phenol derivatives have gained considerable attention for their use as high performance materials often conveniently available from waste streams. The ionic polymerizable 4-vinylphenol derivative sodium styrene sulfate was successfully synthesized. A degradation process over time was observed and elucidated in aging tests. The cationic and radical polymerization kinetics of tetrabutyl ammonium styrene sulfate were analyzed and compared to the common and structurally similar monomer styrene. The ionic character of styrene sulfate introduces exciting features in adhesive systems. In this work, tetrabutyl ammonium styrene sulfate was tested as a comonomer in two acrylate-based adhesive systems with radical curing mechanisms. Both approaches aimed at replacing inert ionic liquids, which may cause a decrease in cohesion, with the ionic comonomer in conductive materials. Thus, an increase in adhesive performance while maintaining ionic conductivity is expected. In the course of these experiments, the potential of styrene sulfate for electrochemical debonding systems was demonstrated as proof-of-concept. Moreover, the use of styrene sulfate in pressure sensitive adhesives results in an increase in adhesive performance and wetting acceleration.

1 Introduction

1.1 General overview of adhesive technologies

Adhesives play an integral role in numerous industrial and consumer applications and are defined as a material used to permanently connect at least two surfaces.[1] Compared to other technologies for assembly methods like sewing or welding, adhesives are preferred mostly due to their superior ratio of time and energy effort against stress resilience.[2] The latter depends on two different factors: cohesive and adhesive forces of the mostly polymeric material.[3] The internal strength of a cured adhesive is described by cohesion and is a result of the chemical bonds within the crosslinking degree and intermolecular interactions.[4] Strong intermolecular interactions like H-bonding and high entanglement densities contribute to the toughness of a material: very hard and brittle materials are usually formed by polymer networks with high cross-linking densities in contrast to highly ductile adhesive layers, e.g. sealants, consisting of polymer chains with strong but reversible intermolecular bonds and entanglements.[1,5] Adhesion on the other hand describes the attraction between adhesive and substrate surface which does not solely depend on the adhesive, but on the mechanical and chemical nature of the surface as well.[6,7] One important factor for adhesion is wetting of a surface by an adhesive.[8,9] Universally, the wetting process is described by a droplet of a liquid on a solid material surface spreading depending on the respective surface energies (Figure 1.1).[10] The formed contact angle decreases with smaller differences in surface energies of adhesive and substrate, resulting in better wettability and consequently adhesion. In addition, adhesive forces are affected by shrinkage of reactive systems resulting in loss of contact area[11] and most importantly intermolecular or covalent bonding between adhesive and substrate.[12,13]

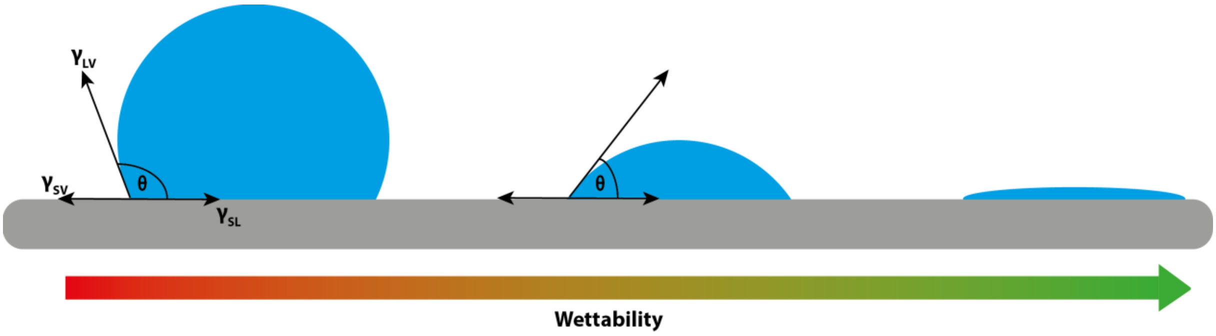

Figure 1.1: Wetting of a surface by a liquid.[10]

Commercial adhesives can be classified as reactive and non-reactive adhesives.[9] Curing of the latter relies on physical mechanisms such as cooling or evaporation of solvent to leave a layer of polymeric material, whereas reactive adhesives consist of monomers or prepolymers which undergo chemical reactions after treatment to form solid polymers.[1,6,14] Typical non-reactive adhesives (Figure 1.2, right) are hot-melt systems, with a broad application field in e.g. packaging and woodworking industries, solvent based adhesives, which include water-based systems for packaging and consumer use, pressure sensitive adhesives (PSAs) in tapes, and plastisols. Reactive adhesives (Figure 1.2, left) are characterized by their respective polymer chain growth mechanism, i.e. polyaddition, polycondensation and polymerization. An example for polyaddition adhesives is polyurethane which is often utilized in body work, glass panel adhering and in the automotive industry. Silanes undergo polycondensation reactions and the resulting highly ductile polymer is well suited for sealing applications. Polymerization adhesives are mostly cured by thermal or irradiation triggers and have a broad array of applications such as coatings, encapsulants, gap fillers and structural adhesives. Until recently, most technologies relied on thermal curing but radiation curing has gained more and more interest due to lower costs in operation[15] and faster curing, making high speed coating applications feasible[16]. With all these technologies combined, the global adhesive market grossed a value of 43.7 billion USD in 2020 and is expected to keep growing in the upcoming years.[17]

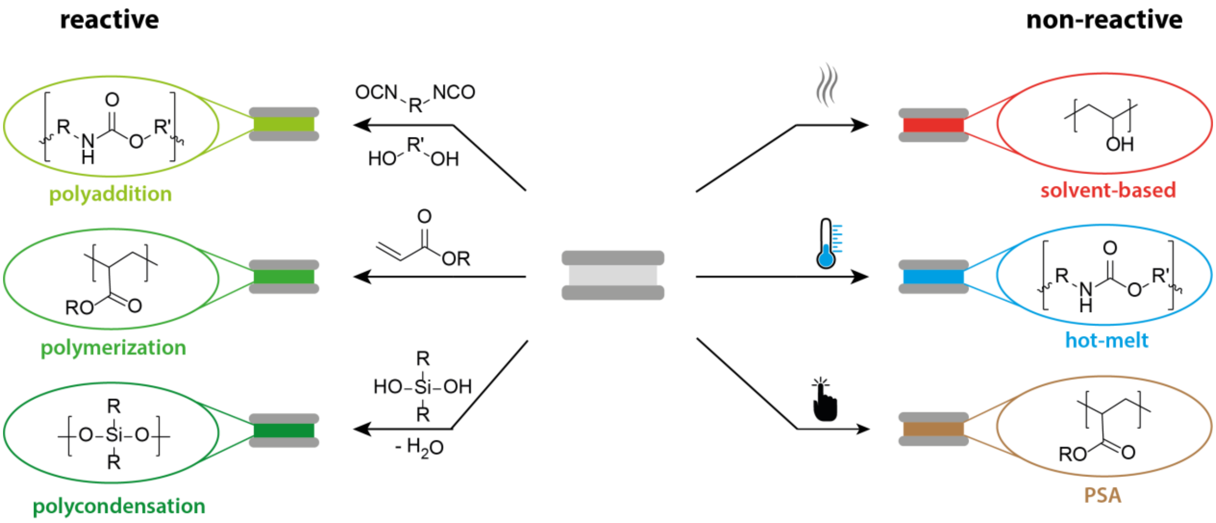

Figure 1.2: Overview of reactive and non-reactive adhesives with exemplary monomer and polymer structures.

Adhesives are not exclusively made of non-reactive polymers or reactive monomers, but are designed in formulations from an array of components to optimize performance and costs.[9] In order to facilitate chemical reactions of monomers, initiators[18] or catalysts[19] are added while maintaining storage stability by adding inhibitors[9]. A common way to reduce production cost of an adhesive is the utilization of filler materials: inert compounds such as barium sulfate or chalk which can beneficially affect material properties.[20] Toughness and impact-resistance of adhesives are often enhanced by the addition of tougheners, reactive, or non-reactive.[21] Both types act either as plasticizers by lowering the glass-transition temperature T_g causing a decrease in brittleness, or as phase-separators to facilitate energy dissipation on impact and to mitigate destruction by micro-fractures.[22] One group of reactive tougheners are prepolymers which are utilized instead of or in addition to small monomer molecules to reduce reactive group concentration and to implement additional structural groups in the final polymer backbone. In addition, compounds, small or polymeric, with high reactive group functionality are added to increase crosslinking density and consequently improving mechanical resistance and rigidity.[23]

Currently, most commercial adhesives rely on monomers and polymers from petroleum resources.[24] Driven by the aspiration to reduce dependence on fossil fuels and decrease carbon dioxide output, many industries have grown to develop products and alter production processes towards a more circular economy.[25] This approach applies to the energy and the chemical production sector alike and aims at refraining from extracting carbon from the earth in the form of gas, oil as well as coal and release it into the atmosphere or the environment. One future vision is well described and promoted by the Renewable Carbon Initiative (RCI).[26] Further important aspects of green chemistry in general are waste prevention and consequently recycling, atom efficiency, energy efficiency, health and safety, and degradability.[27]

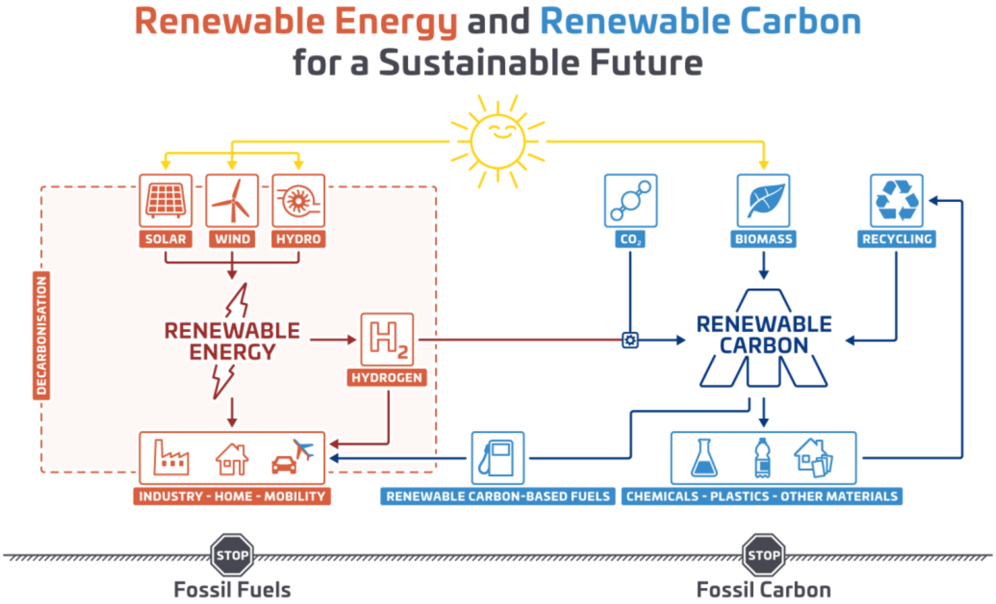

Figure 1.3: Approach for a more circular energy and production industry via renewable resources (provided by RCI, nova-Institut[28]).

An overview of challenges and solution approaches in current green chemistry and its implemented rules was given by Prof. Klaus Kümmerer[29]: A substantial challenge is the huge number of different chemicals in use: about 350,000 different organic compounds are currently available on the market. An example is the utilization of more than 100 different chemicals for the treatment of a football jersey over its whole life cycle. A possible approach to take on this topic is creating lists with well-analyzed compounds with a low impact on the environment and adjust current products to this list as far as possible. The utilization of many chemicals is restricted due to their toxicity. Examples are fire retardants and biocides for facades. Contemporary replacements are mostly used because their effects on health and environment are hardly known and thus there no regulations in place which underlines the necessity for "positive chemical lists". Many harmful chemicals are in use entirely for marketing purposes, i.e. color or odor reasons, which can be reduced dramatically. Moreover, current green chemistry does not properly evaluate the mass streams of products, wastes and their respective compositions in terms of compound separation, disposal, and reutilization. A recommendation by Kümmerer is an improved implementation of chemical research in the economy: Longer life cycles of products, followed by preferably mechanical and if necessary by chemical recycling processes, abstaining from burning wastes in terms of thermal exploitation and separation of compound streams over the whole life cycle of products, especially regarding plastics and metals. This short summary highlights how long the pathway towards a more circular economy still is.

One important step towards a greener adhesive industry, is reduction of energy consumption in application, e.g. by altering processes towards lower curing temperatures or even LED curing if feasible[30], and more importantly, recycling of adhered substrates must become more easily available and hence more prevalent.[31] For recycling, adhered substrates must be separated after use which is extremely difficult, especially for applications with high adhesive strength demands. As a consequence, systems with debonding-on-demand features have been and still are the topic of many research works.[31–34] This topic will be discussed in section 1.3. However, an essential factor is advancing utilization of monomers, polymers, and additives from renewable sources instead of fossil fuels.

1.2 Biobased resources for polymer chemistry and adhesives

Biobased resources for polymer chemistry and adhesives are becoming more and more important in today's world as people and industry become increasingly conscious of their carbon footprint and the environmental impact of everyday products. For this reason, there is a huge market developing for biobased products.[35] Biobased polymers are developed by two different approaches: drop-in replacement of crude oil-based raw materials, and development of new polymers which are not conveniently accessible from fossil feedstocks. Examples for drop-in replacements are polyethylene[36] and polyacrylates[37,38] among others. Currently, there are two main paths for the incorporation of biobased materials as polymer drop-ins: The production of the monomer in question may proceed via novel synthesis routes independent from the fossil fuel industry or raw materials from bio feedstocks are added to oil-based substrates in conventional monomer production. An example is the production of poly(ethylene) (PE) which is commonly produced from ethylene obtained by cracking of petroleum-based naphtha to which a defined amount of bio-naphtha can be added.[35] The bulk of naphtha in this cracking process still originates from fossil fuels, the minimum amount of biobased material in this kind of process is regulated by certification processes. However, the production of substantial amounts of ethylene from ethanol obtained via biomass fermentation is already possible which opens up the route to polyethylene production without any oil-based ethylene.[39]

In contrast, polymers obtained directly from biomass such as cellulose and lignin[40–44] as well as synthesized polyhydroxyl alkanoates[36] are limited to biomass feedstocks. Some monomers can be produced from renewable resources such as corn starch, sugarcane and vegetable oil. One biotech route is processing by fermentation before converting the obtained building blocks into polymers which are subsequently used in industry.[36,45]. One of the most utilized feedstocks is vegetable oil as it available at large scale and a broad array of renewable monomers are processed from it, mostly by modification of the double bonds of plant oil or the respective unsaturated fatty acids.[46] The chemistry of vegetable oils is called oleochemistry and is as old as the chemical industry itself. For instance, by self-metathesis, Wacker oxidation, and epoxidation, monomers for polyesters, polyamides and polycarbonates are produced via oleochemistry.[46] Another important and relevant industrial process is transesterification of the oils which yields biodiesel and glycerol. The latter is a byproduct of this process and can be further utilized either directly for polyester synthesis or converted to e.g. acrylic acid.[38] However, the route towards acrylic acid is not yet commercialized but has been reported under laboratory conditions. Another renewable source to be highlighted is wood. Cellulose and lignin can be obtained and further modified towards novel compounds with natural high molecular masses (s. section 1.2.1) and additionally, aromatic and especially phenolic compounds are obtained from pyrolysis of the crude waste streams (s. section 1.2.2). However, the scope of industrially accessible monomers from biomass is still somewhat narrow and most processes bear limitations regarding sustainability due to utilization of toxic reagents or improvable atom efficiency.[46]

In the adhesive industry, most products were obtained from natural sources about a century ago with some still being in use.[24] A well-known example is animal glue accessible from animal tissue[47], followed by proteins which naturally carry adhesive proteins, e.g. casein in glass bottle labeling,[24] or mixtures of modified starch with water used for glue sticks[24]. Yet, synthesis of polymers with tailorable properties for adhesive applications from renewable building blocks has reached an all-time high of attention in industry and academic research in the last years. Production of diacids and diols for polyester synthesis (s. section 1.2.1) and the utilization as well as conversion of glycerol and fatty acids from vegetable oil have been implemented in industry for years already.[48] Besides the general advantages of biobased feedstocks like reduction of the carbon footprint and lower toxicities, novel monomer structures create opportunities for advances in material and consequently adhesive properties. A prominent example is biodegradable poly(lactide) from bio-based lactides with a global production of 190,000 tons in 2019 which is growing every year.[49] L-3,4-dihydroxyphenylalanine found in mussels has also gained attention. By incorporation into a polyamide adhesive, adhesion to metal surfaces and general adhesive strength underwater were reportedly improved.[50] Another interesting compound is the diol isosorbide, which is derived from glucose and not accessible from oil. It carries four stereo-centers, a singularity which promises interesting properties for a variety of applications in polymer chemistry.[24] Overall, the growing market for adhesives from biobased resources is not only driven by environmental awareness but also by advantages regarding energy efficiency and most importantly new advances in polymer design. Consequently, the demand for research and development of bio feedstock processing keeps growing as the currently available scope of industrial bio-monomers and bio-polymers is still in the early stages of development despite the aforementioned numerous advantages.[46]

1.2.1 Vinyl ethers

A substance class of high interest for current adhesive research are vinyl ethers. These molecules possess a unique combination of properties that make them an attractive alternative for use in many industries, particularly those that are concerned with sustainability or environmentally friendly practices. One reason is the potential production from biobased sources via different routes: Vinyl ethers can be synthesized from a substitution reaction of vinyl chloride with alcoholates or by transvinylation of vinyl esters.[51] The most common approach is the direct vinylation of various alcohol compounds, possibly produced from biomass fermentation,[52] with acetylene to form vinyl ethers[53]. Acetylene can also be potentially produced from renewable sources, i.e. biochar.[54] One advantage of utilizing alcohols for further conversion towards reactive chemicals is the broad array of available structures, ranging from biopolymers such as lignin, cellulose and other sugar alcohols[40–44] to small molecules like 1,3-propane diol or 1,4-butane diol[55]; all of which can be conveniently obtained from agricultural waste streams[56]. Subsequent conversion of industrial available alcohols by vinylation was widely investigated with calcium carbide[57] as well as acetylene[58] among others. Beyond that, polymeric alcohols from biomass were successfully vinylated giving access to high molecular weight vinyl ethers from cellulose[59] and other glucose derivatives[60].

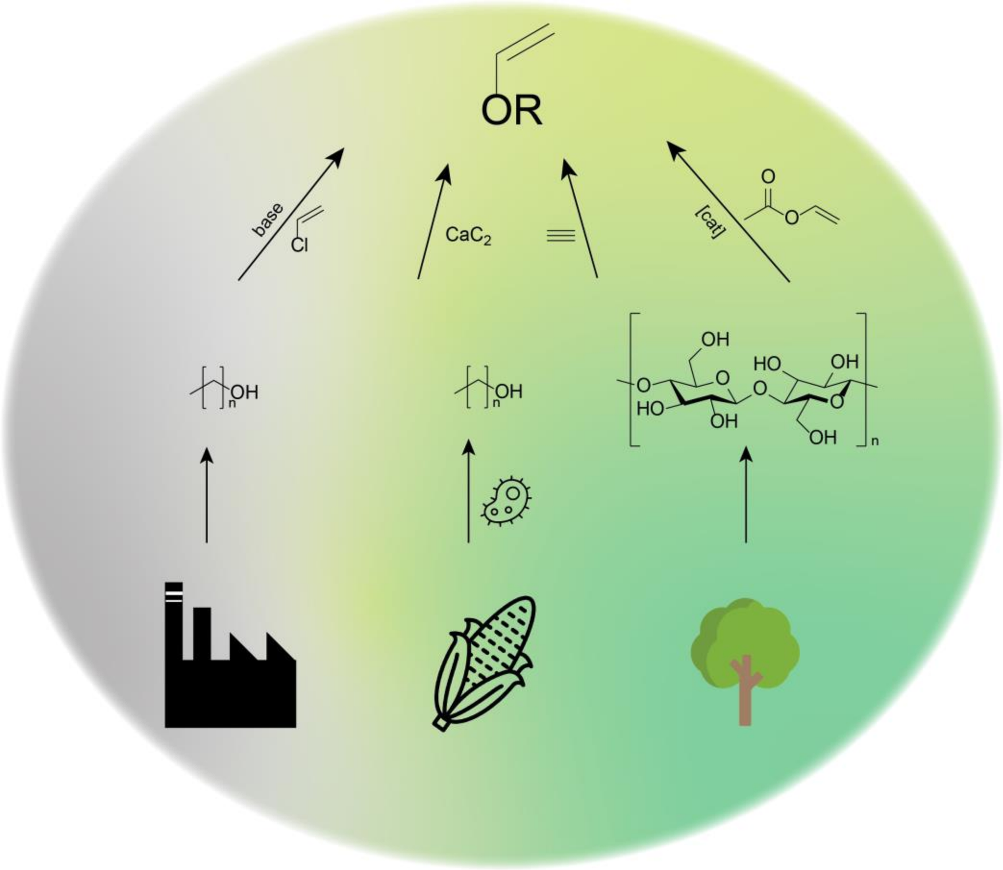

Figure 1.4: Overview of vinyl ether synthesis. Production of alcohols via the industrial route, by fermentation of starch and cellulose from wood. Subsequent conversion into vinyl ethers by substitution of alcoholates with vinyl chloride, vinylation via calcium carbide and acetylene, and metal-catalyzed vinylation.

However, industry contemporarily relies almost completely on vinyl ethers from fossil fuels[61], typically by an addition reaction of acetylene with alcohols at elevated temperatures between 150 °C and 200 °C catalyzed by a base, preferably potassium hydroxide, and high acetylene pressures.[62] The reaction products are purified by distillation which limits this reaction path to small vinyl ether molecules. An attractive strategy for future synthesis of biobased vinyl ethers on an industrial scale is catalytic transfer vinylation, mostly resulting from the versatility in substrates and catalysts, such as mercury, gold, palladium and iridium.[32,63,64] In addition, often moderate reaction conditions are sufficient for satisfactory yields up to 99 %.[64] Vinylation catalyzed by palladium can be conducted at low temperatures, but is limited to aliphatic alcohols whereas utilization of iridium enables the production of e.g. phenolic vinyl ethers at higher temperatures.[32] In summary, the preparation of biobased vinyl ethers is not yet implemented in industry but significant progress was made over the last years to enable large scale production of vinyl ethers conveniently from agricultural waste streams.

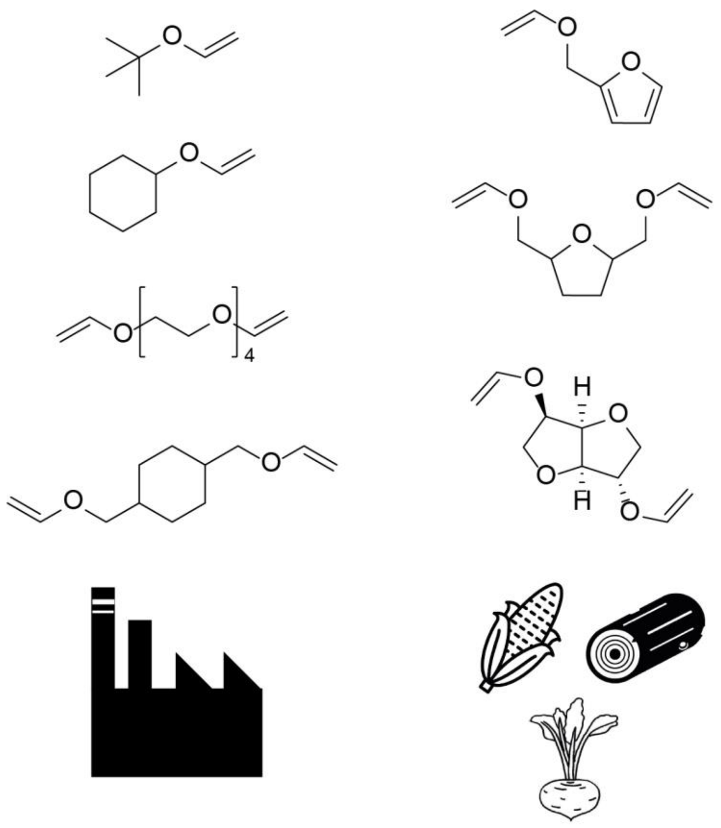

Figure 1.5: Selection of vinyl ether monomers from fossil fuels and potentially renewable sources.[32]

Typically, polyvinyl ethers are prepared by cationic polymerizations which are inhibited by termination and chain transfer reactions with nucleophiles and water. However, the reaction is not inhibited by oxygen and there are no termination reactions between active chain ends and hence cationic polymerizations are considered living polymerizations.[65] Consequently, high monomer conversion is possible even after removing the irradiation source, which makes dark curing feasible.[66] In addition, vinyl ethers are known to achieve considerable deep curing in photoinitiated systems, which is crucial in applications with high layer thicknesses.[67,68] Especially for photocuring applications, vinyl ethers can be seen as competition to well implemented (meth)acrylate systems. In comparison to acrylates, vinyl ethers are preferred in terms of health and safety because of their more pleasant odor, their mostly lower flammability and their typically lower toxicity.[69,70] An example of vinyl ethers being less toxic than acrylates is the comparison of di(ethylene glycol) diacrylate and di(ethylene glycol) divinyl ether. The compounds have identical molecular structures, except for the polymerizable group. Whereas the acrylate is classified as irritating and toxic, the vinyl ether is classified as a non-hazardous substance.[71] Non-hazardous labeling and consumer-friendly handling are one of the main driving forces in industrial applications. Thus, novel vinyl ether-based adhesive systems have a high potential to become an alternative for acrylate systems in applications that benefit from vinyl ether properties. Currently, such applications are scarce, but vinyl ethers are already in use for UV cured inks, coatings and adhesives.[72]

In common commercial adhesives, vinyl ethers are mainly utilized as reactive diluents, e.g. with epoxides.[73] Potential manufacturing of biobased polyols at large industrial scale will help to boost bio-based vinyl ether production, also for adhesives, by conventional acetylene addition or other routes.

Curing of vinyl ether-based adhesives, i.e. the polymerization of vinyl ether moieties typically proceeds in a cationic mechanism.[74,75] Besides the well-known cationic polymerization of vinyl ethers from fossil fuels, Ananikov et al. demonstrated vinyl ether polymerization of biobased terpenes[76] and Brännström et al. prepared polymers from various divinyl ethers obtained from enzymatic processes[77]. Extraordinarily high reactivities were observed which derive from the ether group adjacent to the double bond (Scheme 1.1).[78,79] The neighboring oxygen increases the electron density of the vinyl group and makes it more prone to an addition reaction by an acid which initiates cationic polymerization[80] accompanied by significant heat generation due to the strongly exothermic reaction enthalpy[81]. Ledwith et al.[82] calculated the cationic polymerization enthalpy of ethyl vinyl ether with ΔH_p = -80 kJ/mol which is extraordinarily high compared to e.g. methyl methacrylate with ΔH_p = -54 kJ/mol[83]. This high reactivity is not limited to polymerization reactions but the electron-rich double bond quickly undergoes addition reactions with various nucleophiles such as alcohols, carboxylic acids and thiols.[61] Reactivity and consequently curing time are affected by many factors, such as monomer[84] and initiator structure[85]. The reactivity of alkyl vinyl ethers increases from primary to secondary to tertiary alkyl group substituents.[86] Commonly, vinyl ethers are polymerized by photoinitiation[75,84,87] or initiation by Lewis acids[88], in bulk[89] as well as in organic solvents[90] and in aqueous medium[91]. Moreover, the polymerization process has been refined in terms of polymerization control by utilizing 1,2,3,4,5-pentacarbomethoxycyclopentadiene[92] or by visible light regulation with a RAFT agent[75]. Besides linear polymers from monofunctional monomers, Aoshima et al created GRAFT architectures with cyclic ester comonomers in coordination ring-opening polymerizations.[93] Moreover, vinyl ethers were already copolymerized with styrene in the 1970s but with undesired side reactions, such as Friedel-Crafts addition.[94] These side reactions limit the utilization of aromatic comonomers which are of high interest due to the stabilizing mesomeric effect of the aromatic ring on the carbocation in addition to its alleged positive effect on substrate adhesion. Advances were made by Aoshima et al. by conducting various substitution reactions on phenyl derived vinyl ethers and consequently suppressing undesired Friedel-Crafts side reactions in cationic homopolymerization[95] as well as in copolymerization with benzaldehydes[96].

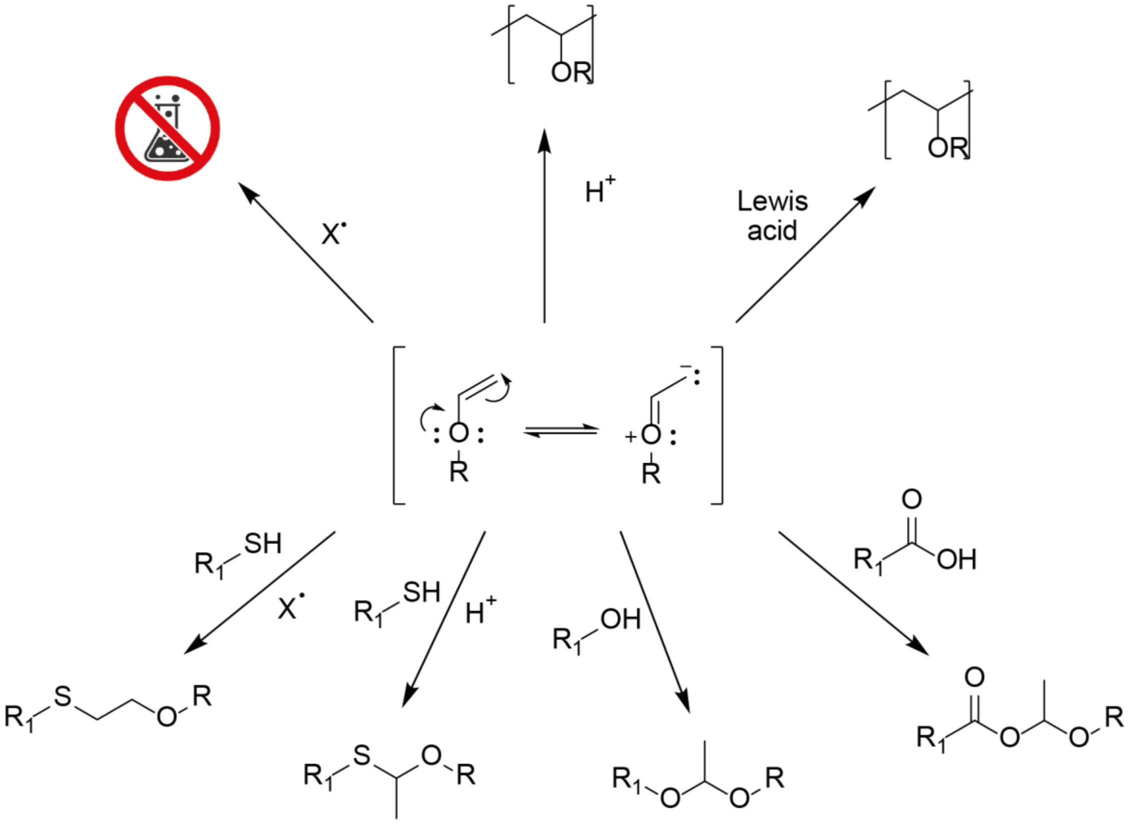

Scheme 1.1: Selection of addition and polymerization reactions of vinyl ethers.

The main focus of vinyl ether homopolymerization in this work lies on cationic photocuring in which reactivity is vastly affected by initiator structure and initiation mode.[97,98] Most commonly, onium salts are utilized and were consequently of high interest in academic research regarding their potential for cationic photoinitiation.[99,100] These compounds act as acid generators upon irradiation which subsequently start polymerization.[78,100,101] An advantage of onium salts is their high photosensitivity combined with high storage stability, making them convenient initiators for adhesive systems. Overall, diaryl iodononium salts exhibit high reactivities and consequently enable short curing times.[99] The photoinitiated decomposition process of diaryl iodonium salts is shown in Scheme 1.3. When absorbing radiation of characteristic wavelength, the cation turns into an excited state which decomposes in two parallel processes, connected by an electron transfer equilibrium. The right reaction path in Scheme 1.2 starts by heterolytic cleavage of the bond between the iodine and an aryl substituent yielding an aryl-cation which further reacts with a nucleophile (R-H) to form a Brønsted acid (AH). The acid may initiate cationic polymerization. As indicated by the left reaction path in Scheme 1.3, if the iodine-aryl bond undergoes homolytic cleavage, an aryl radical and a cationic aryl iodine radical are obtained. The latter reacts with a nucleophile to form the initiating Brønsted acid. Common anions (A^-) are antimony compounds or hexafluorophosphate which also affect the reactivity of the initiator salt.[102] Although onium salts with SbF_6^- or AsF_6^- anions exhibit higher reactivity, the demand for PF_6^- compounds is higher due to their lower toxicity.

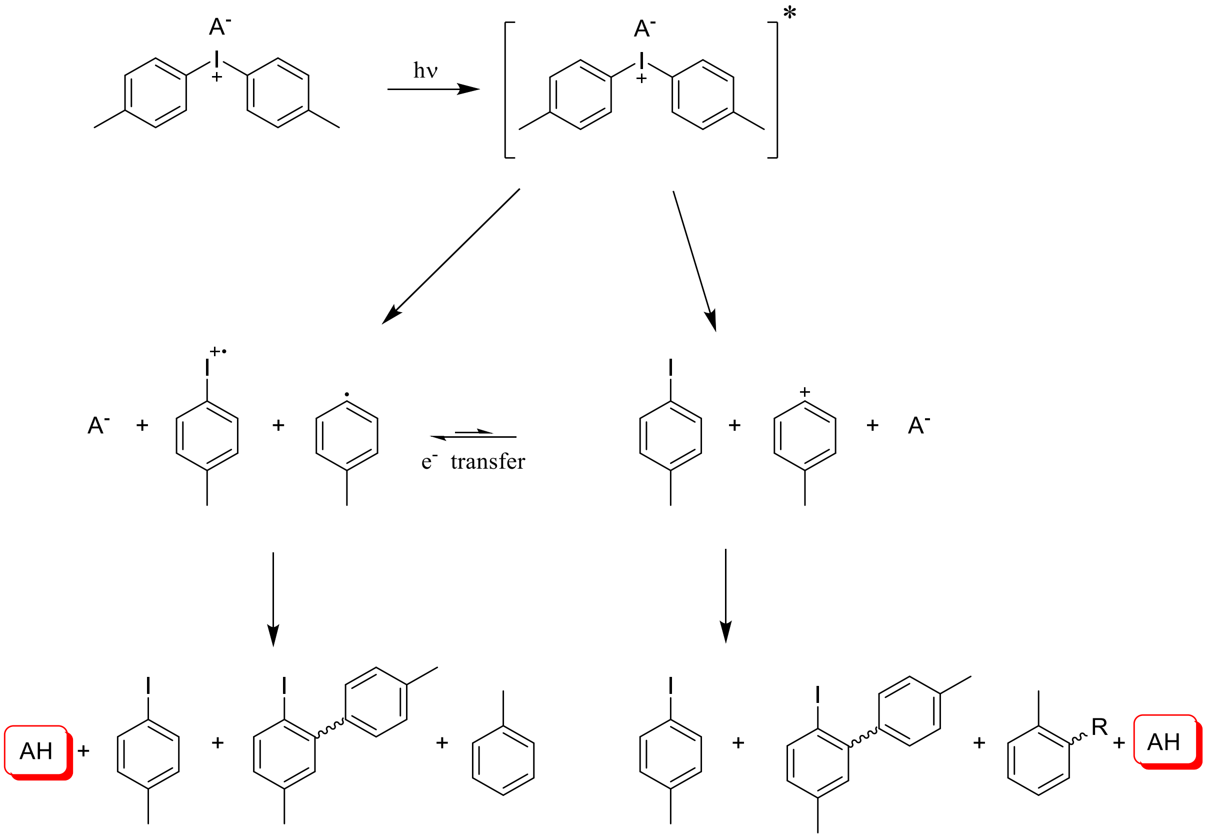

Scheme 1.2: Photoinduced decomposition mechanism of a iodonium (4,4'-Dimethyl-diphenyl iodonium) salt and formation of the active cationic initiator species (AH).[101]

Most onium salts absorb high energy radiation in the UV spectrum[99], which does not fully penetrate transparent plastic substrates like polycarbonate[103]. In addition, the application of UV light in industrial processes has become unpopular because of safety reasons and high energy costs compared to the use of LEDs.[30] As a consequence, photosensitizers with absorption bands in the visual light spectrum are often utilized as co-initiators.[67] The shift in wavelength of the required radiation allows the application of LEDs, resulting in lower energy costs, minimized safety risks and improved substrate penetration. The activation mechanism is shown in Scheme 1.3.[104] The absorption of light by a photosensitizer (PS) forces the PS into an excited state (PS*). The PS* and the onium salt (On^+X^-) form an exciplex, which facilitates an electron transfer from PS* to the onium salt, yielding an onium radical and a PS radical cation. An exciplex is a complex of two atoms or molecules, which is only stable if at least one of the atoms or molecules is in an excited state. The PS radical cation reacts with a hydrogen donor and a photosensitizer cation is formed. This can either directly initiate polymerizations or form an initiating Brønsted acid.[85] Chemically, PS are often aromatic compounds such as benzophenone or anthracene derivates.[104] When selecting a suitable PS for a distinct photoinitiator, the (extended) Rehm-Weller equation (equation 1.2) is taken into account.[85]

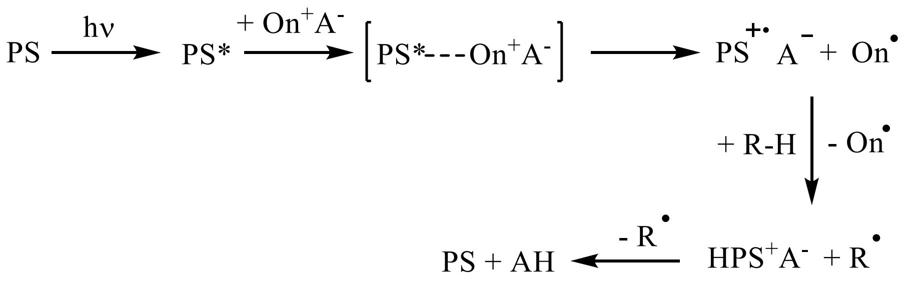

Scheme 1.3: Indirect initiation of cationic polymerizations by formation of an exciplex by an onium salt (On^+A^-) and a photosensitizer (PS).[85,104]

$$\Delta G = F \cdot \left[E^{\mathrm{ox}}_{\frac{1}{2}}(R^{\cdot}) - E^{\mathrm{red}}_{\frac{1}{2}}(\mathrm{On}^+) \right] \tag{1.1}$$

$$\Delta G = F \cdot \left[E^{\mathrm{ox}}_{\frac{1}{2}}(\mathrm{PS}) - E^{\mathrm{red}}_{\frac{1}{2}}(\mathrm{On}^+) \right] - E(\mathrm{PS}^*) \tag{1.2}$$

ΔG is the free Gibbs energy, F is the Faraday constant, $E^{\mathrm{ox}}_{\frac{1}{2}}(\mathrm{PS})$ is the oxidation potential of the photosensitizer, $E^{\mathrm{red}}_{\frac{1}{2}}(\mathrm{On}^+)$ is the reduction potential of the onium and $E(\mathrm{PS}^*)$ is the excitation energy of the photosensitizer. The equation suggests the utilization of PS with low oxidation potentials and high excitation energies. Many anthracene derivates meet these requirements and have been proven to perform well with onium salts.[70]

In addition, cationic polymerization can be mediated by the utilization of radical starters in a mechanism called free radical promoted cationic polymerization.[105] A radical is produced by irradiation or thermal activation of a radical starter which in turn is oxidized by an onium salt to form a carbocation which initiates polymerization instead of a Brønsted acid otherwise formed by onium salt degradation. The efficiency of this process depends on the oxidation potential and is also described by the Rehm-Weller equation. This approach was refined and by addition of (poly)silanes which suppress any oxygen inhibition resulting in a silyl cation initiating species.[106,107] The corresponding activation mechanism is shown in Scheme 1.4.

In contrast to acid initiated polymerization, radical mediated homopolymerization of vinyl ethers is hardly feasible.[108] Under radical conditions, polymers of divinyl ethers were prepared by Kunitake et al. in 1979 by cyclization reactions but with small yields >30 %[109] whereas attempted polymerization of monovinyl ethers results in small oligomers which was discovered by accident in 1983 by Matsumoto et al[110] as vinyl ethers were labeled as unreactive in radical homopolymerization before. However, the limited yields and molecular masses do not result from a lack in reactivity but surprisingly in a massive surplus thereof.

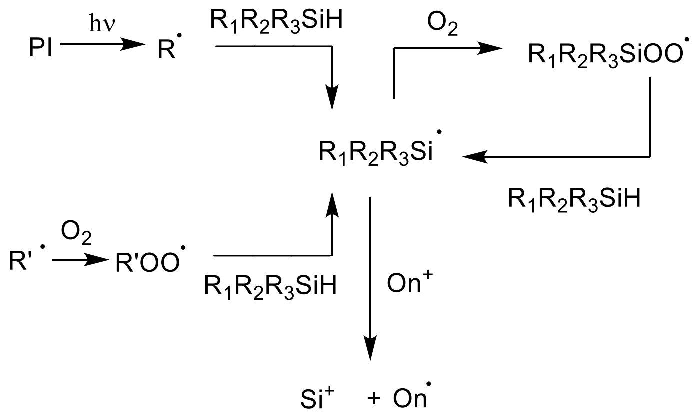

Scheme 1.4: Activation mechanism for silyl-radical mediated cationic polymerization initiation.[107]

By using high photoinitiator concentrations, radical active chain species were observed via electron spin spectroscopy which immediately disappear as soon as irradiation is stopped; an indication for high reactivity towards side and termination reactions.[111] This was further underlined by *ab initio* molecular orbital calculations which imply a divergence from planar sp^2-conformation of typical vinyl radical species in the case of vinyl ethers.[112] In 2008, Matsumoto et al. demonstrated that the rapid termination reactions predominantly proceed by hydrogen abstraction via backbiting followed by β-scission chain transfer and eventual recombination reactions with the resulting alkyl radical acting as an electron acceptor and the propagating chain species as an electron donor.[113] Nonetheless, recent advances made radical homopolymerization of vinyl ethers feasible at first limited to hydroxy-functional vinyl ethers in direct[114] and then extended to most vinyl ethers via RAFT polymerization[80]. In 2019, Sugihara et al. prepared homopolymers from alkyl vinyl ethers in radical homopolymerizations by adding an alkali salt, which results in a decrease in electron density of the double bond by cation-π interactions and thus reduced reactivity as well as in by controlled RAFT polymerizations.[115] A more interesting approach of utilizing vinyl ethers in radical systems for adhesive applications is their copolymerization with electron deficient monomers as adequate reaction partners, such as maleates[68,116] or acrylates[117].

A third relevant way of preparing polymers from vinyl ethers is thiol-ene polyaddition. Nucleophilic thiol moieties react with unsaturated compounds to form the anti-Markownikoff product either under radical conditions[118] or under basic conditions in a Michael-addition reaction[119] with remarkably high reaction rates[120]. In a Michael-addition mechanism, vinyl ethers do not yield significant conversions as the electron-rich double bond disfavors formation of the required anionic intermediate. However, radical thiol-ene “click chemistry” has been known for a long time in this context. In 1905, Posner first described addition reactions between mercaptans and olefins with aliphatic as well as aromatic structures.[121] After years of research, the first polymers with high molecular weight up to 14 kDA and crystalline structures were synthesized in 1948 by photoinitiation without an external initiator[122] and about 30 years later first attempts for industrial use were done[123]. In recent research, thiol-ene chemistry has become more interesting in terms of sustainability mostly due to high regioselectivity and fast reaction rates under mild conditions which include low temperatures and no reaction inhibition in atmospheric environments from oxygen or water in contrast to radical or cationic polymerization.[124] The versatility of polymers from thiol-ene addition has been demonstrated by application as resins for epoxy systems[125], polymers with optic properties[126] and hydrogels for biomedical use[127], just to name a few. The decisive step in radical mediated thiol-ene reactions is the formation of highly reactive thiyl radicals by cleavage of the S-H bond by irradiation, heat or most effectively by utilizing radical initiators which abstract hydrogen upon activation.[128] The resulting radical rapidly reacts with basically any molecule as long as it holds a sterically unhindered double bond. However, differences in reaction rates were observed as electron-rich enes react faster and less exothermic than compounds with an electron deficient double bond.[124] This makes thiol-ene polyaddition an attractive alternative to highly exothermic cationic polymerization of vinyl ethers in adhesive applications. Several biobased thiols have been synthesized and utilized for polymer preparation from biobased lipoic acid[129] or starch[130]. Moreover, a wide array of compounds is potentially available by esterification of biobased alcohols with mercapto acids[131].

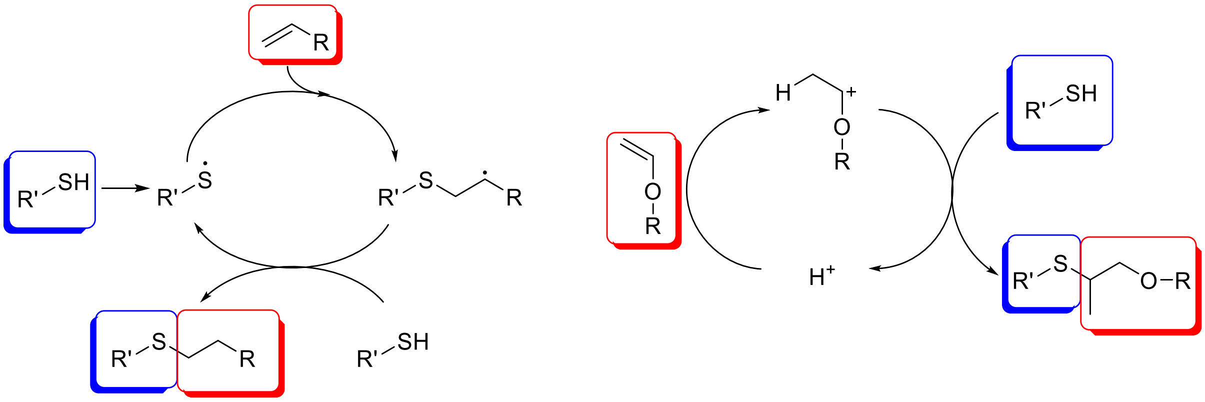

Scheme 1.5: Left: Radical mediated thiol-ene addition reaction of a thiol with a vinyl compound. Right: Acid mediated thiol-ene addition reaction of a thiol with a vinyl ether.

In a radical mediated thiol-ene polyaddition of polyfunctional thiols with polyfunctional vinyl ethers, polymers with thioether linkages are obtained which are expected to be highly flexible in terms of mechanical properties due to the mobility of C-S and C-O bonds. As an alternative, polyaddition under acidic conditions yields polymers with more inelastic thioacetal linkages.[132] Kamigaito et al. showed that the reactions mechanisms compete if radical and cationic initiators are utilized simultaneously resulting in polymers with random distribution of thioether and thioacetal groups.[132] This is of interest as most cationic photoinitiators form a radical intermediate upon irradiation which may lead to a significant share of thioether linkages in the polymer structure even in the absence of radical starters. Another advantage of acid mediated thiol-ene polyaddition is the degradability of the acetal groups adding debond on command and thus recycling features for more sustainable adhesive systems and green polymer chemistry in general.[133]

The highly exothermic cationic polymerization of vinyl ethers is an issue in adhesive applications as too much heat generation causes damage to the cured material as well as to susceptible substrate materials (s. section 3.1.1). This is one of reason why adhesive systems based entirely on vinyl ether functionality have not been developed yet, to the best of our knowledge, and monomer use has been limited to utilization as reactive diluents, especially in epoxide systems. As mentioned in section 1.1, utilizing prepolymers is a well-implemented method to reduce reactive group concentration and consequently reaction enthalpy relative to reaction mass. Hitherto, mostly polyurethanes with vinyl ether functionality were profoundly evaluated and were already synthesized and polymerized via irradiation in 1990 by Lapin et al.[134] In further research reports, vinyl ether polymerization by Lewis acids[135] were demonstrated. Also, kinetic measurements were conducted[136] and even their potential for use in adhesive applications was elucidated[61]. In addition, a number of patents were filed describing vinyl ether functionalized polyurethane resins for coatings[137] and adhesives[138]. Polyurethanes are prepared by polyaddition of multifunctional alcohols with multifunctional isocyanates, typically with two reactive moieties, respectively.[139] Scheme 1.6 shows the preparation of a prepolymer which is formed by polyaddition of a diol with an excess amount of a diisocyanate so terminal isocyanate groups can be end-functionalized with a hydroxy vinyl ether. Aromatic isocyanates react under mild conditions without a catalyst which is often added for less reactive aliphatic isocyanates; the most common catalysts are either organometallic Lewis acids[140] or tertiary amines acting as Lewis bases[141].

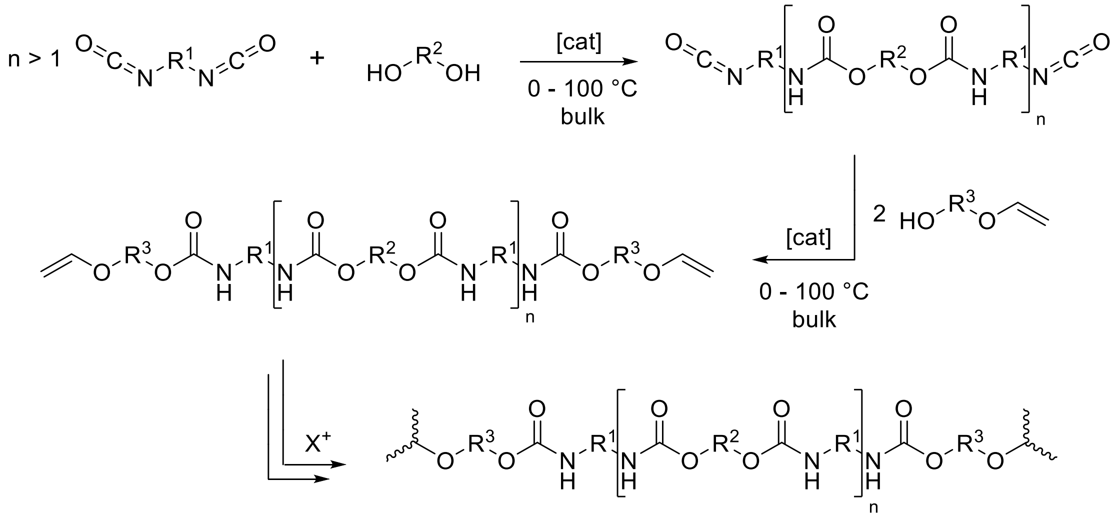

Scheme 1.6: Synthesis and cationic polymerization of a urethane-based prepolymer from a dithiol and a diol, end-functionalized with a hydroxy vinyl ether.

There is a difference in reactivity of vinyl ether moieties in cationic polymerization depending on the prepolymer backbone as kinetics show an inhibition of vinyl ether conversion in polyurethanes from aliphatic diisocyanates compared to aromatic urethane prepolymers.[142–145] This leads to the assumption that urethanes in general may inhibit cationic polymerization by immobilizing the active acidic species due to slight basicity of the carbamate group. Moreover, production of isocyanates from renewable sources is currently an issue to be solved and thus polyurethanes are only partly suitable for sustainable systems.[146] Thus, enlarging the toolbox of potential prepolymers for vinyl ether-based systems is desired.

An interesting choice are hemiacetal esters due to their degradability and potential for high biobased carbon shares. Several synthesis routes for hemiacetal ester compounds were demonstrated. For example, Baeyer-Villiger oxidation of a cyclic ketone with an additional oxygen atom[147], cyclization of a β-hydroxycarboxylic acid with acetaldehyde or a ketone[148], or by an addition reaction of a carboxylic acid with a vinyl ether[149]. In this work, the focus lies on carboxylic acid polyaddition reactions for prepolymer synthesis. Specifically, an excess amount of a divinyl ether is reacted in bulk at about 90 °C with a dicarboxylic acid to form a polymer with vinyl ether end-functionalization to enable further polymerization by cationic initiation as displayed in Scheme 1.7.[32] Under these mild and convenient reaction conditions, full acid conversion can be achieved.[150] By increasing the amount of functional groups per molecule, macromolecular crosslinkers can be obtained. Besides the potential production of vinyl ethers from renewable resources, biobased dicarboxylic acids are already well implemented in research and industry giving access to polymers and consequently reactive components for adhesive systems from 100 % renewable carbon.[151] In addition, hemiacetal ester polymers are well-degradable due to their sensitivity towards hydrolysis of the functional group.[152] This will be further discussed in section 1.3.1.

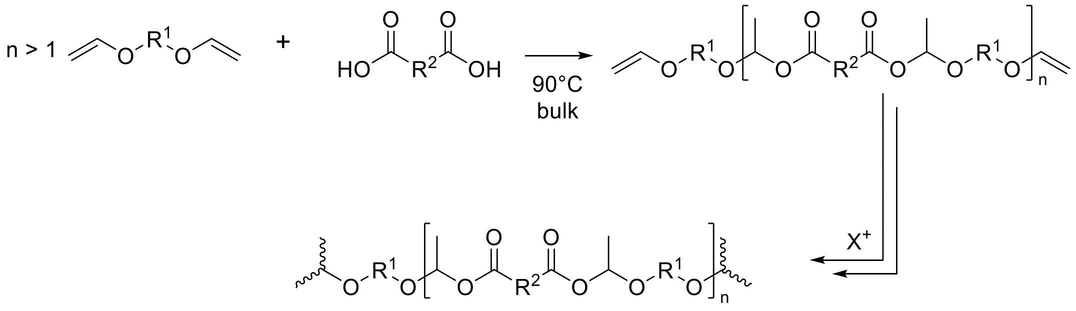

Scheme 1.7: Synthesis and cationic polymerization of a hemiacetal ester-based prepolymer from a dicarboxylic acid and a divinyl ether, given in excess amounts for vinyl ether end-functionalization.

1.2.2 4-Vinylphenol and its derivatives

In literature, polymerizable phenol derivatives have gained considerable attention for their use as an alternative for styrene in polymer chemistry.[153] One reason is the high potential for production from waste streams in the pulp and paper industry as lignin bears many phenolic structures which can be isolated from pyrolytic oils.[154] Starting from the lignin phenylpropane basic unit, alcoholic groups from the alkyl chain are dehydrated and bonds between aromatic rings are cleaved.[154] The product mixture varies depending on reaction conditions and the utilization of organic catalysts like anthraquinone as well as inorganic Cu (II) and Fe (III) salts and oxides under mild alkaline conditions favor production of phenolic aldehyde compounds such as guaiacol and syringol.[154] Moreover, vanillin from lignin is already commercially available[154] although the final purification stage is challenging and currently only feasible by high energy consumption and the use of harmful solvents[155]. Besides their use as value-added flavor and fragrance compounds,[156] the aforementioned phenolic aldehydes can be further modified for polymerization in a Wittig reaction[157] or via a greener route in a Knoevenagel reaction yielding a hydroxycinnamic acid followed by two decarboxylation steps [158] as shown in Figure 1.6. The intermediate hydroxycinnamates can also be obtained by fermentation of lignocellulosic material, adding another green pathway to the production options.[159] In addition, enzymatic decarboxylation of these acids was reported in literature[160] and Myrtollari et al.[161] demonstrated high activity enzymatic decarboxylation as an alternative to current high energy processes.

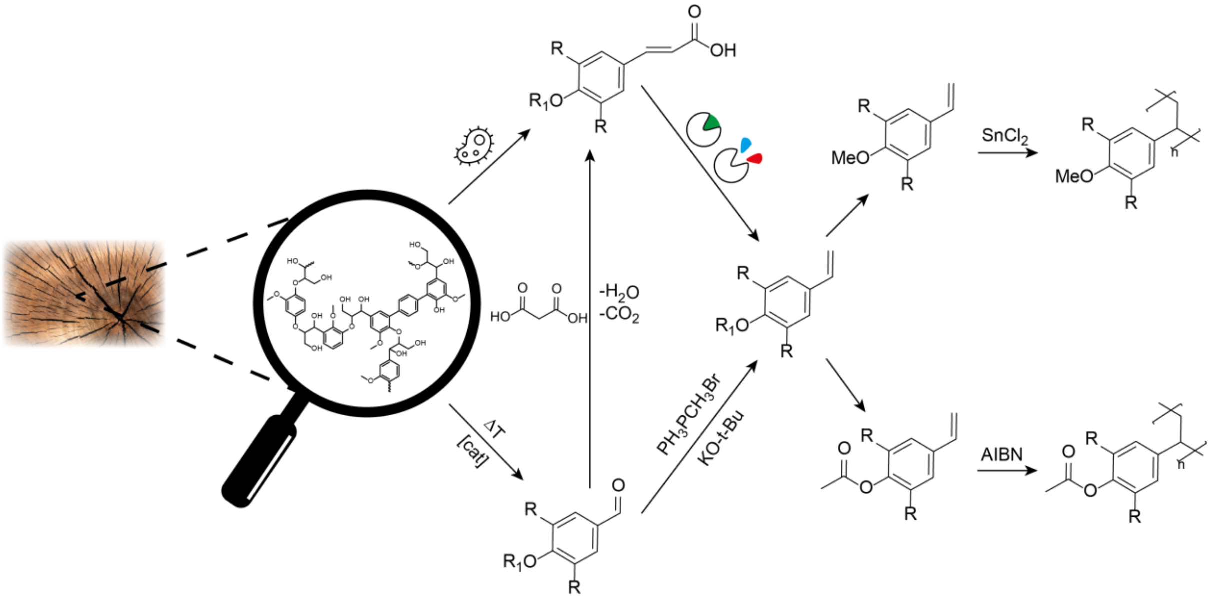

Figure 1.6: Pathways for the synthesis of 4-vinylphenol and derivatives from lignocellulosic waste streams followed by polymerization.

4-vinylphenol (**4VP**) is a simple compound from the class of phenol derivatives with a vinyl group for polymerization reactions similar to the common monomer styrene. A challenge in handling 4VP is its low thermal stability as it is prone to self-polymerization under storage.[162] Typically, this issue is circumvented by protection of the OH group and deprotection after polymerization. Protection of the hydroxyl group does not only increase storage stability but opens up a wide array of post-functionalization possibilities of the aromatic ring and consequently the polymerizable double bond.[153] The electron density of the vinyl group can be altered to adjust the respective monomers for subsequent polymerization as acetylation yields an electron-deficient vinyl compound which performs well in free radical polymerization to form high T_g polymers in high yields.[153] In contrast, high conversions by Lewis acid-mediated cationic polymerization of electron-rich 4-methoxy styrene (**4-MeOS**) has been reported. However, when compared to a isobutyl vinyl ether, a well-studied monomer for cationic polymerization, polymerization of p(4-MeOS) proceeds in a less controlled manner.[163] 4-MeOS is a part of this work in adhesive systems for cationic copolymerization with vinyl ethers which is expected to show high conversion in cationic light curing processes based on the described reports. Furthermore, an interesting compound, which has already been reported for utilization in adhesive systems, is synthesized by a Wittig reaction of 4-hydroxybenzaldehyde followed by allylation of 4-vinylphenol.[157] Akin to 4-MeOS, electron density of the vinyl group in 4-allyloxy-styrene is increased by the alkoxy substituent and thus high reactivities in cationic polymerization were observed.[164] Based on this vinyl-allyl derivative, adhesive systems were developed following two curing stages: cationic photopolymerization and thermal post-curing.[165] In the first step, mainly vinyl groups react to form long polymer chains with allyloxy-phenyl side chains as the allyl groups hardly undergo cationic polymerization (Scheme 1.8). At temperatures above 140 °C, the allyl groups react in a Claisen rearrangement yielding an aldehyde in a keto-enol tautomerization equilibrium. In a final step, phenolic rings in the polymer side chain are crosslinked in acid-catalyzed intermolecular phenol-ene reactions and materials with superior thermal stability are obtained.[164,165] By sulfation of the OH group, p-styrene sulfate is obtained which has not been investigated in literature so far. This ionic monomer is an important part of this work and will be analyzed regarding its synthesis, polymerization behavior, stability, and effect on adhesive features reliant on ionic conductivity. All four described derivates are prepared by functionalization of the OH-group and yet enable completely different curing mechanisms and even additional features. This highlights the versatility of 4VP and underlines the appeal of intensive research of this monomer and its derivatives.

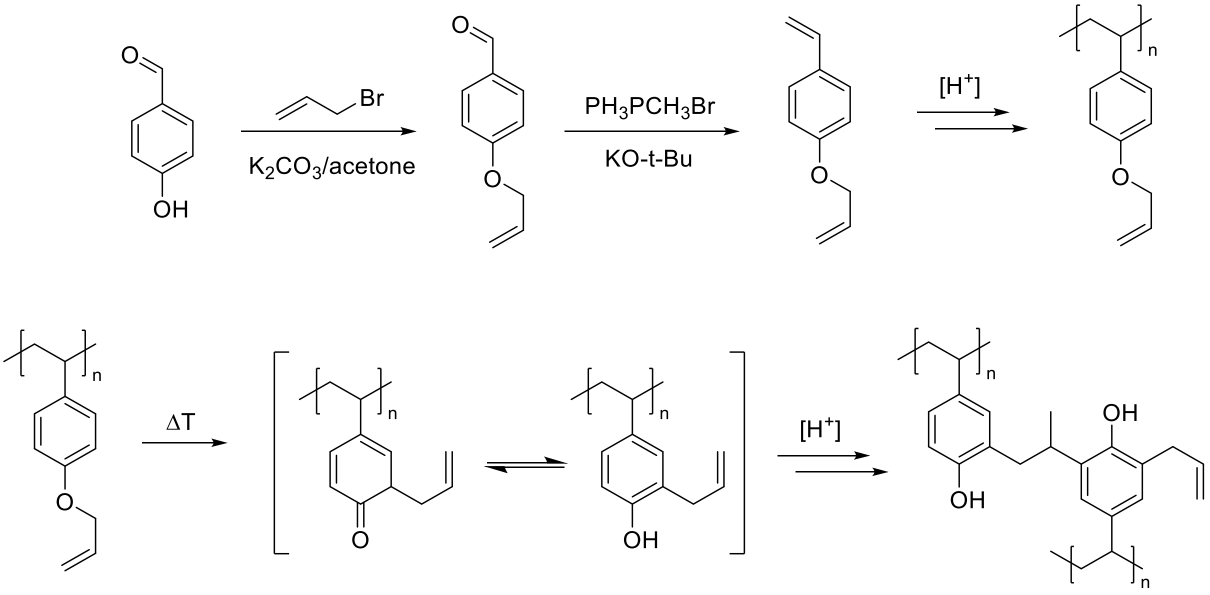

Scheme 1.8: Top: Preparation of 4-allyloxy-styrene from 4-hydroxybenzaldehyde followed by cationic polymerization. Bottom: Thermal crosslinking of poly(4-allyloxy-styrene).

Overall, 4-vinylphenol and its derivatives are interesting for the adhesive industry due several factors: Production from biomass feedstocks has been demonstrated under laboratory conditions as well as environmentally friendly pathways for post-modification and -functionalization. Yet, there is still a long way to go for industrial production at large scale. Depending on the substituents in general and most prominently on the OH-group, polymerization behavior can be tailored, e.g. for high reactivity in cationic polymerization. The latter makes copolymerization with vinyl ethers attractive for adhesive systems characterized by fast curing and high bio-contents. In addition, aromatic structures have been found to increase the intrinsic adhesion of polymers towards substrate surfaces.[166,167]

1.3 Adhesives for debonding-on-demand

Adhesive debonding is a process defined as separation of substrates joined by an adhesive with the help of an external trigger. It can be a result of any external force related to e.g. temperature, pressure, electricity, induction, dissolution or mechanical force.[168] This process has implications for a number of industries, from automotive, electronics, appliance and device industry to biomedical.[168] The main motivations for developing debonding systems is to enable recycling and repair solutions for final products or valuable parts in products such as metals in electronics or paper from packaging. Adhesives should support this or at least do not disturb the recycling process. Another aspect is to facilitate repair and maintenance of products that contain adhesives.[169] One can distinguish between end of life recycling and repair cases to enable longer life cycles. For both scenarios, adhesives must be designed to allow debonding. Currently, debonding is mainly conducted by mechanical or thermal destruction of the adhesive layer which bears difficulties for sensitive substrate materials or by utilization of solvents (s. section 1.3.1). Depending on the chemistry and material properties of an adhesive, these debonding techniques become increasingly difficult with chemically and thermally stable as well as high performance adhesives. In addition, products are usually not designed for adhesive debonding or recycling in general. The adhesive layer is often not accessible without destroying valuable parts of the product or there are simply no recycling processes implemented to deal with the product at the end of its life cycle. Contemporarily, different methodologies to circumvent challenges in destructive debonding techniques are discussed in literature; e.g. reversible systems.[168] By applying an external trigger like heat or radiation, solid polymeric materials can be turned into viscous, almost liquid, layers with no significant cohesive strength which can be re-bonded by other stimuli.[170] One approach is the exploitation of reversible covalent bonding; an example are Diels-Alder bonds which can be cleaved at temperatures above 90 °C, yielding low molecular weight polymers with inferior cohesive strength for easy separation of substrates, followed by re-bonding at room temperature.[171] Moreover, polymers with switchable supramolecular structures are highly promising for debonding, especially in applications with low T_g requirements.[168] Other mentionable debonding technologies are pH-controlled systems based on Schiff base chemistry and catechol groups[172] as well as magnetic field-controlled adhesives[173]. The biggest challenge for extensive material recycling is the adjustment of products and their manufacturing processes to enable debonding processes by design. Research in polymer chemistry and the adhesive industry are necessary to develop adhesives with debonding-on-demand features under mild conditions and without mechanical stress, but also to show the limitations in maintaining high adhesive performances in terms of initial strength as well as ageing stability.[168,169]The latter is an ever-occurring challenge especially in systems designed for debonding by hydrolysis.[174] In theory, this issue is avoided by applying electricity for debonding in electrochemical delamination processes.[175] Both well-implemented approaches are discussed in the following.

1.3.1 Debonding by hydrolysis

Adhesive debonding by hydrolysis is a process used to separate two surfaces that have been bonded together by interaction of the adhesive layer with water.[176] This process has been used in many areas of industry for decades and its use has grown significantly with the advances in modern technology. It is now widely applied in many areas, including medical, automotive, aerospace, and industrial applications.[33,177] Typically, adhesive debonding by hydrolysis is performed by using two different methods: by weakening of the cohesive strength of a polymer by swelling[178] or dissolving[179], as well as by direct cleavage of bonds within the polymer network[180]. The former is the most common method for substrate separation and brings the advantage of a broad application array for many different kinds of adhesives, but often by utilizing organic solvents. However, direct degradation of the polymer network by water is more effective and causes less safety hazards as only water and catalytic amounts of a base or acid are needed. On a downside, polymers containing functional groups degradable by hydrolysis are naturally susceptible to decreases in mechanical strength over time due to reactions with water molecules from the surrounding air.[174] The most common materials affected by direct hydrolysis are aliphatic polyesters made from polyaddition of dicarboxylic acids with diols[181], ring-opening polymerization of lactones, such as caprolactone[34] or γ-butyrolactone[182], or cyclized lactic acids[183]; synthesis and degradation of aromatic polyesters was reported as well[184].

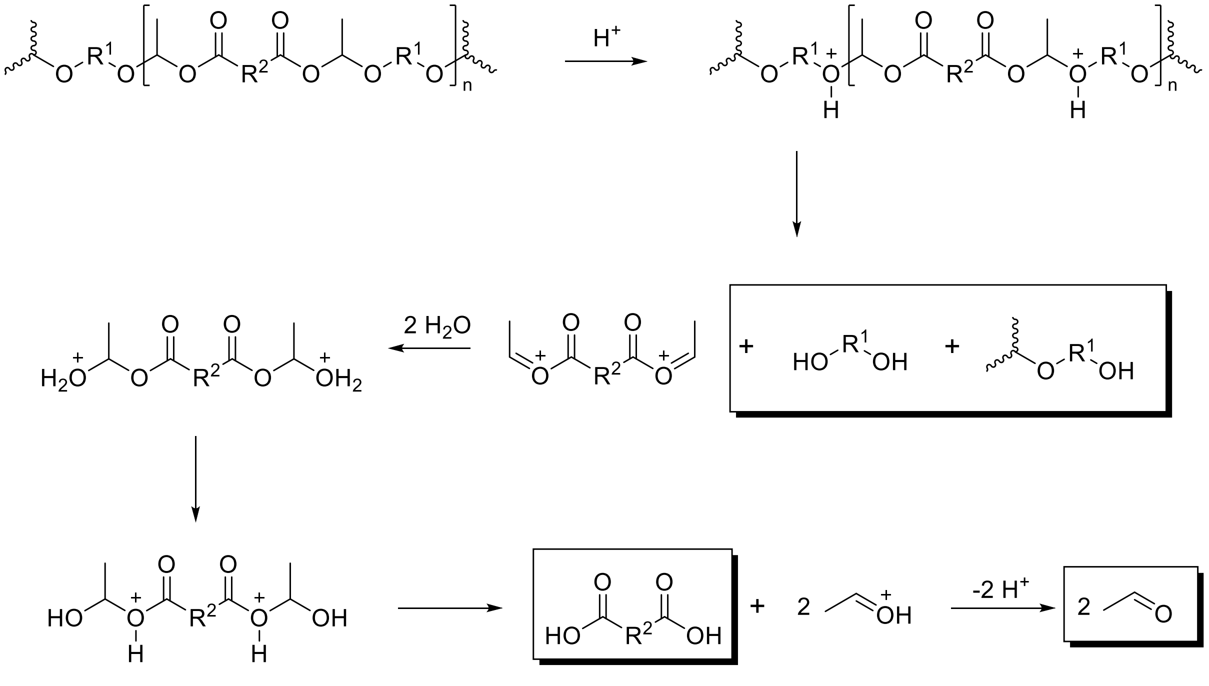

Scheme 1.9: Acid catalyzed hydrolysis of hemiacetal ester moieties in a poly(vinyl ether) network.

Regarding debonding by hydrolysis, the focus of this work lies on degradation of hemiacetal ester moieties in poly(vinyl ether) networks due to convenient prepolymer synthesis and potentially low viscosity compared to urethane prepolymers for better processing. The process of hemiacetal ester hydrolysis has been thoroughly studied in literature[149,152,185] and is illustrated in Scheme 1.9 for a poly(vinyl ether) crosslinked by hemiacetal ester prepolymer chains. Triggered by acidic catalysis, the polymer backbone is cleaved resulting in formation of the diol corresponding to the vinyl ether, the dicarboxylic acid used for hemiacetal ester synthesis, and formaldehyde. The poly(vinyl ether) chains afterwards only exhibit small alcohol terminated side chains instead of hemiacetal ester crosslinks which results in a significant decrease in cohesive strength and thus facilitated substrate debonding in adhesive applications. Moreover, hemiacetal ester can be degraded thermally between 200 °C – 250 °C, yielding additional debonding conditions for acid or water sensitive substrates.[150,186] Recently, cationic polymerization of vinyl ether functionalized hemiacetal ester prepolymers and their thermal as well as acid catalyzed hydrolytic degradation was reported.[32] Surprisingly, the use of aqueous acidic solutions did not result in polymer cleavage but the addition of a polar solvent like acetone or methanol is required. However, the impact on material properties and more specifically on debonding of adhesive joints has not been investigated yet to the best of our knowledge.

1.3.2 Electrochemical debonding

Adhesive electrochemical debonding (**ECD**) or delamination (**EDL**) is a technique that enables the precise removal of bonded materials such as cables, wires, and micro-electronic components from its substrate without causing damage to the substrate.[168] This technique is well established in a wide range of applications within the manufacturing sector, which includes the removal of fragile substrates such as semiconductor devices, high-density memory chips, and printed wiring boards.[187] Electrochemical debonding has several advantages over traditional mechanical debonding approaches, such as reducing the risk of mechanical damage, providing a gentle removal process for fragile substrates, and enabling processing speeds which are significantly faster than alternative methods.[175] The process involves using electricity to remove adhesive bonds between a substrate and the material, usually a cable, wire, or microelectronic component, that is attached to the conductive glued substrates. Starting with the substrate, an electrical potential is applied across the interface between the bond and the substrate, thus creating an electrochemical reaction which breaks the bond.

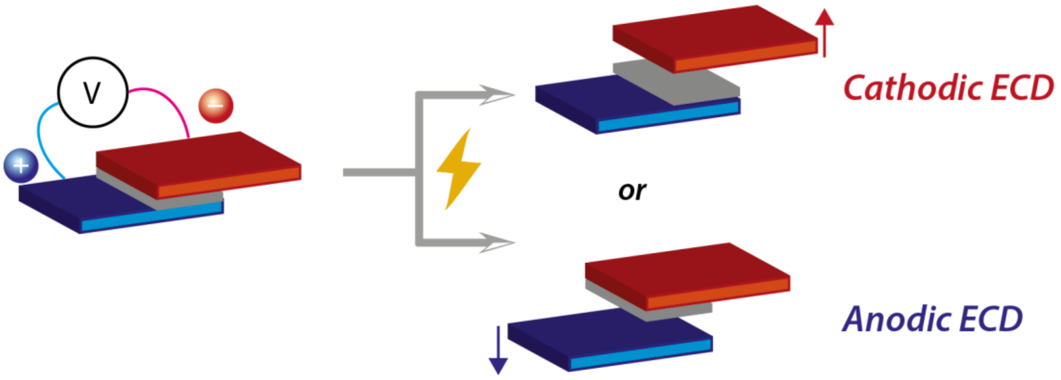

Figure 1.7: Electrochemical debonding (ECD) resulting in separation of either the cathode or the anode from the adhesive layer.

Ionic or electronic conductivity of the adhesive layer is essential, often achieved by the utilization of graphene, solvated salts and ionic liquids[188], which are inert regarding the curing process, or reactive polymerizable ionic liquids (PILs)[189]; examples are given in Figure 1.8. Different mechanisms behind the debonding process were proposed, i.e. phase separation[190], gas emissions[191] or faradaic reactions[192]. A challenge shared by most ECD systems is the limitation to one-sided delamination, either on the cathode or the anode. This makes a second processing step necessary to remove the adhesive layer and consequently weakens the advantages provided by fast and mild adhesive debonding via ECD. However, Chou et al.[193] deeply studied electrochemical debonding of acrylic adhesives with ILs based on imidazolium. They proposed a mechanism starting with diffusion of an ionic liquid towards the electrodes followed by oxidation of a substrate, aluminum in this case, and reduction of the imidazolium cation. As a conclusion, a system must undergo electrochemical reactions on both electrodes in order to successfully debond on both substrates. Generally, the main limitation of this debonding technique lies in the criteria of conductive substrate materials which narrows down the scope of possible products.

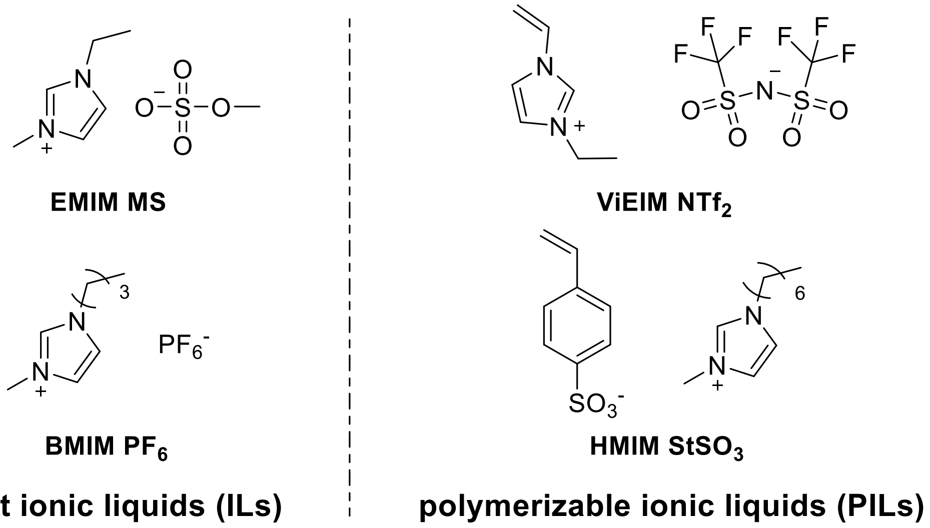

Figure 1.8: Examples of ionic liquids commonly used in adhesives for electrochemical debonding. Left: ILs, 1-ethyl-3-methylimidazolium methylsulfate (EMIM MS) and 1-butyl-3-methylimidazolium hexafluorophosphate (BMIM PF$_6$), do not participate in curing reactions. Right: PILs, 1-vinyl-3-ethylimidazolium bis-(trifluormethylsulfonyl)-imid (ViEIM NTf$_2$) and 1-heptyl-3-methylimidazolium p-styrene sulfonate (HMIM StSO$_3$), undergo polymerization reactions in the curing process of the adhesive.

2 Motivation and Aims

Global industry currently adapts processes towards a more circular economy due to challenges posed by climate change and dependence on fossil fuels. Besides the production of electricity or energy in general from renewable sources, the readjustment of products towards high sustainable carbon contents and more accessible recycling and repair solutions is a driving factor. The compounds and application systems in this thesis are evaluated in the context of adhesives. Whereas companies that use adhesives in their products have to adjust their product design to facilitate recycling by means of adhesive debonding, it is the task of the adhesive industry to develop new systems from biobased feedstocks and evaluate their potentials and limitations. In this work, two potentially biobased materials are investigated: vinyl ethers and 4-vinylphenol derivatives.

The main objective of the investigation of vinyl ethers in this work is to understand the advantages and drawbacks of vinyl ethers in adhesives with a focus on light curing systems. Utilization of vinyl ethers in industry is limited to reactive diluents in cationic reactive formulations at the moment. An important driving factor behind this work is to understand the reasons behind the narrow application scope of vinyl ethers in adhesive systems. Some possible reasons are high production prices and their extraordinarily strong exothermic behavior during curing as well as deficits in adhesion. Intense heat generation can cause material degradation and consequently a loss in cohesion, which must be avoided. Thus, an important goal in this thesis is gaining control of the exothermic cationic polymerization by means of formulation, mostly by reducing the concentration of reactive vinyl ether groups. By developing prototype formulations, the unique characteristics of vinyl ethers will be evaluated in the search for interesting properties and to lay the foundation for new products and adhesive solutions on the market which meet sustainability criteria. To guide the development process, fundamental research on the reactivity and stability of monomers and prepolymers with vinyl ether functionality will be conducted. A major objective of this work is the development of a final vinyl ether prototype formulation based on the insights obtained from the described experiments with good adhesive performance and debonding features.

In academic research, 4-vinylphenol derivatives have gained considerable attention in the last years for high-performance materials obtained from biobased feedstocks. The focus in this thesis lies on 4-methoxy styrene and 4-styrene sulfate. Due to electronic effects of the methoxy group, 4-methoxy styrene is expected to quickly undergo cationic polymerization reactions and will thus be incorporated into vinyl ether adhesive systems with the aim to increase adhesive performance, especially in terms of adhesion. So far, styrene sulfate has not been the target of research in literature to the best of our knowledge. Therefore, the polymerization kinetics of this novel monomer will be investigated and based on these results, potential application fields will be determined. The most outstanding feature of this reactive compound is its ionic character which allows the development of conductive adhesives. Typically, inert ionic liquids are added to formulations to achieve ionic conductivity, but a disadvantage of these compounds is a decrease in adhesive performance. Hence, the main goal of the utilization of styrene sulfate in this work is to facilitate a decrease in ionic liquid additive content to maintain ionic conductivity but improve adhesive performance.

3 Results and Discussion

3.1 Novel vinyl ether-based adhesive systems

3.1.1 Cationic homopolymerization of vinyl ethers

In order to design novel adhesive systems based on vinyl ether functionality, it is crucial to investigate the polymerization behavior of monomers as fundamental building blocks. Besides the choice of monomer, a suitable polymerization initiation system must be identified. As described in section 1.2.1, the first development approach for vinyl ether adhesives aims at light cure applications, and iodonium salts are reportedly well suited for these systems. In pretests, *Omnicat 440* (Bis(4-methylphenyl)iodonium hexafluorophosphate, **PI 440**) by *IGM Resins* was determined as the initiator of choice due to its good solubility in most monomers as well as sufficient reactivity despite its comparably unreactive, but nontoxic anion hexafluorophosphate. For experiments or formulations which require increased reactivity, the photoinitiator *Sylanto 7M-S* ((7-methoxy-4-methylcoumarin-3-yl)phenyl iodonium hexafluoroantimonate, **PI 7MS**) by *Synthos* was utilized due to its higher reactivity influenced by the anion.[102] The photosensitizer Anthracure UVS-1331 (9,10-Dibutoxyanthracene, **PS 1331**) by Kawasaki Kasai Chemicals LTD was added to ensure thorough curing for LED applications with $\lambda = 405$ nm. The respective structures of the initiating and sensitizing compounds are shown in Scheme 3.1.

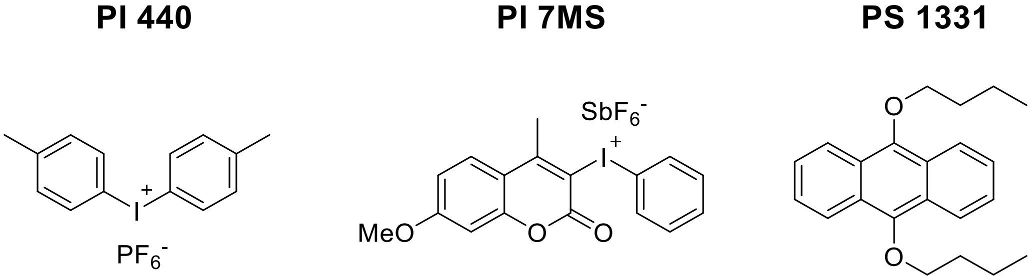

Scheme 3.1: Photoinitiators Bis(4-methylphenyl)iodonium hexafluorophosphate (PI 440, left), 7-methoxy-4-methylcoumarin-3yl)phenyl iodonium hexafluoroantimonate (PI 7MS, middle) and photosensitizer 9,10-Dibutoxyanthracene (PS 1331, right).

In preliminary tests, different PI and PS concentrations were tested regarding reactivity and miscibility. For most application tests in this work, initiator concentrations between 1 – 2 wt% and sensitizer concentrations between 0.3 – 1 wt% were identified for high conversion while keeping the respective concentrations as low as possible. It is worth mentioning that these concentrations are significantly lower than typical initiator concentrations of 3 – 5 wt% in most adhesive applications. First vinyl ether polymerization experiments were performed by adding 1 wt% of PI 440 and 0.3 wt% of PS 1331 to various monomers and initiate polymerization by LED irradiation for 5 seconds. As expected, all monomers show an immediate highly exothermic reaction; an example is shown in Figure 3.1a. Heat generation while curing exceeds the limits of the material's thermal stability and subsequently decomposes the polymer, compromising its mechanical properties in the process. The reaction was accompanied by smoke evolvement and for masses of over one gram of monomer, the reaction mixture ignited. Still, a more thorough look was taken by performing differential scanning calorimetry (DSC) experiments with the same monomer-initiator mixtures as described above. Thermal initiation of the systems starts between 80 °C - 90 °C. However, the samples decompose during measurement which highlights the extensive heat generation by cationic homopolymerization of vinyl ethers and data acquisition was not possible as the reaction takes place in such a violent manner that all sample pans were removed from the measurement setup, most likely due to a small explosion inside the pan. An example is shown in Figure 3.1b.

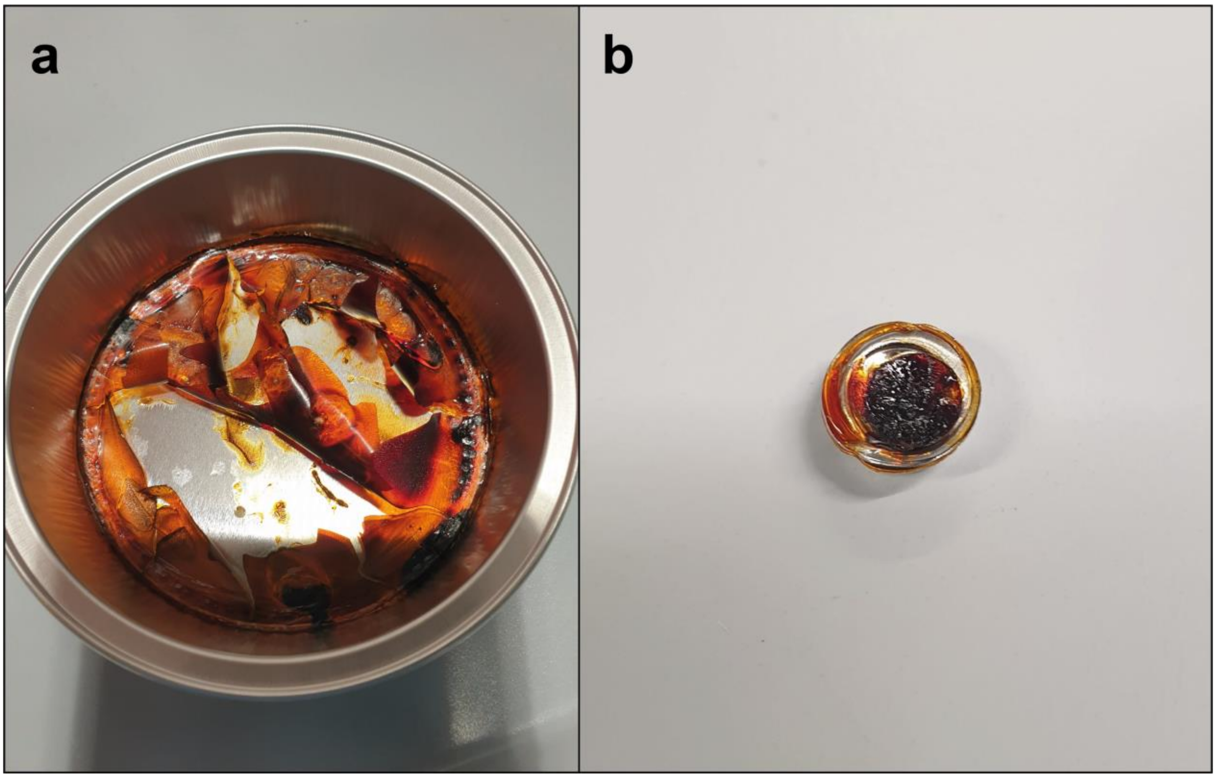

Figure 3.1: Highly exothermic cationic polymerization of vinyl ethers demonstrated by mixture of TEGDVE with 1 wt% of PI 440 and 0.3 wt% of PS 1331 a) after five seconds of LED irradiation in an aluminum pan and b) after DSC measurement.

Still, even in this highly reactive system, valuable insights about curing behavior and material properties of the resulting homopolymers were obtained by rheology experiments. A thin layer (d = 0.200 mm) of a mixture of the respective monomer with 1 wt% of PI 440 was applied to a quartz plate and sheared with a stainless-steel mandrel. The mixture was irradiated with UV light from a mercury lamp and material responses to the applied shear stress were monitored over the curing process. The experimental setup better prevents damage to the polymer by excessive heat generation due to the very thin reactive layer (and consequently low reaction mass) and the good thermal conductivity of the sample holder. Storage modulus *G'*, loss modulus *G''* and dissipation factor tan *δ* over time of two exemplary vinyl ether monomers are shown in Figure 3.2. Additional rheometric data on various monomers can be found in the appendix (Figure 6.1 - Figure 6.11). Both monomers are difunctional but differ in their structure with CDVE bearing a sterically hindered cyclohexyl group between the functional groups compared to the more mobile C_4-alkyl chain of BDVE. Independent from their structure, both monomers polymerize immediately on irradiation and *G'* and *G''* quickly reach a plateau. On account of the living character of the polymerization, the plateau can be interpreted as full vinyl ether conversion. The values of *G'* of the polymers are comparable but *G''* of p(CDVE) is decreased compared to p(BDVE) and consequently the dissipation factor of the latter is significantly increased. This is in line with the expectation that p(BDVE) is softer or more flexible regarding its mechanical properties which can be explained by a more intrinsically flexible polymer structure attributed to the more agile alkyl chain compared to the stiff cyclohexyl structure. Data on material properties obtained from rheometric experiments can be used in formulation development to select the right monomers and respective polymers in order to tailor the technical properties of the cured adhesives. For example, higher concentrations of monomers with lower dissipation factors are utilized to increase the rigidity of a material that is too flexible for an allocated application and vice versa.

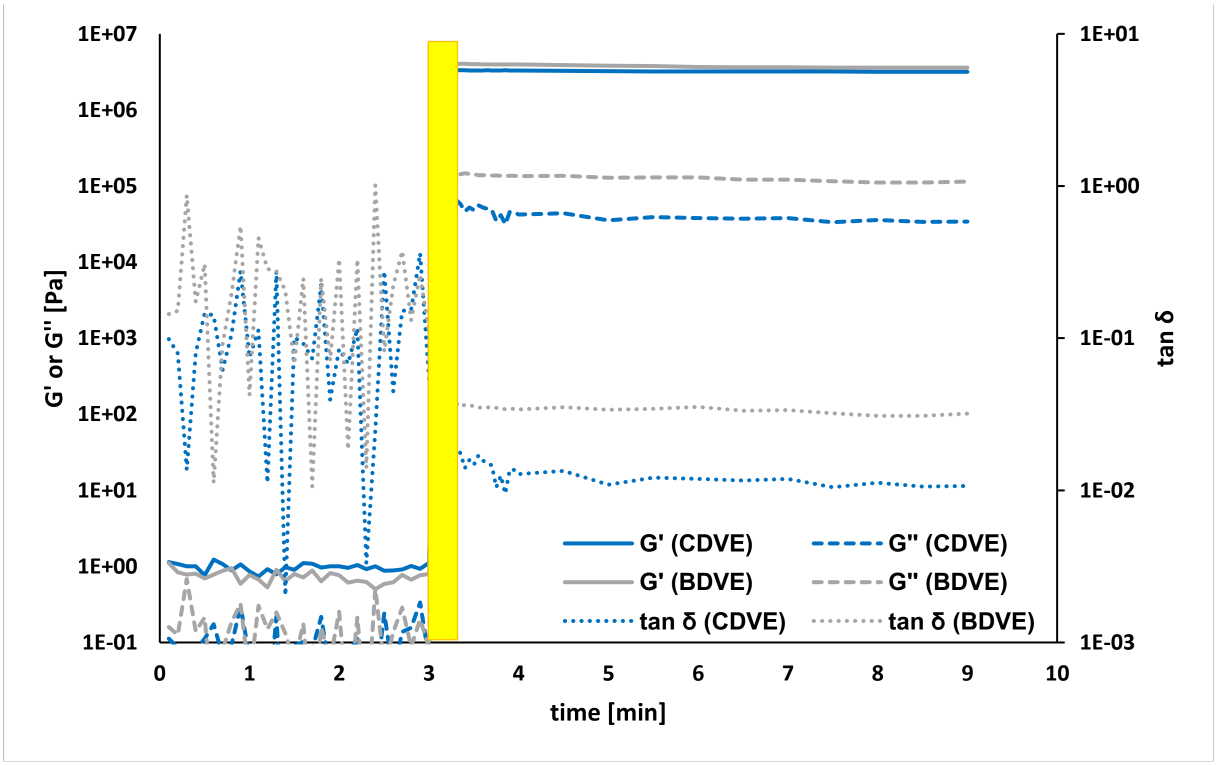

Figure 3.2: Storage modulus *G'* (solid line), loss modulus *G''* (dashed line) and dissipation factor tan *δ* (dotted line) over time of mixtures of divinyl ether monomers BDVE (grey) and CDVE (blue) with 1 wt% of PI 440. To initiate cationic polymerization, the mixtures were irradiated with UV light for 20 seconds indicated by the yellow area.

However, adhesive systems consisting of only small monomers and initiators were ruled out in formulation development due to the highly exothermic nature of vinyl ether cationic polymerization and its subsequent negative impact on mechanical properties. It is imperative to control heat generation for adhesive applications by formulation approaches utilizing filler materials (section 3.1.3) and prepolymers as discussed in the following.

3.1.2 Polyurethane prepolymers in vinyl ether-based adhesives

High functional group reactivity for curing polymerization reactions is strongly desired for adhesive systems, especially for photocuring to ensure fast and high conversion. However, exceedingly strong heat generation due to exothermic polymerization reactions can lead to spontaneous gas formation and decomposition of the material which is detrimental for adhesive performance. This applies to light- as well as thermal curing of small vinyl ether monomers and thus decreasing heat generation during polymerization is vital. Commonly, there are two ways to achieve this goal. Either by adding inert filler materials or by utilizing prepolymers; the latter are relatively small polymers or oligomers with terminal reactive groups. In addition to or instead of small monomer molecules, prepolymers are often utilized to reduce reactive group concentration and to implement additional structural groups from the prepolymer backbone into the polymer chain. In literature, vinyl ether functionalized polyurethane prepolymers usage was often described, even without addition of reactive diluents, i.e. low molecular weight vinyl ether monomers. The general preparation of urethane compounds is explained in section 1.2.1. The syntheses of urethane prepolymers utilized in this work **PU-2** and **PU-3** are described in schemes Scheme 3.2 and Scheme 3.3.

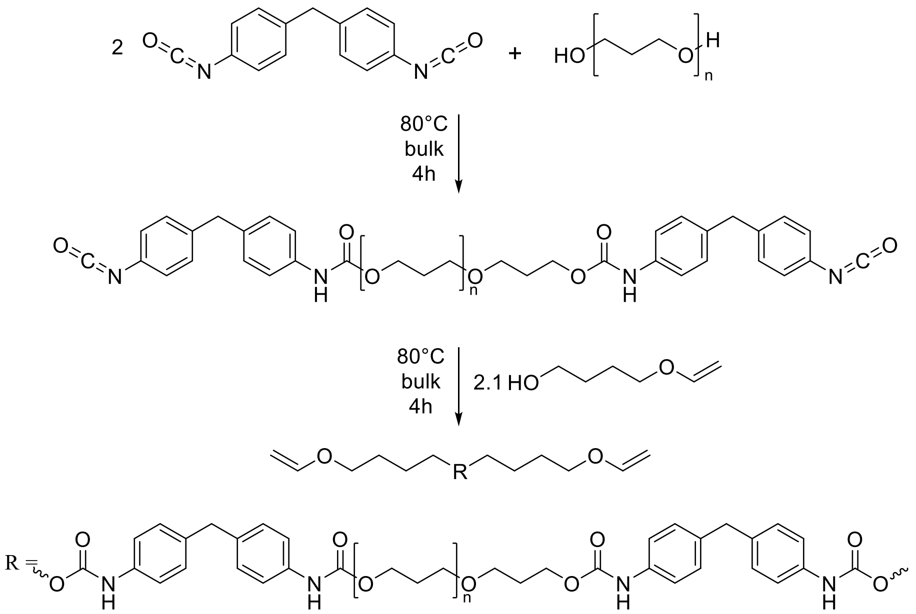

Scheme 3.2: Synthesis of urethane-based difunctional vinyl ether prepolymer PU-2.

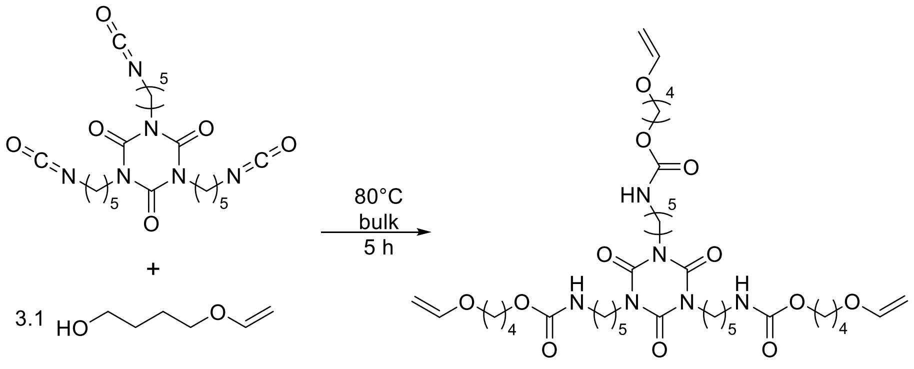

Scheme 3.3: Synthesis of urethane-based trifunctional vinyl ether crosslinker PU-3.

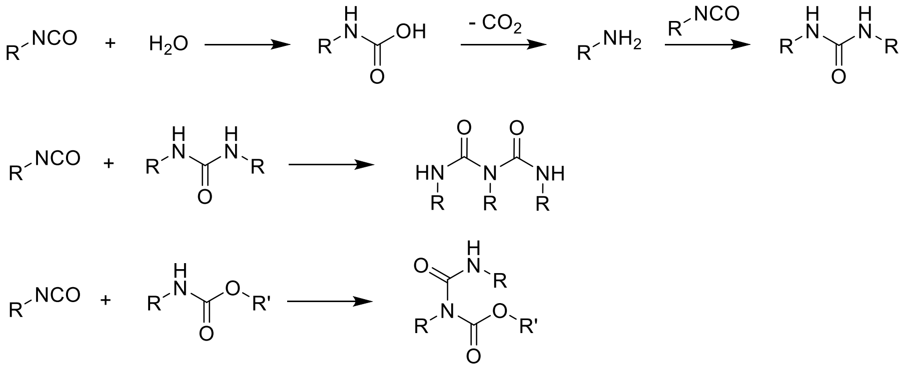

Scheme 3.4: Side reactions of isocyanates with water (top) as well as with urea (middle) and urethane (bottom) moieties.

Both reactions were carried out in bulk at T = 80 °C without a catalyst; the reaction progress was tracked via NCO titration. Full conversion was assumed at an NCO value < 0.1. The difunctional prepolymer PU-2 was prepared by an addition reaction between 4,4'-Methylene diphenyl diisocyanate (**4,4'-MDI**) and a an OH-terminated polyether polyol with $M_n \approx 2700$ Da, which was priorly dried in vacuo, in a first step. In simplified terms, the reaction product is a polyether with 4,4'-MDI endcaps at both ends as anticipated by stoichiometry, but in reality some longer chains, and side products are formed by polyaddition (Scheme 3.4). The obtained product always consists of a mixture between polyether-urethane chains with mostly two or four isocyanate building blocks and small amounts of unreacted diisocyanates. Next, the diisocyanate prepolymer was end-functionalized with 4-Hydroxybutyl vinyl ether (**HBVE**) which yields the final vinyl ether prepolymer PU-2. GPC measurements were carried out to analyze the molecular weight of the final polymeric product (Figure 3.3). The bulk of the signal comes from polymeric material with $M_w = 18800$ Da, $M_n = 10100$ Da & $PD = 1.9$ if only the isolated peak is integrated. Additional peaks from smaller molecules were found with $M_n < 1500$ Da which correspond to urethane compounds without polyether polyol integration and small amounts of byproducts. Hence, data obtained from GPC analysis confirms the hypothesis of formation of polymeric species with several polyether chain segments accompanied by significantly smaller molecules. Yet, the overwhelming bulk of the material can be considered as vinyl ether end-functionalized.

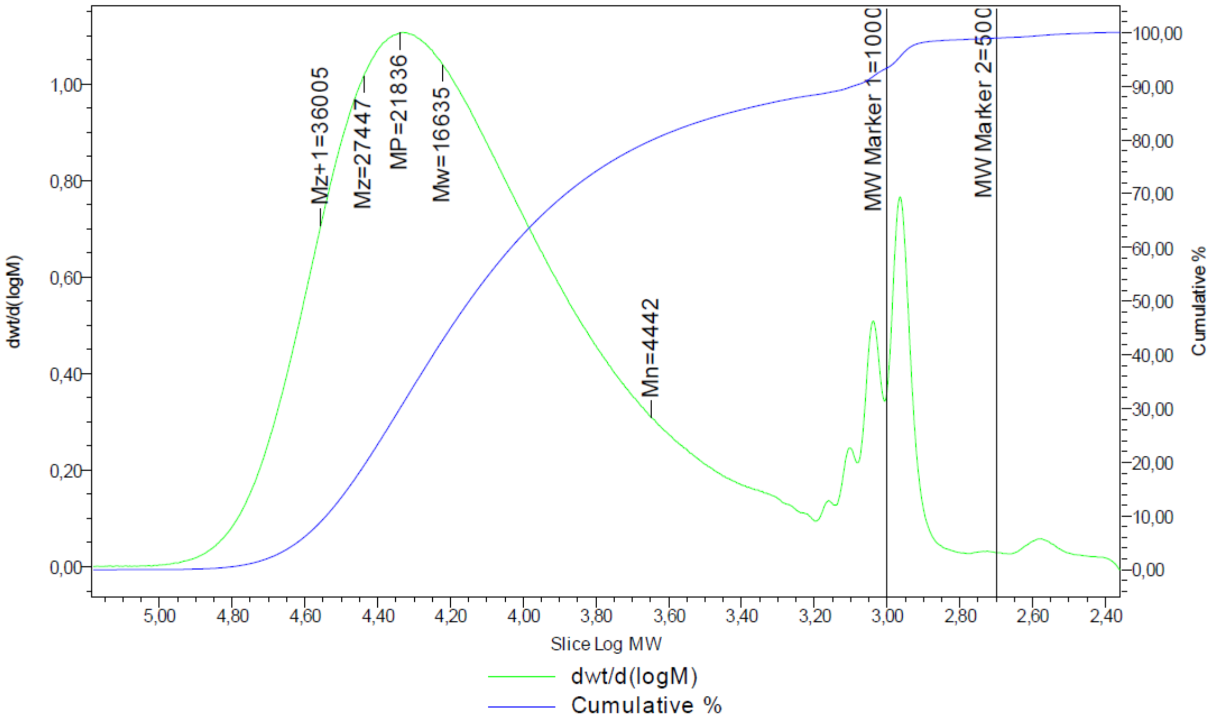

Figure 3.3: Molecular weight distribution curve of PU-2 determined by GPC with polystyrene standard calibration. Integration of the isolated polymeric peak (left) gives M_w = 18800 Da, M_n = 10100 Da & *PD* = 1.9. The full data is listed in Table 6.1.

The macromolecular crosslinker PU-3 was prepared in a single step by an addition reaction of a diisocyanate trimer with HBVE. In both cases, a small excess of hydroxy vinyl ether was added to ensure full isocyanate conversion. It must be noted that isocyanate groups undergo side reactions as described in Scheme 3.4. In a condensation reaction with water, CO_2 is released and urea linkages between two former isocyanate groups are formed which can subsequently react with free isocyanate moieties to yield biuret crosslinks (s. section 3.1.4). As a result, the utilized isocyanate compounds undergo side reactions with water before the reaction is started during storage which are accelerated under prepolymer synthesis conditions. In addition, isocyanates participate in addition reactions with urethane moieties to yield allophanates.[194] Hence, the final product mixture consists of small amounts of unreacted HBVE, urea, biuret and allophanate side products, but mostly the desired polyurethane prepolymers. A full analysis of the product mixture exceeds the scope of this thesis.

An adhesive prototype formulation was developed containing prepolymer **PU-2** and macromolecular crosslinker **PU-3** with urethane backbone structures (Scheme 3.5) as well as two monomers, all of which are vinyl ether functionalized for cationic light curing. The composition of this formulation **F-U** is listed in Table 3.1.

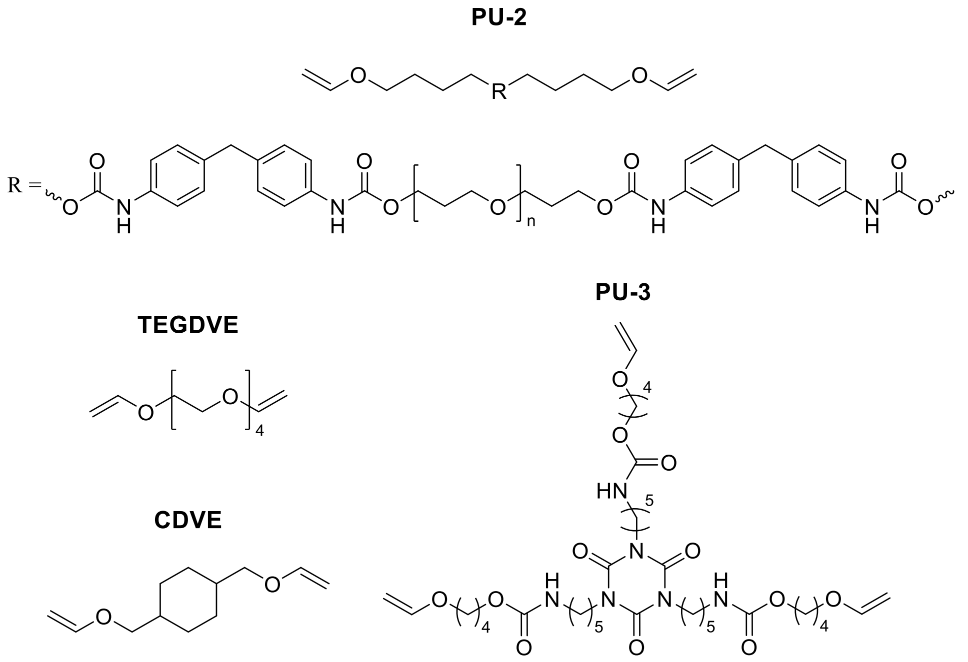

PU-2

TEGDVE

PU-3

CDVE

Scheme 3.5: Chemical structures of urethane based prepolymer PU-2, macromolecular crosslinker PU-3 and divinyl ether reactive diluents TEGDVE and CDVE.

Table 3.1: Composition of urethane-based vinyl ether adhesive formulation F-U in wt%.

Formulation	TEGDVE	CDVE	PU-2	PU-3	PI 440	PS 1331
F-U	20	20	40	20	1.5 phr	0.5 phr

A possible undesired side effect of decreasing vinyl ether concentration is an increase in curing time and decreased vinyl ether conversion in exchange for reduction of heat generation. Irradiation of the liquid formulation F-U with an LED light source for 20 seconds yields a yellowish, non-tacky and solid material (Figure 3.4, left). From visual observation, polymerization starts after 3 seconds of irradiation and appears completed in an instant. 100 % conversion is practically impossible and hard to prove by analytical methods. Material properties were analyzed by tensile testing of specimens cured from F-U (Figure 3.4, right). The maximum stress the material can sustain is σ_{max} = (23.3 ± 0.6) MPa and the strain at break is given as ε_{max} = (10.01 ± 0.02) %; these results imply a somewhat hard, but slightly flexible material. Figure 3.5 shows a categorization of common adhesives based on typical values observed in tensile testing. In comparison, formulation F-U shares mechanical properties with epoxide and polyurethane systems and thus it would be used for applications which require strong but not flexible materials. However, F-U is a prototype adhesive formulation and will mainly serve as a benchmark for more advanced formulations described later in this work.

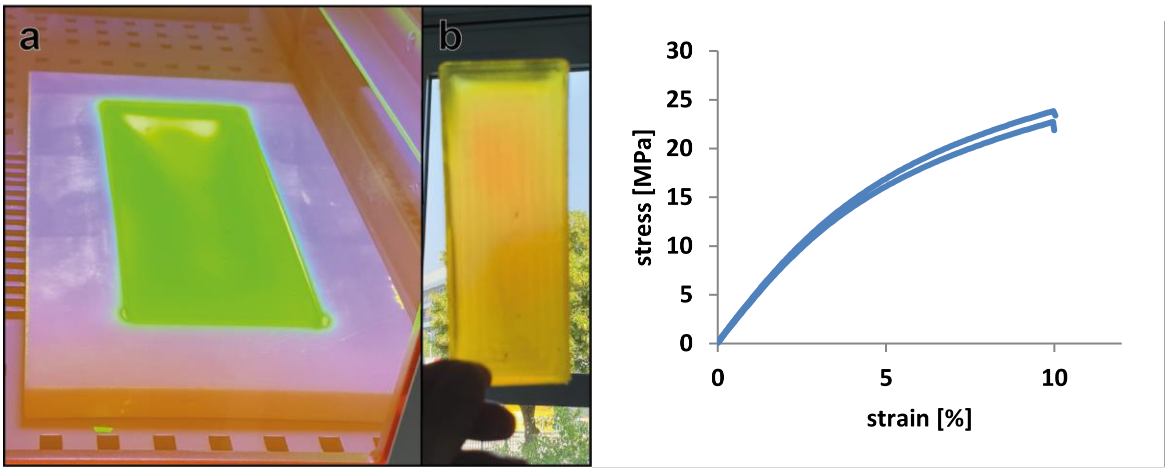

Figure 3.4: Left: LED curing of liquid formulation F-U (a) and the resulting solid, non-tacky material (b). Right: Stress-strain diagram of light-cured urethane-based vinyl ether adhesive formulation F-U.[10]

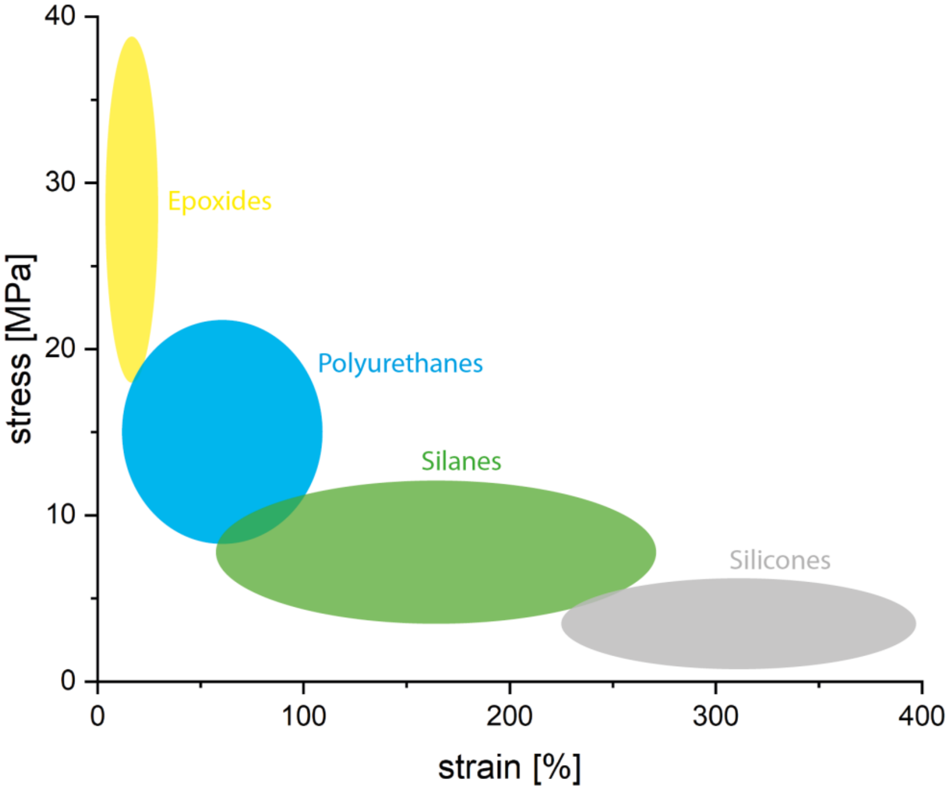

Figure 3.5: Categorization of common adhesives sorted by typical stress-strain behaviors.[195]

The curing process was investigated more deeply by monitoring curing kinetics of formulation F-U in rheology experiments (Figure 3.6). Reaction and monitoring conditions were similar to crude monomer testing described before. The reaction starts immediately on irradiation with an instant sol-gel transition due to fast vinyl ether polymerization. The values of *G'* and *G''* reach a plateau with no further significant change in viscoelastic properties after 20 seconds.

In the lab, a significant decrease in heat generation was observed qualitatively. This is a promising result since utilization of vinyl ether-terminated urethane-based prepolymers for irradiation-curing adhesive systems with vinyl ether functionality can improve the component toolbox by reducing reactive group concentration while still maintaining fast curing. Moreover, no indications for reduced vinyl ether conversion were observed as a solid and most importantly dry material was obtained.

Overall, incorporation of vinyl ether terminated urethane-based prepolymers allows curing of vinyl ether adhesive systems without material degradation by extensive heat generation while maintaining fast curing with high vinyl ether conversion. A prototype formulation was developed which is suitable for applications with high material strength requirements. In the following sections, the utilized prepolymers will be modified to enable additional curing steps, substituted to broaden the material toolbox, and different filler materials were added to the described formulation F-U to further evaluate reduction of heat generation in the curing step.

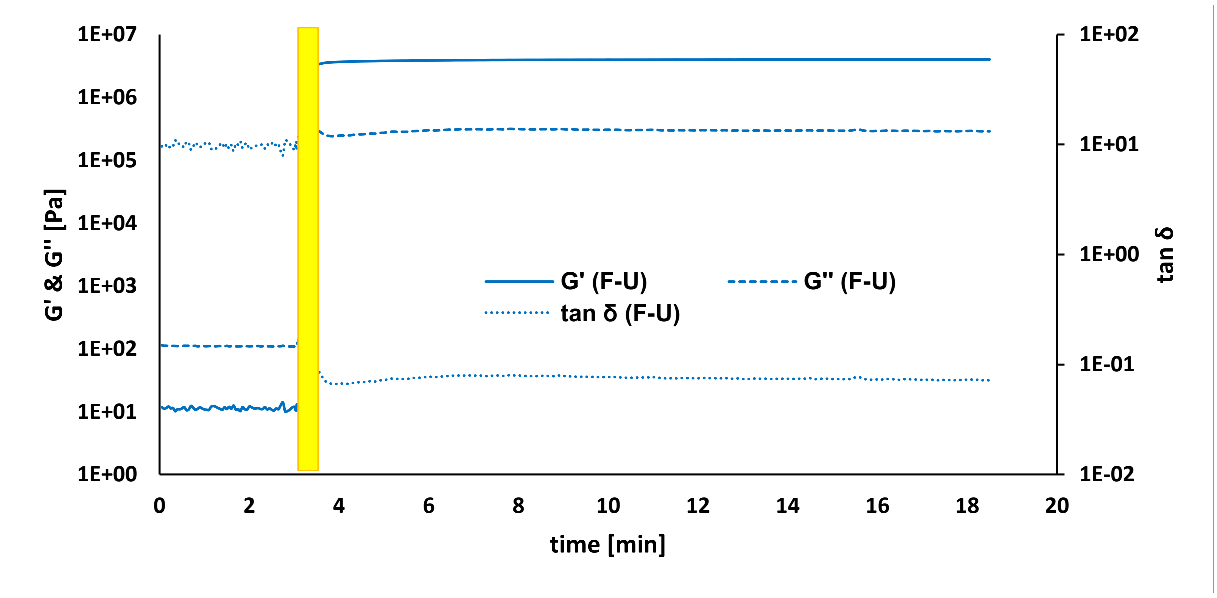

Figure 3.6: Storage modulus *G'* (solid line), loss modulus *G''* (dashed line) and dissipation factor tan *δ* (dotted line) over time of formulation F-U. To initiate cationic polymerization, the sample was irradiated with UV light for 20 seconds indicated by the yellow area.

3.1.3 Controlling exothermic cationic polymerization with filler materials

The use of fillers is very common in the adhesive industry for reasons of reducing reactive group concentration for exothermic curing mechanisms, tailoring mechanical properties of the cured material and most importantly decreasing the cost as most filler materials are very cheap.[9,20] Complementary efforts for controlling the exothermic polymerization behavior by adding various inert filler materials to formulation F-U were made. For quantitative evaluation, the reaction enthalpy was monitored via DSC.[196] The utilized fillers were fumed silica (*Wacker HDK 21*), fused silica (*Denka FB 35*) as well as aluminum oxide (*BAK 40*, *Martoxid 2250*), boron nitride (*Hebofill 490*) and barium sulfate powders. From each mixture, two different samples were analyzed: in liquid form and after irradiating the sample for 20 seconds. By comparing the respective reaction enthalpies ΔH, conclusions can be drawn on vinyl ether conversion by irradiation as ΔH directly correlates with the amount of residual vinyl ether groups reacting by thermal activation. For demonstration, the respective DSC thermograms of F-U are shown in Figure 3.7. The samples were heated from 30 °C to 230 °C in a first heating step (black curve), then cooled down to -50 °C (red curve) and heated up to 230 °C again (blue curve). The utilized iodonium salts are known to initiate cationic polymerizations by UV irradiation.[197] It must be pointed out that research has shown thermal degradation at different temperatures depending on potential reaction partners.[97] In combination with reducing agents, e. g. vinyl ethers, degradation takes place at temperatures as low as 100 °C and with a suitable monomer present, cationic polymerization can be initiated.[198] Usually, curing starts at a certain temperature and polymerization reaction enthalpy ΔH_l can be calculated. If there is unreacted monomer present in the previously UV-cured material, polymerization will continue and the reaction enthalpy ΔH_s is obtained from integration of the respective peak. The ratio $\frac{\Delta H_S}{\Delta H_l}$ equals the degree of cure (**DOC**) and which loosely describes reciprocal vinyl ether conversion in UV curing (equation 3.1).

$$\alpha = 1 - \frac{\Delta H_S}{\Delta H_l} \qquad \textbf{(3.1)}$$

The polymerization is thermally triggered in a first heating step and the bulk of vinyl ether groups is expected to react. Typically, two exothermic peaks are found from the main polymerization step (dark grey) and the post polymerization step (light grey). During the main polymerization step, a crosslinked polymer network is formed and with increasing degree of polymerization and crosslinking, chain mobility decreases which, at some point, results in hindered polymerization as diffusion of active polymer chain ends and monomers drops too low for them to encounter and proceed polymerization. As temperature increases, chain mobility increases and exothermic polymerization continues, resulting in a second peak observed during DSC measurement. The temperature at which polymerization continues is likely linked to T_g of the polymer network. The second and third experimental step were performed to obtain additional data on T_g and residual unreacted components. Due to $\Delta H < 0$ for all observed peaks, the negative enthalpy - ΔH is shown and discussed in the following for better understanding.

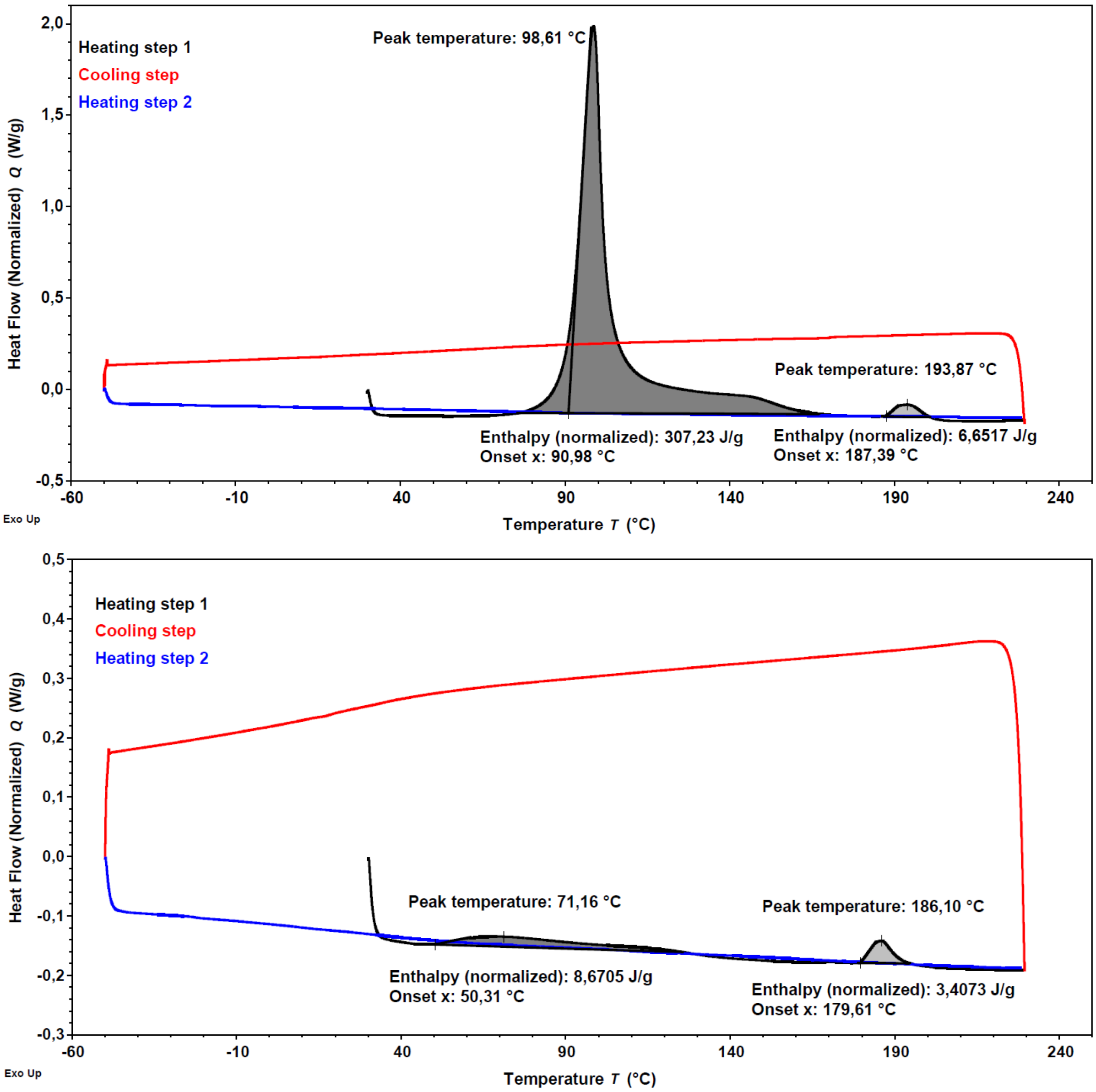

Figure 3.7: DSC thermogram of urethane-based vinyl ether formulation F-U in liquid form (upper) and after irradiation (lower). Typically, two exothermic peaks are found from the main polymerization step (dark grey) and the post polymerization step (light grey).

DSC analysis of formulation F-U in liquid form shows a negative polymerization enthalpy of $-\Delta H_l = 310$ J/g by adding up both peak areas which is considered moderate for adhesive applications. For comparison, typical highly reactive two-part epoxide adhesives exhibit curing enthalpies of about 500 J/g.[199,200] After photocuring, the reaction enthalpy $-\Delta H_s = 12.1$ J/g is naturally significantly lower as the bulk of vinyl ether groups already reacts during pretreatment. From these values the degree of cure of F-U during photocuring was calculated as $\alpha = 0.962$ which is considered adequate but improvable.[199,201] However, further steps to decrease heat generation in the curing process are of interest and additional experiments with several filler materials were carried out; the respective amount of each filler varies due to limits in miscibility and viscosity of the final formulation; the respective thermograms are presented in the appendix (Figure 6.12 - Figure 6.18).

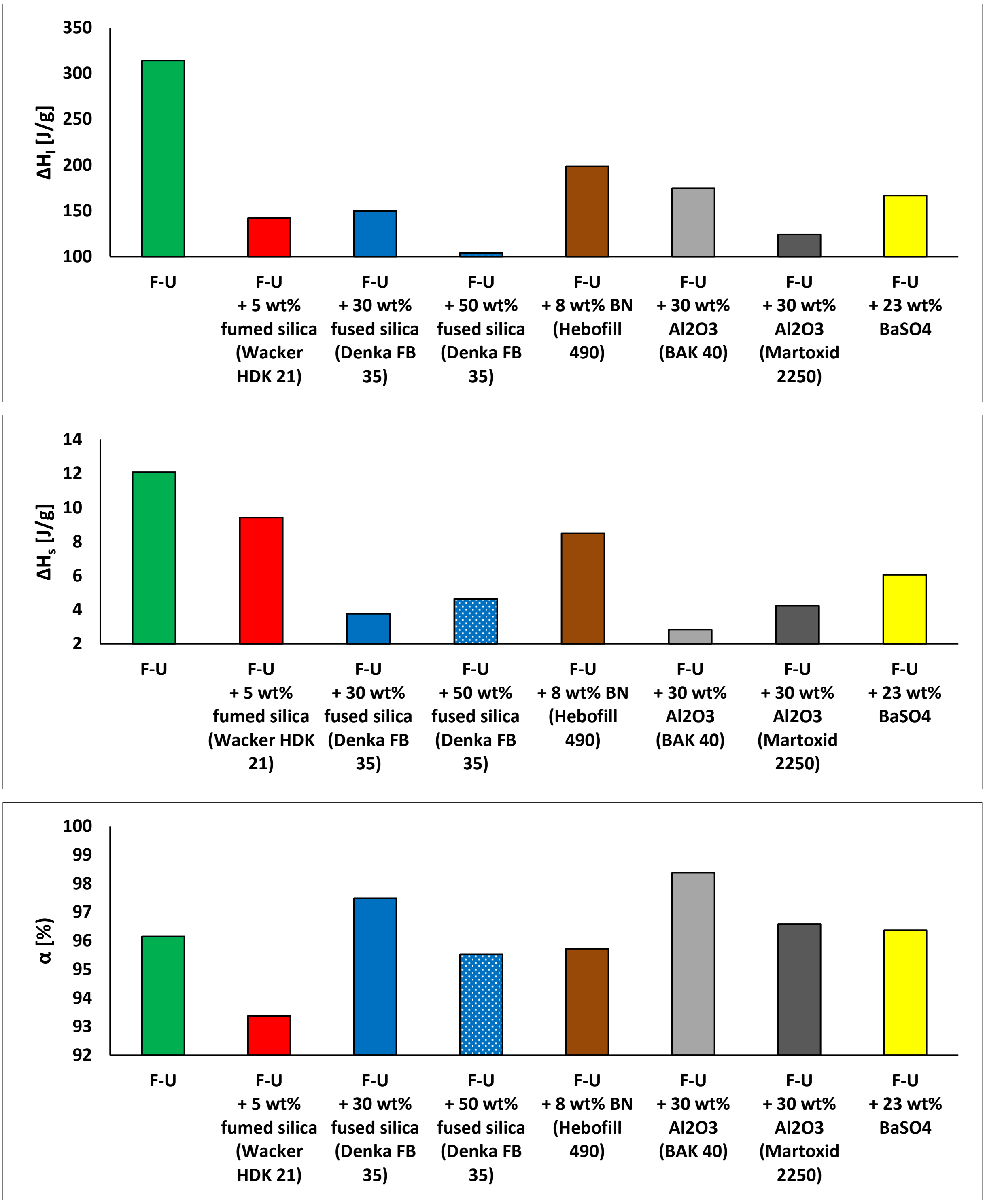

Figure 3.8: Negative reaction enthalpy -*ΔH* of thermal cationic polymerization of urethane-based vinyl ether formulation F-U with various filler materials determined via DSC. The experiments were performed with the liquid formulation (upper) and with the cured material (middle). Degree of cure *α* by irradiation calculated with equation 3.1 (lower). All filler materials were tested at an upper limit of miscibility and viscosity except for the fused silica (blue) which can be added with *w* > 50 wt%.

The negative reaction enthalpies as well as the degree of cure by irradiation α are shown in Figure 3.8. It must be noted that this evaluation method bears certain inaccuracies especially from peak integration and thus small variations of ± 2 % between different mixtures are considered negligible.

As expected, the addition of any filler material causes a significant decrease in $-\Delta H_l$, due to lower reactive group concentration. Still, remarkable differences were found for the various filler materials. Only small amounts of fumed silica, *Wacker HDK 21* in this case, were added due to its strong impact on the viscosity of the formulation. Nevertheless, polymerization enthalpy was cut in half when adding only 5 wt% of the silica. However, addition of fumed silica leads to a significant decrease in DOC from 96.2 % to 93.4 % which is likely due to the afore-mentioned increase in viscosity and consequently hindered reactive group diffusion during polymerization. Similar effects on viscosity were observed for the addition of a boron nitride powder, *Hebofill 290*. Although the effect was not as strong and thus allowing the addition of slightly higher amounts of filler, the decrease in reaction enthalpy is not as drastic: $-\Delta H_l$ is decreased by only about 30 % but in return, the observed reduction in degree of cure is negligible. Remarkably higher amounts of barium sulfate were added, a very common filler material known to also improve material properties such as impact resistance in adhesive systems.[202] $-\Delta H_l$ of F-U containing 23 wt% of barium sulfate is almost cut in half compared to the crude formulation and no considerable changes in DOC were found. However, storage stability of the mixture is an issue as phase separation of reactive components and inert barium sulfate were observed after less than a day. Two different aluminum oxide powders were tested regarding their suitability for vinyl ether UV curing systems by adding 30 wt% of *BAK 40* and *Martoxid 2250,* respectively. The final formulation from F-U and the latter exhibits a massive decrease in polymerization enthalpy by about 60 % with similar conversion by irradiation. In contrast, the addition of *BAK 40* results in a decrease in $-\Delta H_l$ of only about 45 %, but a slight increase in DOC from 96.2 % to 98.4 % was found. Both filler materials showed satisfactory miscibility with the reactive components and cause a significant decrease in heat generation albeit not inhibiting cationic polymerization triggered by LED irradiation. However, fused silica, *Denka FB 35*, showed the best miscibility with vinyl ether formulation F-U, allowing the addition of 50 wt% with a potential to even higher amounts without significantly affecting viscosity or exhibiting storability issues. A mixture of F-U and 30 wt% of this filler reduces reaction enthalpy more than 50 % whereas the addition of 50 wt% cuts it to a third compared to the crude formulation. Moreover, the degree of cure is hardly changed and independent from the tested amount of fused silica. As stated before, the evaluation method utilized for these experiments bears a considerable margin of error and thus slight changes of ± 2 % in DOC are negligible which is the case for almost all tested mixtures. The most important factors are considerable changes in $-\Delta H_l$ and compatibility in terms of mixing as well as storage stability. As a consequence, aluminum oxide powders and especially fused silica have been evaluated to be suitable filler materials for cationic UV curing vinyl ether formulations. They are able to overcome one application challenge as addition leads to a significant decrease in heat generation from polymerization during the curing process as well as a reduction of the overall production cost. Both aspects will be of high importance in future product development work in order to commercialize a vinyl ether-based adhesive product.

3.1.4 Light and moisture dual cure systems

Another approach in reducing highly reactive vinyl ether group concentration is to implement a second curing step with a less exothermic reaction and/or slower curing mechanism. In formulation F-U, all prepolymers were completely functionalized with vinyl ether end groups, but by utilizing substiochiometric amounts of hydroxyalkyl vinyl ethers, such as HBVE, prepolymers with terminal vinyl ether as well as isocyanate groups are obtained. The residual isocyanate groups slowly react with water from the surrounding humid air to amine groups which further react with other isocyanate groups to urea groups to form a densely crosslinked polymer network;[203] the reaction path is described in Scheme 3.7. In an additional step, biuret linkages are formed from an addition reaction of urea with isocyanate groups further increasing crosslinking density. The dual cure concept of this vinyl ether-based adhesive system can be described as follows: In a first cationic photocuring step vinyl ether moieties polymerize to provide a sufficient initial adhesive strength, followed by a second moisture curing step to increase crosslinking and consequently the cohesion of the material for final application requirements. For this approach, the macromolecular crosslinker PU-3 was modified by functionalizing only 30 % of the isocyanate groups (**PU-3a**, Scheme 3.6) and the formulation was adjusted (**F-Ua**, Table 3.2).

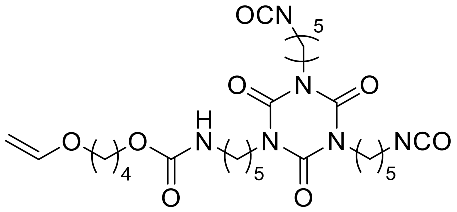

Scheme 3.6: Chemical structure of macromolecular crosslinker PU-3a with 30 % vinyl ether functionalization; 70 % of the isocyanate groups were preserved.

Table 3.2: Composition of a vinyl ether adhesive system with dual cure mechanism F-Ua in wt%.

Formulation	DEGDVE	CDVE	PU-2	PU-3a	PI 440	PS 1331
F-Ua	20	20	20	40	1.5 phr	0.5 phr

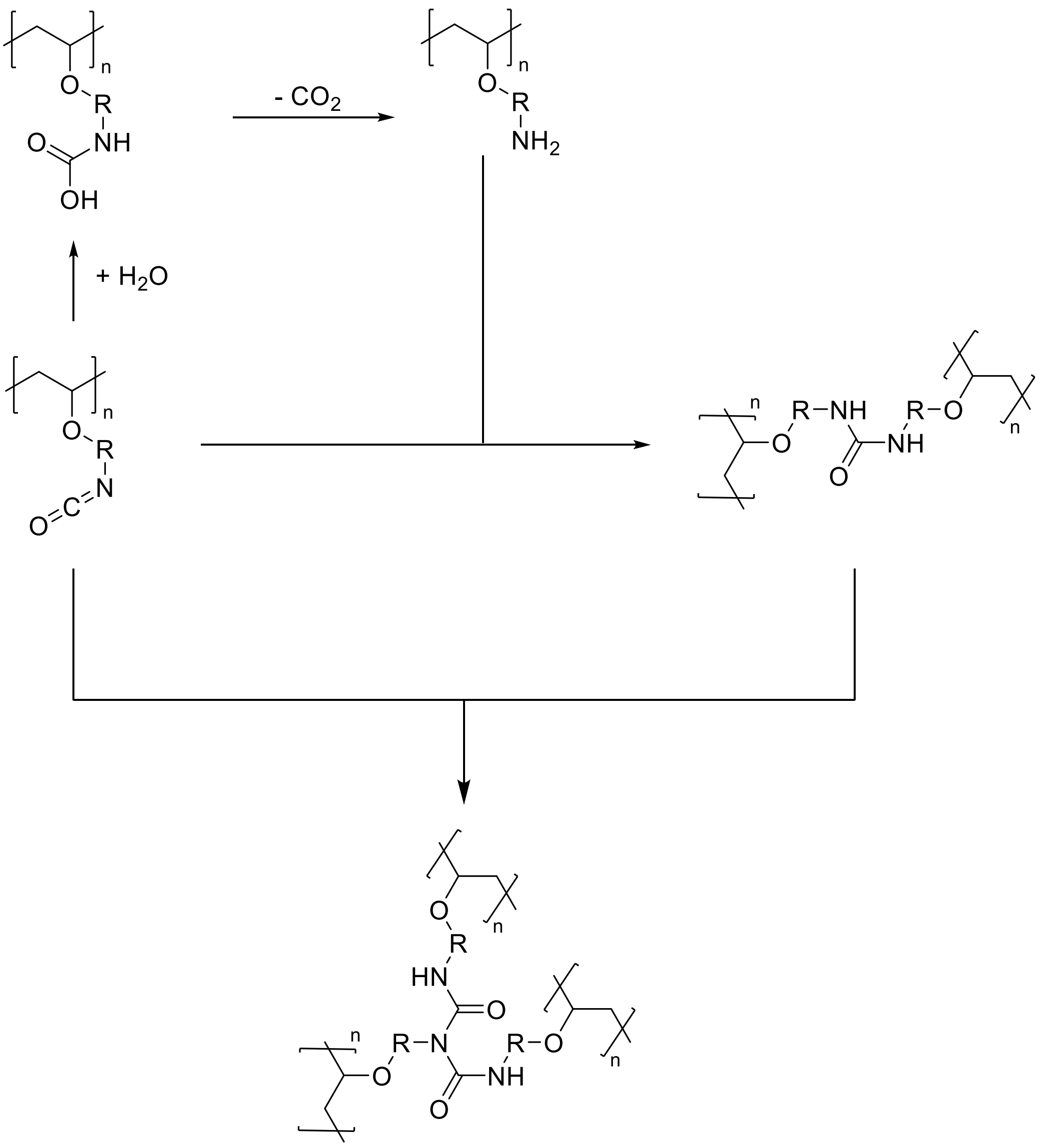

Scheme 3.7: Moisture-driven crosslinking of poly(vinyl ether) chains with terminal isocyanate side chains.

Next, the change in mechanical properties over time was observed to analyze the impact of the second curing step, moisture cure. The liquid formulation was filled into Teflon forms and irradiated with LED light for 20 seconds. DMA measurements (Figure 3.9) and tensile testing experiments (Figure 3.10) were performed one hour after irradiation and after seven days of storage at 23 °C and 50 % RH. After irradiation, a slightly tacky and soft film is obtained, and its viscoelastic and thermal properties are characterized by *G'* (25 °C) = 307.5 MPa and T_g = 60.3 °C. Compared to photocured F-U, the soft- and tackiness can be explained by the significantly lower crosslinking density as the former trifunctional vinyl ether crosslinker is substituted by its monofunctional equivalent. After seven days of moisture curing, the material becomes noticeably harder and more brittle. An increase in both moduli at low to moderate temperatures was observed with *G'* (25 °C) = 1115 MPa. In addition, the glass transition temperature rises to 83.8 °C. A more than threefold increase in storage modulus at room temperature as well as the significant increase in T_g indicates the formation of a more densely crosslinked polymer network by moisture curing of terminal isocyanate groups provided by macromolecular crosslinker PU-3a.

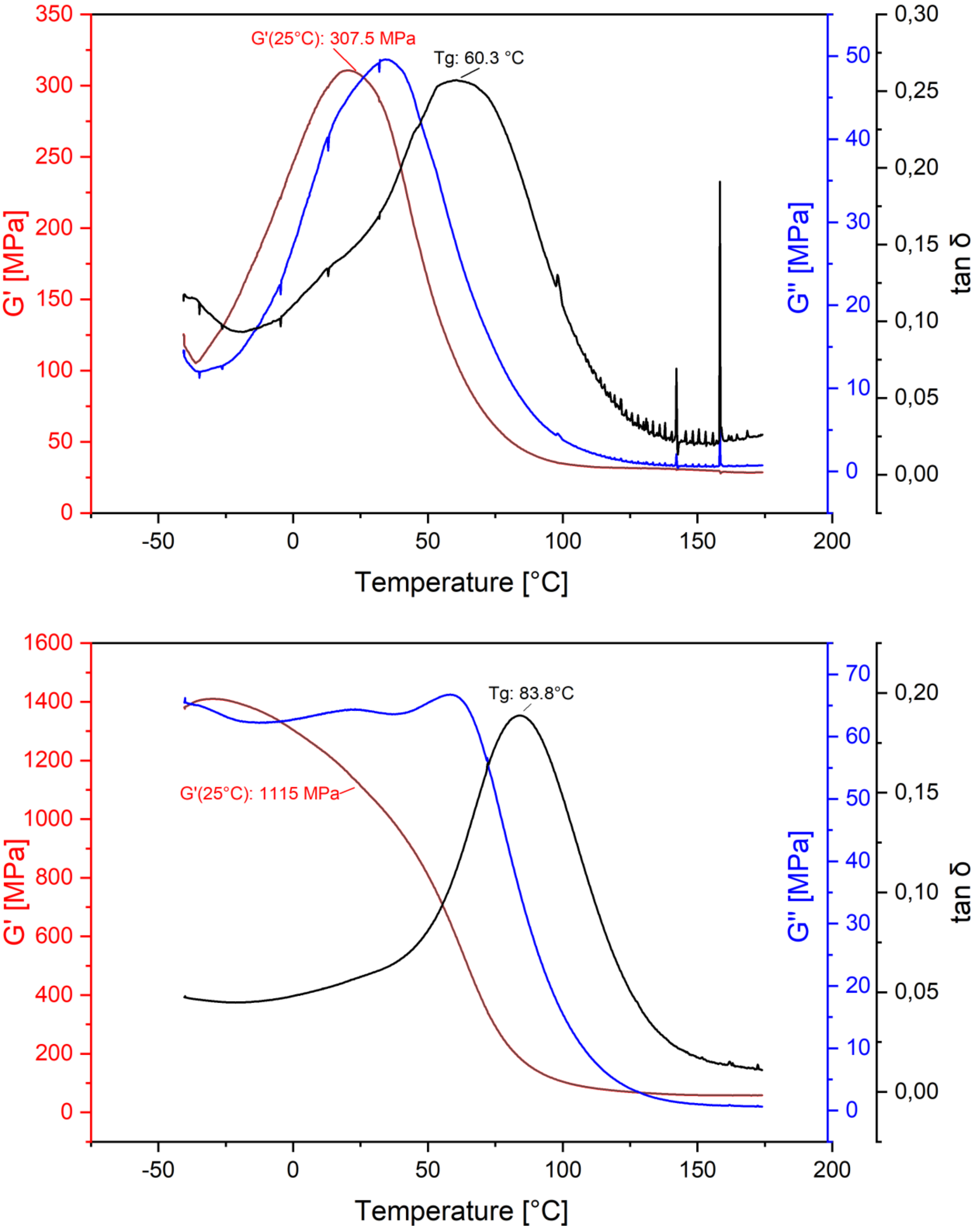

Figure 3.9: DMA thermograms of dual cure formulation F-Ua 1 hour (upper) and 7 days (lower) after photocuring. Moisture-driven post curing results in crosslinking between free isocyanate groups.

This is further emphasized by tensile testing results. After one hour the maximum stress the material can sustain is σ_{max} = (14.6 ± 0.3) MPa and the strain at break is given as ε_{max} = (5 ± 2) %. After 7 days the obtained graphs demonstrate a steeper increase in stress at low elongation which indicates an increase in Young's modulus E. In addition, maximum stress is increased to σ_{max} = (21.8 ± 0.9) MPa whereas strain at break is decreased to ε_{max} = (2.2 ± 0.5) %. The observed change in material properties underlines the hypothesis of densely crosslinked polymer network formation in a moisture driven second curing step resulting in hard and brittle materials. In comparison to single-step curing formulation F-U, there is no significant difference in σ_{max} whereas ε_{max} is significantly decreased for F-Ua which implies a less flexible material resulting from a more densely crosslinked polymer network formed in the second curing step.

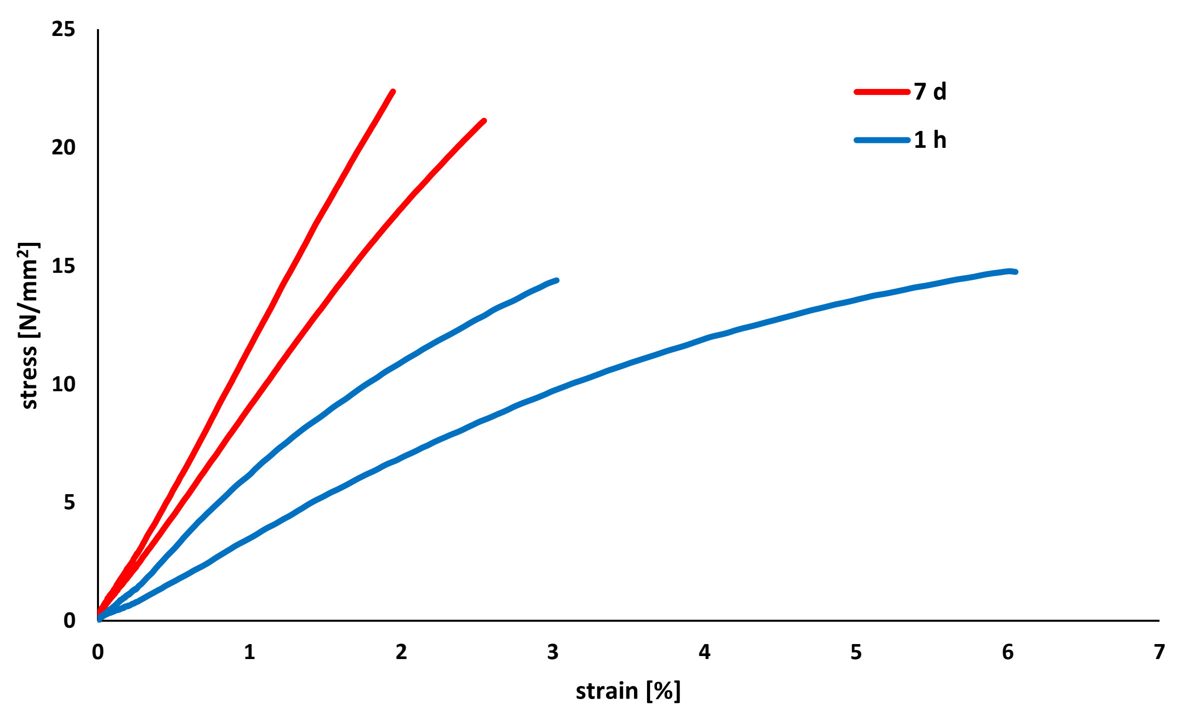

Figure 3.10: Stress-strain diagrams of dual cure Formulation F-Ua 1 hour (blue) and 7 days (red) after photocuring. Moisture-driven post curing results in crosslinking between free isocyanate groups.

The described film specimens were in direct contact with the surrounding air ensuring that humidity access is good enough to allow adequate water diffusion into the material under almost ideal lab conditions. In most applications, there is only a small bond line of the adhesive layer present which limits air contact and consequently the source of water significantly. To investigate possible limitations of the curing mechanism in question and to evaluate adhesive performance under more realistic application conditions, single-lap shear tests were performed. In more detail, different substrates glued by formulation F-Ua were investigated one hour and seven days after photocuring, respectively. The photocuring step necessitates at least one transparent substrate to be present in the joint. Polycarbonate (PC) was selected as it is broadly used for industrial applications in the electronics, medical as well as automotive field. The other utilized substrate materials were Acrylonitrile butadiene styrene (ABS) and polyamide (PA) to investigate adhesion on plastic surfaces, as well as aluminum and steel to estimate adhesive strength on metals. The results are illustrated in Figure 3.11.

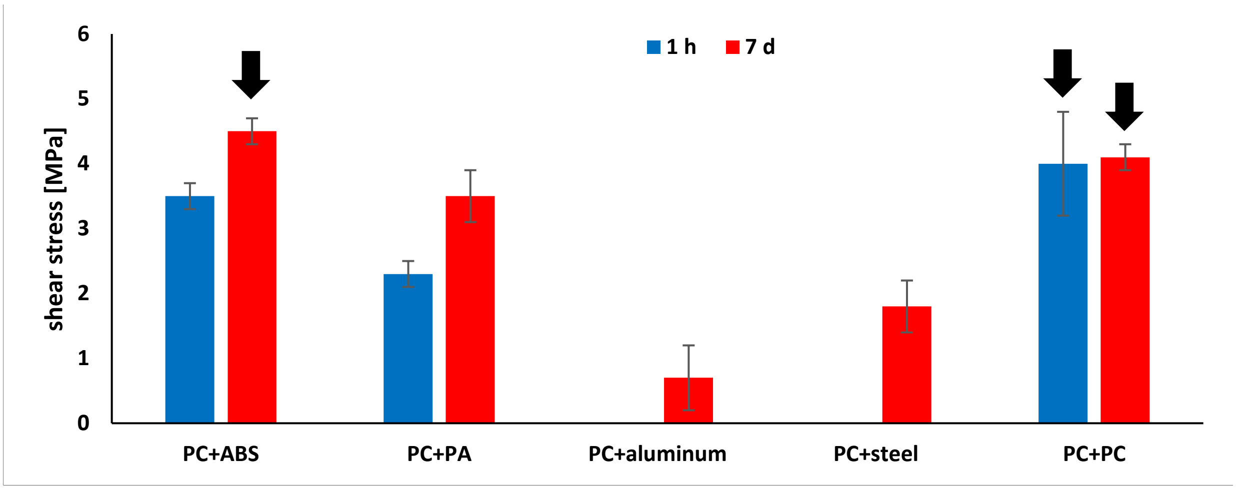

Figure 3.11: Single-lap shear test results of different plastic and metal substrates, glued by dual cure adhesive formulation F-Ua 1 hour (blue) and 7 days (red) after photocuring. The black arrows indicate substrate failure of the specimens during measurement.

On all surfaces, an increase in failure shear stress τ is observed from 1 hour after irradiation to 7 days. On aluminum and steel substrates, adhesive strength is too low for measurement and resulting in separation of substrates even before applying significant shear forces. Overall, significantly higher shear stresses are sustained by the system on plastic surfaces compared to metals. This trend was observed in numerous photocuring vinyl ether systems before, too. Remarkably enough, the adhesive joints of formulation F-Ua on ABS and PC are highly resilient and suffer from substrate failure which is indicated by the black arrows in Figure 3.11. Substrate failure describes breaking of tested substrates during measurement before the adhesive layer cracks or detaches from a substrate surface. In other words, the adhesive is stronger than the substrate. As a next step, the measurement method was adjusted by decreasing the area of the adhesive layer and repeated with PC-PC joints to get an even better picture of the full potential of this prototype formulation. Additionally, it was directly compared to a commercial adhesive, *Loctite UV Eccobond 9060F*. This product is characterized by acrylate and isocyanate functionality and relies on a similar dual cure mechanism: radical photopolymerization of acrylate moieties followed by further crosslinking of polymer chains via moisture driven reactions between isocyanate groups. Single-lap shear experiments were conducted with samples glued by *Loctite UV Eccobond 9060F* 7 days after photocuring; the testing results of both systems are illustrated in Figure 3.12. A distinct trend between the different substrates was found: The acrylate-based adhesive exhibits higher lap shear strength values on metal surfaces whereas the vinyl ether-based system demonstrates superior adhesive performances on plastic surfaces. The most prominent differences and respectively best adhesive performances were observed on steel with a lap shear strength value of δ = (4.3 ± 0.6) MPa by *Loctite UV Eccobond 9060F* and δ = (1.8 ± 0.4) MPa for F-Ua. PC-PC joints achieved δ = (5.7 ± 0.7) MPa for F-Ua compared to merely δ = (2.4 ± 0.6) MPa by the acrylate reference *Loctite UV Eccobond 9060F*. In summary, the overall highest lap shear strength value in this series was accomplished by utilizing a dual cure vinyl ether-based system compared to a similar commercial adhesive. This demonstrates the potential of vinyl ether-based formulations for adhesive applications and also puts emphasis on the need for further research and development of these systems as F-Ua is a rudimentary formulation developed for research purposes and gives a lot of room for more improvement by formulation approaches. Nevertheless, it is a good result to demonstrate an adhesive performance already being comparable or even superior to commercially available adhesives.

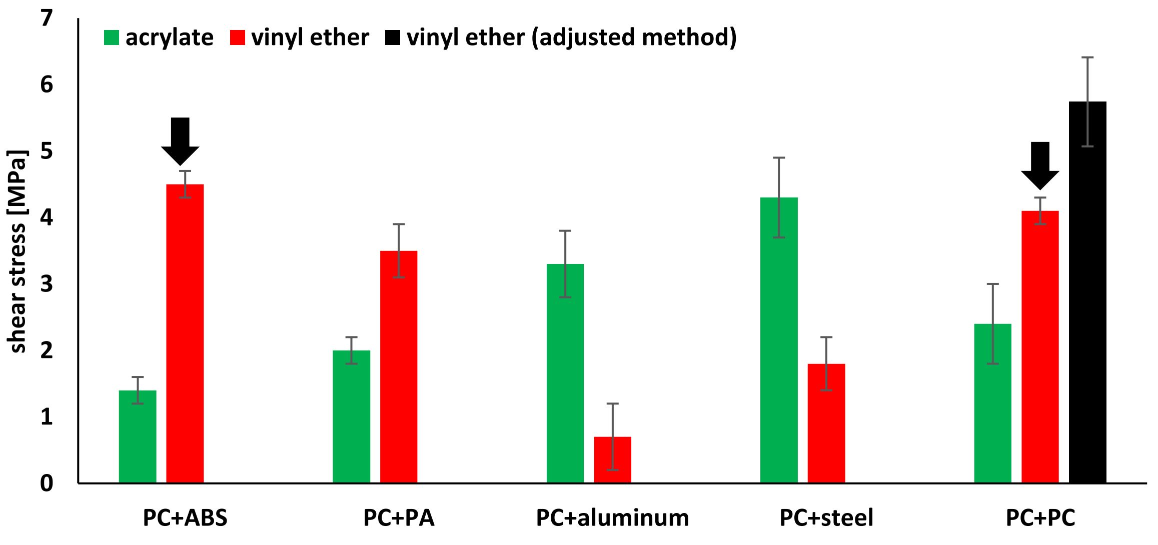

Figure 3.12: Single-lap shear test results of samples, glued by dual cure vinyl ether-based adhesive formulation F-Ua (red) and commercial acrylate-based adhesive *Loctite UV Eccobond 9060F* (green) 7 days after photocuring. The black arrows indicate substrate failure of the specimens during measurement. The experiment was repeated with a smaller adhesive overlap with F-Ua (black) to prevent substrate failure and evaluate the full potential of the vinyl ether adhesive.

3.1.5 Vinyl ethers in two-component thiol-ene adhesives

As explained in section 1.2.1, polyfunctional vinyl ethers undergo thiol-ene polyaddition reactions with polyfunctional thiols to form polymeric structures from long linear chains to densely crosslinked networks depending on monomer functionality. In addition, chain growth may proceed in a radical or cationic mechanism dictated by the utilized initiator which yields different backbone structures as monomers are linked by thioether groups from radical polyaddition opposed to thioacetal linkages formed in cationic mechanisms.[132,204] One advantage of thioacetal backbones is a potential for adhesive debonding systems due to their susceptibility towards hydrolysis.[205] To investigate the potential of biobased vinyl ethers in thiol-ene systems, a benchmark thiol – vinyl ether adhesive formulation was developed. Both thermal- and photoinitiation are possible, but low storage stability is expected due to high reactivities of vinyl ethers with thiols.[123,206] Hence, pretests were performed to develop a reference formulation of a two-component system for subsequent material testing. Tests were performed in aluminum pans with different thiol and vinyl ether components as well as different radical and cationic initiators cured thermally and by irradiation. From these experiments, formulations F-T1 for radical and F-T2 for cationic cure were developed. Their composition is shown in Table 3.3 (entry 1 and 2) with the respective chemical structures of the components illustrated in Scheme 3.8. Respective masses of thiol & vinyl ether component were adjusted to $\frac{n(\mathrm{SH})}{n(\mathrm{VE})} = 0.98$ to ensure high conversion by polyaddition reaction and low odor from thiols due to a slight excess of vinyl ether moieties. However, thermally cured films show higher conversion compared to materials cured by irradiation. The latter exhibit increased tackiness and are generally softer as a result from shorter reaction times at lower temperatures. As a consequence, further material and adhesive testing was limited to thermal initiators *V-65* (2,2'-azobis(2,4-dimethylvaleronitrile) for radical and *K-Pure CXC-1612* for cationic curing. If the latter was utilized, it was dissolved in the thiol part before mixing with the vinyl ether component at 40 °C; if *V-65* was utilized, it was dissolved in the vinyl ether component beforehand.

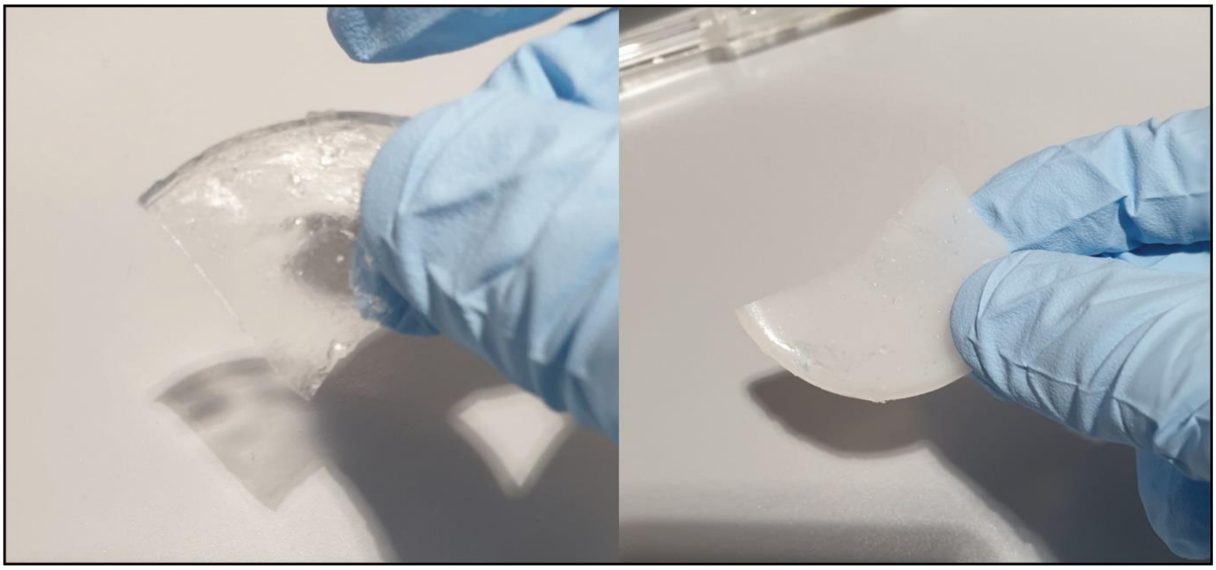

Figure 3.13: Cured films of formulation F-T1 (left) and F-T2 (right).

Table 3.3: Composition of thiol-vinyl ether formulations in wt%. The formulations are separated into a thiol (TMPMP, PETMP, TEMPIC) and a vinyl ether (CDVE, TEGDVE, PU-2, PU-3, PHAE-2) component. The initiator (Init) of F-T1 is *V-65* and the initiator of F-T2(a) is *K-Pure CXC-1612*.

	TMPMP	PETMP	TEMPIC	CDVE	TEGDVE	PU-2	PU-3	PHAE-2	Init	SH/VE
F-T1	10	60	30	40	10	20	30	0	2 phr	0.98
F-T2	0	70	30	30	10	15	25	20	3 phr	0.98
F-T2a	0	70	30	30	10	15	25	20	3 phr	0.71

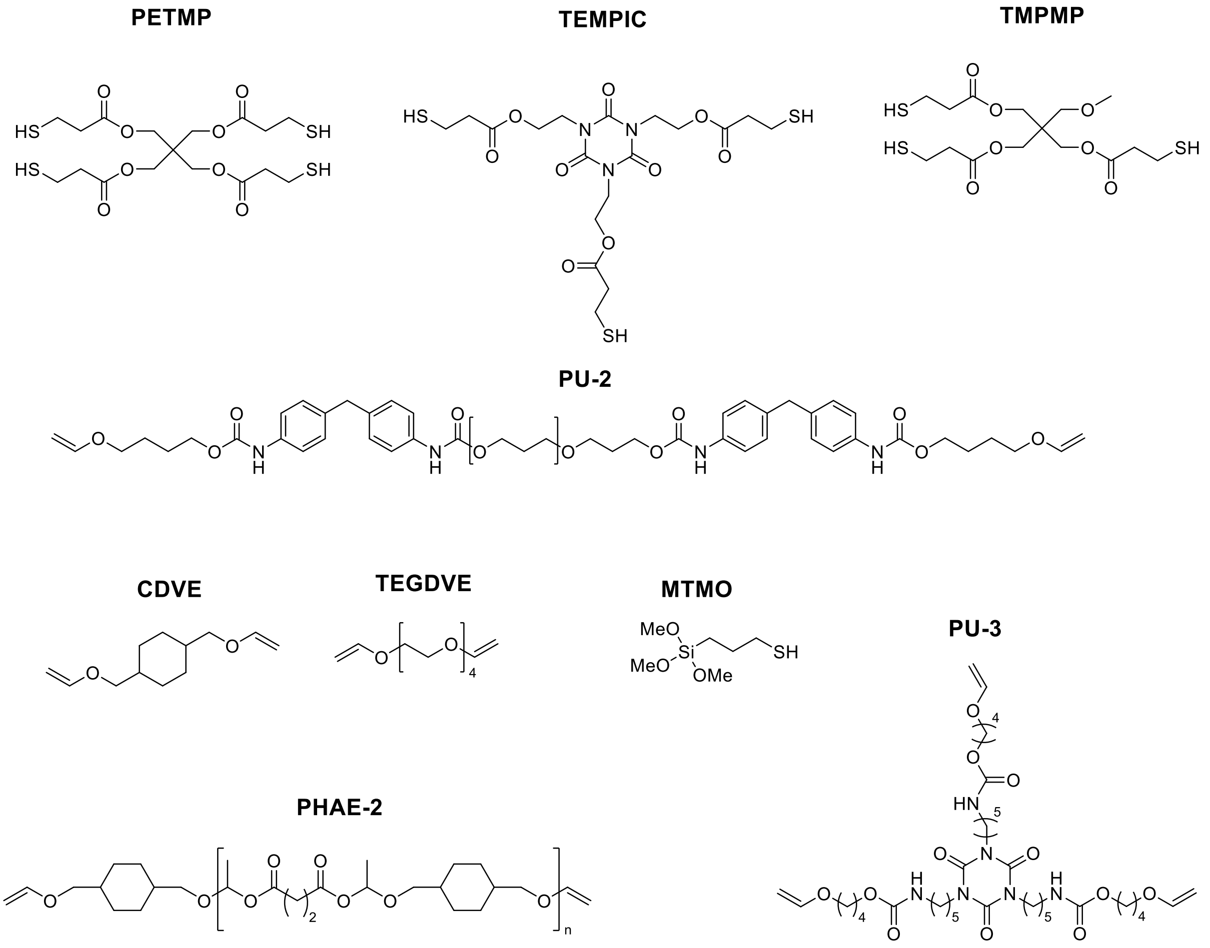

Scheme 3.8: Chemical structures of polyfunctional thiols PETMP, TEMPIC and TMPMP, urethane-based vinyl ether prepolymer PU-2, urethane-based vinyl ether macromolecular crosslinker PU-3, hemiacetal ester-based vinyl ether prepolymer PHAE-2 (further described in section 3.1.7), thiol functionalized silane adhesion promoter *Dynasylan MTMO,* and divinyl ether reactive diluents CDVE and TEGDVE.

Generally, both formulations yield colorless films after curing but cationic formulation F-T2 becomes slightly turbid (Figure 3.13). In addition, differences in curing mechanisms were observed as materials obtained from radical polyaddition are softer and generally weaker than those obtained via cationic polyaddition which is likely due to reduced mobility of thioacetal linkages compared to thioether groups.[132] Specimens from F-T1 and F-T2 were prepared for tensile testing but were not analyzed as the obtained materials are too soft and break due to the pressure applied by clamping the experimental setup. As a consequence, formulation preparation was altered by reducing the amount of thiol component in the final mixture. The aim of this approach was to ensure high thiol conversion in the suspectedly faster cationic thiol-ene polyaddition in a first step and subsequent cationic homopolymerization of excess vinyl ether moieties as depicted in Scheme 3.10. Formulation F-T2 was modified by altering the ratio of the reactive groups to $\frac{n(\mathrm{SH})}{n(\mathrm{VE})}$ = 0.7 (**F-T2a**, Table 3.3 entry 3). Further, it must be noted that 1.5 wt% of a thiol functionalized silane adhesion promoter, *Dynasylan MTMO*, was added to enhance adhesion on substrate surfaces. Silane-based adhesion promoters can form covalent bonds with OH group containing surfaces.[207] Alkoxy groups bonded to the silicon atom are hydrolyzed releasing the respective alcohol as shown in Scheme 3.9. The newly formed OH groups of the silane undergo condensation reactions with themselves as well as with surface hydroxy moieties to covalently bond the silane to a substrate. However, adhesion improvement was also observed without covalent bonding between silane and substrate by coordinative and hydrogen bonding on metals and plastics.[208] Yet bonding between an adhesion promoter and the adhesive polymer network is imperative, in this system ensured by thiol functionalization of the silane.

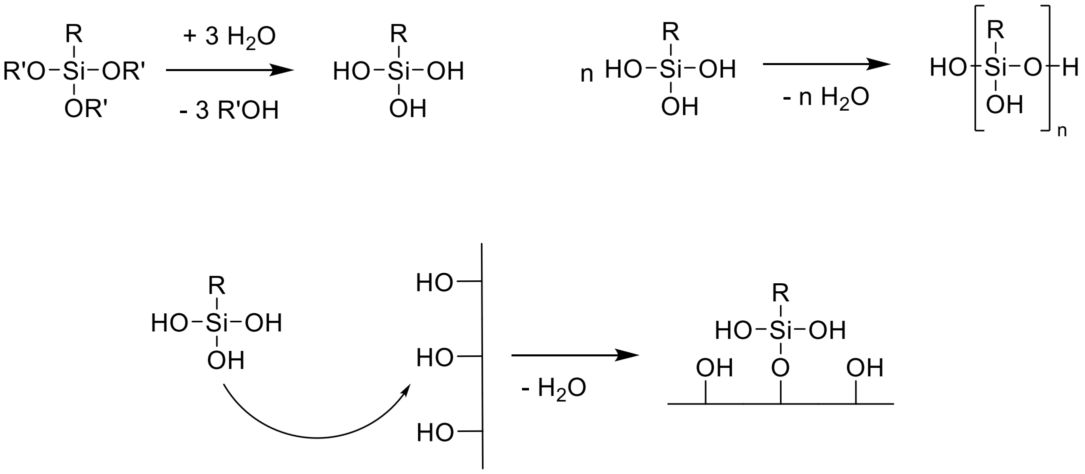

Scheme 3.9: Reaction path of silane-based adhesion promoters. Hydrolysis of alkoxy groups bonded to the silicon atom (top left) followed by silane polycondensation (top right) and covalent bonding to OH groups located on a substrate surface (bottom).

Tensile tests were performed with specimens cured from F-T2a with maximum tensile strength σ_{max} = 6.7 ± 0.7 MPa and elongation at break ε_{max} = 35 ± 2 % (appendix, Figure 6.19). Interestingly, the material is significantly softer and more flexible compared to the 1K vinyl ether formulation F-U indicated by the significant decrease in tensile strength and the massive increase in maximum elongation. Hence, curing of F-T2a results in a less densely crosslinked polymer network despite a similar reactive group concentration in the vinyl ether component. This indicates that material curing proceeds predominantly via thiol-ene polyaddition and not vinyl ether polymerization; this is further underlined by the fact that no odor of non-reacted thiol groups was perceived after the reaction.

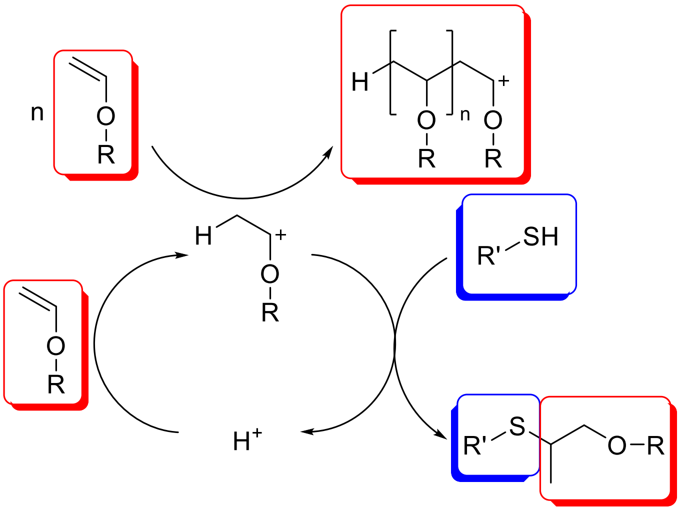

Scheme 3.10: Reaction mechanism of a cationic thiol-ene polyaddition (bottom) with cationic polymerization of excess vinyl ether moieties (top).

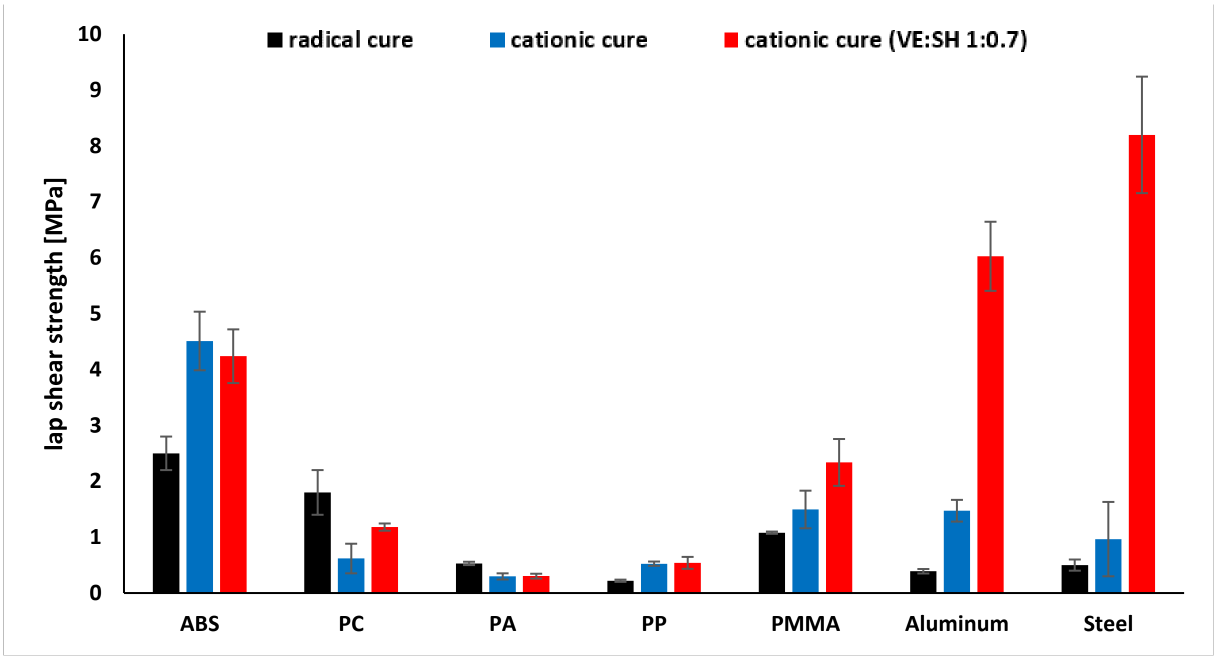

Figure 3.14: Single-lap shear test results of different plastic and metal substrates, glued by a thiol-vinyl ether adhesive formulation thermally cured via radical polyaddition (black) and cationic polyaddition (blue) with a vinyl ether : thiol ratio of 1 : 0.98. In addition, the ratio was changed to 1 : 0.7 (red) and cured via cationic polyaddition.

Single-lap shear tests of radical formulation F-T1 and cationic formulations F-T2 and F-T2a were performed to evaluate the potential of vinyl ethers and the respective curing mechanisms towards adhesive applications (Figure 3.14). Overall, higher lap shear strength values are achieved by cationic curing compared to radically cured formulation FT-1, except for application on PC substrates. It must be noted that adhesive residues on the tested lap shear substrates show a decrease in tackiness from formulation F-T1 to F-T2 to F-T2a. The tackiness most likely results from incomplete curing. Thus, cationic curing additionally results in higher monomer conversion; an increased excess in vinyl ether functionality enhances this effect.

This observation was made for adhesive joints including PMMA, ABS & PC substrates, all of which broke by cohesion failure. Furthermore, the differences in tackiness described above were also seen on PP substrates, but failure mode was found to be adhesion failure. An interesting observation was made on PA. Adhesive residuals from all three systems were slightly wet and hence incomplete curing was assumed. Incomplete cationic curing on polyamide is most likely linked to the nucleophilicity of amide groups present on the substrate surface which results in partial quenching of the active cationic species during polyaddition and polymerization.[209] An overall increase in curing progress was observed on adhesive residuals on aluminum and steel; most likely because of faster heat transfer by metal substrates compared to plastic materials during thermal curing. Investigation of adhesive remains on metal substrates show mixed failure mode with tendencies towards adhesion failure on aluminum and towards cohesion failure on steel (Figure 3.15). Overall, F-T1 shows weak adhesive strength on all substrates as do F-T2 and F-T2a on PC, PA, PP and PMMA with maximum lap shear strength values below 2.5 MPa. However, ABS substrates glued by the cationic formulations F-T2 and F-T2a exhibit lap shear strength values of δ = (4.5 ± 0.9) MPa and δ = (4.2 ± 0.8) MPa, respectively, which is suitable for designated applications already. Yet, highest adhesive strengths are achieved by gluing aluminum and steel joints with F-T2a despite the formerly low values observed on metal surfaces for all vinyl ether-based systems. Strikingly, lap shear strength of aluminum substrates glued by formulations F-T2 and F-T2a increased dramatically from δ = (1.5 ± 0.2) MPa to δ = (6.0 ± 1.2) MPa by increasing the excess of vinyl ether component and adding an adhesion promoter. As no differences in curing progress and mostly adhesion failure mode were observed, the latter likely has a bigger impact on adhesive performance on aluminum surfaces.[13] Although the addition of adhesion promoter also influences adhesive performance on steel, it must be noted that more complete curing by using an excess amount of the vinyl ether component was observed. However, lap shear strength of δ = (8 ± 2) MPa for F-T2a on steel substrates is achieved which is the highest adhesive strength observed for vinyl ether-based systems so far.

In conclusion, radical polyaddition of the tested two-component thiol-vinyl ether systems yield soft and not fully cured materials with weak adhesive performances. By substituting the radical initiator with a cationic initiator, the polyaddition mechanism is altered and thioacetal linkages are formed in contrast to thioether groups found in polymer backbones obtained from radical polyaddition, resulting in hardening of the material by comparison. Higher conversion and a tendency towards cohesive failure mode in lap shear tests highlight the importance of utilizing excess amounts of a vinyl ether part in cationic two-component thiol-vinyl ether systems. This approach yielded the highest lap shear strength values observed so far for vinyl ether-based systems - surprisingly on steel joints.

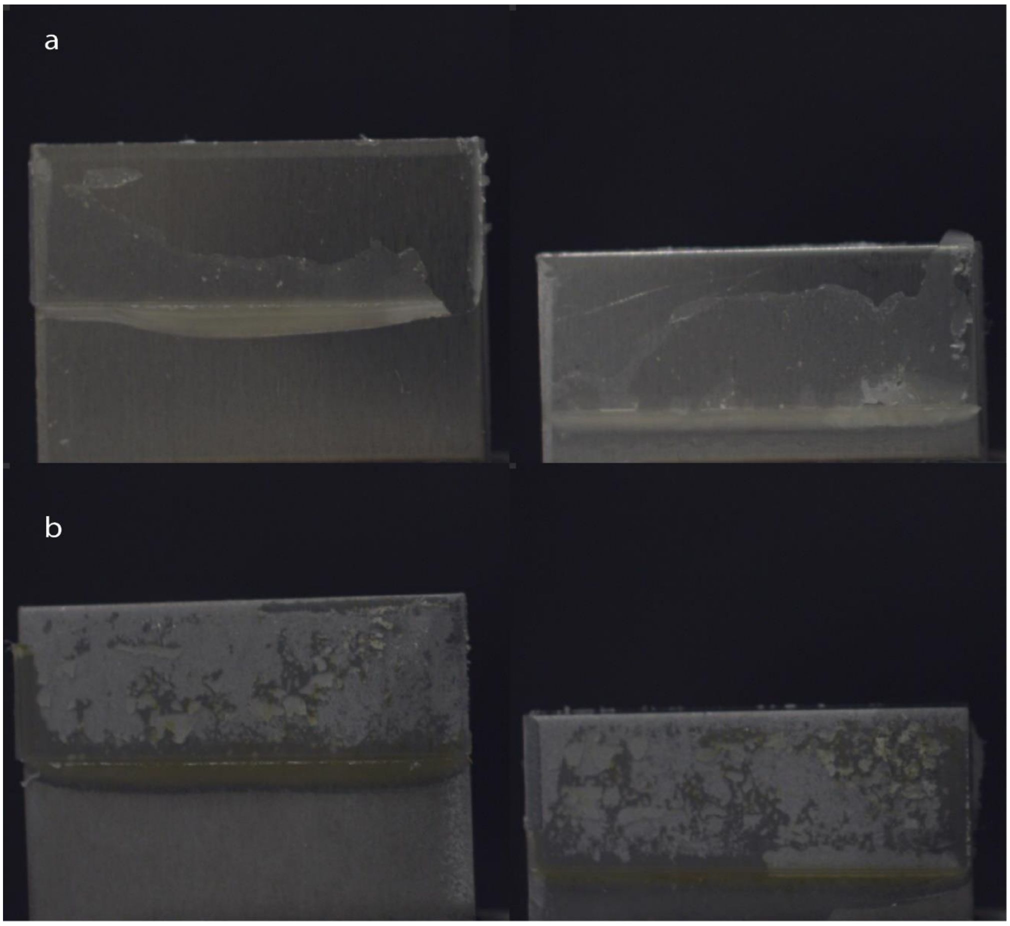

Figure 3.15: Exemplary pictures of adhesive residuals on aluminum (a) and on steel substrates (b). Although both samples show mixed failure mode, adhesion failure is the predominant factor on aluminum opposed to cohesion failure on steel.

The scope of applications for vinyl ethers in adhesive systems has been significantly widened by demonstrating their great potential in two-component systems in combination with thiols as well as their remarkably high adhesive strength on metal surfaces in contrast to prior one-part cationic vinyl ether formulations which clearly favor plastic materials.

3.1.6 Cationic polymerization kinetics of vinyl ether functionalized urethane and hemiacetal esters

After curing urethane-based formulation F-U a noticeable odor of vinyl ether monomers was observed which implies an incomplete conversion of vinyl ether groups in the curing process. As mentioned before, the inhibiting effect of urethane groups on cationic polymerization of vinyl ethers was reported in literature.[142–145] A difference between urethane compounds prepared from aromatic or aliphatic isocyanates was found. Aliphatic isocyanates were described to show a more pronounced inhibition effect on vinyl ether conversion. However, investigation of this difference is not part of this work. Instead, the focus was on differences in cationic vinyl ether polymerization inhibition by urethane groups compared to other functional groups, i.e.

hemiacetal esters. Due to the reported inhibiting effect of urethanes, substituting urethane-based prepolymers with hemiacetal ester compounds aims not only at enabling debonding mechanisms, but also at increasing vinyl ether conversion resulting in improved mechanical properties, less odor and fewer safety concerns regarding the cured material. It is imperative to thoroughly investigate the differences between urethane and hemiacetal ester groups in terms of cationic polymerization kinetics of vinyl ethers in order to fully understand the impact of hemiacetal ester utilization.

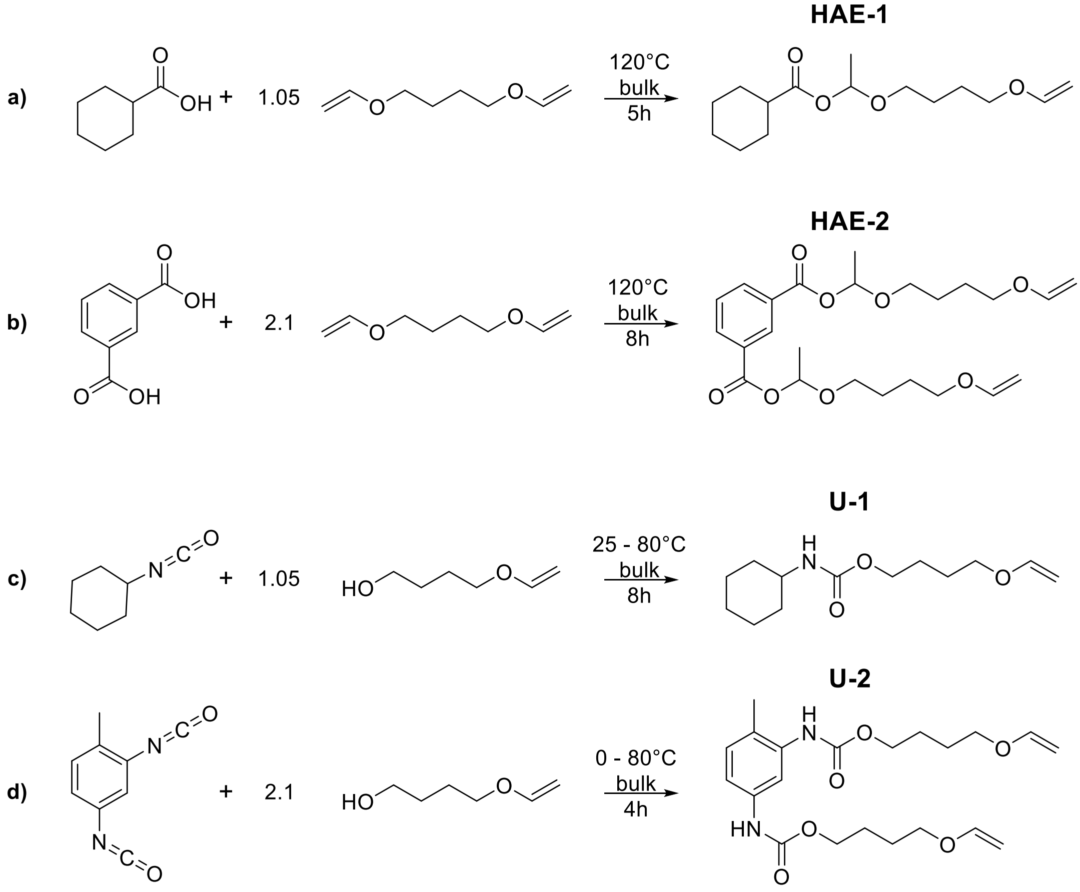

Scheme 3.11: Synthesis of hemiacetal ester and urethane compounds for kinetic measurements in cationic vinyl ether polymerization.

For comparison, two hemiacetal ester and two urethane compounds with terminal vinyl ether functionality were synthesized with similar structures; the respective syntheses are shown in Scheme 3.11. An aliphatic hemiacetal ester with one terminal vinyl ether functionality **HAE-1** was prepared from cyclohexanecarboxylic acid and BDVE, the analog urethane compound **U-1** was synthesized from cyclohexane isocyanate and HBVE. In addition, aromatic difunctional compounds were prepared in a similar manner from isophthalic acid (**HAE-2**) and toluene diisocyanate (**U-2**), respectively. The corresponding ^{1}H-NMR spectra are displayed in Figure 3.16 - Figure 3.17. There are some factors which may sophisticate kinetic measurements depending on the final reaction mixtures: Besides acid conversion and product yield *Y*, both vinyl ether functionalities of BDVE can react with carboxylic acid groups resulting in a decrease in net vinyl ether concentration per gram which leads to a shift in initiator/reactive group concentration impacting kinetic measurements. However, the functional group concentration of hemiacetal esters is unaffected in contrast to acid conversion. The main focus of this experimental series was the potential inhibition by unreactive functional groups and thus the former factor is negligible. In addition, the vinyl ether groups can potentially self-polymerize due to the acidic conditions. ^{1}H-NMR spectra of HAE-1 and HAE-2 show no peaks above 8 ppm which implies full acid conversion, but it must be noted that acid proton signals are not always well visible. Complementary calculations from proton integrals Y_{HAE-1} = 99.1 % and Y_{HAE-2} = 99.5 % further confirm very high yields of the desired products. The ratio of vinyl ether to hemiacetal ester groups was calculated as 90.1 % for HAE-1 and as 92.1 % for HAE-2. But as mentioned above, the small amount of pre-reacted vinyl ether groups hardly affects kinetic measurements. Additionally, these low ratios imply that no self-polymerization of vinyl ether groups occurred. Isophthalic acid is a medium to weak acid with pK_a values of 3.46 and 4.46[210], respectively, and cyclohexanecarboxylic acid is a weak acid with pK_a = 4.9[211]. Most likely both organic acids are too weak to initiate cationic polymerization by deprotonation and subsequent addition to a vinyl group.

The factors of interest in urethane preparation are isocyanate and HBVE conversion as the former influences the concentration of urethane group present in the final sample mixture and the inhibiting effect thereof. Unreacted HBVE may undergo chain transfer reaction in cationic polymerization which slows down the polymerization and yields less densely crosslinked polymer network but does not inhibit it. Calculations from proton integrals result in Y_{U-1} = 98.5 % and Y_{U-2} = 98.8 %. Reactive isocyanate groups typically undergo side reactions at elevated temperatures which make yields of 100 % of the desired urethane compound nearly impossible. However, the achieved yields of both products are very high and all possible effects on cationic polymerization by a very low amount of byproducts are negligible. Moreover, urethane byproducts and reaction mixtures are always present in raw materials for adhesives and tolerated in their corresponding industrial application as described in section 3.1.2. The final reaction mixture of U-1 has a ratio of reacted to unreacted HBVE of 98.7 %, so hardly any free hydroxyl groups are present, and U-2 shows no unreacted HBVE at all. Thus, the reaction mixtures of all four compounds are well suited for kinetic measurements under the described conditions.

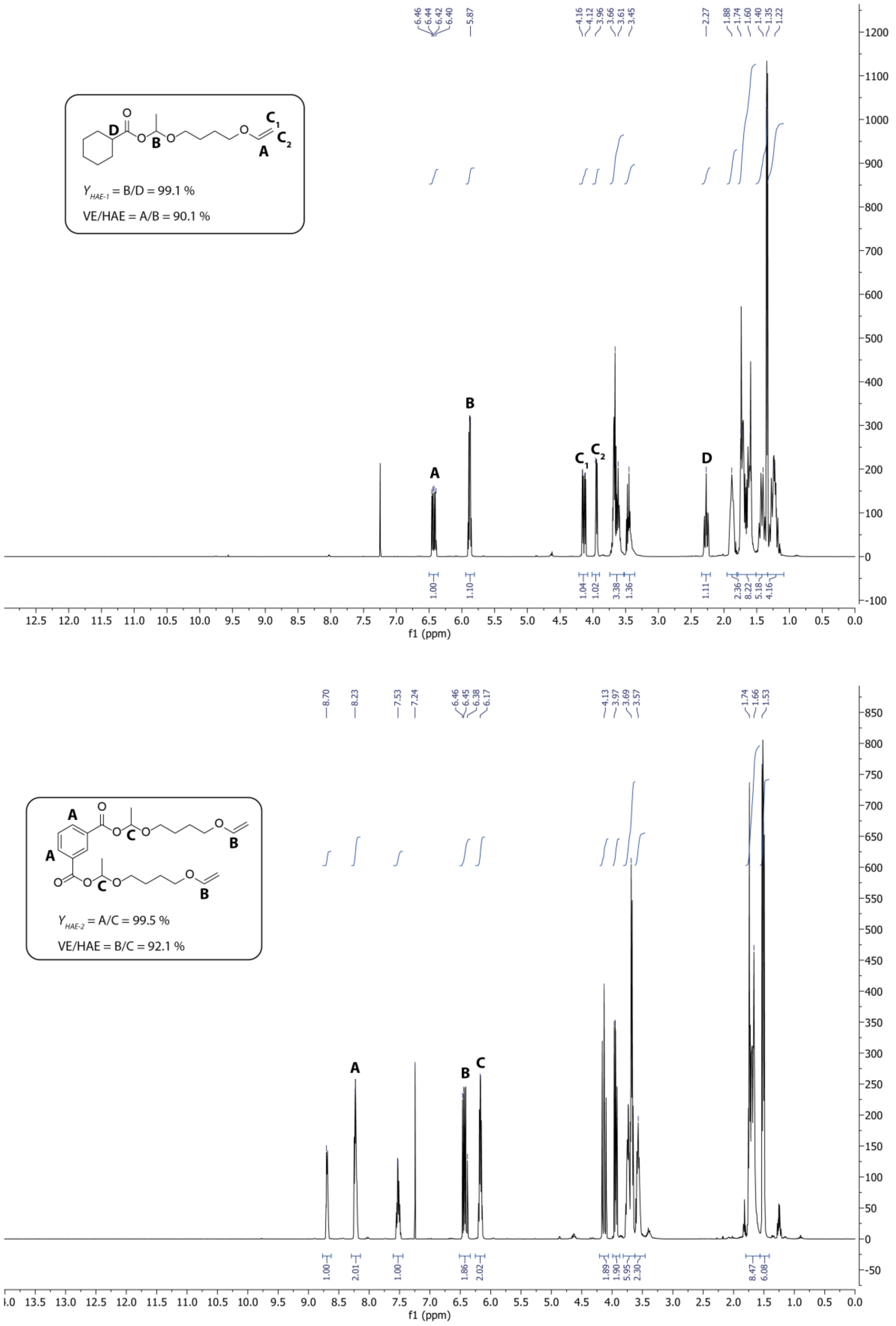

Figure 3.16: ^{1}H-NMR spectra of HAE-1 (upper) and HAE-2 (lower) after reaction in $CDCl_3$. The compounds were utilized without further purification in kinetic measurements.

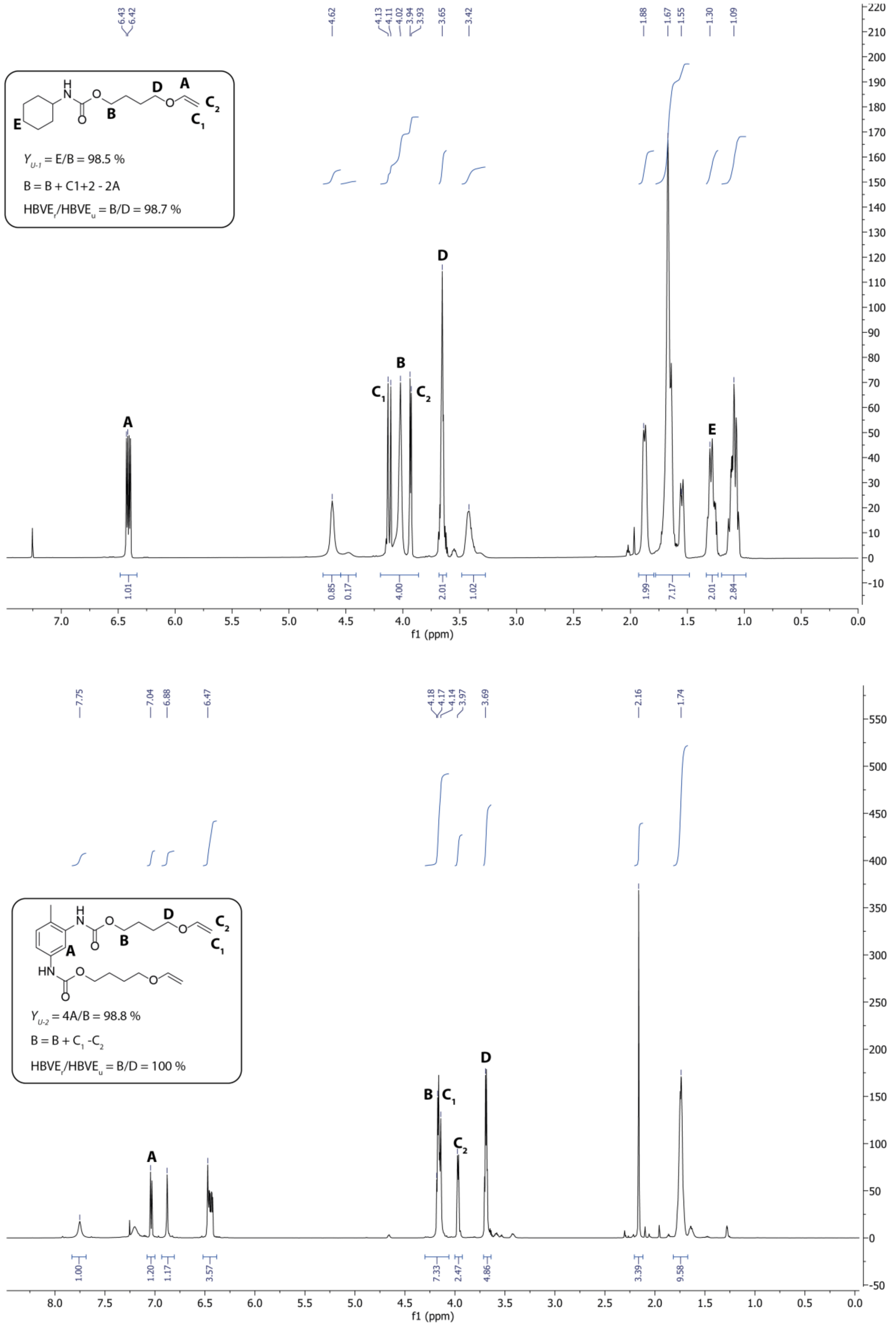

Figure 3.17: ^{1}H-NMR spectra of U-1 (upper) and U-2 (lower) after reaction in $CDCl_3$. The compounds were utilized without further purification in kinetic measurements. No peaks were observed above 8 ppm.

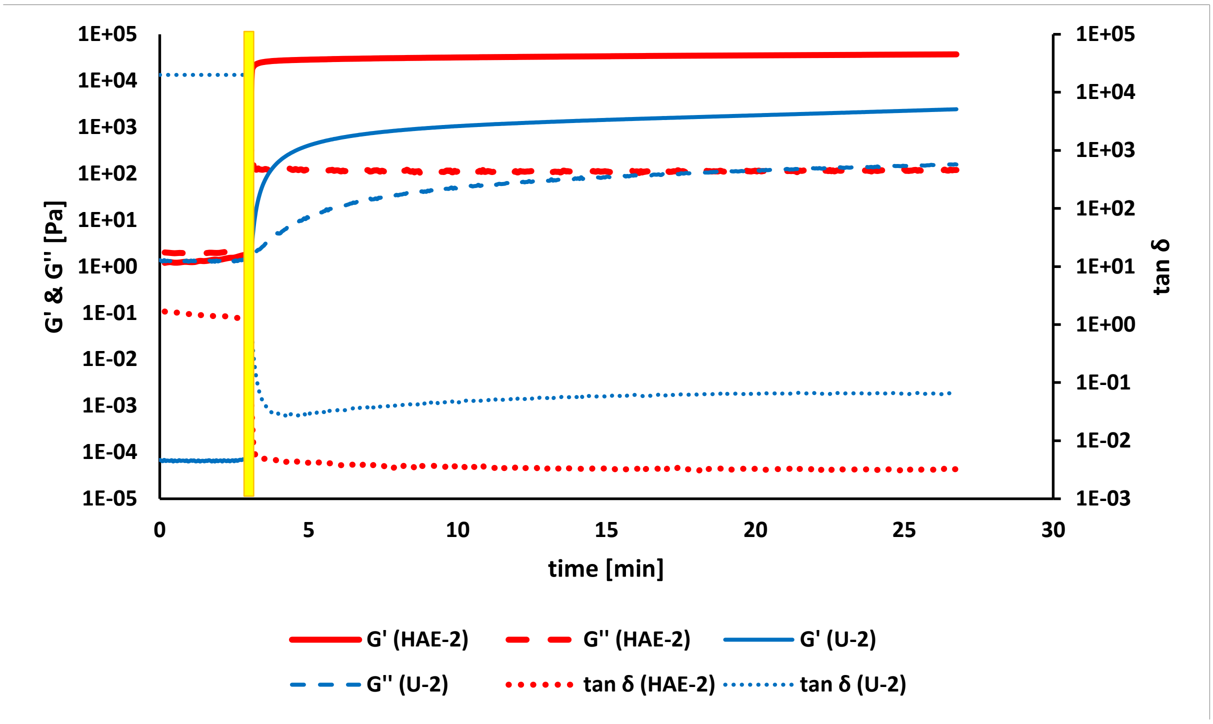

Figure 3.18: Storage modulus *G'* (solid line), loss modulus *G''* (dashed line) and dissipation factor tan *δ* (dotted line) over time of difunctional vinyl ether monomers with hemiacetal ester groups (HAE-2, red) or urethane groups (U-2, blue) with an initiator concentration of w (PI 440) =0.05 wt%. To initiate cationic polymerization, the sample was irradiated with UV light for 3 seconds indicated by the yellow area.

In order to evaluate the inhibiting effect of hemiacetal ester and urethane groups on cationic vinyl ether polymerization, rheometric measurements were carried out. The respective compound was mixed with an initiator solution, consisting of 25 wt% PI 440 in propylene carbonate. The mixtures here were heated to 80 °C for a few minutes to melt the urethane compounds, then properly mixed and finally placed on a preheated quartz plate. After three minutes of shearing for the material to reach a viscoelastic equilibrium state, the samples were irradiated with UV light for three seconds and changes in material properties were monitored over time. The aromatic difunctional compounds HAE-2 and U-2 were polymerized with 0.05 wt% (Figure 3.18) and 0.025 wt% (Figure 3.19) of photoinitiator and compared regarding their curing progress over time.

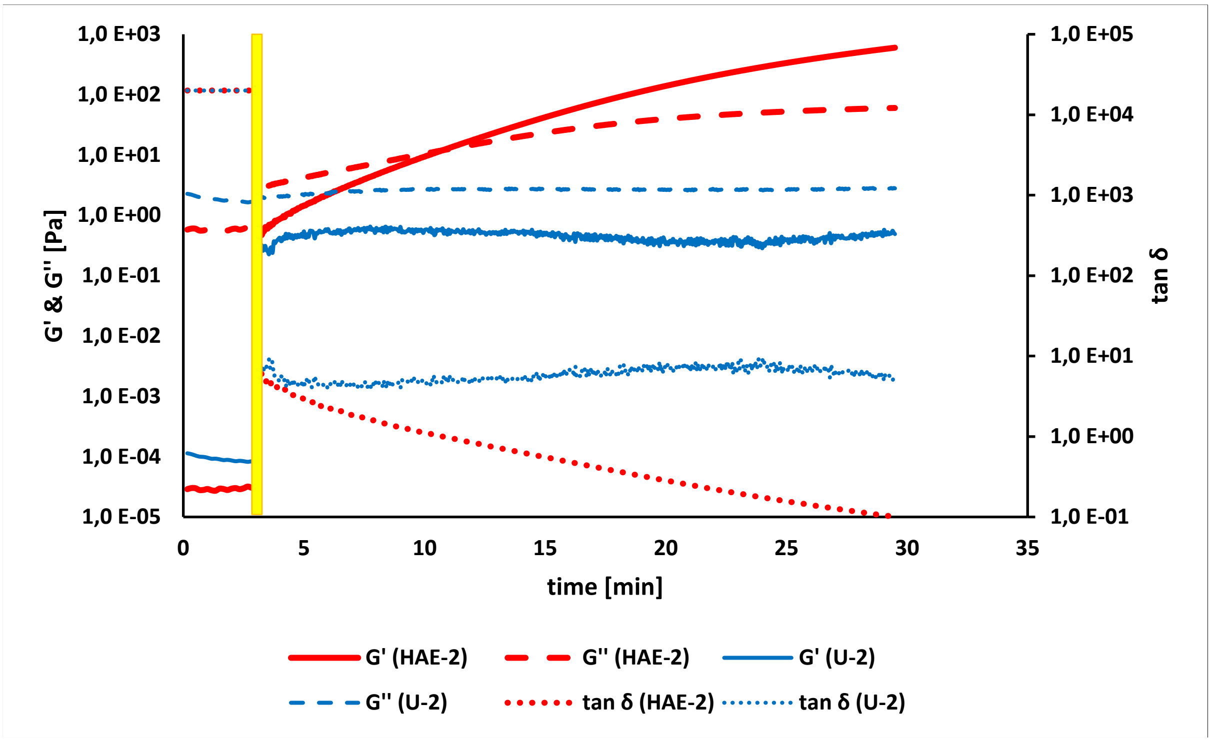

Figure 3.19: Storage modulus *G'* (solid line), loss modulus *G''* (dashed line) and dissipation factor tan *δ* (dotted line) over time of difunctional vinyl ether monomers with hemiacetal ester groups (HAE-2, red) or urethane groups (U-2, blue) with an initiator concentration of w (PI 440) =0.025 wt%. To initiate cationic polymerization, the sample was irradiated with UV light for 3 seconds indicated by the yellow area.

In the first case, both monomers polymerize quickly and undergo sol-gel transition almost instantaneously as soon as irradiation starts. The graphs of storage modulus *G'* and loss modulus *G''* of HAE-2 immediately reach a plateau indicating immediate full conversion, whereas polymerization of U-2 proceeds in a much slower fashion and polymerization is not finished even after 25 minutes of reaction which indicates a possible inhibition of cationic polymerization by urethane groups. The observed decrease in reaction speed is likely due to lower concentrations of active chain ends resulting from immobilization of initiating protons on the urethane group. By decreasing initiator concentration, this effect becomes even more apparent. When using only 0.025 wt% of initiator, *G'* and *G''* of HAE-2 immediately increase on irradiation and polymerization proceeds slowly with a sol-gel transition after about 10 minutes. In contrast, *G'* of U-2 also increases quickly due to UV exposure but stays constant after the light source is turned off and *G''* is hardly affected at all. The course of *G'* of the urethane compound can be explained by a quick first polymerization of vinyl ether groups upon irradiation due to fast formation of an initiating species whereas propagating species are quickly quenched by urethane groups resulting in a stagnation of polymerization and consequently of *G'*. In previous studies, the inhibiting effect of urethane groups was found to be more pronounced if the urethane was synthesized from an aliphatic isocyanate instead of an aromatic one.[142–144] Thus, the observed differences in cationic polymerization of terminal vinyl ether groups of hemiacetal ester and urethane compounds is expected to be even more pronounced. However, a direct comparison between aliphatic and aromatic urethanes is not possible under the described experimental conditions due to the difference in vinyl ether functionality. UV triggered polymerization of HAE-1 and U-1 was monitored with a concentration of 2 wt% and 0.2 wt% of PI 440; the respective rheologic data is presented in Figure 3.20 and Figure 3.21. With high initiator concentration, both compounds undergo an immediate sol-gel transition upon irradiation and moduli values reach a plateau which indicates fast and complete conversion of vinyl ether groups. By decreasing initiator concentration, a distinct difference in curing behavior can be observed. Cationic Polymerization of HAE-1 again proceeds very quickly with full vinyl ether conversion after a few seconds whereas U-2 hardly shows any changes in viscoelastic properties but a very slow increase in *G'* and *G"* starting after about 5 minutes. Hence, a significant difference in polymerization kinetics has been found depending on the functional group in the monomer backbone.

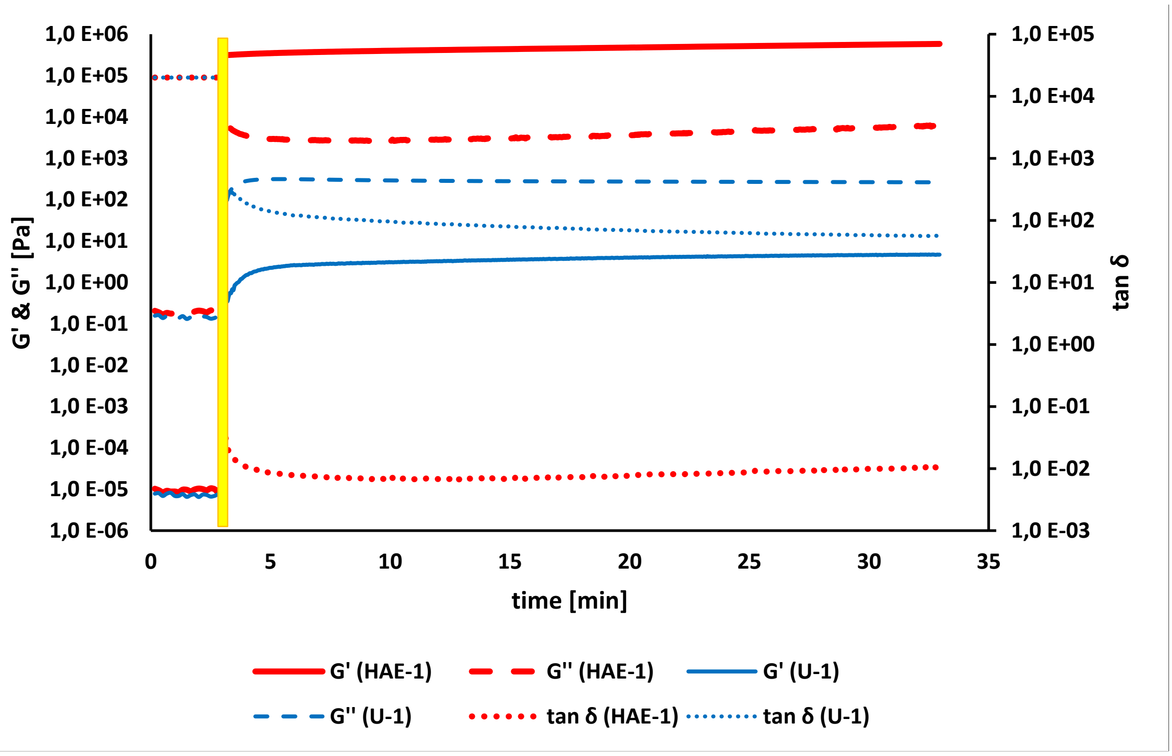

Figure 3.20: Storage modulus *G'* (solid line), loss modulus *G"* (dashed line) and dissipation factor tan *δ* (dotted line) over time of monofunctional vinyl ether monomers with hemiacetal ester groups (HAE-1, red) or urethane groups (U-1, blue) with an initiator concentration of w (PI 440) =2 wt%. To initiate cationic polymerization, the sample was irradiated with UV light for 3 seconds indicated by the yellow area.

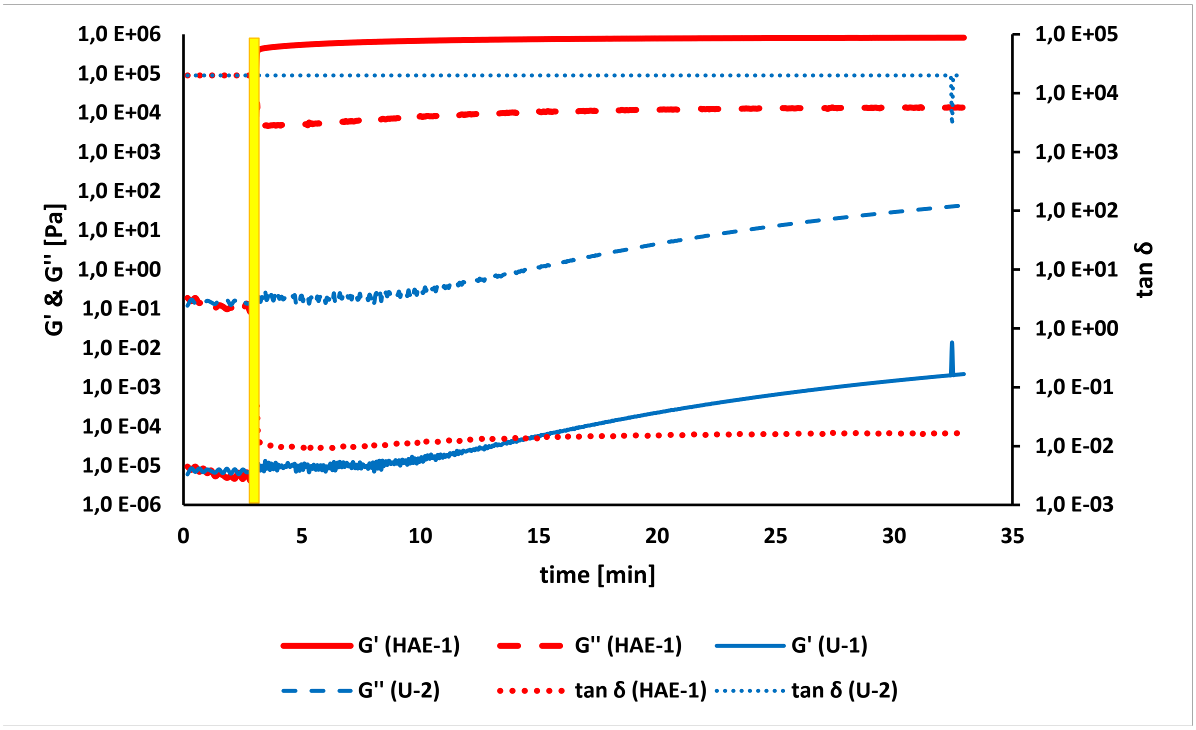

Figure 3.21: Storage modulus *G'* (solid line), loss modulus *G''* (dashed line) and dissipation factor tan *δ* (dotted line) over time of monofunctional vinyl ether monomers with hemiacetal ester groups (HAE-1, red) or urethane groups (U-1, blue) with an initiator concentration of w (PI 440) =0.2 wt%. To initiate cationic polymerization, the sample was irradiated with UV light for 3 seconds indicated by the yellow area.

Although vinyl ethers are known to not yield polymers in radical polymerization, they are highly reactive but undergo termination reactions very fast.[111,113] Thus, the immediate increase in moduli upon irradiation can also be caused by radical polymerization initiated via radical intermediates in initiator decomposition followed by termination reactions. In order to verify this hypothesis, additional rheometric experiments were performed with a mixture of two radical photoinitiators of type I, 1-Hydroxy cyclohexyl phenyl ketone (**PI 184**), and of type II, 4-(4-Methylphenylthio)benzophenone (**PI BMS**). Reaction mixtures with 1 wt% of each radical initiator were prepared and previous kinetic measurements were repeated; the respective data can be found in the appendix (Figure 6.20). None of the utilized monomers react upon irradiation and consequently any impact from radical polymerization can be ruled out. In addition, vinyl ether conversion X in UV-triggered cationic polymerization was examined by ^{1}H-NMR experiments. A propylene carbonate solution with 5 wt% PI 440 was prepared and mixed with hemiacetal ester and urethane monomers with terminal vinyl ether groups and reaction mixtures with 0.1 wt% of PI 440 in regard to the respective monomer were obtained. These mixtures were heated to 80 °C and irradiated with a UV lamp; HAE-1 and U-1 were irradiated for ten seconds, HAE-2 and U-2 for five seconds. ^{1}H-NMR spectra were recorded before and after irradiation. From the spectra, the ratio of integral values of inert (A_x) and vinyl ether protons (A_{VE}) were compared before and after UV exposure following equation 3.2. The respective spectra can be found in the appendix (Figure 6.21 - Figure 6.24) and the results are presented in Table 3.4. Both urethane compounds show hardly any conversion with $X_{U\text{-}1}$ = 0.15 % and $X_{U\text{-}2}$ = 0.62 %. A slight increase in conversion is found for HAE-1 with a conversion of 2.1 % and significantly higher conversions were achieved by HAE-2 with $X_{HAE\text{-}2}$ = 13 %. Again, a distinct trend was observed as vinyl ether monomers with a urethane group hardly undergo cationic polymerization whereas especially hemiacetal ester compound HAE-2 shows significant vinyl ether conversion.

$$X_{VE} = 1 - \frac{\frac{A_{VE}}{A_X}}{\frac{A_{VE,0}}{A_{X,0}}} \qquad \mathbf{(3.2)}$$

Table 3.4: Vinyl ether conversion in photoinitiated cationic polymerization of monomers with hemiacetal ester and urethane monomer backbones determined via ^{1}H-NMR.

	HAE-1	HAE-2	U-1	U-2
Vinyl ether conversion [%]	2.1	13	0.15	0.62

In conclusion, vinyl ether functionalized monomers with hemiacetal ester groups participate in fast cationic polymerization even at very low initiator concentrations. The polymerization is significantly inhibited by the presence of urethane groups in monomer structure explicitly evaluated in kinetic measurements via rheology and vinyl ether conversion determined by ^{1}H-NMR. As a consequence, hemiacetal ester prepolymers are superior to urethane prepolymers for vinyl ether-based adhesive formulations in terms of curing speed and reactive group conversion. Furthermore, hemiacetal ester prepolymers are a good alternative for more sustainable adhesive systems due to the better availability of biobased raw materials for prepolymer synthesis and their potential for debond-on-demand systems.

A draft for a publication is currently in the works about this section. Ideas for the isocyanate and carboxylic acid substrates as well as the radical polymerization approach were provided by Dr. Hendrik Luetzen. The author provided the main idea, the practical work, the evaluations as well as the work approach iterations for the final results.

3.1.7 Hydrolysis of cured hemiacetal ester-based materials

Besides their outstanding reactivity in cationic polymerization, vinyl ether functionalized hemiacetal ester compounds have a potential for utilization in adhesive systems with debonding abilities. In debonding systems, the liquid formulation is cured between two substrate layers e.g. by irradiation or thermal activation providing high adhesive stability which does not degrade over time. By applying an external trigger, the adhesive loses its cohesive and/or adhesive integrity and two glued substrates can be separated and recycled. The development of debonding adhesives is an important part on the pathway to a circular economy and in fighting against climate change. Hemiacetal esters undergo hydrolysis under acidic conditions which makes them a promising compound for such systems. A densely crosslinked network is formed by cationic polymerization of vinyl ether moieties during curing which can be degraded by the addition of water and optimally an acid in catalytic amounts to trigger hemiacetal ester hydrolysis. The polymer backbone breaks into smaller fractions and thus mechanical properties, i.e. cohesion, are significantly weakened. However, materials susceptible to hydrolysis tend to lose cohesion over time due to water from the humid air diffusing into the material and reacting with the respective functional groups to break up crosslinks. It is crucial to find a way to maintain cohesive integrity while keeping the material prone to an external trigger for degradation.

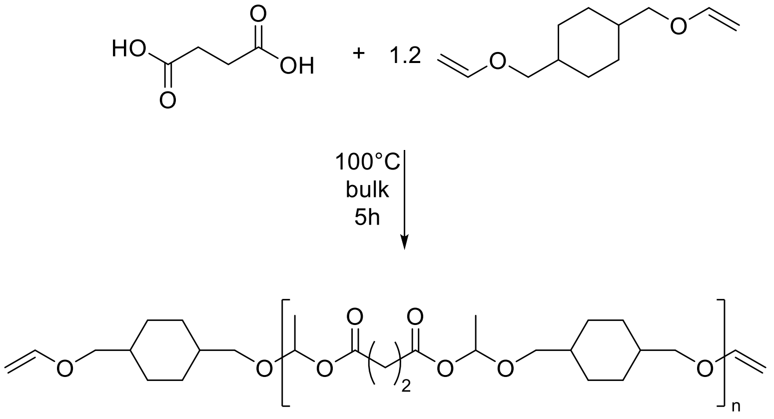

Scheme 3.12: Synthesis of hemiacetal ester-based difunctional vinyl ether prepolymer PHAE-2 from succinic acid and 1,4-Cyclohexandimethanol divinyl ether.

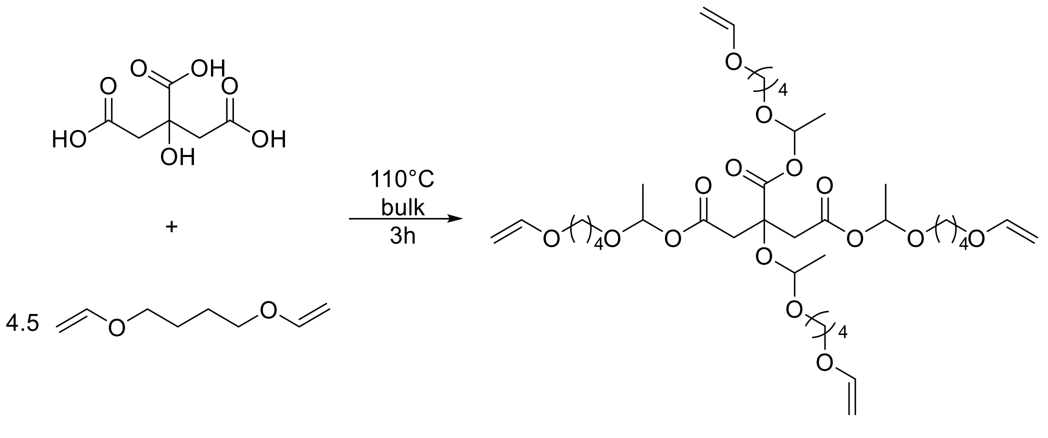

Scheme 3.13: Synthesis of hemiacetal ester- & acetal-based crosslinker PHAE-4 from citric acid and 1,4-Butanediol divinyl ether.

A difunctional hemiacetal ester prepolymer **PHAE-2** was synthesized in a polyaddition reaction between biobased succinic acid and CDVE, the latter given in slight excess to ensure vinyl ether functionality (Scheme 3.12). These building blocks were chosen because of their good availability, although CDVE is only available from fossil fuels so far. In addition, the immobile prepolymer backbone is expected to increase the rigidity of the respective polymer networks in contrast to the typically soft materials obtained from vinyl ethers due to the highly flexible ether group in the polymer main chain. The carboxylic acid groups are fully converted after five hours of reaction, confirmed by ^{1}H-NMR measurements, and the molecular weight is about $M_w \approx 4400$ Da determined via GPC. To enable tailoring of crosslinking density of cured polymer networks, a hemiacetal ester-based crosslinker **PHAE-4** with four terminal vinyl ether groups was prepared in an addition reaction of potentially biobased citric acid (anhydrous) with 1,4-butanediol divinyl ether (**BDVE**), the latter in excess to prevent polyaddition reactions between citric acid molecules which lead to immediate crosslinking and gel formation, which is detrimental for further processing in formulation (Scheme 3.13). In addition to three hemiacetal ester linkages, an additional acetal linkage is formed from the reaction of a vinyl ether with the hydroxy group.[212] The overall conversion of carboxylic acid and hydroxy groups of citric acid was determined via ^{1}H-NMR as X ≈ 80 °C . Consequently, the final product mixture contains unreacted acid groups as well as unreacted BDVE but was used without further purification. From this, a hemiacetal ester-based adhesive formulation with vinyl ether functionality **F-HAE** was developed to evaluate the potentials for adhesive applications in terms of adhesive performance and also debonding capabilities of hemiacetal ester compounds. The composition of formulation F-HAE is shown in Table 3.5 with the respective chemical structures in Scheme 3.14.

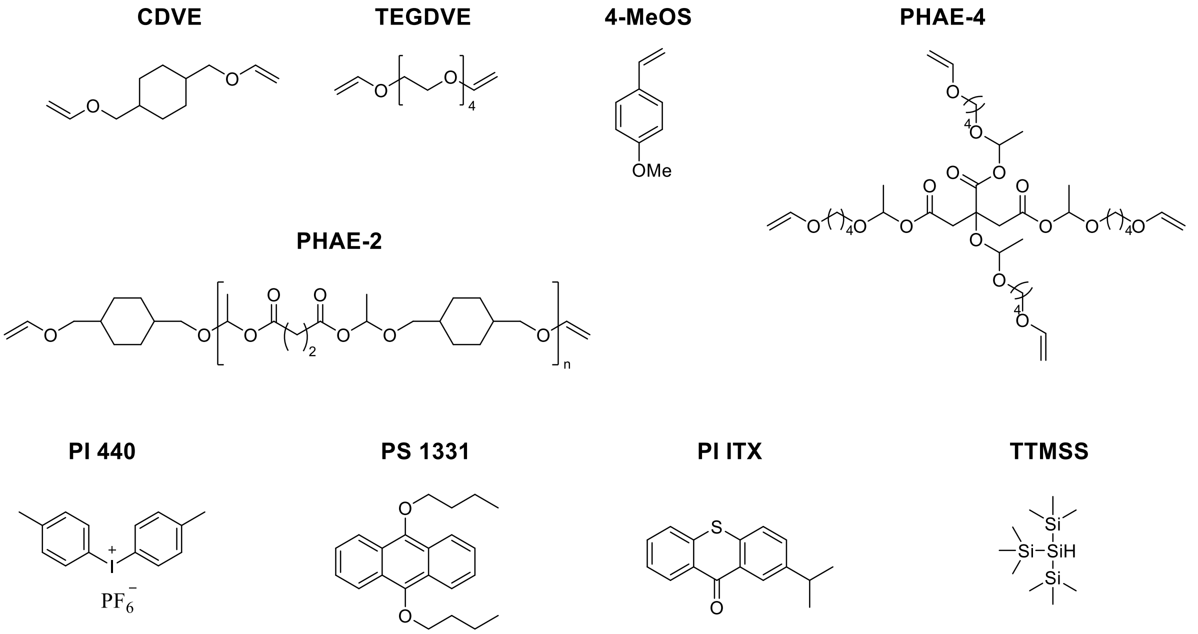

Scheme 3.14: Chemical structures of hemiacetal ester-based vinyl ether prepolymer PHAE-2, hemiacetal ester-based vinyl ether macromolecular crosslinker PHAE-4, vinyl ether reactive diluents CDVE and TEGDVE, 4-Vinylphenol derivative 4-MeOS, cationic photoinitiator PI 440, photosensitizer PS 1331, radical photoinitiator PI ITX and silane TTMSS.

Table 3.5: Composition of hemiacetal ester-based vinyl ether functionalized formulations in wt%. The concentration of the initiators PI 440, PS 1331, PI ITX, TTMSS is given in phr.

	TEGDVE	CDVE	PHAE-2	PHAE-4	4-MeOS	PI 440	PS 1331	PI ITX	TTMSS
F-HAE	15	15	50	20	-	1.5	0.5	-	-
F-HAEa	15	15	50	20	-	1	-	1	3
F-HAEb	15	15	70	-	-	1	-	1	3
F-HAEc	-	-	50	20	30	1.5	0.5	-	-

First, storage stability of the cured material obtained from F-HAE was evaluated by performing DMA experiments with specimens directly after curing and after different storage conditions.[213] For reference, the thermogram of a specimen one hour after preparation is shown in Figure 3.22. The characterizing parameters are storage modulus at 25 °C with *G'* = 796 MPa and glass transition temperature T_g = 60 °C which serve as a reference for complimentary storage stability experiments described later in this section.

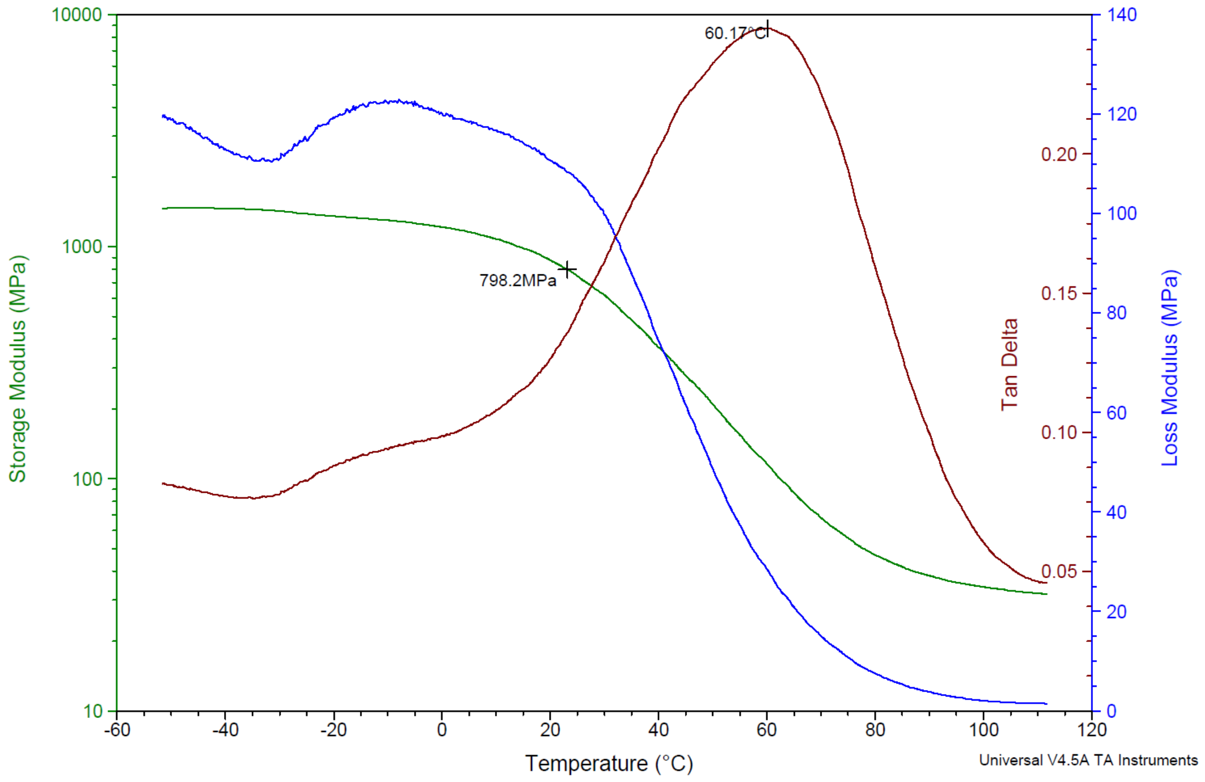

Figure 3.22: DMA thermogram of hemiacetal ester-based formulation F-HAE one hour after photocuring. The characteristics of interest are the temperature at which tan *δ* shows a peak, marking T_g, and the absolute value of *G'* at 25 °C which serves as a benchmark for the mechanical properties of a sample.

One sample of the cured material was stored in an evacuated desiccator for one week and one sample was stored on the lab bench at room temperature. Storage effects on material properties were investigated by DMA. The respective thermograms are shown in Figure 3.24. After one week of storage under dry conditions, hardly any changes in T_g were observed but storage modulus at 25 °C significantly increased to *G'* = 1120 MPa. This indicates further hardening of the material after the curing process which results most likely from a continuation of cationic polymerization due to its living character in the absence of nucleophilic species. Hence, the material does not only hold its cohesive strength over time when stored under dry conditions but becomes more brittle and stronger compared to its state directly after photocuring. In contrast, a significant weakening of the material was observed if stored under air which is highlighted by the results obtained from DMA. Storage modulus at 25 °C drops to 341 MPa which is less than half of what the material exhibits directly after curing. Interestingly, two different glass transition temperatures were found at 23 °C, which is similar to the initial value, and at 62 °C. This phenomenon arises from water diffusing into the material from the outside, degrading the polymer network by hydrolyzing hemiacetal linkages and consequently weakening the material which leads to a decrease in G' and T_g. The second glass transition can be explained by the diffusion behavior of the water which penetrates the material from the surface and goes deeper towards the core over time and thus hemiacetal ester degradation follows a gradient with an unaffected core in the center of the material at the point of measurement. This hypothesis is backed by differences in the optical appearance of the core of the material and the surrounding layer (Figure 3.23). Overall, the material becomes brighter over time and opaquer. This discoloration gradient is attenuated in the core of the material which supports the aforementioned hypothesis. After longer storage times the second glass transition at the initial value is expected to vanish. However, it must be further elucidated if the weakening of the material certainly results from hemiacetal ester hydrolysis or other unexpected factors as discussed later in this section.

Figure 3.23: Cured samples of formulation F-HAE. Left: Shortly after curing. Right: After one week of storage. A distinct discoloration takes place: the material becomes brighter over time. In the right picture, an attenuated discoloration gradient can be seen on the inside of the sample.

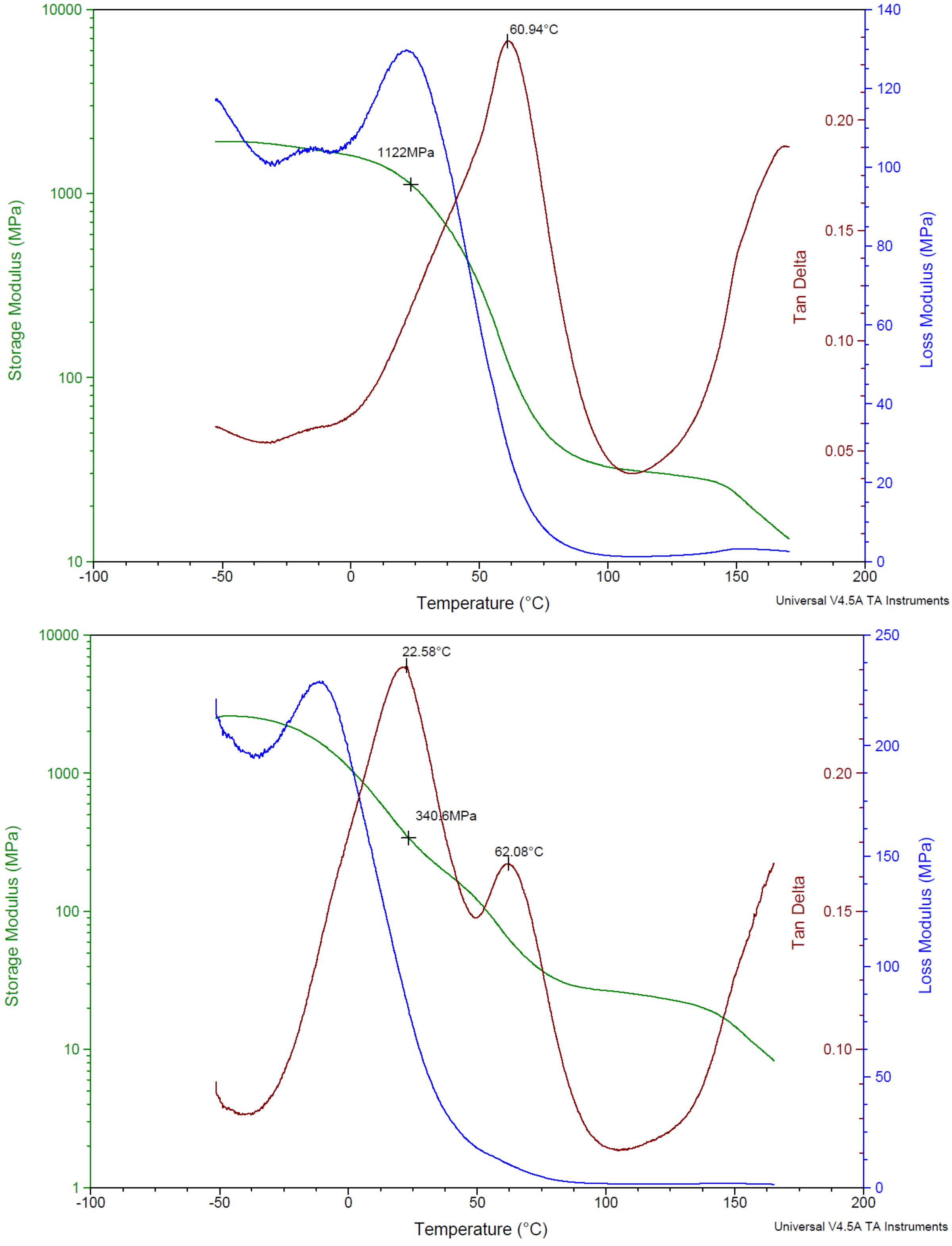

Figure 3.24: DMA thermogram of formulation hemiacetal ester-based formulation F-HAE after photocuring and storage for one week in an evacuated desiccator (upper) or under air (lower).

Table 3.6: Tensile test results of specimens cured from hemiacetal ester-based vinyl ether functionalized formulation F-HAE. The specimens were stored in a desiccator for one week, under air for one week or stored under air for one week, followed by one week in a desiccator, respectively with maximum stress σ_{max} and elongation at break ε_{max}.

Conditions	σ_{max} [MPa]	ε_{max} [%]
1W dry	25 ± 5	4.3 ± 0.5
1W air	7 ± 2	5 ± 2
1W air/1W dry	6 ± 2	6 ± 3

In addition, tensile tests were carried out with specimens cured from F-HAE under different storage conditions to obtain a more thorough picture of material degradation. Specimens were analyzed after photocuring and one week of storage under dry conditions, one week under air as well as one week under air followed by one week in a desiccator. The latter gives insight into the reversibility of the mechanical changes of hemiacetal ester polymer networks. The results are shown in Table 3.6, the stress-strain graphs can be found in the appendix (Figure 6.24). After one week of dry storage of the material, maximum tensile strength σ_{max} is about 25 MPa which is comparable to materials obtained from F-U and strain at break ε_{max} is cut in half to about 4.3 %. Consequently, the formed hemiacetal ester polymer network is less flexible than a similar urethane-based material. Upon irradiation, no significant differences in curing time or heat generation were observed between urethane-based formulation F-U and hemiacetal ester-based formulation F-HAE. The inhibiting effect of the urethane groups on cationic vinyl ether polymerization reported in the previous section mostly affects the late curing stage and would become more apparent with lower initiator concentrations. However, the described results do not allow a direct comparison between the effect of hemiacetal ester and urethane backbone structures on mechanical properties due to differences in prepolymer building block structures and molecular weight as well as crosslinker functionality. In contrast to the high tensile strength of the material when stored under dry conditions, σ_{max} drops to about 7 MPa with no significant change in ε_{max} when stored under air which underlines the effect of humidity on material degradation observed in DMA experiments. In an additional experiment, the specimens were first stored under air for one week, followed by one week of storage in a desiccator before measurement. Compared to specimens measured without the second storing stage, tensile strength and maximum elongation do not change significantly. Thus, downstream drying of the material has no effect on its mechanical properties which indicates that material softening does not result from swelling by water molecules or a plasticizing effect but an irreversible chemical reaction, such as hydrolysis.

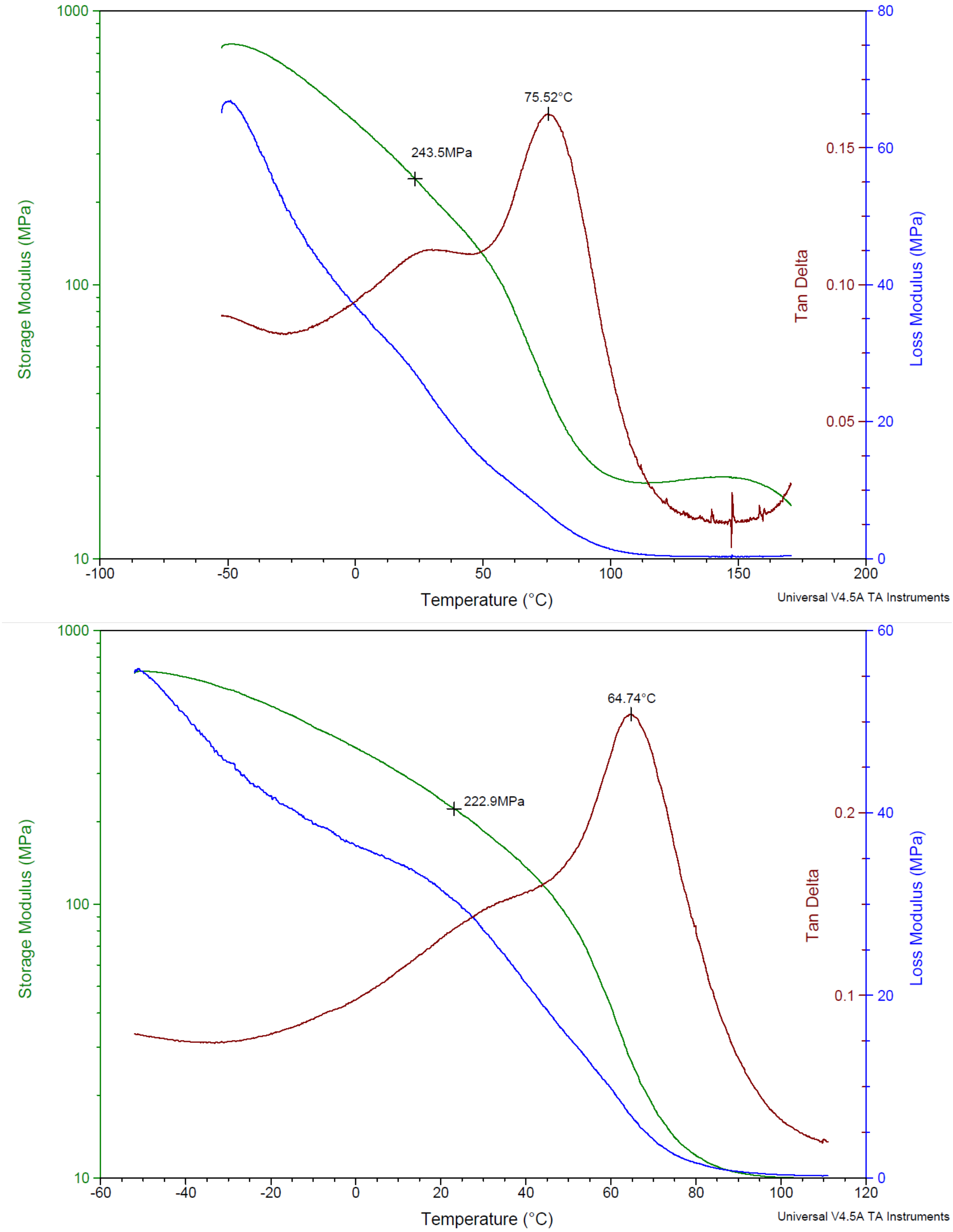

Figure 3.25: DMA thermograms of formulation urethane-based formulation F-U after photocuring and storage for one week in an evacuated desiccator (upper) or under air (lower).

In order to evaluate the role of hemiacetal ester groups in the polymer backbone on material weakening under air, an analogue DMA tests series was carried out with formulation F-U which does not contain any hemiacetal ester groups but is based on urethane prepolymers. Two samples of F-U were photocured and stored for one week either in a desiccator or under air and DMA experiments were performed (Figure 3.25). Under dry conditions, T_g of the cured material reaches 76 °C whereas glass transition of the material stored under air takes place at only 65 °C. This is likely due to favored conditions for cationic polymerization under vacuum as water from the surrounding air may act as a chain transfer agent or a weak inhibitor. G' is also slightly increased if the material is stored in a desiccator but only by about 20 MPa. However, the course of the graph of tan δ does not change depending on storage conditions which implies no gradient in degradation throughout the material. Overall, the insignificant differences in storage modulus and consistent dissipation factor behavior over temperature indicate no degradation of the material by surrounding air. This underlines the theory that the observed changes in mechanical properties for hemiacetal ester-based materials result from hydrolysis of these groups by surrounding air. The considerable weakening of the material under mild conditions highlights the susceptibility of hemiacetal ester groups towards hydrolysis and shows a need for improvement of formulation F-HAE for their use in adhesive applications. Under real application conditions, the material likely weakens too easily to ensure high adhesive performance over time and thus a way must be found to inhibit material degradation by water from the surrounding air.

There are several approaches to deal with the aforementioned issue of material degradation. One is that the adhesive can be sealed by a hydrophobic layer after curing to stop any water from diffusing into the material.[214] Another approach might be to add water scavenging additives, such silanes which react with any water coming in contact with the adhesive or conventional desiccants, typically activated charcoal or zeolites.[215] Another way is to remove any acid, which may act as a catalyst for hydrolysis, after curing. The first approach limits the scope of application as the bond line to be sealed is not necessarily accessible and also adds another step to production. The second approach does increase the time of storage stability, but the issue remains over a long period of time as soon as the water scavenging capabilities of the additives are depleted. Thus, removing hydrolysis catalyzing acidic species seems to be the most promising approach to effectively deal with the issue of material degradation by moisture over time in the described system. Experiments were performed to investigate if the material is affected by acidic conditions when coming into contact with water. A film was cured from F-HAE and placed into a deionized water bath equipped with a pH-meter. The pH immediately fell from 5.5 to 4.5 which implies that a significant amount of acid is present under wet/humid conditions and acid catalyzed hydrolysis is thus very likely.

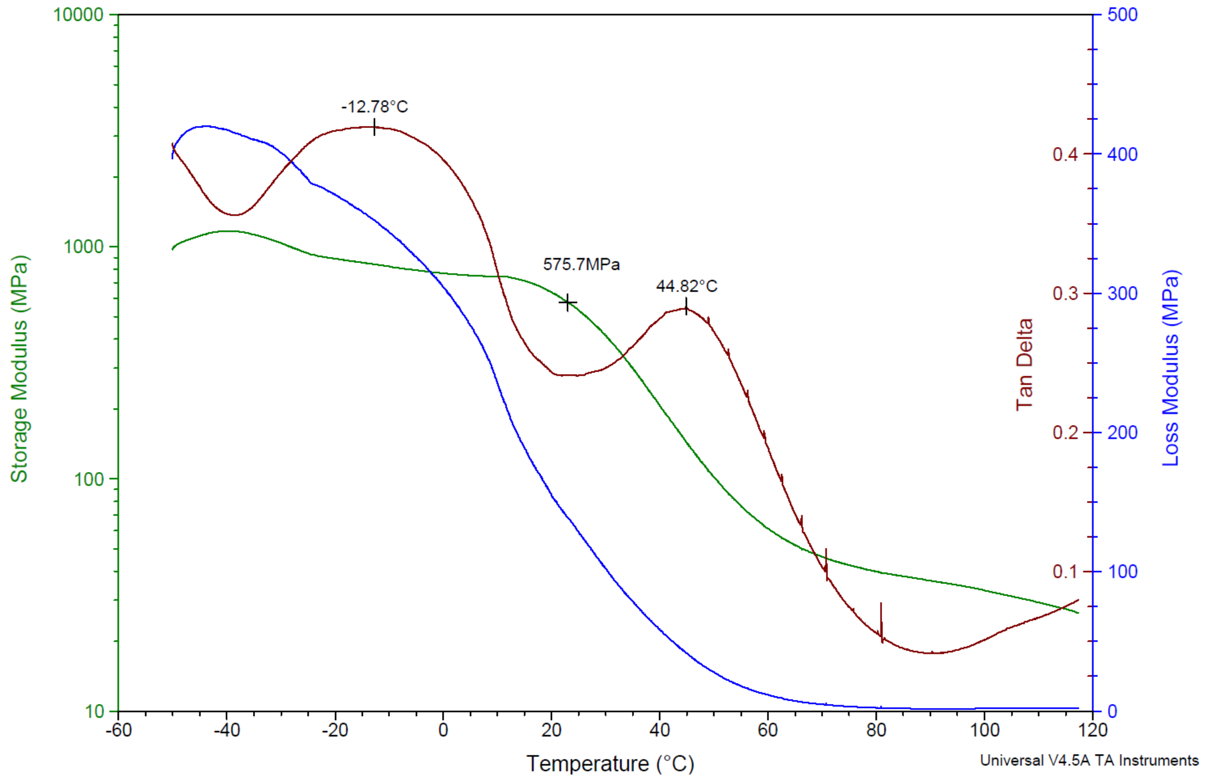

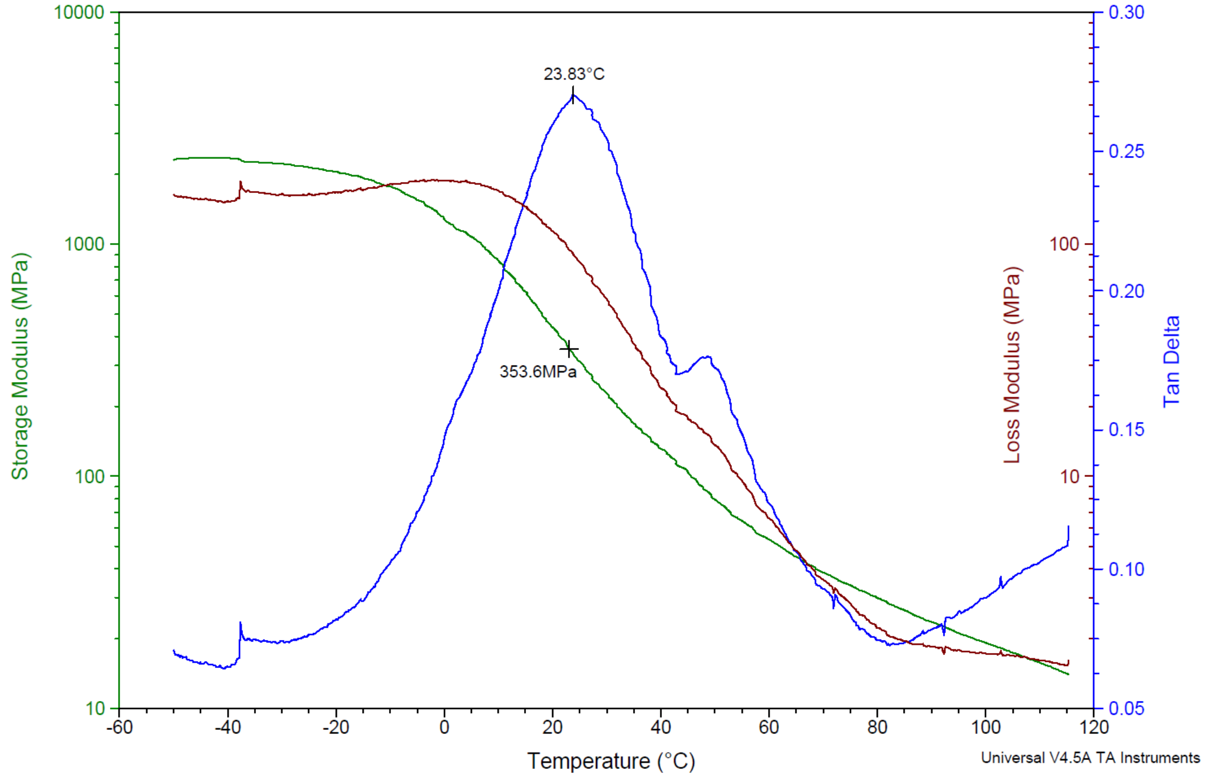

Figure 3.26: DMA thermograms of hemiacetal ester-based formulation F-HAEa one hour after silyl-mediated photocuring (upper) and after one week of storage at 23 °C with 50 %RH (lower).

As described in section 1.2.1, the utilized photoinitiators create an active H^+ on irradiation which initiates cationic polymerization. It is possible to quench the acid by adding latent bases, such as encapsulated amines, which are almost inert at room temperature and consequently do not inhibit cationic polymerization in the first curing step but set free an acid quenching base after thermal activation.[216] However, these latent amines are not completely inert at room temperature and significantly inhibit cationic polymerization in the photocuring step. This approach was investigated in basic curing experiments. When adding 0.5 wt% of latent base *Technicure LC 80* to F-HAE, significant amounts of unreacted liquid formulation components were found after photocuring. Polymerization inhibition became more apparent with increasing layer thickness. In addition, no significant changes in material weakening by storage were observed. Therefore, the most promising approach is to change the initiating species from a free proton to a sterically more hindered ion which may initiate polymerization but not catalyze hydrolysis. This can be achieved by utilizing an initiator system consisting of a cationic photoinitiator, most preferably an iodonium ion, a radical photoinitiator and a silane. The initiating mechanism is described in section 1.2.1 and yields a silyl cation instead of a proton which initiates polymerization but is highly unlikely to catalyze hemiacetal ester hydrolysis. The initiation system of hemiacetal ester-based formulation F-HAE was altered (Table 3.5, entry 2) and DMA experiments were performed to evaluate the impact of silyl initiation on material degradation. Specimens of formulation **F-HAEa** were analyzed directly one hour after photocuring and after one week of storage at 23 °C with 50 %RH. The respective thermograms are shown in Figure 3.26. Surprisingly, two glass transitions were observed for the material shortly after photocuring at -13 °C and at 45 °C. This may indicate inhomogeneous curing or the formation of two different polymer networks, possibly competing preferred cationic polymerization with less preferred radical polymerization. In addition, $G' = 576$ MPa is significantly lower than G' of the material cured conventionally. Storage modulus and both glass transition temperatures being decreased by utilizing a silyl initiation system indicates a less dense polymer network resulting from less favored polymerization conditions. After 1 week of storage under humid conditions, one main glass transition was found at 24 °C, which is similar to the one observed from cured F-HAE, with another partial transition at around 45 °C. Moreover, storage modulus G' decreases to 354 MPa; a value comparable to cured F-HAE as well. The striking similarities between the mechanical properties of materials which only differentiate in their initiation systems strongly suggests that utilizing the chosen initiator package does not resolve the issue of hemiacetal ester hydrolysis and the resulting material degradation. The serious impact of hydrolysis on the material properties is further highlighted by results from tensile testing of specimens from cured F-HAEa (Figure 3.27). One hour after curing maximum tensile strength $\sigma_{max} = 21 \pm 5$ MPa and elongation at break $\varepsilon_{max} = 2.5 \pm 0.7$ % of the material are comparable to fully cured F-Ua. However, after one week of storage at 23 °C and 50 %RH, maximum tensile strength drops to $\sigma_{max} = 3.7 \pm 0.2$ MPa and elongation at break increases to $\varepsilon_{max} = 6.0 \pm 0.2$ %. This change in mechanical properties to an inferior tensile strength underlines the massive impact of hydrolysis on the material despite a change in initiation. One conclusion from these observations is a lack of efficiency in the initiation process to convert all formed protons so silyl cations as initiating species, but it is also possible that an acidic species emerges from one of the components in the formulation which is discussed in the following.

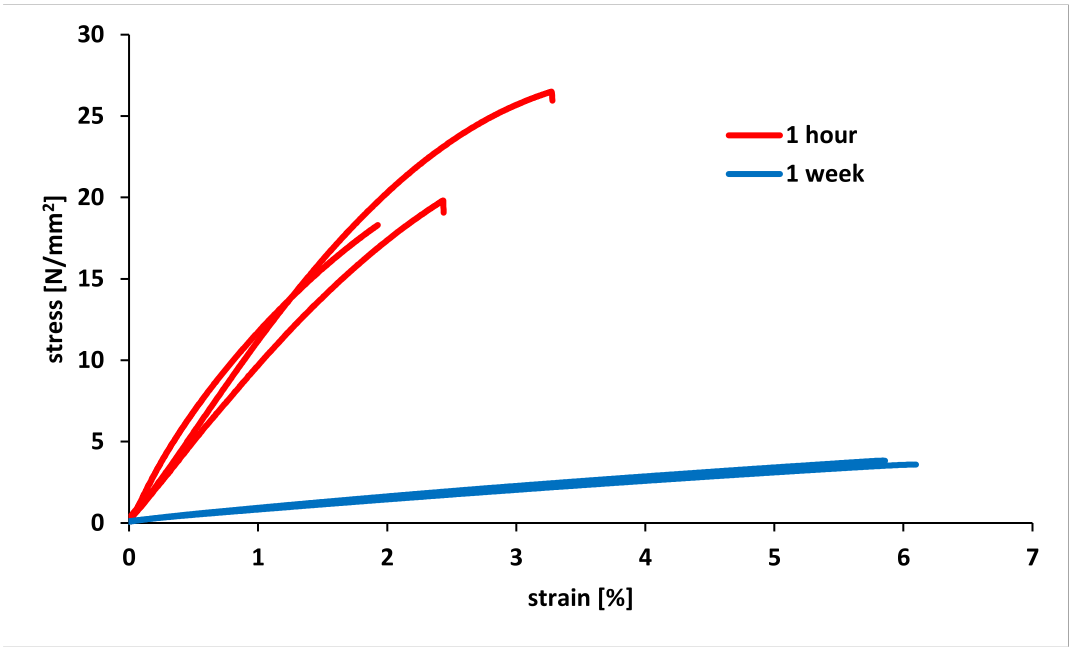

Figure 3.27: Stress-strain diagrams of hemiacetal ester-based formulation F-HAEa one hour after silyl-mediated photocuring (red) and after one week of storage at 23 °C and 50 %RH (red).

The hemiacetal ester-based macromolecular crosslinker PHAE-4 is synthesized from citric acid and the typical conversion of carboxylic and alcoholic groups, determined via ^{1}H NMR, is typically around 80 %. Consequently, there are still free carboxylic acid groups present in the formulation which are deprotonated when encountering water molecules.[217] Hence, F-HAEa was modified by removing PHAE-4 but still utilizing the silyl initiation system (**F-HAEb**). DMA measurements were carried out with specimens of cured F-HAEb one hour after photocuring and after one week of storage at 23 °C and 50 %RH; the respective thermograms are displayed in Figure 3.28. Shortly after curing, the storage modulus of the material at 25 °C is G' = 1640 MPa and T_g = 47 °C. Strikingly, G' is increased threefold compared to the same system including crosslinker PHAE-4, which indicates a massive increase in stiffness of the material by changing the formulation. Despite high vinyl ether functionality of the crosslinker, its impact on material brittleness is lower compared to PHAE-2 which either results from increased vinyl ether conversion due to miscibility advantages or the generally stiff polymer backbone of PHAE-2. However, the main focus of this experiment lies on a change in hydrolysis tendencies.

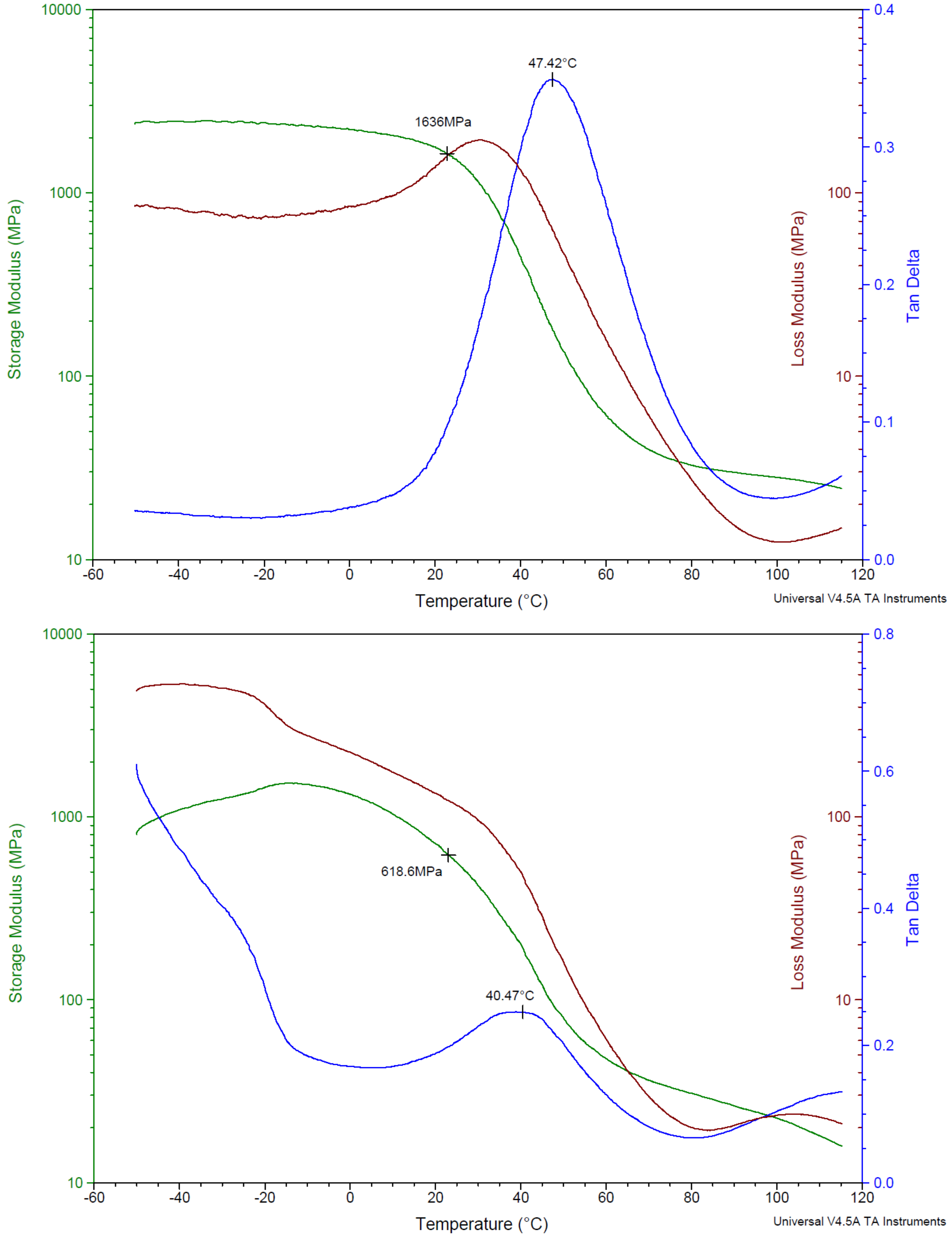

Figure 3.28: DMA thermograms of hemiacetal ester-based, PHAE-4 free formulation F-HAEb one hour after silyl-mediated photocuring (upper) and one week of storage at 23 °C with 50 %RH (lower).

After one week of storage, *G’* at 25 °C is decreased to 619 MPa and the glass transition temperature is slightly lowered by about 7 °C. These findings, once more, indicate polymer network degradation and hence no significant correlation between free carboxyl groups of

PHAE-4 and hydrolysis catalysis in the observed system can be made. One can conclude that the present catalyst for hydrolysis is the proton formed during initiator decomposition when exposed to irradiation. Modification of the initiation system aimed at inhibiting proton formation and create silyl cation species for polymerization instead but does not result in an increase in storage stability of the polymer network which implies an insufficient conversion of H^+ species to silyl cations during irradiation most likely due to fast degradation of the iodonium salt and consequently no full substitution of the initiating species.

In summary, utilizing hemiacetal ester-based prepolymers with vinyl ether functionalization leads to adhesive systems with high vinyl ether conversion and tunable material properties by simple means of formulation. Materials obtained from these systems exhibit storage moduli at room temperature over 1600 MPa which indicates materials with high cohesive power in adhesive applications. In addition, the potential of the evaluated compounds for debonding systems is great as material degradation caused by hemiacetal ester hydrolysis was observed even under mild conditions. However, the high susceptibility towards hydrolysis also implies that one important aim of future research is to increase storage stability of the cured material while maintaining debond-on-demand features. This was not achieved by modifying the initiation system via utilizing a radical photoinitiator and a silane to substitute the initiating proton with a silyl cation. The still present H^+ species catalyzes hemiacetal ester hydrolysis which results in material degradation even under mild conditions.

3.1.8 Final prototype

In the previous chapters, the impact of hemiacetal ester hydrolysis on material degradation has been shown in regard to the crude cured material. However, it is necessary to evaluate the effect of this phenomenon under adhesive application conditions. Hence, polycarbonate substrates were selected as one of the most important light cure plastics and glued by applying F-HAE. With these samples, single-lap shear tests were performed. The experiments showed that the utilized system yields lap shear strength values of $\delta = (1.6 \pm 0.4)$ MPa and complete adhesion failure with the adhesive layer itself being intact but completely detached from one substrate surface. In order to comprehensively evaluate the debonding capabilities of hemiacetal ester-based adhesive systems, it is reasonable to first improve adhesion to facilitate the observation of high impact debonding effects. As described in section 1.2.2, one reason for the utilization of 4-vinylphenol derivatives is their proposed effect on adhesion.[166,167] Thus, F-HAE was modified by substituting vinyl ether monomers TEGDVE and CDVE with 4-methoxy styrene (**4-MeOS**) to evaluate its impact on adhesion and material properties (**F-HAEc,** Table 3.5). 4-MeOS was chosen due to its +M- effect by the methoxy group which increases electron density in the vinyl double bond and consequently increases reactivity in cationic polymerization.[218] First, the overall mechanical properties were analyzed followed by an evaluation of the effect of hydrolysis on the material. The liquid formulation F-HAEc was photocured and tensile tests were performed (Figure 3.29).

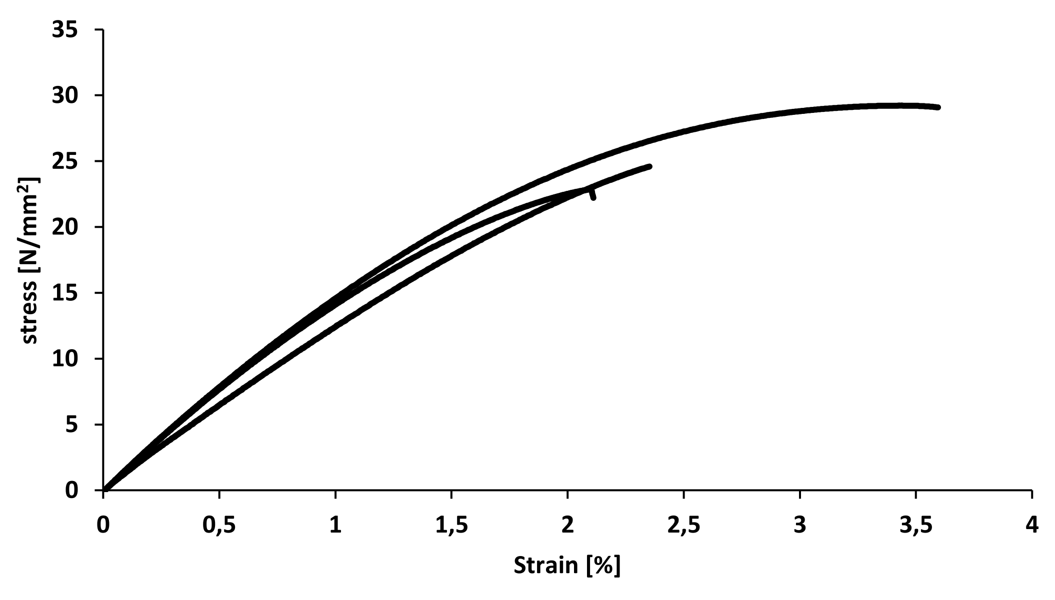

Figure 3.29: Stress-strain diagram of hemiacetal ester-based formulation F-HAEc one hour after photocuring.

Compared to F-HAE, the obtained material is expected to be more elastic mostly due to substitution of difunctional vinyl ether monomers with a monofunctional styrene monomer resulting in a less dense polymer network. Surprisingly, similar maximum tensile strength values of $\sigma_{max} = 26 \pm 3$ MPa but significantly lower strain at break $\varepsilon_{max} = 2.6 \pm 0.6$ % were found. Hence, the substitution of monomers results in a less ductile material after curing which likely results from the more rigid polymer backbone formed by polymerization of the vinyl group of 4-MeOS opposed to vinyl ether groups which form highly flexible alkyl ether linkages between monomeric units. Complementary DMA experiments were performed to analyze the mechanical properties more thoroughly and to gain insight into material degradation by hemiacetal ester hydrolysis. Figure 3.30 shows the respective thermograms of specimens from formulation F-HAEc one hour after photocuring and after one week of storage at 23 °C and 50 %RH. Shortly after curing, the material's storage modulus at room temperature is G' (25 °C) = 772 MPa and exhibits a glass transition at T_g = 54 °C; both values are slightly decreased compared to cured F-HAE but in a similar range. After one week of storage, the material massively weakens as G' at 25 °C drops to 22.3 MPa and T_g drops to 15 °C and thus material degradation is accelerated which is further highlighted by the missing second peak in the graph of tan δ arising from the unaffected core of the material observed before. Surprisingly, hydrolysis of the hemiacetal ester polymer network takes place faster by substituting CDVE and TEGDVE with 4-MeOS.

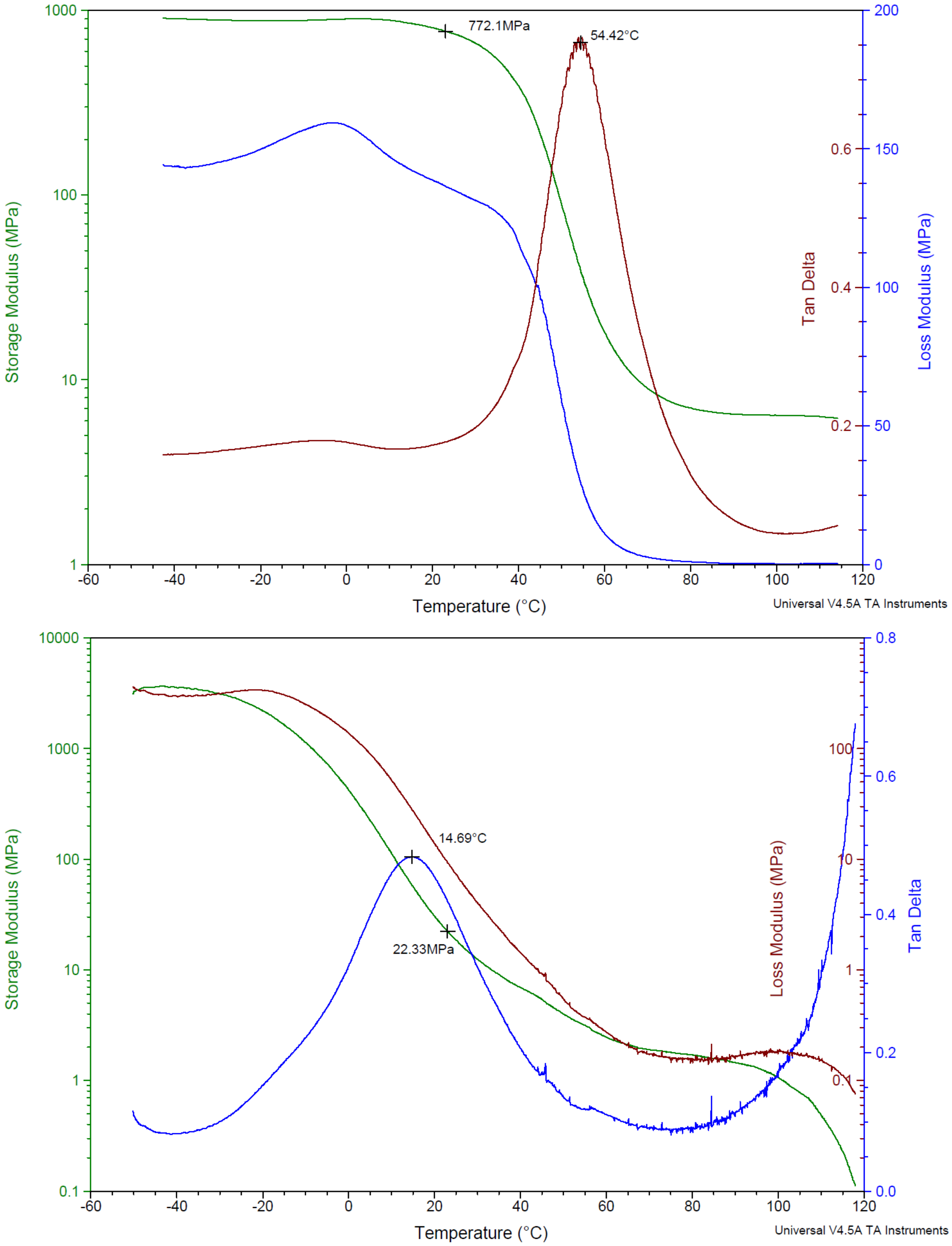

Figure 3.30: DMA thermograms of hemiacetal ester-based formulation F-HAEc one hour after photocuring (upper) and after one week of storage at 23 °C with 50 %RH (lower).

Neither of the monomers participate in hydrolysis themselves or of hemiacetal ester linkages, hence this effect must arise from either a change in catalyst or water activity. On the one hand, the material might become more hygroscopic by leaving out hydrophobic CDVE but on the other hand, TEGDVE is expected to increase hygroscopicity of the cured material more strongly than 4-MeOS due to the polarity of TEGDVE derived from its five ether groups. A decrease in activity of the free acid catalyst by stabilization is highly unlikely. For this, the proton must be, at least partially, immobilized at a functional group. The aromatic ring of 4-MeOS is more likely to immobilize an H^+ compared to the ether groups of poly(vinyl ether) chains. However, this is contradicted by the experimental results. Another explanation is increased diffusion of water and catalyst through the polymer network due to increased polymer mobility indicated by the slight decrease in T_g of F-HAEc compared to F-HAE. Overall, the present experimental data does not allow a concise conclusion about the observed phenomenon and additional experiments must be carried out to thoroughly investigate the underlying process of hydrolysis and ultimately find a way to protect the material from degradation by water in adhesive applications.

Table 3.7: Single-lap shear results of adhesive joints glued by hemiacetal ester-based formulations F-HAE and F-HAEc one hour after photocuring or one week of storage under warm and humid conditions after photocuring with stress at break δ.

Formulation	Substrates	Storage conditions	δ [MPa]
F-HAE	PC	no storage	1.6 ± 0.4
F-HAE	PC	1W, 40 °C, 80 %RH	-
F-HAEc	PC	no storage	6.2 ± 0.6
F-HAEc	PC	1W, 40 °C, 80 %RH	0.8 ± 0.3
F-HAEc	PMMA	no storage	2.9 ± 0.5

As mentioned before, the effect of humid air on hemiacetal ester polymer networks is expected to be lower in an adhesive application with a thin bond line compared to the previously performed tests with full surface contact of the material to air. However, gluing PC substrates with F-HAE yields adhesive joints with insufficient adhesive performance, mainly due to low adhesion. The utilization of 4-MeOS aims at increasing adhesion and enabling a profound investigation of the debonding capabilities of hemiacetal ester-based adhesive formulation. Single-lap shear tests were carried out with PC and PMMA adhesive joints glued with F-HAEc; the results are displayed in Table 3.7. By substituting vinyl ether monomers TEGDVE and CDVE with 4-MeOS, the adhesive strength is massively increased as stress at break δ is almost quadrupled to 6.2 ± 0.6 MPa when measured one hour after curing. The desired effect on adhesion of 4-MeOS is adequately pronounced which results in a formulation suitable for most photocuring adhesive applications on polycarbonate in terms of initial adhesive strength. In addition, the adhesive performance on PMMA substrates is also greatly improved as all former vinyl ether-based photocuring systems showed $\delta < 1$ MPa. In order to investigate the debond-on-demand potential of this system, the adhesive joints were stored for one week at 40 °C and 80 %RH which is considered as harsh conditions for stability tests in humid environments for adhesive applications. These conditions allow insight into storage stability under extreme conditions as well as susceptibility to external triggers for debonding. PC-PC samples prepared from F-HAE immediately fall apart when being slightly moved and thus exhibiting complete debonding. Although the initial adhesive strength was relatively low, these results still emphasize the high potential of hemiacetal ester-based adhesives for debonding systems. A similar effect was observed for F-HAEc with stress at break $\delta = 0.8 \pm 0.3$ MPa. The very humid and warm conditions reduce the adhesive strength by a factor of more than six, so the substrates can be easily separated by hand. However, the material does not completely decompose under these harsh conditions which shows that the adhesive system is not suitable for applications with elevated temperatures and high humidity but has a certain resilience for possible applications requiring mild conditions.

The conclusion taken from these results is dichotomous: the observed material degradation under the used conditions shows that although the adhesive layer does not completely disintegrate, it is significantly weakened. This highlights the importance of developing ways to increase storage stability of the cured material in future research. Hence, hemiacetal ester hydrolysis by moisture must be inhibited but stay available by application of an external trigger, e.g. soaking in aqueous hydrochloric acid. Yet, the developed hybrid system of vinyl ether functionalized hemiacetal ester prepolymers and 4-Vinylphenol derivative 4-MeOS shows excellent adhesive performance on PC substrates and a very high potential for debond-on-demand applications. Based on this highly promising prototype formulation, a high-performance adhesive system with great potential for debond-on demand features and high bio-contents can be developed. The discussed results show the aptitude of vinyl ether-based systems, especially in combination with hemiacetal ester prepolymers, for a greener adhesive industry and a more circular economy. In addition, an example for the significant impact of utilizing potentially bio-based 4-vinylphenol derivatives has been shown, in this case by increasing substrate adhesion. However, only 4-MeOS has been discussed in this work so far, but a broad variety of compounds is available from 4-vinylphenol feedstocks, e.g. ionic sulfate compounds. These are discussed in the following chapters regarding their chemical stability and effect on different adhesive systems.

3.2 Biobased 4-vinylphenol derivatives in adhesive systems

3.2.1 Degradation and stabilization of sodium styrene sulfate

The interest in derivatives of 4-vinylphenol in polymer chemistry derives from the potential renewable feedstock and a plethora of interesting properties for polymer design as described in section 1.2.2. The impact of neutral 4-MeOS on adhesion especially on plastics was described in the previous chapter. However, the main focus of this work lies on an ionic derivative: *p*-styrene sulfate. Ionic species are attractive for specific adhesive applications as they increase the ionic conductivity of a polymer which enables electrochemical debonding features (s. section 1.3.2). Moreover, implementation of ionic comonomers is expected to increase adhesion on metal surfaces.[219] If one part of the ion pair is polymerizable, properties such as conductivity can be tailored by counterion exchanges which, if chosen carefully, do not interfere with polymerization.[220]

First, sodium p-styrene sulfate (SSS) was synthesized by sulfation of 4-vinylphenol in DMF followed by a cation exchange as described in Scheme 3.15.[221] An important factor in this synthesis is working under dry conditions as the product is susceptible to hydrolysis which will be discussed extensively in this section. After synthesis, the product was purified by extraction with DCM followed by column chromatography. A white powder was obtained with an isolated yield of 67 %. The corresponding ^{1}H-NMR spectrum is shown in Figure 3.31. This preparation method was not chosen to develop a process for production at an industrial scale but to obtain material for the investigation of its properties.

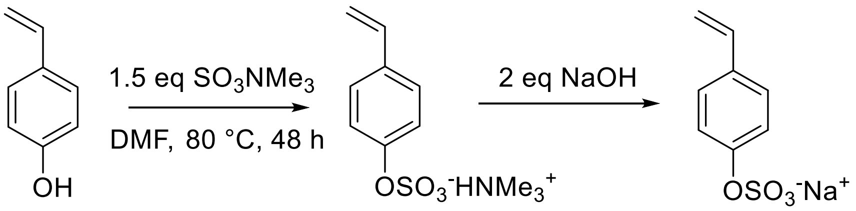

Scheme 3.15: Synthesis of sodium p-styrene sulfate. Sulfation of 4-vinylphenol in DMF followed by a cation exchange with sodium hydroxide.

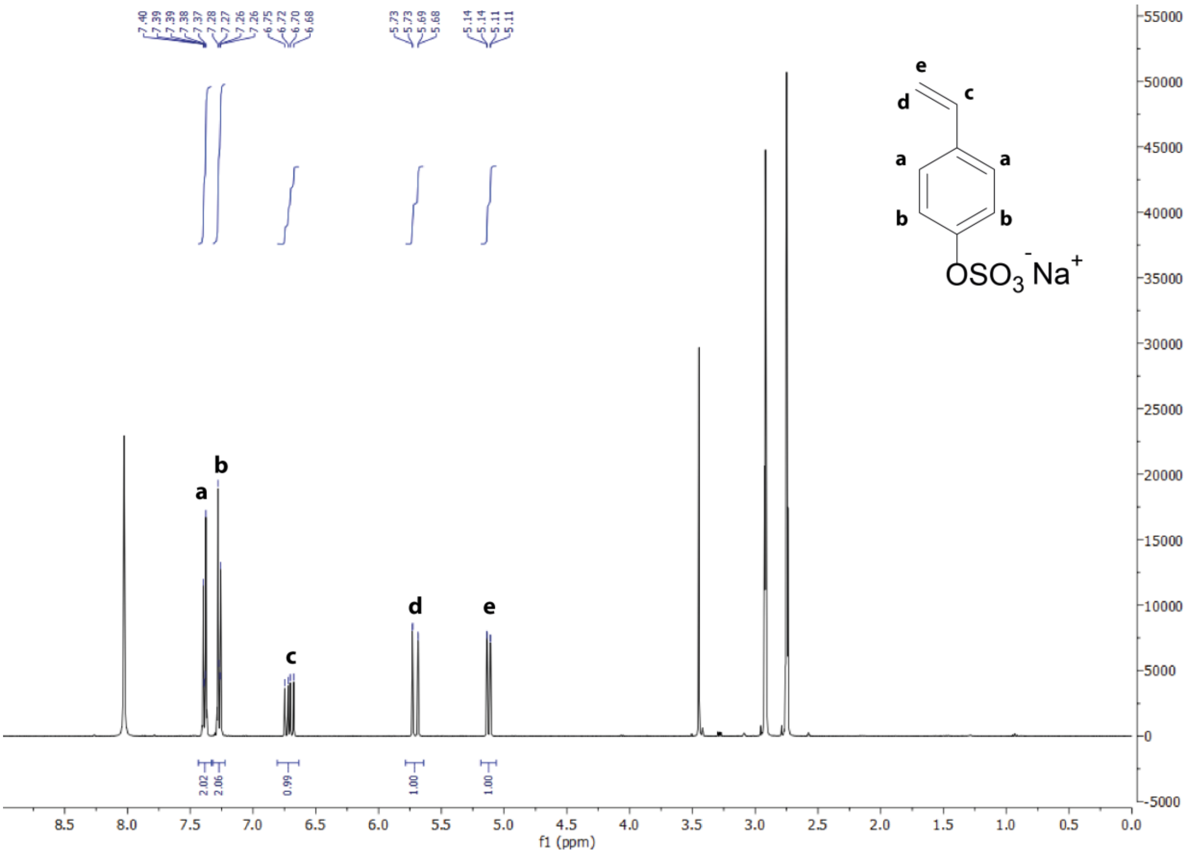

Figure 3.31: ^{1}H-NMR spectra of sodium p-styrene sulfate in DMF-d_7 directly after synthesis. The peaks at 8 ppm, 2.9 ppm & 2.7 ppm correspond to DMF and the peak at 3.5 ppm corresponds to water. No peaks were observed above 8.5 ppm.

If SSS was stored at RT, a discoloration from white to pink after a few days and to purple after a few weeks was observed. In addition, it became drastically difficult to dissolve the compound in a number of solvents, except for DMF and in low concentrations in DMSO. This change in material was not expected and as mentioned in section 1.2.2, there are no reports in literature on (sodium) styrene sulfate. As a consequence this alteration was investigated thoroughly. ^{1}H-NMR spectra of the original product and at several stages of discoloration were recorded up to 100 days of storage (Figure 3.32). The spectra which are not shown in this section can be found in the appendix (Figure 6.26 - Figure 6.28) Surprisingly, the ^{1}H-NMR spectrum reveals drastic changes compared to the initial compound which implies complete degradation of SSS after 100 days. The characteristic vinyl peaks at 5.2, 5.75 and 6.75 ppm disappear as well as the sharp and defined aromatic proton peaks between 7.25 – 7.5 ppm. Instead, broad peaks around 6.7 ppm as well as between 0.8 – 1.5 ppm newly emerge. Broad peaks are often found in ^{1}H-NMR spectra of polymers.[222] Hence, the disappearance of the signals assigned to vinyl group protons indicates conversion, i.e. polymerization, thereof. This hypothesis is further supported by the fact that the broad peaks were found only in the spectrum of the discolored sample. A first assumption was that the peak group between 0.8 - 1.5 ppm corresponds to the main alkyl polymer chain analogous to polystyrene[222] and the peaks at 6.7 ppm correspond to aromatic protons in the polymer side chains.

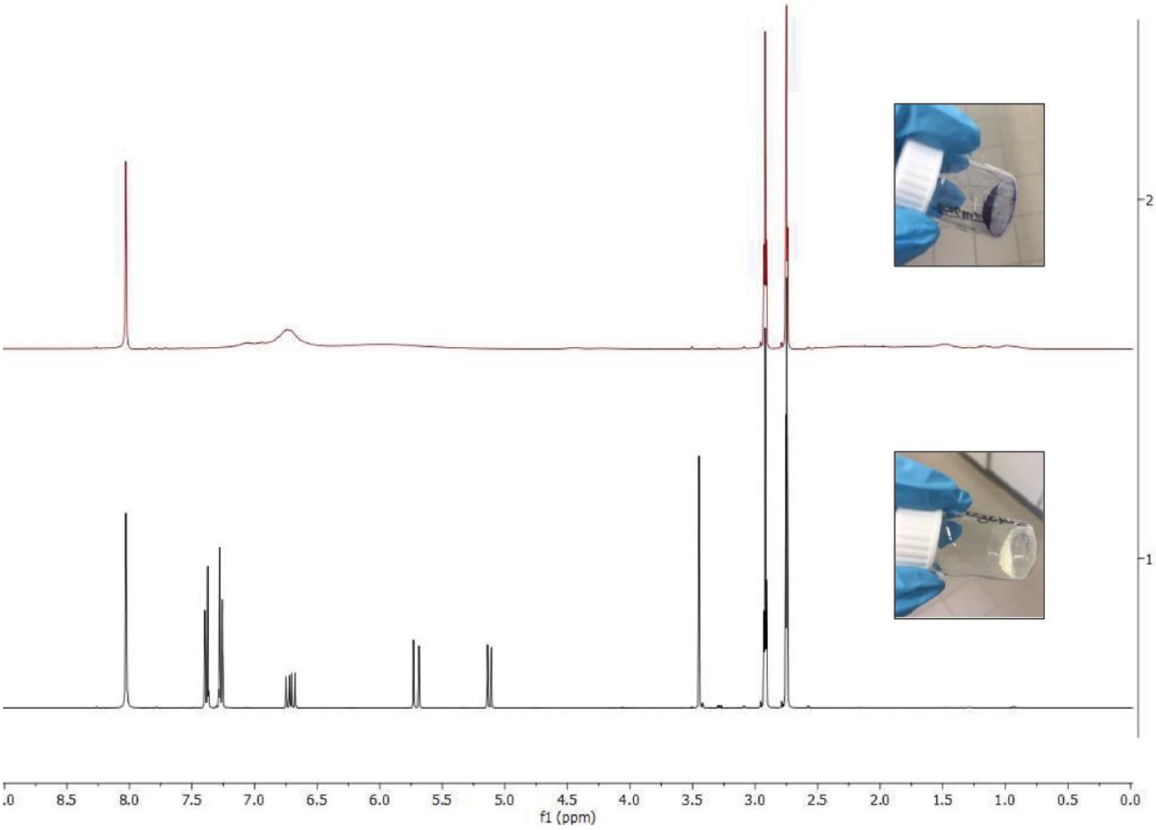

Figure 3.32: ^{1}H-NMR spectra of sodium p-styrene sulfate in DMF-d$_7$ directly after synthesis (bottom) and after 100 days of storage (top). The initially white powder turns purple over time. All vinyl peaks vanish over time, the aromatic peaks shift to lower δ values and become broader. No peaks were observed above 8.5 ppm.

Insight on the aging process was gained from spectra after a several days of storage. No changes were observed after three or even seven days. Figure 3.33 shows the respective NMR spectra directly after synthesis, after 10 and after 15 days of storage. After 10 days, new sharp peaks were found at 5.0, 5.6, 6.8 and 7.3 ppm. Due to the similar multiplicity of the adjacent vinyl and aromatic proton signals, it can be assumed that the newly found peaks correspond to the same functional groups but with altered electronic shielding resulting in the observed change in chemical shift. In this case, all proton peaks are shifted to slightly lower *δ* values, except for the protons originally adjacent to the sulfate group exhibiting a more pronounced downshift. Due to the high multiplicity of the peak corresponding to the single vinyl proton adjacent to the aromatic ring, the shifted peak is only partially visible as a small shoulder in the lower shift region of the original signal. However, no broad polymeric peaks were observed after 15 days of storage. Thus, although the characteristic proton peaks exhibit an alteration in chemical shift, no indication for vinyl conversion was found and consequently no or hardly any polymerization reactions have occurred yet. The change in electronic shielding of all protons, most pronounced for the proton adjacent to the sulfate group, implies that the electronic properties of the aromatic ring change over time.

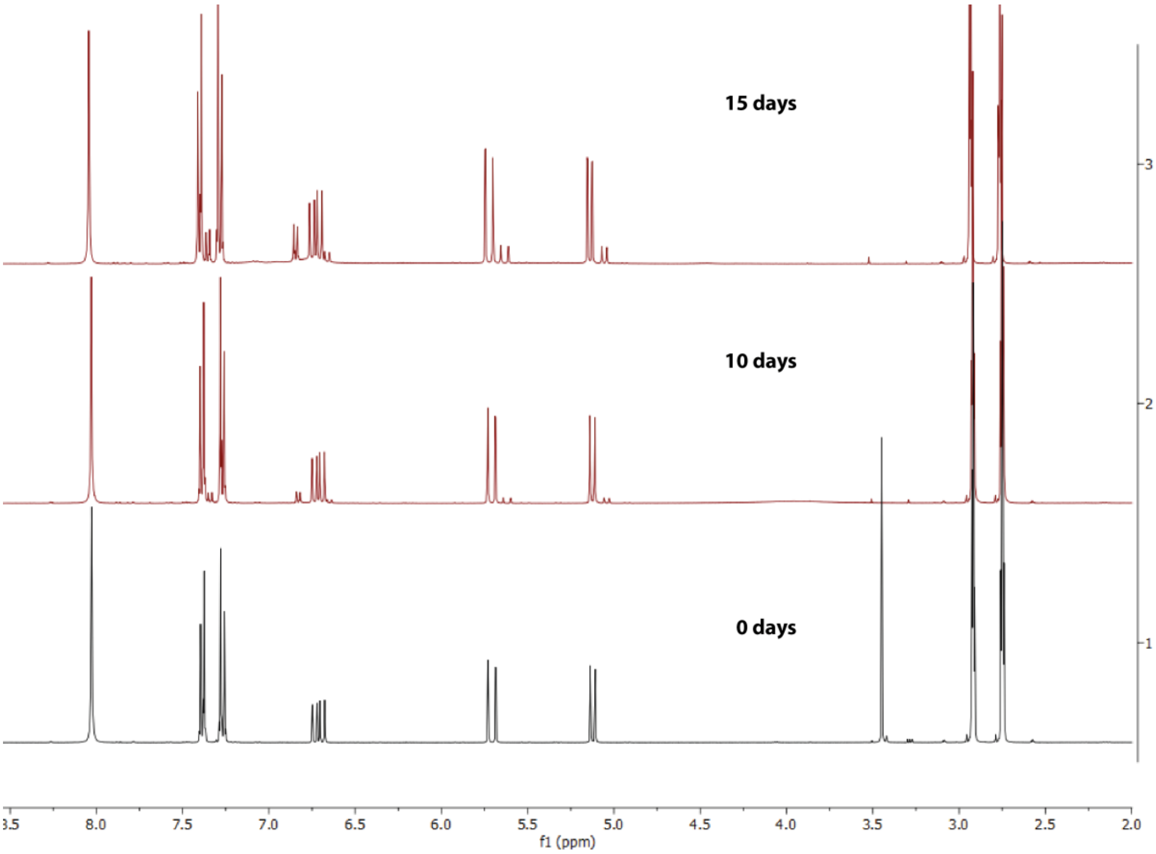

Figure 3.33: ^{1}H-NMR spectra of sodium p-styrene sulfate in DMF-d_7 directly after synthesis (bottom), after 10 days (middle) and after 15 days of storage (top). New vinyl and aromatic peaks emerge over time.

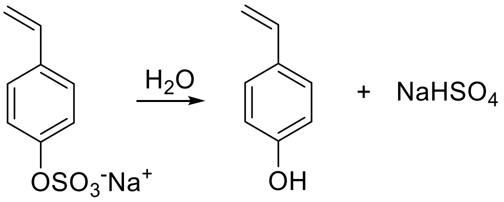

Scheme 3.16: Hydrolysis of sodium *p*-styrene sulfate.

The most likely explanation for this pronounced shift in electronic shielding of the protons adjacent to the sulfate group is hydrolysis. This reaction of the aromatic sulfate with water yields 4-vinylphenol (**4VP**) and sodium bisulfate as described in Scheme 3.16. NMR spectra of 4VP in DMSO-d_6 were recorded as a reference and the ^{1}H-NMR spectrum is shown in Figure 3.34. A direct comparison of chemical shift values of the respective peaks is not possible due to the utilization of different solvents.

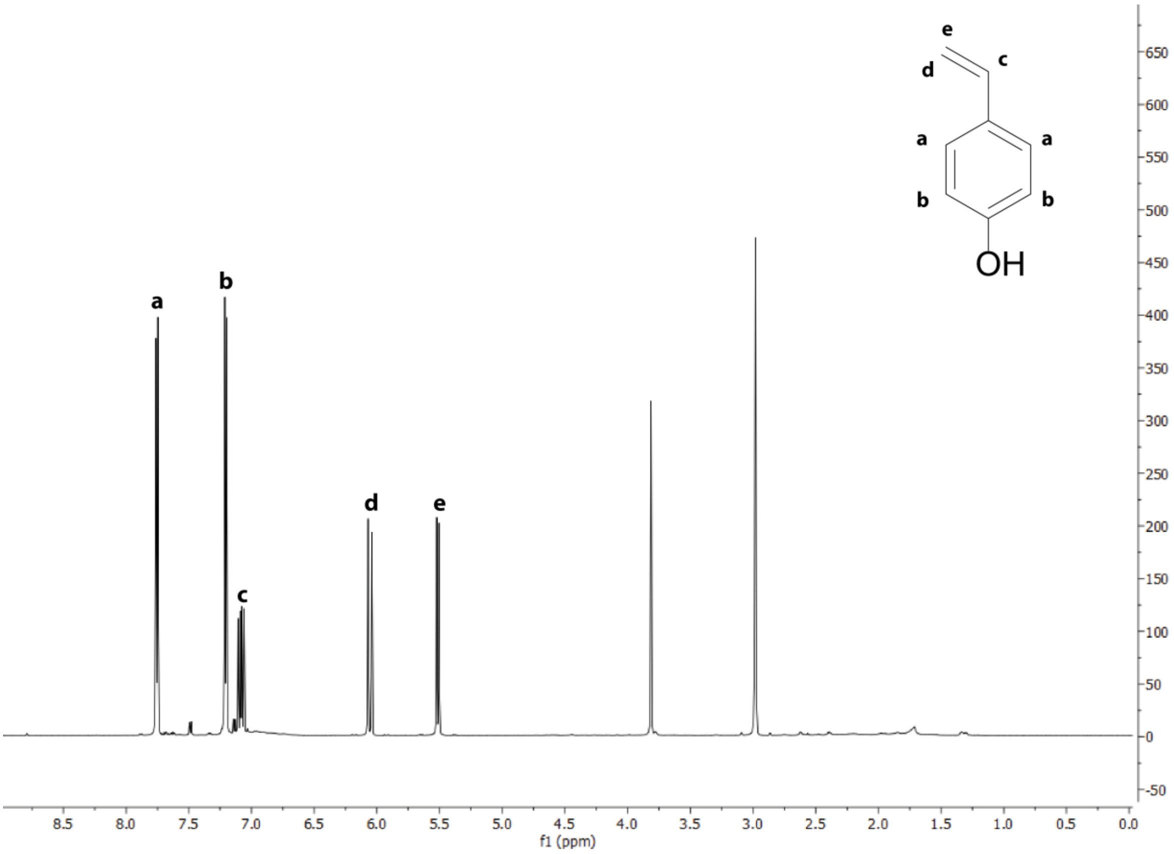

Figure 3.34: ^{1}H-NMR spectrum of 4-vinylphenol in DMSO. The peak corresponding to the proton adjacent to the OH-group is located very closely to the respective peak of the CH-vinyl proton. The solvent residual peak is located at 2.9 ppm and the water peak at 3.8 ppm.

Yet, a very prominent similarity between the spectrum of 4VP and the newly found signals in discolored SSS samples was observed. The aromatic peak **b** of 4VP is found only slightly upshifted compared to the CH-vinyl proton peak **c** which resembles the newly formed peak at 6.8 ppm for SSS after storage. This supports the hypothesis of sulfate group hydrolysis over time yielding 4VP. However, no significant broad polymeric peaks were observed after 15 days, and the vinyl peaks are still very prominent. Thus, the hydrolysis of SSS is the first isolated step in the degradation process. Figure 3.35 shows ^{1}H-NMR spectra of SSS after 50 and 100 days of storage. After 50 days, the number of broad peaks is vastly increased compared to 15 days, but vinyl peaks can still be found. After 50 more days, no more vinyl peaks are observable in the ^{1}H-NMR spectrum and broad peaks in the aromatic region at about 6.7 ppm as well as in the aliphatic region between 0.8 – 1.5 ppm increase in intensity. At this stage, the degradation can be considered completed. As mentioned before, it is likely that the final degradation product is of polymeric nature indicated by vinyl group conversion and broad ^{1}H-NMR peaks. The self-polymerization of 4VP in the solid state has been reported in the literature, but the mechanism was not yet completely illuminated. Polymerization via cationic propagation was proposed by Whitehead et al.[162]. They found out that the addition of radical initiators hardly altered polymerization of the monomer in solution and p(4VP) was formed also in the absence of an initiator. No self-polymerization but typical radical polymerizations were observed if the hydroxyl group is replaced by a methyl group. In addition, self-polymerization does not occur if the hydroxyl group is located in meta position. Thus, a cationic mechanism initiated by intra- or intermolecular proton transfer was proposed which is highly favored if the hydroxyl group is located in ortho or para position due to an increase in electron density of the vinyl group by resonance stabilization. most likely proceeding in a cationic mechanism.[162] In this specific system, acidic sodium bisulfate is formed in the first hydrolysis step which can protonate the 4VP vinyl group and consequently initiate cationic polymerization as shown in Scheme 3.17. The typically fast cationic polymerization is slowed down by diffusion limitations of the material in solid state. Still, complete conversion of the vinyl groups under ambient conditions in solid state is remarkable because of the limited diffusion and the general sensitivity of cationic polymerizations.

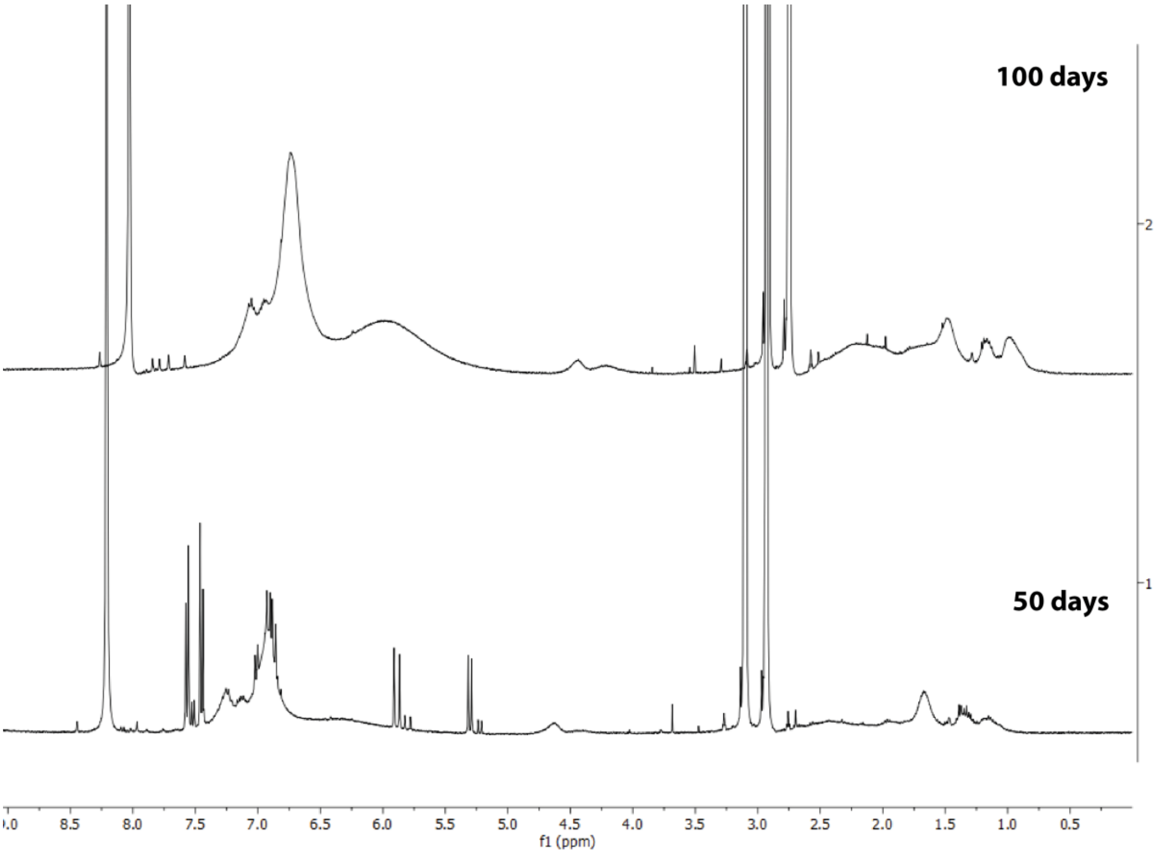

Figure 3.35: ^{1}H-NMR spectra of sodium p-styrene sulfate in DMF-d_7 after 50 days (bottom) and after 100 days (top) of storage. All vinyl peaks vanish over time, broad polymeric peaks increase in intensity.

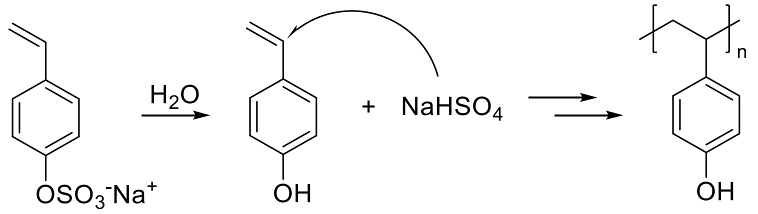

Scheme 3.17: Hydrolysis of sodium p-styrene sulfate followed by cationic self-polymerization of 4-vinylphenol initiated by sodium hydrogen sulfate.

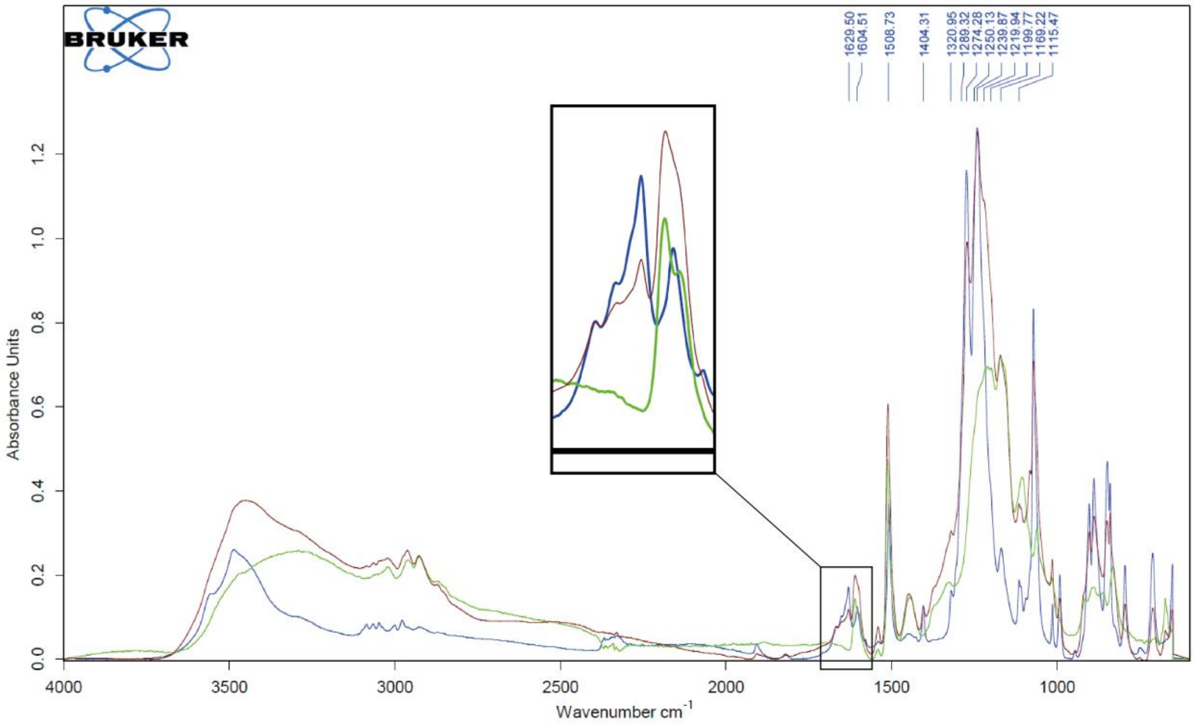

Figure 3.36: ATR-IR spectra of sodium p-styrene sulfate particles. Different particles were picked for surface analysis by IR microscopy. Comparison of white (blue), light purple (black) and dark purple (green) particles. The most prominent change is the significant decrease in intensity of the absorption band at 1630 cm^{-1} which can be assigned to a vinyl C=C stretching vibration (left peak in the inlay).

This hypothesis was further examined by IR measurements. Particles of SSS after 14 days of storage with different degrees of discoloration were analyzed and IR spectra were recorded and are displayed in Figure 3.36. White colored, light purple colored and dark purple colored particles were manually separated and analyzed, respectively. The white particles were considered as equal to the starting material to facilitate qualitative interpretation of the degradation process accompanied by particle discoloration. General changes in intensity over the whole spectra were observed which is common for solid state ATR-IR spectroscopy. The absorption band of interest for the investigated system can be found at 1630 cm^{-1} and can be assigned to a vinyl C=C stretching vibration.[223] A small difference in intensity of this band occurred when comparing white and light purple particles, especially in relation to the neighboring band at 1605 cm^{-1} which can be assigned to the C=C stretching vibration of the aromatic ring. This change in absorbance intensity indicates vinyl group conversion but most certainly not to a full extent for light purple particles. Strikingly, the absorption band at 1630 cm^{-1} is no longer present in the spectrum of the dark purple particles which implies full vinyl conversion. From these results it can be concluded that the degree of discoloration of SSS directly correlates with the degradation process, in this case linked to vinyl group conversion. However, p(4VP) is typically a white powder so the discoloration must result from another effect and not just polymerization. The discoloration was not more intense at the surface or the center of the bulk material but well distributed which implies that deterioration takes place simultaneously all over the material without a distinct spatial starting point. Moreover, the proposed reaction steps of hydrolysis followed by vinyl polymerization do not proceed separately but somewhat simultaneously in regard to the bulk of the material. However, no direct information about polymer formation can be concluded from the IR spectra, but the spectrum of a dark purple particle is very similar to a spectrum of p(4VP) (taken from ATR spectrum library) which further supports the proposed hypothesis regarding the degradation product (Figure 6.29). Additional differences in absorption band form and signal intensity between the different stages of discoloration as well as p(4VP) were found in the region between 1100 – 1300 cm^{-1} which can be assigned to different sulfate vibrations. This will be elucidated later in this section.

In order to verify polymer formation, GPC measurements were performed with SSS after 100 days of storage. Two samples were measured in THF, and molecular mass distribution values were calculated from polystyrene standard calibration. The molecular weight distribution curve of one sample is shown in Figure 3.37 and the averaged values are listed in Table 3.8. A distinct polymer peak was found which makes up the bulk of the recorded material accompanied by some peaks in the low molecular weight region which are negligible. Two values for the respective M are given in Table 3.8, one considering the full chromatogram for peak integration and a corrected value only referring to the polymeric peak. The latter is used to limit the discussion on the polymeric parts. First, the presence of polymeric material validates the aforementioned hypothesis of vinyl group conversion by polymerization. The obtained polymers are of small to medium size with M_w = (5860 ± 130) Da and M_n = (4340 ± 60) Da which corresponds to about 35 monomeric units per polymer chain on average. Regarding the polymerization conditions, the calculated polydispersity of 1.4 % is low. As the reaction takes place in a completely uncontrolled manner in the solid state, significantly higher values were expected. However, the proposed hypothesis for SSS degradation by sulfate group hydrolysis followed by vinyl group conversion via, most presumably cationic, polymerization was confirmed by NMR, IR and GPC measurements. Yet, the discoloration of the material is of much interest to better understand the degradation process and is discussed in the following paragraph.

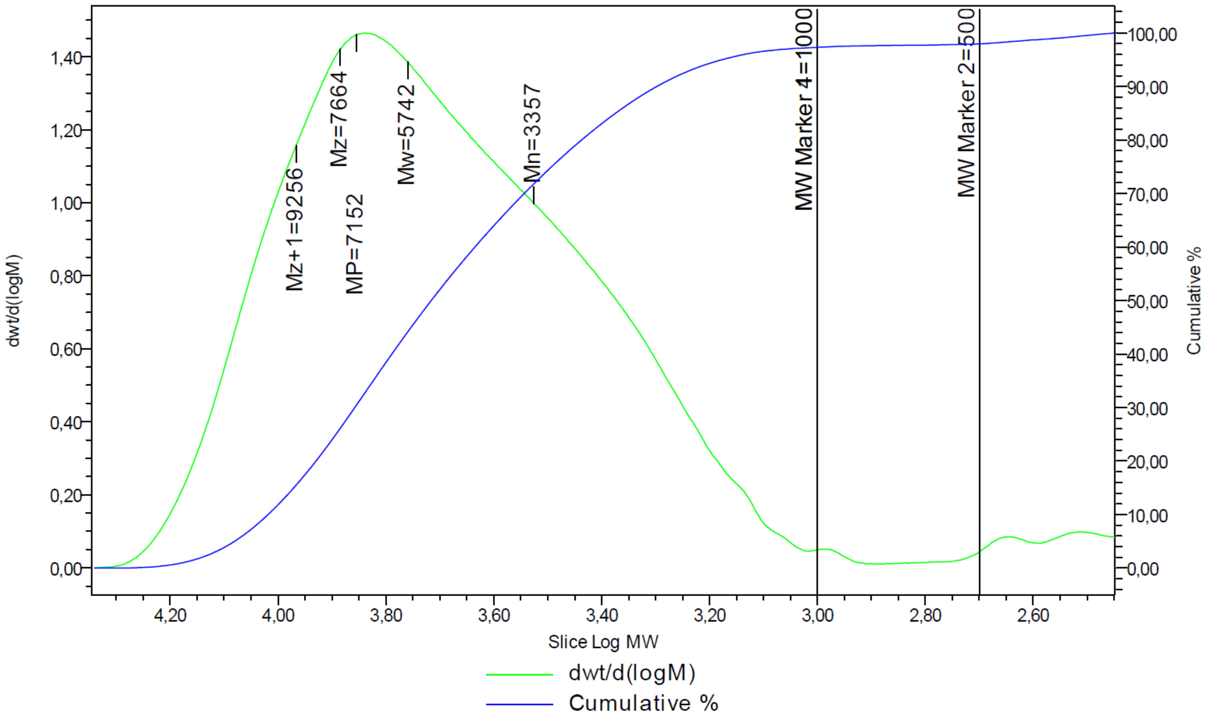

Figure 3.37: Molecular weight distribution curve of an SSS sample after 100 days of storage determined by GPC with polystyrene standard calibration.

Table 3.8: Molecular weight distribution of SSS after 100 days of storage calculated from the full chromatogram and corrected by isolation of the polymeric peak. Data was obtained via GPC and averaged from two separate measurements.

	M_w [Da]	M_n [Da]	M_P [Da]	Polydispersity
full	5620 ± 120	3310 ± 50	7010 ± 140	1.7
corrected	5860 ± 130	4340 ± 60	7010 ± 140	1.4

The discoloration accompanying the degradation of SSS cannot be explained by any of the yielded products in the process described above as 4VP, $NaHSO_4$ and p(4VP) are colorless solids. Thus, either unexpected side reactions occur, or complexes of these compounds are formed which contribute to the purple color. In order to examine the latter, mixtures of sodium hydrogen sulfate monohydrate with p(4VP), phenol and polystyrene were prepared and crushed with mortar and pestle. No discoloration was observed if phenol or polystyrene were used. Additional IR measurements were performed to check for macroscopically undetected changes in molecular structure (appendix, Figure 6.30 & Figure 6.31) but no significant differences between the isolated compounds and the respective mixtures thereof were found. However, $NaHSO_4 * H_2O$ and p(4VP) took on a pinkish color while grinding, which became more apparent when scratching the material off the mortar with a spatula. The discoloration intensified by dispersing the mixture in acetone followed by evaporation of the solvent as displayed in Figure 3.38. The lack of discoloration observed with phenol instead of p(4VP) implies that the polymeric structure plays an important role in color formation because any effects on possible side reactions by the alkyl main chain are negligible. Thus, complex formation favored by interlinked phenolic side chain species instead of isolated phenols seems likely. However, no changes were observed for a mixture of polystyrene and sodium hydrogen sulfate monohydrate which implies that the aromatic character of the side chain species is not solely responsible for discoloration but the OH substituent contributes significantly either by coordination of the group itself towards another species or by its electronic effects, e.g. +M effect, on the aromatic ring.

Figure 3.38: p(4-vinylphenol) and sodium hydrogen sulfate monohydrate were grinded with pestle and mortar. Left: Dispersion in acetone. Right: After solvent evaporation.

Subsequent IR measurements of the discolored mixture were carried out and the obtained spectrum was compared to the spectra of the respective isolated compounds (Figure 3.39). Several differences were observed: The sharp double peak **a** found at 3550 cm^{-1} for NaHSO4 * H_2O vanishes in the corresponding crushed sample. The absorption band corresponds to OH stretching vibrations of water in a crystalline structure, in this case in combination with sodium hydrogen sulfate. By mixing and crushing, this crystalline structure is destroyed which explains the disappearance of this specific absorption band. The most significant change is the change in peak shape and intensity of the bands between 1100 – 1300 cm^{-1}. These high intensity peaks can be generally assigned to various sulfate vibrations either protonated, deprotonated, or bonded to organic molecules.[224] The sulfate groups as well as OH deformation vibrations by water contribute to the absorption bands **c** between 1200 – 1300 cm^{-1} of sodium hydrogen sulfate monohydrate. In the same region, p(4VP) shows absorption bands originating from small amounts of moisture but mostly the OH group of the phenol side chains.

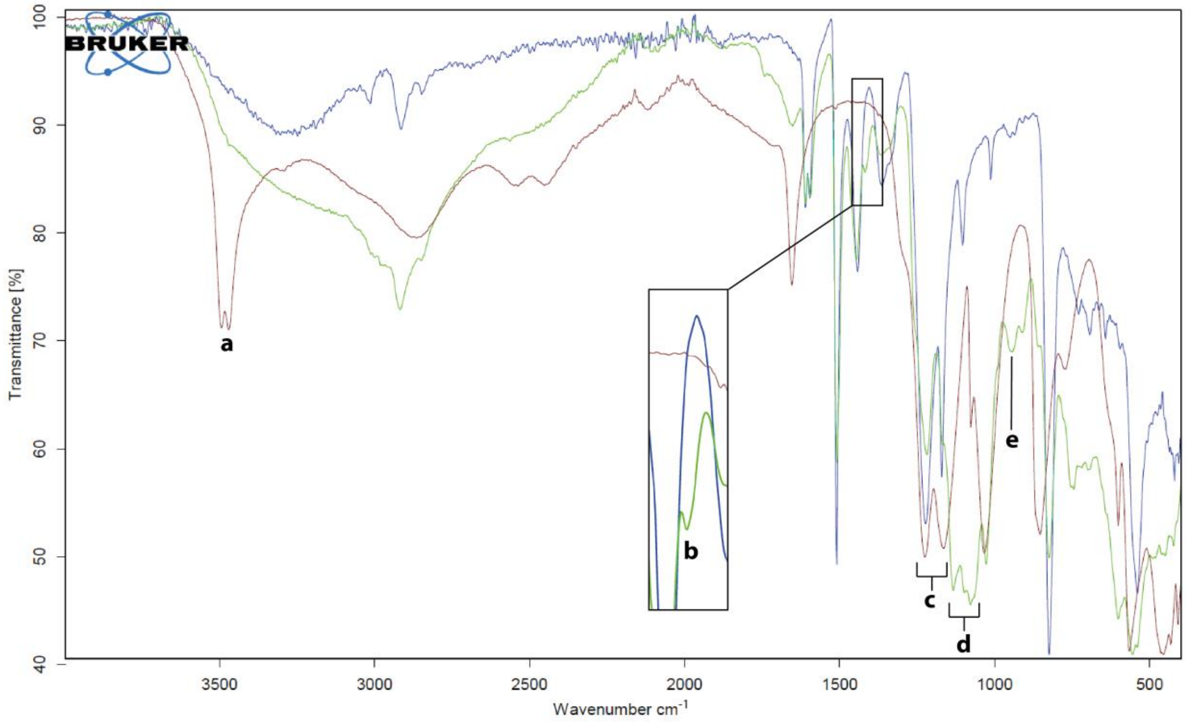

Figure 3.39: FTIR spectra of sodium hydrogen sulfate monohydrate (dark red), p(4-vinylphenol) (blue) and a grinded mixture thereof (green). The peaks at 1100 – 1200 cm^{-1} are only present in the grinded mixture and can be assigned to deprotonated sulfate anions.

There are small differences in shape and intensity of the peaks compared to the sulfate salt, but both are summarized as the peak group **c** in this discussion. As expected, these bands are also present in the spectrum of the grinded mixture, but a new peak group **d** between 1100 – 1200 cm^{-1} emerges. These peaks were also found in the spectra of the isolated compounds but with much less intensity, especially in comparison to the neighboring peak group **c**. Moreover, the shape of the absorption bands is altered. As both groups are, at least partially, assigned to sulfate vibrations the observed change can be seen as a shift in vibrations of the sulfate groups. More precisely, deprotonation of hydrogen sulfate seems very likely.[224] As a consequence, the proton must bond to another compound, in this case either water or p(4VP). There are two indications for protonation of the latter: two new peaks were found in the spectrum of the grinded mixture with **b** at 1460 cm^{-1} which can be assigned to C=C stretching vibration of the aromatic ring and **e** at 910 cm^{-1} which can be assigned to C-H vibrations of the aromatic ring. A change in the aromatic ring structure can be caused by protonation or sulfation of either the ring itself or the OH substituent. Sulfation of the OH group is highly unlikely as temperatures around 80 °C and several hours of reaction time are needed even in solution. In addition, the obtained phenyl sulfate compound is very unstable as demonstrated before in this section. Furthermore, sulfation of the aromatic ring is also hardly possible as direct addition/substitution reactions between sulfate and phenyl moieties have not been reported yet to the best of our knowledge. The most likely explanation for the observed changes in ring structure is protonation of the ring itself. The positive charge on the resulting cation is well stabilized by resonance effects of the aromatic ring further supported by the OH-substituent which generally increases the electron density of the phenyl ring due to its +M effect as described in Scheme 3.18. As mentioned before, the polymeric structure contributes to the discoloration which implies that a complex of the stabilized positively charged side chain species is formed most likely with the deprotonated SO_4^{2-} anion in the center. The formation of this complex can result in the observed pink or purple color of the material. However, to verify this assumption, further analytics must be performed which are not part of this work.

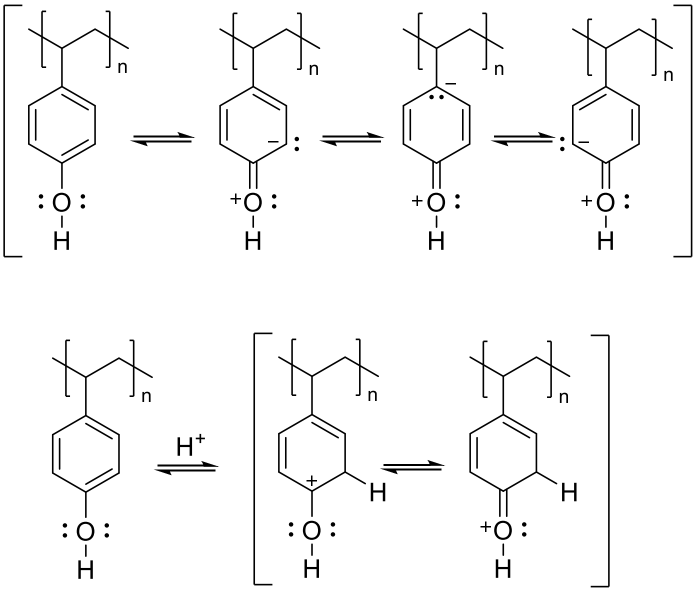

Scheme 3.18: Resonance structures of p(4VP) unprotonated (top) and protonated in ortho position (bottom).

The degradation process of sodium styrene sulfate has been thoroughly investigated in this section. Based on these findings, two different ways of stabilizing this interesting monomer for industrial use were developed. First, self-polymerization of 4VP in solid state was reported before already and stabilization was achieved by storing the monomer in solution. Typically, MeOH or propylene glycol are used.[162] Consequently, SSS was dissolved in MeOH with a concentration of 40 %w/w. Storage stability was analyzed by taking samples, adding a few drops of deuterated methanol and performing ^1H NMR measurements directly after solution preparation and after 4 months of storage at room temperature. The respective spectra are shown in Figure 3.40. No changes in the proton spectrum were found after this time. The high intensity solvent peaks do not superimpose any signals from SSS allowing a good comparison. Due to its high polarity, there is always a significant amount of water present in methanol, if not dried beforehand. Yet, no indications for sulfate hydrolysis were found. Hence, stabilization of SSS by dissolving it even in polar solvents with water impurities is an easy way to improve its storage stability.

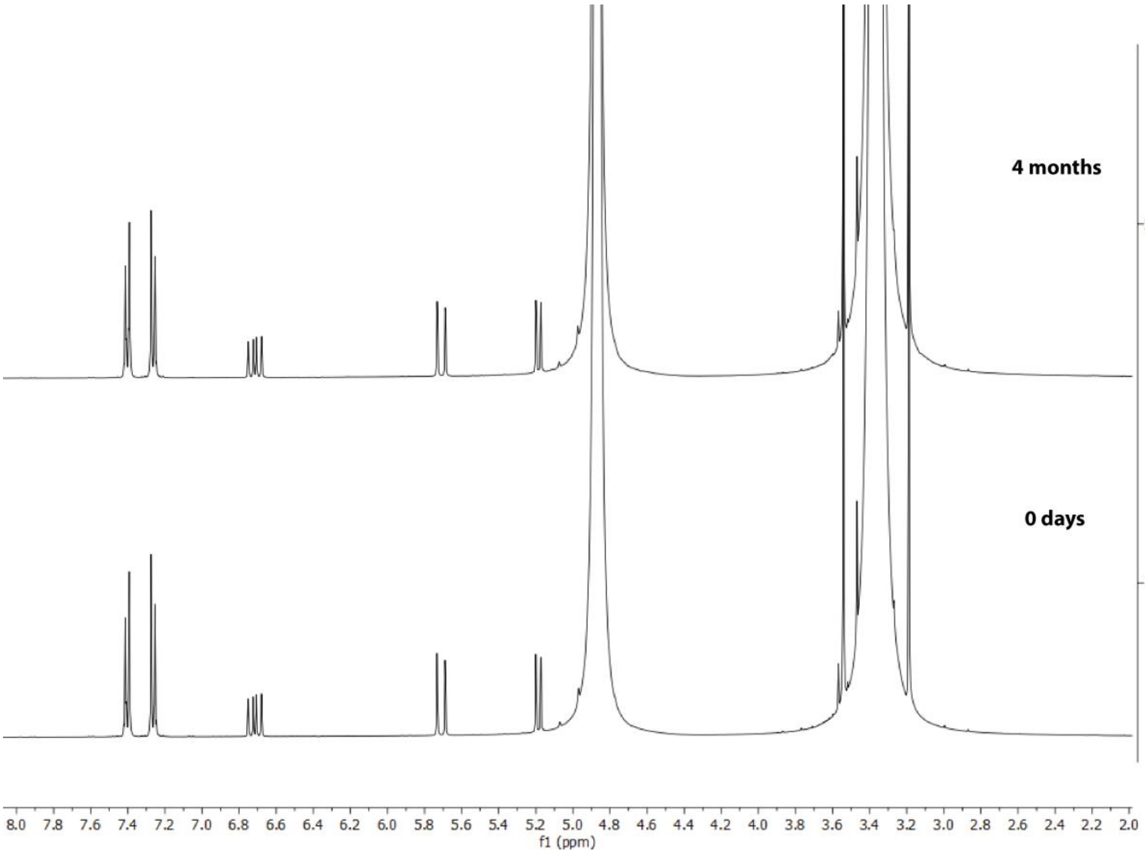

Figure 3.40: ^{1}H-NMR spectra of sodium p-styrene sulfate dissolved in methanol. A few drops of MeOH-d$_4$ were added for measurement. No implications of SSS degradation were found.

However, the low stability of SSS can still become an issue even if used directly after solvent evaporation and it is beneficial to store it solvent-free due to cost and environment reasons. Thus, another attempt was made to stabilize p-styrene sulfate in a more permanent way. By exchanging sodium with a rather nonpolar organic cation, the compound becomes more hydrophobic and consequently reactions with water become less likely. Furthermore, the utilization of such a cation improves the solubility of the monomer in organic media like most reactive mixtures in adhesive systems which is highly beneficial for most formulation approaches. In this work, tetrabutyl ammonium (TBA) was utilized as the cation. As described in Scheme 3.19[221], p-styrene sulfate was synthesized from 4VP and an aqueous tetrabutyl ammonium hydroxide solution was added to perform the cation exchange. The final product was purified via extraction with DCM and column chromatography in 95:5 DCM:MeOH with a typical yield of 60 %. A white powder was obtained with high purity as confirmed by ^{1}H-NMR analysis (Figure 3.41).

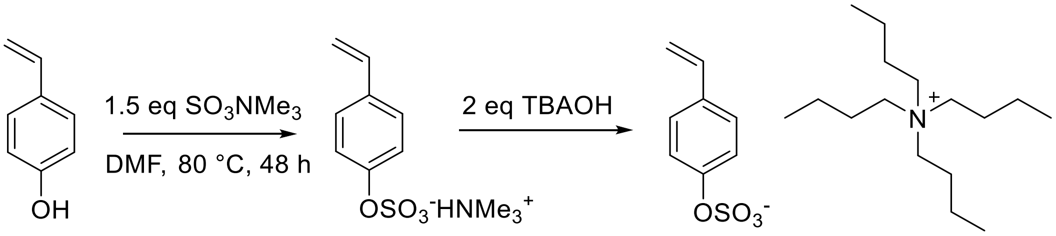

Scheme 3.19: Synthesis of tetrabutyl ammonium p-styrene sulfate from 4-vinylphenol.

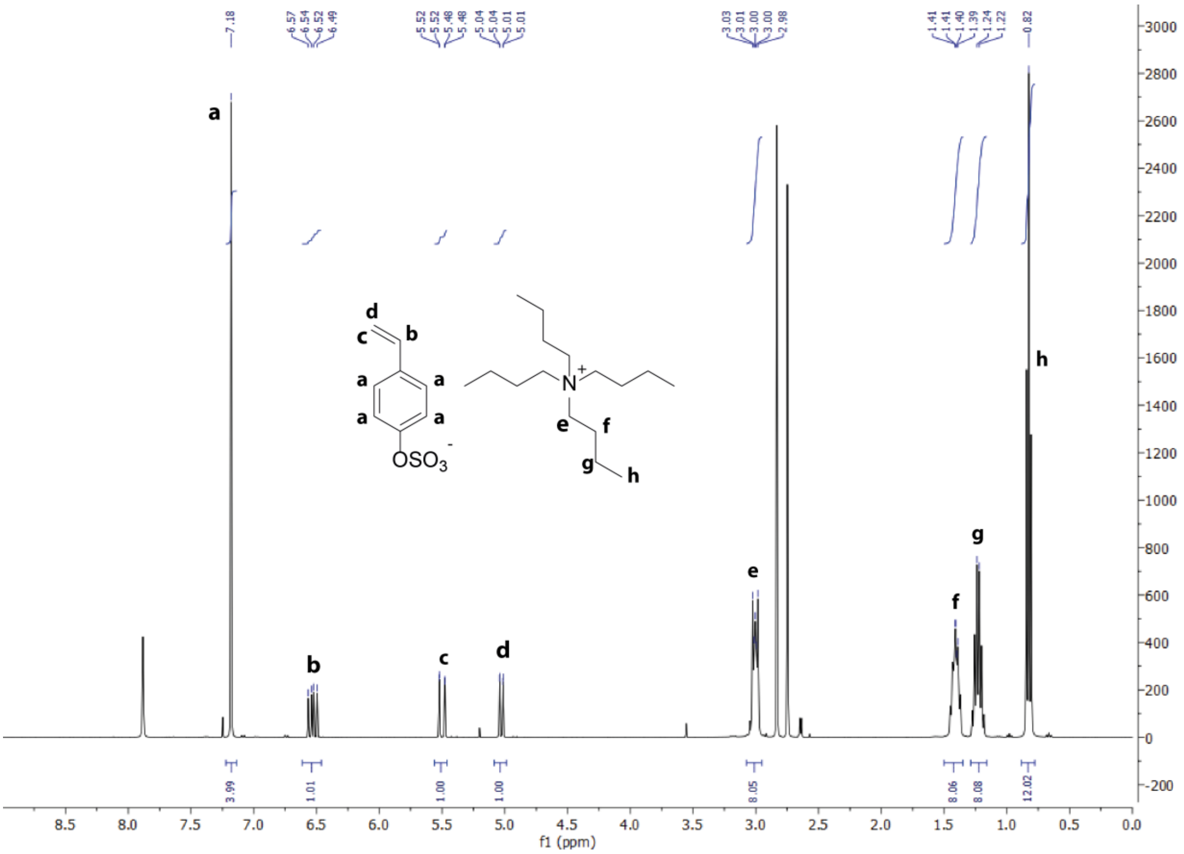

Figure 3.41: ^1H-NMR spectrum of tetrabutyl ammonium p-styrene sulfate in $CDCl_3$. The peaks at 7.9 ppm, 2.8 ppm & 2.7 ppm correspond to residual DMF from synthesis.

The storage stability of TBASS was examined via ^1H-NMR spectroscopy directly after synthesis and product isolation in $CDCl_3$ as well as after 6 months of storage in solid state at $T = 4 - 8$ °C in DMSO-d_6; Figure 3.42 shows the corresponding spectra. Apart from small amounts of residual DMF from synthesis, no difference in proton signals were found. Thus, p-styrene sulfate was successfully stabilized which is a very interesting and notable result. By this route, the novel reactive sulfate monomer can be much easier used in industrial development work in the field of adhesives and coatings. By implementing a nonpolar organic counterion, a more hydrophobic compound is obtained which is less prone to hydrolysis and subsequent self-polymerization giving one solution to stabilize styrene sulfate.

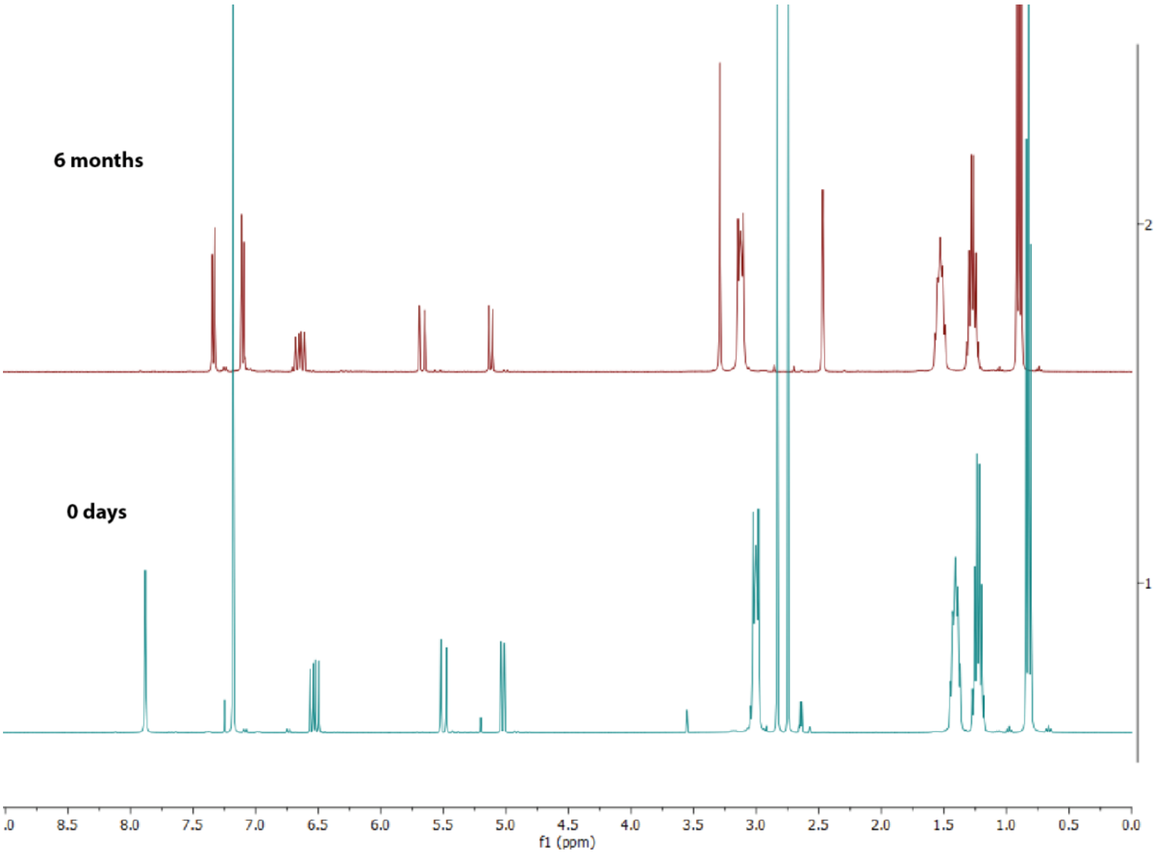

Figure 3.42: ^{1}H-NMR spectra of tetrabutyl ammonium p-styrene sulfate. Bottom: Spectrum recorded directly after synthesis in $CDCl_3$. The peaks at 7.9 ppm, 2.8 ppm & 2.7 ppm correspond to residual DMF from synthesis which was removed in vacuo afterwards. Top: Spectrum recorded after 6 months of storage in DMSO-d_6. The peak at 3.4 ppm corresponds to water. No significant changes in TBASS signals were observed.

In conclusion, sodium p-styrene sulfate degrades over time if stored under ambient conditions at room temperature. The proposed mechanism of sulfate group hydrolysis followed by self-polymerization was confirmed via ^{1}H-NMR, IR, and GPC measurements. It is likely that polymerization proceeds in a cationic mechanism initiated by sodium hydrogen sulfate formed in the hydrolysis step. The compound was stabilized by storing it in MeOH and by creating a more hydrophobic salt via cation exchange: sodium was substituted with tetrabutyl ammonium. The resulting compound is well suitable as an ionic derivative of 4-vinylphenol for adhesive applications in terms of miscibility with common monomers organic media, which is very useful in the materials industry. The following section deals with the investigation of TBASS in cationic as well as in radical polymerizations. Finally, TBASS was implemented in two different adhesive systems.

3.2.2 Polymerization kinetics of styrene sulfate

In order to find a suitable adhesive system for the implementation of p-styrene sulfate, it is important to analyze its polymerization behavior in terms of reaction rate and conversion to provide a more effective direction for applications development. The most common reactive curing techniques in industry are cationic and especially radical polymerization. Polymerization kinetics of TBASS were compared to styrene. The latter was chosen for comparison because of the structural similarity. It is a well implemented monomer in industry that has been thoroughly investigated in literature regarding its polymerization kinetics, in radical[225] as well as cationic[226] and even in anionic[227] mechanisms. Conclusions on the effect of sulfate substitution on the polymerization behavior of the aromatic vinyl compound can be drawn. As mentioned above, styrene is polymerizable independently from how the propagating species are charged. Depending on the substitution of the aromatic ring, cationic or anionic mechanisms can be favored. If the substituting group is withdrawing electrons, the monomer reacts faster in anionic polymerization and cationic polymerization is favored if the functional group is donating electrons to the π-system.

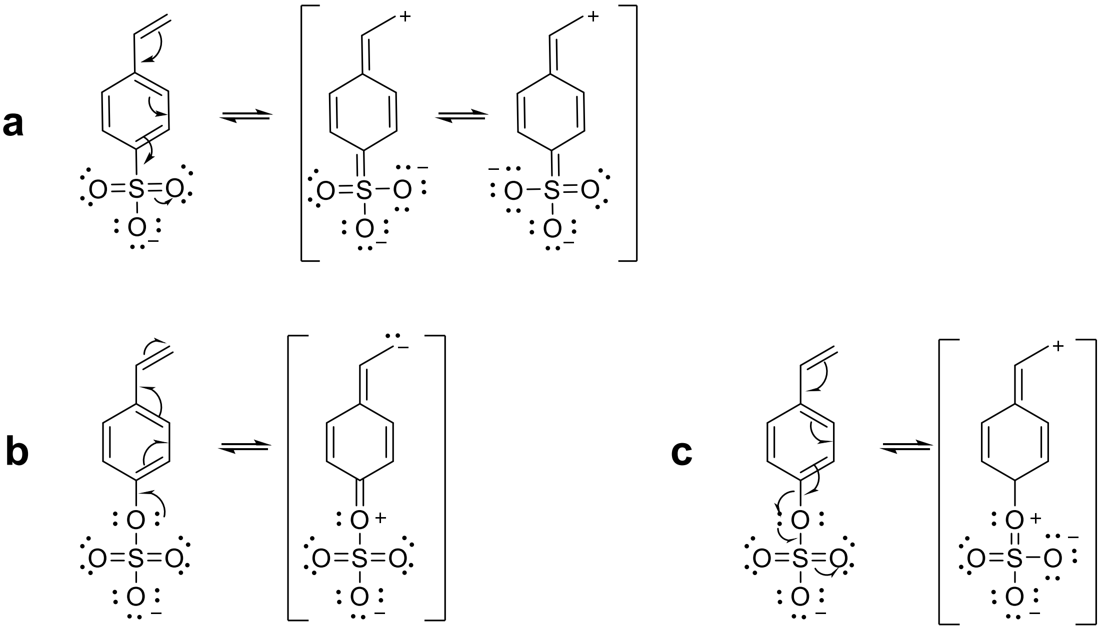

Scheme 3.20: Resonance structures describing the electron withdrawing effect of a sulfonate group on styrene (a) and the electron withdrawing (b) or donating (c) effect in question by a sulfate group.

For example, p-styrene sulfonate reportedly performs well in radical[228] and anionic[229] polymerization. The sulfonate group withdraws electrons by the inductive effect of electronegative oxygen atoms and additionally by a negative mesomeric (-M) effect. The latter has the bigger impact on the electron density of the vinyl group. The resonance structures shown in Scheme 3.20a carry positively charged vinyl groups which quickly react with anionic initiators and consequently also anionic propagating species, resulting in fast initiation and monomer conversion in anionic polymerization. However, the effect of a sulfate substituent is not clear. By its inductive effect, electron density is decreased which promotes anionic polymerization. This is further amplified by a possible -M effect, as displayed in Scheme 3.20c which proceeds via non-existent intermediates, i.e. five valence electrons at the α-oxygen atom between the sulfur and the aromatic ring which decreases the probability of the resulting resonance structure. In contrast, a +M effect, as shown in Scheme 3.20b, is likely and the resulting carbanion monomer is expected to perform well in cationic polymerization.

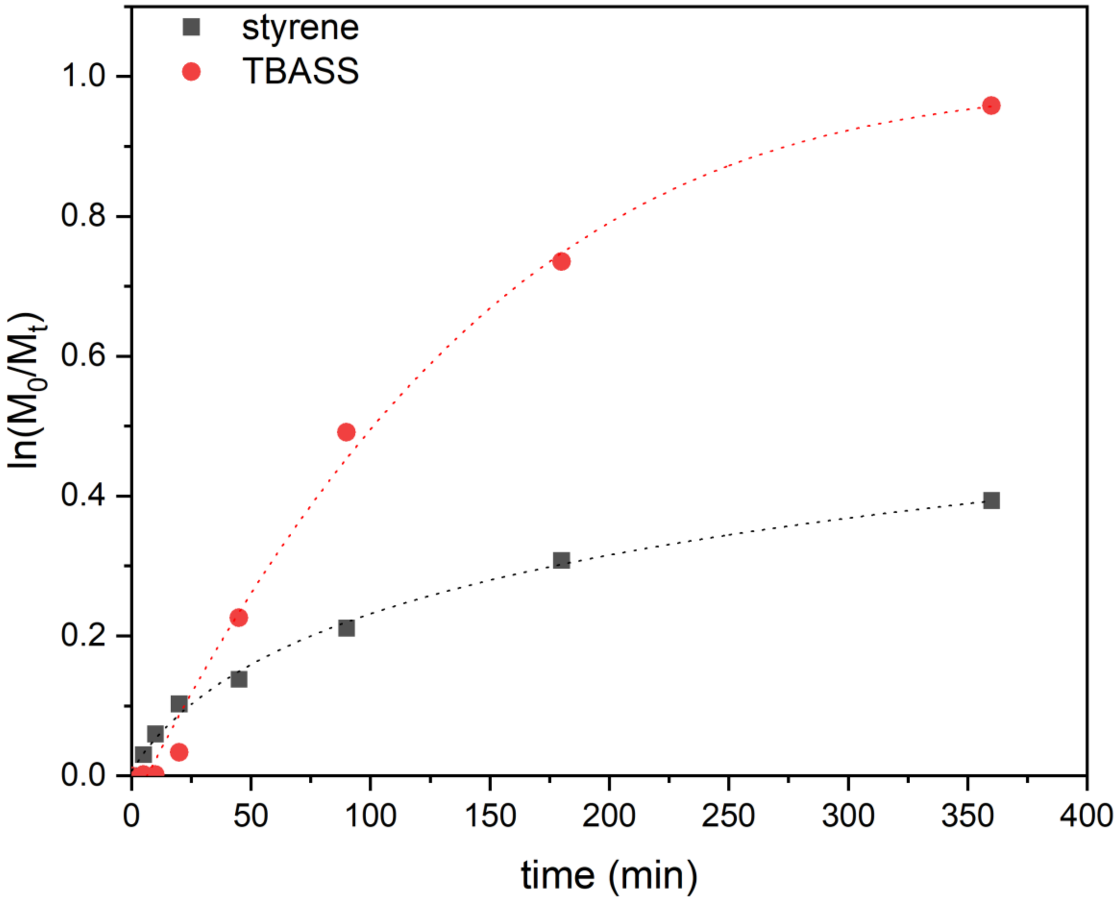

Figure 3.43: Kinetic plots of ln (M_0/M_t) versus time for radical polymerization of styrene (dark grey) and TBASS (red). Polymerizations were carried out with M_0 = 0.5 mol/L and c (AIBN)/c (monomer) = 0.01 at T = 80 °C.

Radical solution polymerizations of TBASS and styrene were performed and conversion over time was monitored by ^{1}H NMR; the spectra can be found in the appendix (Figure 6.32 - Figure 6.49). The monomers were dissolved in purified DMSO at a low concentration of 0.5 mol/L to minimize diffusion effects by an increase in viscosity during polymerization. The radical initiator was azobisisobutyronitrile (**AIBN**) with $\frac{c(\text{AIBN})}{c(\text{monomer})}$ = 0.01. A small amount of dimethyl terephthalate was added as an internal NMR standard. After dissolving all components, the solutions were degassed by three freeze-pump-thaw cycles and kept under nitrogen atmosphere, a sample was taken as a starting point and the reaction flasks were placed in a preheated oil bath at 80 °C. The samples were instantly frozen with liquid nitrogen to quench the reaction. Monomer conversion was determined via ^{1}H-NMR. Figure 3.43 shows the kinetic plot for the radical polymerization of both monomers; final conversion after 24 hours and molecular weight distribution values for both polymerization techniques are listed in Table 3.9. The latter were obtained by GPC analysis, but p(TBASS) was not measurable as the polymer did not dissolve in the solvents available for GPC measurements.

Table 3.9: Polymerization time *t*, monomer conversion *X* and molecular weight distribution values (M_w, M_n, *PD*) for the resulting polymers of radical and cationic polymerization experiments of styrene and TBASS. Conversions were determined via ^{1}H-NMR and molar mass distribution values via GPC. p(TBASS) was not fully dissolvable in the available solvents for GPC analysis, so no data on p(TBASS) were obtained.

	M_w [Da]	M_n [Da]	*PD* [%]	*X* [%]	*t* [min]
styrene, radical	6244 ± 3	3774 ± 3	1.7	42	1440
TBASS, radical	-	-	-	78	1440
styrene, cationic	21190 ± 20	7730 ± 10	2.7	66	180
TBASS, cationic	-	-	-	3	180

Radical polymerization of styrene starts quickly but slows down over time reaching a final conversion of 42 % and with M_w = 6244 ± 3 Da and a polydispersity of 1.7. The somewhat low conversion is typical for free radical polymerization of styrene in solution, whereas conversions over 95 % are achieved in bulk.[230] The low molecular weight results from low monomer conversion and the polydispersity is also typical for the experimental setup. The steep slope in the first minutes indicates fast initiation rates of AIBN towards styrene. After some time, the conversion rate drops significantly which is most likely due to a decreasing active chain end concentration caused by radical termination reactions which is a natural limitation to monomer conversion in radical polymerization. It must be noted that styrene termination rates are high compared to other typical monomers, e.g. acrylates.[231] However, termination mainly proceeds via primary radical termination due to steric hindrance by the bulky aromatic ring side chains.[232] In contrast, TBASS polymerization starts slowly but accelerates massively between 20 – 45 minutes of reaction; the graph shows an even steeper slope than that of styrene in the first minutes of reaction. In addition, polymerization proceeds at a steady rate for a long time causing the course of the graph until about 120 minutes to be almost linear. Afterwards, the polymerization rate decreases over time but slower than for styrene with a final conversion of 78 % after 24 hours. The slow start of the polymerization implies a low initiation rate of AIBN towards TBASS which results in a slow buildup of propagating chain species. However, after some time the polymerization rate gets remarkably high compared to styrene and the inevitable deceleration in conversion rate in free radical polymerization is less prominent. From these observations, it is reasonable to assume that the termination reaction rates of TBASS are significantly lower than those of styrene resulting in a comparably high concentration of the propagating species over the course of the polymerization. A decrease in termination rates can be explained by a more pronounced steric hindrance by the sulfate group attached to the aromatic ring. To conclude, radical polymerization of TBASS starts slowly compared to styrene but proceeds at higher reaction rates over time with less prominent termination reactions which leads to higher monomer conversion.

The cationic solution polymerizations of styrene and TBASS were carried out in chloroform with an equally low monomer concentration of 0.5 mol/L. The reactions were initiated by boron trifluoride etherate (**BTFE**) with $\frac{c(\mathrm{BTFE})}{c(\mathrm{monomer})} = 0.05$. A small amount of dimethyl terephthalate was added as an internal standard for ^{1}H-NMR measurements. All compounds and glass wares were dried before the reaction which was carried out at 0 °C. Prior to the addition of BTFE, a sample was taken as a starting point. All samples were added instantly to a solution of dibutyl amine in chloroform to quench the reaction.

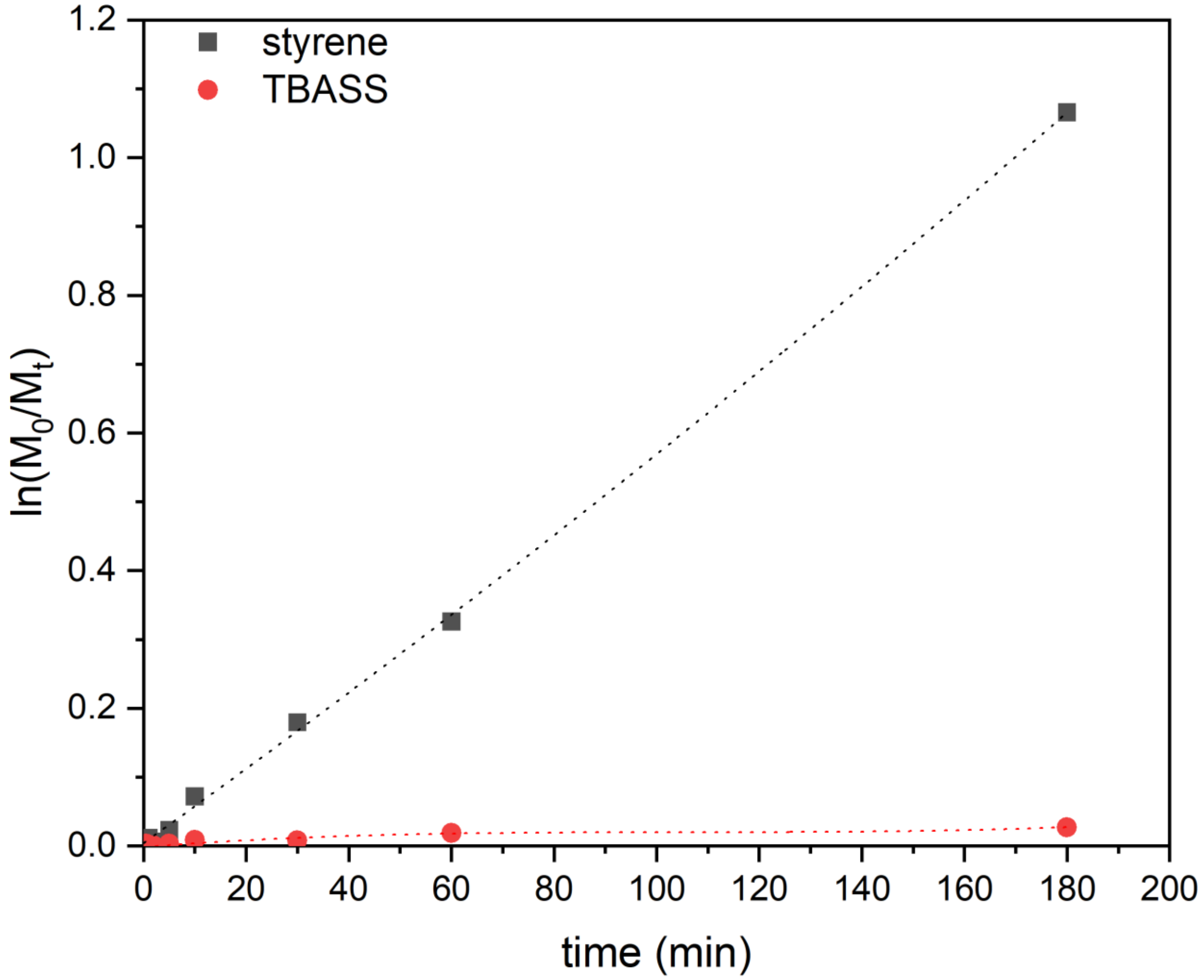

Figure 3.44: Kinetic plots of ln (M_0/M_t) versus time for cationic polymerization of styrene (dark grey) and TBASS (red). Polymerizations were carried out with M_0 = 0.5 mol/L and c (BTFE)/c (monomer) = 0.05 at T = 0 °C.

Figure 3.44 shows the kinetic plots of the cationic polymerization of both monomers, the ^{1}H-NMR spectra can be found in the appendix (Figure 6.50 - Figure 6.67). Styrene conversion proceeds linearly with a final conversion of 66 % after 180 minutes, M_w = 21190 ± 20 Da and a polydispersity of 2.4. The conversion is slightly higher than reported in similar experimental setups[233] and polydispersity is in a common range[234]. The linear course of the graph indicates no significant impact on polymerization by termination reactions which is common for cationic polymerization as, in contrast to radical polymerization, two active chain ends cannot undergo termination; only nucleophilic molecules and water can cause termination reactions. This is one reason for the measured high molecular weight, and also implies that higher conversions can be achieved by means of longer reaction times. Surprisingly, TBASS hardly reacts in cationic polymerization with a final conversion of only 3 % after 180 minutes. Possible reasons for that are impurities in solvent, initiator, or internal standard which, however, can be ruled out as the same dried and purified batches were used for both polymerizations. Impurities in the monomer, e.g. TBAOH from synthesis or 4VP from sulfate hydrolysis, are also highly unlikely as it was purified thoroughly and no indications for significant amounts of impurities can be drawn from the ^{1}H-NMR spectrum of TBASS. Another possible explanation is quenching of the initiating or propagating species by the sulfate anion of the monomer itself. By protonation of the sulfate, cationic polymerization is not able to start or propagate. So far, cationic polymerization of various cationic monomers has been reported.[235] Yet, no articles about cationic polymerization of anionic monomers have been published to the best of our knowledge. In order to evaluate the probability of a potential inhibition effect, the pK_a value of the organic sulfate group must be taken into account. As it is not available for this specific monomer, it must be approximated. Inorganic sulfuric acid is a very strong acid with pK_a = - 6.6 for the first deprotonation and the resulting HSO_4^- is a strong acid with pK_a = 2.0.[236] The structurally similar sulfurous acid has significantly lower pK_a values of 1.8 and 7.2, respectively.[236] The acidity of the species is influenced by the organic substituent. Benzenesulfonic acid is a much stronger acid than its inorganic counterpart in both stages of deprotonation with pK_a = -6.5.[237] The anion obtained by deprotonation of the acid is stabilized by resonance effects with the aromatic ring. If this effect is applied to styrene sulfate, it is very likely that the protonated acid form is a strong or very strong acid. For comparison, cationic polymerization of butadiene initiated by sulfuric acid at very low temperatures, T = -75 °C, has been reported.[238] Thus, quenching of the cationic polymerization by protonation of the sulfate group is unlikely. As a consequence, the inhibition of cationic polymerization of TBASS is probably attributed to electronic effects, i.e. withdrawing of electrons from the π-system by an inductive and a -M effect by the sulfate group as depicted in Scheme 3.20c.

In conclusion, radical polymerization of TBASS is characterized by faster reaction rates and higher monomer conversion compared to styrene, mainly attributed to a decrease in termination reactions. In contrast, TBASS does not undergo cationic polymerization, most likely due to electronic effects from the sulfate group. Therefore, the implementation of TBASS as a monomer in adhesive systems with radical curing mechanisms is advised. Although reaction rates and conversion in homo- and copolymerization can differ significantly, utilization of TBASS will be limited to radical copolymerization with acrylates in this work and will be discussed in the following chapters.

3.2.3 Styrene sulfate for electrochemical debonding

In the aspiration for development of a more circular economy, the demand for sustainable adhesive systems steadily increases. One approach is the implementation of adhesives with debonding features as described in section 1.3. The 4-vinylphenol derivate p-sodium styrene sulfate is an interesting monomer for systems for electrochemical debonding or delamination (**EDL**) due to its ionic character. Typically, ionic liquids (**ILs**) are added to a formulation to ensure ionic conductivity which is critical for the delamination process. However, inert ILs are known to decrease adhesive performance because they act as a plasticizer for the polymer network and, in addition, experiments in industry have shown that ILs tend to diffuse out of the cured adhesive over time which makes the material lose its mechanical integrity as well as efficiency in the debonding process. By substituting inert ILs with polymerizable ionic liquids (**PILs**) or reactive ionic monomers in general, both undesired effects can potentially be overcome. In order to investigate the utilization of TBASS in adhesives for EDL purposes, two acrylate-based reactive systems were picked for reference, one with PILs and one with an IL. The structures of the ionic components are displayed in Scheme 3.21 and the composition of the respective formulations with and without TBASS are given in Table 3.10. All formulations were used to glue aluminum substrates and were cured thermally with a radical initiator benzoyl peroxide (**BPO**) at 80 – 120 °C.

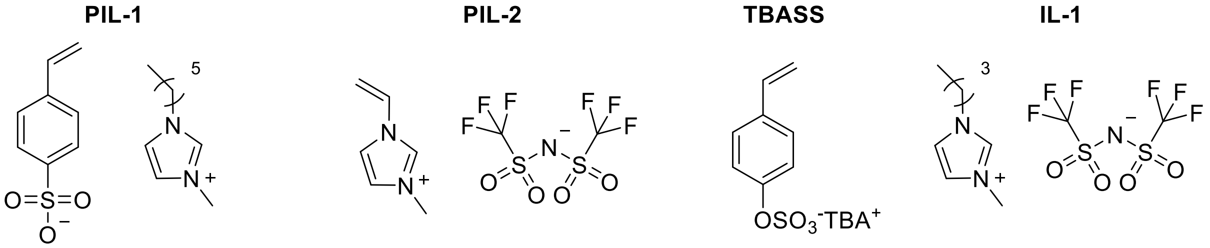

Scheme 3.21: Chemical structures of 1-hexyl-3-methylimidazolium styrene sulfonate (PIL-1), 1-vinyl-3-methylimidazolium bistriflimide (PIL-2), tetrabutyl ammonium p-styrene sulfate (TBASS) & 1-butyl-3-methylimidazolium bistriflimide (IL-1) used in acrylate-based systems for electrochemical debonding.

Table 3.10: Compositions of formulations for electrochemical debonding in wt%. PES-A is a difunctional acrylate with a polyester urethane oligomeric backbone, HAA is a hydroxyalkyl acrylate, AP is an adhesion promoter and BPO is benzoyl peroxide, a thermal radical initiator.

Formulation	PES-A	HAA	AP	BPO	PIL-1	PIL-2	IL-1	TBASS
F-PIL-1	30	17	3	2	11	37	-	-
F-PIL-2	30	17	3	2	-	37	-	11
F-IL-1	47	26	5	3	-	-	19	-
F-IL-2	47	26	5	3	-	-	-	19

In the reference system containing polymerizable ionic liquids **F-PIL-1**, only the structurally related **PIL-1** 1-hexyl-3-methylimidazolium styrene sulfonate was substituted by TBASS. First, impedance measurements of the resulting formulation **F-PIL-2** were performed to examine changes in ionic conductivity by TBASS (Figure 3.46, left). The specific resistivity *ρ* was calculated from impedance *Z* in the plateau region as shown in Figure 3.45 by using equation 3.3 with *A* being the overlapping area of the glued substrates and *d* the layer thickness.

$$\rho = \frac{Z \cdot A}{d} \qquad \textbf{(3.3)}$$

$$\kappa = \frac{1}{\rho} \qquad \textbf{(3.4)}$$

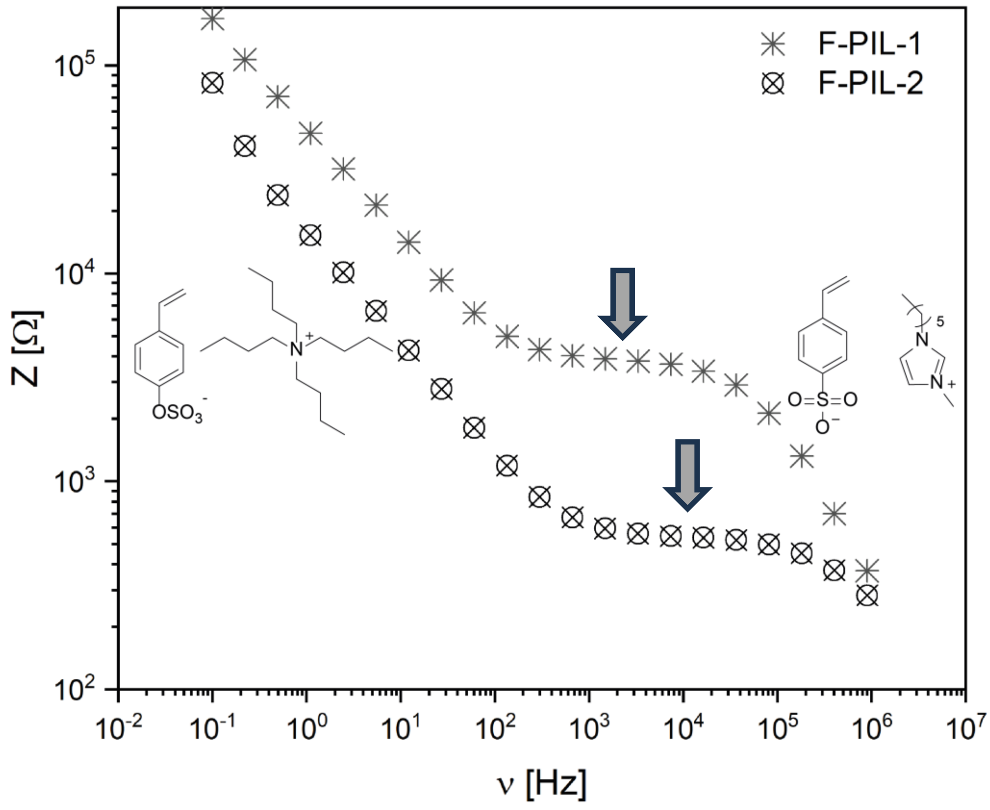

Figure 3.45: Impedance versus frequency plot from impedance measurements of aluminum substrates glued with F-PIL-1 (cross) or F-PIL-2 (circle). The arrows mark the plateau region from which resistivity *ρ* was calculated.

A significant decrease in resistivity was observed if PIL-1 is replaced by TBASS and consequently an increase in $\frac{1}{\rho}$,i.e. in conductivity κ (equation 3.4). This increase likely results from faster diffusion of ionic species through the polymer network towards the electrodes. There are two possible explanations for higher ion mobility in this system: On one hand, the overall molecular diffusion is increased in a polymer network with decreased T_g by incomplete curing and due to lower monomer conversion. A drastic intrinsic change in T_g of the polymer by substituting styrene sulfonate with structurally related styrene sulfate is unlikely. On the other hand, the cations of TBASS and PIL-1 differ significantly in size and form which allows changes in mobility mostly via ion hopping.[239]

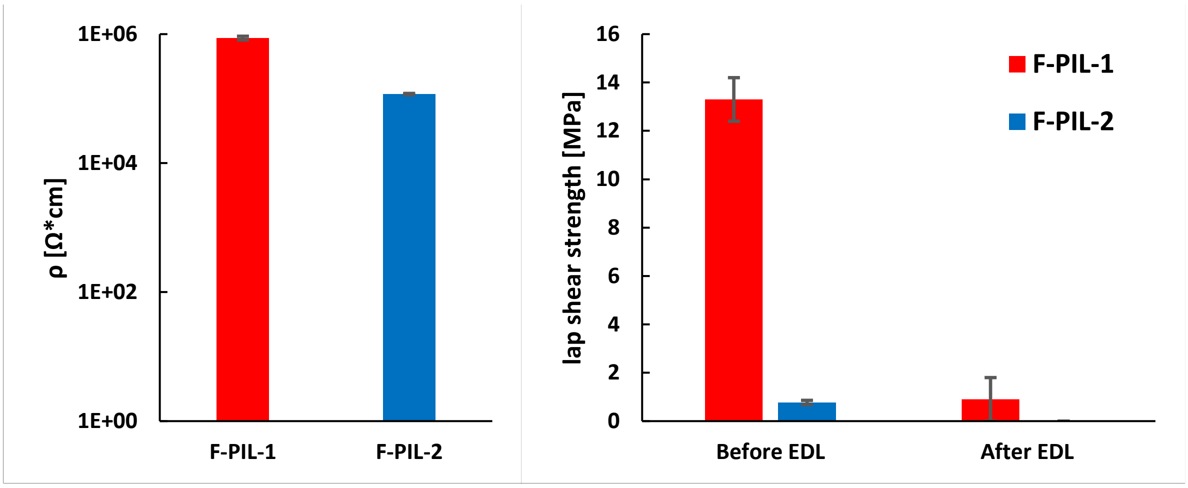

Figure 3.46: Comparison in conductivity and electrochemical delamination effect of formulations with polymerizable ionic liquids with PIL-1 (red) or TBASS (blue). Left: Specific resistivity ρ at 25 °C of aluminum substrates glued with the respective formulation. Right: Lap-shear strength values of aluminum substrates glued with the respective formulation before and after electrochemical delamination (EDL).

However, an increase in conductivity is a promising advantage regarding EDL efficiency which was evaluated in single-lap shear experiments (Figure 3.46, right). Aluminum substrates were glued by thermal curing of the respective formulation and analyzed before and after the EDL process. For debonding, a current with a voltage of 30 V was applied to the opposed substrates for 20 minutes. An initial lap-shear strength of the reference system F-PIL-1 of (13.3 ± 0.9) MPa was found which was decreased by over 90 % after applying voltage. By replacing PIL-1 with TBASS, the adhesive performance deteriorates massively with an initial lap-shear strength of (0.77 ± 0.09) MPa; failure mode of all samples was determined as cohesive failure. This drastic drop in cohesion does not only imply incomplete conversion of TBASS but inhibition of radical polymerization in general. This is an unexpected behavior, because of the high reactivity of TBASS in radical polymerization reported in section 3.2.2. Copolymerization with acrylates was not investigated, but even if no chain propagation between acrylate and TBASS active chain ends takes place, an inhibition of the respective polymerizations was not expected. Hence, a possible explanation for this phenomenon is the altered initiation from azo-initiator AIBN to peroxide-initiator BPO. Jiang et al.[232] reported that termination of BPO-initiated styrene polymerization proceeds predominantly by chain transfer reactions with BPO which leads to low monomer conversion if a high ratio of $\frac{c(\mathrm{BPO})}{c(\mathrm{monomer})}$ is used. Regarding the debonding features, the aluminum substrates separate immediately upon application of a current on the system which does show an effect by EDL, but no reasonable conclusion on efficiency can be drawn due to the low initial adhesive strength.

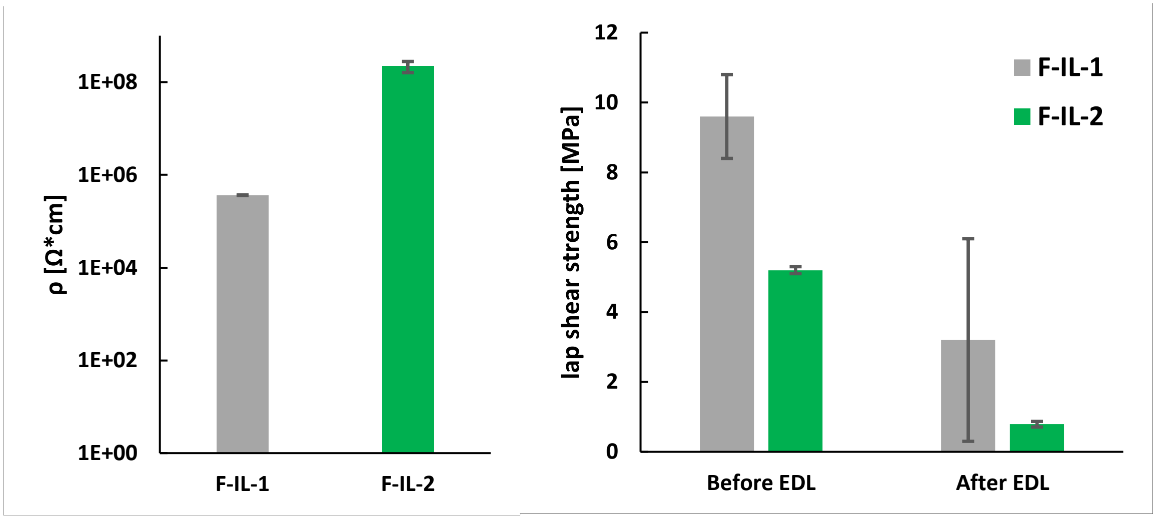

Figure 3.47: Comparison in conductivity and electrochemical delamination effect of formulations with IL-1 (grey) or TBASS (green). Left: Specific resistivity *ρ* at 25 °C of aluminum substrates glued with the respective formulation. Right: Lap-shear strength values of aluminum substrates glued with the respective formulation before and after electrochemical delamination (EDL).

Yet, these findings present critical issues on the use of TBASS in acrylate-based peroxide-initiated systems and the same inhibition phenomenon is expected to be found in F-IL-2 curing. In this formulation, an inert ionic liquid is replaced by TBASS. Figure 3.47 (left) shows an increase in resistivity by more than two orders of magnitude by TBASS utilization. This decrease in conductivity and hence in ion diffusion results from the vast difference in mobility between a free ionic liquid and TBASS which is, at least partially, incorporated into a polymer. The effect of EDL on the reference system F-IL-1 is weaker than for F-IL-2 with a decrease in lap shear strength of about 60 % (Figure 3.47, right); the absolute values must be taken with a grain of salt because of the high error in the measurements. Again, lower adhesive performances were observed if TBASS was utilized instead of the ionic liquid but to a much lower extent. The initial lap shear strength of F-IL-2 was δ_0 = (5.2 ± 0.1) MPa which decreased by about 85 % to δ_{EDL} = (0.79 ± 0.08) MPa during the debonding process. In this system, curing can be seen as partially successful with a decent initial adhesive strength. However, adhesive performance is still significantly weakened compared to F-IL-1 which indicates partial inhibition of radical polymerization which is further underlined by the cohesive failure mode in lap shear testing before EDL (Figure 3.48, left). Yet, there is a big improvement compared to F-PIL-2. The most striking difference between these systems is the absence of 1-vinyl-3-

methylimidazolium bistriflimide (**PIL-2**) and the polymerization of which might be mostly interfered with by TBASS. Nevertheless, the use of BPO as a radical initiator for TBASS (co)polymerization seems to be the main issue regarding curing inhibition. However, the goal of TBASS implementation was to evaluate its suitability in adhesive systems with electrochemical debonding features. F-IL-2 shows a decent starting adhesive strength and a vast decrease thereof by EDL. In addition, investigation of the adhesive residuals showed an explicit switch in failure mode in single-lap shear testing from cohesive before to adhesive failure after applying voltage (Figure 3.48). This shift towards adhesion failure implies that a delamination process has occurred, and the adhesive was mostly removed from one electrode without destroying the cohesive integrity of the material. Therefore, the potential of TBASS for electrochemical debonding systems as a substitution for inert ionic liquids was demonstrated.

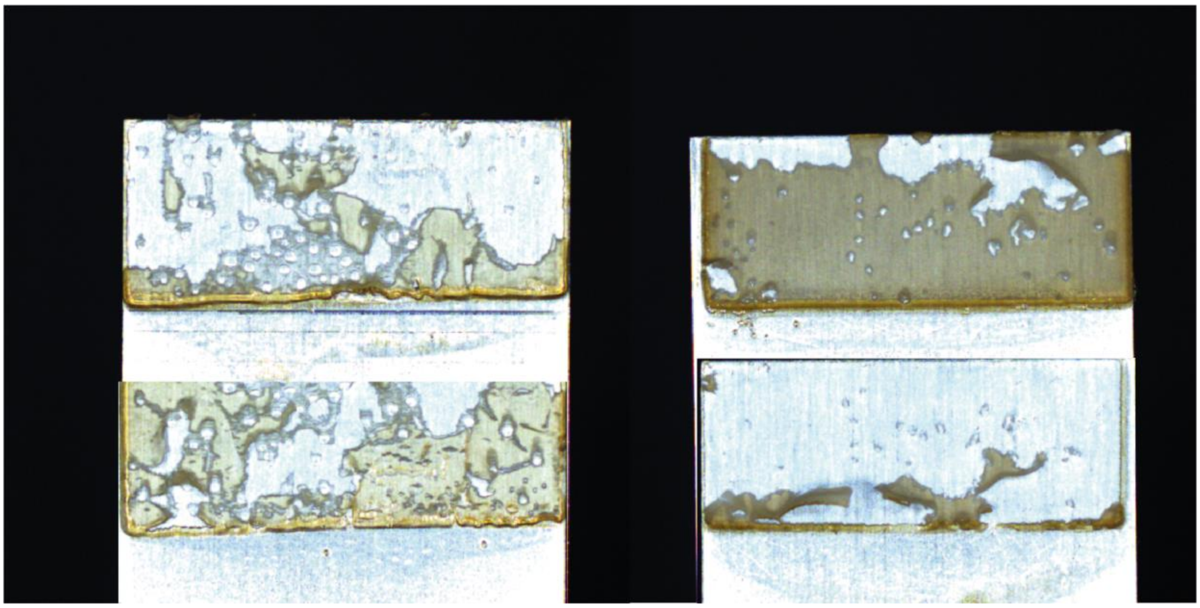

Figure 3.48: Adhesive residuals on aluminum substrates glued by F-IL-2 after single-lap shear measurement before (left) and after (right) EDL. The matching substrate parts are displayed beneath each other.

In general, the implementation of TBASS in acrylate-based reactive systems with EDL features leads to a decrease in activity of the utilized monomers in radical polymerization to a moderate or even a critical extent. This inhibition is likely caused by the incompatibility of TBASS with radical initiator BPO, but no conclusion can be drawn regarding the exact reasons behind this phenomenon. The described experiments were carried out in the context of a scouting project at the end of this work. Hence, no deep investigation of the inhibition effects and consequently the general polymerization of TBASS with BPO was done. However, by replacing an inert IL with TBASS, an adhesive system was created with a decent initial adhesive performance and an efficient delamination process resulting in a decrease in lap shear strength by about 85 %; the substrates can be separated by hand. Thus, the potential of TBASS as a substitution for free ionic liquids for adhesives with electrochemical debonding capabilities has been demonstrated. Further experiments with different radical initiators, preferably azo-initiators, are reasonable to better understand the underlying issues. In the following chapter, the implementation of TBASS in such a system is discussed but not in the context of EDL.

3.2.4 Preparation and characterization of PSAs with styrene sulfate

Another possible field of application for ionic tetrabutylammonium p-styrene sulfate is conductive pressure sensitive adhesives (**PSAs**), e.g. for medical patches which are able to record electrocardiograms. PSAs are polymers with glass-transition temperatures well below application temperature, so the non-reactive adhesive can be applied without further curing and reapplied which is advantageous for a lot of tapes. Due to their low T_g, PSA polymers are still mobile at application temperature and final adhesive strength is built up over time by diffusion of the polymer chains and subsequent substrate wetting. In order to enable ionic conductivity, inert ionic liquids are often added to the synthesized polymers, but a drawback of these systems is a decrease in adhesive performance, i.e. peel strength, by IL addition. A possible approach to decrease the amount of added IL is to utilize ionic comonomers, to preserve ionic conductivity but improve adhesive strength in the final product. Several (meth)acrylate monomers were copolymerized with TBASS in different concentrations: without the ionic comonomer for reference, with 0.5, 1.5 & 5.0 wt% of styrene sulfate. Radical solution polymerization was initiated by AIBN and carried out in a batch reactor with constant monomer and initiator solution feed in ethyl acetate under reflux. The comonomers and an indicative composition is given in Scheme 3.22. The obtained polymer solution was further diluted with ethyl acetate, ethanol, and isopropyl alcohol. The monomer conversion was determined by GC measurements: as demonstrated in Table 3.11. Hardly any residual (meth)acrylate monomers were detected via GC and consequently monomer conversion in all batches was very high regardless of TBASS concentration. Therefore, styrene sulfate does not inhibit radical-mediated acrylate polymerization in this system. Complementary LC analyses were performed to analyze TBASS conversion, but any signal intensities were too low to evaluate. Hence, it is assumed that TBASS has also participated in copolymerizaion, which is supported by the findings from section 3.2.2.

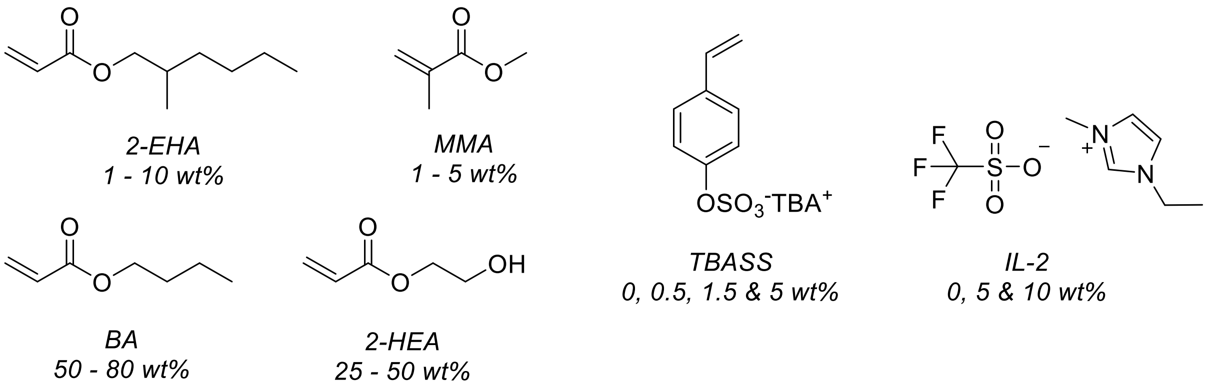

Scheme 3.22: Composition of acrylate-TBASS copolymers for PSA applications. Acrylate monomers 2-ethylhexyl acrylate (2-EHA), methyl methacrylate (MMA), butyl acrylate (BA) & 2-hydroxyethyl acrylate (2-HEA) were utilized. The ionic liquid 1-ethyl-3-methyldimidazolium triflate (IL-2) is added after copolymerization prior to film preparation.

Table 3.11: Residual monomer analysis via GC for copolymerization of several acrylates with different concentrations of TBASS. The values describe the residual monomer concentration in % (wt./wt.).

w (TBASS) [wt%]	2-EHA %	MMA %	BA %	2-HEA %	TBASS %
0	0.03	< 0.02	0.48	0.02	-
0.5	0.03	< 0.02	0.52	0.02	-
1.5	0.03	< 0.02	0.49	0.02	-
5	0.03	< 0.02	0.48	< 0.02	-

In order to determine the respective molecular weight distribution of each polymer, two GPC analyses were commissioned which yielded strikingly different results (Figure 3.49, Table 3.12). The obtained data is incongruent in terms of absolute molecular weight values, which is common in GPC analysis, but also regarding the trends in M_w against styrene sulfate concentration. $M_{w,1}$ decreases almost by a whole order of magnitude if only 0.5 wt% of TBASS is copolymerized and continues to drop with increasing styrene sulfate content. In contrast, $M_{w,2}$ increases with growing TBASS concentration. The very same trend is observed for the respective polydispersity values with the exception of PD_2 for *w* (TBASS) = 0.5 wt%. GPC is a relative analysis method which means that the absolute values must be taken with a grain of salt. However, trends observed in the data reflect the differences between different polymers well. The occurrence of antithetic trends in the same polymers implies drastic differences in the experimental setup or procedure. However, in both GPC experiments the same column material was utilized, just with slightly different pore sizes (*PLgel MIXED A* and *B* by *Varian*). Thus, interactions of the ionic compounds with the column material can be ruled out. Although tetrahydrofuran (THF) was used as the eluent in all measurements, a difference in concentration is a possible explanation for the results. Unfortunately, sample concentration was not provided for both measurements which were carried out by external accredited analytical departments. However, a change in concentration of the ionic species can result in altered coiling behavior, i.e. an increase of the Stokes radius of the polymer under more favorable solvation conditions as depicted in Figure 3.50.[240] This effect will be discussed in more detail later in this section.

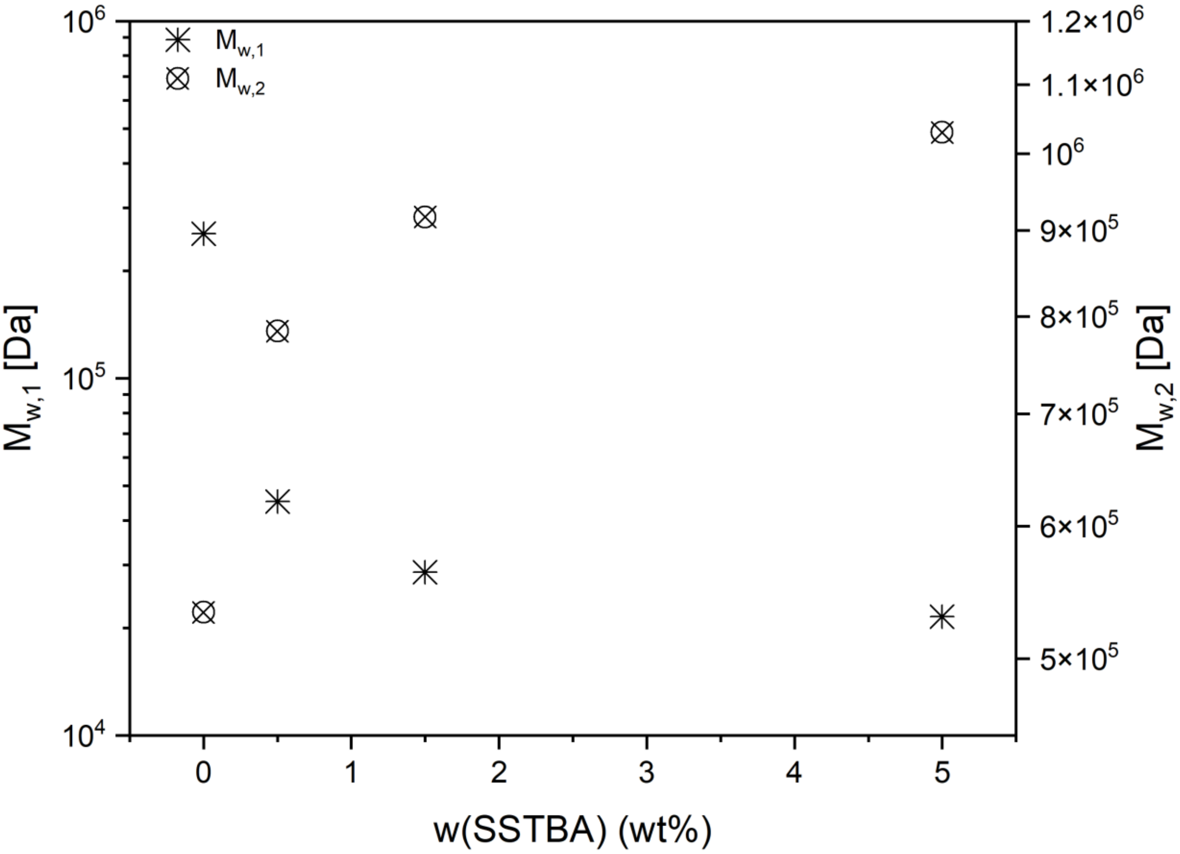

Figure 3.49: Molecular weight distribution of acrylate-TBASS copolymers. Two measurements were commissioned at different locations with different outcomes. No significant changes in measurement methodology were made.

Table 3.12: Molecular weight distribution of acrylate-TBASS copolymers. Two measurements were commissioned at different locations with different outcomes. No significant changes in measurement methodology were made.

w (TBASS) [wt%]	$M_{w,1}$ g/mol	$M_{w,2}$ g/mol	PD_1	PD_2
0	$2.5 * 10^5$	$5.3 * 10^5$	13.3	18.91
0.5	$4.5 * 10^4$	$7.8 * 10^5$	5.8	16.73
1.5	$2.9 * 10^4$	$9.2 * 10^5$	5.3	26.21
5	$2.2 * 10^4$	$1.0 * 10^6$	4.8	30.38

Yet, trends in the molecular weight distribution of polymers can also be approximated by viscosity measurements. It has been widely reported that the viscosity of a polymer solution or polymer melt increases with the average molecular weight of the polymer.[241] This relation is described by the Mark-Houwink equation:

$$[\eta] = KM^{\alpha} \tag{3.5}$$

with the intrinsic viscosity $[\eta]$ and two polymer-solvent dependent parameters K and α. The relative viscosity (**RV**), compared to crude ethyl acetate, of the polymer solutions was measured; the results are shown in Figure 3.51. A slight decrease in *RV* was found from 0 to 0.5 wt% of TBASS followed by a continuous decrease with growing styrene sulfate content. The first decrease in viscosity is too moderate to be reasonably correlated with a vast drop in molecular weight as indicated by $M_{w,1}$ data. It must be noted that the implementation of ionic groups in the polymer chain effectively turns the otherwise neutral polymer into a polyelectrolyte which results in a number of alterations in solution and melt behavior. On one hand, strong ionic interactions between the chains can increase the viscosity of the system depending on the grade of dissociation of the anionic side chain and the free cation.[242] On the other hand, interactions between polymer chains and solvent change. If the intermolecular interactions between a polymer and a solvent are highly energetically favorable, the polymer acts as an ideal chain (Figure 3.50, right) in a theta solvent; $\alpha = 0.5$ in equation 3.5.[243] When the polymer-solvent interactions become less favorable, polymer-polymer self-interactions increase which causes the polymer to coil (Figure 3.50, left). The implementation of ionic side chains can reportedly result in an alteration in coiling behavior, induced by changes in polymer-solvent interactions but also by electrostatic repulsion effects between the charged side chain groups which cause the polymer coils to expand.[244] The form of the polymer coils in solution significantly influences viscosity and especially molecular weight measurements. In GPC experiments, the Stokes radii of the polymers are measured.[245] Ionic groups in the polymer chain can lead to unwinding of the polymer coils in the utilized solvent and thus the measured molecular weight appears higher than it actually is compared to polymers with fewer or without ionic groups. However, the effect of the ionic groups on the interaction between the polymers and the GPC solvent, THF, cannot be reliably predicted and thus a concise conclusion about the effect of TBASS on the polymerization process cannot be drawn.

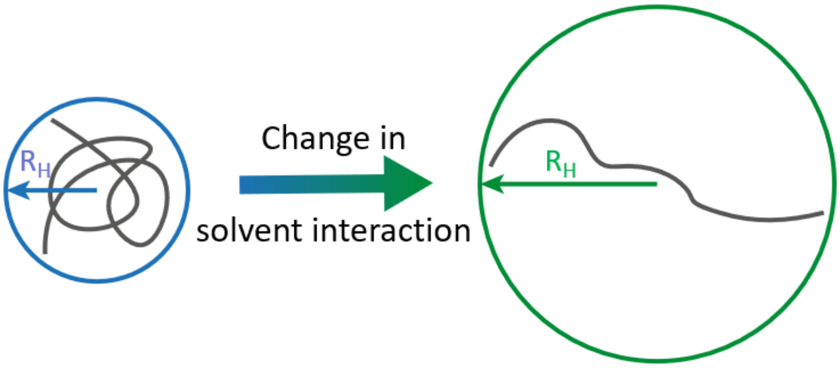

Figure 3.50: Schematic depiction of increase in Stokes radius R_h by changes in solvent-polymer interactions resulting from e.g. implementation of ionic side chains.

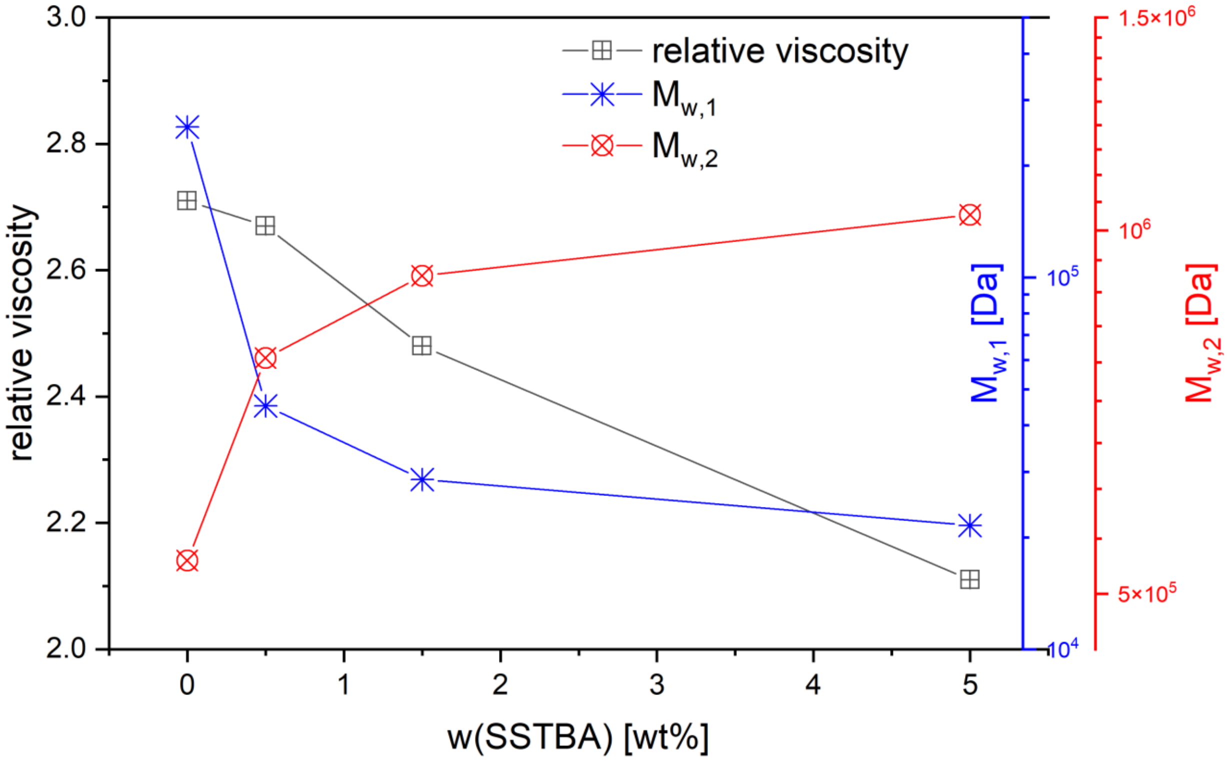

Figure 3.51: Molecular weight distribution of acrylate-TBASS copolymers (blue, red) compared to relative viscosity (black, reference: crude ethyl acetate) of the respective polymer solutions. Typically, there is a correlation between *RV* and M_w. A reasonable correlation was not found.

Although data on the molecular weight of the synthesized polymers is difficult to obtain, information about whether TBASS copolymerizes with the utilized acrylates or not was gained. As mentioned before, an inhibition of acrylate and/or TBASS polymerization can be ruled out. However, if styrene sulfate homopolymerizes, the obtained polymer chains are significantly smaller than the acrylate copolymers. This hypothesis is based on three assumptions described in equation 3.6 – 3.8. First, styrene sulfate concentration in the reaction mixture must be much lower than acrylate concentration which is the case for all performed polymerization procedures. Second, the ratio of termination reaction rate coefficient k_t to propagation rate coefficient k_p of TBASS must be roughly equal to the respective ratio of the acrylates. Asua *et al.* reported higher ratios for styrene compared to butyl acrylate.[231] Kinetic measurements in 3.2.2 showed that this ratio is lower for TBASS than for styrene. Yet, a precise prediction about assumption two cannot be made but it is fair to assume that the termination to propagation ratio of TBASS is not vastly higher than the respective ratio of the acrylate monomers which is the only case in which the underlying hypothesis must be dismissed. However, assumption three is more decisive on the final polymer chain length: the ratio of termination by combination to termination by disproportionation or chain transfer reactions of TBASS must be lower or equal to the respective ratio of acrylates. The point of this assumption is that combination yields one long polymer chain instead of two shorter chains obtained from other termination reactions. In literature, termination behavior of acrylates has been reported with very high combination rates[246] even up to 100 %[247]. In contrast, termination of styrene is dominated by chain transfer reactions, whereas combination reactions are observed only to a small extent, which is mostly associated with the bulky styrene side chains.[232] This effect is likely enhanced by the sulfate substituent at the aromatic ring, thus termination by combination of TBASS active chain ends is not a dominant factor. In conclusion, it is assumed that the acrylate polymer chains obtained from a solution with at least 95 wt% of acrylate monomers which polymerize, if at all, not much slower than TBASS and terminate mostly by combination are much longer than the chains obtained from the hypothetical parallel homopolymerization of TBASS.

$$c(\mathrm{TBASS}) \ll c(\mathrm{acrylates}) \qquad \textbf{(3.6)}$$

$$\frac{k_t(\mathrm{TBASS})}{k_p(\mathrm{TBASS})} \approx \frac{k_t(\mathrm{acrylates})}{k_p(\mathrm{acrylates})} \qquad \textbf{(3.7)}$$

$$\frac{k_{t,c}(\mathrm{TBASS})}{k_{t,x}(\mathrm{TBASS})} \leq \frac{k_{t,c}(\mathrm{acrylates})}{k_{t,x}(\mathrm{acrylates})} \qquad \textbf{(3.8)}$$

$$D = KM_w^{-\alpha} \qquad \textbf{(3.9)}$$

The diffusion coefficient *D* of a polymer chain in solution decreases with increasing molecular weight as described by equation 3.9.[248] As a consequence, if TBASS does not copolymerize with the acrylates in the performed polymerization experiments, *D* of the homopolymer chains must be lower than *D* of the acrylate polymer chains. By Diffusion Ordered 2D-NMR spectroscopy (DOSY) a diffusion coefficient can be assigned to a proton signal in a spectrum. In DOSY NMR a magnetic pulsed field gradient is applied to the sample.[249] The self-diffusion of molecules through the gradient field results in changes in signal intensity. From this change in intensity, a diffusion coefficient can be calculated and correlated to a ^{1}H-NMR signal.[250] In ^{1}H-NMR the proton signals of the aromatic ring of styrene sulfate were found at 6.9 ppm and 7.2 ppm (Figure 3.41) and a characteristic proton signal of a polyacrylate side chain is located at 4.0 ppm.

A sample was taken from the polymer solution with 5 wt% of TBASS, dried, dissolved in $CDCl_3$ and DOSY NMR measurements were performed; the results are displayed in Figure 3.52. The broad form of the aromatic proton signals suggest polymerization of TBASS.[222] In addition, the diffusion coefficients of the aromatic protons and the acrylate protons are within the same range which implies copolymerization. However, the measurements were performed at room temperature and with a short delay in pulse sequence of 50 ms. A fit of the signal shows hardly any decrease in signal intensity correlated to field gradient strength. Typically, intensity decays exponentially according to the self-diffusion behavior of the measured molecules. Without a substantial decay, diffusion of the long polymer chains is too slow for the measurement technique and the obtained D values do not represent the actual diffusion but only the limitations of the used procedure.[251,252]

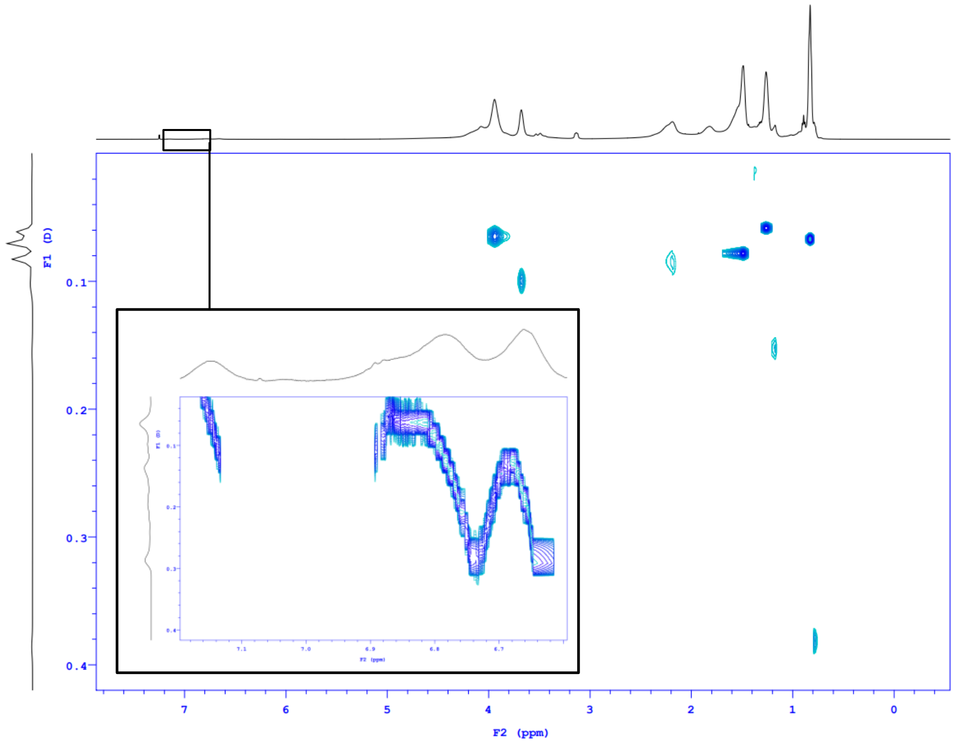

Figure 3.52: ^{1}H 2D DOSY NMR spectrum of acrylate-TBASS copolymer with 5 wt% of TBASS. The diffusion coefficient *D* (y-axis) directly correlates to polymer chain length. Measurements were performed in $CDCl_3$ at RT with a delay in pulse sequence of 50 ms.

Hence, the measurements were repeated at 50 °C to accelerate polymer self-diffusion and the delay in pulse sequence was increased to 800 ms to give the polymer more time between impulses to diffuse through the sample tube. Also, the solvent was changed to DMSO-d_6 to allow measurements with elevated temperatures. The signal intensity decay was plotted against field gradient strength as shown in Figure 3.53. An exponential decay was found with almost no signal observable at high field gradient strengths which is considered crucial for diffusion coefficient calculations.[251] By an exponential fit of the signal decay, D was calculated for the aromatic proton signal at 6.619 ppm with D_{ss} = (0.77 ±0.03) * 10^{-10} m^2/s and the acrylate proton signal at 3.976 ppm with D_a = (0.84 ±0.05) * 10^{-10} m^2/s. The values are not only within the same range but within their respective error margins. From this data, it can be concluded that TBASS copolymerizes with acrylate monomers and ionic side chains are implemented into the long polymer chains. This deduction on the structure of the synthesized polymers for PSA application will be used to interpret their behavior in application discussed in the following section.

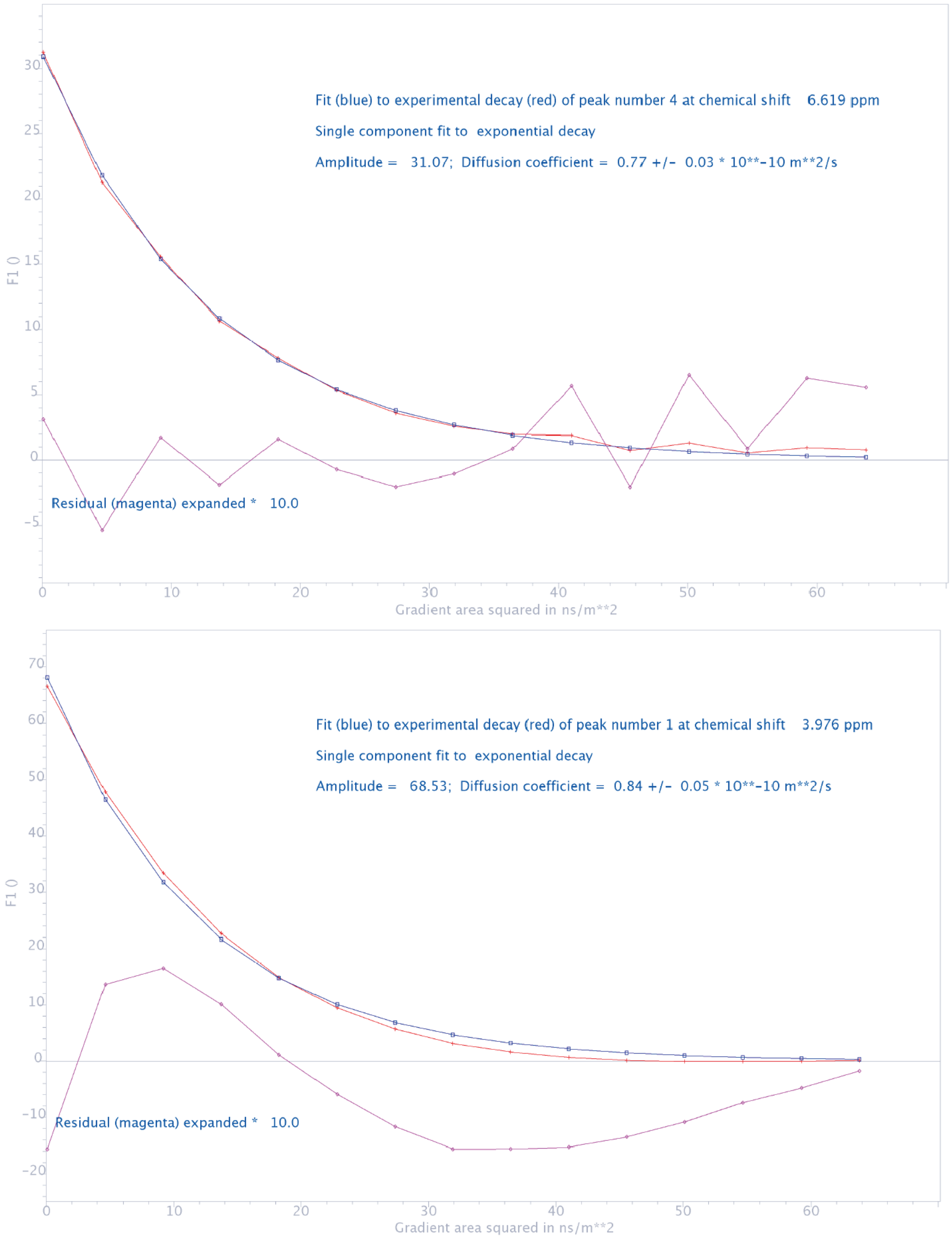

Figure 3.53: Data fitting of signal decay in DOSY NMR measurements of an acrylate-TBASS copolymer with 5 wt% TBASS measured in DMSO-d_6 at 50 °C with a delay in pulse sequences of 800 ms. Temperature and delay are increased to facilitate reproducible values for *D* for high molecular weight polymers. Top: aromatic ^{1}H signal corresponding to TBASS units. Bottom: aliphatic ^{1}H signal corresponding to acrylate units.

3.2.5 Styrene sulfate in conductive PSAs

For application testing, an intermolecular crosslinker, aluminum acetyl acetonate (Al(acac)$_3$), was added to polymer solutions which increases shear strength and overall cohesion of the PSA.[253] The final solutions were homogeneously applied on silicone paper, dried and transferred to a quartz plate for rheometric measurements to analyze the viscoelastic behavior over a temperature ramp. Figure 3.54 shows the dissipation factor tan δ of all four polymers plotted against temperature, plots of storage modulus G' and loss modulus G'' can be found in the appendix (Figure 6.79 - Figure 6.82). The peak of tan δ marks the glass-transition temperature; T_g values of all investigated polymers are within the same range at -2 °C ≤ T_g ≤ 5 °C. However, a general increase in tan δ above T_g was observed. This implies a softening of the material with growing styrene sulfate content. In polymer systems, the same effect can be assumed from increasing T_g values which were not observed. The behavior of the PSAs at higher temperatures can also be caused by changes in entanglement density in the systems. Cohesion of polymer melts is dominated by intermolecular interactions of entangled polymer chains.[254] Thus, the observed softening of the PSAs at high temperatures can be attributed to lower entanglement densities which can result from two different factors: On one hand, electrostatic repulsion of the ionic side chains causes the polymer coils to expand which leads to a less entangled polymer network. On the other hand, the force needed to detach entanglements decreases with polymer chain length.[255] Additional rheological experiments on the entanglement behavior of the polymer melts were carried out. Frequency sweep measurements were performed in which the polymers disentangle at different frequencies, depending on entanglement density and intermolecular interactions, under given shear forces. It was attempted to calculate the entanglement molecular weight based on the reptation model by Doi and Edwards[256] and de Gennes[257] but all recent models on quantification of entanglements in polymer melts are limited to homopolymers with narrow molecular weight distributions.[258] As a consequence, no consistent data of the investigated polymers with four to five different comonomers and high polydispersity was obtained. As it was not possible to quantify the molecular weight distribution or entanglement behavior, a concise conclusion on the underlying mechanism of material softening at high temperatures cannot be drawn at this point. In future research approaches, additional light-scattering experiments can be a way to obtain information about the molecular weight distribution. In light-scattering experiments, the respective M_w values are also calculated from the respective Stokes radii of the polymers, but the form factor $P(q)$ can also be approximated which gives information about the coiling behavior of the polymers.[259] By a correlation of these values, a trend in molecular weight distribution of the polymers depending on the styrene sulfate concentration can be seen.

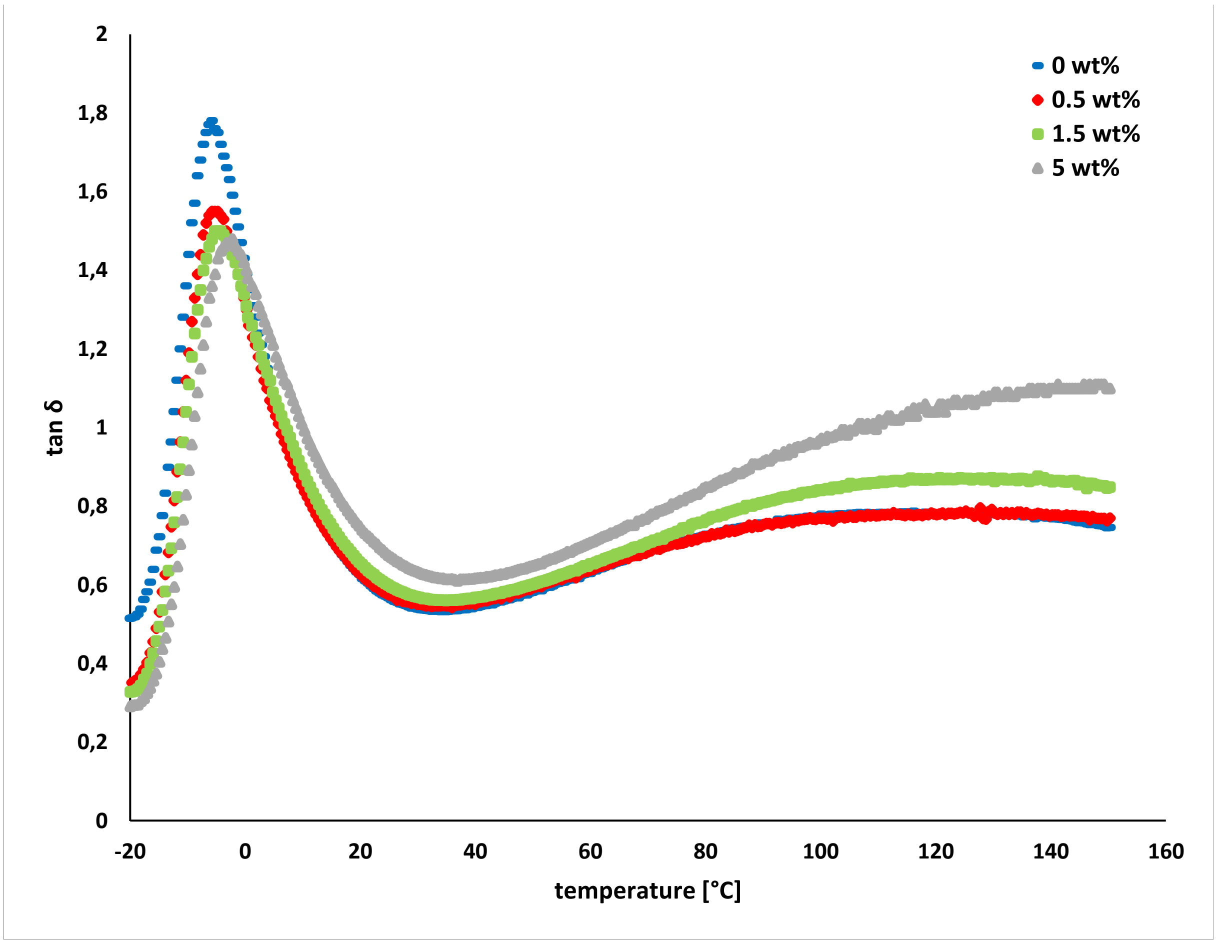

Figure 3.54: Dissipation factor tan δ versus temperature of acrylate-TBASS copolymers with 0 (blue), 0.5 (red), 1.5 (green) & 5 wt% (grey) of TBASS. Data was obtained from rheometric oscillatory experiments.

A possible application for the investigated PSAs is as an adhesive for ECG medical patches with built-in electrodes for long-term examinations. For the electric signal of the heartbeat to be conducted to electrodes, the adhesive needs to have electronic, or in this case ionic, conductivity. Typically, this is achieved by adding an ionic liquid to the PSA. On the downside, the addition of an IL causes a cutback in cohesion and consequently adhesive performance. Thus, the implementation of ionic TBASS in the polymer chain aims at decreasing the amount of utilized IL and consequently enhancing adhesive performance while maintaining ionic conductivity. Samples were prepared with 0 wt%, 5 wt% and 10 wt% of 1-ethyl-3-methylimidazolium triflate (**IL-2**, Scheme 3.22) added. The impedance, or the inverse conductivity, of a material when an alternating current is applied, of the PSAs was measured at a frequency range of 900000 Hz ≤ v 0.1 Hz. The data generated from impedance measurements can be found in the appendix and the specific resistivity ρ was calculated with equation 3.3; the obtained data is presented in Figure 3.55. The resistivity of the system significantly decreases by two magnitudes by adding only 0.5 wt% of styrene sulfate. This increase in conductivity continues in a flattened manner with increasing concentrations of the ionic comonomer. However, when IL is added to the system, the impact of styrene sulfate is no longer observable. A concentration of 5 wt% of ionic liquid decreases the resistivity by more than four magnitudes compared to the completely neutral polymer. Most likely, this high impact masks the influence on conductivity by ionic groups in the polymer chain. An additional 5 wt% of IL-2 further decreases resistivity but to a smaller extent to about 2 * 10^6 Ω*cm. A typical requirement for ECG medical patches is ρ = 1.3 10^6 Ω*cm which is almost met. Although the implementation of small amounts of TBASS in the polymer results in a significant increase in ionic conductivity, the effect dampens with increasing styrene sulfate concentration highlighted by the fact that the difference between 0.5 wt% and 1.5 wt% of TBASS is about as prominent as between 1.5 wt% and 5 wt%. In addition, the effect of 5 wt% of IL-2 is much more pronounced so ionic comonomer contents up to 5 wt% do not have a significant effect on conductivity in the range of application requirements. Most likely, a more significant effect is observed by utilizing higher amounts of styrene sulfate which might cause a significant decrease in cohesion as implied by rheological experiments discussed above. Still, the addition of more TBASS or IL-2 is needed to meet industrial requirements for ECG medical patches. However, this work focuses on the general impact of styrene sulfate on the PSA system and experiments with higher styrene sulfate content were not conducted. In addition, styrene sulfate is currently not available on an industrial scale and high concentrations of the ionic monomer in potential products are unlikely at this moment.

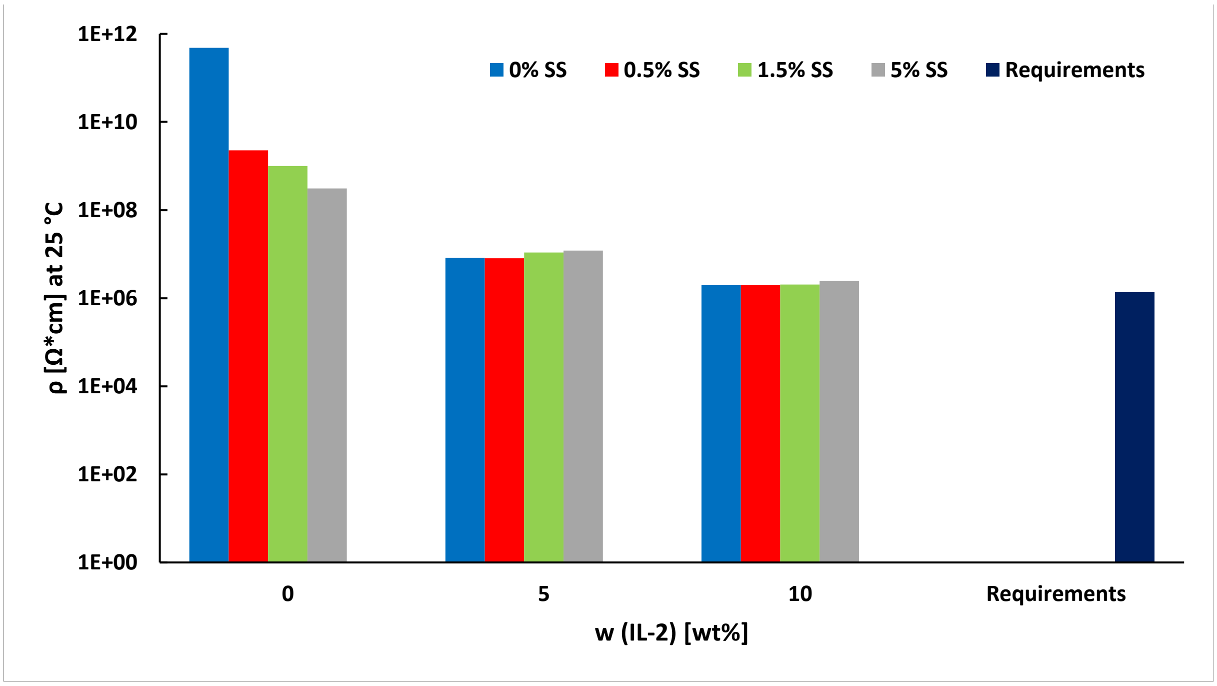

Figure 3.55: Specific resistivity ρ at 25 °C of acrylate-TBASS copolymers with 0 (blue), 0.5 (red), 1.5 (green) & 5 wt% (grey) of TBASS with different amounts of IL-2 added. The requirements for a typical ECG medical patch are shown in dark blue. Data was obtained from impedance measurements by gluing substrates coated with a conductive ink with the copolymer PSA system.

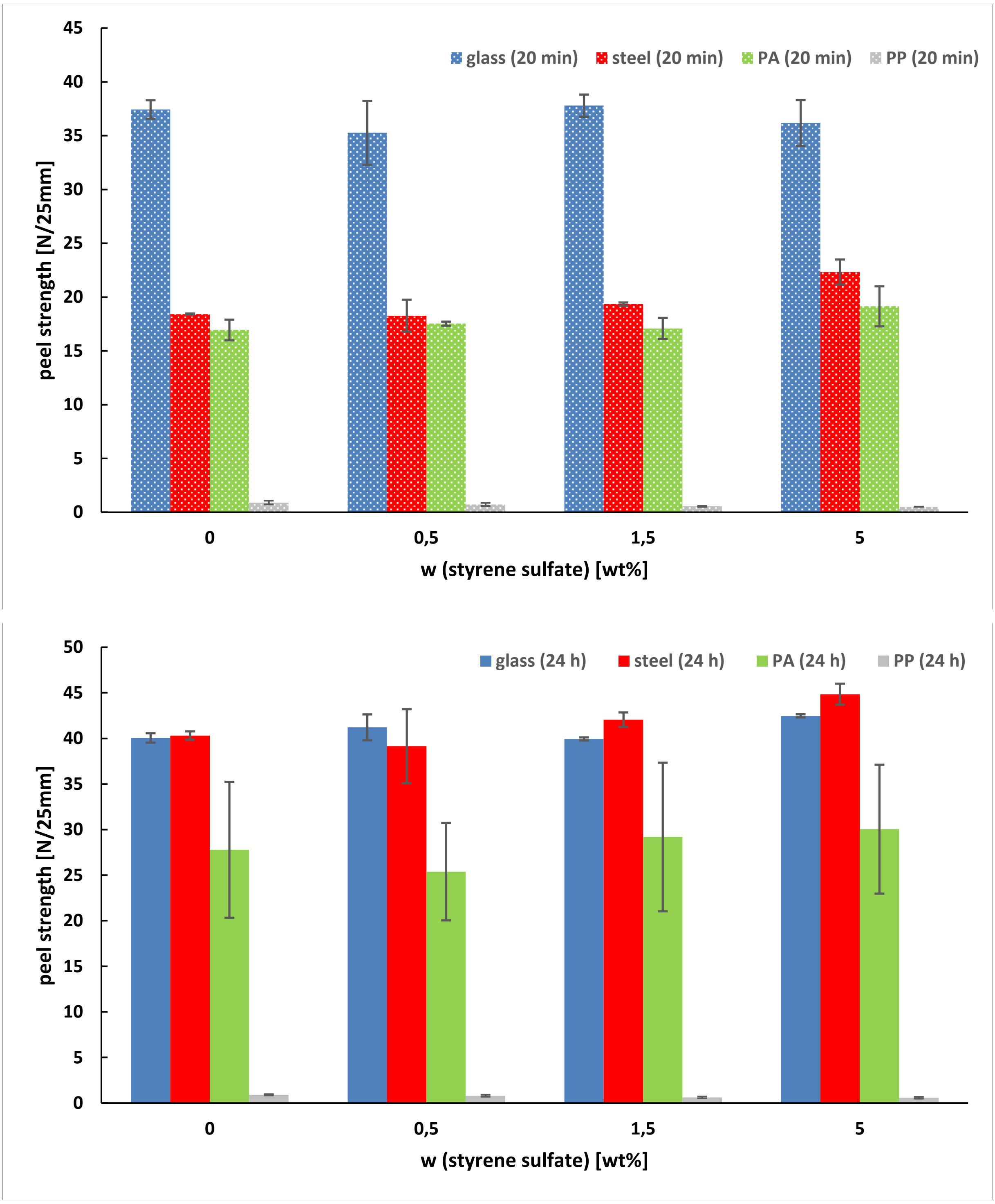

Figure 3.56: 180° peel strength values of acrylate-TBASS copolymers with 0, 0.5, 1.5 & 5 wt% of TBASS on glass (blue), steel (red), polyamide (green) & polypropylene (grey). Samples were measured 20 minutes (top) and 24 hours (bottom) after application. A general increase in peel strength was observed over time.

In order to investigate the impact of styrene sulfate on the adhesive performance of the PSAs, 180 ° peel tests of all polymers were performed on glass, steel, a polar plastic (polyamide (**PA**)), and a nonpolar plastic (polypropylene (**PP**)); the results are presented in Figure 3.56. The different substrates were chosen to investigate a broad array of potential applications and the impact of styrene sulfate on adhesion on the different surfaces.

Measurements were carried out at RT 20 minutes and 24 hours after application. As application temperature is above T_g for all samples, the polymer chains are mobile and need to build up adhesive strength over time by wetting. After 20 minutes, peel strength of all samples on glass is significantly higher than on any other substrates with $\sigma_p \approx 37$ N/25 mm followed by comparable values on steel and PA around 18 N/25 mm for w(TBASS) < 5 wt%. Independent from sample and wetting time, the measured peel strength values on PP were negligibly small at around 1 N/25 mm. After 20 minutes, no significant differences in peel strength were observed related to styrene sulfate content of the polymer on glass, PA, and PP. However, an increase in adhesive performance was found on steel with growing concentration of TBASS. This trend on the different substrates is also consistent 24 hours after application and the enhancing effect of the ionic comonomer on steel becomes even more pronounced. In general, peel strength increases at a higher wetting time on glass, PA, and especially on steel. In conclusion, the implementation of styrene sulfate does not impair the adhesive performance of the investigates PSAs but even improves peel strength on steel substrates which can be attributed to ionic interactions of the sulfate groups with the metal surface.

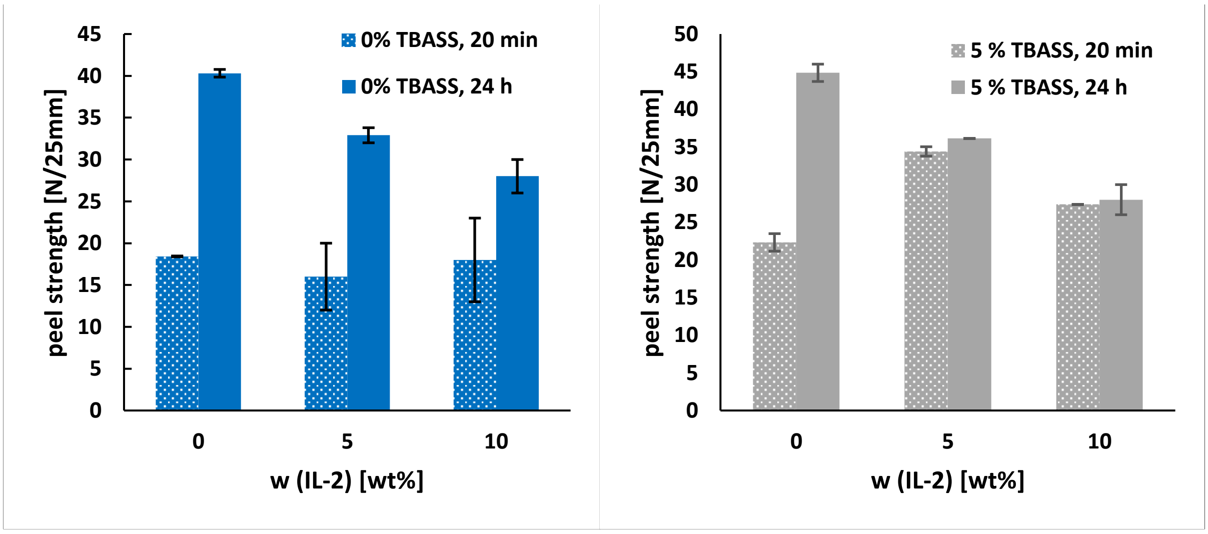

Figure 3.57: 180° peel strength values acrylate-TBASS copolymers with 0 (left), & 5 wt% (right) of TBASS with different amounts of IL-2 added. Samples were measured 20 minutes (dotted) and 24 hours (solid) after application. A synergetic effect between TBASS and IL-2 significantly accelerates peel strength buildup.

Comprehensive 180 ° peel tests were performed with PSAs containing 5 wt% and 10 wt% of IL-2 added, respectively. Overall, the addition of the ionic liquid significantly decreases peel strength of all systems and on all substrates; the data can be found in the appendix (Figure 6.86 - Figure 6.99). However, the most interesting observation was made on steel. The left side of Figure 3.57 shows peel strength values of the PSA without styrene sulfate 20 minutes and 24 hours after application. Overall, a significant increase in peel strength is observed over time: from 18 N/25 mm to 32 N/25 mm with 5 wt% IL. In contrast, final peel strength is almost reached after 20 minutes in a corresponding system with 5 wt% styrene sulfate and the increase over time is negligible from 34 N/25 mm to 36 N/25 mm (Figure 3.57, right). This fast buildup of final adhesion on the substrate is only observed if both styrene sulfate and IL are present in the system which indicates an unexpected synergetic effect. In addition, Loop Tack experiments on steel substrates validate these results (Figure 3.58). Without ionic liquid, the application tack decreases with increasing styrene sulfate content but increases if IL is added. The data obtained from 180° peel tests on glass and PA substrates also implies quick buildup of adhesion if the ionic monomer and the IL are both utilized. Thus, it results from an intrinsic effect of the adhesive. The fast wetting of the substrates by the adhesive indicates high mobility of the polymer chains and consequently low entanglement density in systems with styrene sulfate and IL. This fast buildup in peel strength is favorable for applications which require high initial adhesive performances.

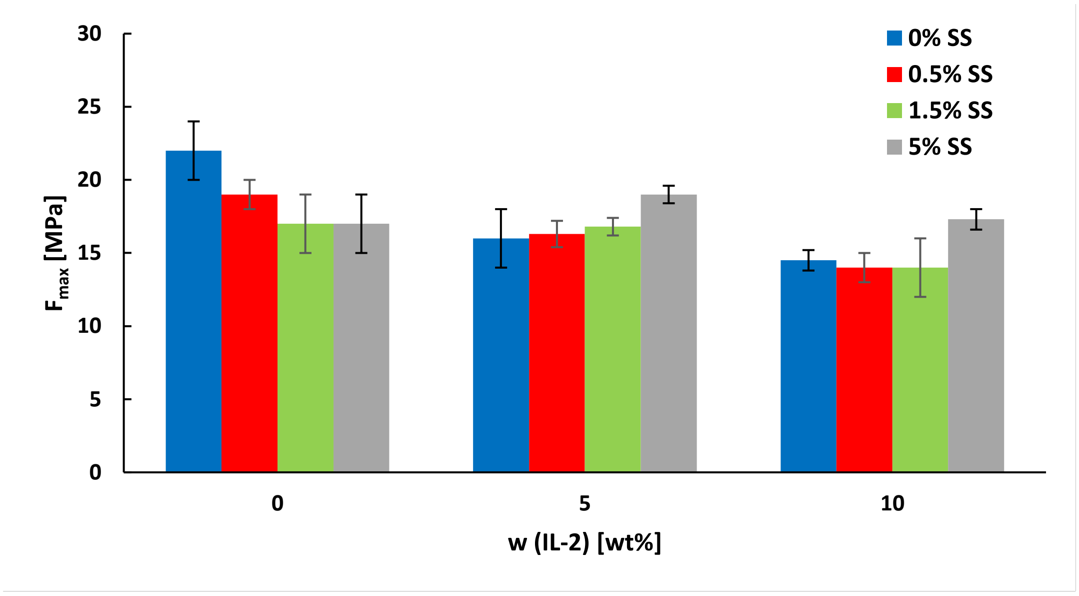

Figure 3.58: Loop tack results of acrylate-TBASS copolymers with 0 (blue), 0.5 (red), 1.5 (green) & 5 wt% (grey) of TBASS on steel substrates with different amounts of IL-2 added. The higher maximum force F_{max}, the faster is the wetting process of the substrate surface by the PSA copolymer.

In conclusion, TBASS was copolymerized with different acrylate comonomers for an ionically conductive PSA system. Although it was not possible to determine the molecular weight distribution of the polymers, copolymerization was confirmed by DOSY NMR analysis. As anticipated, conductivity of the PSA increases with increasing styrene sulfate content, but the effect of IL addition is much more pronounced and superimposes any contribution by TBASS in mixed systems at *w* (TBASS) ≤ 5 wt%. Implementation of the ionic comonomer does not diminish the adhesive performance and even increases peel strength on steel substrates. This indicates that the utilization of higher amounts of TBASS for conductivity increase is feasible without losing adhesive performance, and thus a system with decreased free ionic liquid content is conceivable. In addition, a synergistic effect between styrene sulfate and the ionic liquid was observed which causes very fast wetting of substrate surfaces. A patent has been filed for PSAs with TBASS and similar salts as comonomers. The basic idea for the patent was provided by Dr. Adrian Brandt and Philipp Ernst. The author is responsible for all practical works, evaluations, and work progress iterations. As a consequence, the author holds a 60 % share of the invention.

4 Conclusion and Outlook

In the aspiration to adjust current industrial products towards the establishment of a more circular economy, adhesive research should focus on showing advantages and drawbacks of novel adhesive systems with high renewable carbon content and debonding features. In this context, this thesis aimed at the evaluation of vinyl ethers and 4-vinylphenol derivatives in adhesive systems. Both substance classes are partially available from biobased feedstocks at the moment. The investigation of vinyl ethers was focused on the development of novel reactive formulations, with a focus on light triggered cationic polymerization, to elucidate their potential as the main functionality in adhesives. In addition, debonding by hydrolysis was tested by utilizing vinyl ether-functionalized hemiacetal ester prepolymers. One of these systems was combined with the 4-VP derivative 4-MeOS. Another derivative, styrene sulfate, was synthesized, stabilized, and incorporated in well-known acrylate-based adhesive formulations.

Novel vinyl ether-based adhesive systems

The main objective of this thesis concerning the introduction of vinyl ethers in novel adhesive systems is to understand and subsequently control vinyl ether polymerization. Various vinyl ether monomers were homopolymerized by initiation with iodonium salts which are well-established as cationic photoinitiators. In bulk experiments, intense heat generation was observed which results from the exothermic cationic polymerization of vinyl ethers. The resulting material degradation renders high mass fractions of small vinyl ethers monomers as impractical in adhesive formulations. However, extensive rheological data on the respective homopolymers was gathered by monitoring the curing process in rheometric experiments. As an alternative, urethane-based prepolymers were synthesized and a prototype formulation was developed with decreased reactive group concentration. By LED irradiation, a homogeneous and well-cured material was obtained with mechanical properties typically associated with epoxide or polyurethane adhesives, i.e. strong but not flexible materials. Thus, an adhesive formulation was developed with moderate amounts of heat released in the light-triggered cationic polymerization while maintaining fast curing. Furthermore, various filler materials were added to this adhesive formulation and evaluated in terms of miscibility, viscosity increase as well as reduction of heat and vinyl ether conversion. A guiding classification was outlined regarding the suitability of each filler with the presented vinyl ether system in terms of thermal control and mass fraction limitations. The objective of controlling heat generation in cationic vinyl ether curing has been met by utilization of prepolymers and fillers.

The scope of vinyl ether curing mechanisms was expanded by adding a second moisture cure step after photopolymerization. A urethane-based crosslinker was synthesized with one vinyl ether and two free isocyanate moieties on average and a novel formulation was developed.

The impact of crosslinking reactions between isocyanate groups in the presence of water on material and adhesive properties was demonstrated. The formulation was compared to a commercial acrylate-based product with identical curing steps and found to be comparable and even superior to the commercial product regarding their adhesive performance on plastic substrates. A disadvantage of the tested vinyl ether-based systems is low adhesion on metal surfaces. By the implementation of a different curing mechanism, polyaddition with thiols, this drawback was circumvented. The created two-component formulation achieved high lap shear strength values on aluminum and especially on steel by thermal cationic-mediated thiol-ene curing. However, there is still considerable room for improvement regarding vinyl ether systems with moisture and thiol-ene curing mechanisms. Via formulation approaches, the adhesive performance can be increased, more sustainability criteria can be met and productions costs can be lowered.

The two classes of prepolymers, polyhemiacetal esters and polyurethanes, in this work were compared regarding possible inhibition of vinyl ether polymerization in kinetic experiments. Two hemiacetal ester and urethane model compounds were synthesized, respectively. Cationic polymerization of the urethane compounds is significantly slower as demonstrated in rheometric measurements. Further confirmation was obtained via NMR spectroscopy. These results support the hypothesis of inhibition of cationic polymerization by urethane groups which was hinted at in the literature already. Moreover, they indicate more efficient curing processes in vinyl ether adhesive systems in which hemiacetal ester prepolymers are utilized instead of polyurethanes. The effect of hydrolysis on cured hemiacetal ester-based materials was analyzed to elucidate potential debonding by hydrolysis features. The developed formulations initiated by iodonium salts and by silyl-mediated photoinitiation systems showed high susceptibility towards hydrolysis even under mild conditions. However, attempts at controlling the hydrolysis process by limiting debonding to activation from external triggers were not successful. Finally, a 4-vinylphenol derivative, 4-methoxy styrene, was incorporated into a final prototype formulation based on vinyl ether-functionalized hemiacetal ester prepolymers. 4-MeOS significantly increases adhesion, as intended, and therefore it is an interesting compound for future formulation approaches in cationic systems. However, material degradation by hydrolysis was observed under mild conditions similar to previous findings arising from the utilized hemiacetal ester prepolymers. These results imply a high potential for hemiacetal ester-based formulations for adhesives with debonding by hydrolysis features. Yet, more research must be conducted to increase storage stability after curing and limit material degradation to hydrolysis triggered by external activation. Possible approaches are the utilization of water-scavenging additives or a change in initiation to radical mechanisms.

Biobased 4-vinylphenol derivatives in adhesive systems

The ionic polymerizable 4VP derivative sodium styrene sulfate was successfully synthesized. Discoloration and changes in solubility over time were observed and aging tests monitored via NMR and infrared spectroscopy were conducted. In solid state, the sulfate group is hydrolyzed by water from the surrounding air and the resulting sodium bisulfate initiates cationic self-polymerization of the vinyl groups. After 100 days of storage in an open container at room temperature, the process is finished with poly(4-vinylphenol) as the main product. Sodium styrene sulfate can be stabilized by storing it in solution, e.g. in methanol, or by a cation exchange. Sodium was substituted with tetrabutyl ammonium which does not only enhance storage stability but also increases miscibility of the ionic monomer with other reactive organic media like acrylates. This marks an important step in the utilization of styrene sulfate in potential application systems. The cationic and radical polymerization kinetics of tetrabutyl ammonium styrene sulfate were analyzed and compared to the common and structurally similar monomer styrene. Higher activity and conversion of TBASS compared to styrene was found in radical polymerization, most likely due to a decrease in termination reaction rates. In contrast, TBASS hardly undergoes cationic polymerization which results from a decrease in electron density of the vinyl group induced by electronic effects of the sulfate substituent.

As a consequence, TBASS was tested as a comonomer in two acrylate-based adhesive systems with radical curing mechanisms. Both approaches aimed at replacing inert ionic liquids, which can decrease cohesion, in conductive materials with the ionic comonomer and thus increasing adhesive performance while maintaining ionic conductivity. By substituting a polymerizable ionic liquid, styrene sulfonate, with TBASS in a formulation with electrochemical debonding features, the curing process is strongly impaired. If an inert ionic liquid is replaced by TBASS in a similar formulation, polymerization inhibition is also observed but to a lesser extent. Yet, an adhesive with considerable adhesive strength was developed which responds with a massive decrease in lap shear strength to the application of voltage. Hence, the potential of TBASS in adhesive systems with electrochemical debonding features was demonstrated as proof-of-concept. The inhibition of radical polymerization can be caused by initiation by a peroxide initiator BPO opposed to the azo-initiator AIBN utilized in kinetic experiments. However, deeper investigations must be carried out to confirm this hypothesis, e.g. via kinetic experiments with various radical initiators. From there, TBASS can be used in suitable reactive formulations to develop novel adhesive systems with electrochemical debonding features.

Moreover, TBASS was copolymerized with (meth)acrylates, to prepare a pressure sensitive adhesive. In the azo-initiated reaction, no inhibition of the radical polymerization was observed as determined via gas chromatography and copolymerization of styrene sulfate with acrylate monomers was confirmed in DOSY NMR experiments. The effect of the ionic comonomer on conductivity, material and adhesive properties was investigated for different TBASS concentrations. Surprisingly, no changes in T_g depending on the concentration of the ionic monomer was observed in rheometric measurements, but a softening of the material at high temperatures with increasing styrene sulfate content. The desired increase in ionic conductivity was achieved as a decrease in resistivity by two magnitudes was observed in impedance measurements when copolymerizing only 0.5 wt% of TBASS. Ionic conductivity is further increased but in a flattened manner with increasing styrene sulfate concentration. Yet, the addition of inert ionic liquid results in a more intense rise in conductivity which masks any impact caused by TBASS. Remarkably, the addition of styrene sulfate does not only prevent a decrease in adhesive performance but intrinsically increases it. An increase in peel strength was observed with increasing styrene sulfate concentration, most prominently on steel substrates, independent from ionic liquid addition. Moreover, an interesting synergetic effect was observed between styrene sulfate and the inert ionic liquid. Maximum peel strength was reached after a short period of time if w (TBASS) ≥ 5 wt% and an ionic liquid was added. Thus, the wetting process is significantly accelerated by this effect which likely results from an expansion of the polymer coils and consequently higher mobility of the polymer chains with lower entanglement densities. Although the effect of the utilized amounts of TBASS on ionic conductivity cannot compete with an inert ionic liquid, significant increases in conductivity were demonstrated by incorporation of the ionic monomer into an acrylate-based pressure sensitive adhesive. Furthermore, TBASS does not only not impair adhesive performance but increases peel strength, especially on steel, and is able to accelerate substrate wetting. As a consequence, a patent was filed on the use of TBASS in pressure sensitive adhesives. In subsequent research approaches, higher concentrations of the ionic comonomer can be used to investigate the full potential and limitations of its use in this particular adhesive system in terms of conductivity and adhesive performance.

5 Methods and Materials

5.1 Materials

Methanol (EMPLURA, Supelco), acetonitrile (≥ 99.9 %) and dichloromethane (DCM, UniSolv, Supelco) were purchased from VWR. Dimethyl sulfoxide(DMSO, ≥ 99.5 %), chloroform (anhydrous, ≥ 99 %), methanol (anhydrous, ≥ 99.8 %) and dimethyl formamide (DMF, anhydrous, ≥ 99 %) were purchased from Sigma-Aldrich. Propylene carbonate (≥ 99.0 %) was acquired from Merck.

Omnicat 440, Omnirad ITX, Omnirad 184 and Omnirad BMS were provided by IGM Resins. K-Pure CXC was provided by King Industries. Sylanto 7MS was provided by Synthos. Boron trifluoride diethyl etherate (BTFE, for synthesis), 2,2'-azobis(2-methylprpionitrile) (AIBN, ≥ 98 %), benzoyl peroxide (BPO, with 25 wt% H_2O, for synthesis), $Al(acac)_3$ (≥ 99 %) and tris(trimethylsilyl)silane (TTMSS, ≥ 97 %) were acquired from Sigma-Aldrich. Anthracure UVS-1331 was provided by Kawasaki Kasei Chemicals Ltd.

1-hexyl-3-methylimidazolium styrene sulfonate (PIL-1), 1-vinyl-3-methylimidazolium bistriflimide (PIL-2), 1-butyl-3-methylimidazolium bistriflimide (IL-1) and 1-ethyl-3-methylimidazolium triflate (IL-2) were acquired from IoLiTec.

2-Hydroxy ethyl acrylate (2-HEA), methyl methacrylate (MMA), 2-ethylhexyl acrylate (2-EHA) and n-butyl acrylate (BA) were provided by the Henkel production site in Antwerpen with a purity of ≥ 98 %.

Sulfur trioxide trimethylamine complex (≥ 99 %), dimethyl terephthalate (≥ 99 %, recrystallized from acetonitrile prior to use), poly(4-vinylphenol) (M_w ≈ 25000 Da), phenol (≥ 99.0 %), tetrabutylammonium hydroxide solution (40 wt% in H_2O), dibutylamine (≥ 98 %), sodium hydrogen sulfate monohydrate (≥ 99 %) and sodium hydroxide (pellets, EMPLURA) were acquired from Sigma-Aldrich. Styrene (GPR Rectapur) was purchased from VWR. 3-mercaptopropyl trimethoxysilane (Dynasylan MTMO) was acquired from Evonik Industries.

4-hydroxybutyl vinyl ether (HBVE), 1,4-cyclohexanedimethanol divinyl ether (CDVE), di(ethylene glycol) divinyl ether (DEGDVE), tri(ethylene glycol) divinyl ether (TEGDVE), cylcohexyl vinyl ether (CVE) and 1,4-butanediol divinyl ether (BDVE) were provided by BASF SE. Tris[2-(3-mercaptopropionyloxy) ethyl] isocyanurate (THIOCURE TEMPIC) and pentaerythritol tetra(3-mercaptopropionate) (THIOCURE PETMP) were acquired from Thiochem/Bruno Bock GmbH. 4-methoxy styrene (4-MeOS) was purchased from Sigma-Aldrich, 4-vinylphenol (4VP, for synthesis) was provided by Sumitomo Chemicals.

Wacker HDK 21 was provided by Wacker Chemie AG, Denka FB 35 was provided by Denka Company Ltd.. HeBoFill 490 was provided by Henze BNP. BAK 40 was provided by Ya'an Bestry Performance Materials corp. Martoxid TM-2250 was provided by Huber Materials. $BaSO_4$ was provided by Sachtleben Minerals GmbH.

Cyclohexane carboxylic acid (98 %), cyclohexyl isocyanate (≥ 98 %) was purchased from Sigma-Aldrich. Toluene diisocyanate (TDI, Unate T-100) was acquired from Umax Chemicals. Polyether polyol Velvetol H2700 was provided by Allessa GmbH. Pentamethylene diisocyanate trimer Desmodur eco N7300 and 4,4'-methylene diphenyl diisocyanate (MDI, Desmodur 44 MC Flakes) were acquired from Evonik Industries. Isophthalic acid (≥ 99 %) was purchased from ThermoFisher Scientific. succinic acid (Biosuccinium) was provided by Roquette. Citric acid (anhydrous, ≥ 99 %) was acquired from Brenntag.

The substrates used for testing of adhesive and debonding properties are aluminum alloy 7075 (80 mm x 25 mm x 2,0 mm), steel type DD11 (80 mm x 25 mm x 2,0 mm), polypropylene (PP, 80 mm x 25 mm x 4,0 mm), polyamide 6 (PA, 80 mm x 25 mm x 4,0 mm), acrylonitrile butadiene styrene (ABS, 80 mm x 25 mm x 4,0 mm), polycarbonate (PC, 80 mm x 25 mm x 4,0 mm) and poly(methyl methacrylate) (PMMA, 80 mm x 25 mm x 4,0 mm).

5.2 Syntheses and polymerizations

Preparation of difunctional polyether urethane prepolymer PU-2. The reaction was carried out in a three-necked flask with a reflux condenser and an overhead stirrer. The stoichiometry of the polyol polyether Velvetol H2700 and 4,4'-methylene diphenyl diisocyanate (4,4-MDI) was calculated for isocyanate end functionalization, i.e. a ratio of $\frac{\mathrm{NCO}}{\mathrm{OH}} = \frac{2.10}{1}$. The diol prepolymer was dried under decreased pressure at 80 °C for an hour before adding the isocyanate. The reaction was carried out under nitrogen atmosphere at 80 °C in the flask and its progress was tracked by NCO content titration. After the first reaction was completed, 4-Hydroxybutyl vinyl ether (HBVE) was added for end functionalization of the polymer chains with $\frac{\mathrm{OH}}{\mathrm{NCO}} = \frac{1.10}{1}$. The reaction was considered finished when an NCO value < 0.1 % was determined.

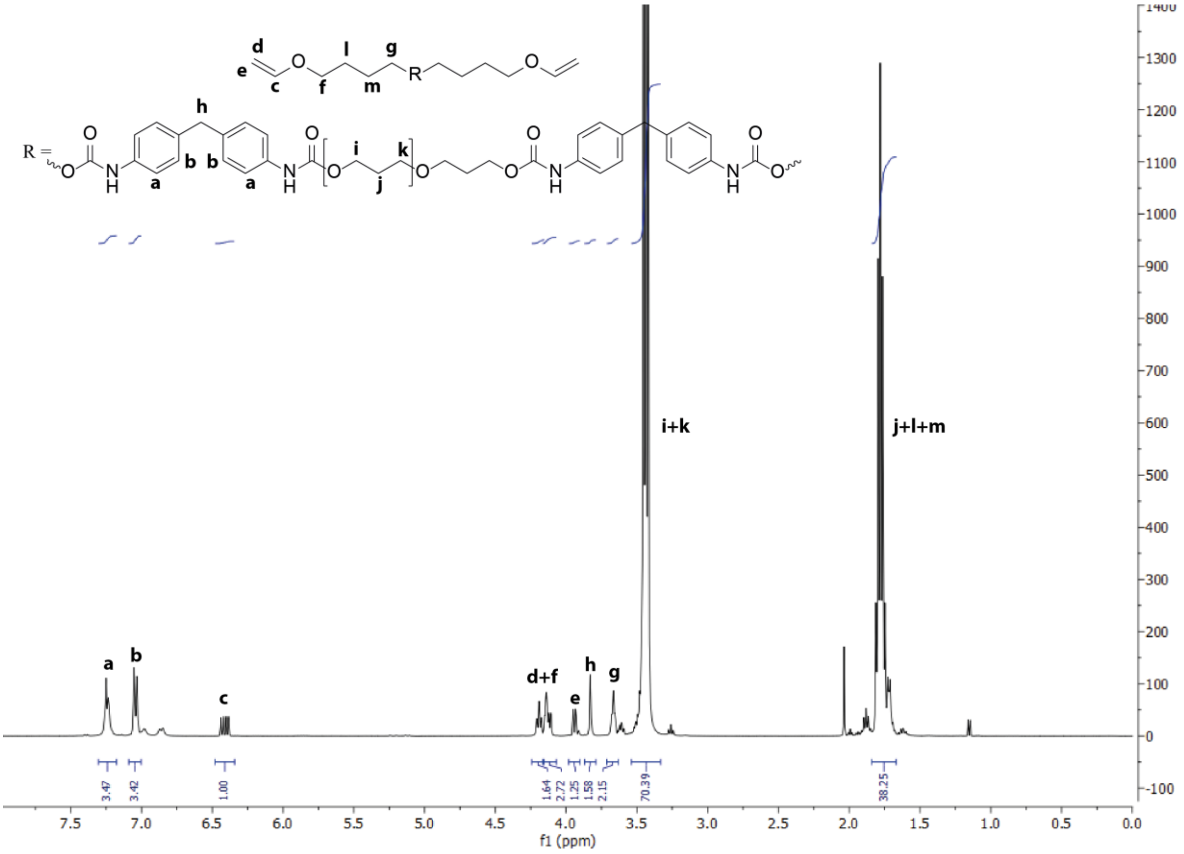

Figure 5.1: ^{1}H NMR spectrum of difunctional polyether urethane prepolymer PU-2 in $CDCl_3$. There are small unidentified peaks which result from common impurities in isocyanate compounds and side products from urethane synthesis. No peaks were observed above 7.5 ppm.

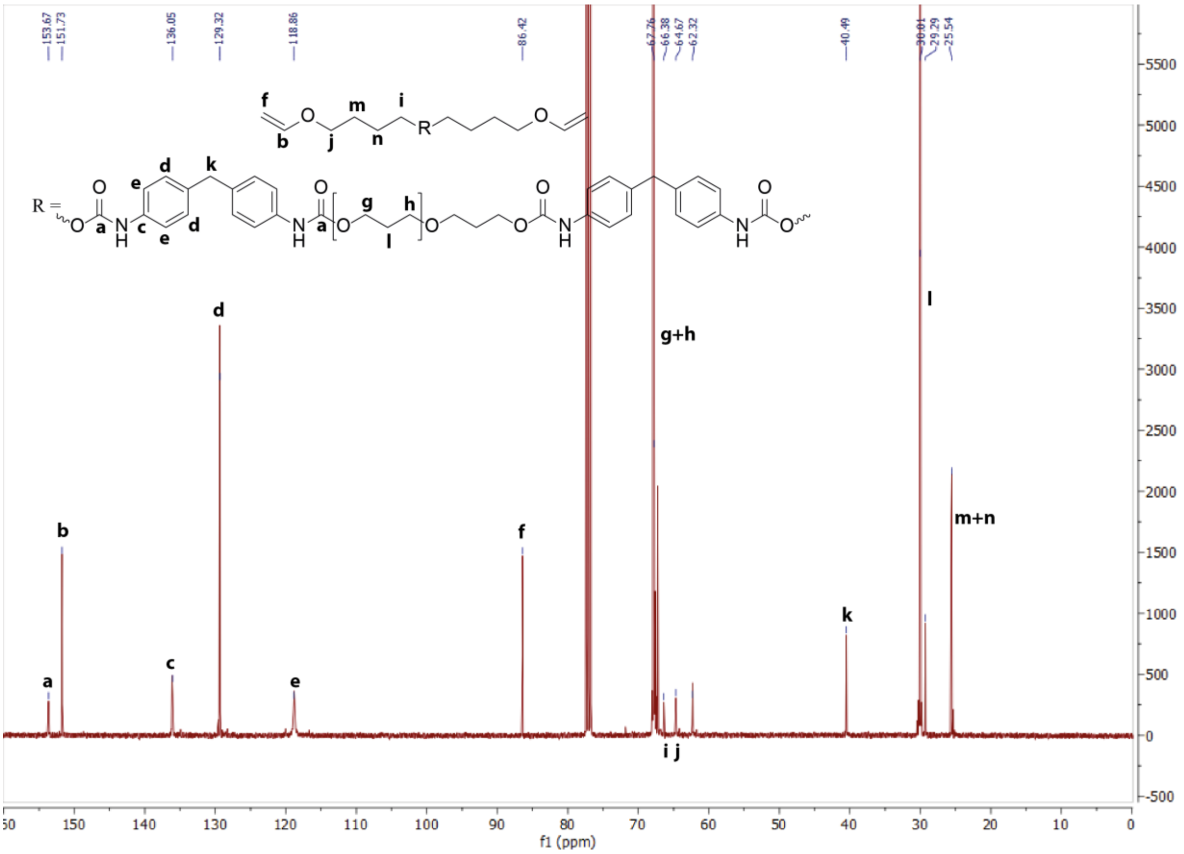

Figure 5.2: ^{13}C-NMR spectrum of difunctional polyether urethane prepolymer PU-2 in CDCl$_3$. There are small unidentified peaks which result from common impurities in isocyanate compounds and side products from urethane synthesis. No peaks were observed above 160 ppm.

Preparation of urethane macromolecular crosslinker PU-3a/b. The reaction was carried out in a three-necked flask with a reflux condenser and an overhead stirrer. The stoichiometry of the pentamethylene diisocyanate trimer Desmodur eco N7300 and 4-Hydroxybutyl vinyl ether (HBVE) was calculated **a)** for vinyl ether end functionalization, i.e. a ratio of $\frac{\mathrm{OH}}{\mathrm{NCO}} = \frac{1.10}{1}$ or **b)** for 33 % vinyl ether end functionalization, i.e. a ratio of $\frac{\mathrm{OH}}{\mathrm{NCO}} = \frac{1}{3}$. The reaction was carried out under nitrogen atmosphere at 80 °C and its progress was tracked by NCO content titration. The reaction was considered finished when **a)** an NCO value < 0.1 % or **b)** an NCO value ≈ 12.9 % was determined.

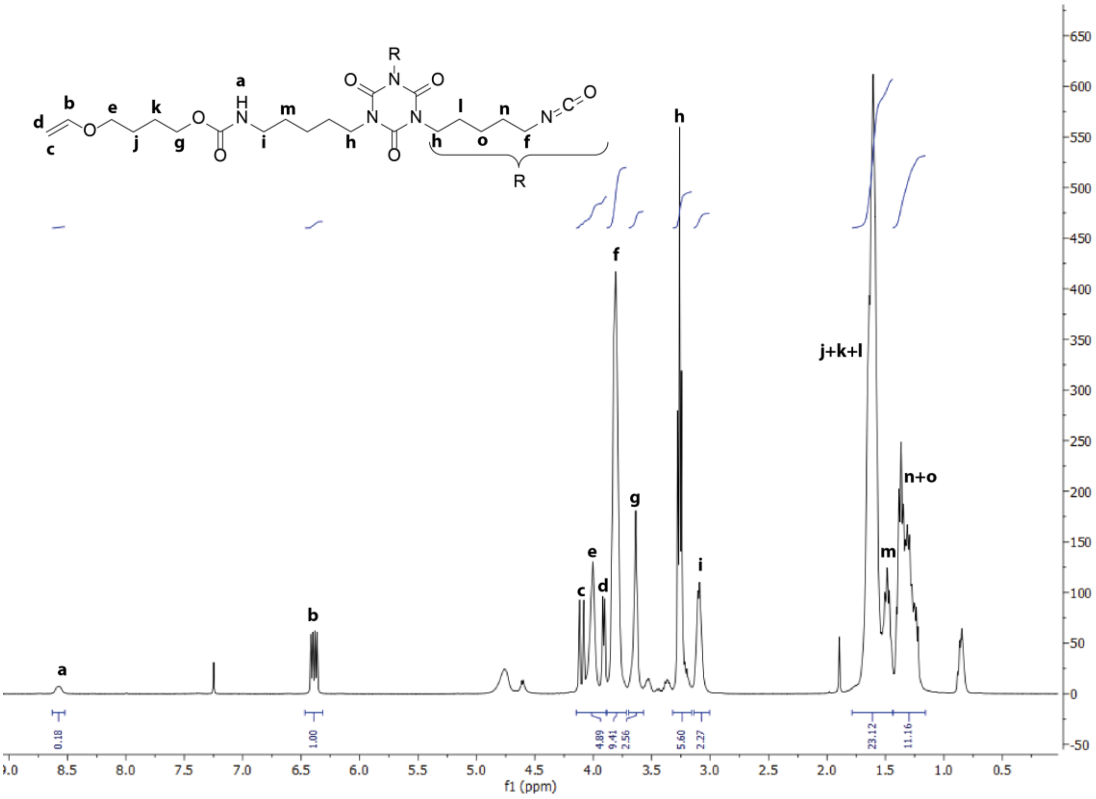

Figure 5.3: ^{1}H NMR spectrum of difunctional polyether urethane macromolecular crosslinker PU-3b in $CDCl_3$. The ratio of reacted to unreacted isocyanate is given by the integral ratio i/f. There are small unidentified peaks which result from common impurities in isocyanate compounds and side products from urethane synthesis.

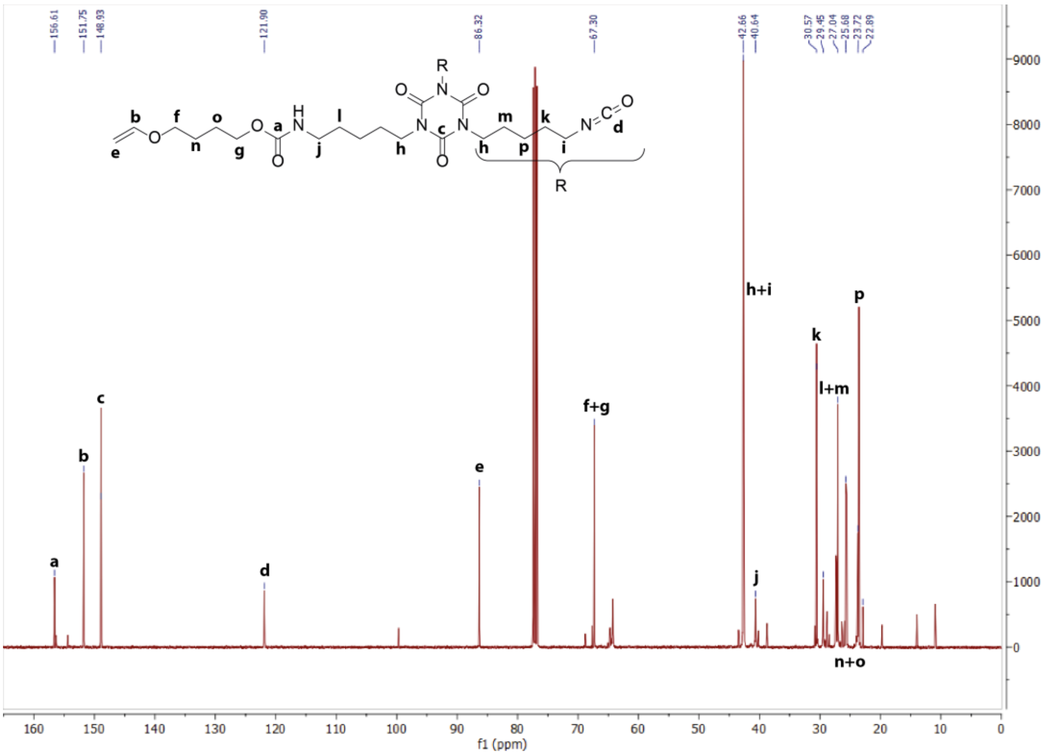

Figure 5.4: ^{13}C NMR spectrum of difunctional polyether urethane macromolecular crosslinker PU-3b in $CDCl_3$. There are small unidentified peaks which result from common impurities in isocyanate compounds and side products from urethane synthesis.

General preparation of difunctional hemiacetal ester prepolymers. The reactions were carried out in a three-necked flask with a reflux condenser and an overhead stirrer. The stoichiometries of dicarboxylic acid and divinyl ether were calculated for $\frac{n(\mathrm{VE})}{n(\mathrm{COOH})} = 1.2$. The reaction was carried out at 90 °C oil bath temperature while stirring at 200 RPM for about 3 hours.

Preparation of difunctional hemiacetal ester prepolymer PHAE-2. The reaction was carried out in a three-necked flask with a reflux condenser and an overhead stirrer. The stoichiometry of succinic acid and 1,4-cyclohexane dimethanol divinyl ether was calculated for $\frac{n(\mathrm{VE})}{n(\mathrm{COOH})} = 1.2$. The reaction was carried out at 100 °C oil bath temperature while stirring at 200 RPM for 5 hours. Molecular weight was determined by GPC with $M_{n,1} \approx 2300$ Da and ^{1}H NMR spectroscopy with $M_{n,2} \approx 1500$ Da.

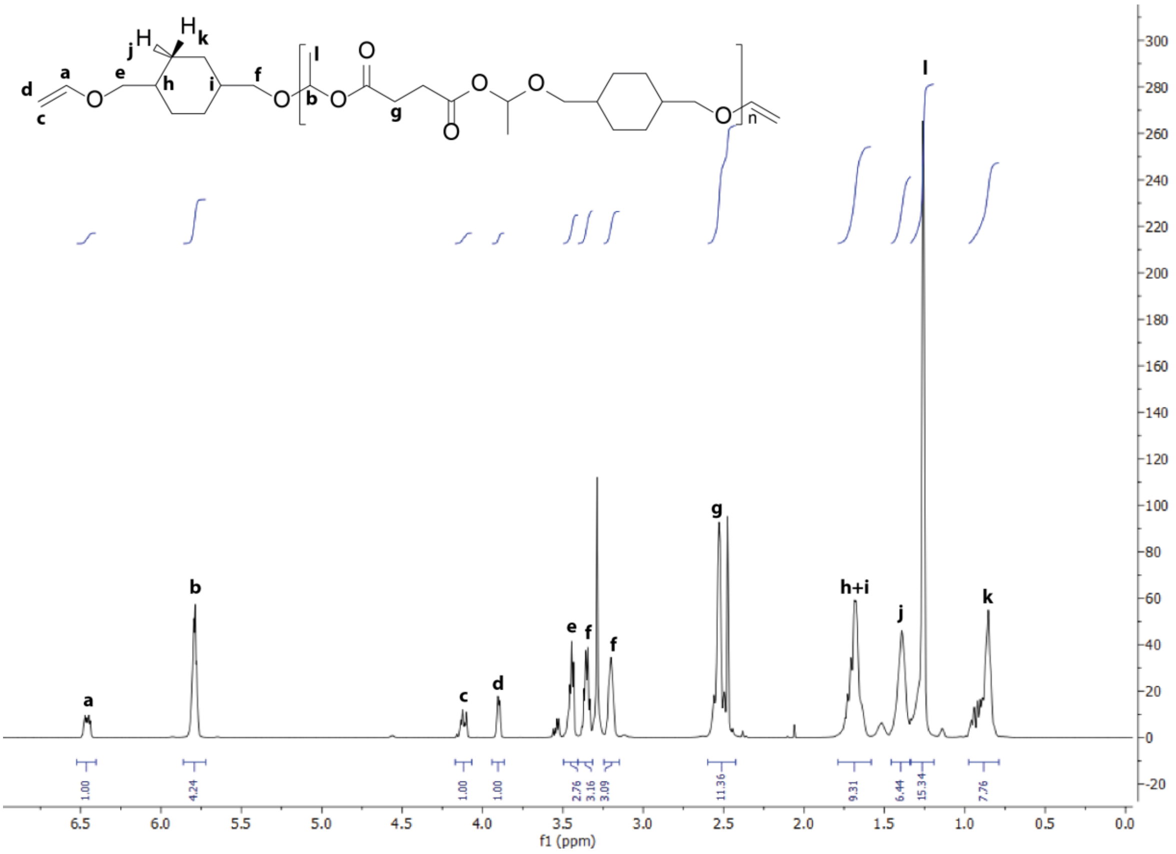

Figure 5.5: ^{1}H NMR spectrum of difunctional hemiacetal ester prepolymer PHAE-2 in DMSO-d$_6$. The most important proton signals of the structure are labeled. The molecular weight distribution value M_n can be calculated from the integral ratio a/b. The labels j and k correspond to the differently shifted protons of the cyclohexyl ring due to its chair conformation.

Preparation of difunctional hemiacetal ester macromolecular crosslinker PHAE-4. The reaction was carried out in a three-necked flask with a reflux condenser and an overhead stirrer. All glass ware was dried in the oven at T = 120 °C under reduced pressure over night. The setup was assembled while constantly flushing with nitrogen. Citric acid was dried at RT and reduced pressure over night. 1,4-butanediol divinyl ether (BDVE) was dried by storing it under molecular sieve (4 Å). The stoichiometry of the reactants was calculated for $\frac{n(\mathrm{VE})}{n(\mathrm{COOH})} = 1.2$ and the reactants were added while sustaining a dry environment in the flask. The reaction was carried out at 100 °C oil bath temperature while stirring at 200 RPM for 2.5 hours. Conversion of citric acid was determined via ^{1}H NMR spectroscopy with a typical value of $X \approx 80$ %. Small amounts of unreacted BDVE were found.

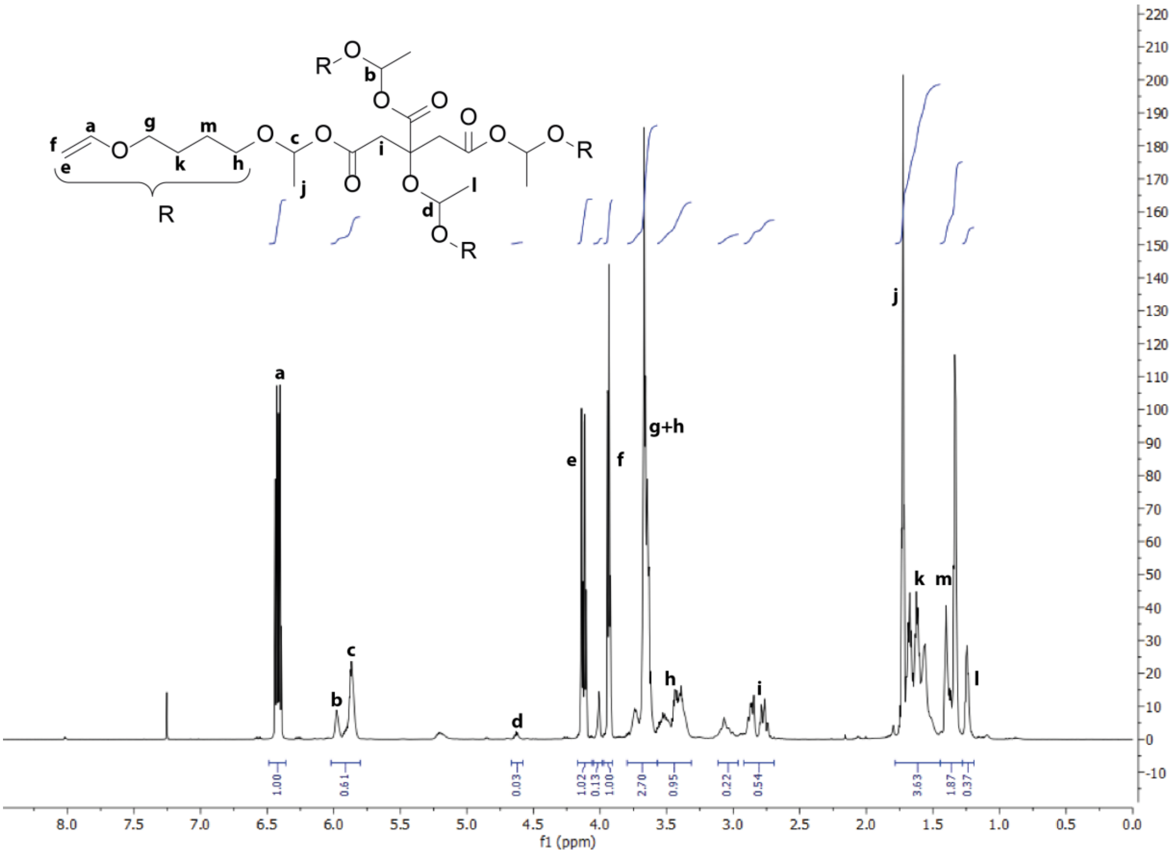

Figure 5.6: ^{1}H NMR spectrum of difunctional hemiacetal ester prepolymer PHAE-2 in CDCl$_3$. Conversion X can be calculated from the integral ratio (b+c+d)/i. There are many slightly shifted and overlapping signals as the final product is a mixture of product and unreacted substrates. Although there is unreacted present, no carboxylic acid proton peaks were found above 8 ppm.

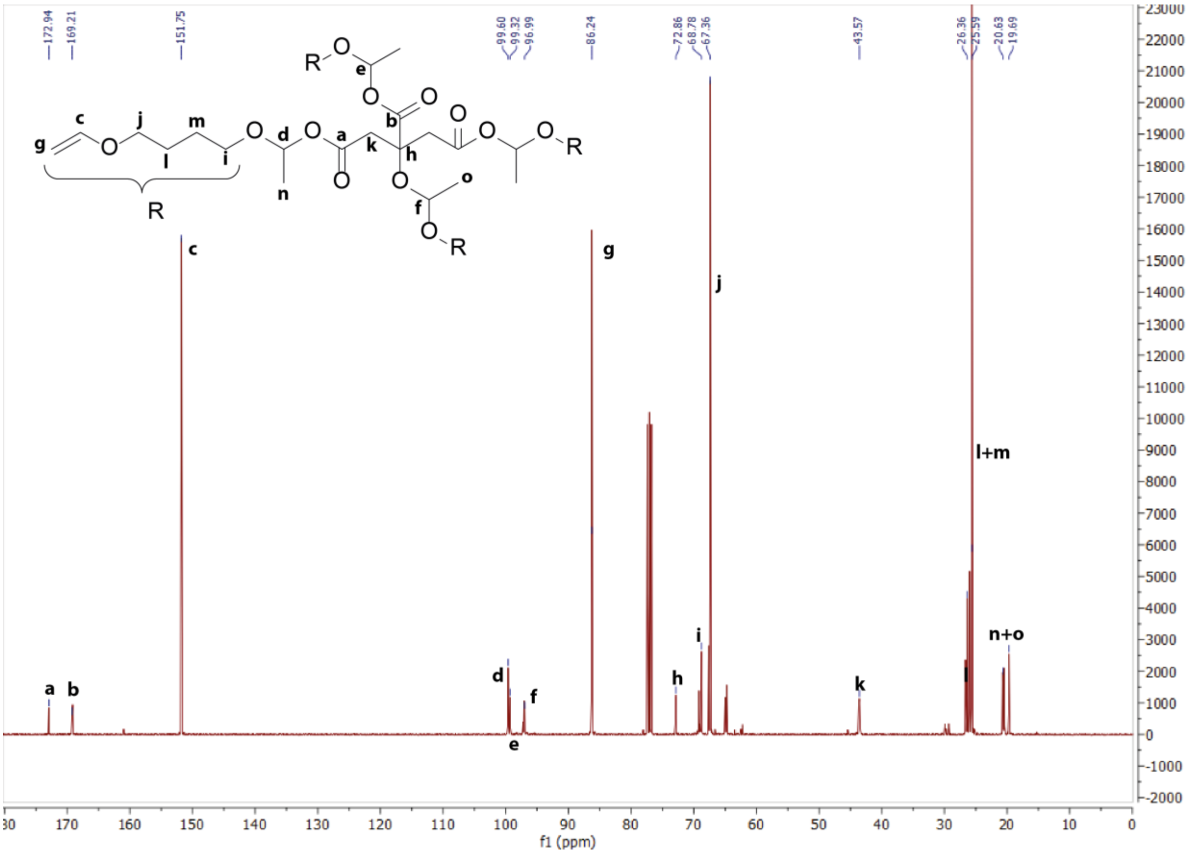

Figure 5.7: ^{13}C NMR spectrum of difunctional hemiacetal ester prepolymer PHAE-2 in CDCl$_3$. There are many slightly shifted and overlapping signals as the final product is a mixture of product and unreacted substrates.

Preparation of 1-(4-(vinyloxy)butoxy)ethyl cyclohexanecarboxylate (HAE-1). Butanediol divinyl ether (BDVE, 6.10 g, 42.9 mmol) was dried over molecular sieve before the reaction and weighed into a three-necked flask. Cyclohexanecarboxylic acid (CHCA, 5.0 g, 39 mmol) was added while constantly flushing with nitrogen. The stoichiometry of the reactants was calculated for $\frac{n(\mathrm{BDVE})}{n(\mathrm{CHCA})} = 1.05$. The flask was equipped with an overhead stirrer, and a reflux condenser. The reaction mixture was stirred at 250 RPM and kept under nitrogen atmosphere. The reaction is finished after 5 h at 120 °C oil bath temperature.

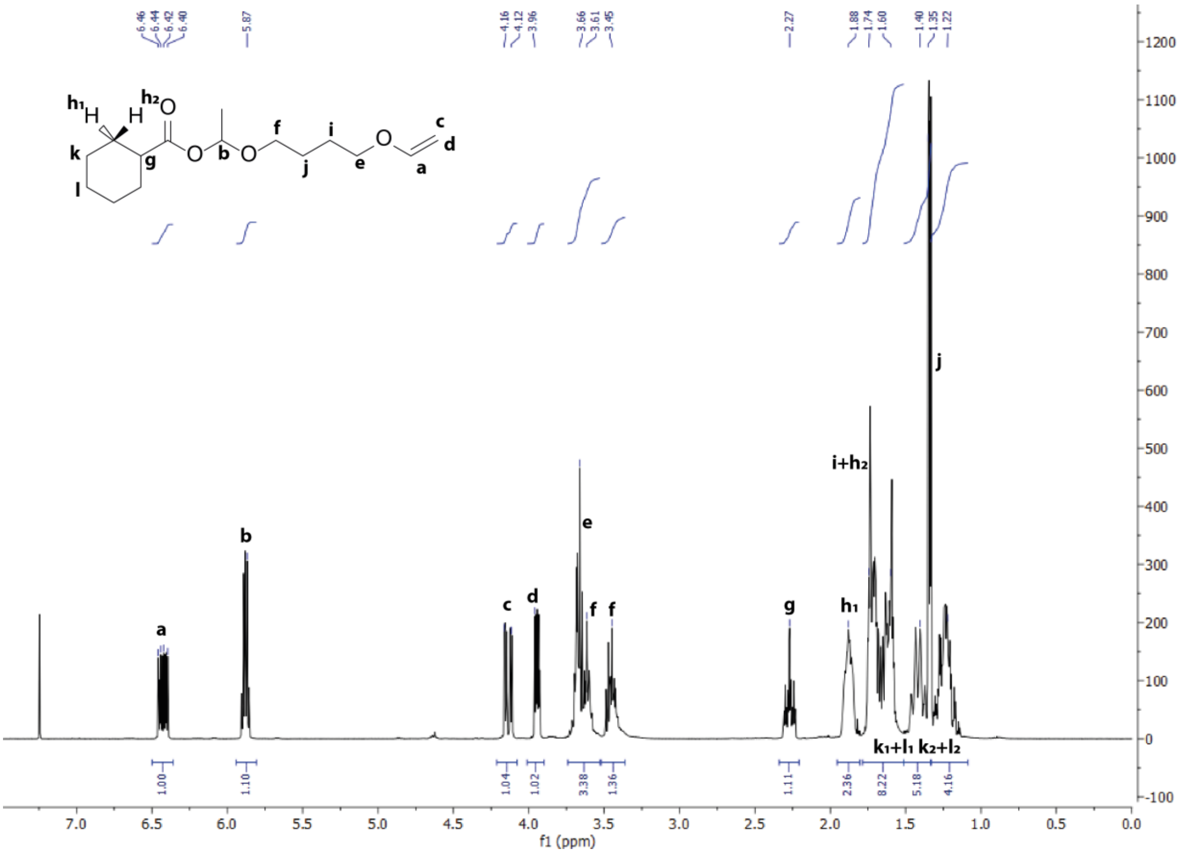

Figure 5.8: ^{1}H-NMR spectrum of vinyl ether-functionalized hemiacetal ester HAE-1 in $CDCl_3$. No peaks were observed above 7.5 ppm.

Preparation of bis(1-(4-vinlyoxy)butoxy)ethyl) isophthalate (HAE-2). Butanediol divinyl ether (BDVE, 18.0 g, 126 mmol) was dried over molecular sieve before the reaction and weighed into a three-necked flask. Isophthalic acid (IA, 10.0 g, 60.2 mmol) was added while constantly flushing with nitrogen. The stoichiometry of the reactants was calculated for $\frac{n(\mathrm{BDVE})}{n(\mathrm{IA})} = 2.1$. The flask was equipped with an overhead stirrer, and a reflux condenser. The reaction mixture was stirred at 250 RPM and kept under nitrogen atmosphere. The reaction is finished after 8 h at 120 °C oil bath temperature.

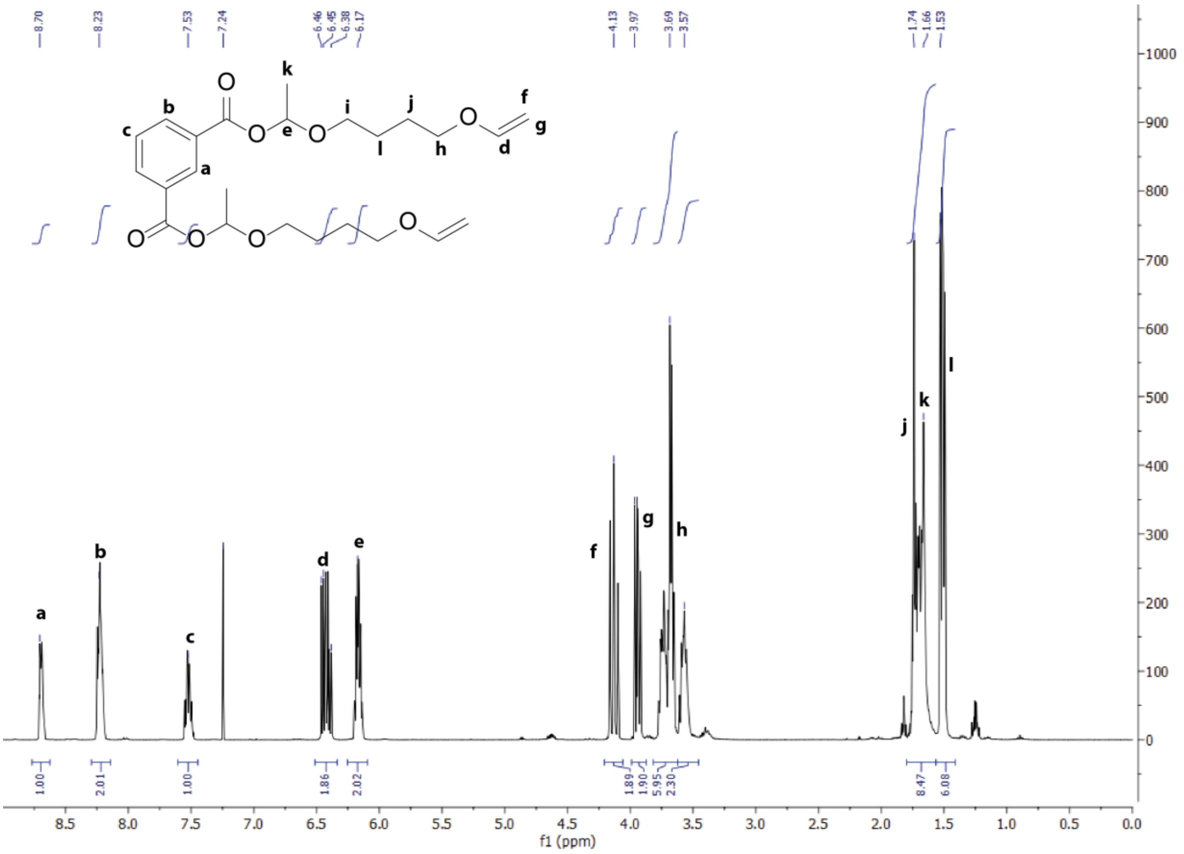

Figure 5.9: ^{1}H-NMR spectrum of vinyl ether-functionalized hemiacetal ester HAE-2 in $CDCl_3$. No peaks were observed above 9 ppm.

Preparation of 4-(vinyloxy)butyl cyclohexylcarbamate (U-1). 4-Hydroxybutyl vinyl ether (HBVE, 5.10 g, 43.9 mmol) was dried over molecular sieve before the reaction and weighed into a three-necked flask and cyclohexane isocyanate (CHI, 5.0 g, 40 mmol) was added while constantly flushing with nitrogen. The stoichiometry of the reactants was calculated for $\frac{n(\mathrm{HBVE})}{n(\mathrm{CHI})} = 1.05$. The flask was equipped with an overhead stirrer, and a reflux condenser. The reaction mixture was stirred at 250 RPM and kept under nitrogen atmosphere. The solution was stirred and slowly heated to 80 °C oil bath temperature. The reaction was considered finished when an NCO value < 0.1 % was determined, typically after 8 hours.

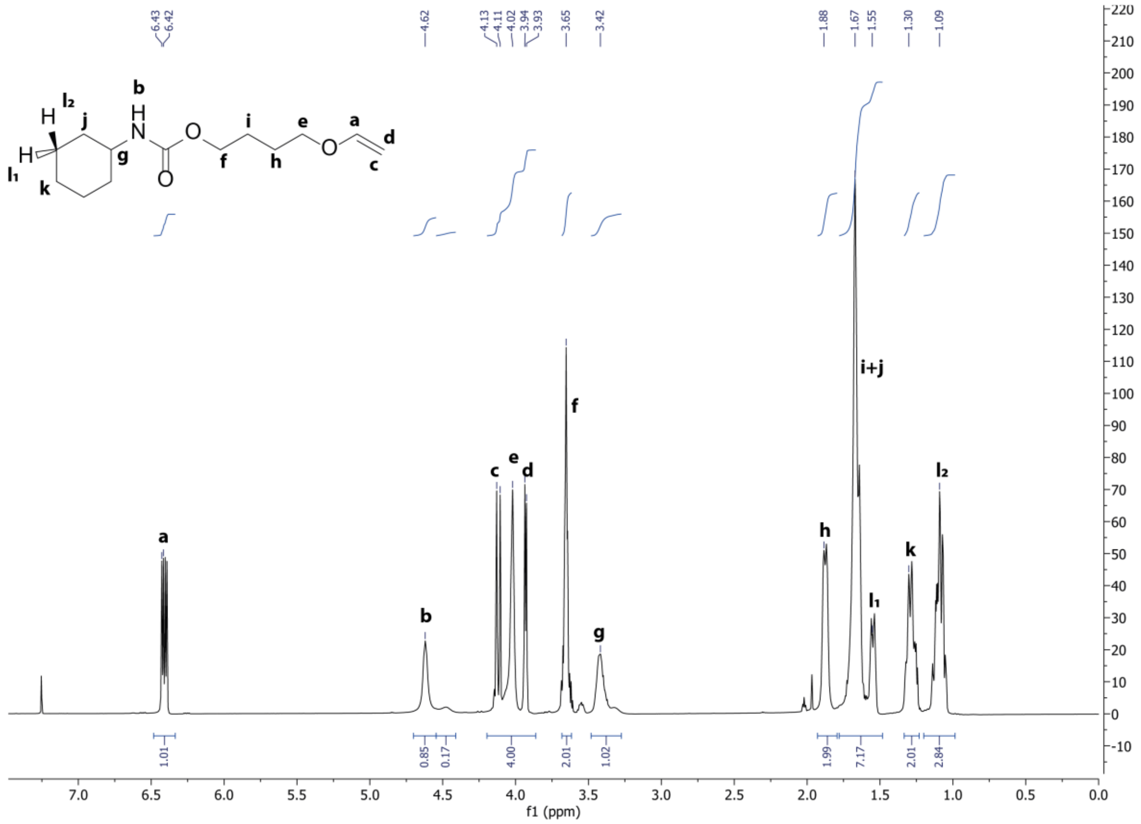

Figure 5.10: ^{1}H-NMR spectrum of vinyl ether-functionalized urethane U-1 in $CDCl_3$. No peaks were observed above 8 ppm.

Preparation of bis(4-vinyloxy)butyl) (4-methyl-1,3-phenylene)dicarbamate (U-2). 4-Hydroxybutyl vinyl ether (HBVE, 7 g, 60.3 mmol) was dried over molecular sieve before the reaction and weighed into a three-necked flask and toluene diisocyanate (TDI, 5 g, 28.7 mmol) was added while constantly flushing with nitrogen. The stoichiometry of the reactants was calculated for $\frac{n(\mathrm{HBVE})}{n(\mathrm{TDI})} = 2.1$. The flask was equipped with an overhead stirrer, and a reflux condenser. The reaction mixture was stirred at 250 RPM, kept under nitrogen atmosphere, and cooled immediately due to much heat generation by the exothermal reaction. Afterwards, the solution was stirred and slowly heated to 80 °C oil bath temperature. The reaction was considered finished when an NCO value < 0.1 % was determined, typically after 4 hours.

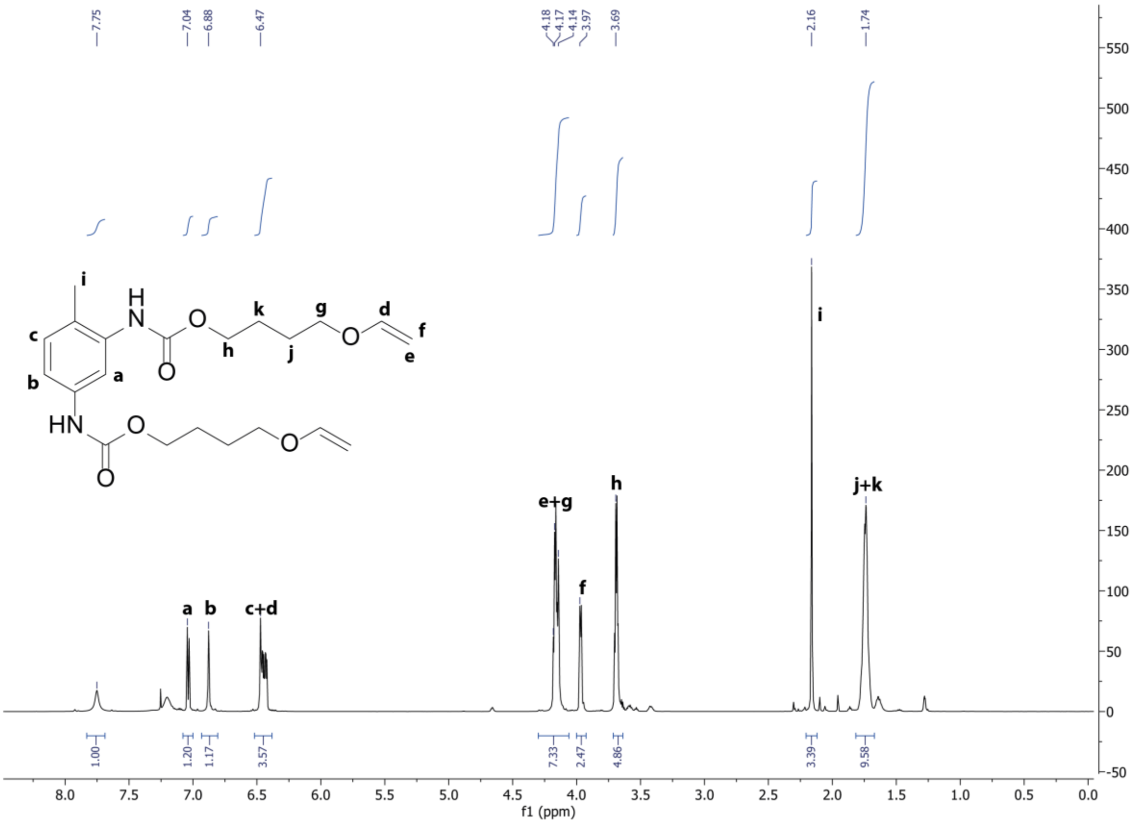

Figure 5.11: ^{1}H-NMR spectrum of vinyl ether-functionalized urethane U-2 in $CDCl_3$. No peaks were observed above 8 ppm.

Preparation of sodium styrene sulfate. The reaction was carried out in a three-necked flask with a reflux condenser and a magnetic stirrer. All glass ware was dried in the oven at T = 120 °C under reduced pressure over night. The setup was assembled while constantly flushing with nitrogen. 4-Vinylphenol (4-VP, 2.85 g, 23.75 mmol) and sulfur trioxide trimethylamine complex (SO_3NMe, 6.61 g, 47.5 mmol, 2.0 eq) were dried for two hours in vacuo at room temperature. The reactants were added to the flask and dissolved in 40 mL of anhydrous DMF. The reaction was stirred at T = 80 °C oil bath temperature for 72 hours. The reaction was cooled down to RT and the solvent was evaporated under reduced pressure. The residue was dissolved in 200 mL of anhydrous methanol and NaOH (dried under reduced pressure, 1.9 g, 47.5 mmol, 2.0 eq) was added. The reaction mixture was stirred for one hour at room temperature. The precipitates were removed by filtration and purified by column chromatography in 95:5 DCM:MeOH to 3:1 DCM:MeOH. The product was dried in vacuo and solidified to an off-white solid. Isolated yield: 67%. ^{1}H-NMR spectra can be found in section 3.2.1.

Preparation of tetrabutylammonium styrene sulfate. The reaction was carried out in a three-necked flask with a reflux condenser and a magnetic stirrer. All glass ware was dried in the oven at T = 120 °C under reduced pressure over night. The setup was assembled while constantly flushing with nitrogen. 4-Vinylphenol (4-VP, 6.0 g, 50,0 mmol) and sulfur trioxide trimethylamine complex (SO_3NMe, 10.5 g, 75.0 mmol, 1.5 eq) were dried for two hours in vacuo at room temperature. The reactants were added to the flask and dissolved in 60 mL of anhydrous DMF. The reaction was stirred at T = 80 °C oil bath temperature for 72 hours. The reaction was cooled down to RT. 1.1 eq of tetrabutylammonium hydroxide (TBA OH, 40 % aqueous solution) was added and stirred for one hour. More water was added, and the solution was extracted 4 times with DCM. The solvent was evaporated and the product was purified by column chromatography in 95:5 DCM:MeOH. The product was dried in vacuo and solidified to an off-white solid. Isolated yield: 60%. ^{1}H-NMR spectra can be found in section 3.2.1.

Preparation of polystyrene for FTIR analysis. The reaction was carried out in a round bottom flask equipped with a reflux condenser. Styrene (5.0g, 48 mmol) and AIBN (0.79 g, 4.8 mmol) were dissolved in 30 mL of DMSO. The solution was stirred at T = 80 °C for 8 hours. The solvent was evaporated and the obtained polymer was analyzed via GPC with $M_w \approx 17000$ Da and $PD = 2.2$.

Preparation of PSA polymer solutions with different styrene sulfate content. Two mixtures, an initial and a feed monomer solution, containing ethyl acetate, 2-ethylhexyl acrylate (2-EHA), methyl methacrylate (MMA), 2-hydroxyethyl acrylate (2-HEA), n-butyl acrylate (BA) and tetrabutylammonium styrene sulfate (TBA SS) were prepared. In addition, two mixtures, an initial and a feed initiator solution, consisting of ethyl acetate and azobisisobutyronitril (AIBN) were weighed out. All mixtures were prepared four times with different compositions, respectively, as shown in Scheme 3.22. Initial batch monomer and initiator solution were filled into a *SYSTAG FlexyCUBE* reactor with a reflux condenser and tubes, connected to a pump, were placed in the feed solutions. The initial reaction solutions were stirred with an overhead stirrer at 250 RPM and heated to 80 °C for 15 minutes. Afterwards, the monomer feed solutions were added over two hours as well as the initiator feed solution over four hours. Thereafter, the mixtures were stirred for another two hours; temperature was set at 80 °C over the whole process. In the last step, the reaction mixture was cooled down to room temperature and a dilution solution, consisting of ethanol, ethyl acetate and isopropanol, was added and the final polymer solution was obtained.

Free radical polymerization of styrene and tetrabutylammonium styrene sulfate (TBA SS). The solvent DMSO was distilled before the reaction for purification. Styrene was freshly distilled two days before polymerization to remove the inhibitor. The flask with the distilled monomer was covered in aluminum foil and stored in the freezer. TBASS was synthesized as described above. AIBN was recrystallized twice from methanol prior to use and stored in the freezer. Solvent, monomer, Dimethyl terephthalate and AIBN were added to a three-necked flask and stirred until a clear solution was obtained. The reaction mixture was prepared with *c* (monomer) =0.50 mol/L and $\frac{c(\text{AIBN})}{c(\text{monomer})} = 0.01$. Three degassing circles were performed before putting the reaction flask, equipped with a reflux condenser and a septum, in a preheated oil bath with *T* = 80 °C. Before samples were taken, the syringes were flushed with the inert gas atmosphere inside the flask two times. The samples were transferred into glass vials. Polymerization was stopped by freezing the sample with liquid nitrogen and storing it in a Dewar vessel with dry ice until NMR analysis was performed.

Living cationic polymerization of styrene and tetrabutylammonium styrene sulfate (TBA SS). The solvent chloroform (anhydrous) was used as received. Styrene was freshly distilled two days before polymerization. The flask with the distilled monomer was covered in aluminum foil and stored in the freezer under molecular sieve. TBASS was synthesized as described above. The reaction was carried out in a Schlenk-flask, equipped with a septum. All glass ware and magnetic stirrers were dried in the oven at T = 120 °C under reduced pressure over night. The reaction mixture was prepared with *c* (monomer) =0.50 mol/L and added under nitrogen atmosphere. Afterwards, Dimethyl terephthalate was added and dissolved. The solution was cooled to T = 0 °C and the initiator was added with $\frac{c(\text{BTFE})}{c(\text{monomer})} = 0.05$. Before samples were taken, the syringes were flushed with the inert gas atmosphere inside the flask two times. The samples were transferred into glass vials filled with a solution of dibutylamine in chloroform for quenching. The samples were stored in the freezer at T = -18 °C until NMR analysis was performed.

Curing of cationic adhesives with photoinitiators. To reduce the water content, a small amount of p-toluenesulfonyl isocyanate was added to all adhesive formulations with cationic curing mechanism. The crude specimens or adhesive joints were irradiated by an LED with λ = 405 nm for 20 seconds, followed by thermal postcuring for 45 minutes at 80 °C. Crude specimens for DMA and stress-strain analysis were cured on level three and specimens for single-lap shear testing were cured on level one (s. Table 5.1).

Table 5.1: Irradiance E_{ir} and radiant exposure H_e with 10 seconds of irradiation on the first (LED 1) and third (LED 3) level of the LED setup and in the UV chamber in mW/cm^2 3: 10s 397 mW/cm2 & 3658 mJ/cm2; 1: 10s 775 mW/cm2 & 7009 mJ/cm2.

	E_{ir} [mW/cm^2]	H_e [mJ/cm^2]
LED 1	775	7009
LED 3	397	3658
UV	87	

Curing of cationic adhesives with thermal initiators. All adhesive formulations with cationic thermal curing mechanisms were polymerized by placing the respective material in an oven at T = 100 °C for 45 minutes.

Radical curing of adhesives with electrochemical debonding properties. All adhesive formulations tested for electrochemical debonding properties were cured by placing the respective adhesive joints in an oven at T = 80 °C for 15 minutes and subsequently at T = 120 °C for 30 minutes for postcuring.

Preparation of PSA films. The PSA films for property testing were prepared by applying the respective polymer solution on an etched polyethylene foil which was grounded with vacuum pump on an *elcometer 4340 Automatic Film Applicator*. Film thickness was adjusted to obtain films with a coating weight ρ_A of 30g/m^2. Calculation was based on data obtained from prior solid content determination experiments. After application, the film was dried in an oven at 115 °C for 5 min and covered with silicone paper.

5.3 Analytical methods

NCO titration. First, the blank value was determined via titration. Three drops of a bromophenol blue–methanol solution were added to 50 mL of acetone. The solution was titrated with hydrochloric acid (c =0.1 mol/L) until a change in color from blue to yellow was observed and the used volume $V_{NCO,a}$ of hydrochloric acid was noted. A sample with $m_{sample} \approx 0.3$ g was taken from of the reaction mixture and dissolved in 50 mL acetone. Three drops of a bromophenol blue–methanol solution were added and the solution was stirred. It was titrated with hydrochloric acid (c = 0.1 mol/L) until a change in color from blue to yellow was observed and the used volume $V_{NCO,b}$ of hydrochloric acid was noted. The NCO value was calculated by using equation(5.1). Titrations were performed manually with a *Witeg Titrex 2000*.

$$\text{NCO value} = \frac{\left(\boldsymbol{V_{NCO,a}} - \boldsymbol{V_{NCO,b}}\right) * \boldsymbol{M}(\textbf{NCO}) * \boldsymbol{c}(\textbf{HCl}) * \textbf{100\%}}{\boldsymbol{m_{sample}}} \tag{5.1}$$

Nuclear magnetic resonance (NMR) spectroscopy. All samples were dissolved in a deuterated solvent and measured with an *Agilent MR400*. ^{1}H spectrums were recorded with v = 400 Hz.

Diffusion Ordered NMR Spectroscopy (DOSY). In DOSY NMR a magnetic pulsed field gradient is applied to the sample as illustrated in Figure 5.12.[249] First, the magnetic spins of all nuclei are aligned on the transverse plane by a 90° pulse followed by application of a magnetic field with a gradient in field strength G_n along the z-axis of the sample tube which causes the previously aligned spins to de-phase depending on their spatial location along the gradient field. This is called the encoding step. Afterwards, the molecules in the sample solution are allowed to diffuse through the tube for a defined diffusion or delay time t_d. A homogeneous 180° pulse is applied to reverse spins without changing the phase of the respective nuclei spins which are then refocused by applying, G_n again. If the nuclei have not diffused along the z axis, the second gradient field application would completely negate spin dephasing. By diffusion along the field gradient, a signal intensity decay is measured on data acquisition. A series of pulse sequences is measured with different field strength gradients and signal attenuation is correlated to t_d. which allows calculation of diffusion coefficient *D* linked to a specific signal in the ^{1}H NMR spectrum. The described method is simplified, most modern techniques use more complicated pulse sequences to allow analyses of macromolecules and increase data resolution.[260]

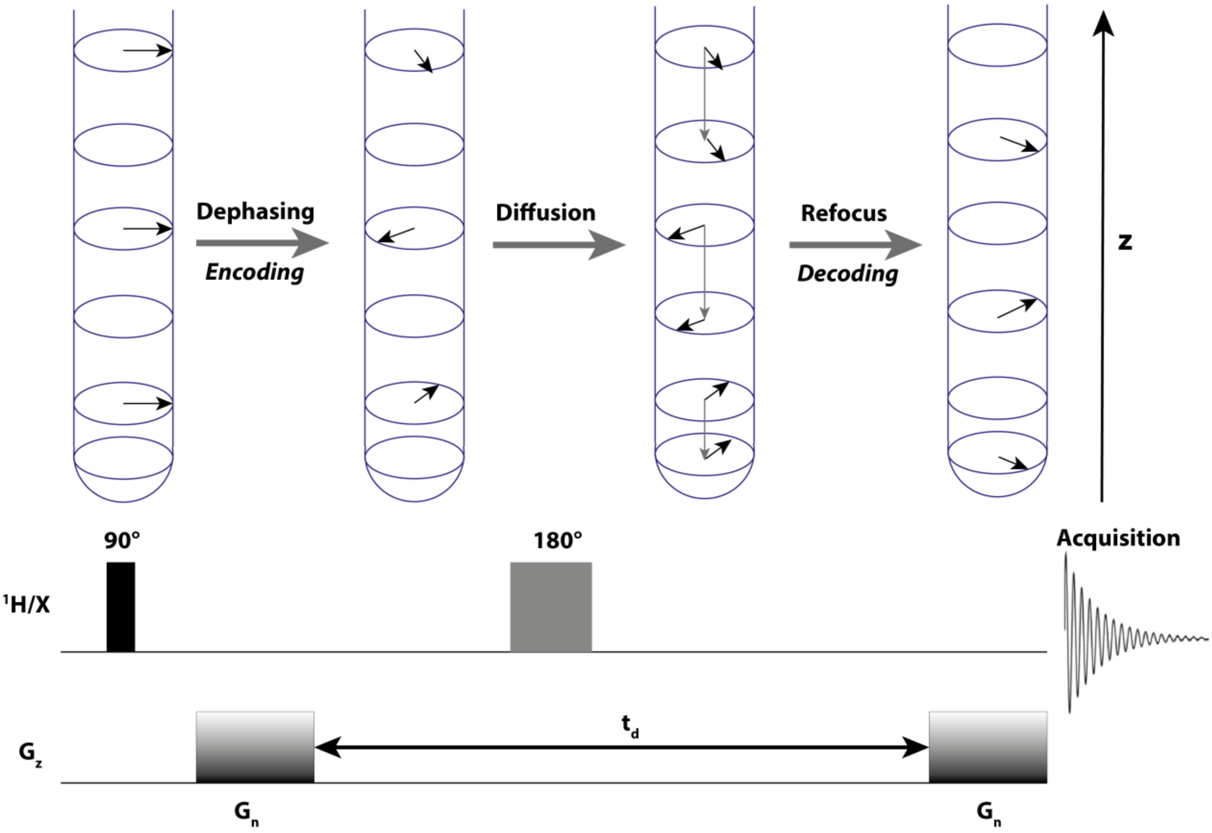

Figure 5.12: Simple pulse sequence using a spin echo in DOSY NMR measurements.

Infrared spectroscopy (IR). IR spectra were recorded with an *FT-IR Alpha* by Bruker with a platinum ATR crystal. Spectral analyses were performed with *OPUS* software by Bruker.

Impedance measurements of PSA films. For each PSA polymer, two 2 x2 cm testing strips were applied to substrates coated with conductive ink *LOCTITE EDAG PF 407C*. The two substrates were then glued with an angle of 180° and impedance measurements at a frequency range $9*10^6$ Hz ≤ v ≤ 0.1 Hz were performed with an *Autolab PGSTAT302N* potentiostat. The resistivity ρ was calculated as shown in equation 1 with the measured impedance Z, overlap area A and layer thickness d.

$$\boldsymbol{\rho = \frac{Z \cdot A}{d}} \qquad \textbf{(5.2)}$$

Impedance measurements of bonded aluminum substrates prior to EDL. The substrates were cleaned with isopropanol beforehand. Then, two substrates were joined and grounded with an initial layer thickness of d_a ≤ 106 µm and an area of A = 100 mm^2 of the adhesive between them. The layer thickness was set by utilizing glass beads. The samples were cured thermally at 80 °C for 15 minutes followed by 30 minutes at 120 °C. After cooling, the impedance was measured as described above.

Electrochemical delamination (EDL) of bonded aluminum substrates. The samples were prepared as described for impedance measurements above. A multimeter was connected to a *EA-PSI 5080-20 A* power supply by Elektro-Automatik. One substrate was linked to the cathode and the other to the anode with alligator clamps. A current with a voltage of 30 V was applied for 20 minutes. Afterwards, the substrates were analyzed in single-lap shear tests.

Gel permeation chromatography (GPC). The samples were dissolved in THF for several hours at 40 °C and eluted in THF on a series of *PLgel MIXED B* columns (polystyrene-divinylbenzene) by Varian at 40 °C. Signals were detected with a *Waters 2414 Refractive Index detector*. This procedure was done for all samples, except for $M_{w,2}$ and PD_2 in section 3.2.4 in which a *PLgel MIXED A* column by Varian was used. Molecular weight distribution values were calculated from calibration with polystyrene standards *EasyCal* by Polymer Laboratories.

Thermal analysis. The most established method to examine the thermal properties of a material is differential scanning calorimetry (DSC). In DSC, a sample is heated and cooled, while the change in heat flow is measured, which gives qualitative and quantitative insight into morphologic changes in the material like glass-transition, crystallization and melting.[261] Morphologic changes cause a transient change in heat flow depending on its free Gibbs energy. The glass-transition temperature T_g of a polymer material indicates crosslinking degree and, possibly, monomer conversion. The experiments in this work were performed with a *TAI Discovery Series* device. DSC samples were placed into a pan which was closed with a lid afterwards. The lid was pierced with a needle before measurement for pressure release. All analyses were performed with a heating rate of 10 K/min and under nitrogen atmosphere. Polymerization enthalpy as well as peak temperature of the corresponding exothermic peaks were calculated by integration via *TA Instruments TRIOS* software.

Stress-strain analysis. Bulk specimens (Figure 5.14a, 40 mm x 3.5 mm x 1 mm) were clamped and stretched, while measuring the occurring forces and elongation.[262] Bulk specimens were prepared by pouring the respective formulation in a Teflon mold. The material was cured depending on its curing mechanism. Analyses were performed with a *Zwick Z050* device, a *XForce HP* (30 kN) measuring cell and *MultiXtens* extensiometer. The specimens were placed in the device automatically by a *UR 5E* robot by *Universal Robots*.

Single-lap shear tests. To investigate adhesive properties, single-lap shear tests were performed (Figure 5.13). The substrates were cleaned with isopropanol beforehand. Then, two substrates were joined and grounded with an initial layer thickness of $d_a \leq 106$ µm and an area of A = 100 mm^2 of the adhesive between them. The layer thickness was set by utilizing glass beads. The adhesive layer was cured depending on its curing mechanism. The adherents were pulled at 10 mm/min. The tensile stress, required to force joining failure, was measured. The tests were performed with a *Zwick Z050* device and a *XForce HP* (30 kN) measuring cell. The specimens were placed in the device automatically by a *UR 5E* robot by *Universal Robots*.

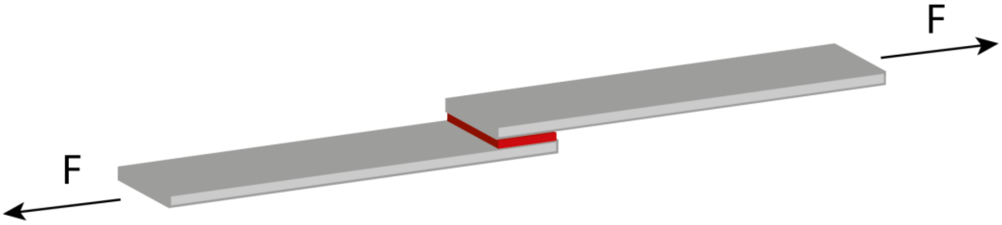

Figure 5.13: Concept of single-lap shear tests. Pulling of a lap-shear sample. The adhesive is colored red.

Dynamic mechanical analysis. Dynamic mechanical analysis (DMA) is a method to determine mechanical and thermal properties of a material at the same time. A bulk sample is exposed to sinusoidal tensile stress and the strain is measured.[262] In these analyses, the viscoelastic properties are observed while altering the temperature. Significant changes in small temperature intervals indicate morphologic changes. The samples were prepared by filling the respective formulation into a Teflon mold (adjustable length, 1 cm wide, 0,4 cm deep) and curing by irradiation from both sides and post-curing for 45 min at 80 °C. The analyses in this work were performed with a *TA Instruments DMA Q800* with a single cantilever clamp, an oscillating strain of 0.1 % and a frequency of 1 Hz.

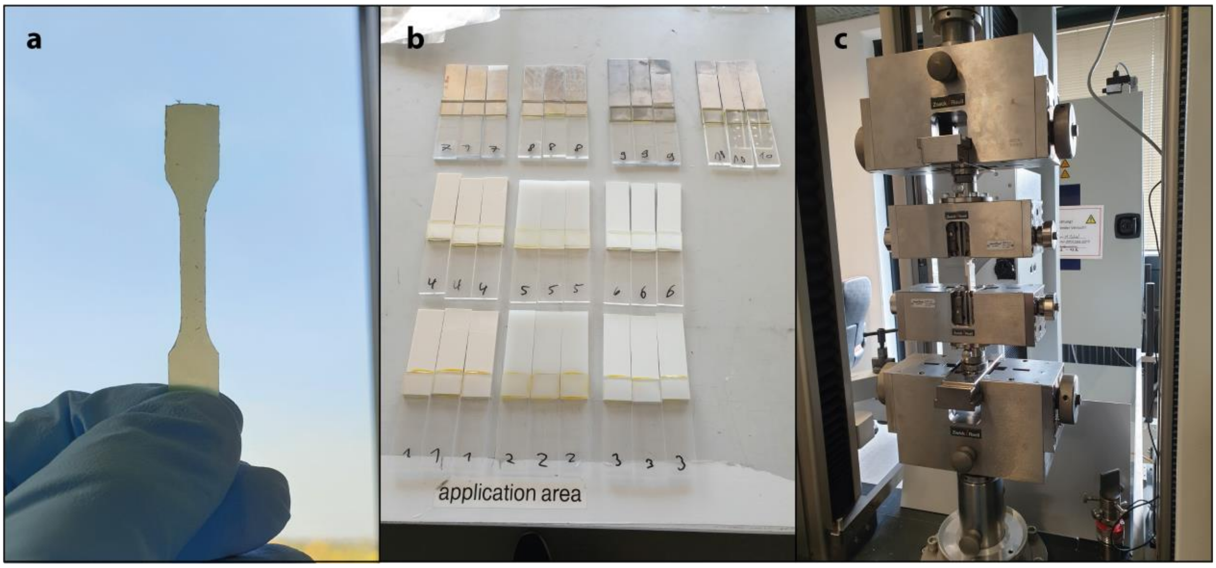

Figure 5.14: Photos of (a) "dog bone" sample for tensile testing; (b) adhered single lap shear specimens; (c) *ZwickRoell Z100* testing machine.

180 ° peel test of PSA films. The testing substrates were thoroughly cleaned with Persil solution, ethyl acetate and acetone and acclimated at 23 °C and 50 % RH for at least 5 hours. For each crude polymer solution or polymer-ionic liquid blend, three 150 x 25 mm test strips were applied to the substrates and a 2 kg weight was rolled over the strip to increase wetting on the substrate. The substrates and the loose end of the applied testing strip were vertically clamped in a *Zwick Z100*. The testing strip was pulled at a 180° angle at 300 mm/min for 80 mm and the applied force was measured. This measurement was performed 20 minutes and 24 hours after application.

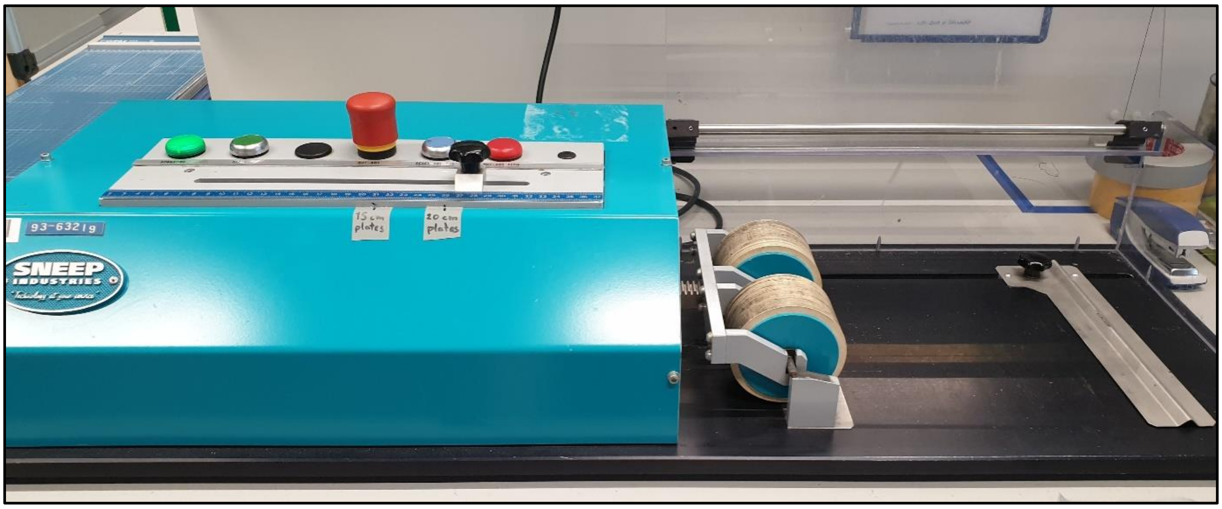

Figure 5.15: Device to applicate testing strips to substrates for 180° peel tests.

Loop tack test of PSA films. For each system three 150 x 25 mm testing strips were clamped in a loop form with a *Zwick Z100* after removing the silicone paper cover. and lowered onto a substrate at 300 mm/min until full contact between the film and the substrate is reached. Then the testing strip is pulled back upwards, and the force required to remove the strip is measured.

Rheology analysis. Rheology analysis can be used to investigate fluids and viscoelastic solids.[263] There are many possible measurement techniques for a rheometer, e.g. the oscillating shearing of an adhesive while curing. The flow behavior of the liquid and the viscoelastic properties of the cured material are examined and the development during the curing process can be observed. Viscoelastic properties are described by complex shear modulus *G*. *G* is calculated from storage modulus *G'*, representing elastic properties, and loss modulus *G''*, representing viscous properties; shown in equation (5.3).[263]

$$\boldsymbol{G = G' + iG''} \tag{5.3}$$

$$\boldsymbol{tan\ \delta = \frac{G''}{G'}} \tag{5.4}$$

In this work, rheology experiments were performed at 30 °C, if not stated otherwisel, with an *Anton Paar Rheometer MCR 302*, a *D-PP25* mandrel (if not stated otherwise), a starting adhesive thickness of 0.200 mm, a shear deformation of 0.1 % and a shear rate of 10 rad/s. Except for experiments discussed in section 3.1.1, shear deformation was 10 % for the first three minutes.

Cationic polymerization kinetics of urethane and hemiacetal ester prepolymers via rheology. Di-p-tolyliodonium hexafluorophosphate (PI 440) was dissolved in propylene carbonate before the reaction in a solution with 25 wt% of the initiator. Initiator solution and monomers were weighed into a glass vial and heated to T = 80 °C to melt the urethane monomers. The mass of the initiator alternated depending on the experiment. After 30 minutes, a sample was taken from the oven and mixed thoroughly; all samples were homogeneous. The experiments were carried out at T = 75 °C with an *Anton Paar Rheometer MCR 302*, a *D-PP25* mandrel, an initial gap of 0.200 mm, a shear deformation of 2 % (10 % for the first three minutes) and a shear rate of 10 rad/s. The respective samples were placed on a preheated quartz plate. After establishing an initial gap of 0.200 mm, the sample was trimmed. The sample was irradiated after 3 minutes with a *Omnicure S 2000 SC* light source for 3 seconds.

Radical polymerization kinetics of urethane and hemiacetal ester prepolymers via rheology. Hydroxycyclohexyl phenyl ketone and 4-(4-Methylphenylthio)benzophenone were dissolved in propylene carbonate before the reaction in a solution with respectively 10 wt% of each initiator. Initiator solution and monomers were weighed into a glass vial and heated to T = 80 °C to melt the urethane monomers. The mass of each initiator was 1 wt% in regard to the monomer. After 30 minutes, a sample was taken from the oven and mixed thoroughly; all samples were homogeneous. The experiments were carried out at T = 75 °C with an *Anton Paar Rheometer MCR 302*, a *D-PP25* mandrel, an initial gap of 0.200 mm, a shear deformation of 2 % (10 % for the first three minutes) and a shear rate of 10 rad/s. The respective samples were placed on a preheated quartz plate. After establishing an initial gap of 0.200 mm, the sample was trimmed. The sample was irradiated after 3 minutes with a *Omnicure S 2000 SC* light source for 3 seconds.

Cationic polymerization kinetics of urethane and hemiacetal ester prepolymers via NMR spectroscopy. Di-p-tolyliodonium hexafluorophosphate (PI 440) was dissolved in propylene carbonate before the reaction in a solution with 5 wt% of the initiator. Initiator solution, internal standard dimethyl terephthalate and monomers were weighed into a glass vial and heated to T = 80 °C to melt the urethane monomers. In regard to the monomer, the mass of the initiator was 0.1 wt% and the mass of the internal standard 2 wt%. After 30 minutes, a sample was taken from the oven and mixed thoroughly; all samples were homogeneous. A small sample was taken for reference. Afterwards, the glass vial was placed into a *Loctite ZETA 7401* UV chamber with a 400 W Hg-UV-Lamp. The irradiance inside the chamber was measured and is given in Table 5.1. U-1 and HAE-1 were irradiated for 10 seconds; U-2 and HAE-2 were irradiated for 5 seconds. Afterwards, the samples were kept at RT, ^{1}H-NMR spectra were recorded 2 hours after irradiation.

Solids content of PSA solutions. About 1.5 g of a sample were put into a dried aluminum pan and kept in the oven at 150 °C for one hour. The solids content was calculated from the weight loss due to solvent and residual monomer evaporation.

Relative viscosity of PSA polymer solutions. The samples were diluted with EtOAc to create solutions with a fixed solids content. 10.0 mL of the respective solution was filled into the glass equipment. The solution was channeled through the apparatus with compressed air and the time the solution needed to flow back was measured and compared to crude EtOAc. The experiments were performed at 19.9 °C, monitored with a *ViscoSystem AVS 350* and repeated 6 times for each sample.

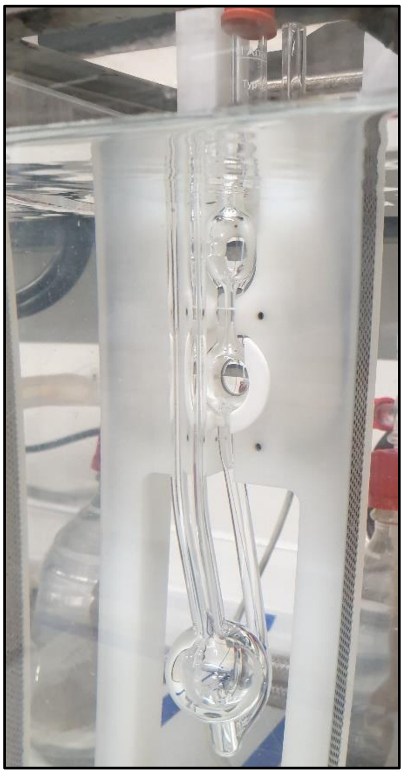

Figure 5.16: Glass equipment for relative viscosity measurements.

6 Appendix

Table 6.1: Molecular weight distribution values of P-U2 determined via GPC. Two samples were measured resulting in two values for each peak.

	M_w [Da]	M_n [Da]	M_P [Da]	Polydispersity
Peak 1	18946	10198	22633	1.9
Peak 1	18696	1077	21836	1.9
Peak 2	1478	1477	1451	1.0
Peak 2	1474	1472	1445	1.0
Peak 3	1291	1289	1276	1.0
Peak 3	1282	1280	1263	1.0
Peak 4	1105	1103	1099	1.0
Peak 4	1097	1095	1091	1.0
Peak 5	901	893	928	1.0
Peak 5	894	886	920	1.0
Peak 6	547	544	549	1.0
Peak 6	529	526	531	1.0
Peak 7	380	373	378	1.0
Peak 7	376	371	376	1.0
Peak 8	269	268	297	1.0
Peak 8	258	258	253	1.0

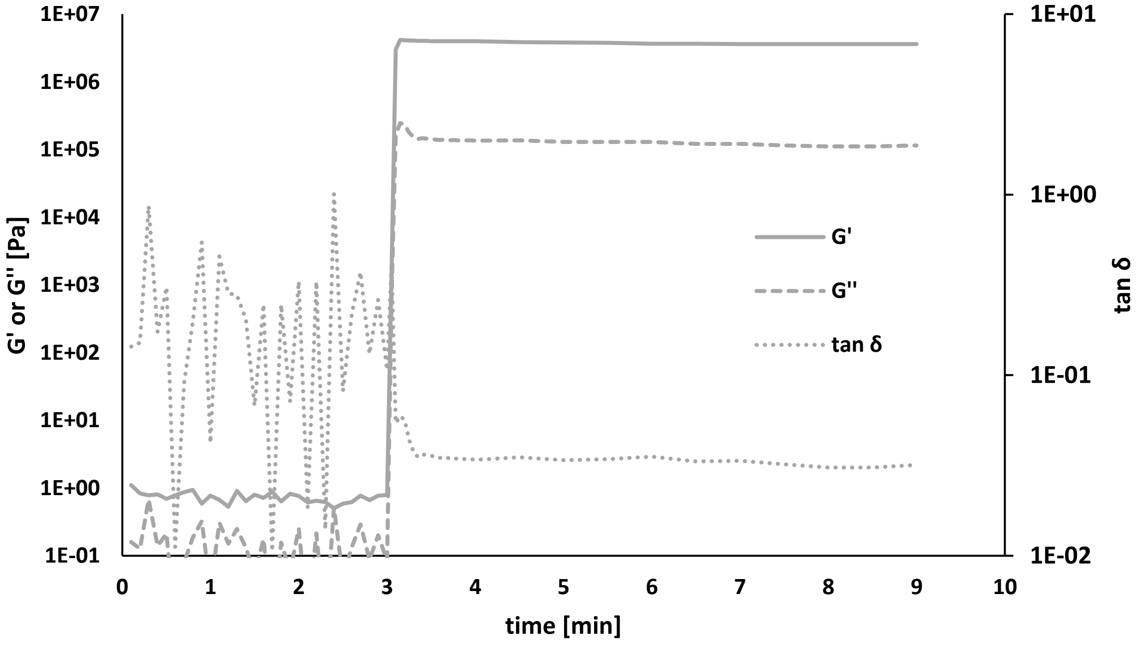

Figure 6.1: Storage modulus *G'* (solid line), loss modulus *G''* (dashed line) and dissipation factor tan *δ* (dotted line) over time of mixtures of vinyl ether monomer BDVE (grey) with 1 wt% of PI 440. To initiate cationic polymerization, the mixtures were irradiated with UV light for 20 seconds after 3 minutes of oscillation.

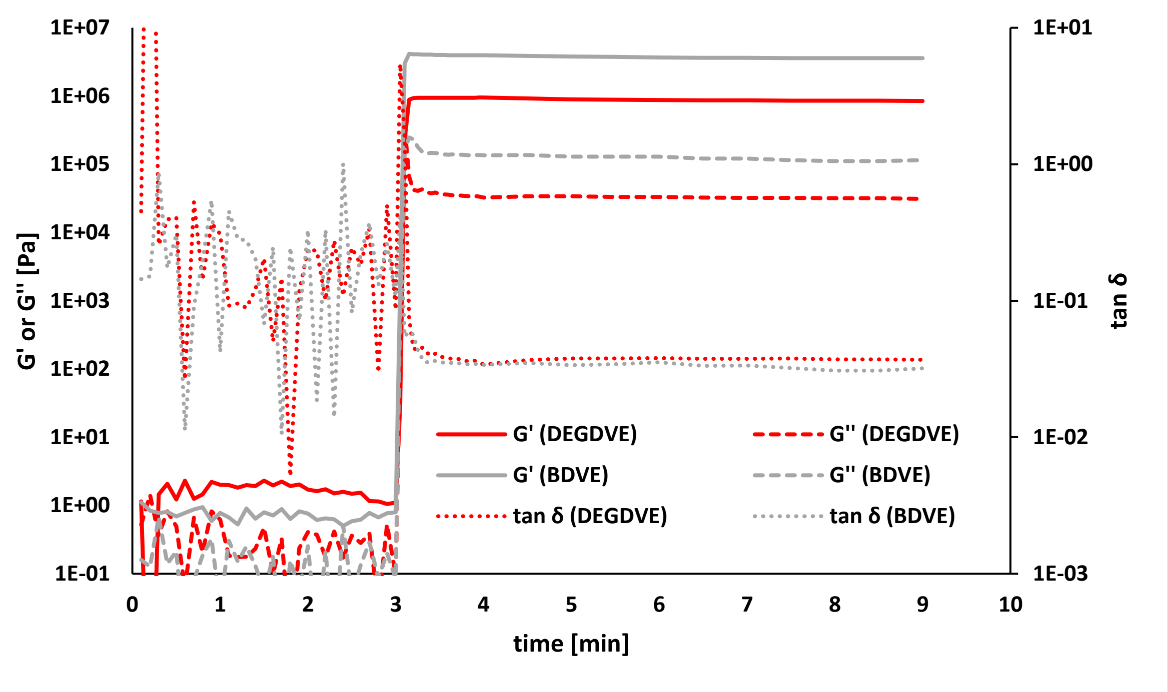

Figure 6.2: Storage modulus *G'* (solid line), loss modulus *G''* (dashed line) and dissipation factor tan *δ* (dotted line) over time of mixtures of vinyl ether monomers DEGDVE (red) and BDVE (grey) with 1 wt% of PI 440. To initiate cationic polymerization, the mixtures were irradiated with UV light for 20 seconds after 3 minutes of oscillation.

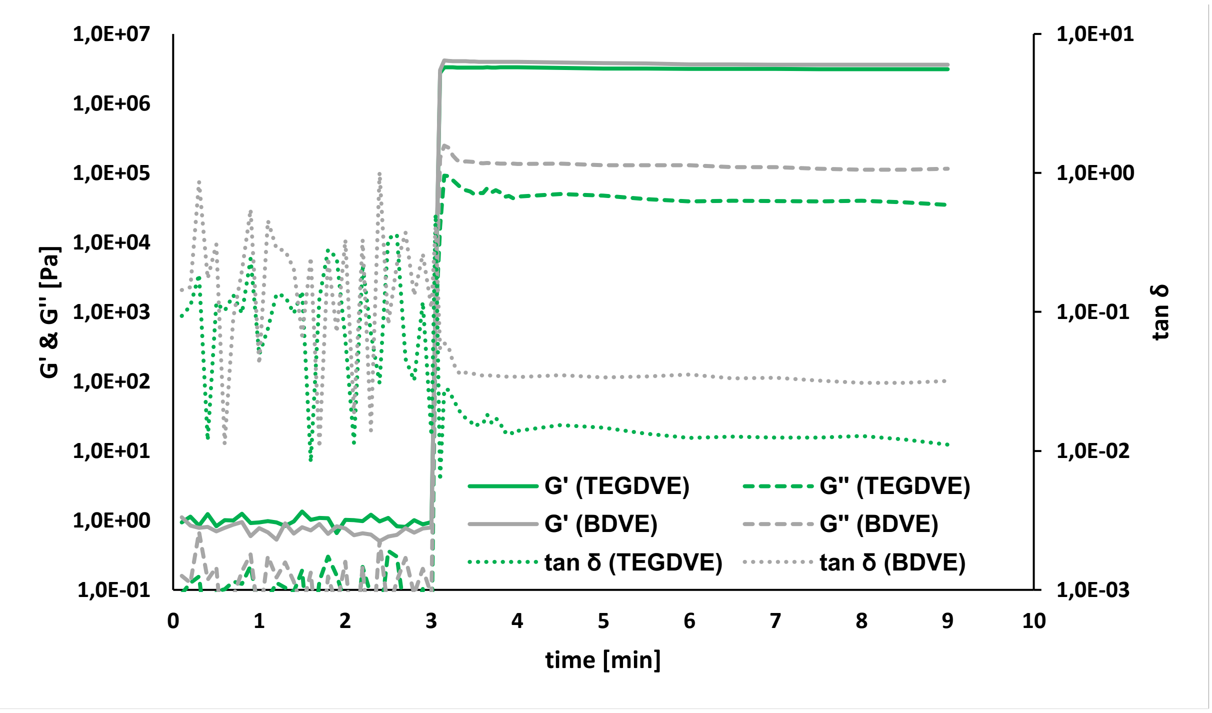

Figure 6.3: Storage modulus *G'* (solid line), loss modulus *G''* (dashed line) and dissipation factor tan *δ* (dotted line) over time of mixtures of vinyl ether monomers TEGDVE (green) and BDVE (grey) with 1 wt% of PI 440. To initiate cationic polymerization, the mixtures were irradiated with UV light for 20 seconds after 3 minutes of oscillation.

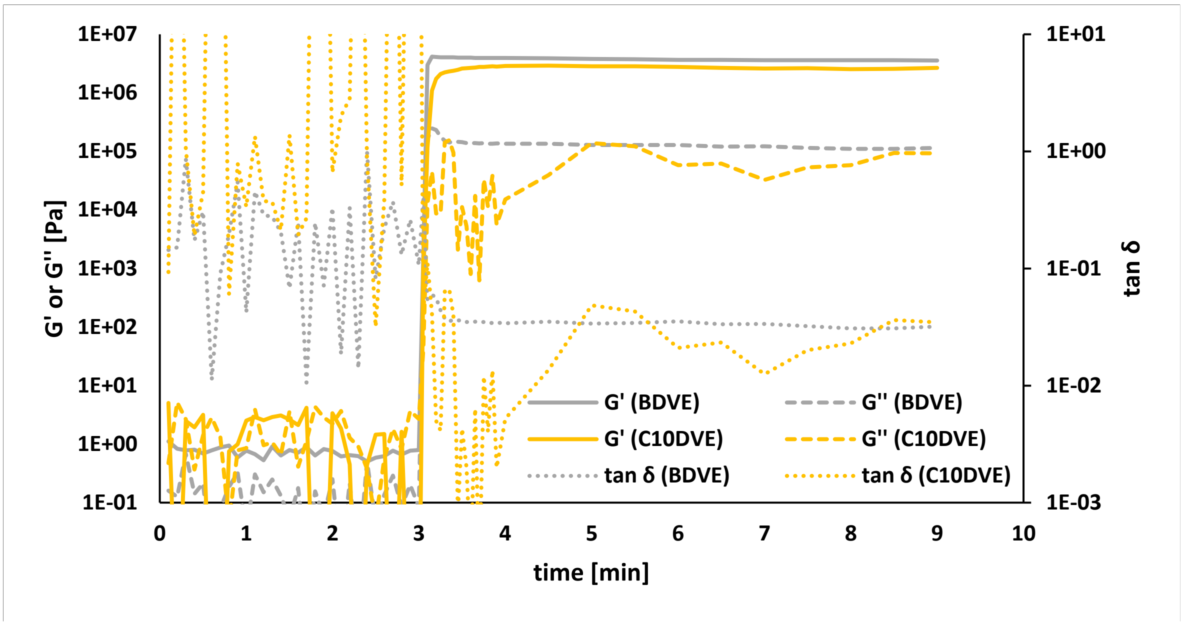

Figure 6.4: Storage modulus *G'* (solid line), loss modulus *G''* (dashed line) and dissipation factor tan *δ* (dotted line) over time of mixtures of vinyl ether monomers C10DVE (orange) and BDVE (grey) with 1 wt% of PI 440. To initiate cationic polymerization, the mixtures were irradiated with UV light for 20 seconds after 3 minutes of oscillation.

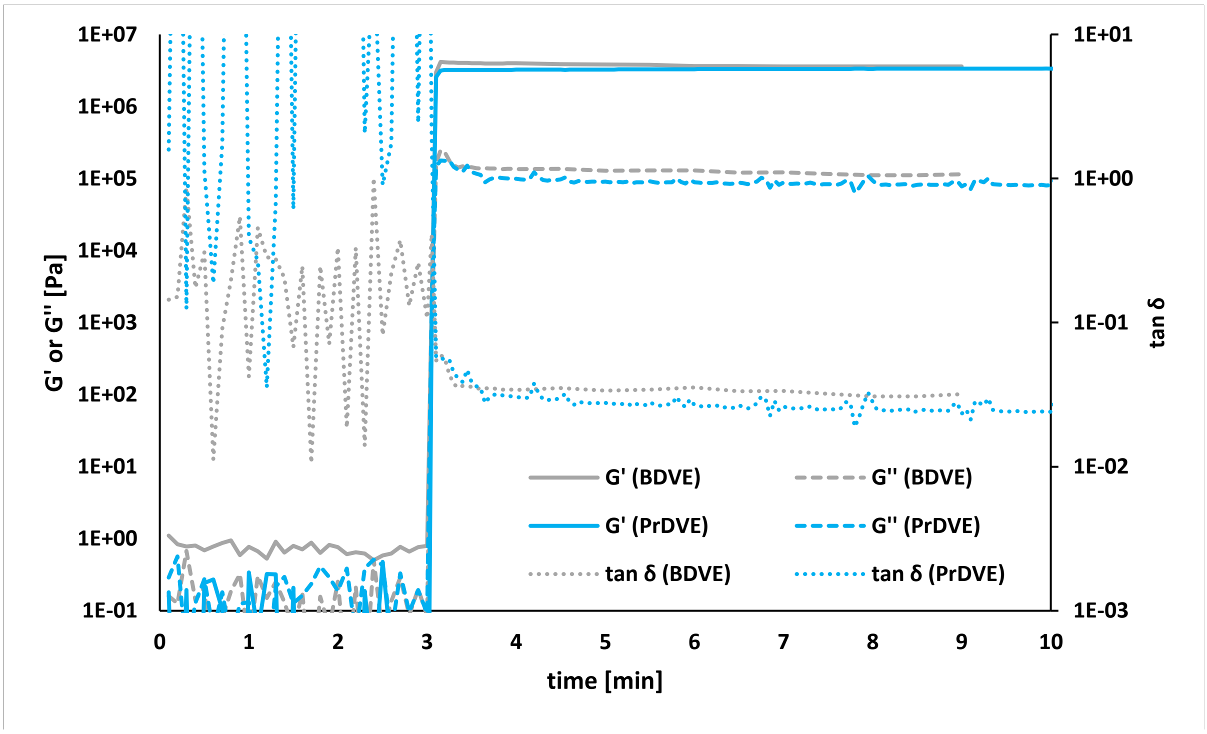

Figure 6.5: Storage modulus *G'* (solid line), loss modulus *G''* (dashed line) and dissipation factor tan *δ* (dotted line) over time of mixtures of vinyl ether monomers PrDVE (light blue) and BDVE (grey) with 1 wt% of PI 440. To initiate cationic polymerization, the mixtures were irradiated with UV light for 20 seconds after 3 minutes of oscillation.

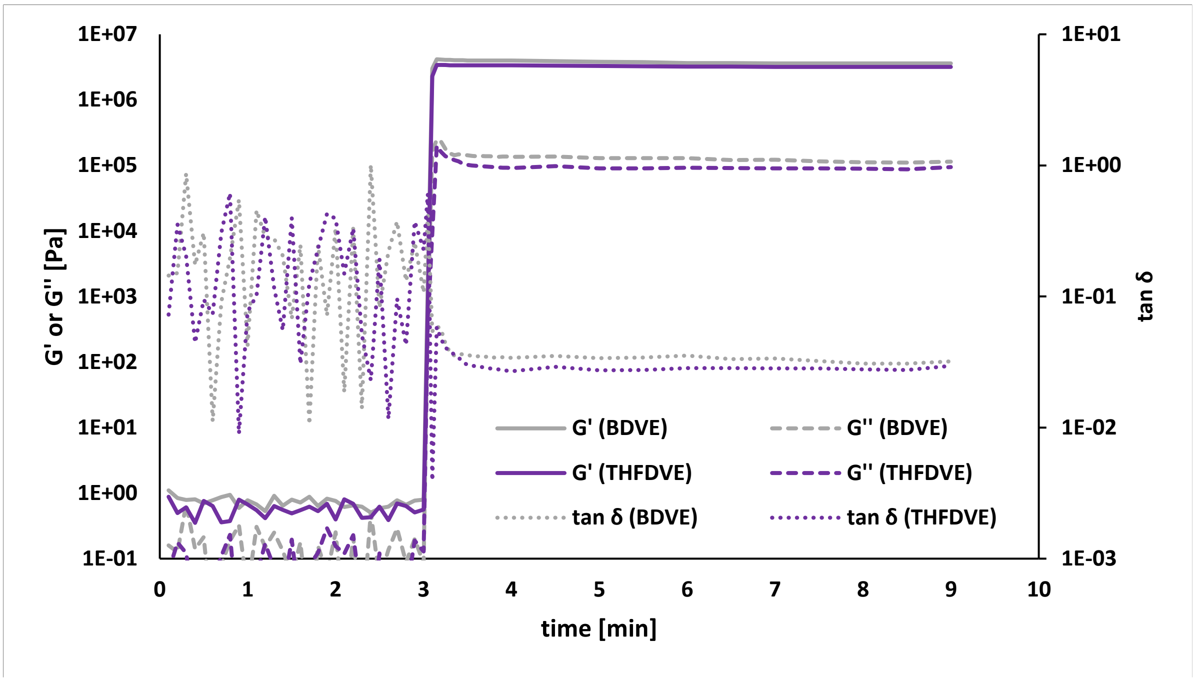

Figure 6.6: Storage modulus *G’* (solid line), loss modulus *G’’* (dashed line) and dissipation factor tan *δ* (dotted line) over time of mixtures of vinyl ether monomers THFDVE (purple) and BDVE (grey) with 1 wt% of PI 440. To initiate cationic polymerization, the mixtures were irradiated with UV light for 20 seconds after 3 minutes of oscillation.

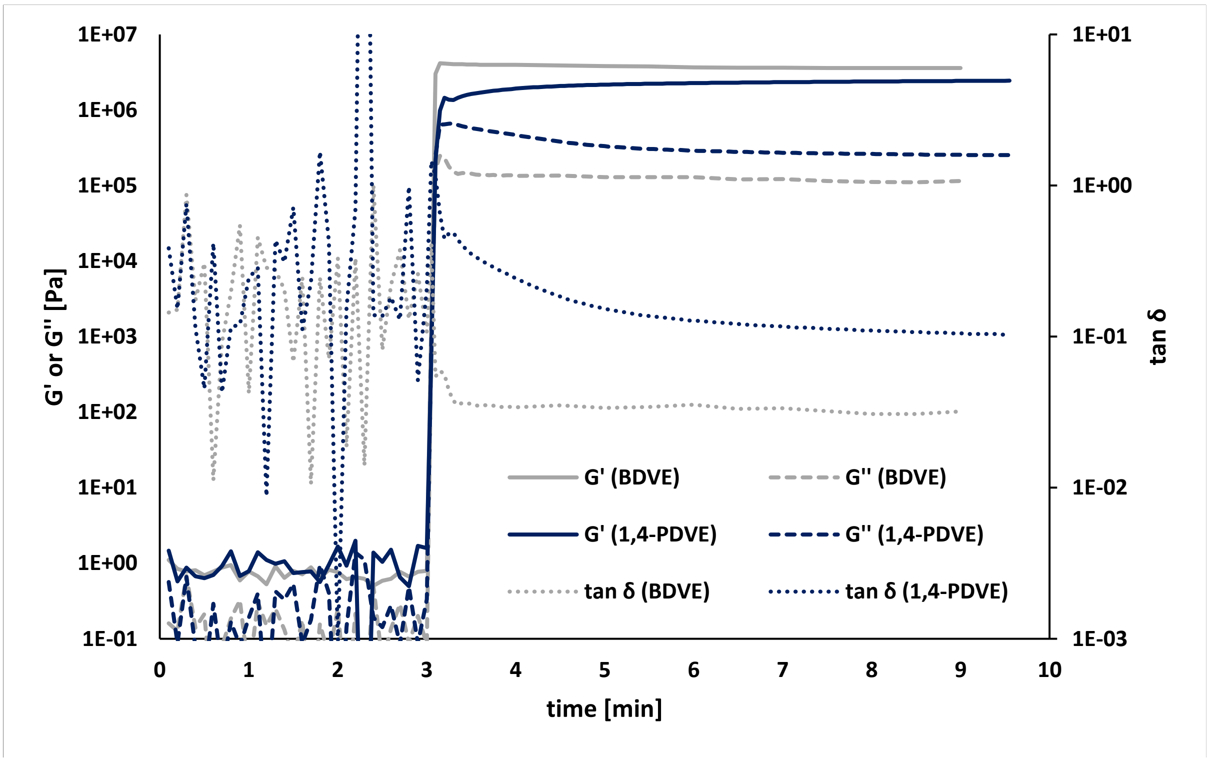

Figure 6.7: Storage modulus *G’* (solid line), loss modulus *G’’* (dashed line) and dissipation factor tan *δ* (dotted line) over time of mixtures of vinyl ether monomers 1,4-PDVE (dark blue) and BDVE (grey) with 1 wt% of PI 440. To initiate cationic polymerization, the mixtures were irradiated with UV light for 20 seconds after 3 minutes of oscillation.

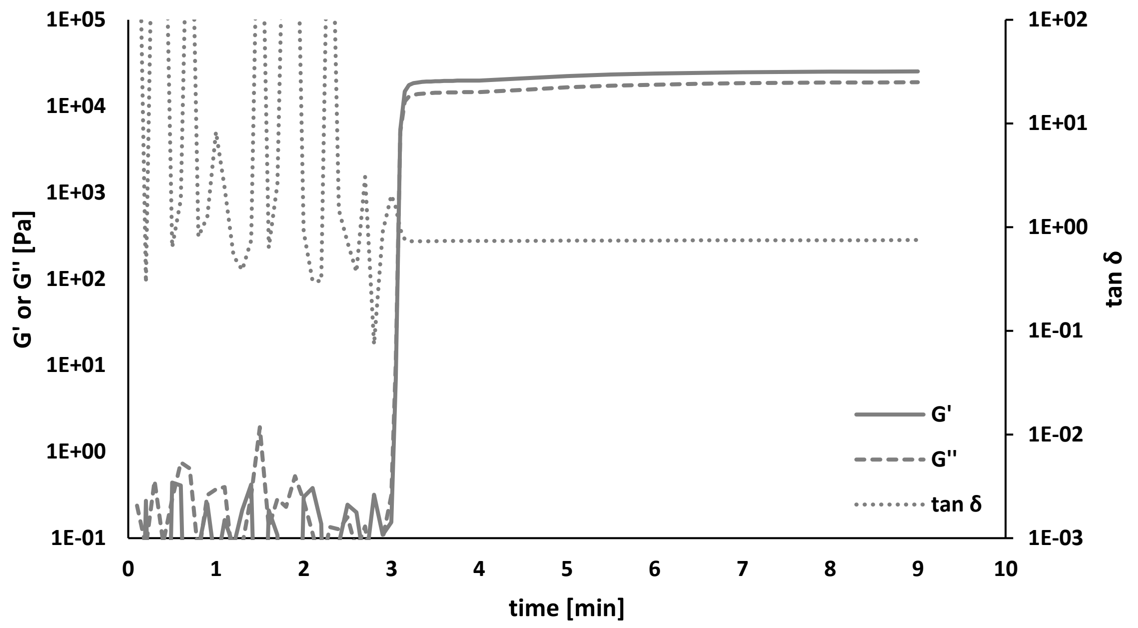

Figure 6.8: Storage modulus *G'* (solid line), loss modulus *G''* (dashed line) and dissipation factor tan *δ* (dotted line) over time of mixtures of vinyl ether monomer IBVE (dark grey) with 1 wt% of PI 440. To initiate cationic polymerization, the mixtures were irradiated with UV light for 20 seconds after 3 minutes of oscillation.

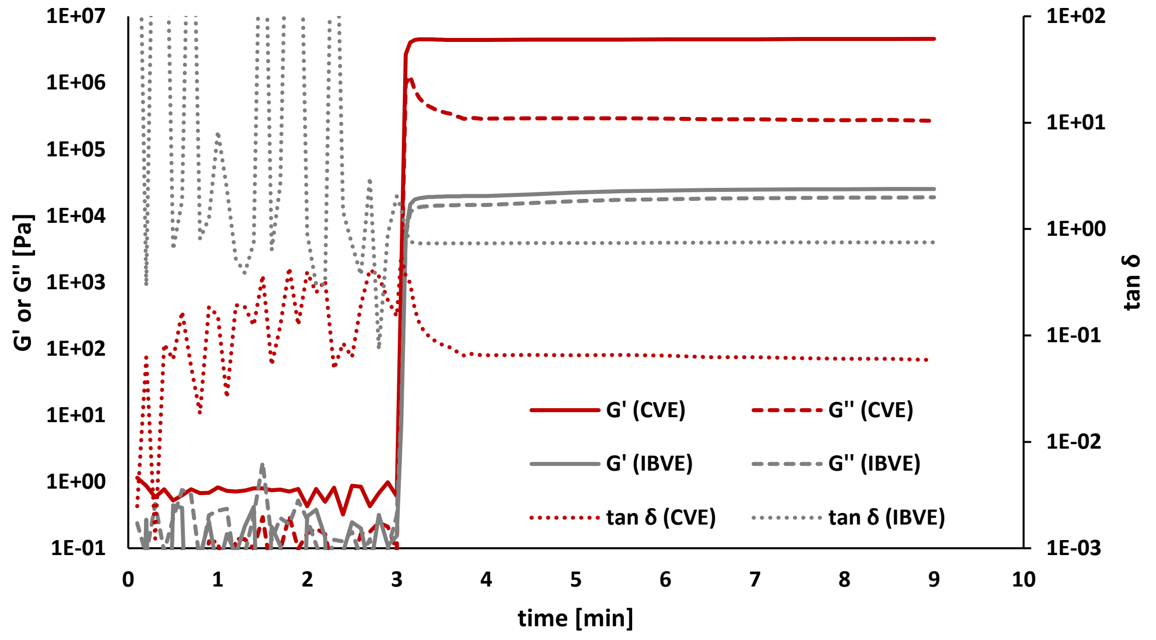

Figure 6.9: Storage modulus *G'* (solid line), loss modulus *G''* (dashed line) and dissipation factor tan *δ* (dotted line) over time of mixtures of vinyl ether monomers IBVE (dark grey) and CVE (dark red) with 1 wt% of PI 440. To initiate cationic polymerization, the mixtures were irradiated with UV light for 20 seconds after 3 minutes of oscillation.

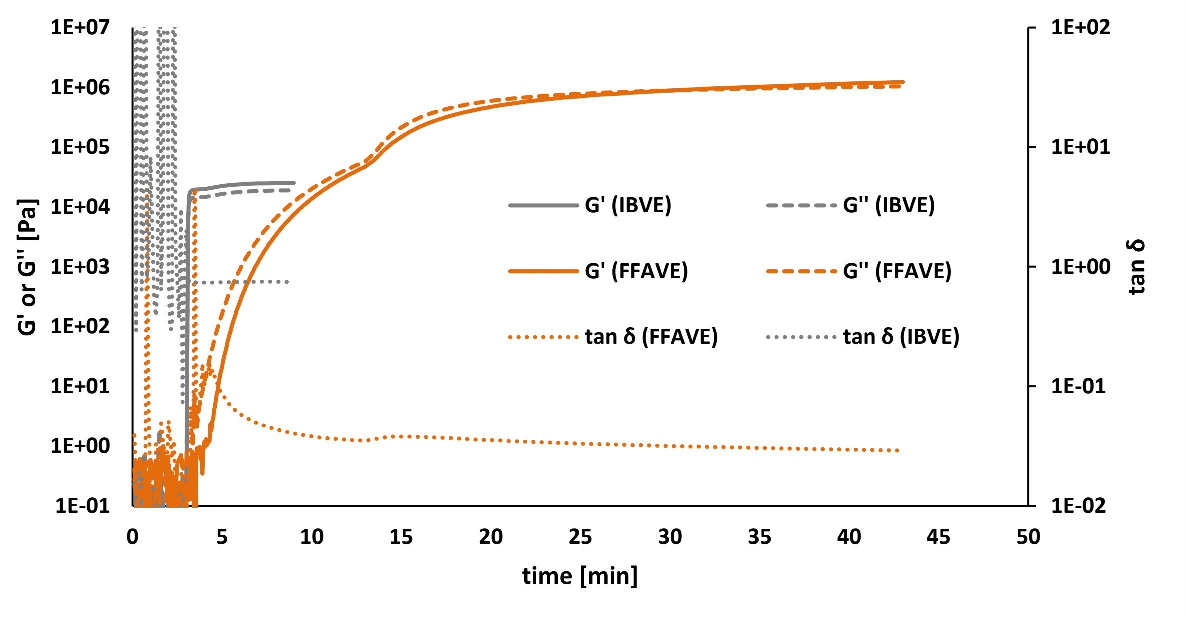

Figure 6.10: Storage modulus *G'* (solid line), loss modulus *G''* (dashed line) and dissipation factor tan *δ* (dotted line) over time of mixtures of vinyl ether monomers IBVE (dark grey) and CVE (dark red) with 1 wt% of PI 440. To initiate cationic polymerization, the mixtures were irradiated with UV light for 20 seconds after 3 minutes of oscillation.

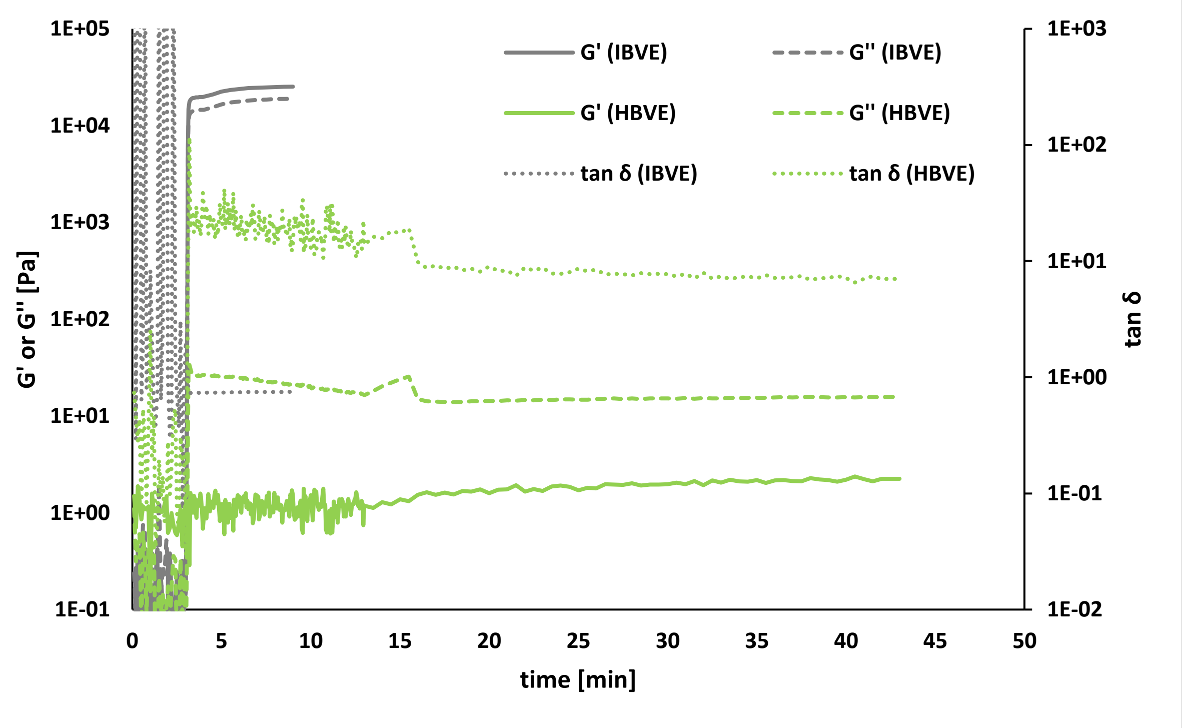

Figure 6.11: Storage modulus *G'* (solid line), loss modulus *G''* (dashed line) and dissipation factor tan *δ* (dotted line) over time of mixtures of vinyl ether monomers IBVE (dark grey) and HBVE (light green) with 1 wt% of PI 440. To initiate cationic polymerization, the mixtures were irradiated with UV light for 20 seconds after 3 minutes of oscillation.

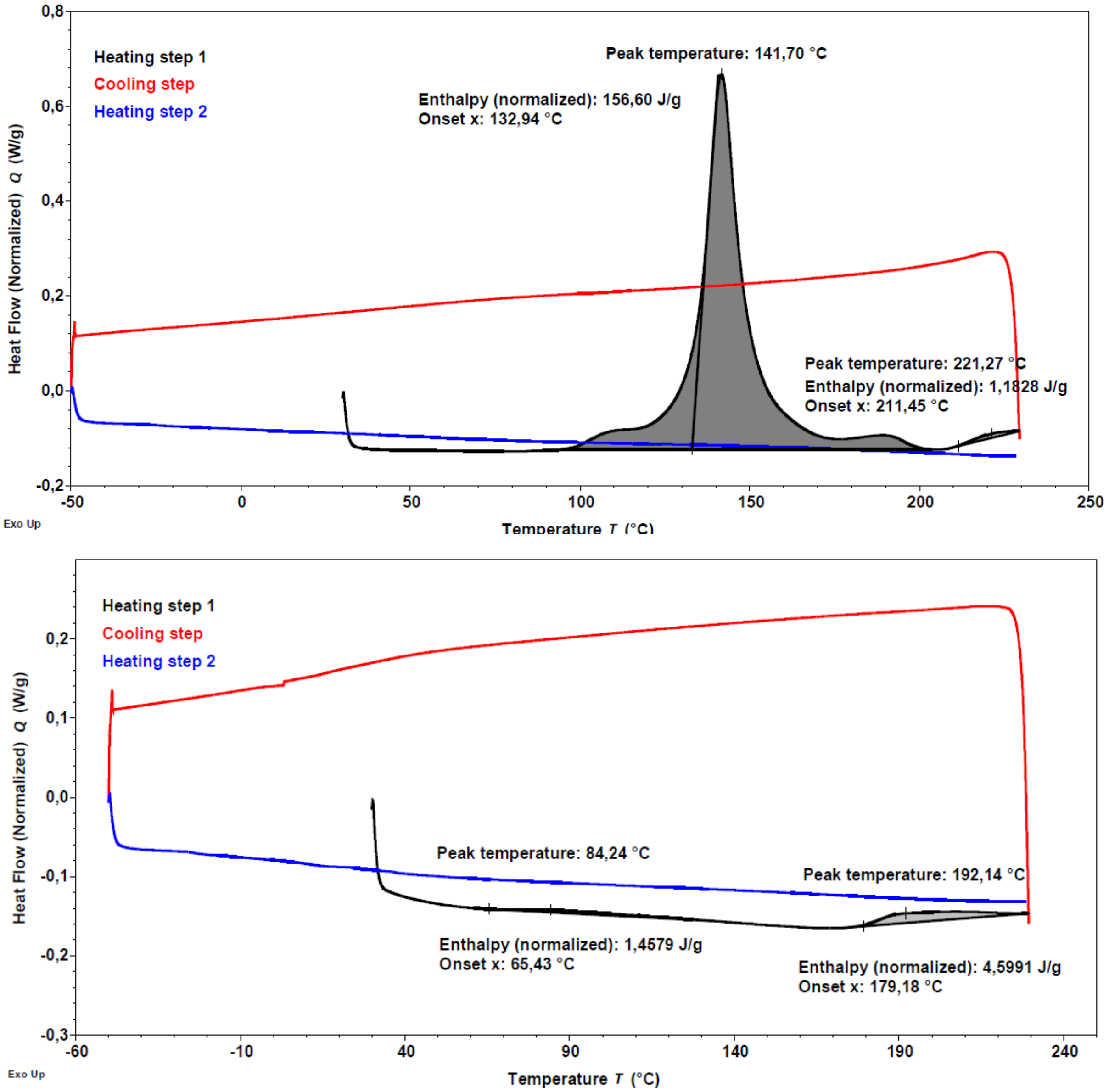

Figure 6.12: DSC thermogram of urethane-based vinyl ether formulation F-U with 23 wt% of $BaSO_4$ in liquid form (upper) and cured (lower).

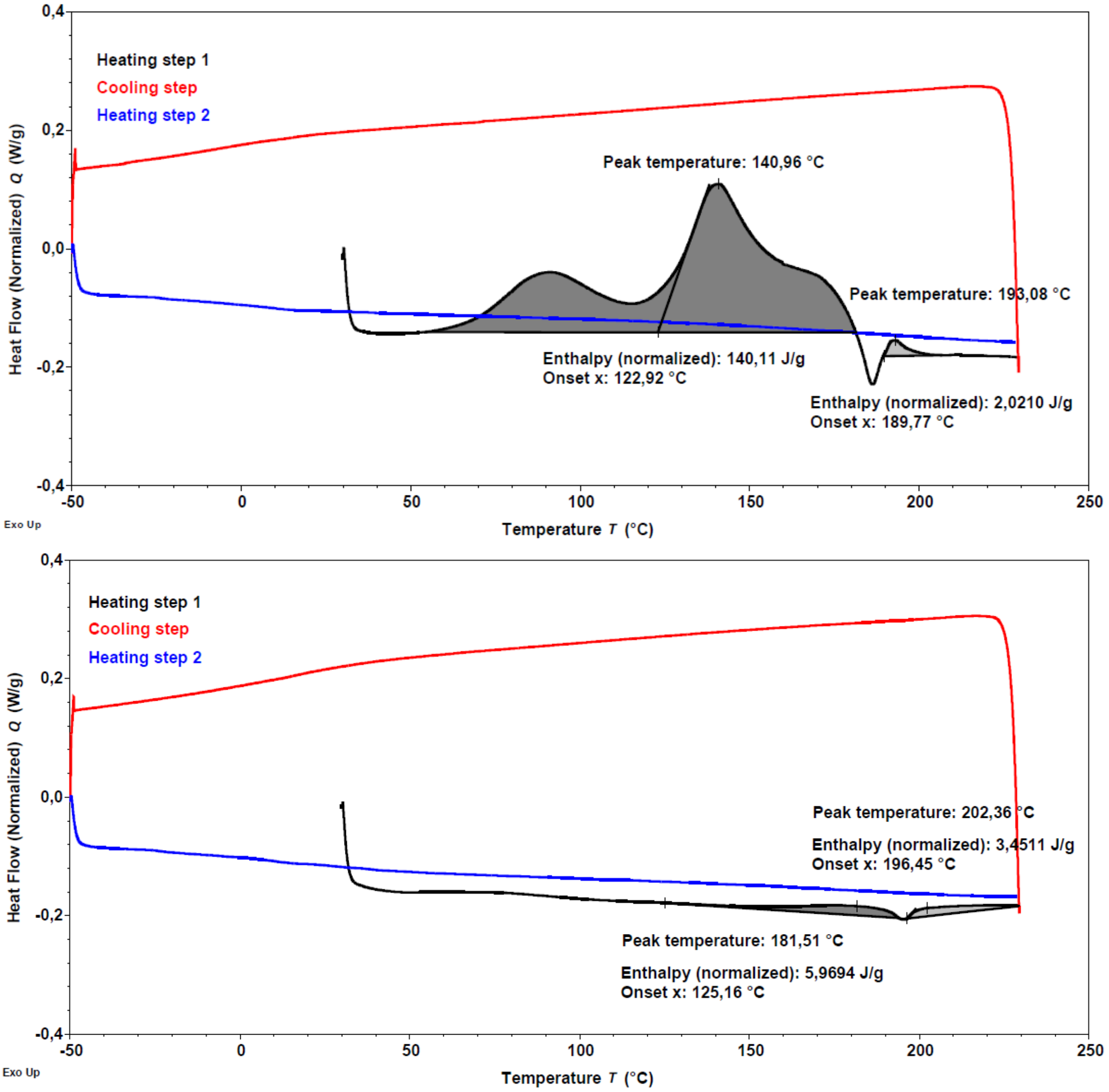

Figure 6.13: DSC thermogram of urethane-based vinyl ether formulation F-U with 5 wt% of Wacker HDK 21 in liquid form (upper) and cured (lower).

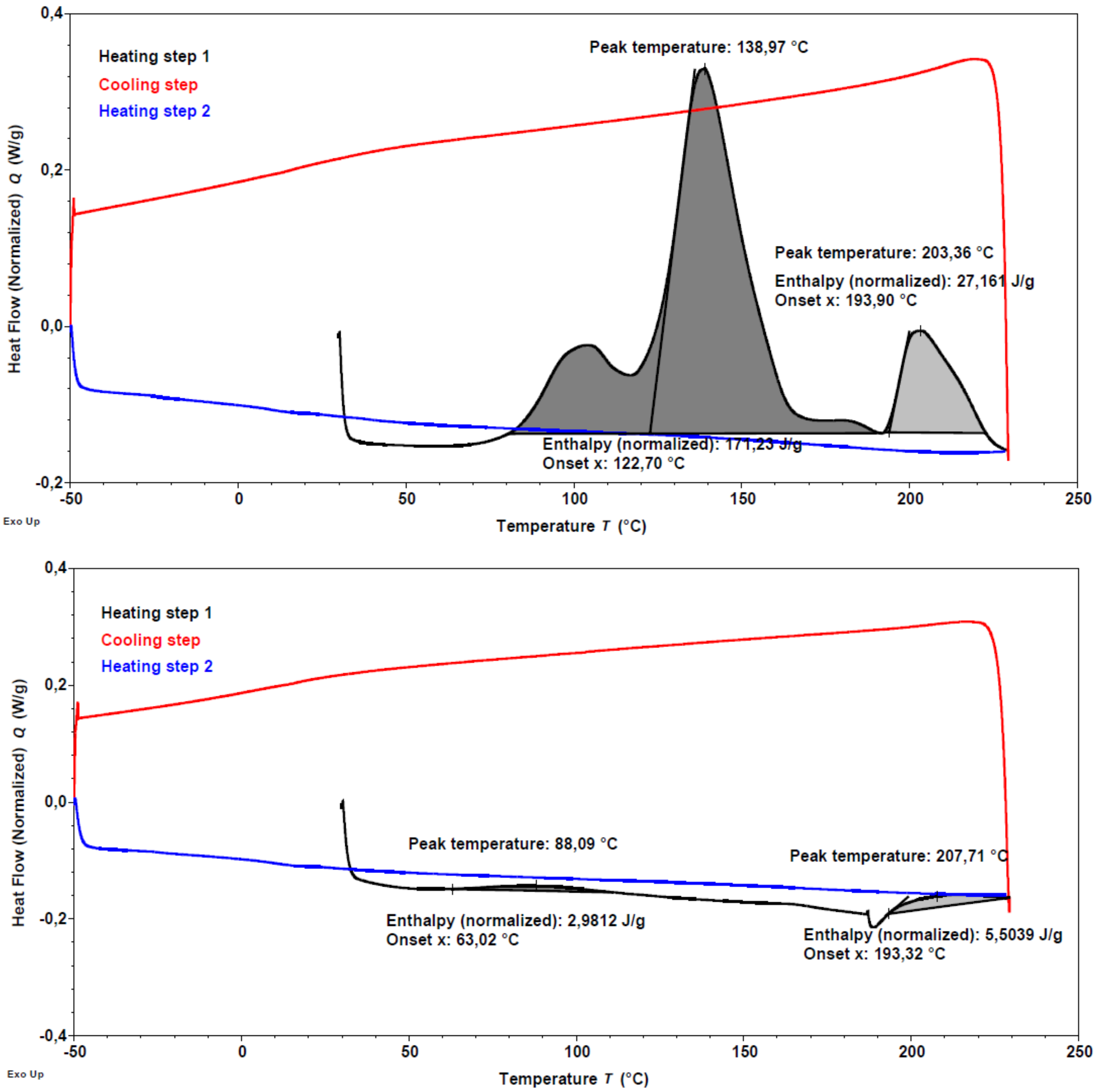

Figure 6.14: DSC thermogram of urethane-based vinyl ether formulation F-U with 8 wt% of Hebofill 490 in liquid form (upper) and cured (lower).

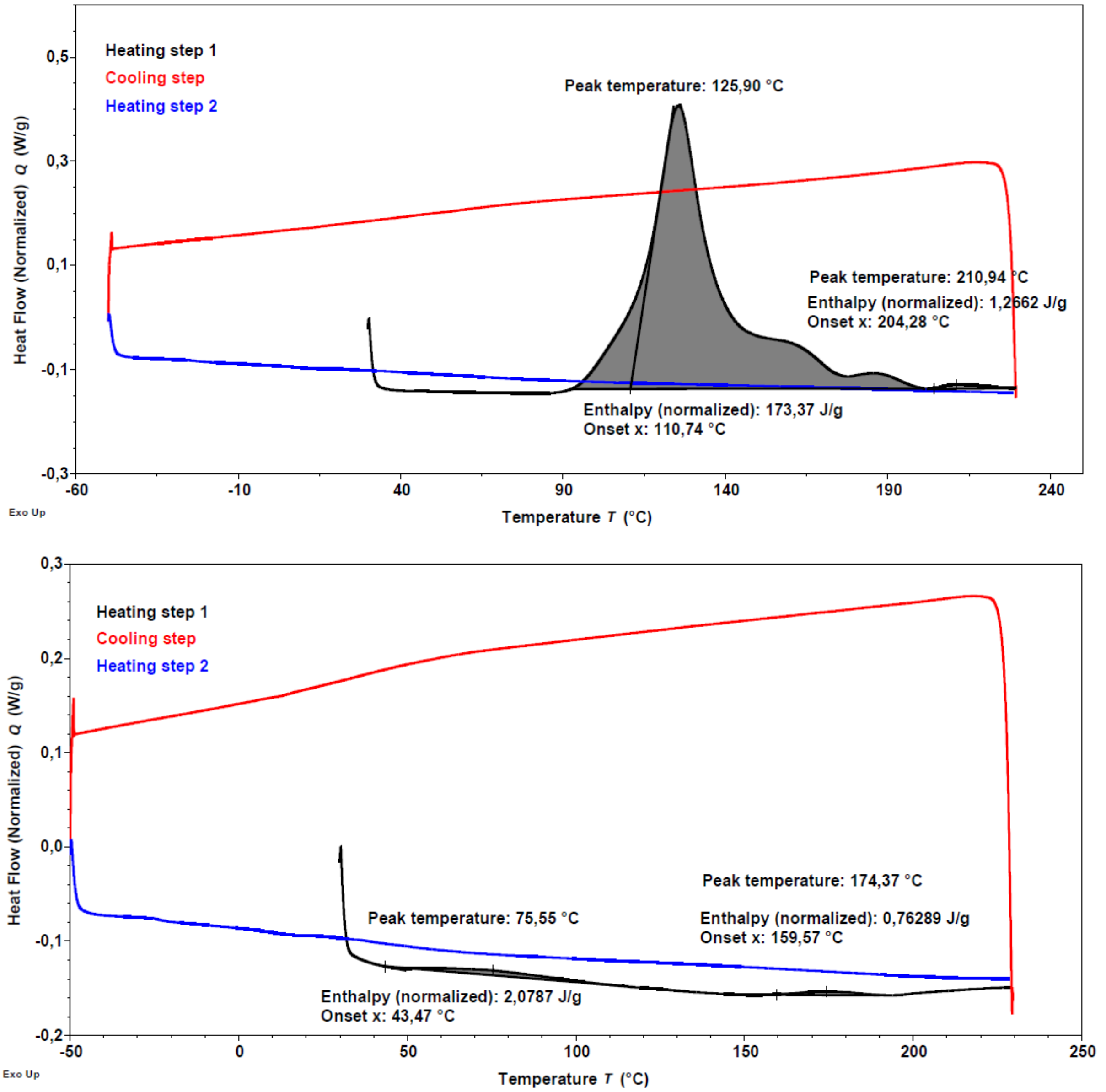

Figure 6.15: DSC thermogram of urethane-based vinyl ether formulation F-U with 30 wt% of BAK 40 in liquid form (upper) and cured (lower).

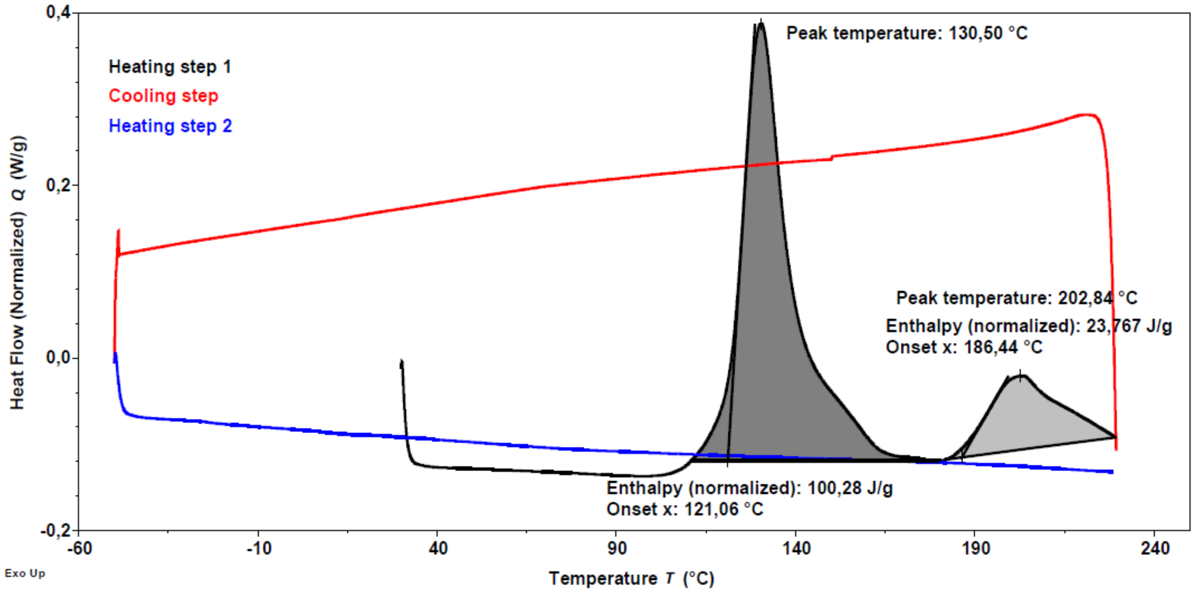

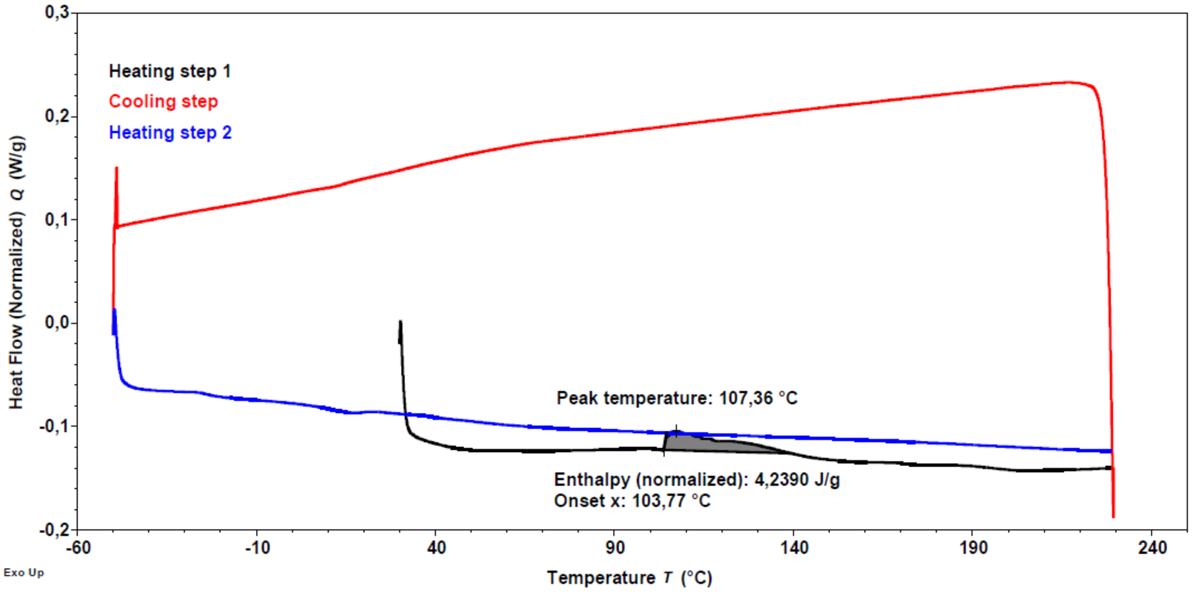

Figure 6.16: DSC thermogram of urethane-based vinyl ether formulation F-U with 30 wt% of Martoxid 2250 in liquid form (upper) and cured (lower).

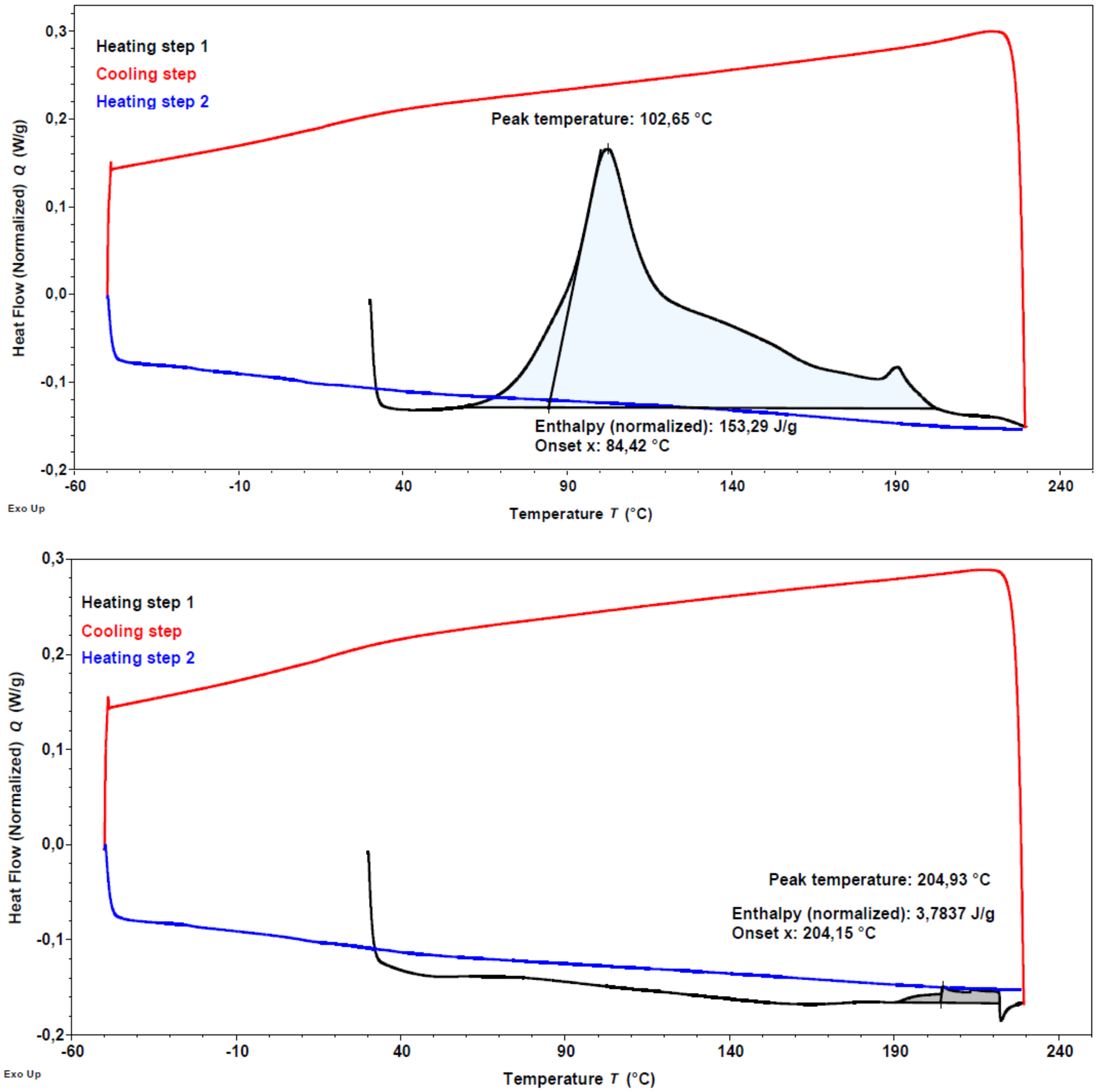

Figure 6.17: DSC thermogram of urethane-based vinyl ether formulation F-U with 30 wt% of Denka FB 35 in liquid form (upper) and cured (lower).

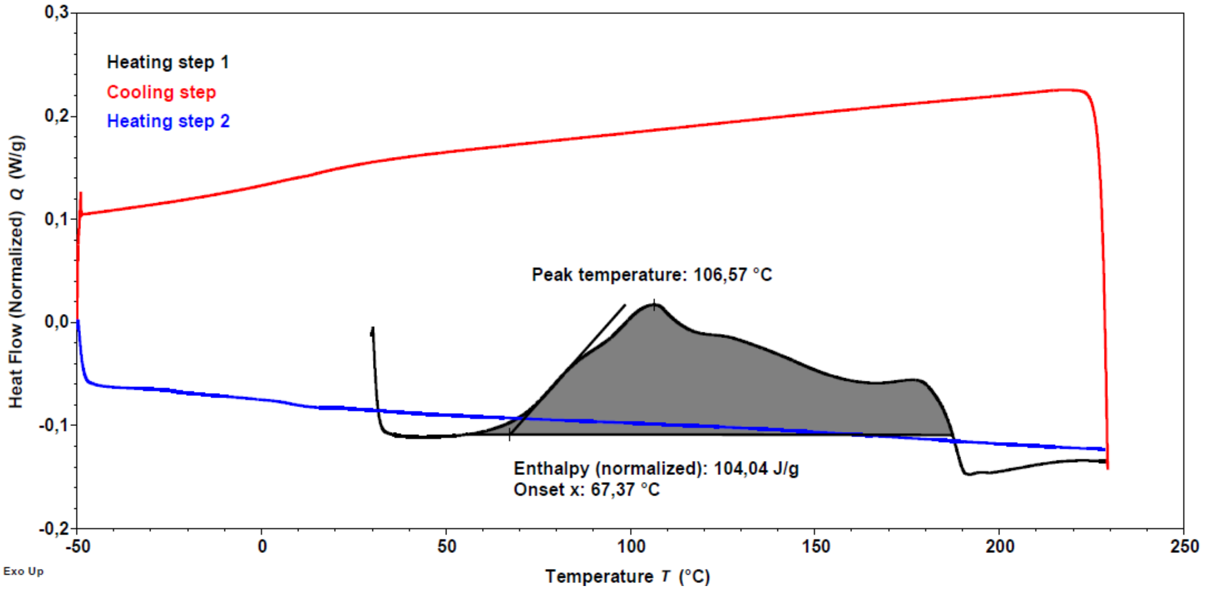

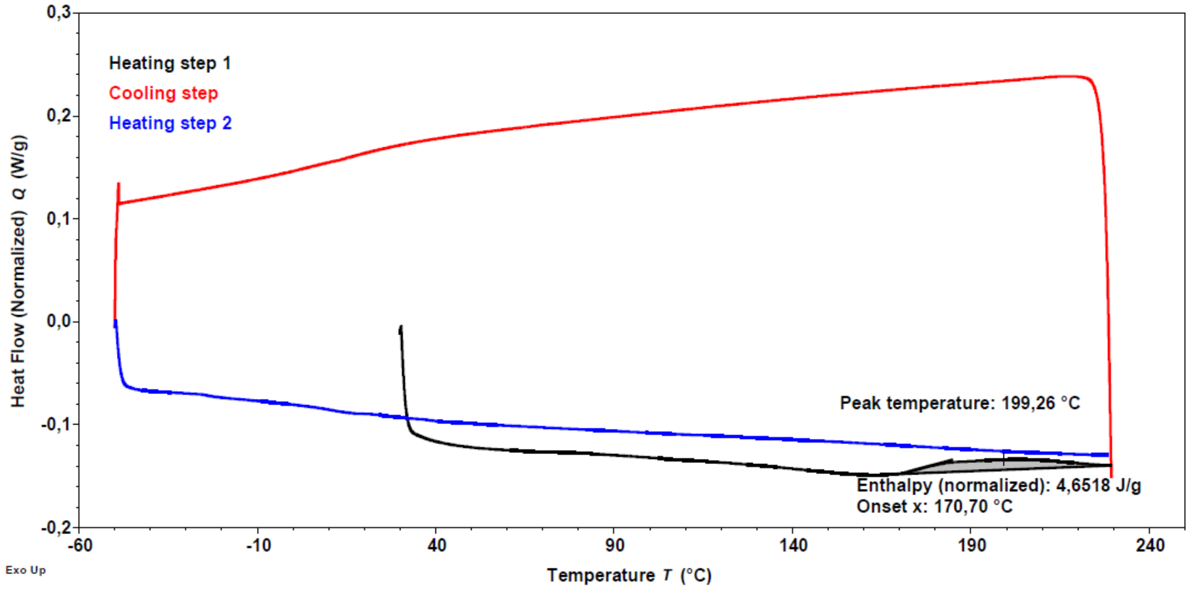

Figure 6.18: DSC thermogram of urethane-based vinyl ether formulation F-U with 50 wt% of Denka FB 35 in liquid form (upper) and cured (lower).

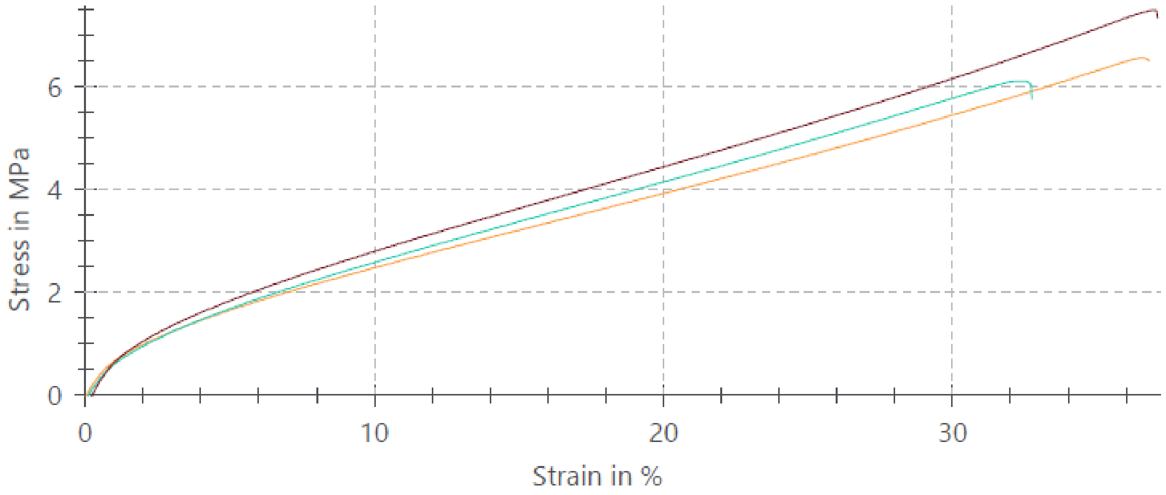

Figure 6.19: Stress-strain diagram recorded in tensile testing of specimens from cured F-T2a.

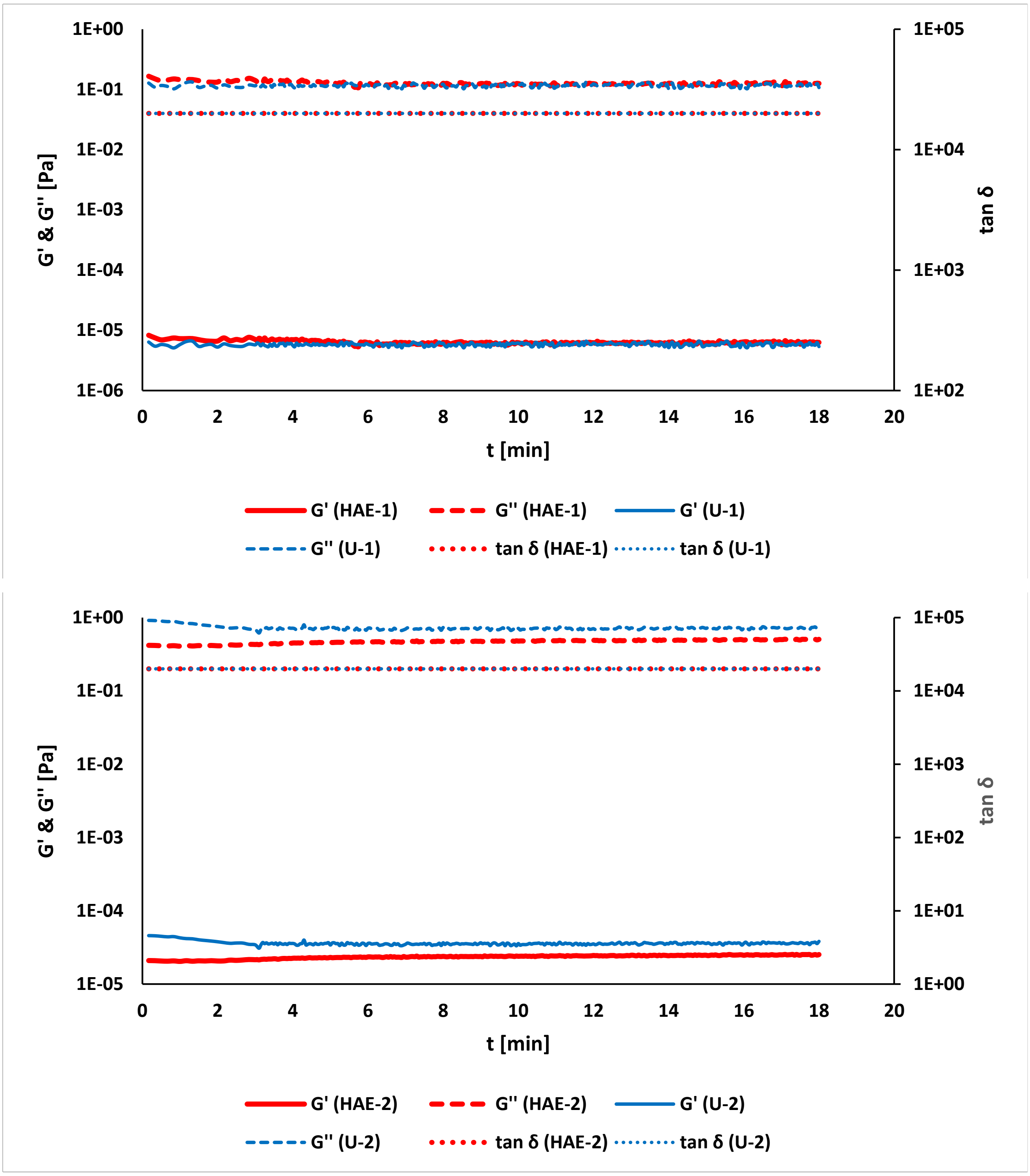

Figure 6.20: Storage modulus *G'* (solid line), loss modulus *G''* (dashed line) and dissipation factor tan *δ* (dotted line) over time of monofunctional (top) and difunctional (bottom) vinyl ether monomers with hemiacetal ester groups (red) or urethane groups (blue) with an initiator concentration of w (PI 184) = w (PI BMS) =1 wt%. To initiate cationic polymerization, the sample was irradiated with UV light for 3 seconds indicated by the yellow area.

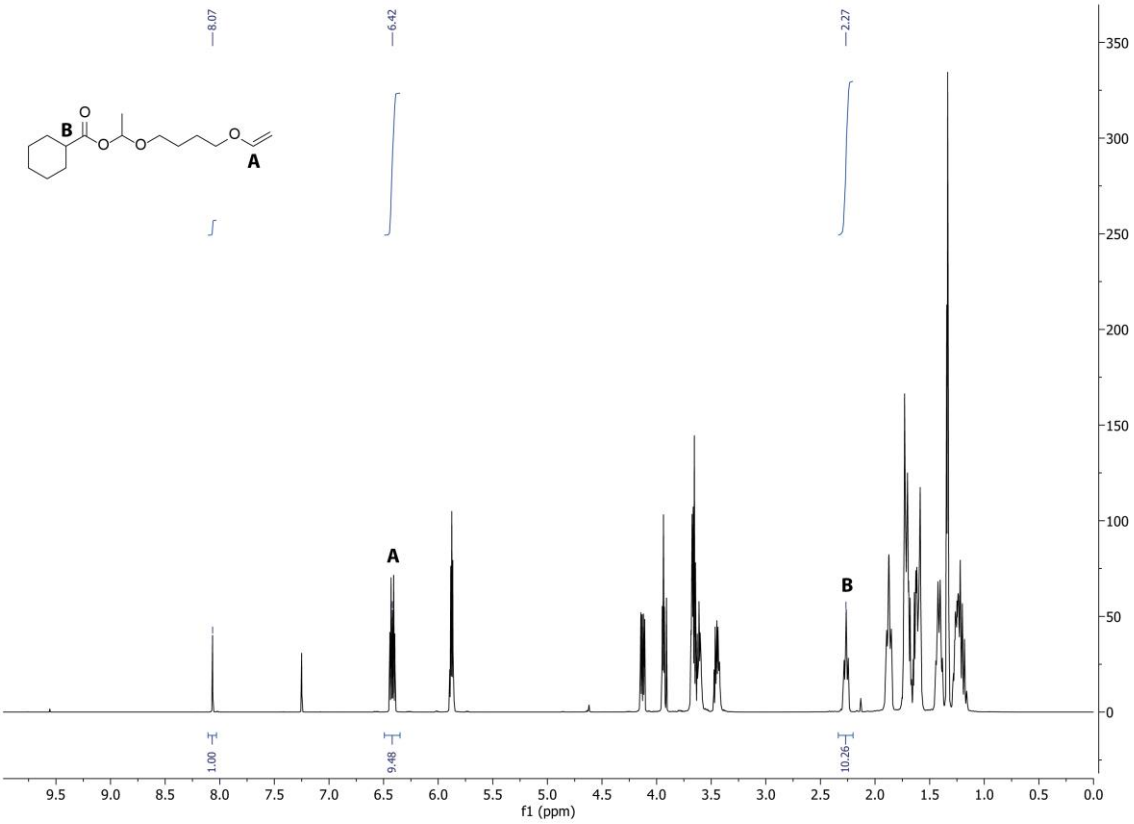

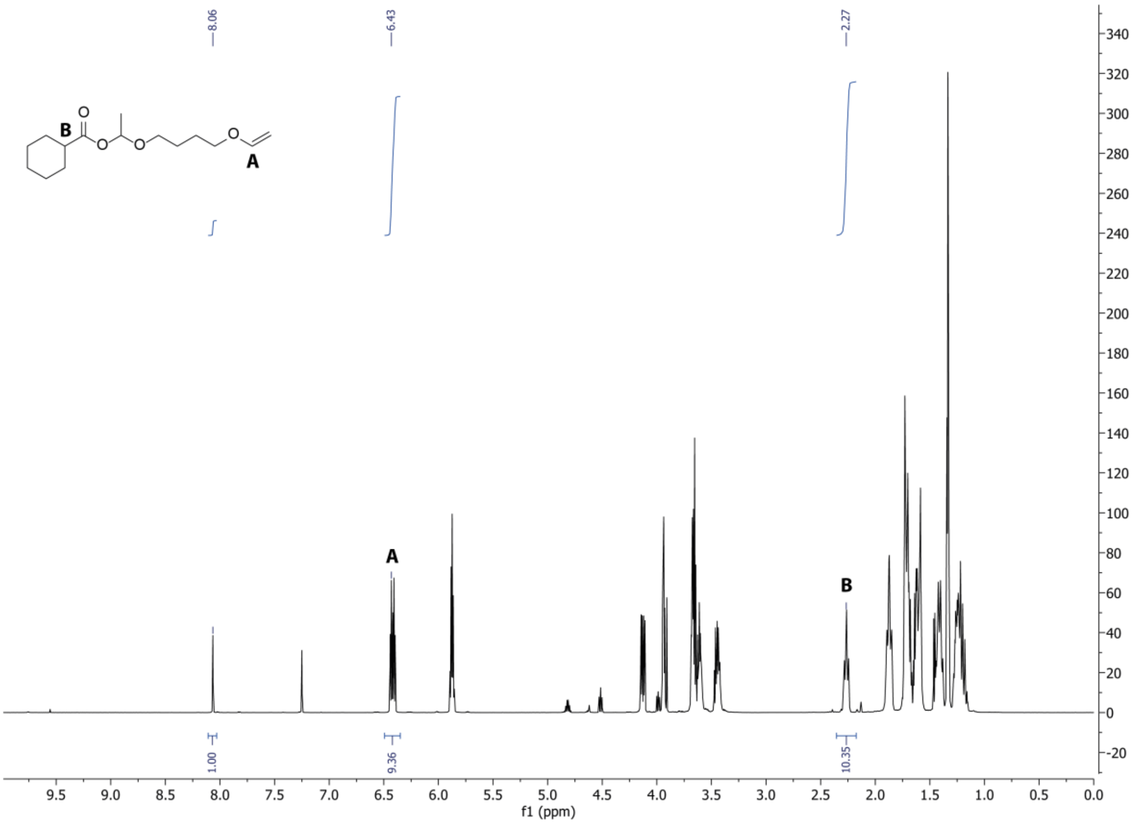

Figure 6.21: ^{1}H NMR spectra of HAE-1 before (top) and after (bottom) irradiation for determination of conversion in cationic photopolymerization.

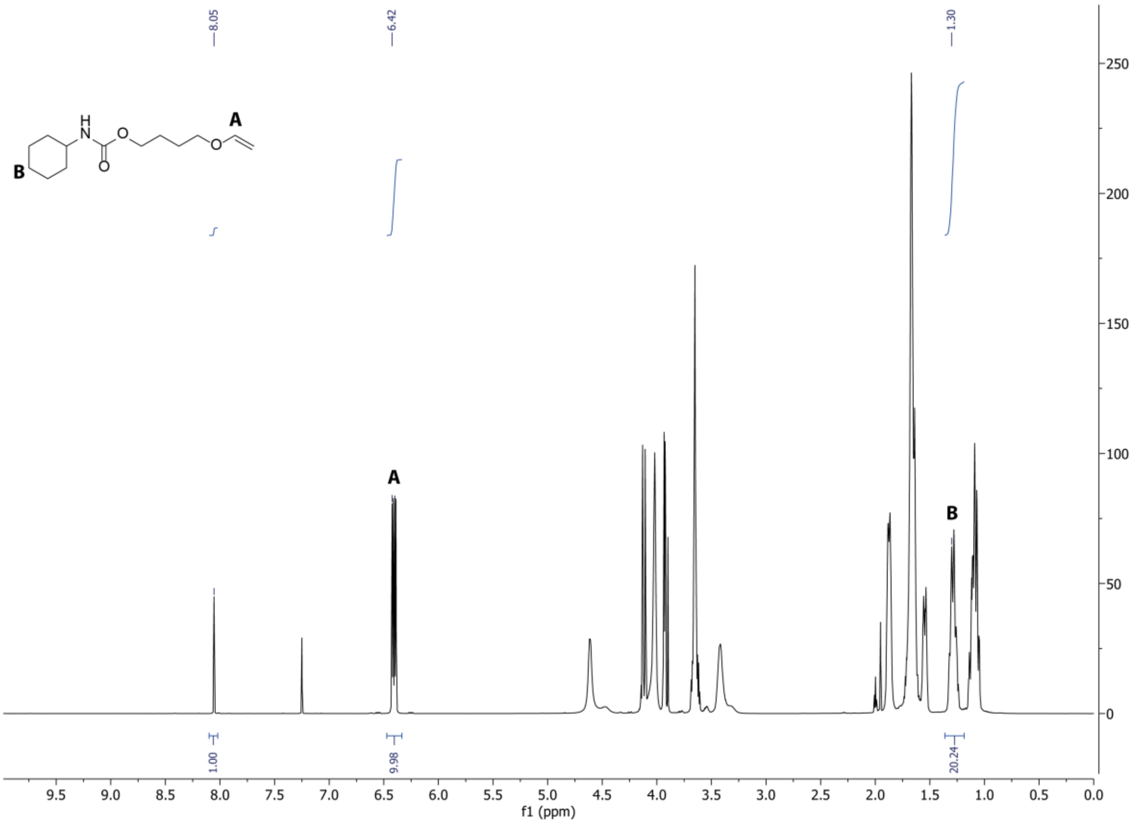

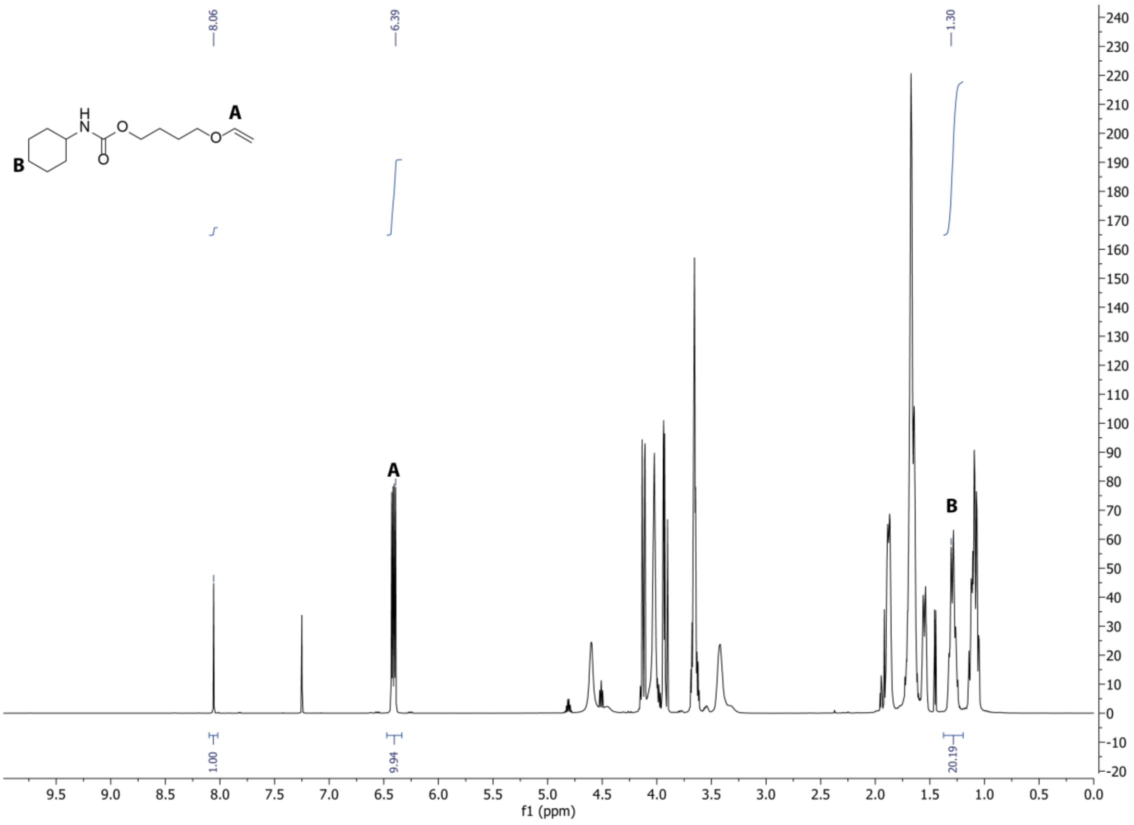

Figure 6.22: ^{1}H NMR spectra of U-1 before (top) and after (bottom) irradiation for determination of conversion in cationic photopolymerization.

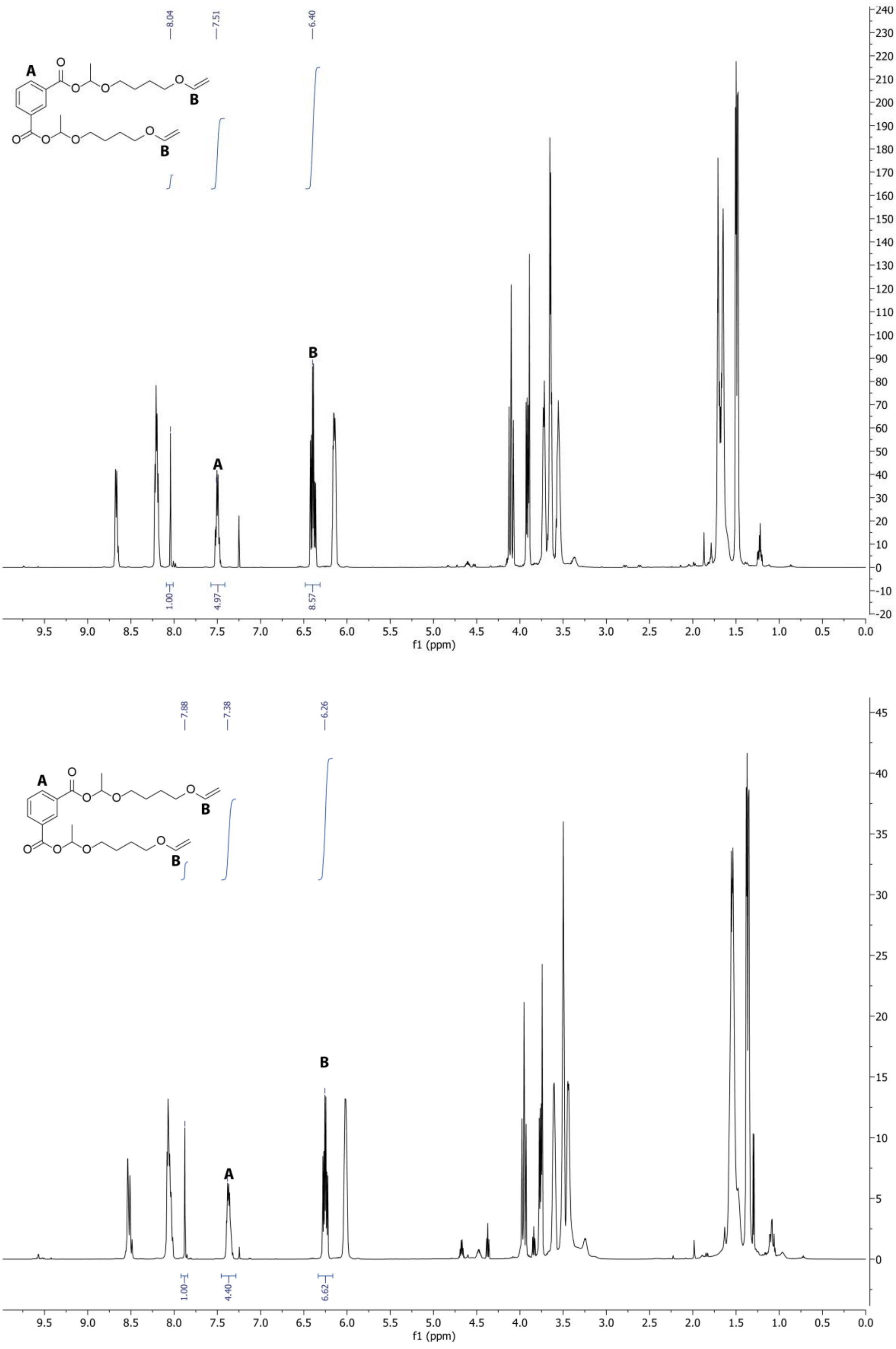

Figure 6.23: ^{1}H NMR spectra of HAE-2 before (top) and after (bottom) irradiation for determination of conversion in cationic photopolymerization.

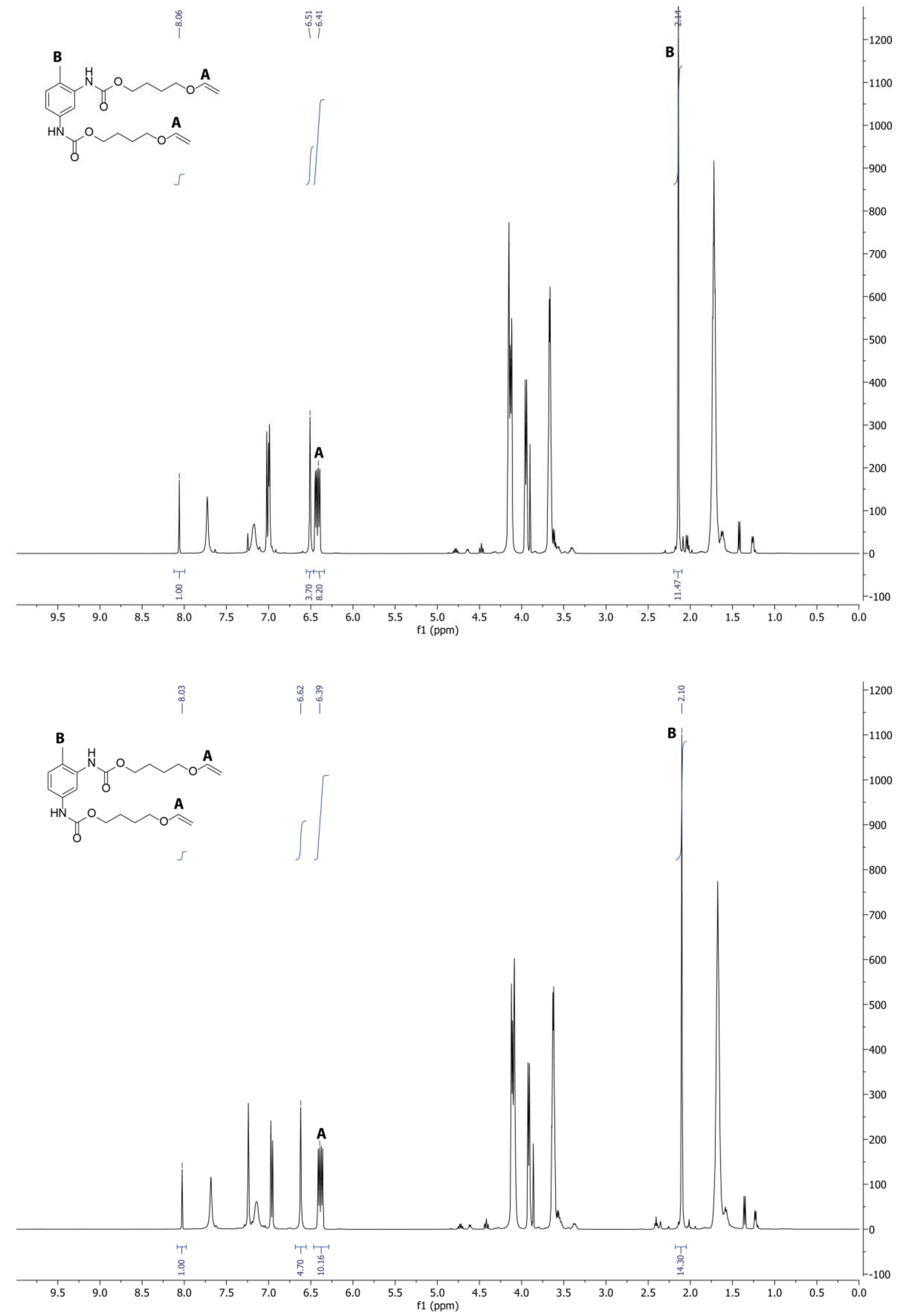

Figure 6.24: ^{1}H NMR spectra of U-2 before (top) and after (bottom) irradiation for determination of conversion in cationic photopolymerization.

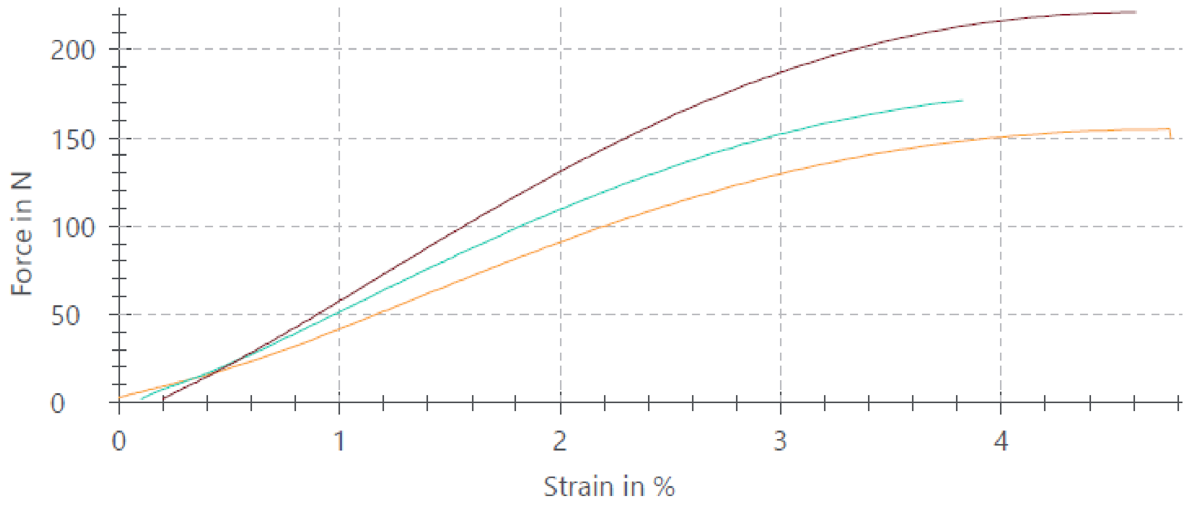

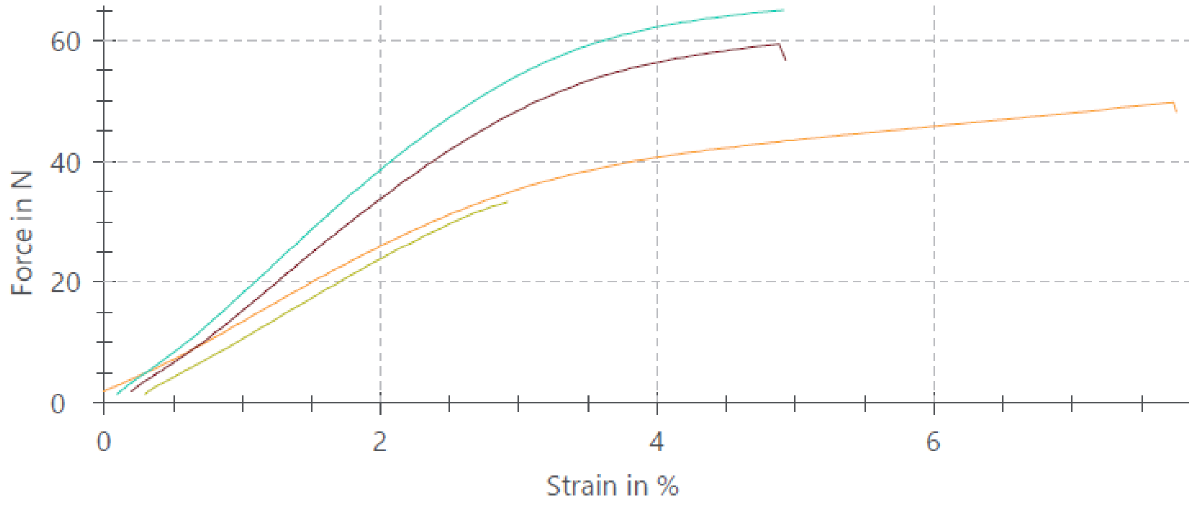

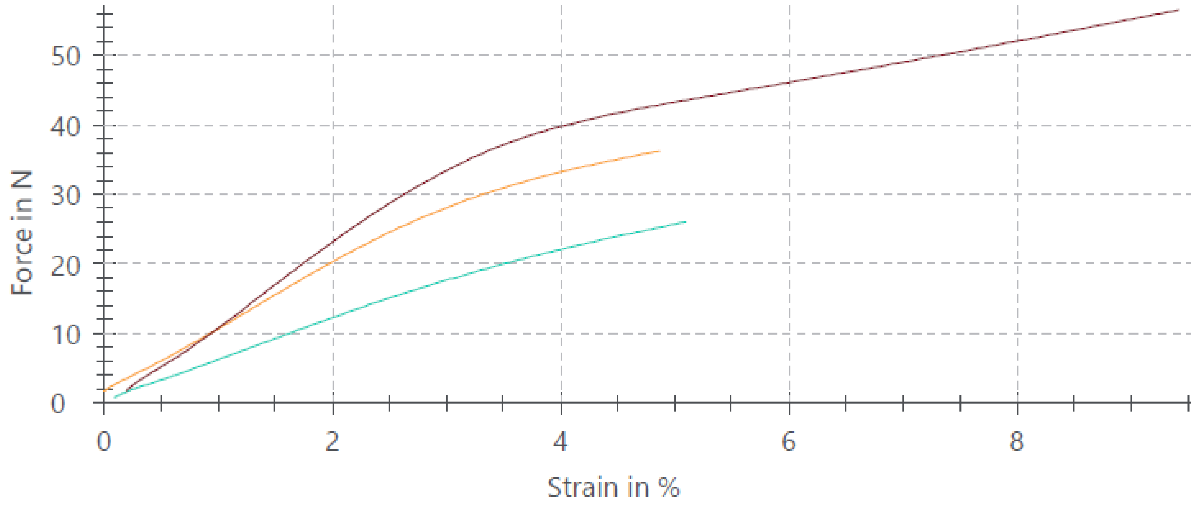

Figure 6.25: Stress-strain diagrams obtained from Tensile tests of specimens cured from hemiacetal ester-based vinyl ether functionalized formulation F-HAE. The specimens were stored in a desiccator for one week (top), under air for one week (middle) or stored under air for one week, followed by one week in a desiccator (bottom), respectively.

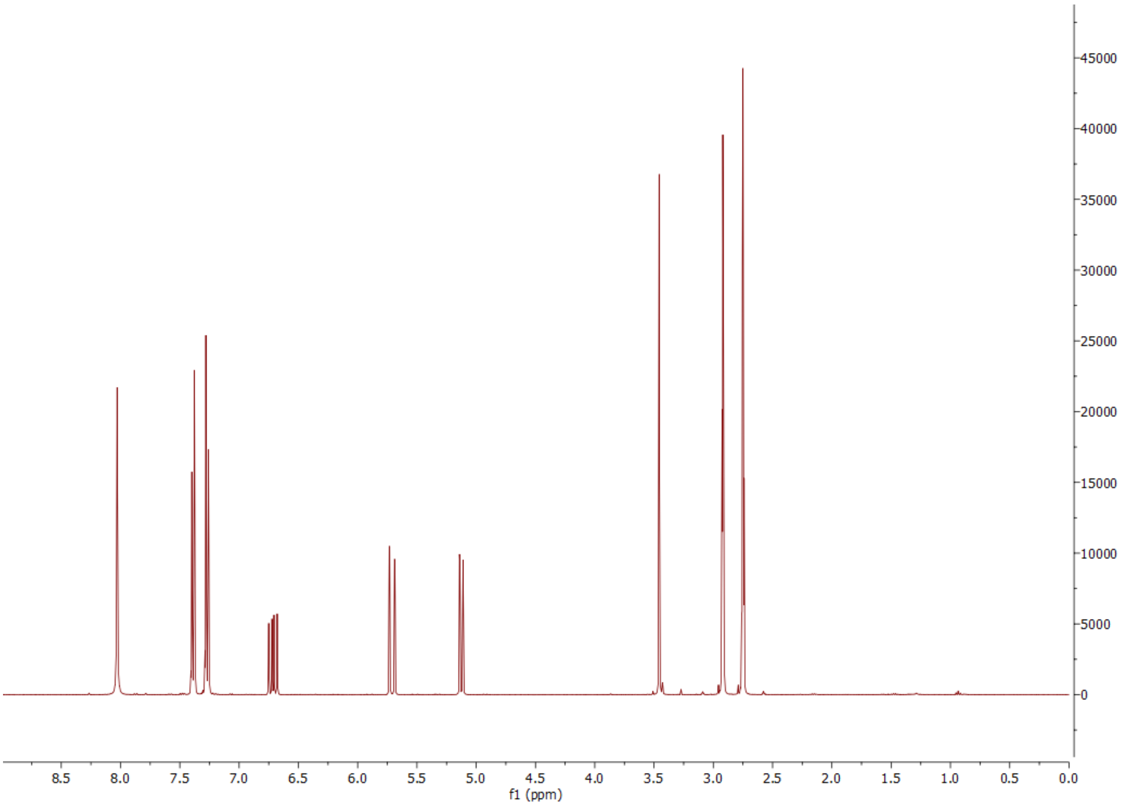

Figure 6.26: ^{1}H-NMR spectra of sodium p-styrene sulfate in DMF-d_7 after three days of storage.

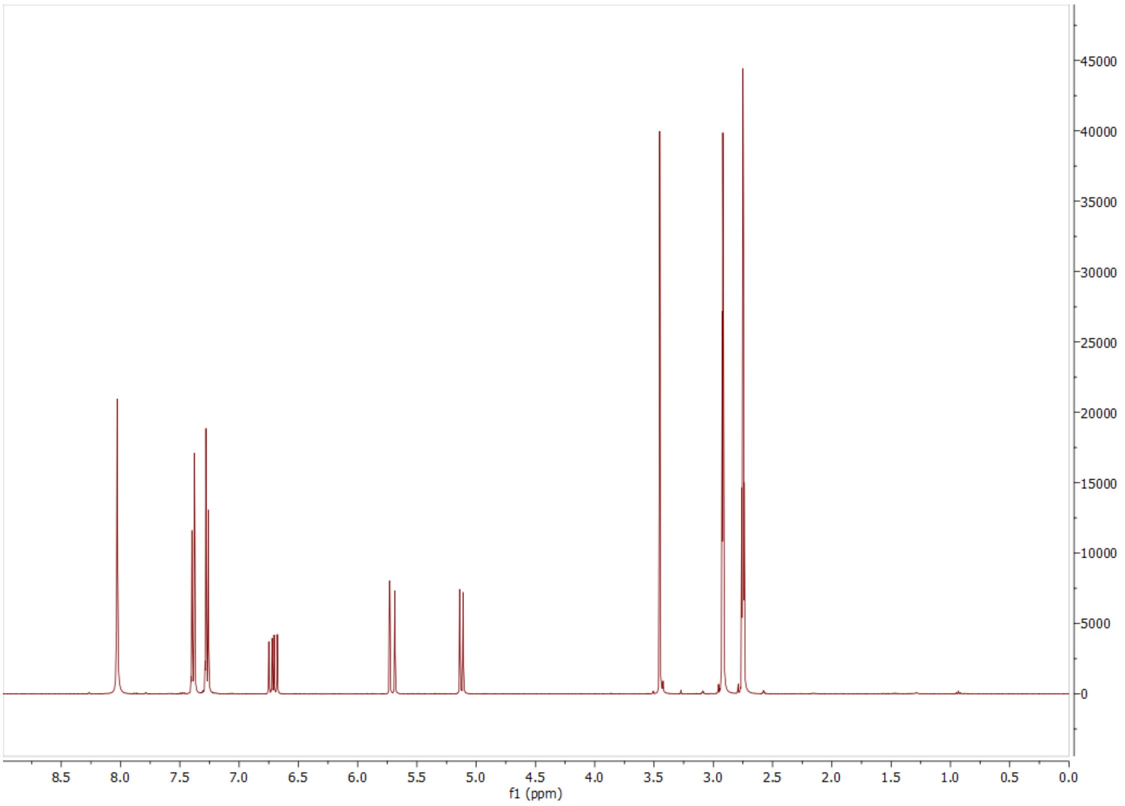

Figure 6.27: ^{1}H-NMR spectra of sodium p-styrene sulfate in DMF-d_7 after seven days of storage.

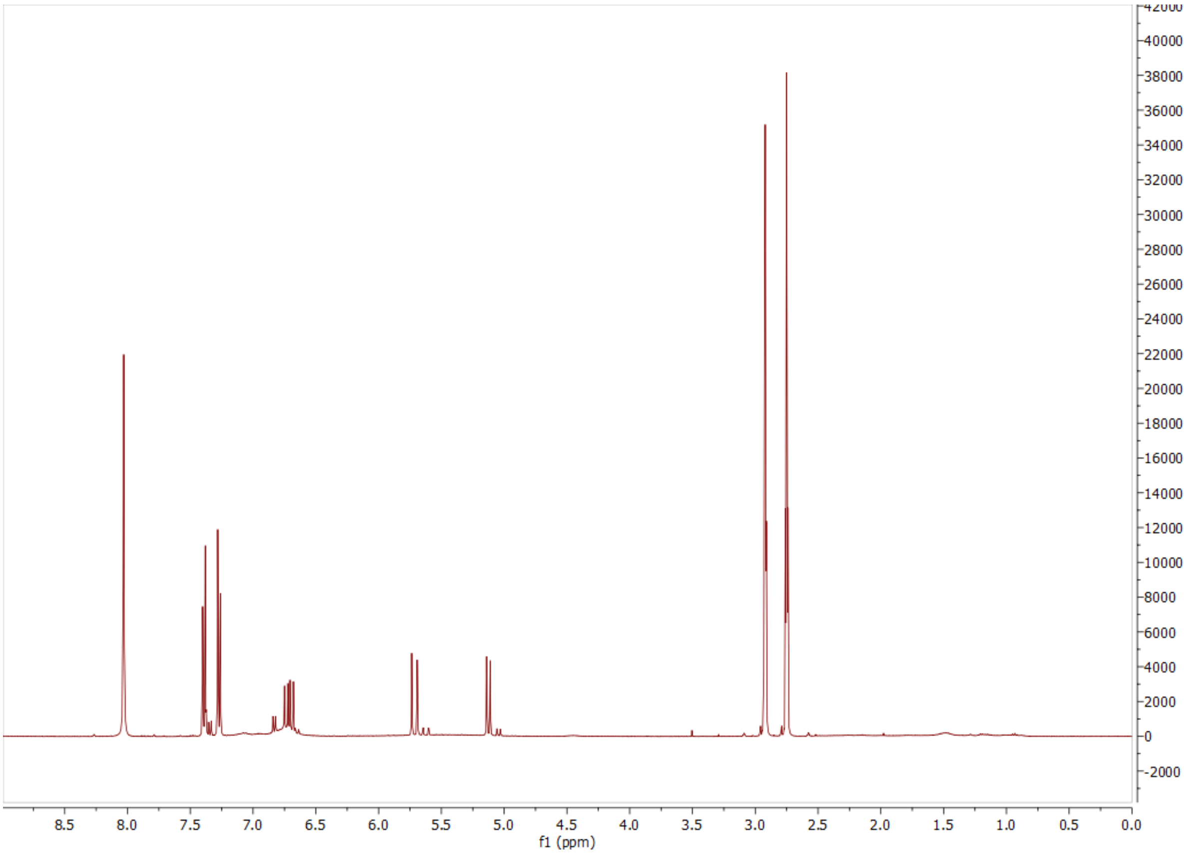

Figure 6.28: ^{1}**H-NMR spectra of sodium p-styrene sulfate in DMF-d$_7$ after 24 days of storage.**

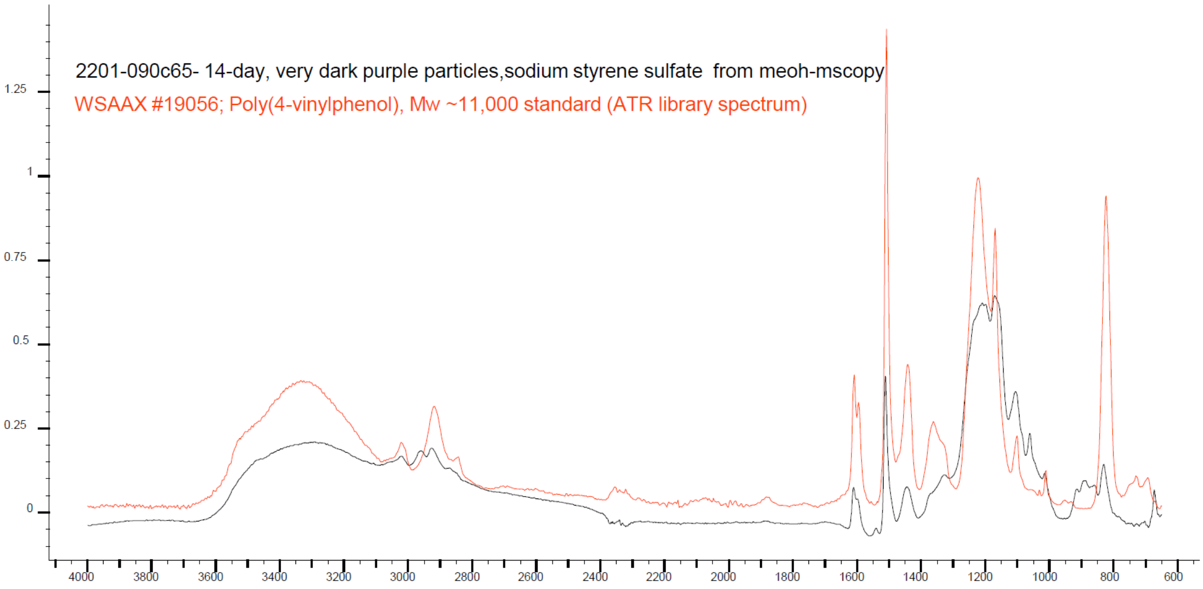

Figure 6.29: IR spectrum of dark purple colored particles of SSS after 14 days of storage compared to poly(4-vinylphenol) (taken from ATR spectrum library).

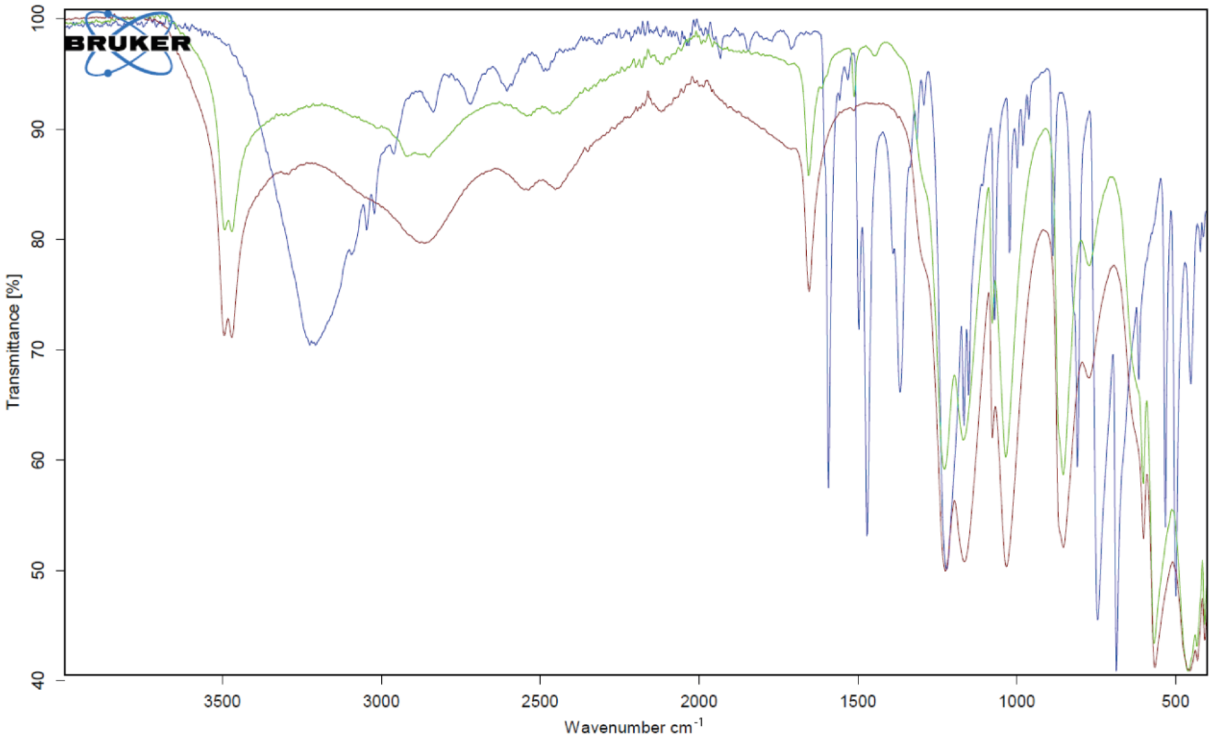

Figure 6.30: FTIR spectra of sodium hydrogen sulfate monohydrate (dark red), phenol (blue) and a grinded mixture thereof (green).

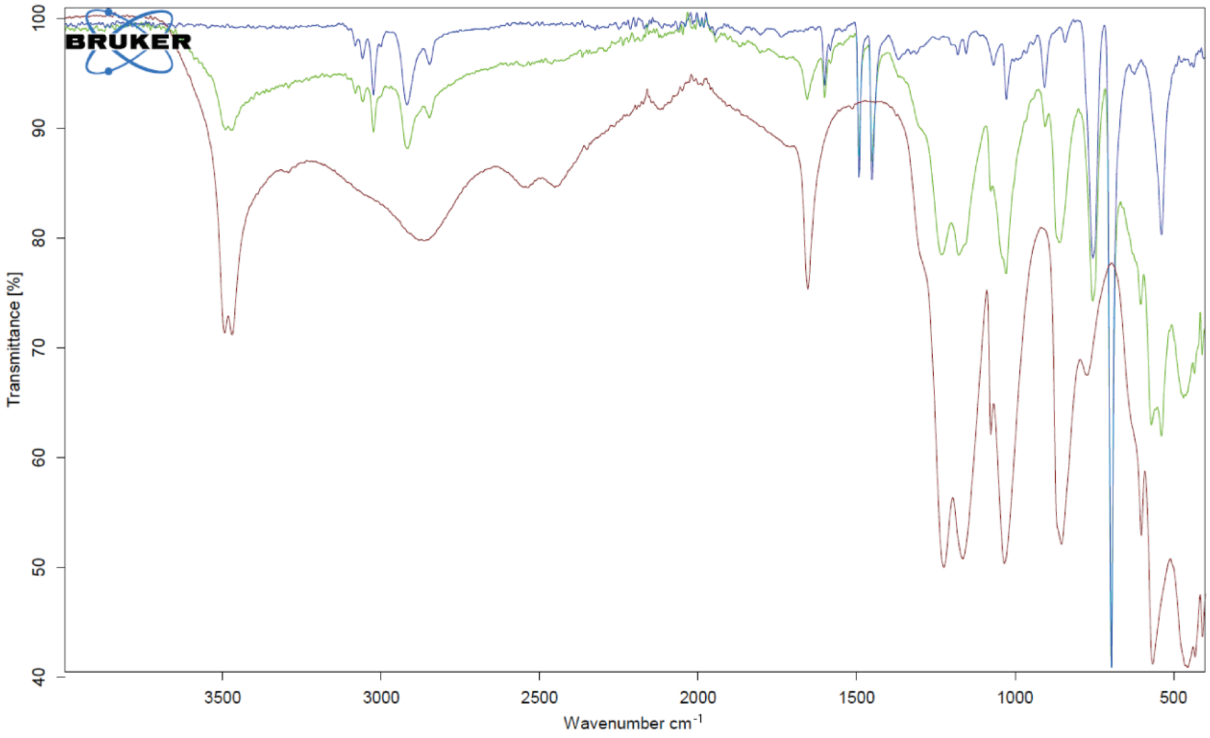

Figure 6.31: FTIR spectra of sodium hydrogen sulfate monohydrate (dark red), polystyrene (blue) and a grinded mixture thereof (green).

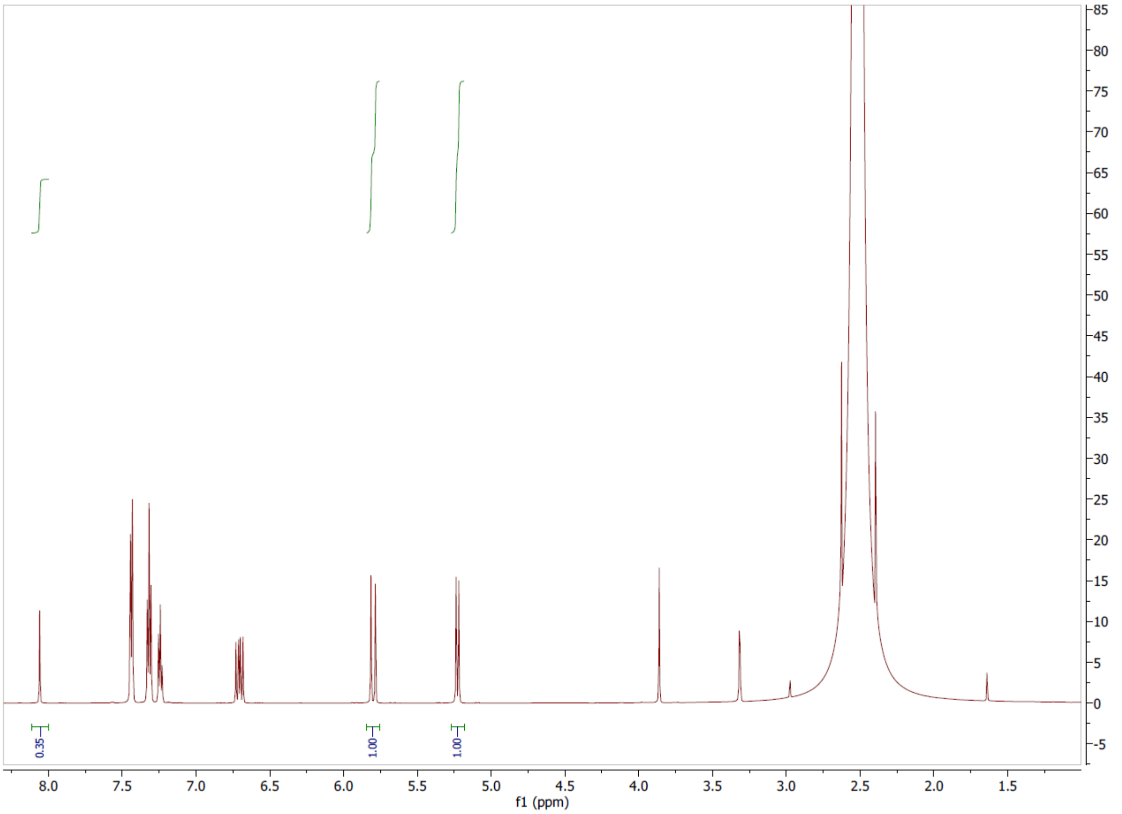

Figure 6.32: ^{1}H NMR spectrum for kinetic measurements of the free radical polymerization of styrene at *t* = 0 min.

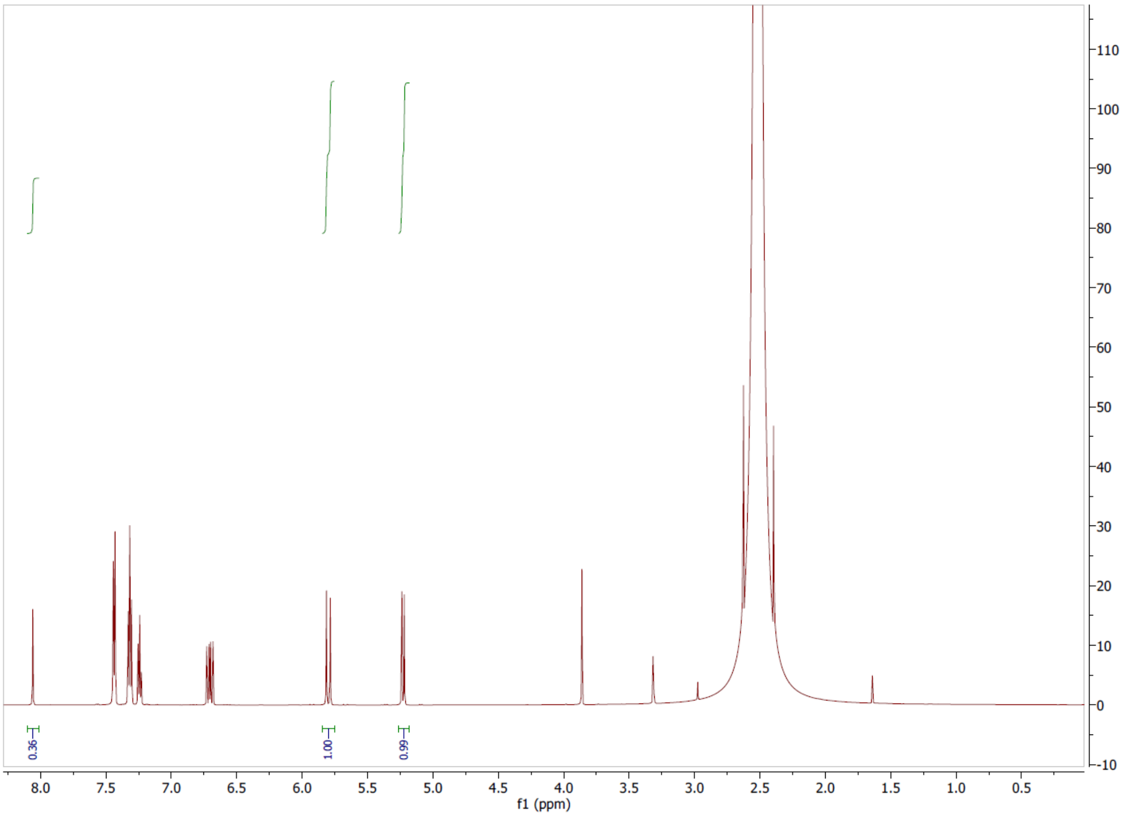

Figure 6.33: ^{1}H NMR spectrum for kinetic measurements of the free radical polymerization of styrene at *t* = 5 min.

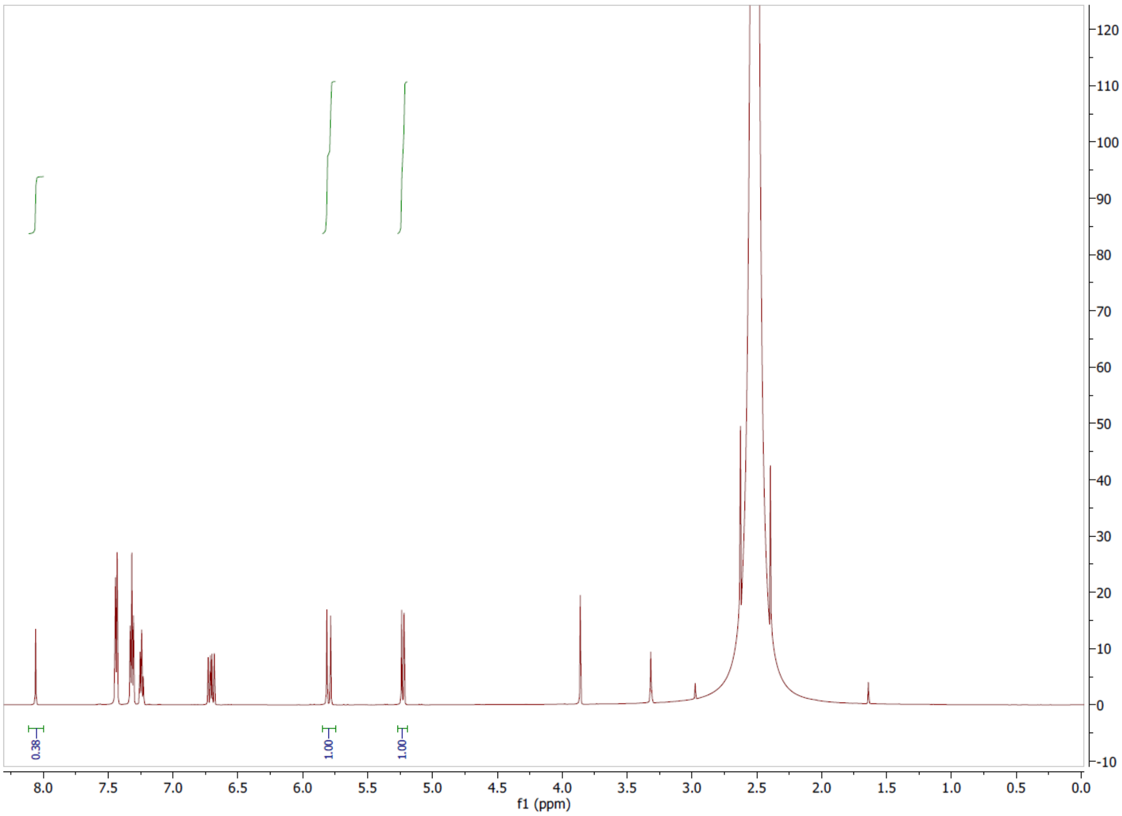

Figure 6.34: ^{1}H NMR spectrum for kinetic measurements of the free radical polymerization of styrene at *t* = 10 min.

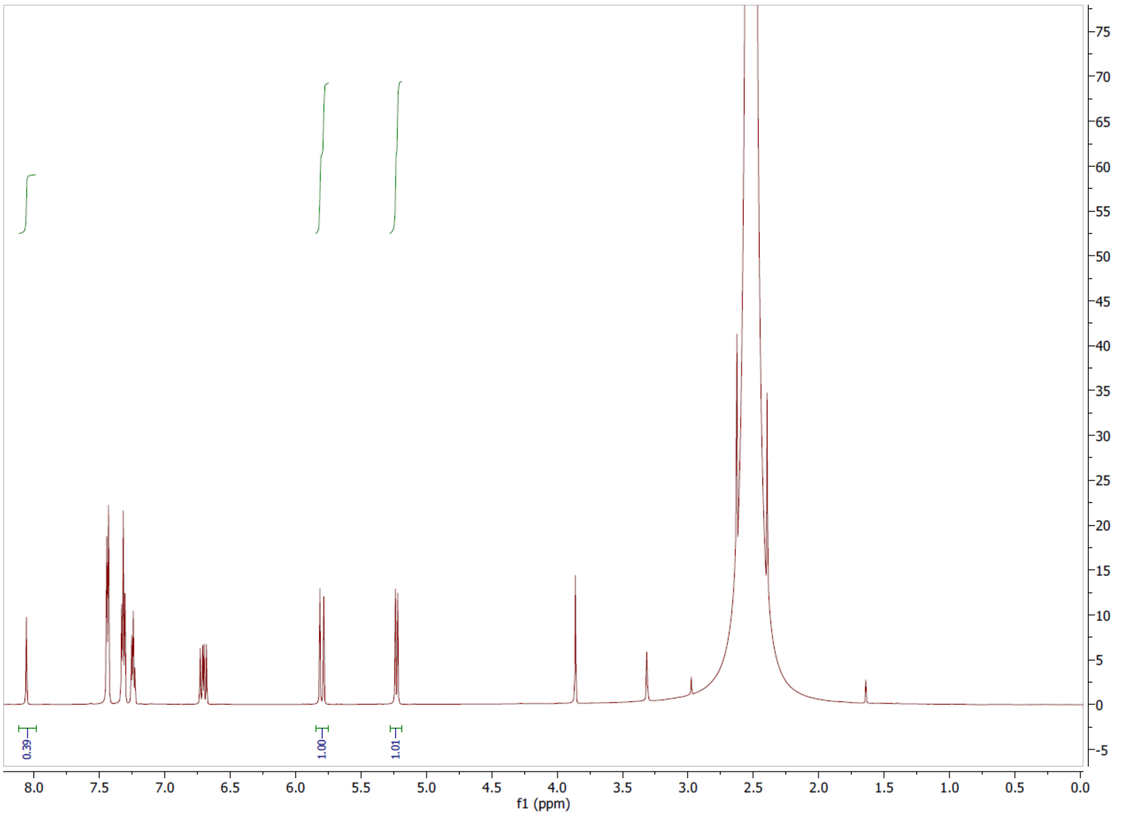

Figure 6.35: ^{1}H NMR spectrum for kinetic measurements of the free radical polymerization of styrene at *t* = 20 min.

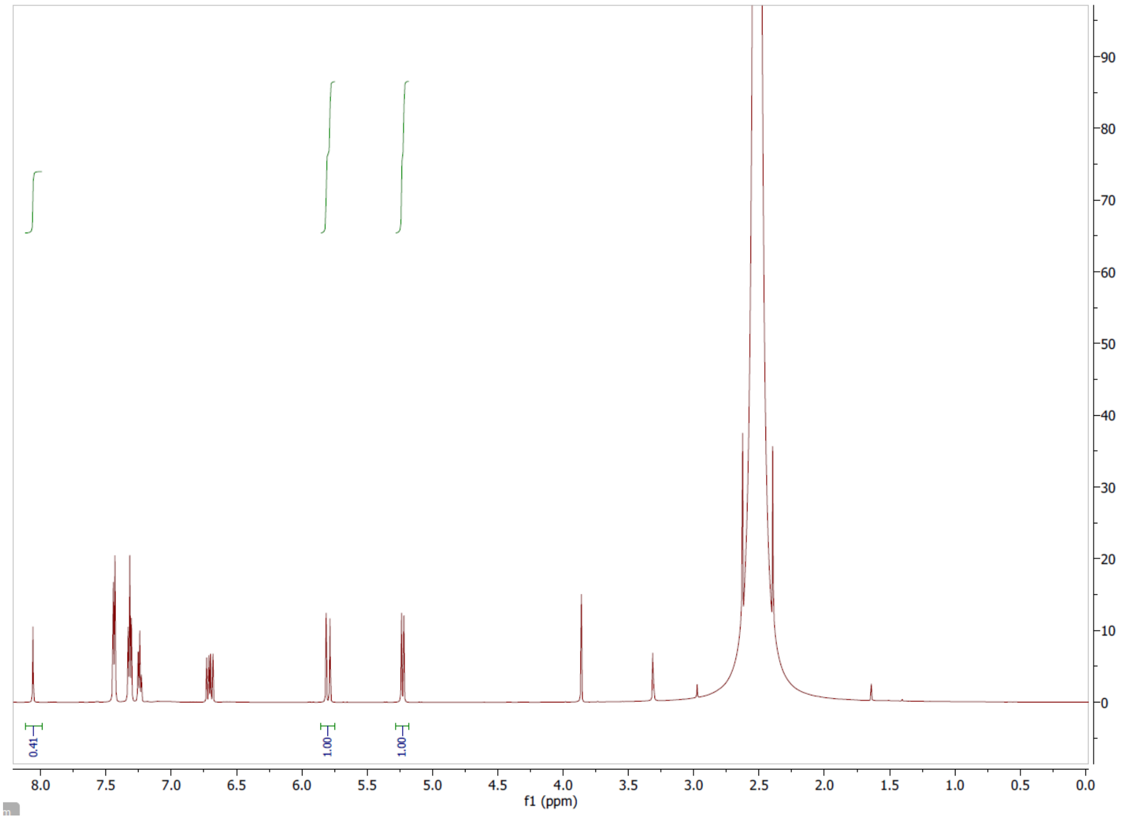

Figure 6.36: ^{1}H NMR spectrum for kinetic measurements of the free radical polymerization of styrene at *t* = 45 min.

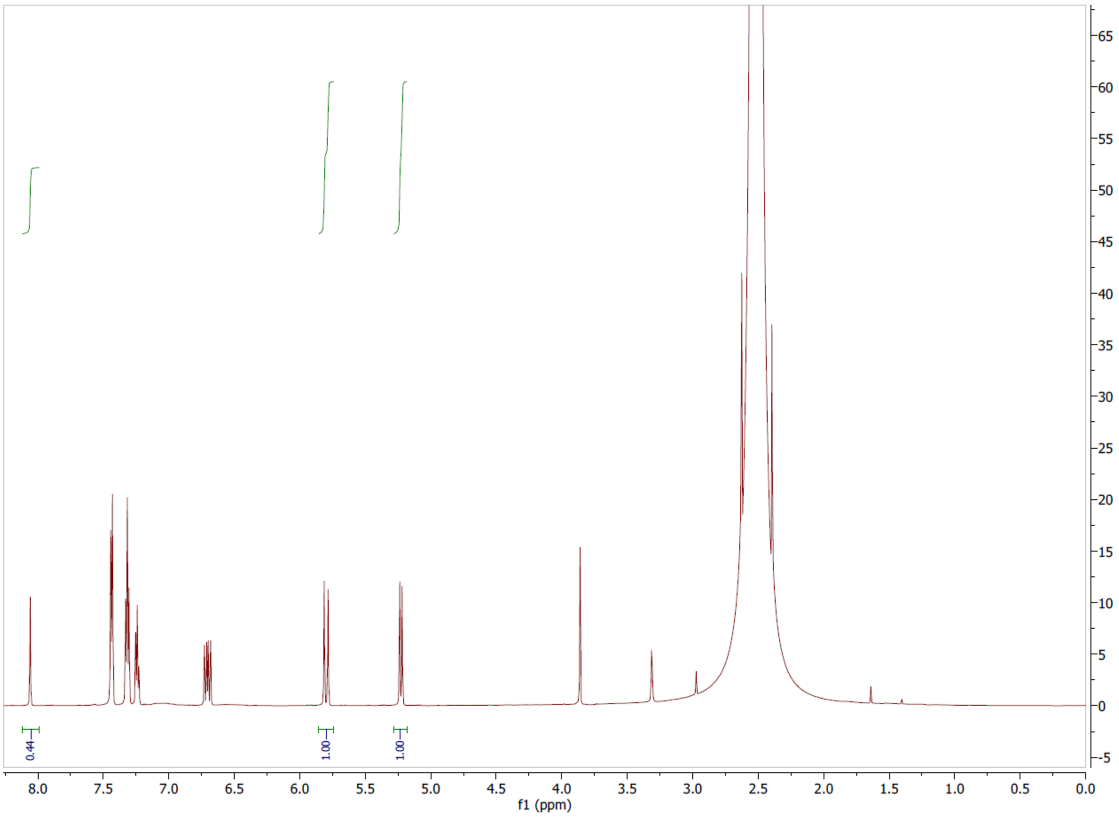

Figure 6.37: ^{1}H NMR spectrum for kinetic measurements of the free radical polymerization of styrene at *t* = 90 min.

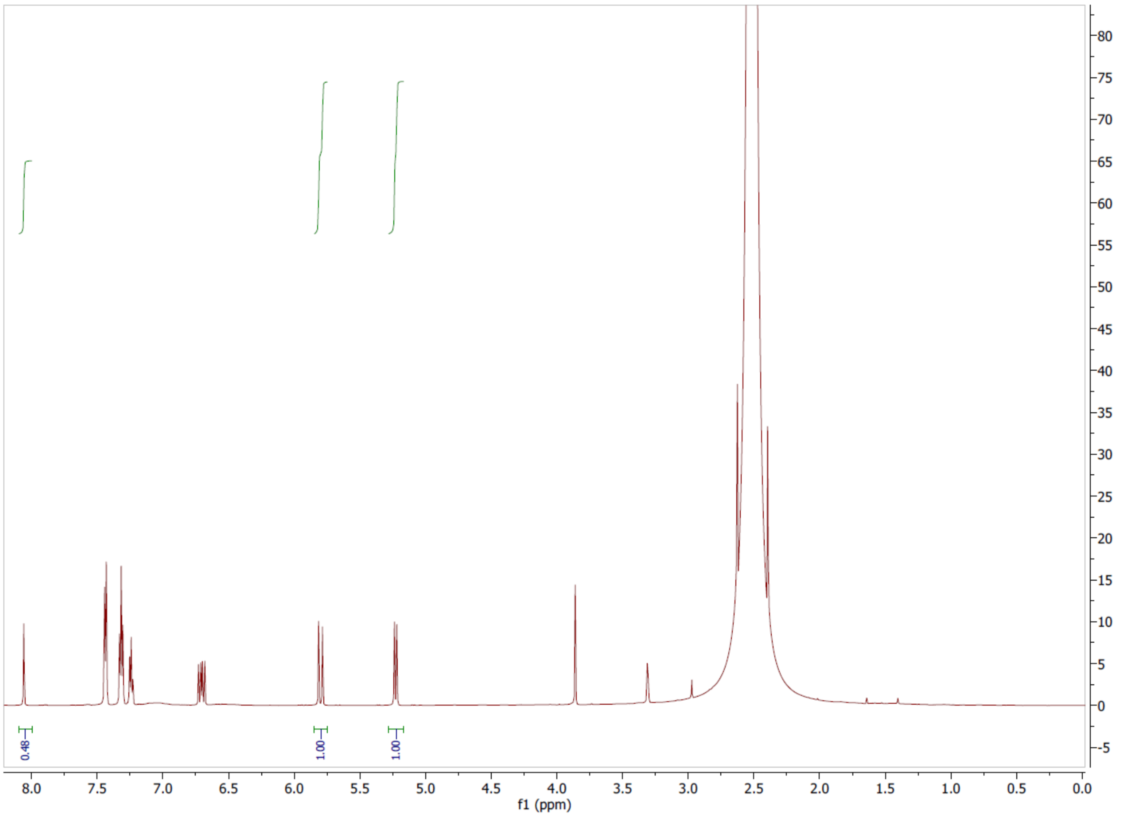

Figure 6.38: ^{1}**H NMR spectrum for kinetic measurements of the free radical polymerization of styrene at *t* = 180 min.**

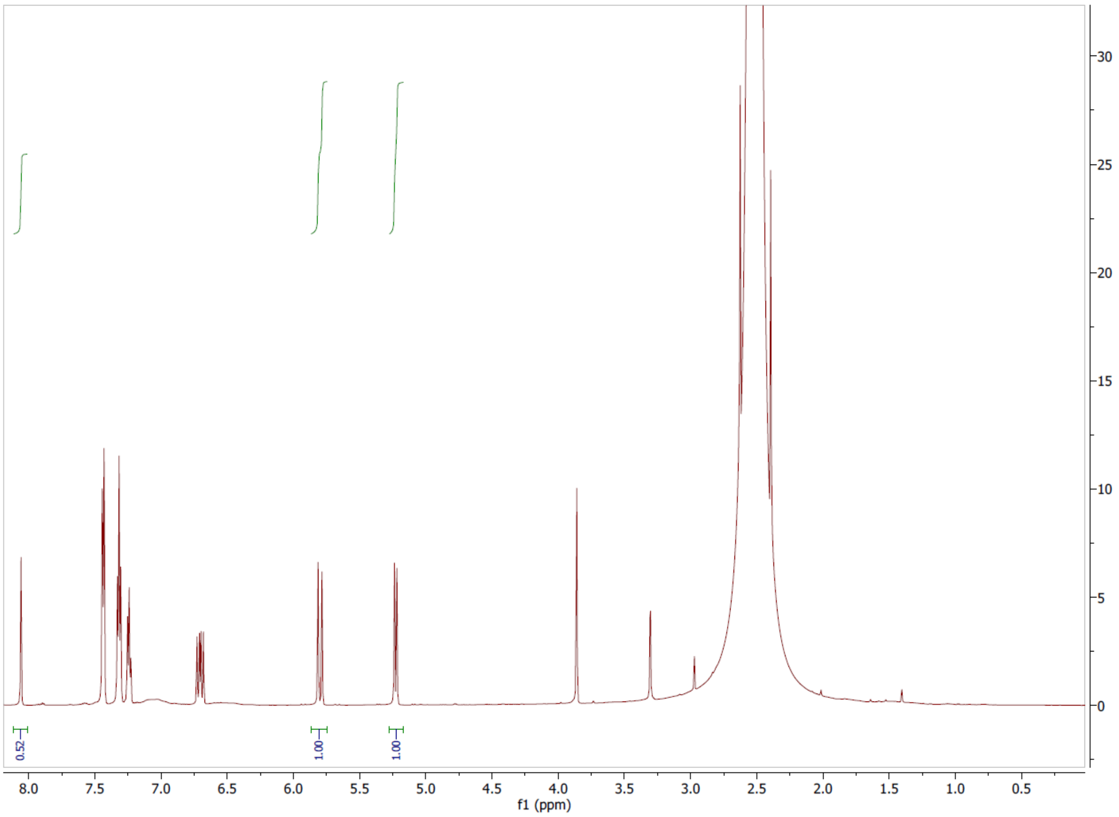

Figure 6.39: ^{1}**H NMR spectrum for kinetic measurements of the free radical polymerization of styrene at *t* = 360 min.**

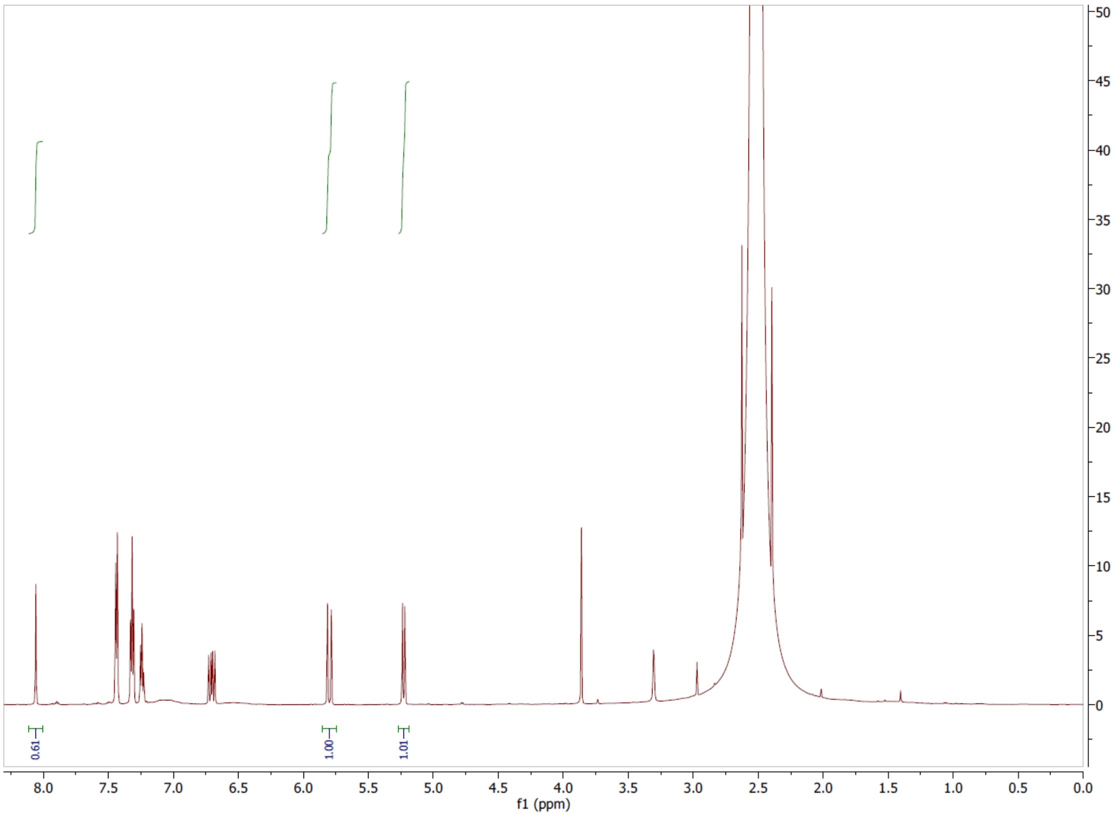

Figure 6.40: ^{1}H NMR spectrum for kinetic measurements of the free radical polymerization of styrene at *t* = 1440 min.

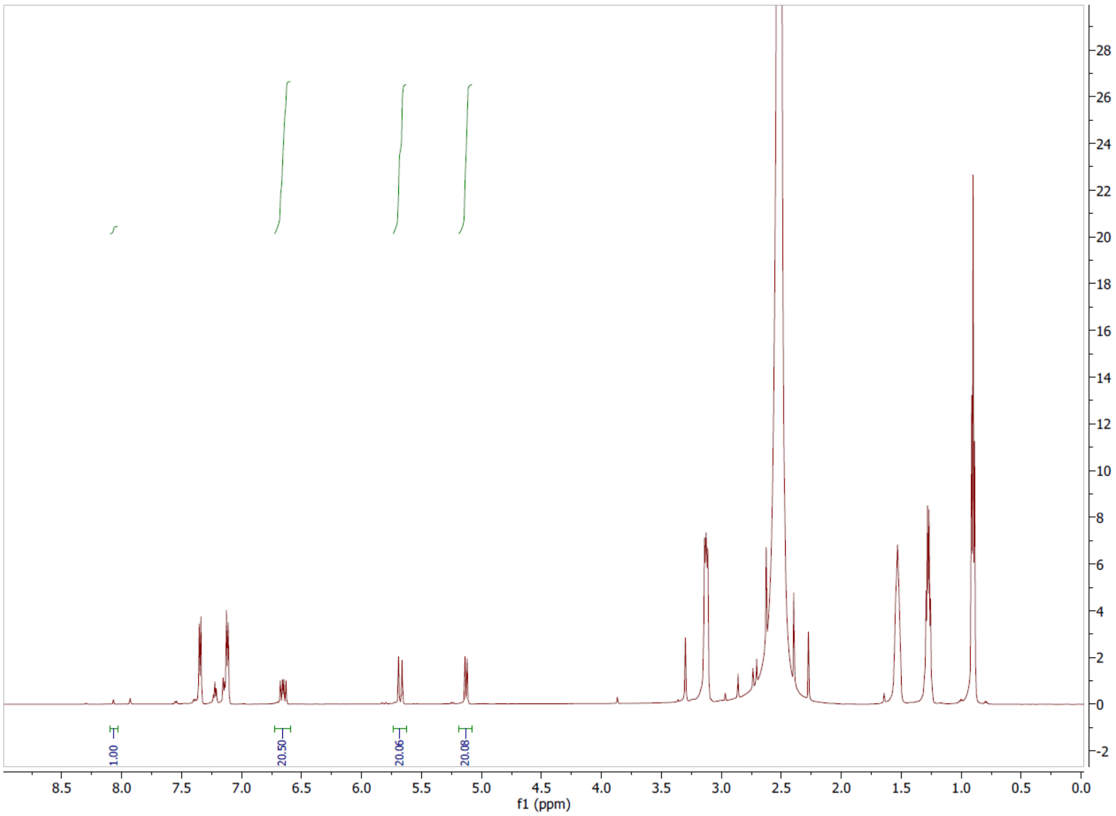

Figure 6.41: ^{1}H NMR spectrum for kinetic measurements of the free radical polymerization of TBASS at *t* = 0 min.

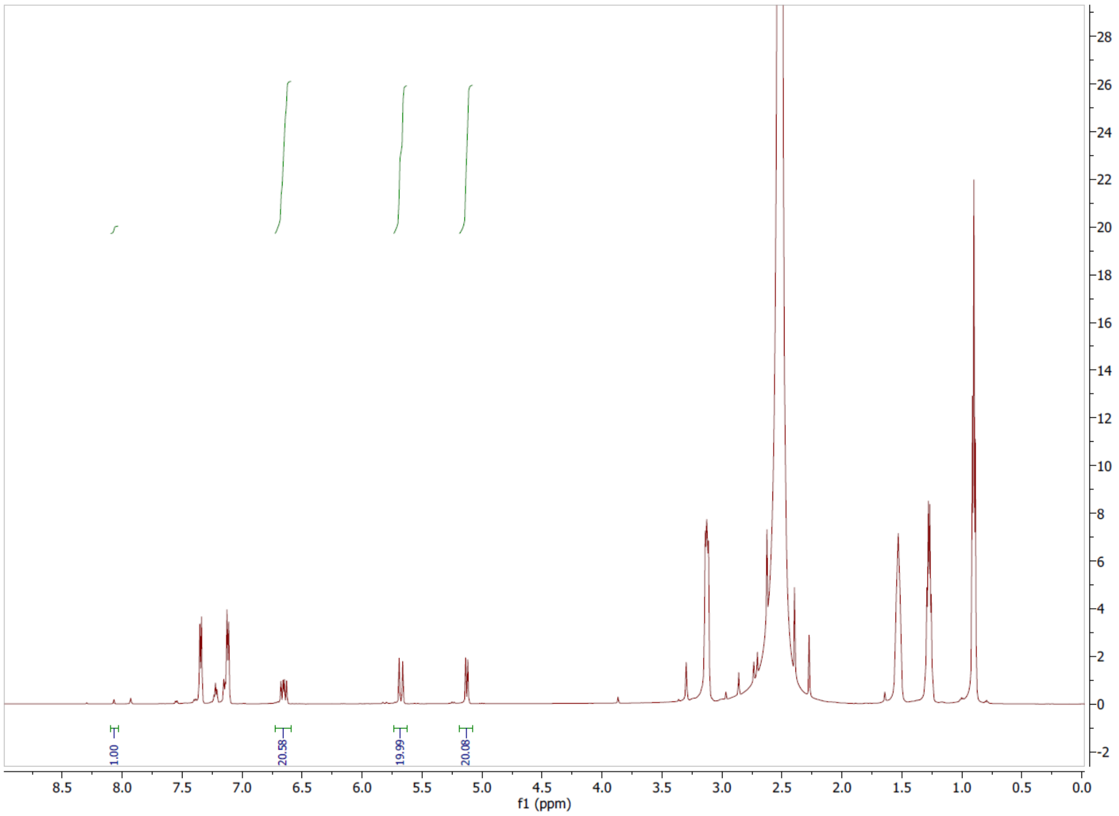

Figure 6.42: ^{1}H NMR spectrum for kinetic measurements of the free radical polymerization of TBASS at *t* = 5 min.

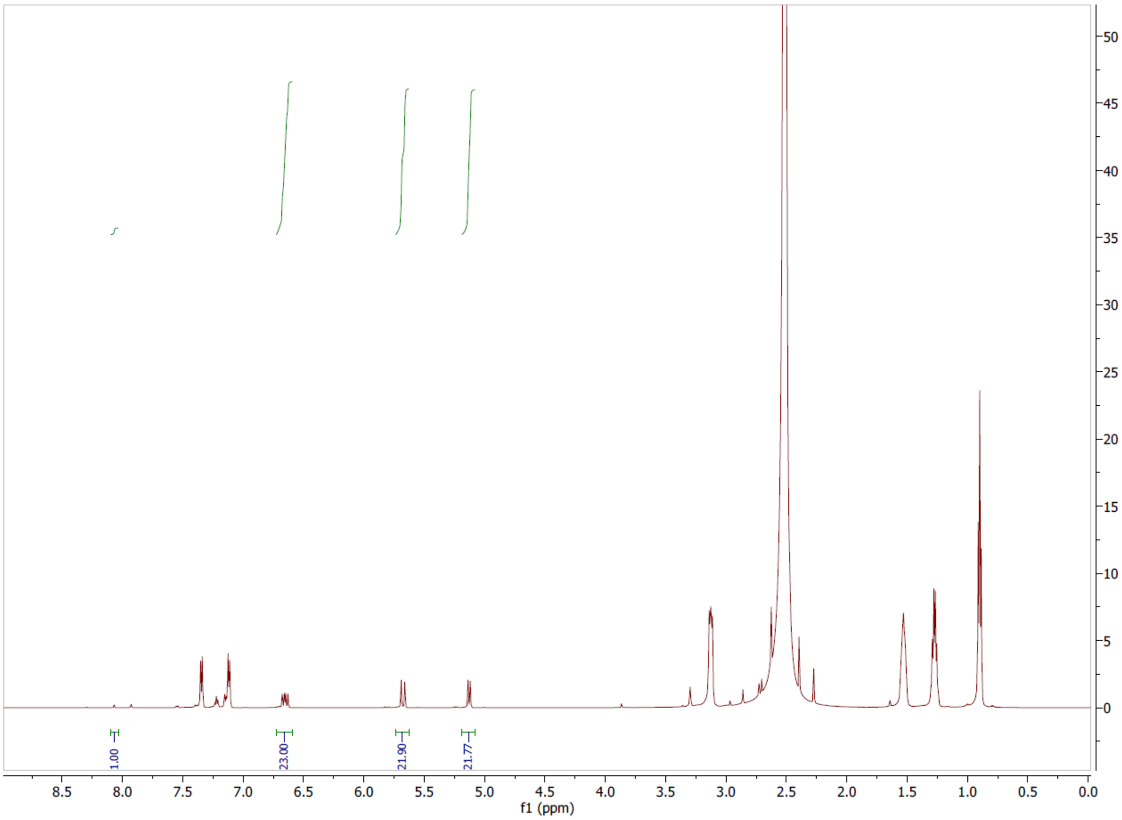

Figure 6.43: ^{1}H NMR spectrum for kinetic measurements of the free radical polymerization of TBASS at *t* = 10 min.

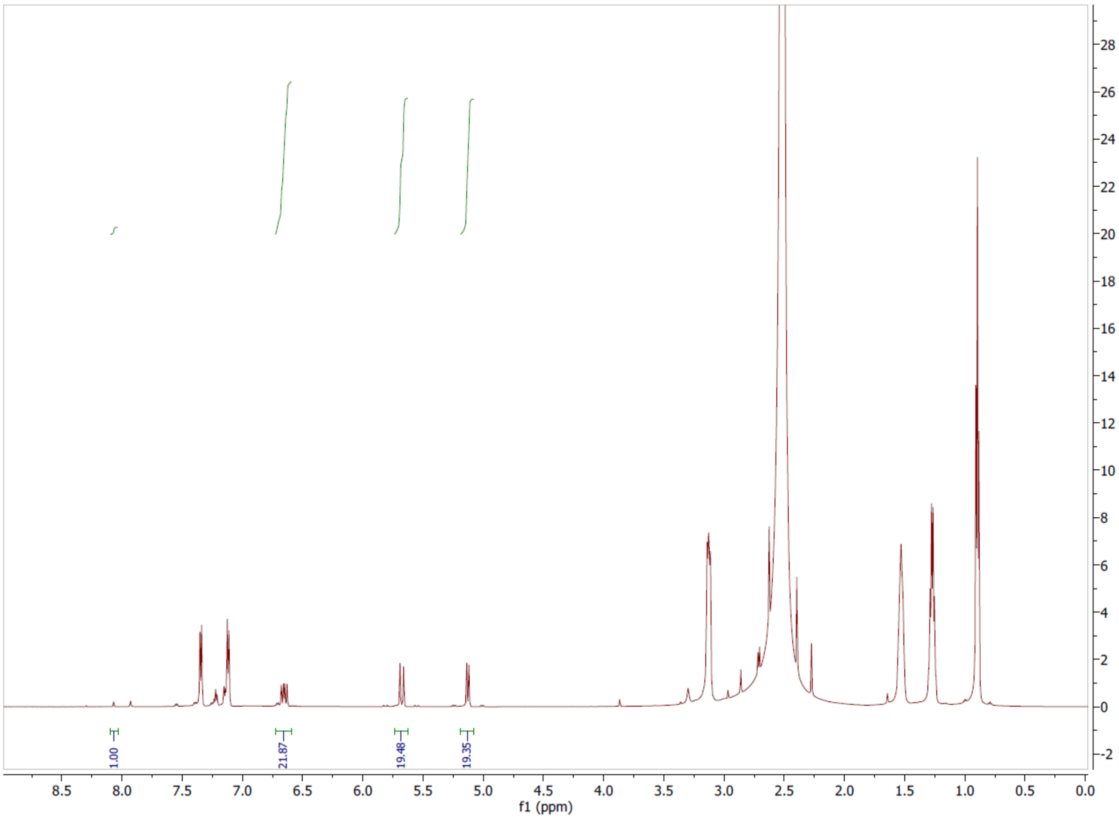

Figure 6.44: ^{1}H NMR spectrum for kinetic measurements of the free radical polymerization of TBASS at *t* = 20 min.

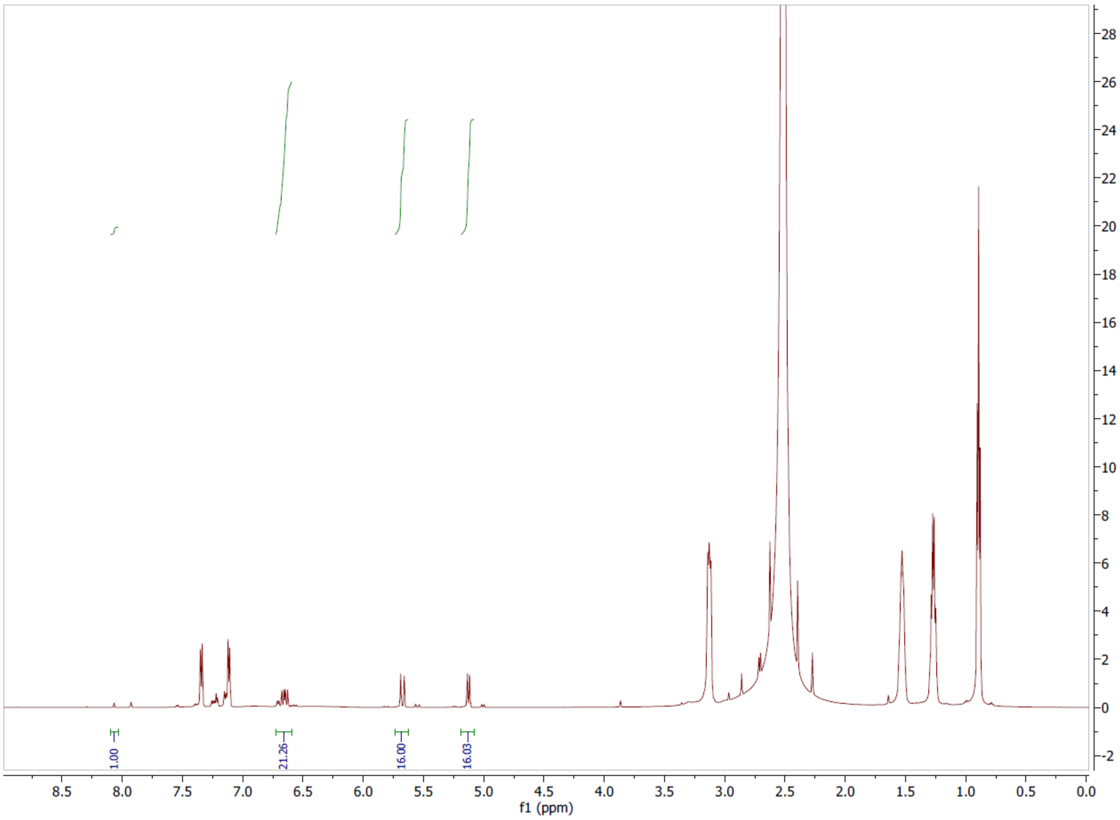

Figure 6.45: ^{1}H NMR spectrum for kinetic measurements of the free radical polymerization of TBASS at *t* = 45 min.

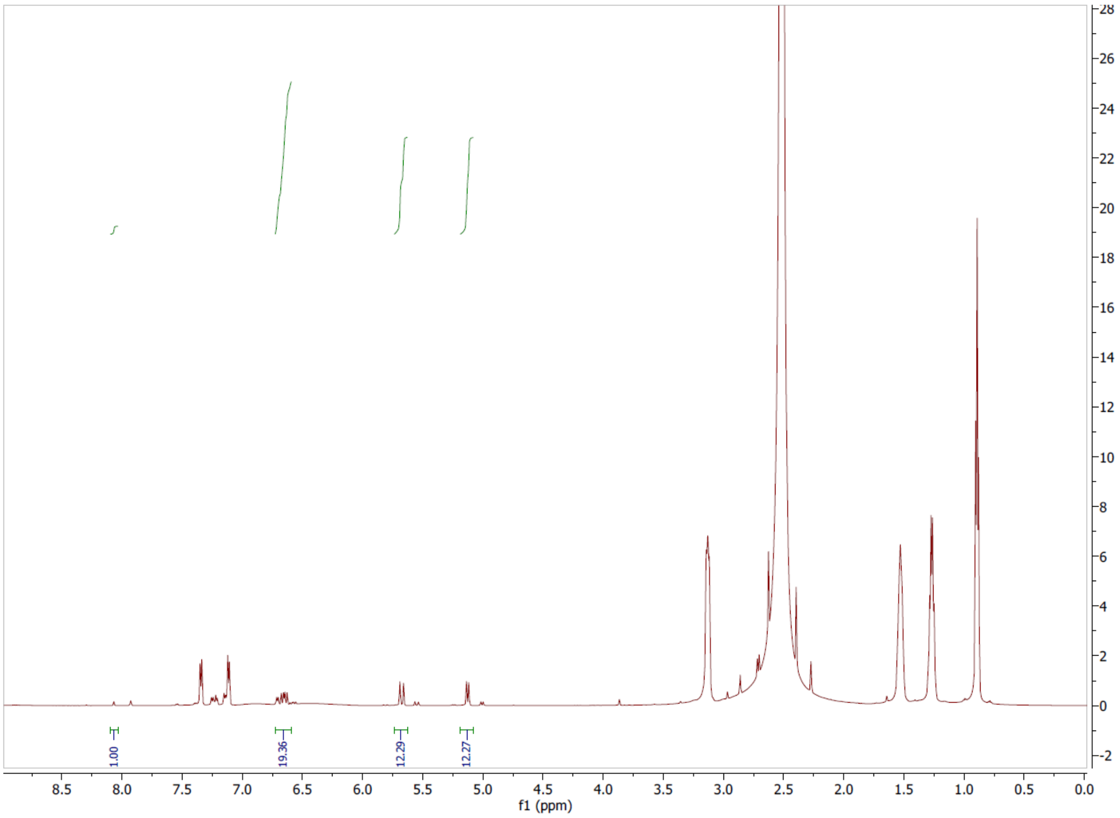

Figure 6.46: ^{1}H NMR spectrum for kinetic measurements of the free radical polymerization of TBASS at *t* = 90 min.

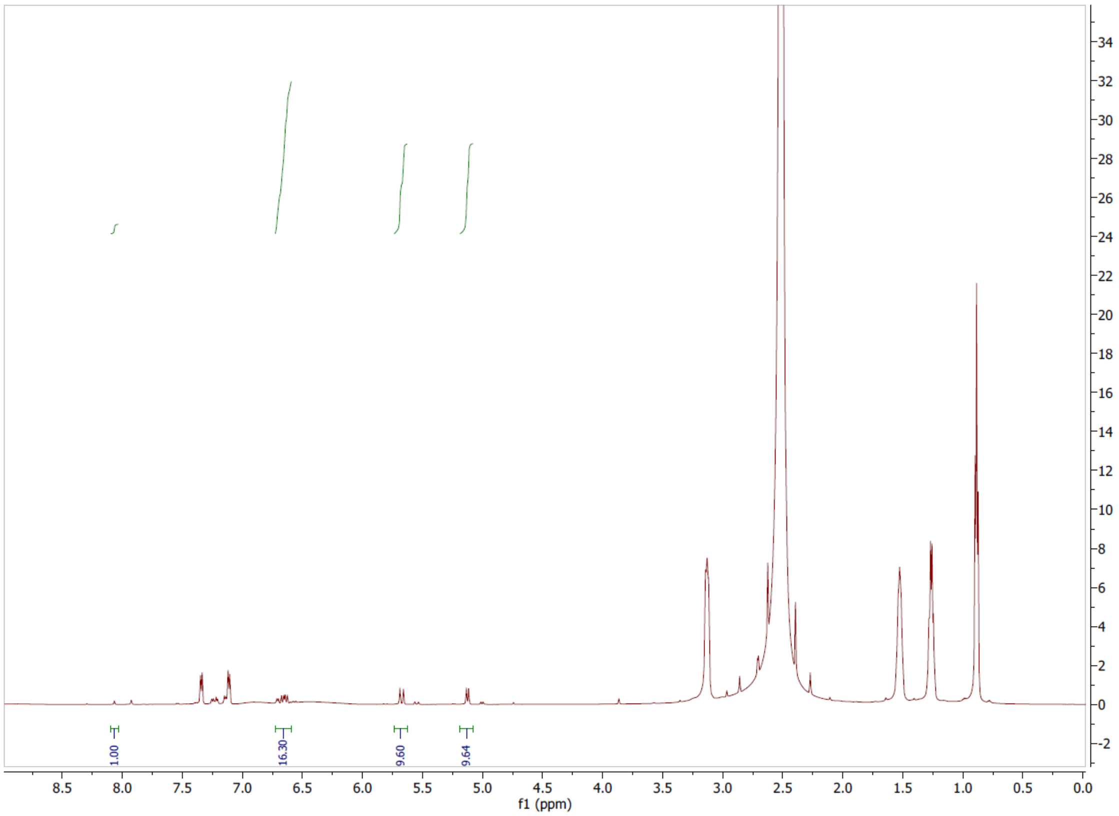

Figure 6.47: ^{1}H NMR spectrum for kinetic measurements of the free radical polymerization of TBASS at *t* = 180 min.

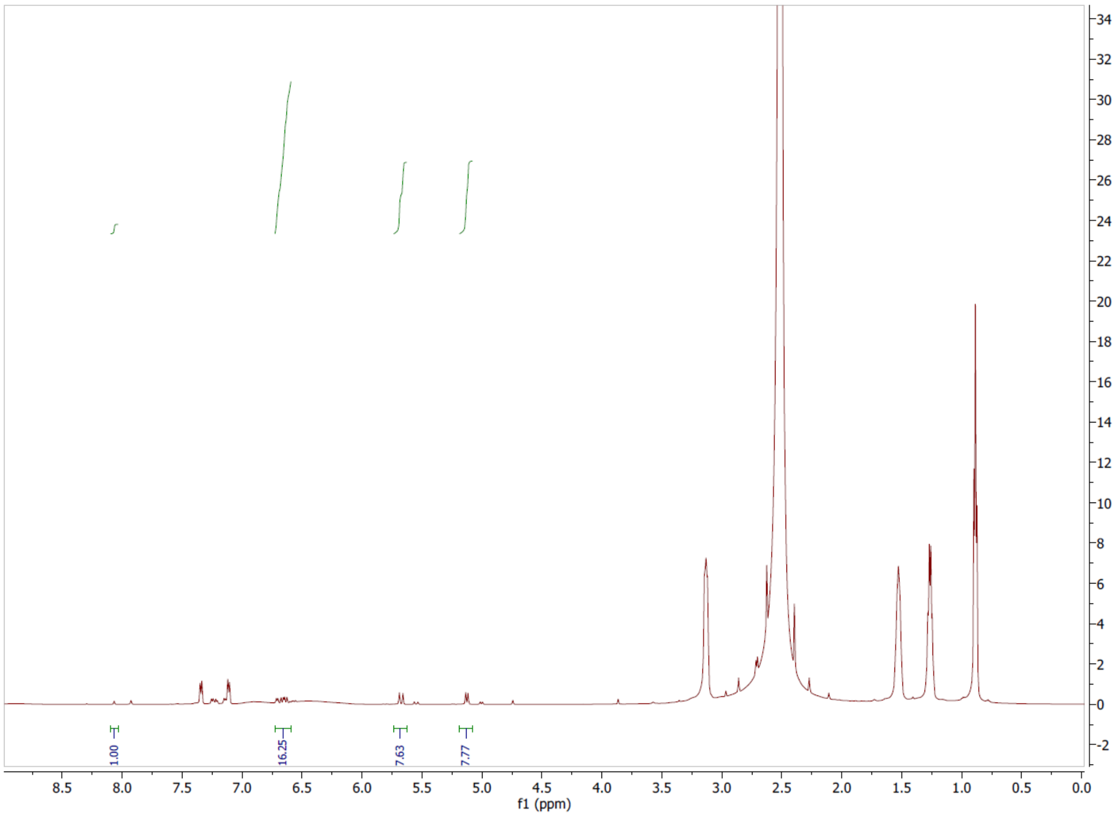

Figure 6.48: ^{1}H NMR spectrum for kinetic measurements of the free radical polymerization of TBASS at *t* = 360 min.

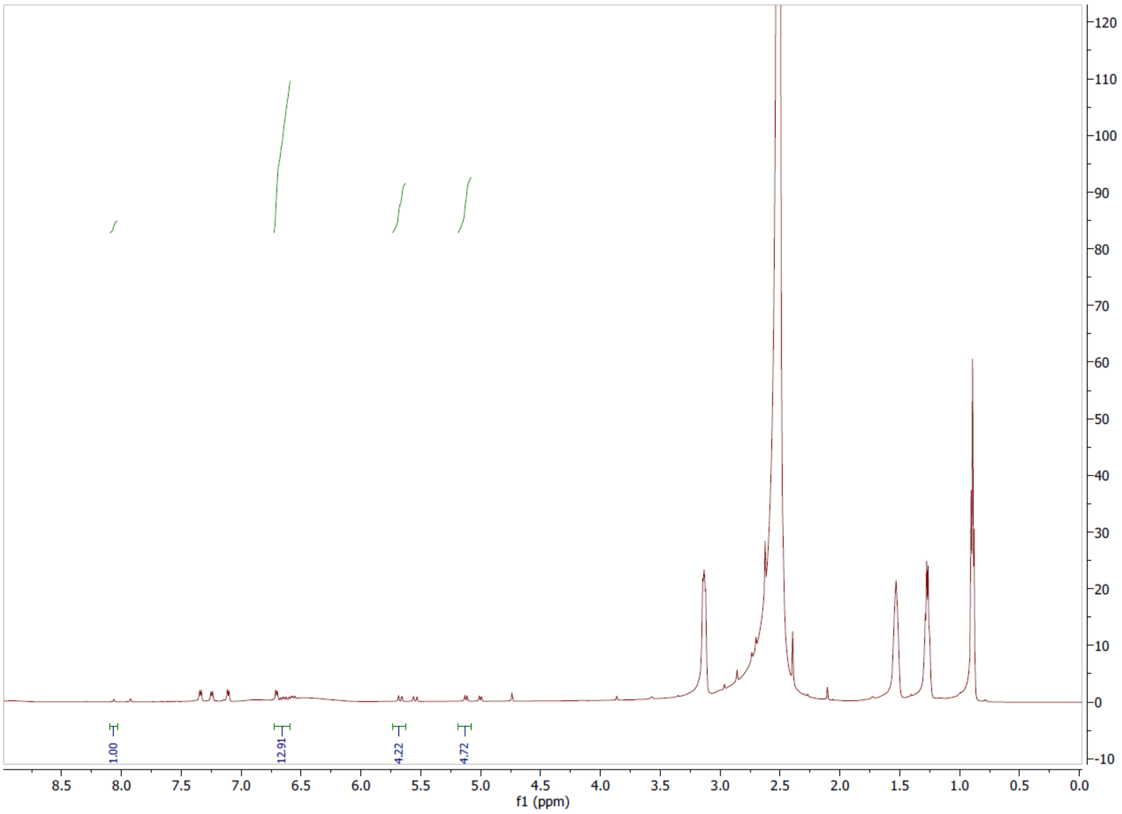

Figure 6.49: ^{1}H NMR spectrum for kinetic measurements of the free radical polymerization of TBASS at *t* = 1440 min.

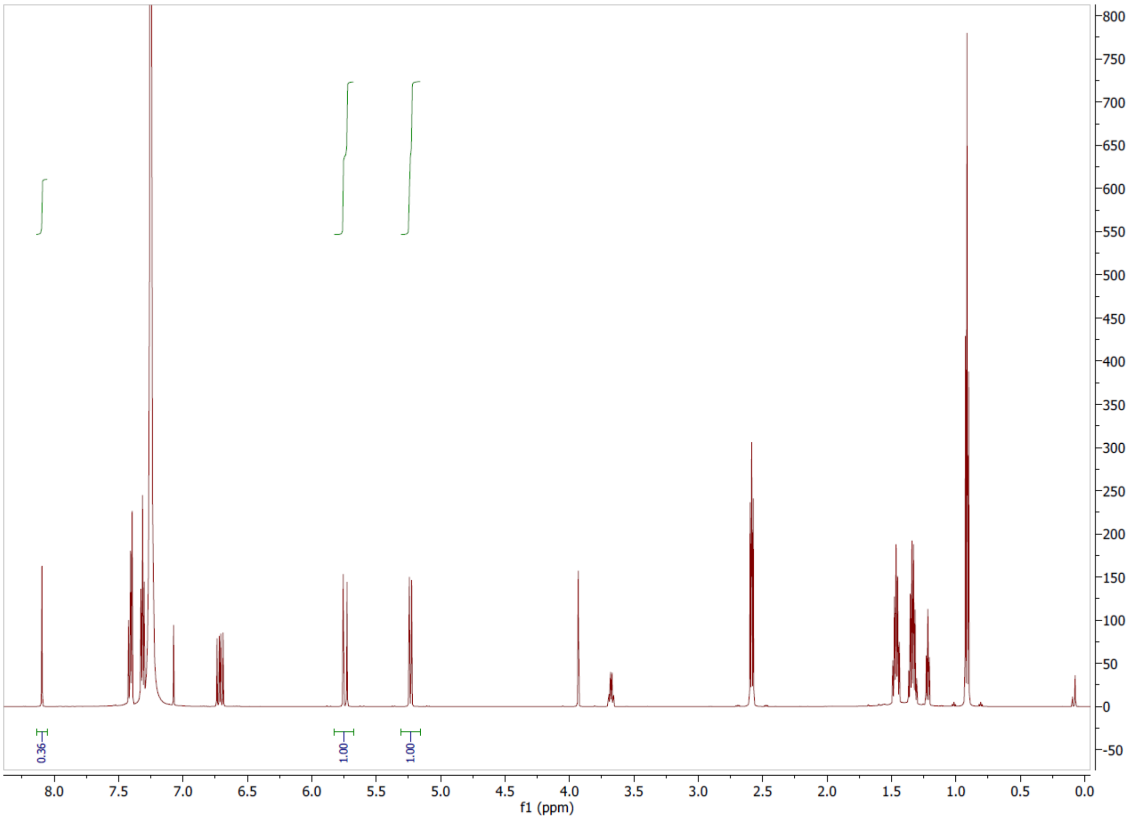

Figure 6.50: ^{1}H NMR spectrum for kinetic measurements of the cationic polymerization of styrene at *t* = 0 min.

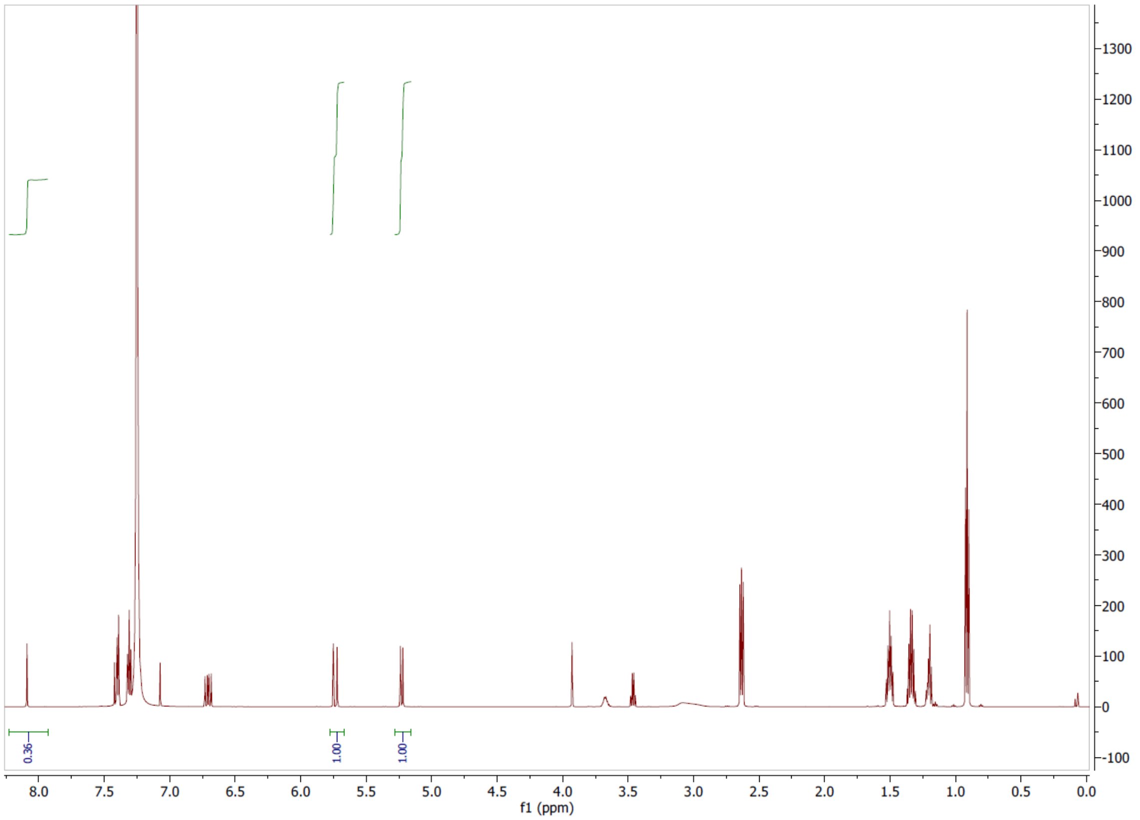

Figure 6.51: ^{1}H NMR spectrum for kinetic measurements of the cationic polymerization of styrene at *t* = 0.5 min.

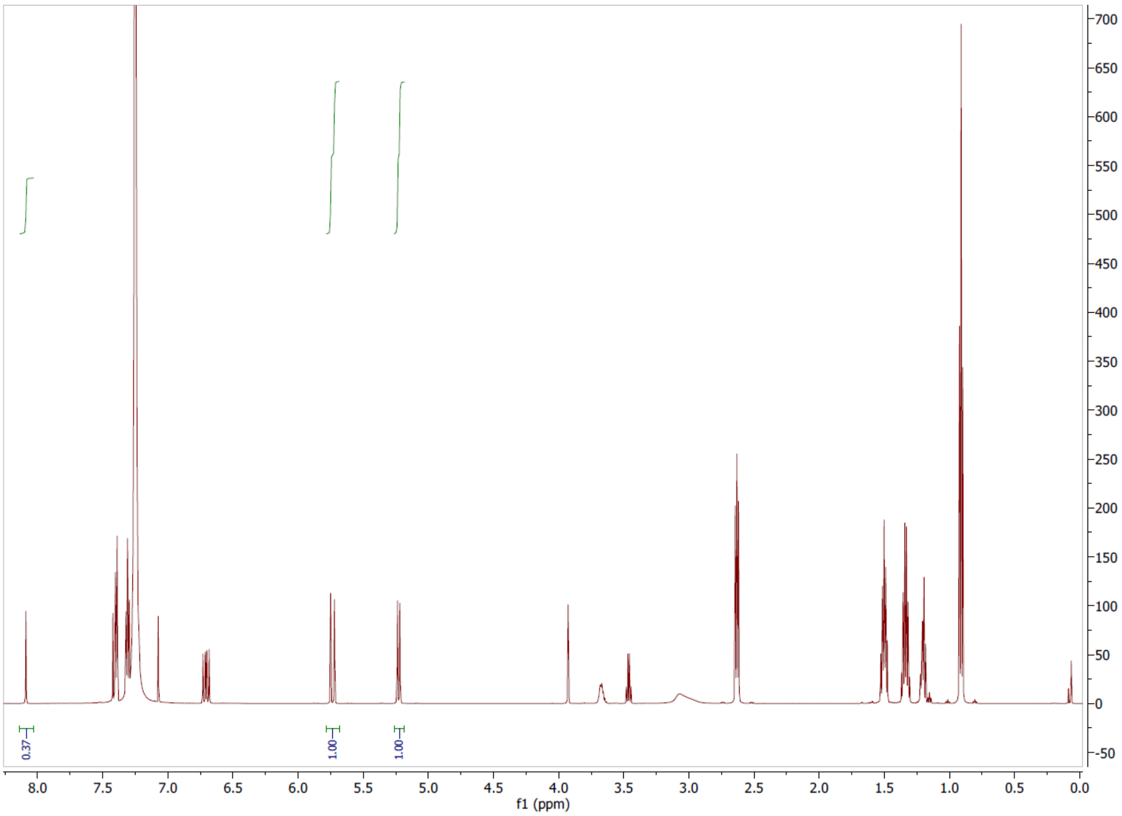

Figure 6.52: ^{1}H NMR spectrum for kinetic measurements of the cationic polymerization of styrene at *t* = 1 min.

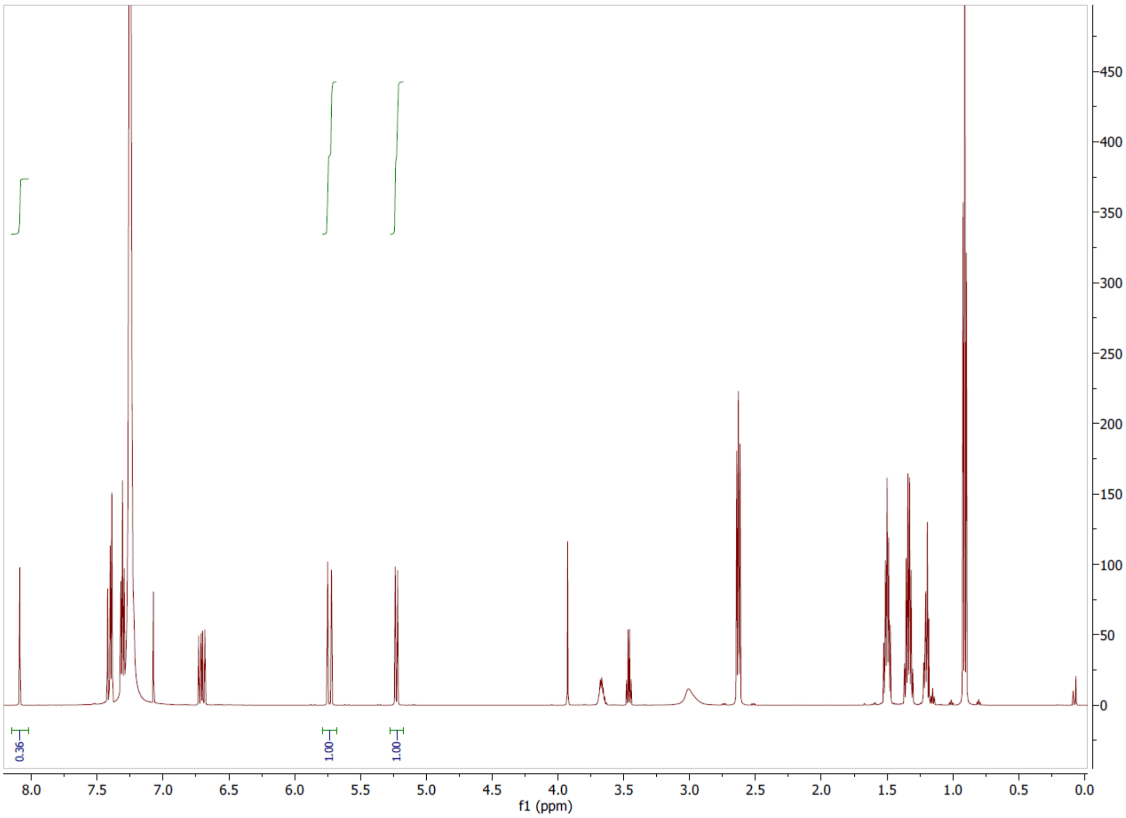

Figure 6.53: ^{1}H NMR spectrum for kinetic measurements of the cationic polymerization of styrene at *t* = 2 min.

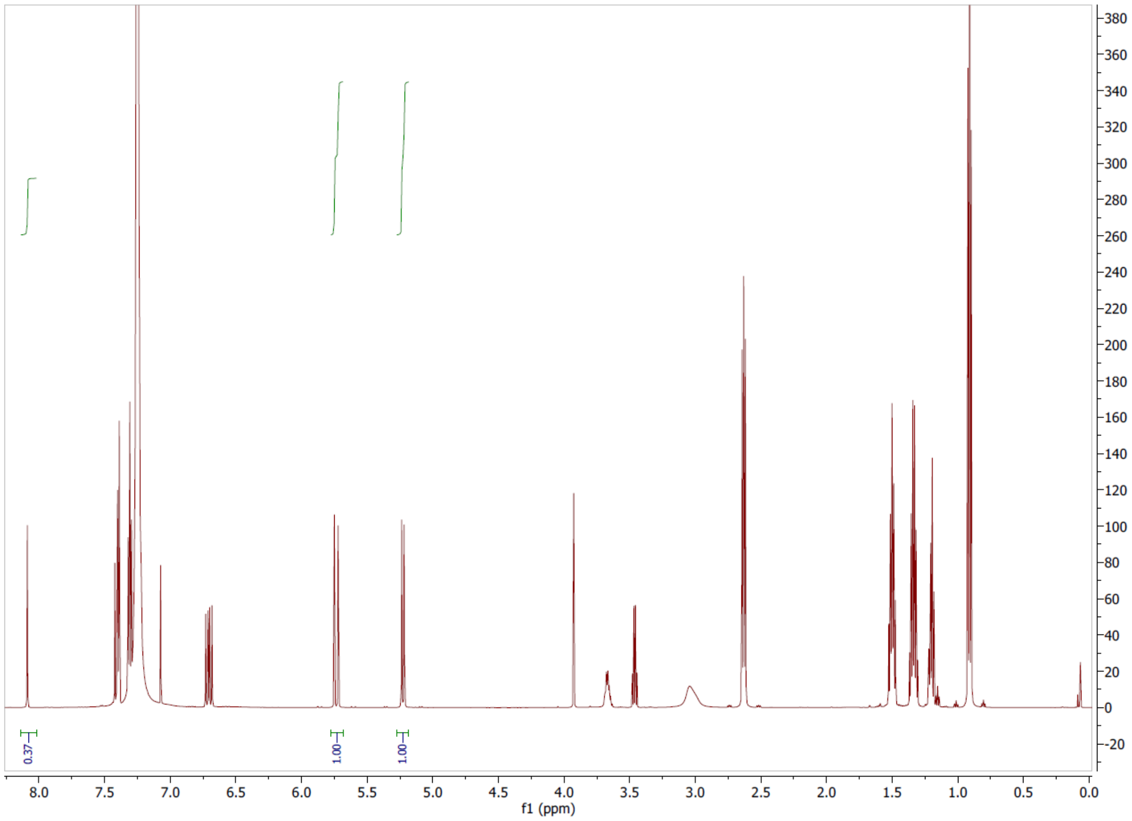

Figure 6.54: ^{1}H NMR spectrum for kinetic measurements of the cationic polymerization of styrene at *t* = 5 min.

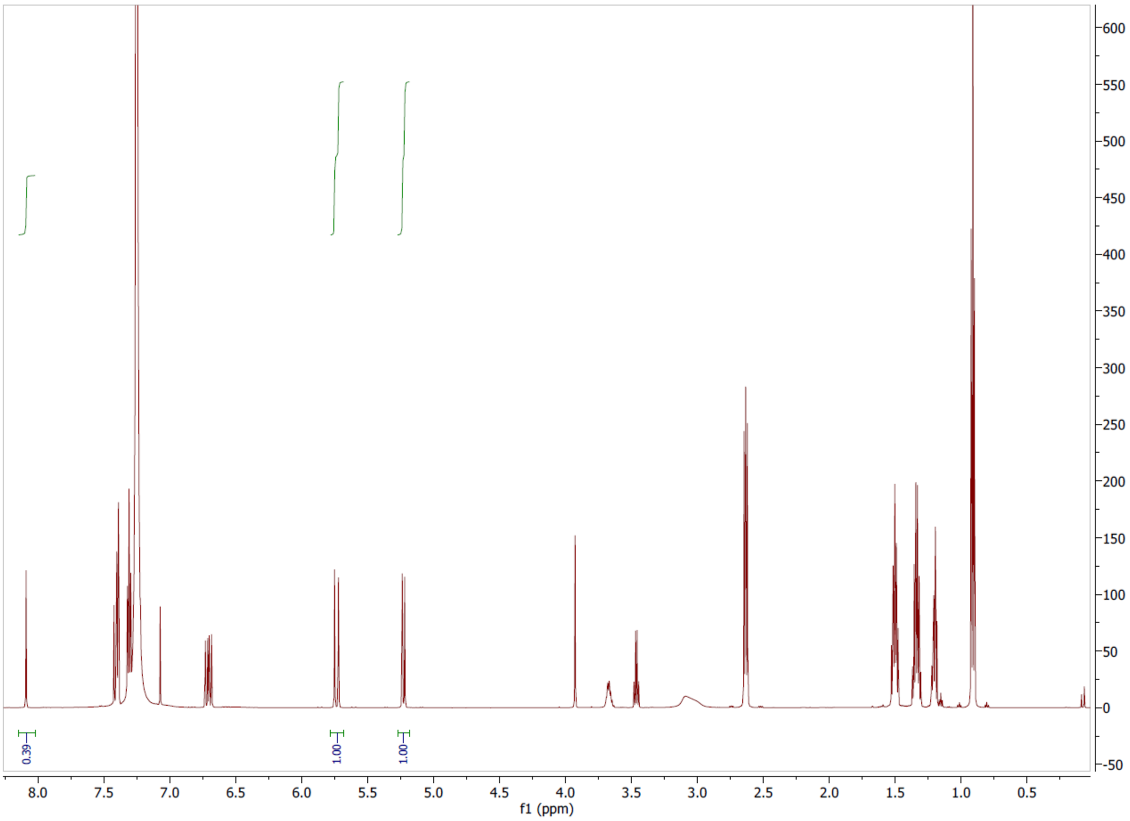

Figure 6.55: ^{1}H NMR spectrum for kinetic measurements of the cationic polymerization of styrene at *t* = 10 min.

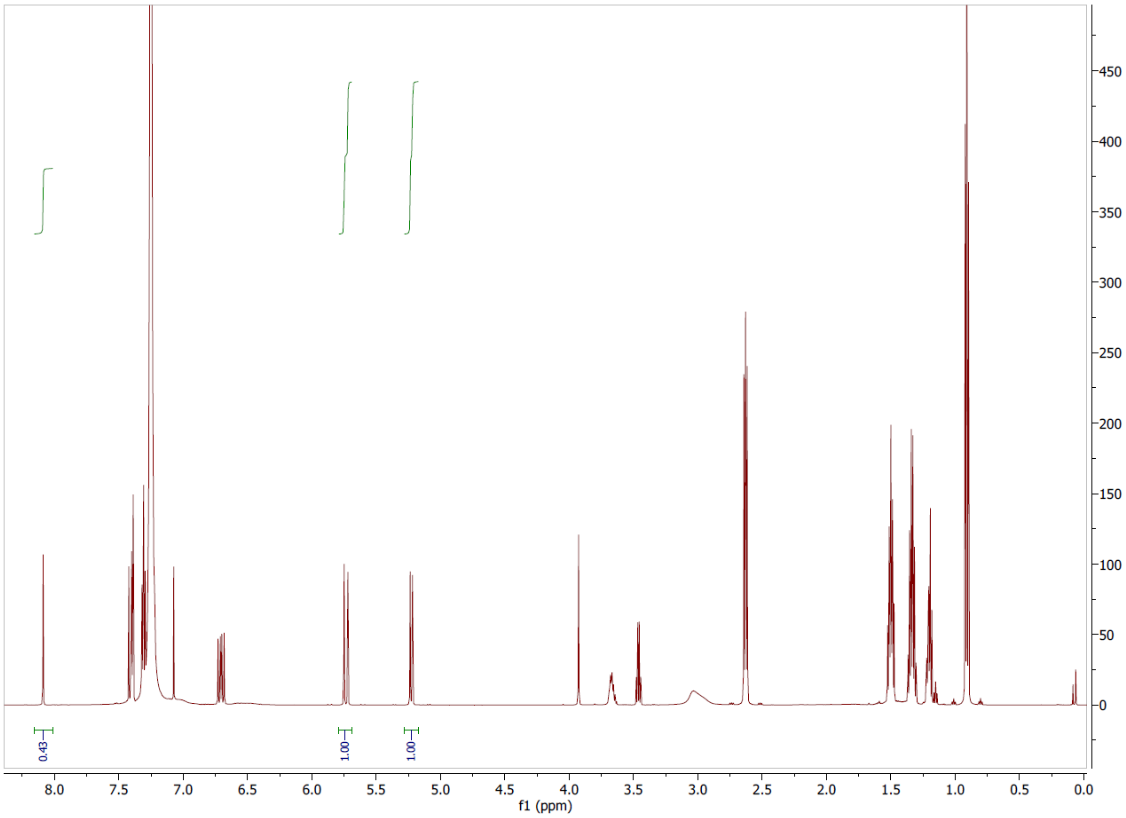

Figure 6.56: ^{1}H NMR spectrum for kinetic measurements of the cationic polymerization of styrene at t = 30 min.

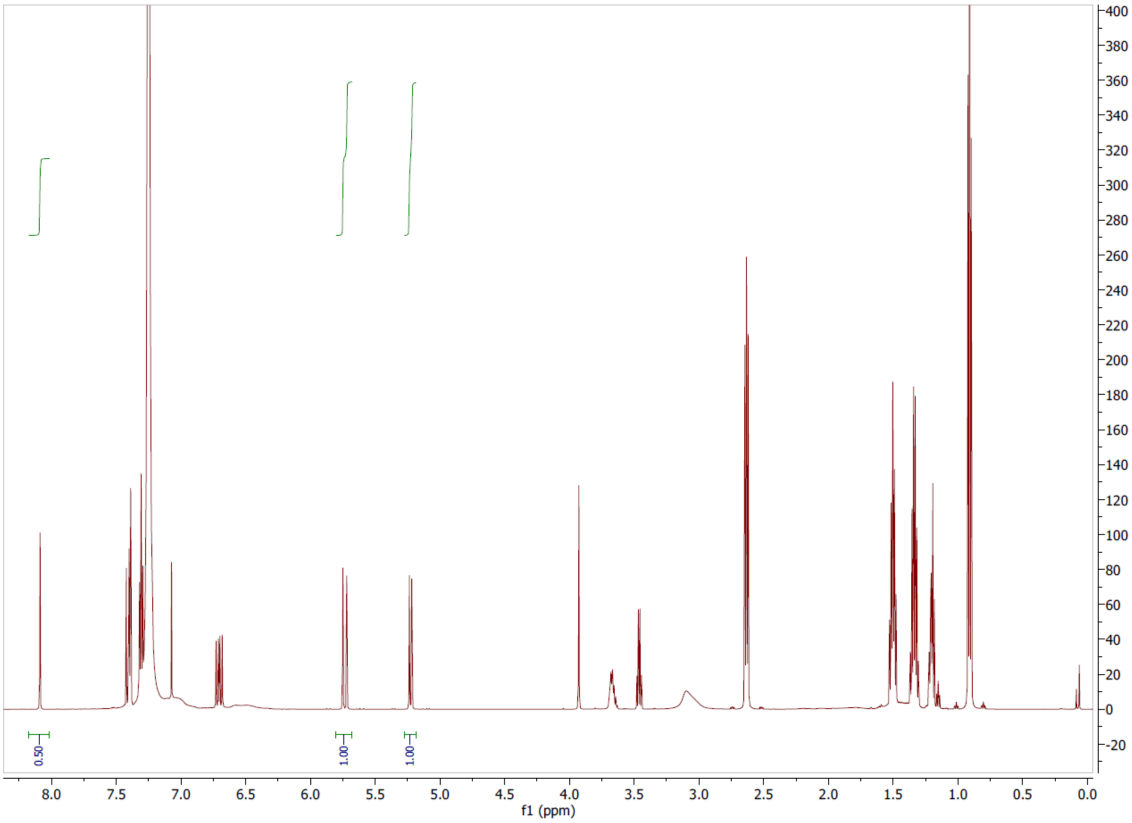

Figure 6.57: ^{1}H NMR spectrum for kinetic measurements of the cationic polymerization of styrene at t = 60 min.

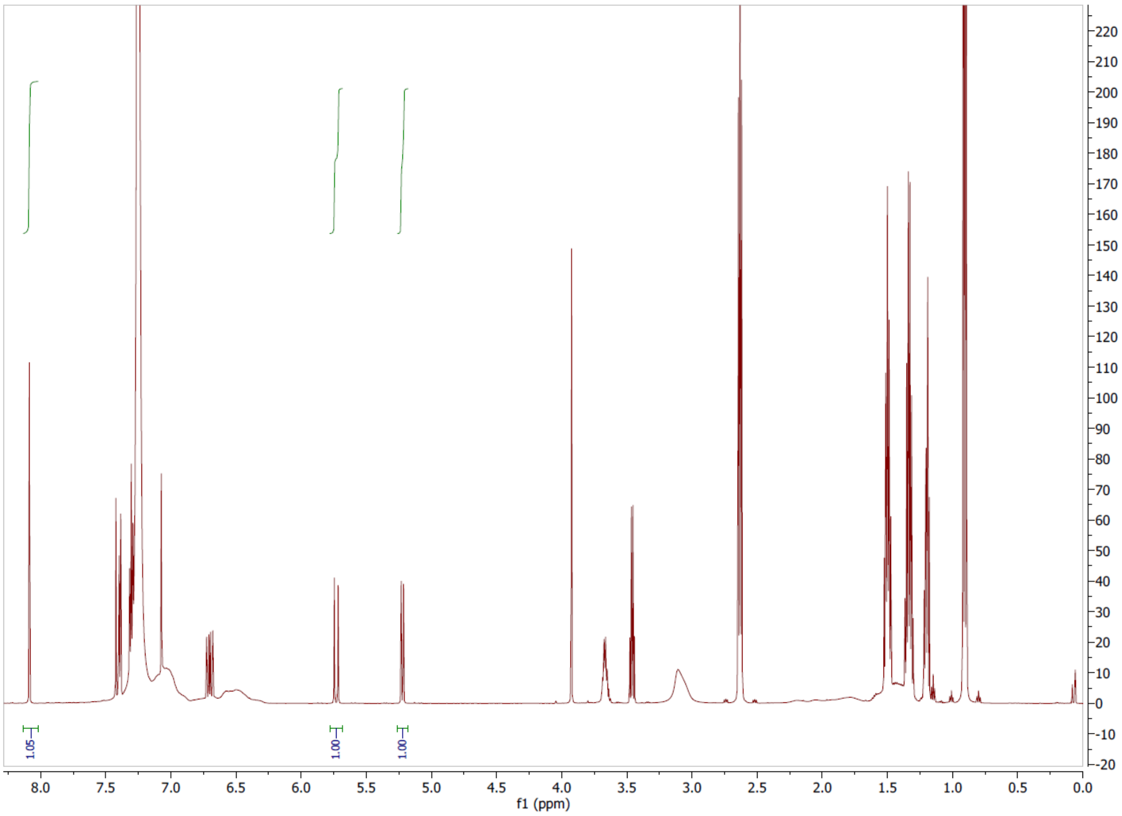

Figure 6.58: ^{1}H NMR spectrum for kinetic measurements of the cationic polymerization of styrene at *t* = 180 min.

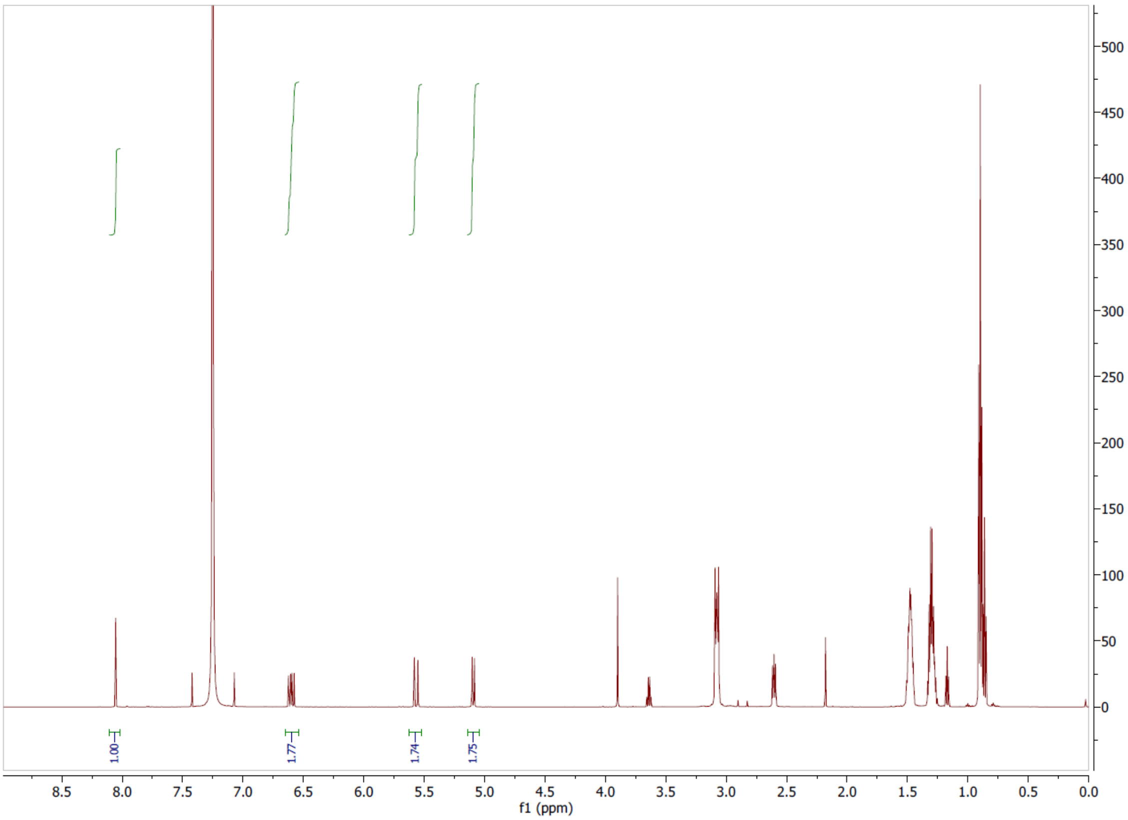

Figure 6.59: ^{1}H NMR spectrum for kinetic measurements of the cationic polymerization of TBASS at *t* = 0 min.

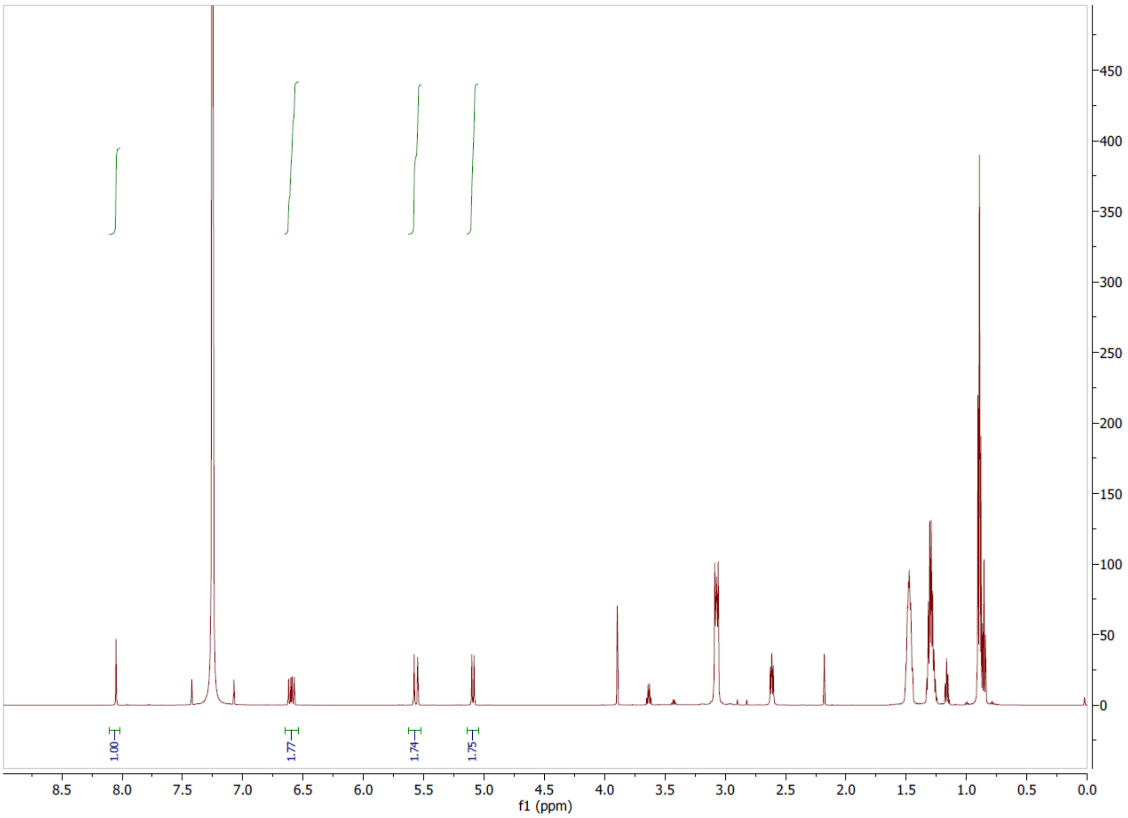

Figure 6.60: ^{1}H NMR spectrum for kinetic measurements of the cationic polymerization of TBASS at *t* = 0.5 min.

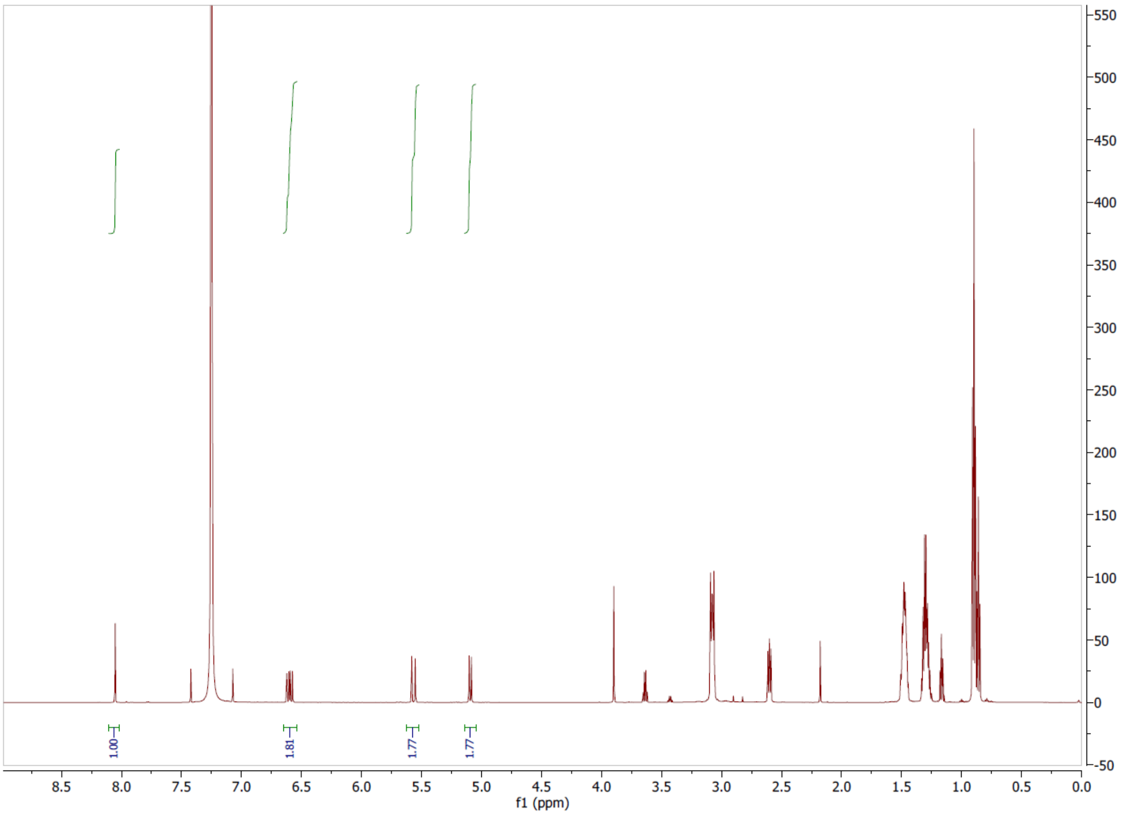

Figure 6.61: ^{1}H NMR spectrum for kinetic measurements of the cationic polymerization of TBASS at *t* = 1 min.

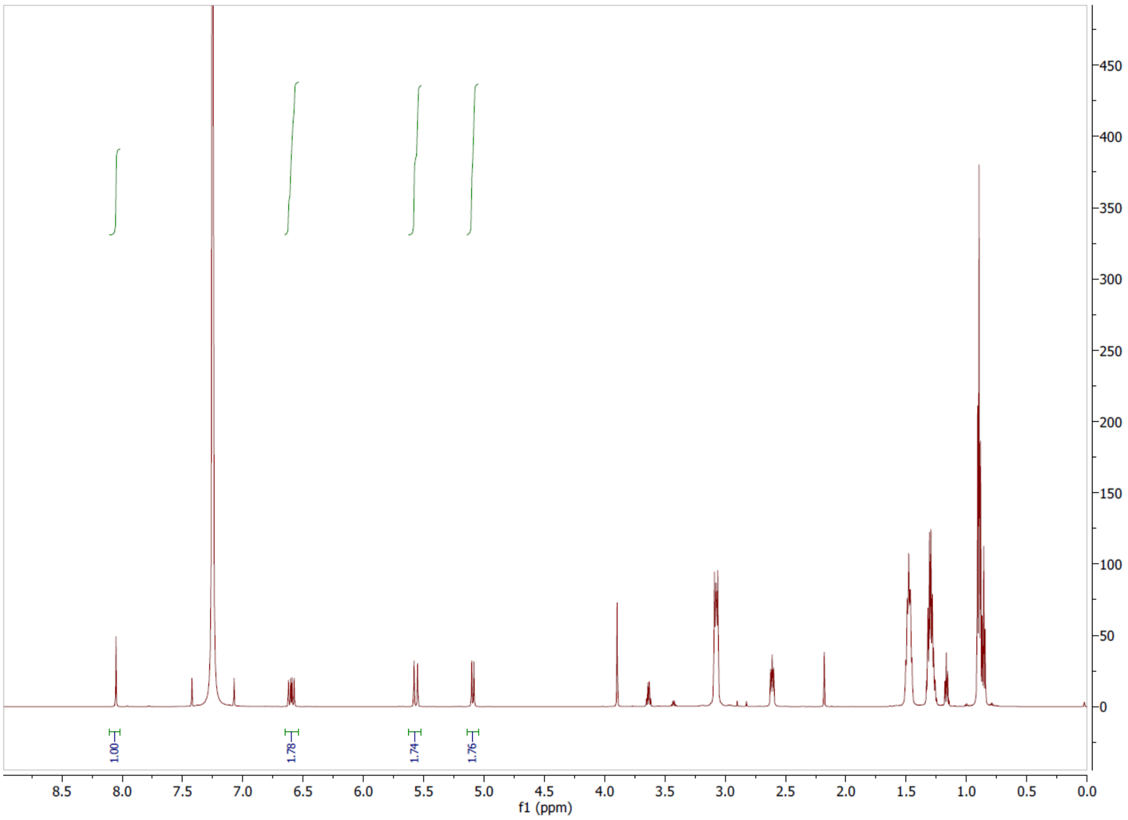

Figure 6.62: ^1H NMR spectrum for kinetic measurements of the cationic polymerization of TBASS at *t* = 2 min.

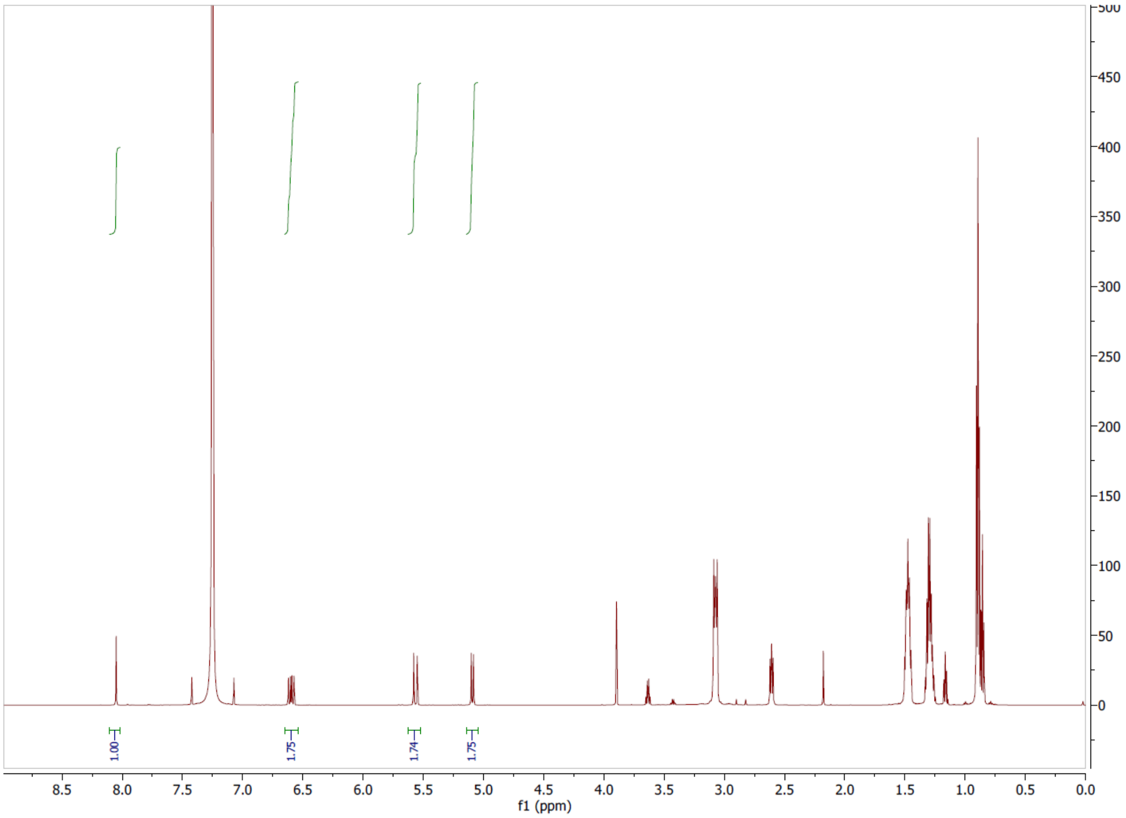

Figure 6.63: ^1H NMR spectrum for kinetic measurements of the cationic polymerization of TBASS at *t* = 5 min.

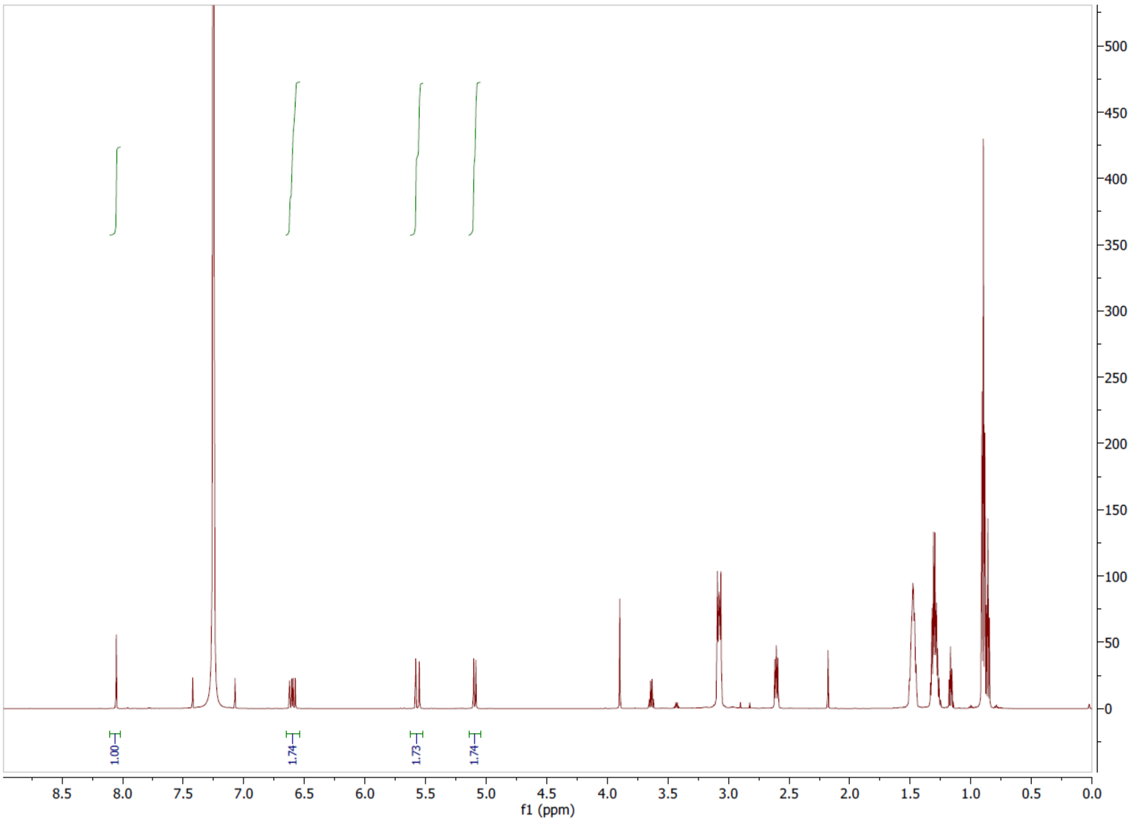

Figure 6.64: ^{1}H NMR spectrum for kinetic measurements of the cationic polymerization of TBASS at *t* = 10 min.

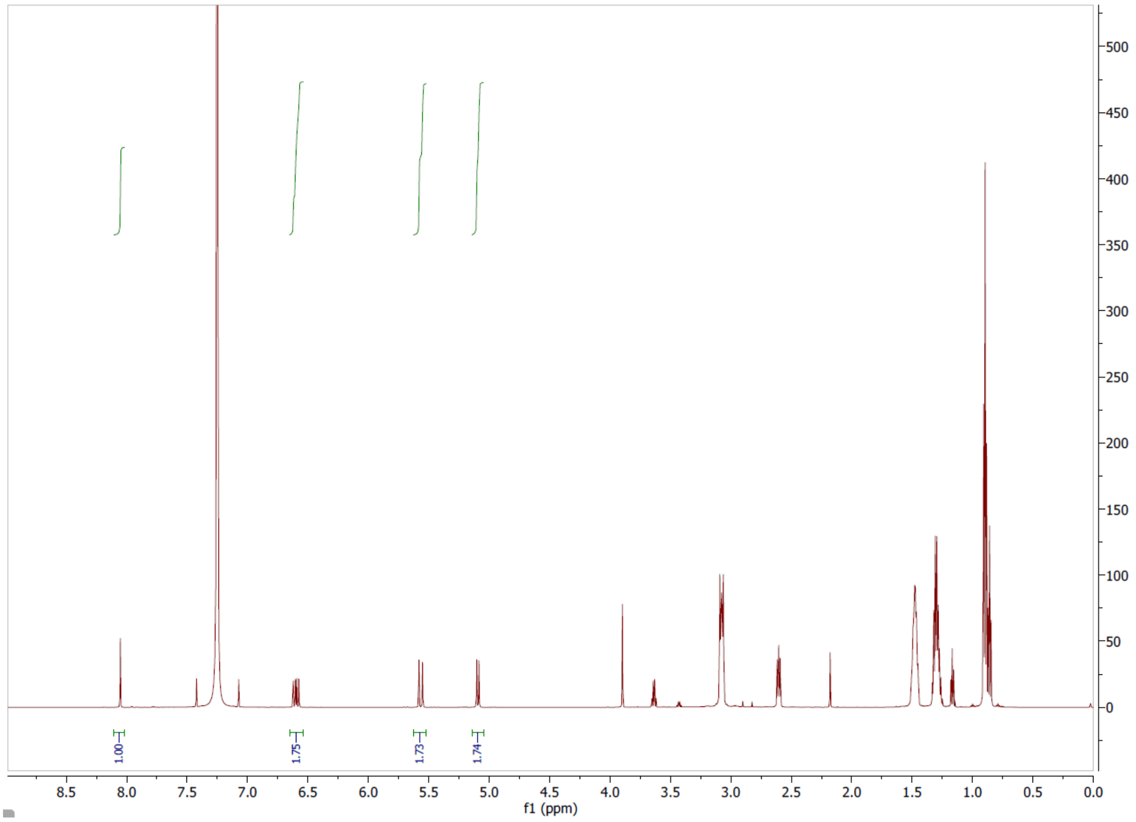

Figure 6.65: ^{1}H NMR spectrum for kinetic measurements of the cationic polymerization of TBASS at *t* = 30 min.

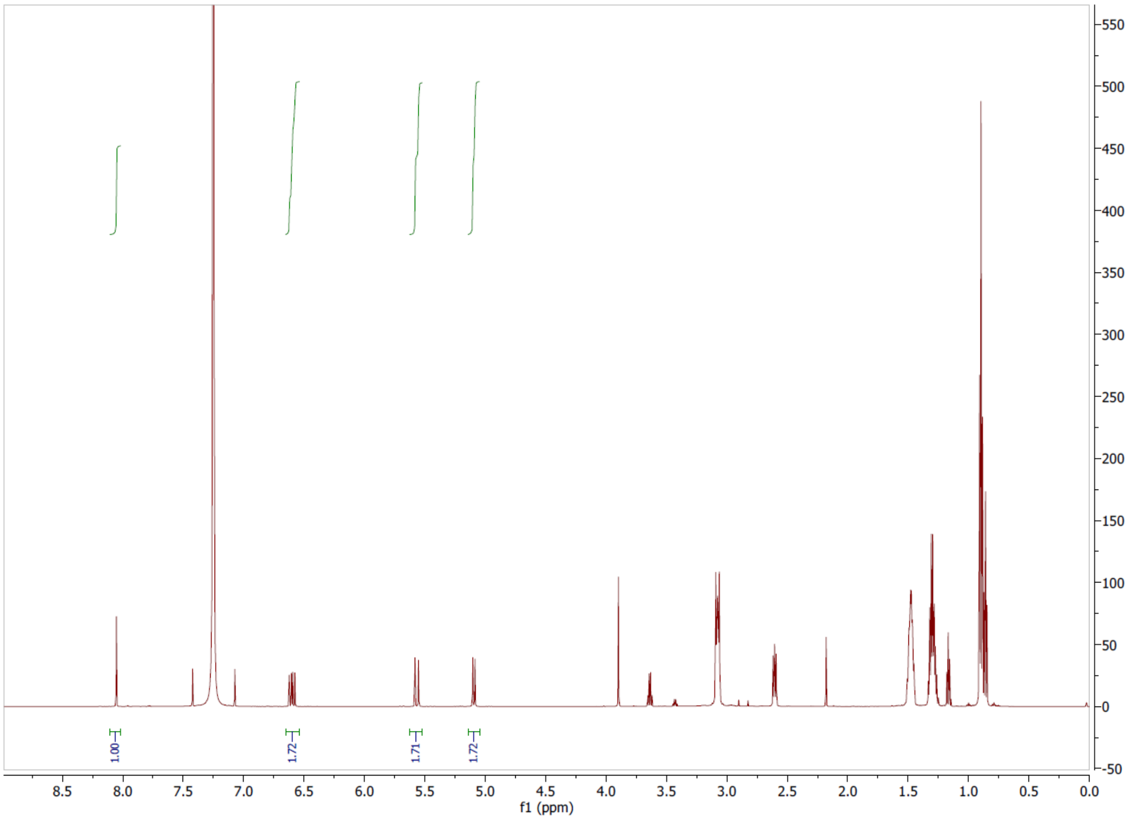

Figure 6.66: ^{1}H NMR spectrum for kinetic measurements of the cationic polymerization of TBASS at *t* = 60 min.

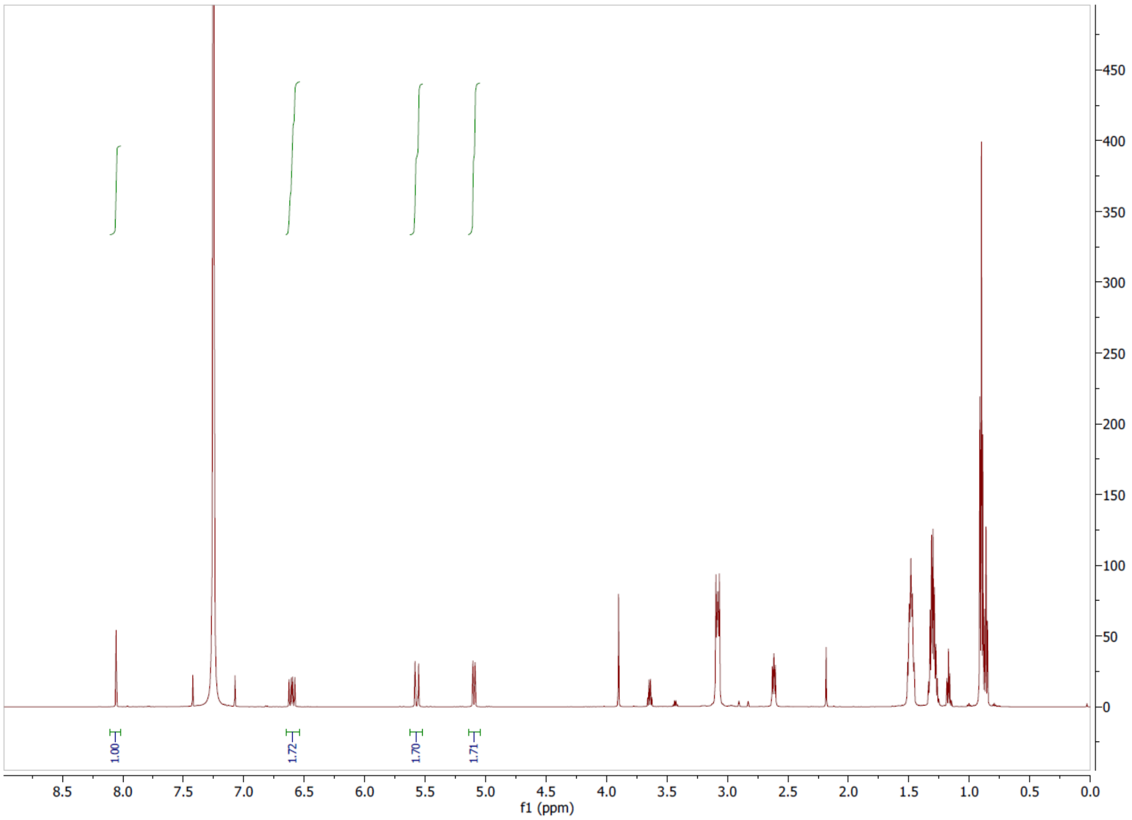

Figure 6.67: ^{1}H NMR spectrum for kinetic measurements of the cationic polymerization of TBASS at *t* = 180 min.

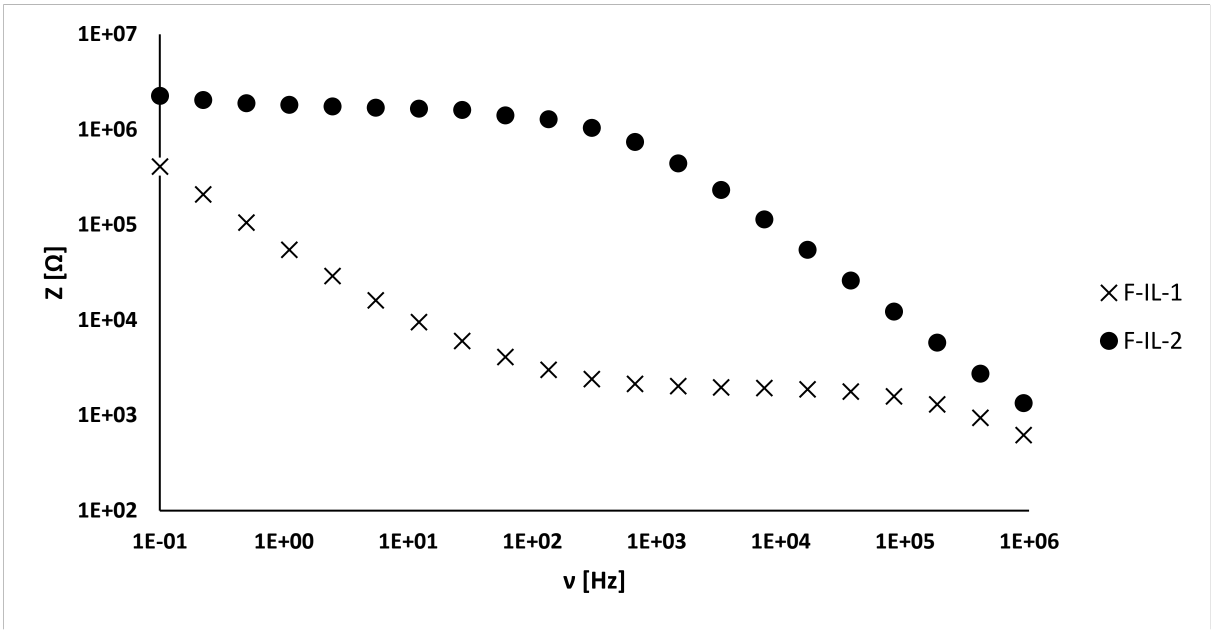

Figure 6.68: Impedance versus frequency plot from impedance measurements of aluminum substrates glued with F-IL-1 (cross) or F-IL-2 (circle).

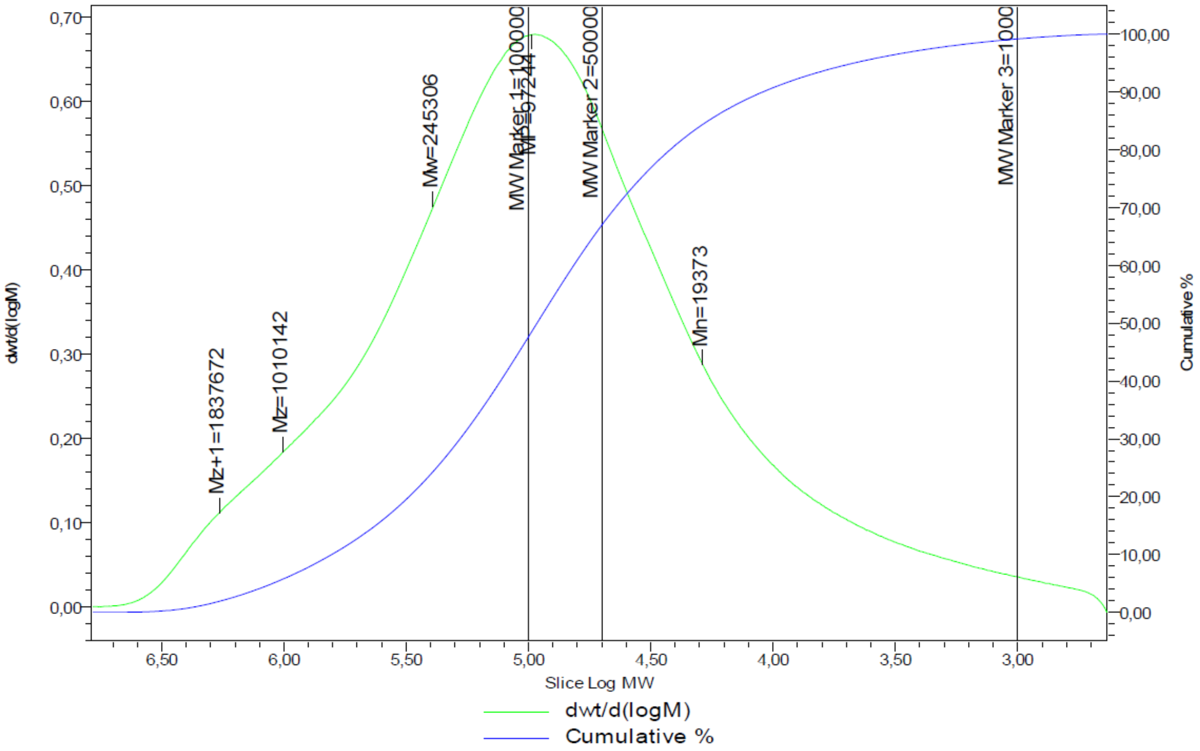

Figure 6.69: Molecular weight ($M_{w,1}$) distribution curve determined via GPC of a PSA with *w* (TBASS) = 0 wt%.

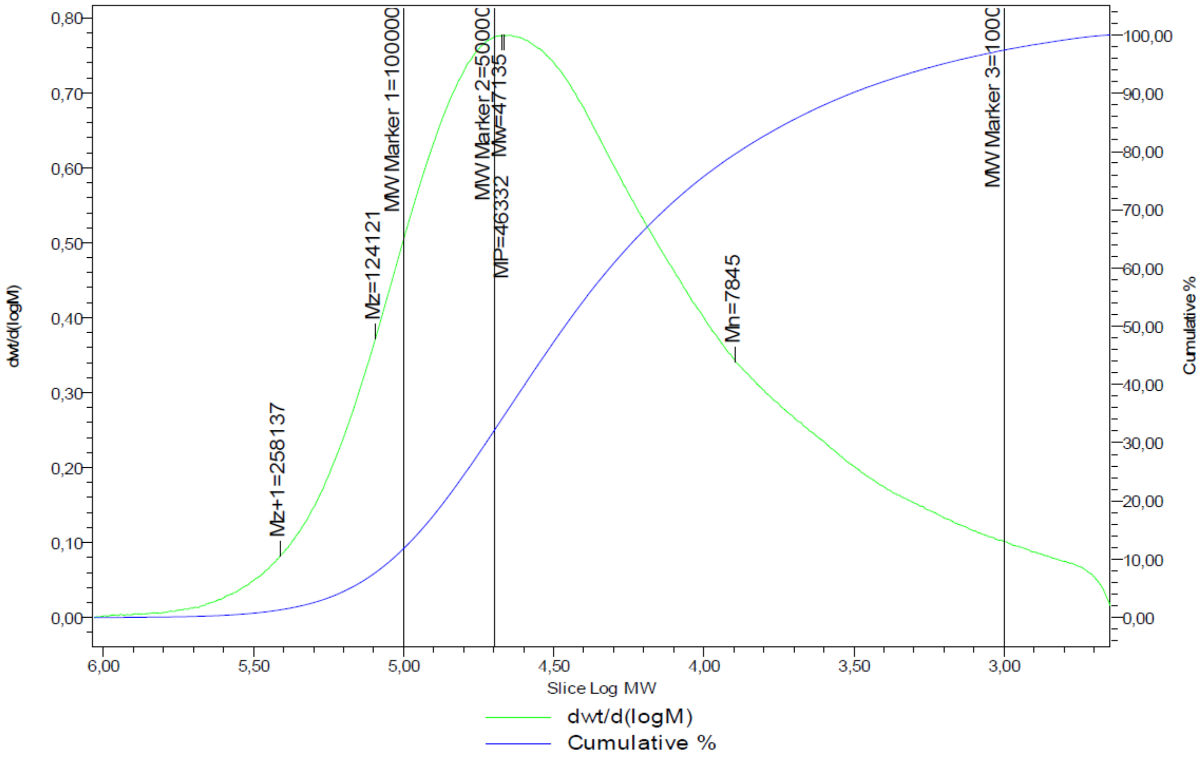

Figure 6.70: Molecular weight ($M_{w,1}$) distribution curve determined via GPC of a PSA with *w* (TBASS) = 0.5 wt%.

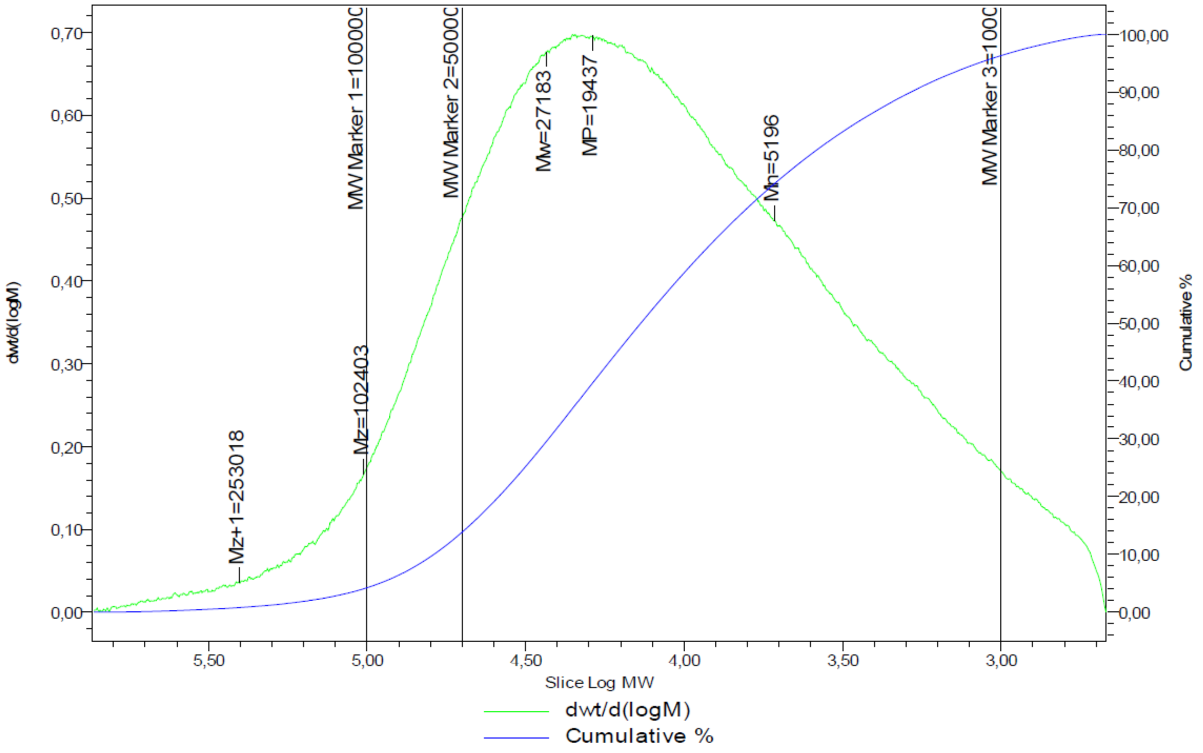

Figure 6.71: Molecular weight ($M_{w,1}$) distribution curve determined via GPC of a PSA with *w* (TBASS) = 1.5 wt%.

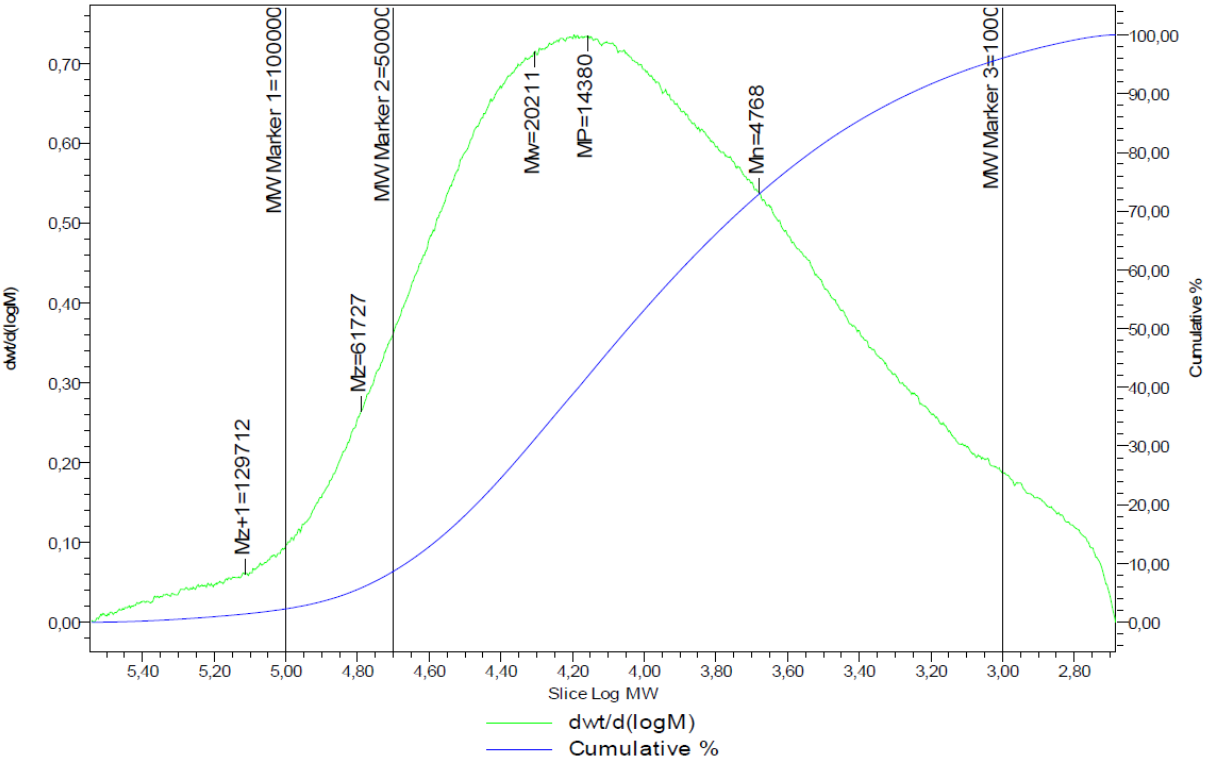

Figure 6.72: Molecular weight ($M_{w,1}$) distribution curve determined via GPC of a PSA with *w* (TBASS) = 5 wt%.

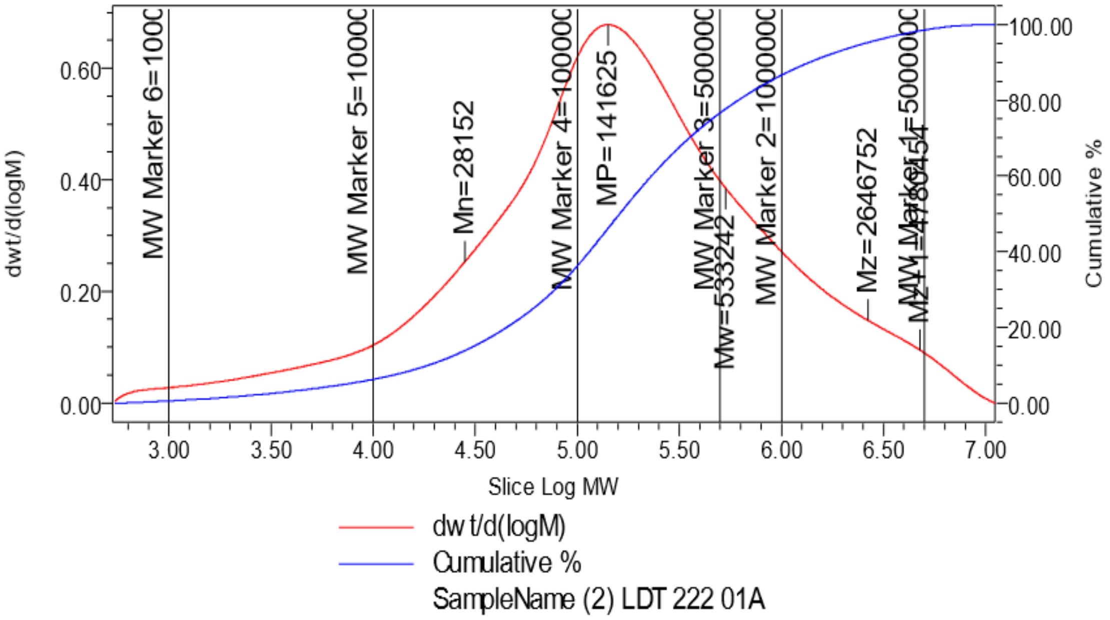

Figure 6.73: Molecular weight ($M_{w,2}$) distribution curve determined via GPC of a PSA with *w* (TBASS) = 0 wt%.

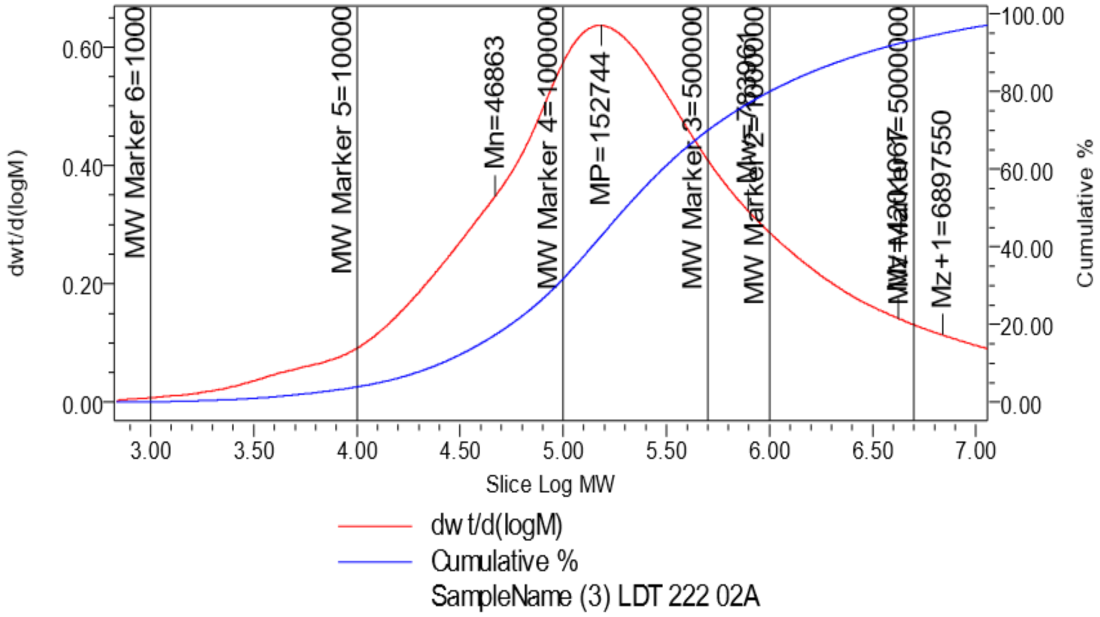

Figure 6.74: Molecular weight ($M_{w,2}$) distribution curve determined via GPC of a PSA with *w* (TBASS) = 0.5 wt%.

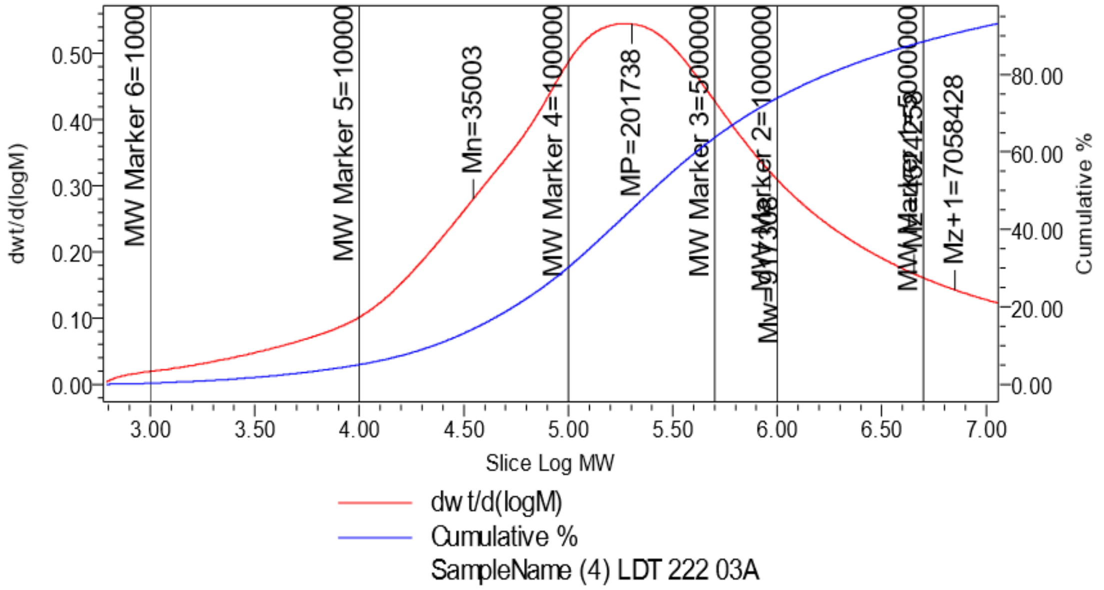

Figure 6.75: Molecular weight ($M_{w,2}$) distribution curve determined via GPC of a PSA with *w* (TBASS) = 1.5 wt%.

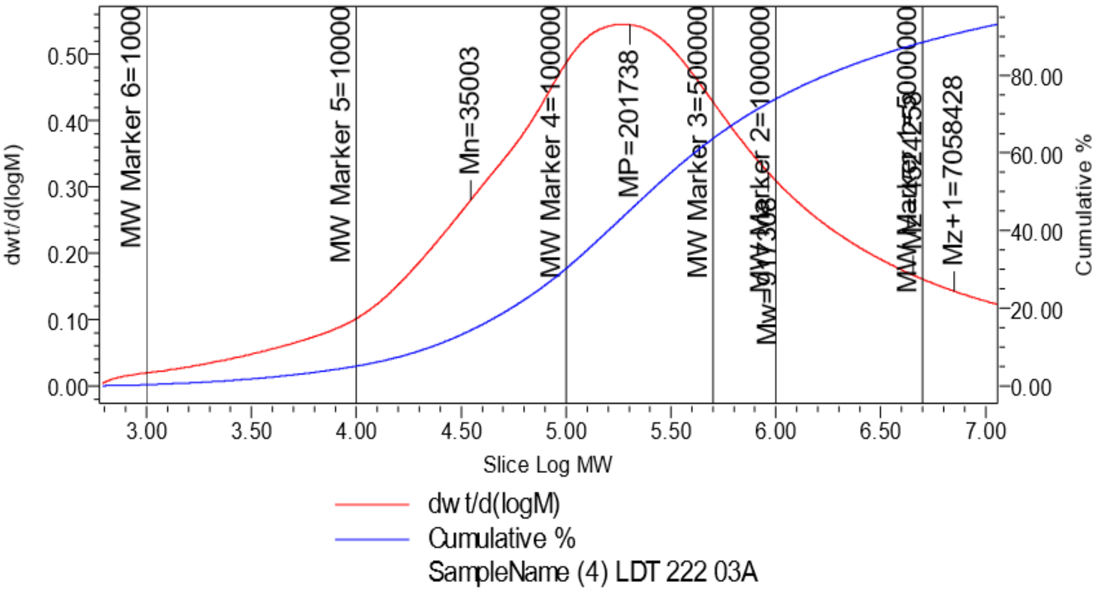

Figure 6.76: Molecular weight ($M_{w,2}$) distribution curve determined via GPC of a PSA with *w* (TBASS) = 5 wt%.

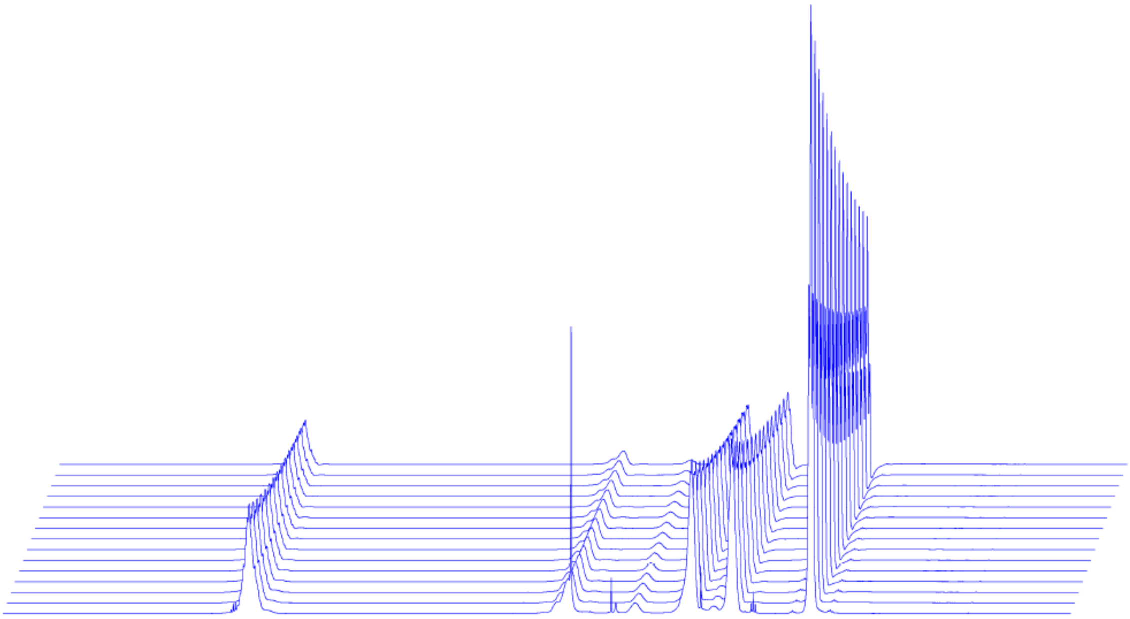

Figure 6.77: Visualization of signal decay with increasing field strength gradient from the front to the back.

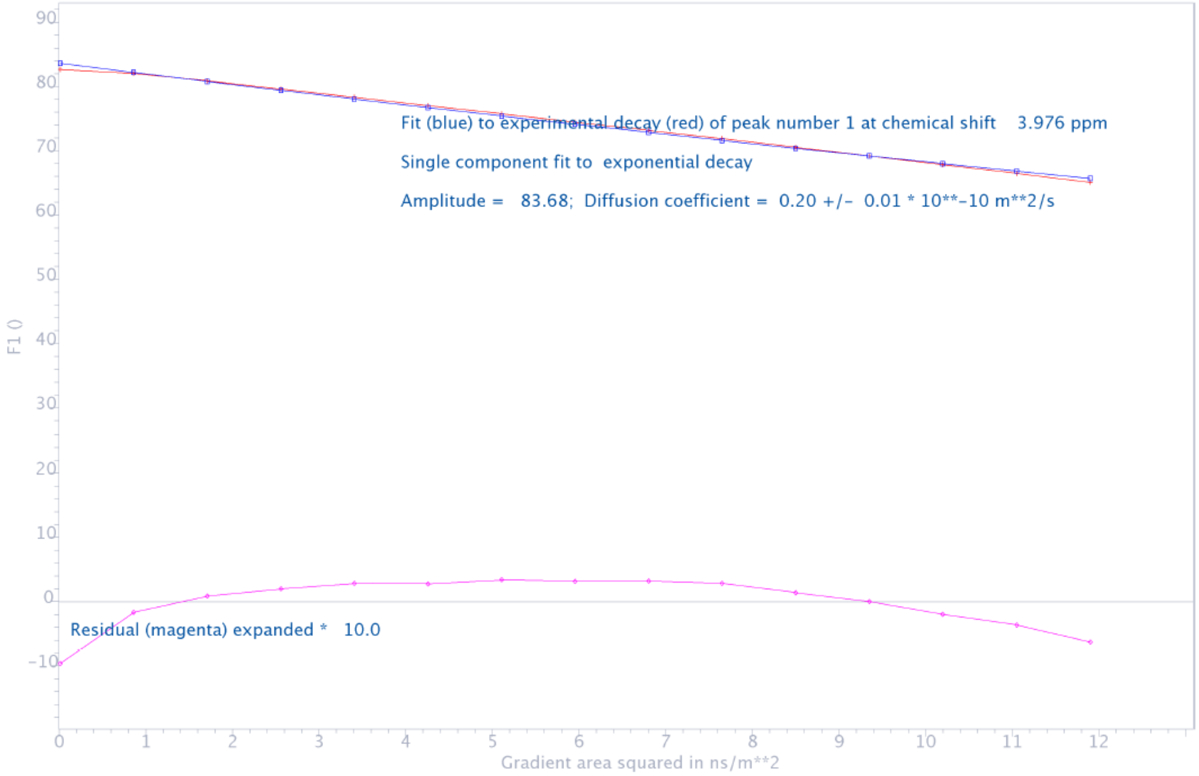

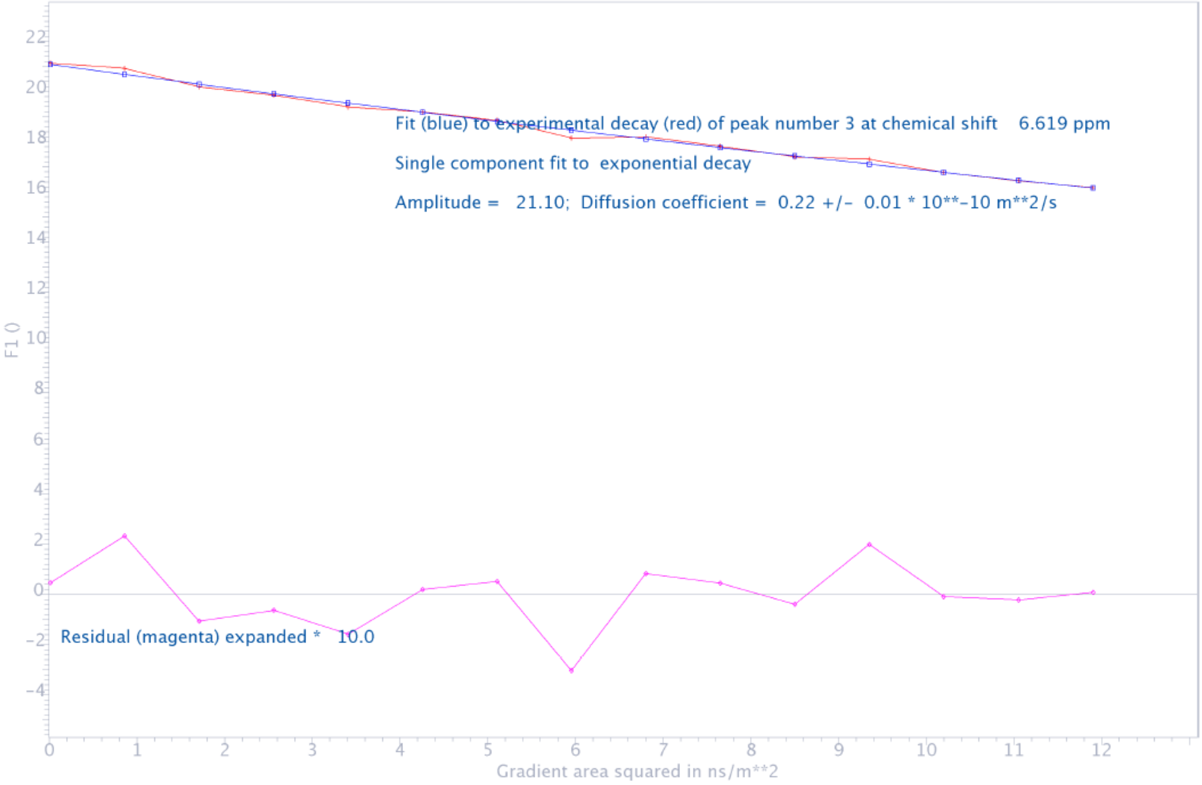

Figure 6.78: Data fitting of signal decay in DOSY NMR measurements of an acrylate-TBASS copolymer with 5 wt% of TBASS measured in DMSO-d_6 at 50 °C with a day in pulse sequences of 150 ms.

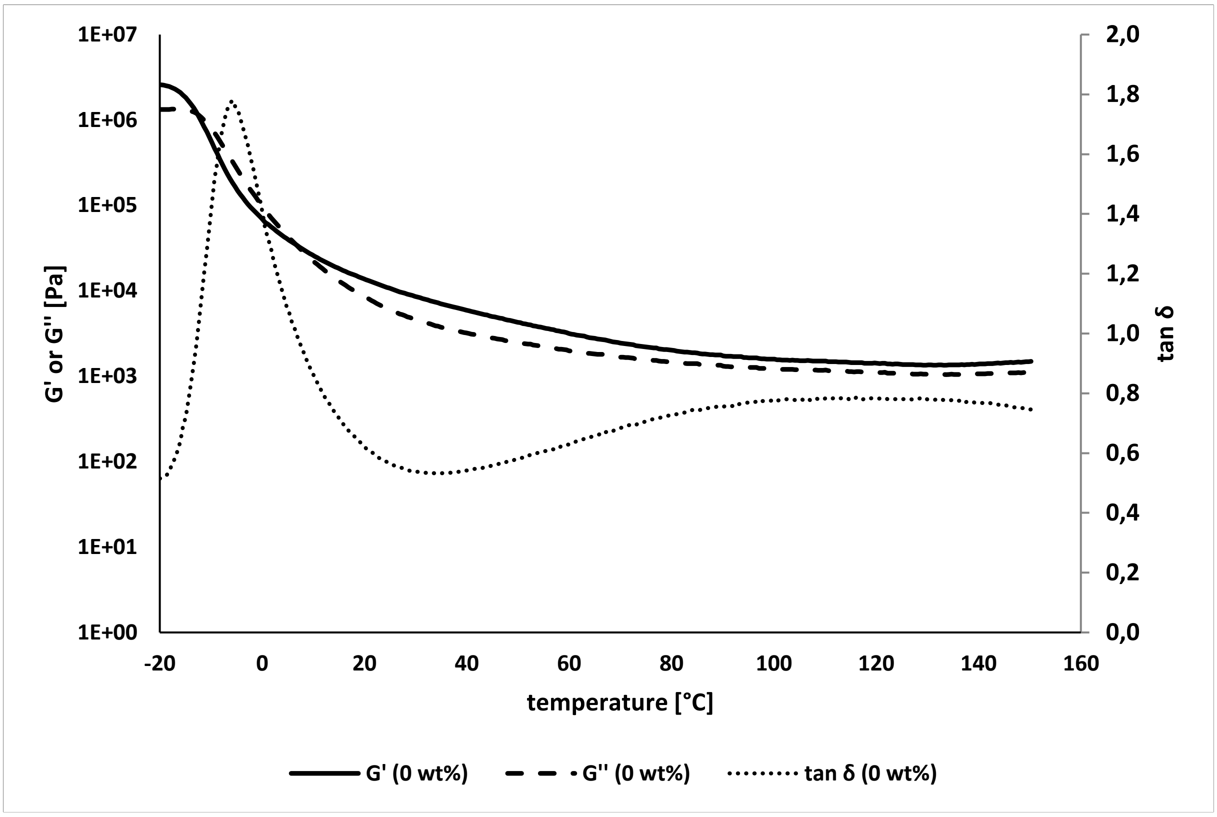

Figure 6.79: Storage modulus G' (solid line), loss modulus G'' (dashed line) and dissipation factor tan *δ* (dotted line) of a PSA with *w* (TBASS) = 0 wt%.

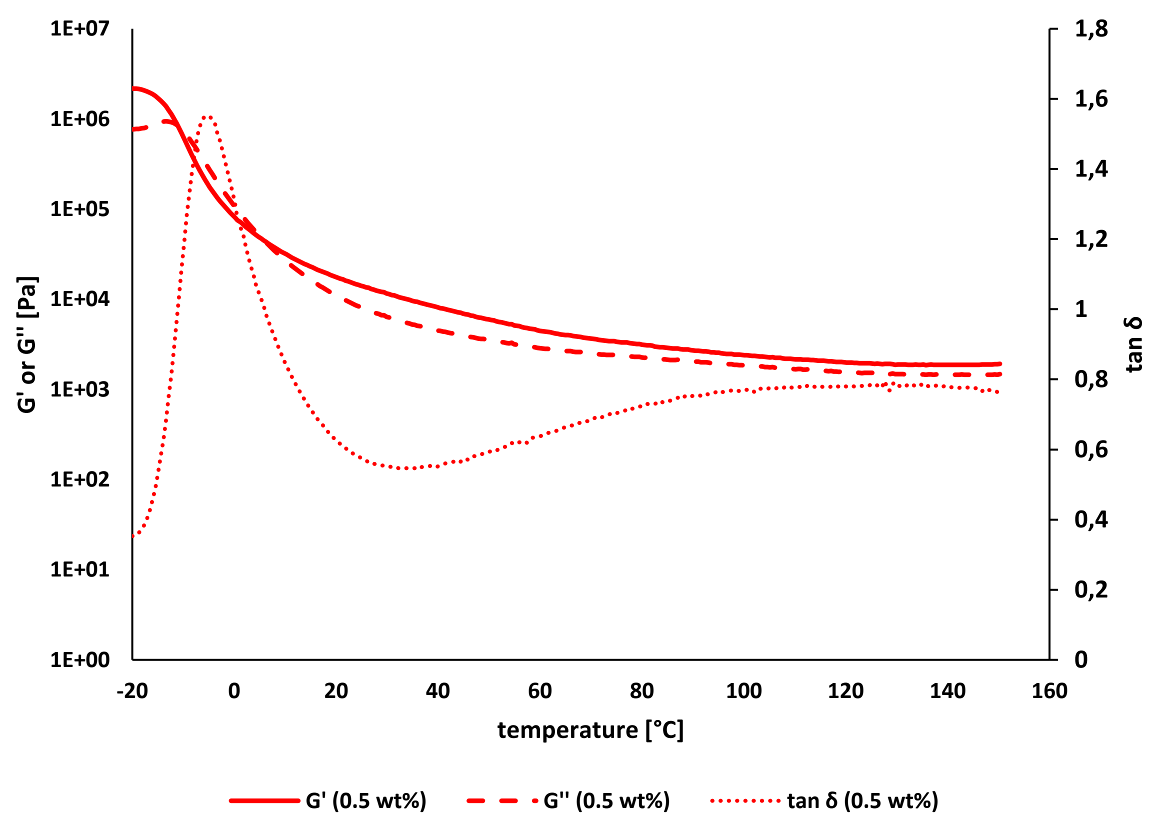

Figure 6.80: Storage modulus G' (solid line), loss modulus G'' (dashed line) and dissipation factor tan *δ* (dotted line) of a PSA with *w* (TBASS) = 0.5 wt%.

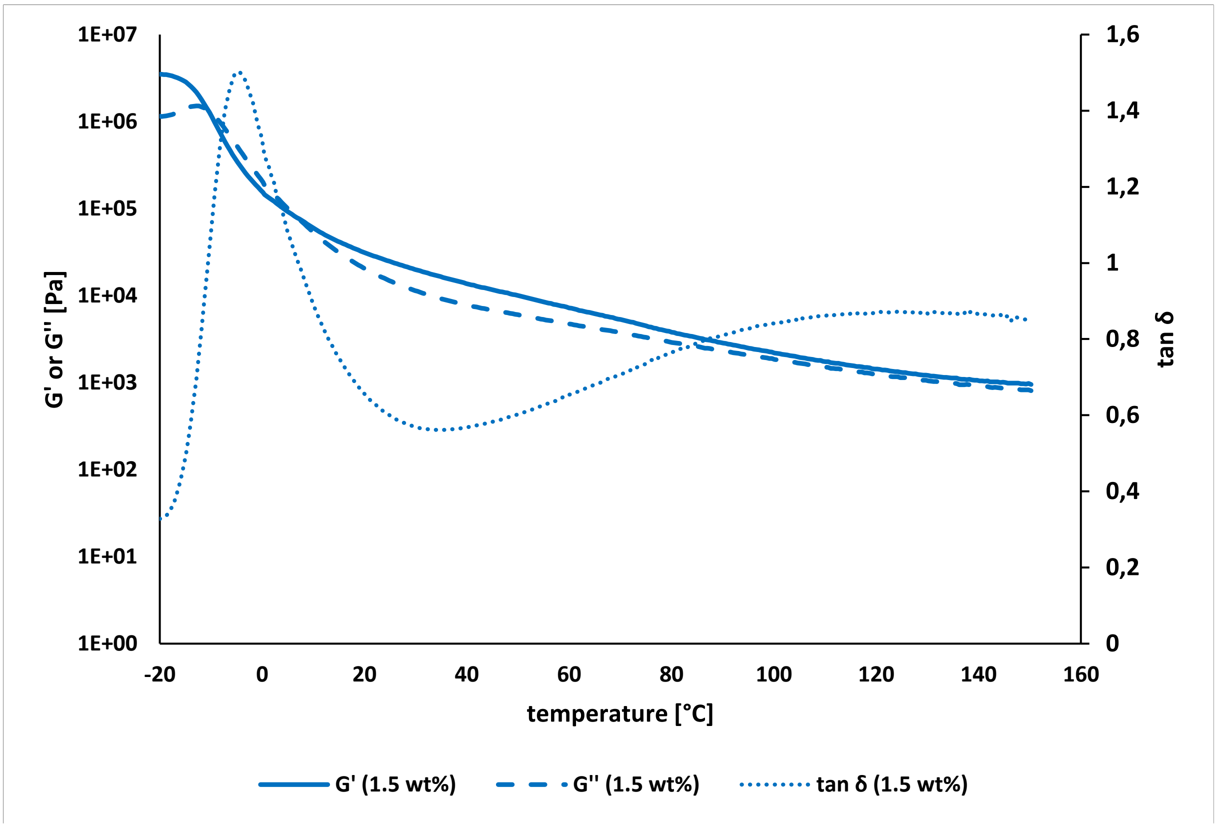

Figure 6.81: Storage modulus G’ (solid line), loss modulus G’’ (dashed line) and dissipation factor tan *δ* (dotted line) of a PSA with *w* (TBASS) = 1.5 wt%.

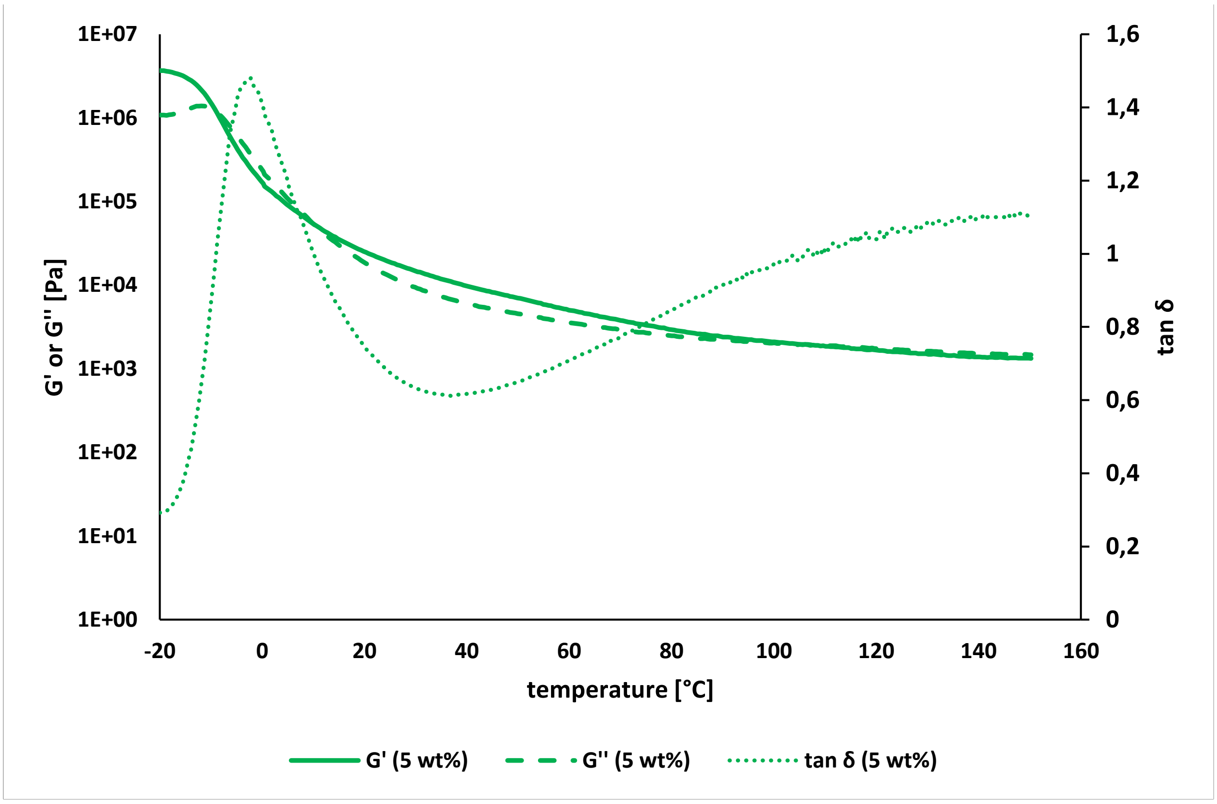

Figure 6.82: Storage modulus G’ (solid line), loss modulus G’’ (dashed line) and dissipation factor tan *δ* (dotted line) of a PSA with *w* (TBASS) = 5 wt%.

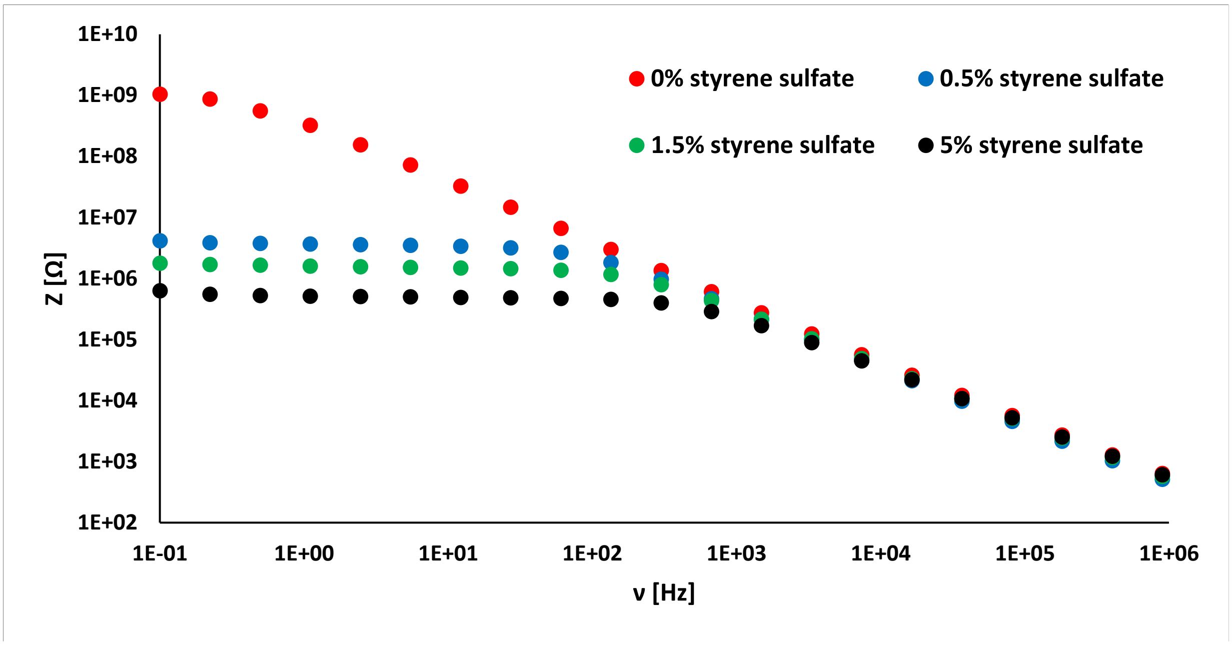

Figure 6.83: Impedance plotted against frequency of PSAs with 0 (red), 0.5 (blue), 1.5 (green) & 5 wt% (black) of TBASS without IL.

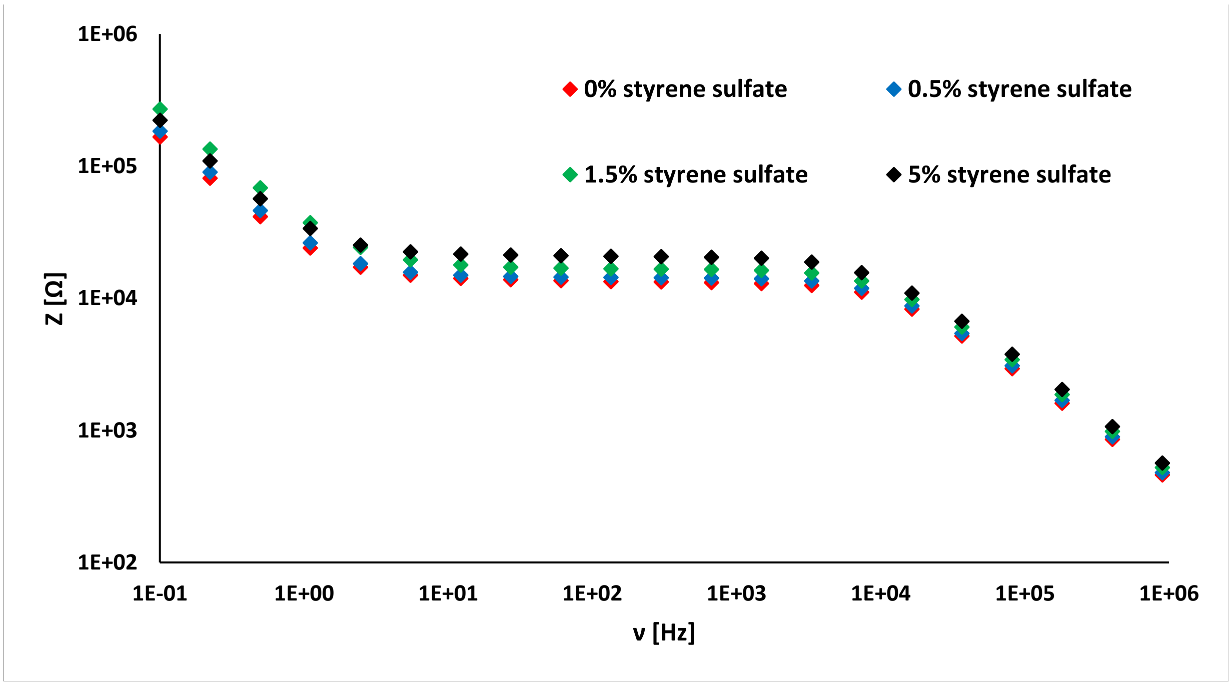

Figure 6.84: Impedance plotted against frequency of PSAs with 0 (red), 0.5 (blue), 1.5 (green) & 5 wt% (black) of TBASS with 5 wt% of IL-2 added.

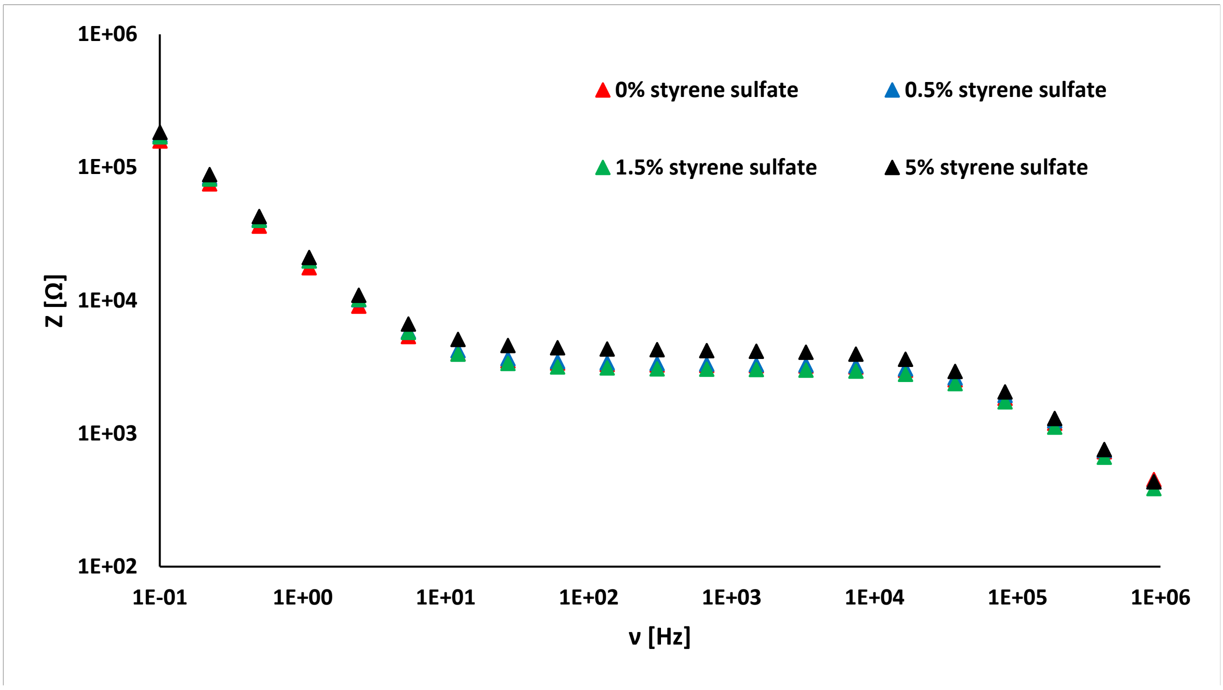

Figure 6.85: Impedance plotted against frequency of PSAs with 0 (red), 0.5 (blue), 1.5 (green) & 5 wt% (black) of TBASS with 5 wt% of IL-2 added.

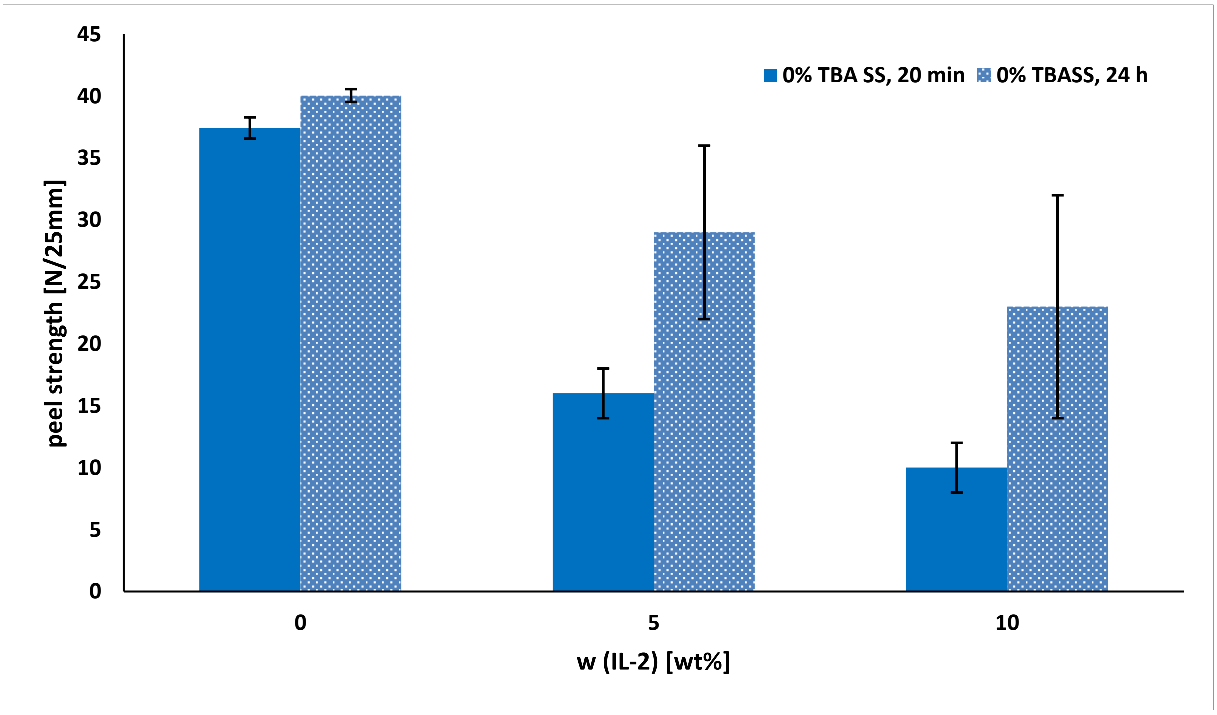

Figure 6.86: 180° peel strength values of a PSA with w (TBASS) = 0 wt% and different amounts of IL-2 added on glass. Measurements were performed 20 minutes (solid) and 24 hours (dashed) after application.

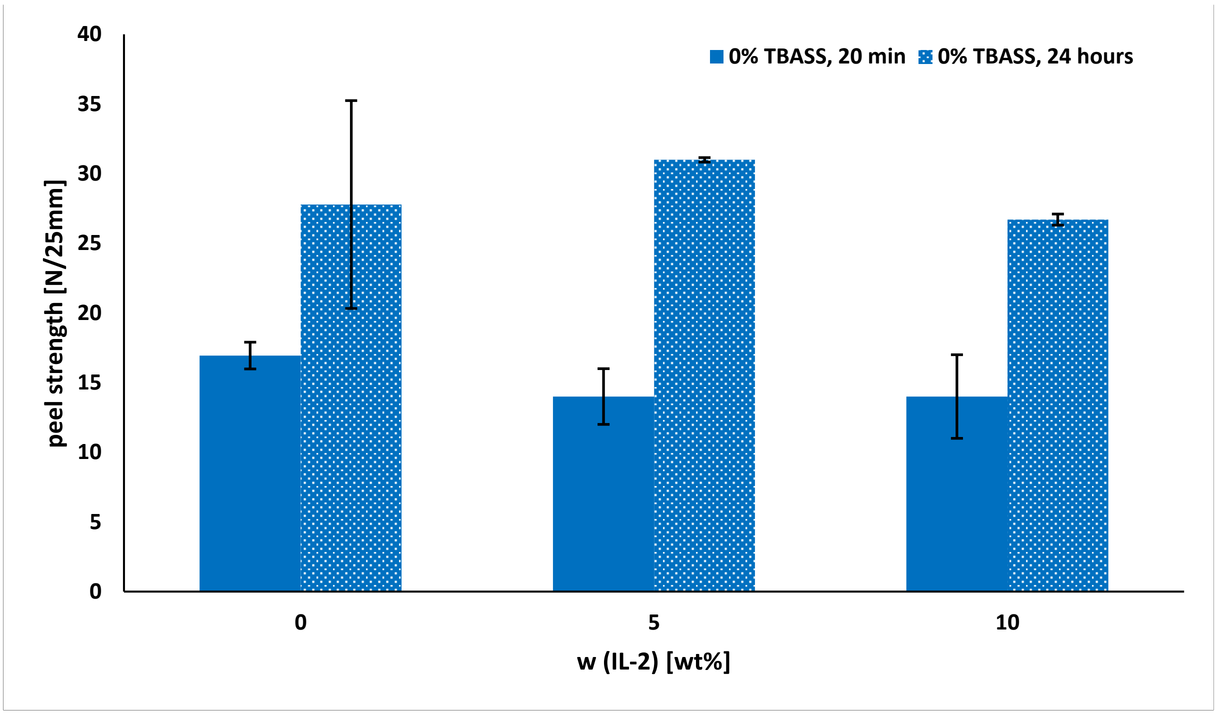

Figure 6.87: 180° peel strength values of a PSA with w (TBASS) = 0 wt% and different amounts of IL-2 added on PA. Measurements were performed 20 minutes (solid) and 24 hours (dashed) after application.

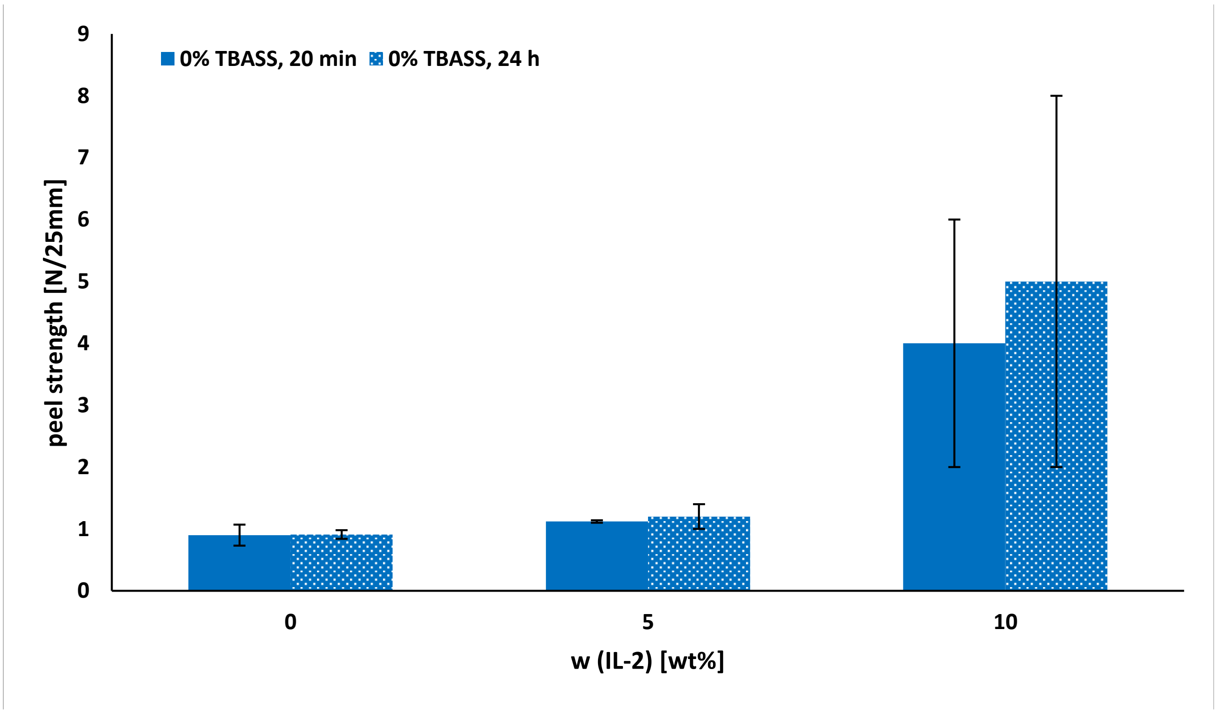

Figure 6.88: 180° peel strength values of a PSA with w (TBASS) = 0 wt% and different amounts of IL-2 added on PP. Measurements were performed 20 minutes (solid) and 24 hours (dashed) after application.

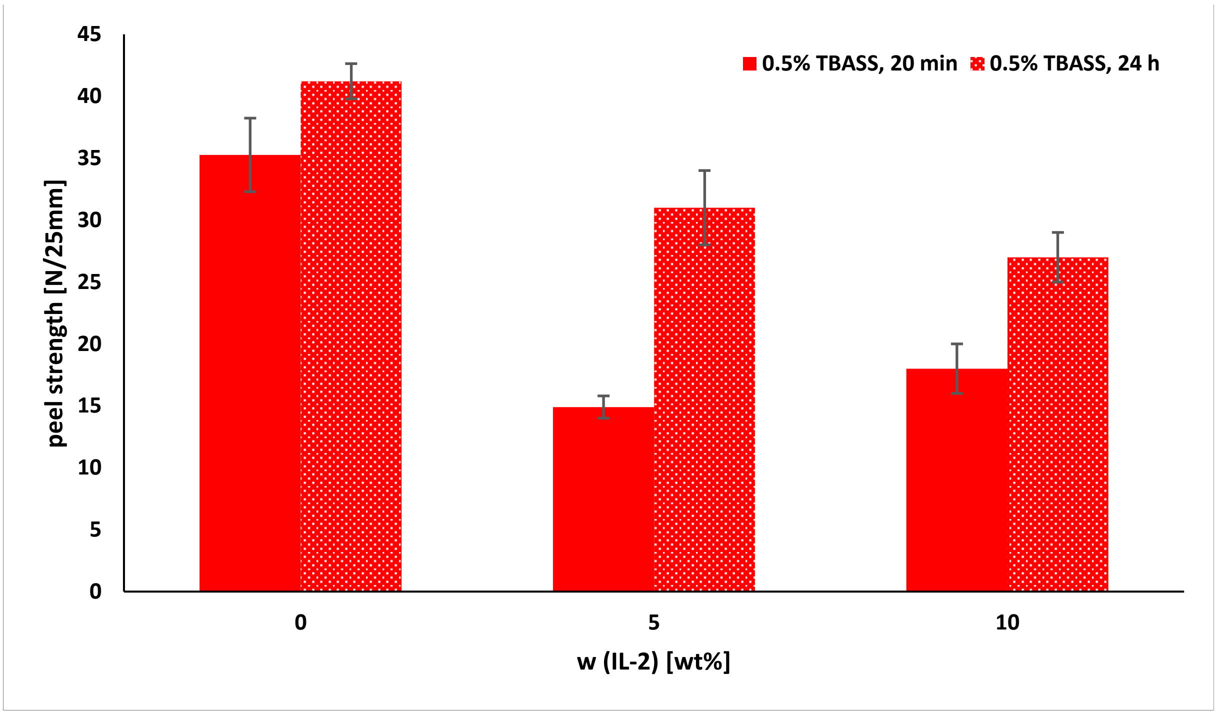

Figure 6.89: 180° peel strength values of a PSA with w (TBASS) = 0.5 wt% and different amounts of IL-2 added on glass. Measurements were performed 20 minutes (solid) and 24 hours (dashed) after application.

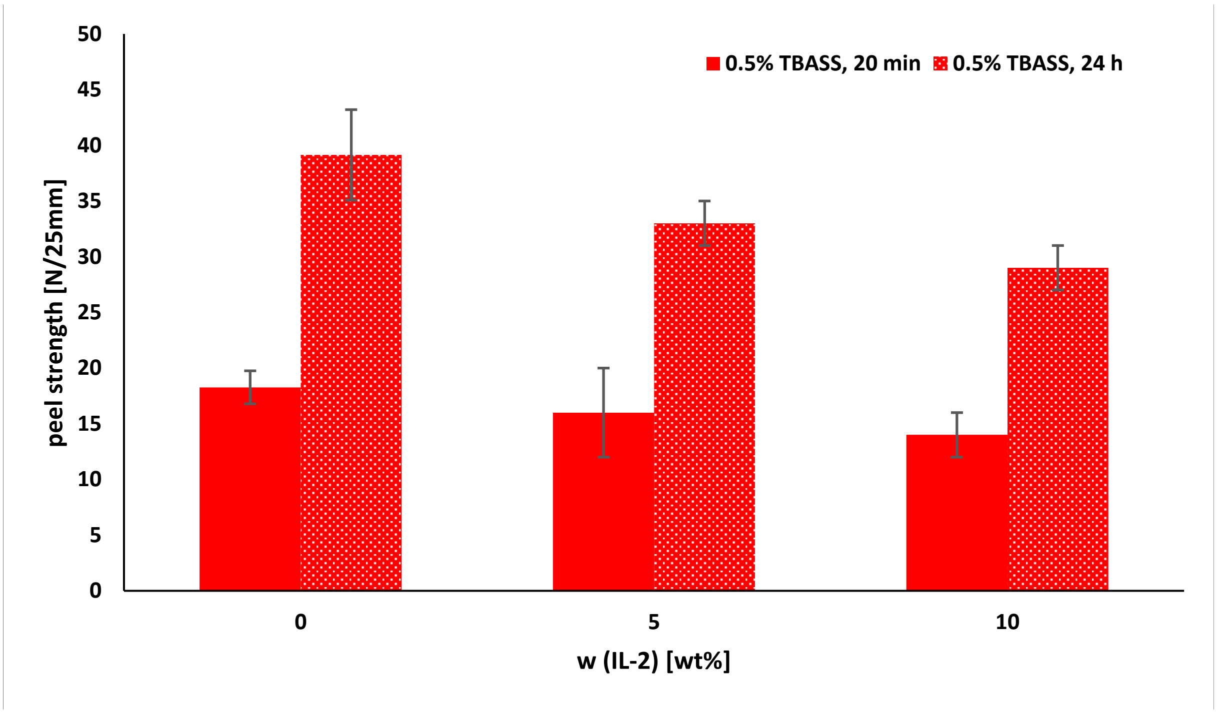

Figure 6.90: 180° peel strength values of a PSA with w (TBASS) = 0.5 wt% and different amounts of IL-2 added on steel. Measurements were performed 20 minutes (solid) and 24 hours (dashed) after application.

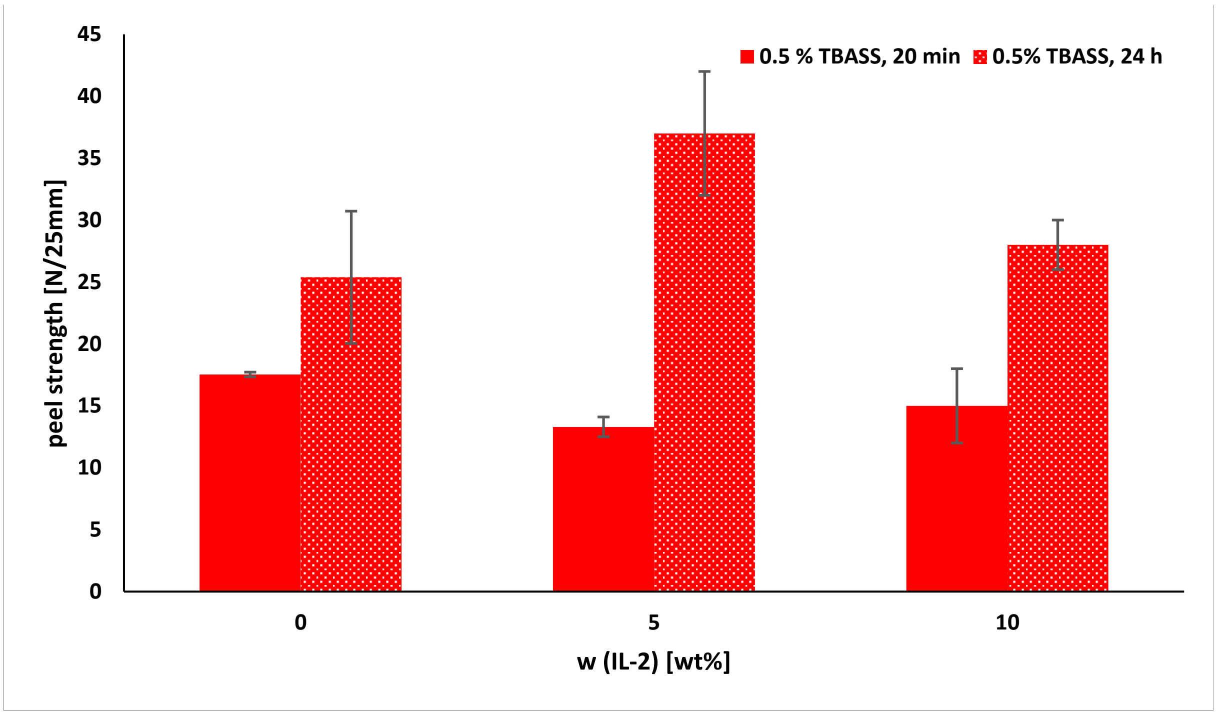

Figure 6.91: 180° peel strength values of a PSA with w (TBASS) = 0.5 wt% and different amounts of IL-2 added on PA. Measurements were performed 20 minutes (solid) and 24 hours (dashed) after application.

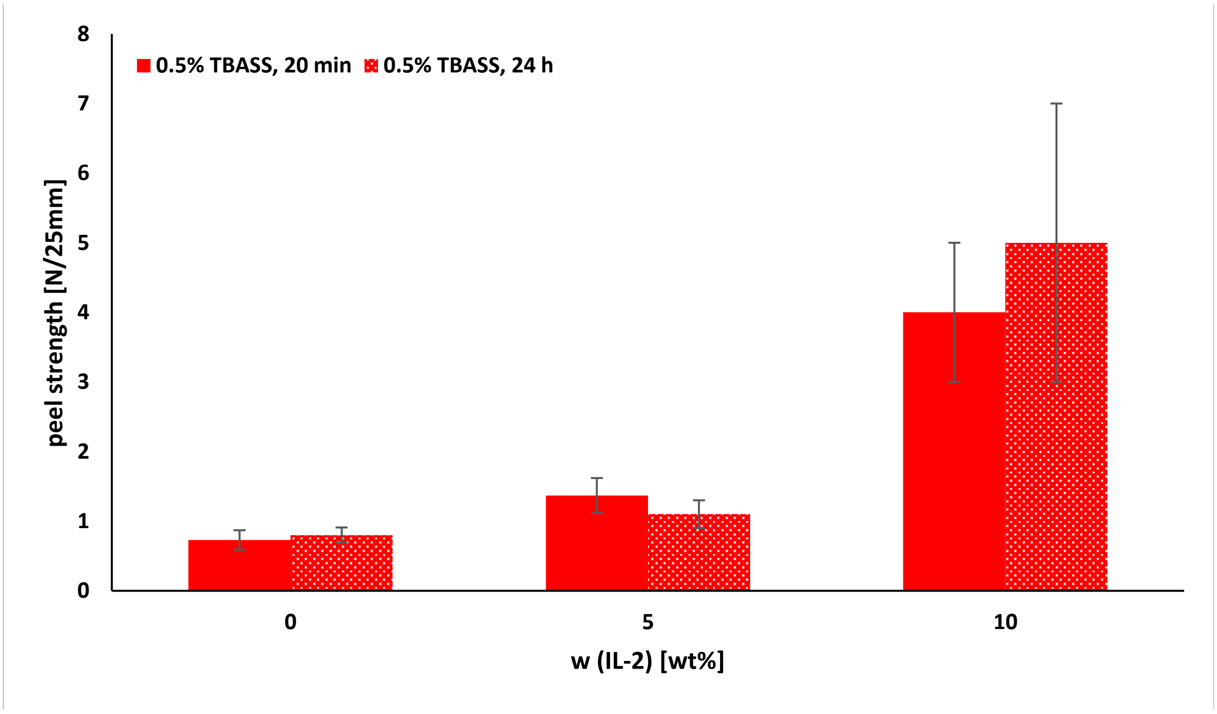

Figure 6.92: 180° peel strength values of a PSA with w (TBASS) = 0.5 wt% and different amounts of IL-2 added on PA. Measurements were performed 20 minutes (solid) and 24 hours (dashed) after application.

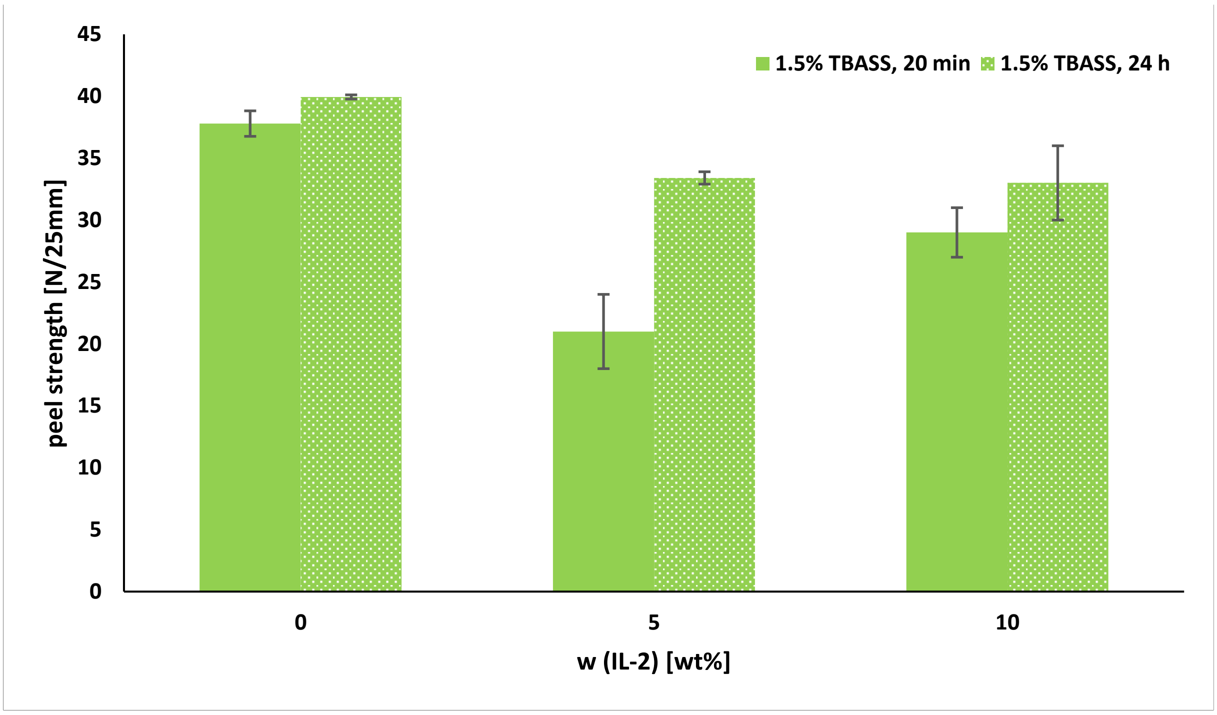

Figure 6.93: 180° peel strength values of a PSA with w (TBASS) = 1.5 wt% and different amounts of IL-2 added on glass. Measurements were performed 20 minutes (solid) and 24 hours (dashed) after application.

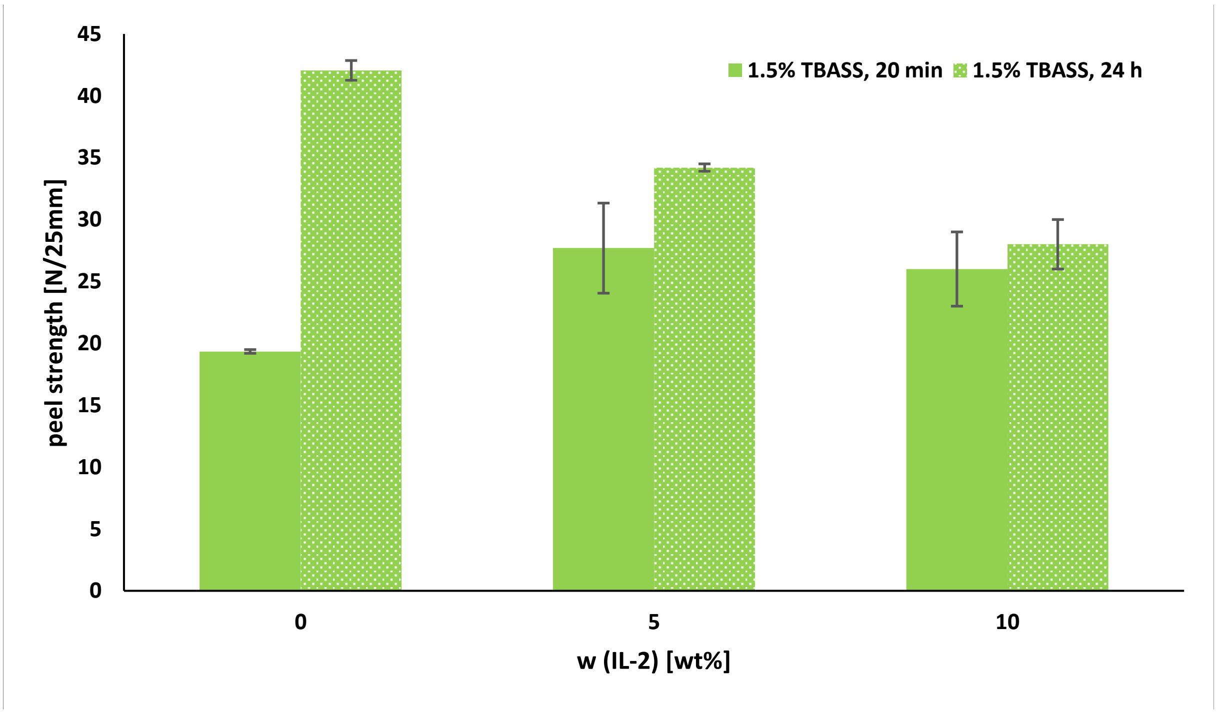

Figure 6.94: 180° peel strength values of a PSA with w (TBASS) = 1.5 wt% and different amounts of IL-2 added on steel. Measurements were performed 20 minutes (solid) and 24 hours (dashed) after application.

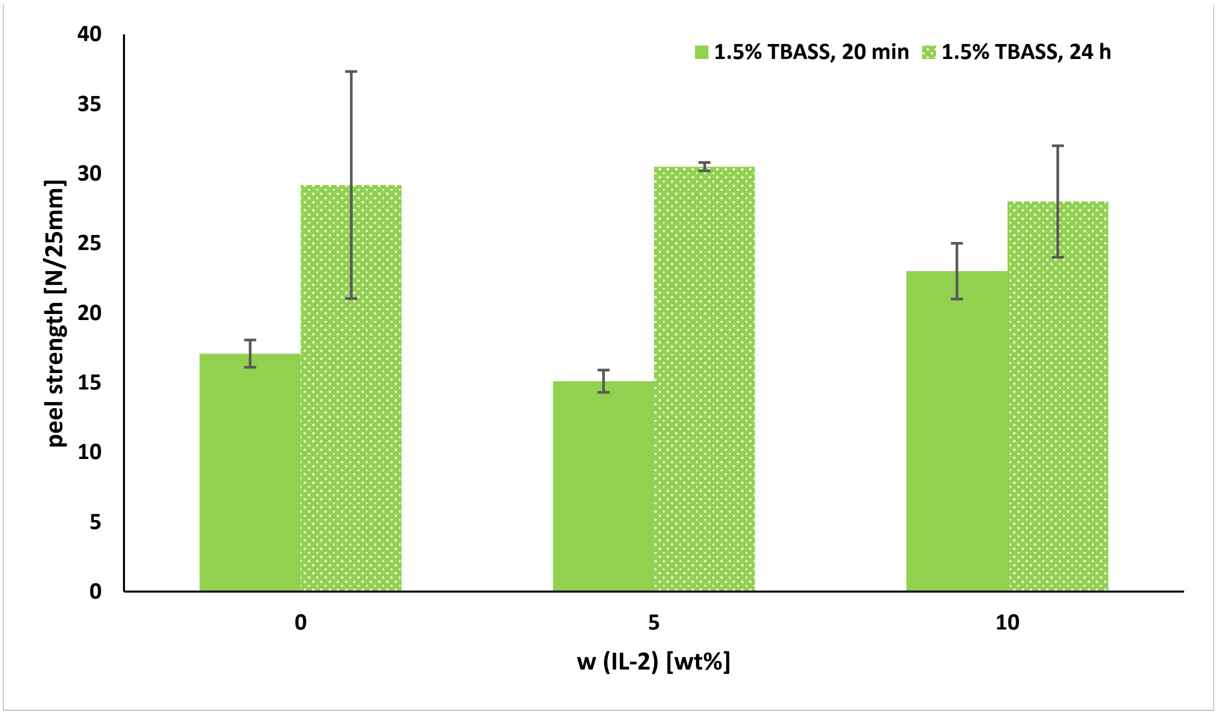

Figure 6.95: 180° peel strength values of a PSA with w (TBASS) = 1.5 wt% and different amounts of IL-2 added on PA. Measurements were performed 20 minutes (solid) and 24 hours (dashed) after application.

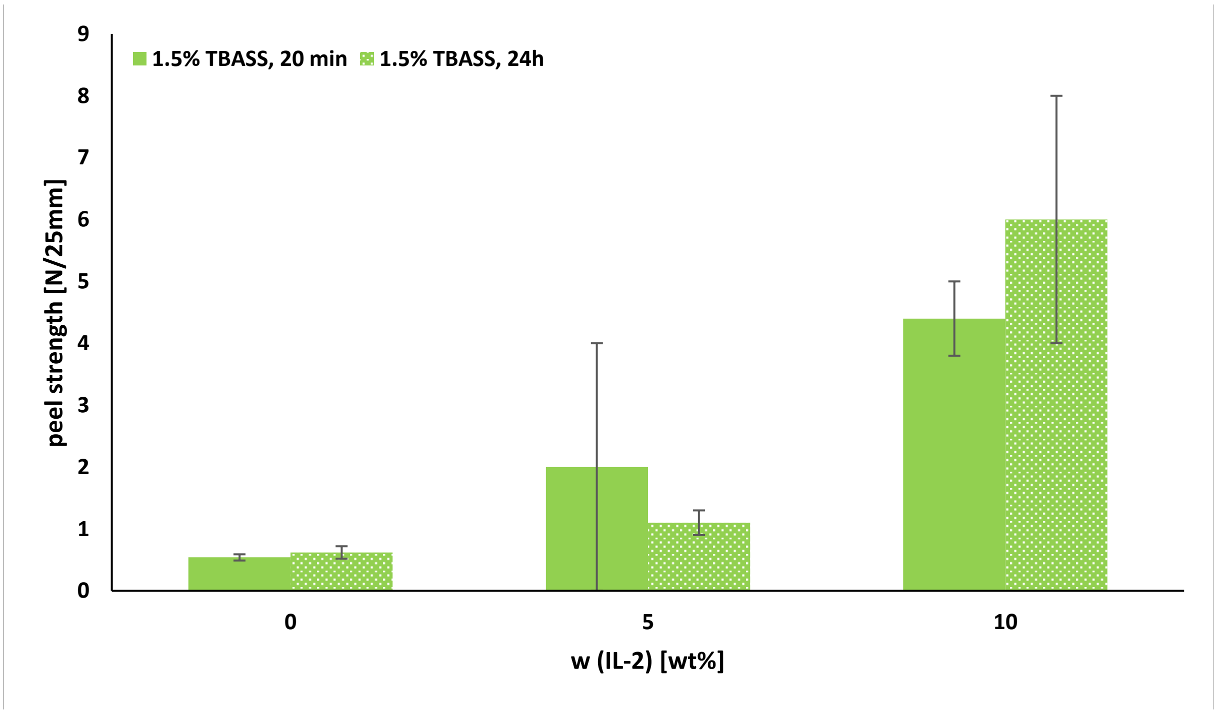

Figure 6.96: 180° peel strength values of a PSA with w (TBASS) = 1.5 wt% and different amounts of IL-2 added on PP. Measurements were performed 20 minutes (solid) and 24 hours (dashed) after application.

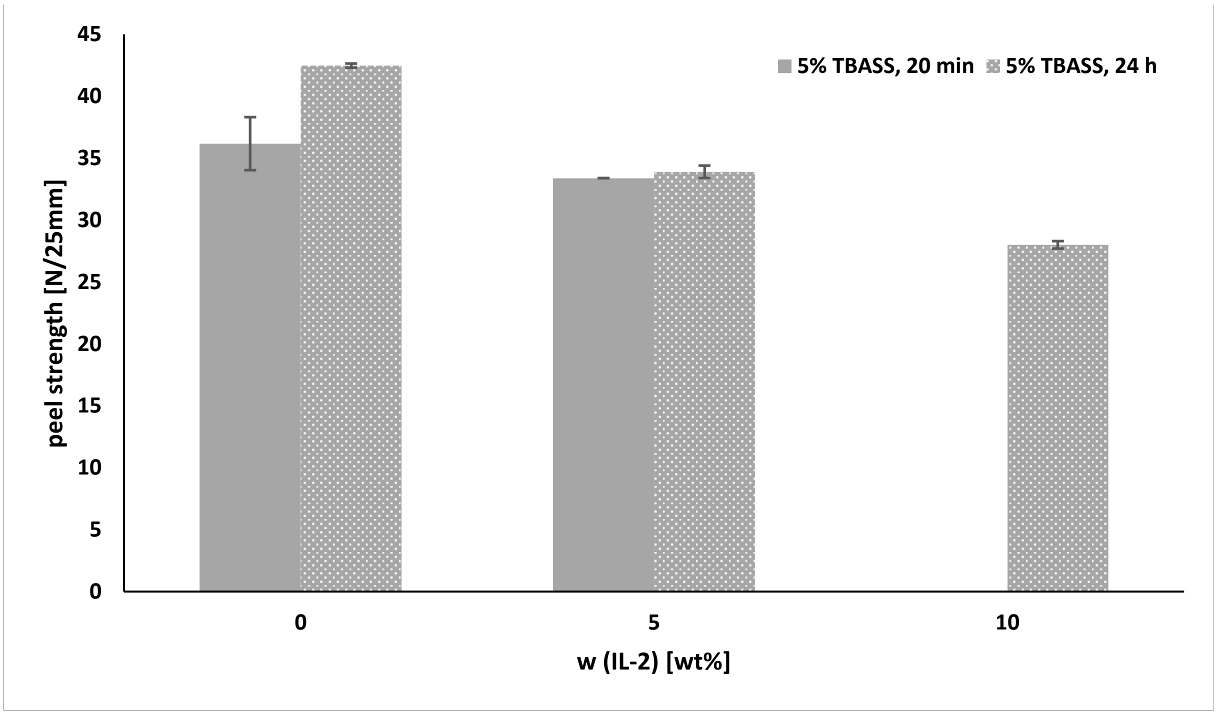

Figure 6.97: 180° peel strength values of a PSA with w (TBASS) = 5 wt% and different amounts of IL-2 added on glass. Measurements were performed 20 minutes (solid) and 24 hours (dashed) after application.

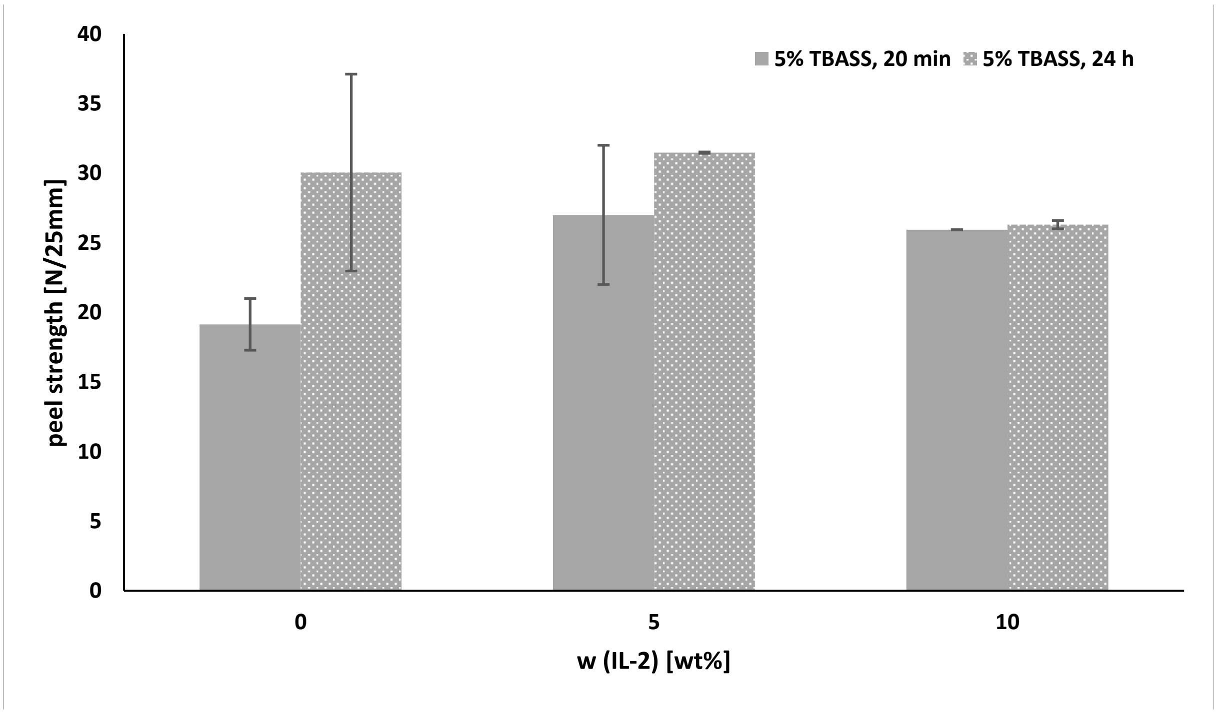

Figure 6.98: 180° peel strength values of a PSA with w (TBASS) = 5 wt% and different amounts of IL-2 added on PA. Measurements were performed 20 minutes (solid) and 24 hours (dashed) after application.

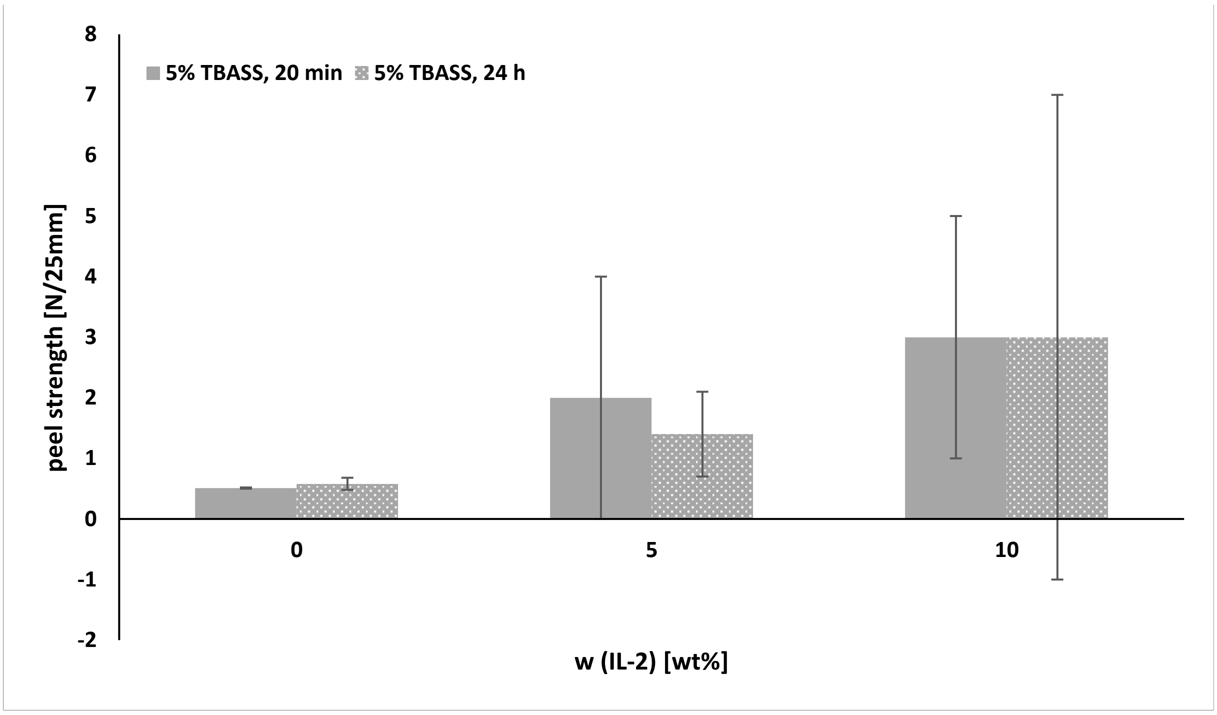

Figure 6.99: 180° peel strength values of a PSA with w (TBASS) = 5 wt% and different amounts of IL-2 added on PP. Measurements were performed 20 minutes (solid) and 24 hours (dashed) after application.

Literature

[1] E. M. Petrie, *Handbook of adhesives and sealants*, McGraw-Hill, New York, **2009**.

[2] B. Müller, W. Rath, *Formulating adhesives and sealants. Chemistry, physics and applications*, Vincentz Network, Hannover, **2010**.

[3] J. A. von Fraunhofer, *International Journal of Dentistry* **2012**, *2012*, 951324.

[4] L. A. Girifalco, *Statistical Mechanics of Solids*, Oxford University Press, New York, **2003**.

[5] N. Platzer, *J. Polym. Sci. B Polym. Lett. Ed.* **1982**, *20*, 459.

[6] A. J. Kinloch, *Adhesion and adhesives. Science and technology*, Chapman and Hall, London, **1994**.

[7] Y. Peykova, S. Guriyanova, O. V. Lebedeva, A. Diethert, P. Müller-Buschbaum, N. Willenbacher, *International Journal of Adhesion and Adhesives* **2010**, *30*, 245.

[8] M. Toyama, T. Ito, H. Nukatsuka, M. Ikeda, *Journal of Applied Polymer Science* **1973**, *17*, 3495.

[9] W. Brockmann, P. L. Geiß, J. Klingen, K. B. Schroeder, *Adhesive bonding. Materials, applications and technology*, Wiley-VCH, Weinheim, **2009**.

[10] M. Kropff, *Master thesis*, RWTH Aachen, Aachen, **2020**.

[11] a) K. Kendall, *J. Phys. D: Appl. Phys.* **1973**, *6*, 1782; b) C. J. Kleverlaan, A. J. Feilzer, *Dental Materials* **2005**, *21*, 1150; c) D. Truffier-Boutry, S. Demoustier-Champagne, J. Devaux, J.-J. Biebuyck, M. Mestdagh, P. Larbanois, G. Leloup, *Dental Materials* **2006**, *22*, 405.

[12] Y. Iyengar, D. E. Erickson, *Journal of Applied Polymer Science* **1967**, *11*, 2311.

[13] W. D. Bascom, *Macromolecules* **1972**, *5*, 792.

[14] a) J. M. Hung, Chu, W. K., Zhang, Y. S., Cole, I., EP 1611219 A1, **2006**; b) P. F. Abate, V. I. Rodriguez, R. L. Macchi, *Journal of dentistry* **2000**, *28*, 437.

[15] V. Kottisch, Q. Michaudel, B. P. Fors, *J. Am. Chem. Soc.* **2017**, *139*, 10665.

[16] G. Cohen, *RadTech Report* **2012**, *2012*, 44.

[17] K. Ahuja, S. Bayas, can be found under https://www.gminsights.com/industry-analysis/adhesives-and-sealants-market-report, **2020**.

[18] Y.-J. Park, D.-H. Lim, H.-J. Kim, D.-S. Park, I.-K. Sung, *International Journal of Adhesion and Adhesives* **2009**, *29*, 710.

[19] P. Merz, R. Dux, D. Grichting, US 6025029, **1997**.

[20] S. Clauβ, K. Allenspach, J. Gabriel, P. Niemz, *Wood Sci Technol* **2011**, *45*, 383.

[21] a) A. Lutz, D. Schneider, US 7625977 B2, **2009**; b) C. D. Weber, D. R. Egan, US 2009/0099312 A1, **2009**.

[22] a) K. Xiao, L. Ye, *Polymer Engineering & Science* **2000**, *40*, 2288; b) J. Wang, H. Zhang, Y. Miao, L. Qiao, X. Wang, F. Wang, *Polymer* **2018**, *138*, 211; c) M. Kotoul, J. Vrbka, *Theoretical and Applied Fracture Mechanics* **2003**, *40*, 23.

[23] T. Okamatsu, *Polymer* **2002**, *43*, 721.

[24] L. A. Heinrich, *Green Chem.* **2019**, *21*, 1866.

[25] R. A. Sheldon, M. Norton, *Green Chem.* **2020**, *22*, 6310.

[26] a) M. Carus, L. Dammer, A. Raschka, P. Skoczinski, C. vom Berg, *Renewable Carbon–Key to a Sustainable and Future-Oriented Chemical and Plastic Industry*, **2020**; b) P. Ruiz, P. Skoczinski, A. Raschka, N. Hark, M. Carus, A. Özgen, J. Kern, N. Plum, *Carbon Dioxide (CO2) as Feedstock for Chemicals, Advanced Fuels, Polymers, Proteins and Minerals*, nova-Institut GmbH, **2023**.

[27] P. T. Anastas, J. C. Warner, *Green chemistry*. *Theory and practice*, Oxford University Press, Oxford, **2000**.

[28] Renewable Carbon Initiative, "Renewable Energy and Renewable Carbon for a Sustainable Future - Graphic", can be found under https://renewable-carbon.eu/publications/product/renewable-energy-and-renewable-carbon-for-a-sustainable-future-%e2%88%92-graphic/, **2020**.

[29] K. Kümmerer, *CHEManager* **2023**, *2023*, 10.

[30] J. V. Crivello, J. H. W. Lam, *Sci., Polym. Chem. Ed.* **1978**, *1978*, 2441.

[31] K. R. Mulcahy, A. F. R. Kilpatrick, G. D. J. Harper, A. Walton, A. P. Abbott, *Green Chem.* **2022**, *24*, 36.

[32] Brian Spiegelberg, *Dissertation*, Universität Rostock, Rostock, **2022**.

[33] N. D. Blelloch, H. J. Yarbrough, K. A. Mirica, *Chemical science* **2021**, *12*, 15183.

[34] J.-T. Dong, W.-K. Zou, F. Chen, Q. Zhao, *Chin J Polym Sci* **2018**, *36*, 953.

[35] P. Skoczinski, M. Carus, G. Tweddle, P. Ruiz, D. de Guzman, J. Ravenstijn, H. Käb, N. Hark, L. Dammer, *Industrial Biotechnology* **2023**, 185.

[36] R. P. Babu, K. O'Connor, R. Seeram, *Prog Biomater* **2013**, *2*, 8.

[37] a) X. XU, J. LIN, P. CEN, *Chinese Journal of Chemical Engineering* **2006**, *14*, 419; b) J. G. H. Hermens, A. Jensma, B. L. Feringa, *Angewandte Chemie International Edition* **2022**, *61*, e202112618.

[38] K. Avasthi, A. Bohre, M. Grilc, B. Likozar, B. Saha, *Catal. Sci. Technol.* **2020**, *10*, 5411.

[39] V. Siracusa, I. Blanco, *Polymers* **2020**, *12*.

[40] F. Cheng, H. Bayat, U. Jena, C. E. Brewer, *Journal of Analytical and Applied Pyrolysis* **2020**, *147*, 104780.

[41] A. P. Tathod, P. L. Dhepe, *Bioresource Technology* **2015**, *178*, 36.

[42] L. Urbina, M. Á. Corcuera, N. Gabilondo, A. Eceiza, A. Retegi, *Cellulose* **2021**, *28*, 8229.

[43] M. Wu, J. Peng, Y. Dong, J. Pang, X. Zhang, *Industrial Crops and Products* **2021**, *172*, 114013.

[44] R. Volpe, A. A. Zabaniotou, V. Skoulou, *Energy Fuels* **2018**, *32*, 8420.

[45] H. Nakajima, P. Dijkstra, K. Loos, *Polymers* **2017**, *9*, 523.

[46] A. Llevot, P.-K. Dannecker, M. von Czapiewski, L. C. Over, Z. Söyler, M. A. R. Meier, *Chemistry – A European Journal* **2016**, *22*, 11510.

[47] H. B. Sweatt, *J. Chem. Educ.* **1946**, *23*, 192.

[48] C. Zhang, T. F. Garrison, S. A. Madbouly, M. R. Kessler, *Prog Polym Sci (Oxford)* **2017**, *71*, 91.

[49] E. Balla, V. Daniilidis, G. Karlioti, T. Kalamas, M. Stefanidou, N. D. Bikiaris, A. Vlachopoulos, I. Koumentakou, D. N. Bikiaris, *Polymers* **2021**, *13*, 1822.

[50] I. Manolakis, B. A. J. Noordover, R. Vendamme, W. Eevers, *Macromolecular rapid communications* **2014**, *35*, 71.

[51] E. Hofmann, H.-J. Klimisch, R. Backes, R. Vogelsang, L. Franz, R. Feuerhake, *Ullmann's Encyclopedia of Industrial Chemistry* **2011**.

[52] a) D. H. Blount, US 6908995, **2005**; b) M. I. Sherman, C. L. Elmore, US 4612286A, **1986**; c) R. W. Torget, K. L. Kadam, T. Hsu, G. P. Philippidis, C. E. Wyman, US 5124417, **1995**.

[53] W. Reppe, *Justus Liebigs Ann. Chem.* **1956**, *601*, 81.

[54] a) V. H. Agreda, *Fuel* **1990**, *69*, 132; b) A. M. Smith, A. B. Ross, *Algal Research* **2016**, *16*, 1.

[55] W. Sabra, C. Groeger, A.-P. Zeng in *Bioreactor Engineering Research and Industrial Applications I*, Springer, Berlin, Heidelberg, **2015**, pp. 165–197.

[56] a) A. J. Adebayo, J. K. Ogunjobi, O. O. Oluwasina, L. Lajide, *Chemistry Africa* **2023**, 1; b) I. Panovic, C. S. Lancefield, D. Phillips, M. J. Gronnow, N. J. Westwood, *ChemSusChem* **2019**, *12*, 542; c) A. P. Tathod, P. L. Dhepe, *Bioresource Technology* **2015**, *178*, 36.

[57] S. P. Teong, A. Y. H. Chua, S. Deng, X. Li, Y. Zhang, *Green Chem.* **2017**, *19*, 1659.

[58] V. V. Voronin, M. S. Ledovskaya, A. S. Bogachenkov, K. S. Rodygin, V. P. Ananikov, *Molecules* **2018**, *23*, 2442.

[59] B. A. Trofimov, L. A. Oparina, L. N. Parshina, M. Y. Khil’ko, A. P. Tantsyrev, G. P. Aleksandrova, *Cellulose* **2013**, *20*, 1201.

[60] B. A. Trofimov, L. N. Parshina, L. A. Oparina, A. P. Tantsyrev, M. Y. Khil'ko, O. V. Vysotskaya, A. V. Stepanov, N. K. Gusarova, J. Henkelmann, *Tetrahedron* **2007**, *63*, 11661.

[61] S. Kirschbaum, *Dissertation*, Johannes Gutenberg-Universität Mainz, Mainz, **2015**.

[62] E. H. W. Reppe, *Chemie Ingenieur Technik* **1950**, *22*, 273.

[63] a) M. Bosch, S. Handerson, M. Schlaf, *Journal of Carbohydrate Chemistry* **2008**, *27*, 103; b) H. Lüssi, *HCA* **1966**, *49*, 1684; c) A. Nakamura, M. Tokunaga, *Tetrahedron Letters* **2008**, *2008*, 3729; d) B. Spiegelberg, H. Jiao, R. Grauke, C. Kubis, A. Spannenberg, A. Brandt, A. Taden, H. Beck, S. Tin, J. G. Vries, *Adv Synth Catal* **2022**, *364*, 1251.

[64] T. Hirabayashi, S. Sakaguchi, Y. Ishii, *Advanced Synthesis & Catalysis* **2005**, *347*, 872.

[65] S. Aoshima, S. Kanaoka, *Chemical reviews* **2009**, *109*, 5245.

[66] B. Golaz, V. Michaud, Y. Leterrier, J.-A.E. Månson, *Polymer* **2012**, *53*, 2038.

[67] J.-D. Cho, J.-W. Hong, *Journal of Applied Polymer Science* **2004**, *93*, 1473.

[68] C. Decker, D. Decker, *Polymer* **1997**, *38*, 2229.

[69] a) C. Decker, T. Nguyen Thi Viet, H. Pham Thi, *Polym. Int.* **2001**, *50*, 986; b) M. Z. Fiume, *Internation journal of toxicology* **2002**, *2002*, 1; c) S. Geukens, A. Goossens, *Contact Dermatitis* **2001**, *44*, 153; d) H. F. Smyth, C. P. Carpenter, C. S. Weil, U. C. Pozzani, J. A. Striegel, J. S. Nycum, *American Industrial Hygiene Association Journal* **1969**, *30*, 470.

[70] E. W. Nelson, T. P. Carter, A. B. Scranton, *Macromolecules* **1994**, *27*, 1013.

[71] a) *Di(ethylene glycol) diacrylate - safety data sheet*, **2020**; b) *Di(ethylene glycol) divinyl ether - safety data sheet*, **2020**.

[72] BASF SE, "The broadest portfolio of vinyl monomers", **2019**.

[73] a) A. R. Jagtap, A. More, *Polym. Bull.* **2022**, *79*, 5667; b) K. Yurugi, A. Fukada, K. Matsukawa, US 6767980 B2, **2004**.

[74] A. Kanazawa, S. Kanaoka, S. Aoshima, *Chem. Lett.* **2010**, *39*, 1232.

[75] V. Kottisch, Q. Michaudel, B. P. Fors, *Journal of the American Chemical Society* **2016**, *138*, 15535.

[76] S. A. Metlyaeva, K. S. Rodygin, K. A. Lotsman, D. E. Samoylenko, V. P. Ananikov, *Green Chem.* **2021**, *23*, 2487.

[77] S. Brännström, M. Finnveden, N. Razza, M. Martinelle, E. Malmström, M. Sangermano, M. Johansson, *Macromol. Chem. Phys.* **2018**, *219*, 1800335.

[78] J. V. Crivello, D. A. Conlon, *Journal of Polymer Science: Polymer Chemistry Edition* **1983**, *21*, 1785.

[79] a) V. Kottisch, Q. Michaudel, B. P. Fors, *Journal of the American Chemical Society* **2017**, *139*, 10665; b) J. G. Woods in *Radiation Curing*, Springer, Boston, MA, **1992**, pp. 333–398.

[80] S. Sugihara, Y. Kawamoto, Y. Maeda, *Macromolecules* **2016**, *49*, 1563.

[81] E. W. Nelson, J. L. Jacobs, A. B. Scranton, K. S. Anseth, C. N. Bowman, *Polymer* **1995**, *36*, 4651.

[82] A. Ledwith, E. Lockett, D.C. Sherrington, *Polymer* **1975**, *16*, 31.

[83] A. G. Evans, E. Tyrrall, *J. Polym. Sci.* **1947**, *2*, 387.

[84] C. Decker, C. Bianchi, D. Decker, F. Morel, *Progress in Organic Coatings* **2001**, *42*, 253.

[85] Y. Yağci, I. Reetz, *Progress in Polymer Science* **1998**, *23*, 1485.

[86] K. Hatada, K. Nagata, H. Yuki, *Bulletin of the chemical society of Japan* **1970**, *1970*, 3195.

[87] S. C. Lapin in *Radiation Curing*, Springer, Boston, MA, **1992**, pp. 241–271.

[88] a) K. Kojima, M. Sawamote, T. Higashimura, *Macromolecules* **1989**, *1989*, 1552; b) M. Kamigaito, Y. Maeda, M. Sawamoto, T. Higashimura, *Macromolecules* **1993**, *26*, 1643.

[89] M. Sangermano, G. Malucelli, R. Bongiovanni, A. Priola, U. Annby, N. Rehnberg, *European Polymer Journal* **2002**, *38*, 655.

[90] H. Shimomoto, D. Fukami, S. Kanaoka, S. Aoshima, *J. Polym. Sci. A Polym. Chem.* **2011**, *49*, 2051.

[91] S. V. Kostjuk, F. Ganachaud, *Accounts of chemical research* **2010**, *43*, 357.

[92] V. Kottisch, J. O'Leary, Q. Michaudel, E. E. Stache, T. H. Lambert, B. P. Fors, *Journal of the American Chemical Society* **2019**, *141*, 10605.

[93] M. Higuchi, A. Kanazawa, S. Aoshima, *Macromolecules* **2020**, *53*, 3822.

[94] a) S.-C. Chu, G. B. Butler, *Journal of Polymer Science: Polymer Chemistry Edition* **1978**, *1978*, 1375; b) K. Hayashi, S. Okamura, *Polymer Journal* **1973**, *1973*, 495.

[95] T. Asakawa, A. Kanazawa, S. Aoshima, *Macromolecules* **2020**, *53*, 6887.

[96] Y. Ishido, R. Aburaki, S. Kanaoka, S. Aoshima, *Macromolecules* **2010**, *43*, 3141.

[97] J. V. Crivello, T. P. Lockhart, J. L. Lee, *Journal of Polymer Science: Polymer Chemistry Edition* **1983**, *21*, 97.

[98] N. P. Hacker, D. V. Leff, J. L. Dektar, *J. Org. Chem.* **1991**, *56*, 2280.

[99] J. V. Crivello, *Journal of Polymer Science Part A: Polymer Chemistry* **1999**, *37*, 4241.

[100] J. V. Crivello, J. H. W. Lam, *Macromolecules* **1977**, *10*, 1307.

[101] J. L. Dektar, N. P. Hacker, *J. Org. Chem.* **1990**, *55*, 639.

[102] K. Morio, H. Murase, H. Tsuchiya, T. Endo, *Journal of Applied Polymer Science* **1986**, *32*, 5727.

[103] A. L. Andrady, N. D. Searle, L. F.E. Crewdson, *Polymer Degradation and Stability* **1992**, *35*, 235.

[104] Klessinger, Martin, Michl, Josef, *(No Title)*.

[105] a) M. A. Tasdelen, J. Lalevée, Y. Yagci, *Polym. Chem.* **2020**, *11*, 1111; b) Y. Bi, D. C. Neckers, *Macromolecules* **1994**, *27*, 3683; c) Y. Yagci, W. Schnabel, *Die Makromolekulare Chemie, Rapid Communications* **1987**, *8*, 209; d) J. Lalevée, H. Mokbel, J.-P. Fouassier, *Molecules (Basel, Switzerland)* **2015**, *20*, 7201.

[106] a) Y. Yağci, I. Kminek, W. Schnabel, *European Polymer Journal* **1992**, *1992*, 387; b) Y. Yağci, W. Schnabel, *Makromol. Chem. Macromol. Symp.* **1992**, *1992*, 133.

[107] J. Lalevée, M.-A. Tehfe, F. Morlet-Savary, B. Graff, X. Allonas, J. P. Fouassier, *Progress in Organic Coatings* **2011**, *70*, 23.

[108] M. D. Lechner, K. Gehrke, E. H. Nordmeier, *Makromolekulare Chemie*, Birkhäuser Basel, Basel, s.l., **2003**.

[109] M. Tsukino, T. Kinitake, *Macromolecules* **1979**, *12*, 387.

[110] A. Matsumoto, T. Nakana, M. Oiwa, *Makromol. Chem., Rapid Commun.* **1983**, *1983*, 277.

[111] M. Kamachi, K. Tanaka, Y. Kuwae, *Journal of Polymer Science Part A: Polymer Chemistry* **1986**, *1986*, 925.

[112] M. Imoto, S. Sakai, T. Ouchi, *J. Chem. Soc., Japan* **1985**, *1985*.

[113] T. Kumagai, C. Kagawa, H. Aota, Y. Takeda, H. Kawasaki, R. Arakawa, A. Matsumoto, *Macromolecules* **2008**, *41*, 7347.

[114] S. Sugihara, A. Yoshida, S. Fujita, Y. Maeda, *Macromolecules* **2017**, *50*, 8346.

[115] S. Sugihara, A. Yoshida, T.-A. Kono, T. Takayama, Y. Maeda, *Journal of the American Chemical Society* **2019**, *141*, 13954.

[116] L. Zhang, L. Liu, Y. Chen, *J. Appl. Polym. Sci.* **1999**, *74*, 3541.

[117] C. Decker, D. Decker, *Journal of Macromolecular Science, Part A* **1997**, *34*, 605.

[118] K. Griesbaum, *Angew. Chem. internat. Edit.* **1970**, *1970*, 273.

[119] J. W. Chan, C. E. Hoyle, A. B. Lowe, M. Bowman, *Macromolecules* **2010**, *43*, 6381.

[120] T. O. Machado, C. Sayer, P. H.H. Araujo, *European Polymer Journal* **2017**, *86*, 200.

[121] T. Posner, *Ber. Dtsch. Chem. Ges.* **1905**, *38*, 646.

[122] C. S. Marvel, R. R. Chambers, *J. Am. Chem. Soc.* **1948**, *70*, 993.

[123] C. E. Hoyle, T. Y. Lee, T. Roper, *Journal of Polymer Science Part A: Polymer Chemistry* **2004**, *42*, 5301.

[124] C. E. Hoyle, C. N. Bowman, *Angewandte Chemie International Edition* **2010**, *49*, 1540.

[125] R. Auvergne, M. Desroches, S. Clerc, S. Carlotti, S. Caillol, B. Boutevin, *Reactive and Functional Polymers* **2012**, *72*, 393.

[126] a) Q. Li, H. Zhou, C. E. Hoyle, *Polymer* **2009**, *50*, 2237; b) N. A. Feidenhans'l, J. P. Lafleur, T. G. Jensen, J. P. Kutter, *ELECTROPHORESIS* **2014**, *35*, 282.

[127] J. J. Roberts, S. J. Bryant, *Biomaterials* **2013**, *34*, 9969.

[128] M. Claudino, KTH Royal Institute of Technology, **2011+0200**.

[129] L. Pezzana, M. Sangermano, *Progress in Organic Coatings* **2021**, *157*, 106295.

[130] H. Şeker, E. Çakmakçi, *Journal of Polymer Science* **2020**, *58*, 1105.

[131] a) Y. Labat in *A John Wiley & Sons, Inc., publication* (Eds.: I. John Wiley & Sons, J. I. Kroschwitz, R. E. Kirk, D. F. Othmer, A. Seidel), Wiley-Interscience, Hoboken, NJ, **2004**; b) X. Wang, W. Li, S. Wang, Q. Wang, L. Li, H. Wang, T. Qiu, *Chinese Journal of Chemical Engineering* **2021**, *36*, 111.

[132] M. Uchiyama, M. Osumi, K. Satoh, M. Kamigaito, *Angewandte Chemie International Edition* **2020**, *59*, 6832.

[133] a) M. Uchiyama, Y. Murakami, K. Satoh, M. Kamigaito, *Angewandte Chemie* **2023**, *135*, e202215021; b) Q. Li, S. Ma, N. Lu, J. Qiu, J. Ye, Y. Liu, S. Wang, Y. Han, B. Wang, X. Xu et al., *Green Chem.* **2020**, *22*, 7769.

[134] S. C. Lapin in *ACS Symposium Series* (Eds.: C. E. Hoyle, J. F. Kinstle), American Chemical Society, Washington, DC, **1990**, pp. 363–381.

[135] T. Namikoshi, T. Hashimoto, T. Kodaira, *J. Polym. Sci. A Polym. Chem.* **2004**, *42*, 2960.

[136] P. Feng, W. Li, Y. Zou, *J. Appl. Polym. Sci.* **2014**, *131*, n/a-n/a.

[137] S. A. Shama, E. S. Poklacki, J. M. Zimmermann, US 4956198 A, **1990**.

[138] a) J. H. Udding, A. E. Wolters, US 2004/0072964 A1, **2004**; b) H. Kroener, E. Schupp, E. Wistuba, O. Aydin, E. Schwarzenbach, K. Schnell, EP 0617102 B1, **1997**.

[139] a) E. Delebecq, J.-P. Pascault, B. Boutevin, F. Ganachaud, *Chemical reviews* **2013**, *113*, 80; b) M. Szycher, *Szycher's handbook of polyurethanes*, CRC Press, Boca Raton, Fla., **1999**.

[140] a) W. Denissen, M. Droesbeke, R. Nicolaÿ, L. Leibler, J. M. Winne, F. E. Du Prez, *Nat Commun* **2017**, *8*, 14857; b) R. P. Houghton, A. W. Mulvaney, *Journal of Organometallic Chemistry* **1996**, *518*, 21; c) R. Lomölder, F. Plogmann, P. Speier, *Journal of Coatings Technology* **1997**, *69*, 51.

[141] a) M.-C. Chang, S.-A. Chen, *Journal of Polymer Science Part A: Polymer Chemistry* **1987**, *25*, 2543; b) H. Q. Waleed, M. Csécsi, V. Konyhás, Z. R. Boros, B. Viskolcz, Z. Fejes, B. Fiser, *Phys. Chem. Chem. Phys.* **2022**, *24*, 20538.

[142] C. Decker, *Acta Polym.* **1994**, *45*, 333.

[143] C. Decker, C. Bianchi, D. Decker, F. Morel, *Progress in Organic Coatings* **2001**, *42*, 253.

[144] C. Decker, *Polymer International* **1998**, *45*, 133.

[145] S. C. Lapin **1992**, *1992*, 241.

[146] J. Niesiobędzka, J. Datta, *Green Chem.* **2023**, *25*, 2482.

[147] a) A. E. Neitzel, M. A. Petersen, E. Kokkoli, M. A. Hillmyer, *ACS Macro Letters* **2014**, *3*, 1156; b) A. Narumi, M. Yamada, Y. Unno, J. Kumaki, W. H. Binder, K. Enomoto, M. Kikuchi, S. Kawaguchi, *ACS Macro Letters* **2019**, *8*, 634.

[148] M. Okada, H. Sumitomo, M. Atsumi, *Macromolecules* **1984**, *17*, 1840.

[149] E. Ruckenstein, H. Zhang, *Journal of Polymer Science Part A: Polymer Chemistry* **2000**, *2000*, 1848.

[150] Y. Nakane, M. Ishidoya, T. Endo, *J. Polym. Sci. A Polym. Chem.* **1999**, *37*, 609.

[151] a) R.-T. Zeng, Y. Wu, Y.-D. Li, M. Wang, J.-B. Zeng, *Polymer Testing* **2017**, *57*, 281; b) X. Zhang, Y. Zhao, Y. Liu, J. Wang, Y. Deng, *Appl Microbiol Biotechnol* **2020**, *104*, 4259.

[152] R. R. Gallucci, R. C. Going, *J. Org. Chem.* **1982**, *1982*, 3517.

[153] J. van Schijndel, D. Molendijk, K. van Beurden, L. A. Canalle, T. Noël, J. Meuldijk, *European Polymer Journal* **2020**, *125*, 109534.

[154] C. Amen-Chen, H. Pakdel, C. Roy, *Bioresource Technology* **2001**, *79*, 277.

[155] M. I. F. Mota, P. C. Rodrigues Pinto, J. M. Loureiro, A. E. Rodrigues, *Separation & Purification Reviews* **2016**, *45*, 227.

[156] a) S. Mathew, T. E. Abraham, S. Sudheesh, *Journal of Molecular Catalysis B: Enzymatic* **2007**, *44*, 48; b) S. van Beek, F. G. Priest, *Applied and environmental microbiology* **2000**, *66*, 5322.

[157] J. G. Woods, M. Masterson, US 005633411, **1997**.

[158] a) J. van Schijndel, L. A. Canalle, J. Smid, J. Meuldijk, *OJPC* **2016**, *06*, 101; b) J. van Schijndel, L. Canalle, D. Molendijk, J. Meuldijk, *Synlett* **2018**, *29*, 1983.

[159] H. Gu, Y. Zhu, Y. Peng, X. Liang, X. Liu, L. Shao, Y. Xu, Z. Xu, R. Liu, J. Li, *Biotechnol Biofuels* **2019**, *12*, 268.

[160] a) A. R. Goodey, R. S. Tubb, *Microbiology* **1982**, *128*, 2615; b) P. Gramatica, B. M. Ranzi, P. Manitto, *Bioorganic Chemistry* **1981**, *10*, 14; c) A. K. Schweiger, N. Ríos-Lombardía, C. K. Winkler, S. Schmidt, F. Morís, W. Kroutil, J. González-Sabín, R. Kourist, *ACS Sustainable Chem. Eng.* **2019**, *7*, 16364.

[161] H. Terholsen, K. Myrtollari, M. Larva, C. Möller, A. Taden, R. Kourist, U. T. Bornscheuer, D. Kracher, *ChemBioChem* **2023**, e202300207.

[162] R. H. Still, A. Whitehead, *Journal of Applied Polymer Science* **1977**, *1977*, 1199.

[163] A. Kanazawa, S. Shibutani, N. Yoshinari, T. Konno, S. Kanaoka, S. Aoshima, *Macromolecules* **2012**, *45*, 7749.

[164] J. Woods, M. Masterson, C. McArdle, J. Burke in *ACS Symposium Series* (Eds.: C. E. Hoyle, J. F. Kinstle), American Chemical Society, Washington, DC, **1990**, pp. 107–120.

[165] W. J. Steinkraus, WO 98/14487, **1998**.

[166] T. Miwa, R. Tawata, S. Numata, *Polymer* **1993**, *34*, 621.

[167] K. Xu, J. C. Selby, M. A. Shannon, J. Economy, *Journal of Applied Polymer Science* **2004**, *92*, 3843.

[168] M. D. Banea, *rev adhes adhesives* **2019**, *7*, 33.

[169] M. D. Banea, da Silva, Lucas F. M., Campilho, Raul D. S. G., C. Sato, *The Journal of Adhesion* **2014**, *90*, 16.

[170] C. Heinzmann, S. Coulibaly, A. Roulin, G. L. Fiore, C. Weder, *ACS Applied Materials & Interfaces* **2014**, *6*, 4713.

[171] J. H. Aubert, *The Journal of Adhesion* **2003**, *79*, 609.

[172] B. Jin, G. Zhang, J. Lian, Q. Zhang, X. Zhan, F. Chen, *J. Mater. Chem. A* **2019**, *7*, 12266.

[173] Z. Liu, F. Yan, *Advanced Science* **2022**, *9*, e2200264.

[174] J. E. Pickett, D. J. Coyle, *Polymer Degradation and Stability* **2013**, *98*, 1311.

[175] I. Bibi, H. Ahmad, A. Farid, H. Iqbal, N. Habib, M. Atif, *Materials Today Communications* **2023**, *35*, 106293.

[176] a) C. L. Jenkins, H. M. Siebert, J. J. Wilker, *Macromolecules* **2017**, *50*, 561; b) K. L. van Landuyt, J. de Munck, A. Mine, M. V. Cardoso, M. Peumans, B. van Meerbeek, *Journal of dental research* **2010**, *89*, 1045.

[177] D. Hofmann, M. Entrialgo-Castaño, K. Kratz, A. Lendlein, *Advanced Materials* **2009**, *21*, 3237.

[178] J. H. Waite, N. H. Andersen, S. Jewhurst, C. Sun, *The Journal of Adhesion* **2005**, *81*, 297.

[179] R. Puligadda, S. Pillalamarri, W. Hong, C. Brubaker, M. Wimplinger, S. Pargfrieder, *MRS Online Proceedings Library (OPL)* **2006**, *970*, 0970-Y04-09.

[180] H. Zhang, T. Zhao, P. Duffy, Y. Dong, A. N. Annaidh, E. O'Cearbhaill, W. Wang, *Advanced healthcare materials* **2015**, *4*, 2260.

[181] a) T. Kijchavengkul, R. Auras, M. Rubino, S. Selke, M. Ngouajio, R. T. Fernandez, *Polymer Degradation and Stability* **2010**, *95*, 2641; b) K. S. Seo, J. D. Cloyd, *Journal of Applied Polymer Science* **1991**, *42*, 845.

[182] Z. Cui, B. H. Lee, B. L. Vernon, *Biomacromolecules* **2007**, *8*, 1280.

[183] a) N. F. Zaaba, M. Jaafar, *Polym Eng Sci* **2020**, *60*, 2061; b) G. Gorrasi, R. Pantani in *Synthesis, Structure and Properties of Poly(lactic acid)*, Springer, Cham, **2017**, pp. 119–151.

[184] T. Kaneko, T. H. Thi, D. J. Shi, M. Akashi, *Nature Mater* **2006**, *5*, 966.

[185] a) J. Mizuguchi, T. Hashimoto, M. Urushisaki, T. Sakaguchi, *Kobunshi Ronbunshu* **2013**, *2013*, 602; b) A. E. Neitzel, L. Barreda, J. T. Trotta, G. W. Fahnhorst, T. J. Haversang, T. R. Hoye, B. P. Fors, M. A. Hillmyer, *Polym. Chem.* **2019**, *10*, 4573.

[186] E. Khosravi, F. Iqbal, O. M. Musa, *Polymer* **2011**, *52*, 243.

[187] J. Jeong, *Journal of Adhesion and Interface* **2018**, *2018*, 84.

[188] S. Leijonmarck, A. Cornell, C.-O. Danielsson, T. Åkermark, B. D. Brandner, G. Lindbergh, *International Journal of Adhesion and Adhesives* **2012**, *32*, 39.

[189] A. Sierra-Romero, K. Novakovic, M. Geoghegan, *Langmuir* **2022**, *38*, 15476.

[190] J. S. Berg, C. H. Reynolds, J. Lin, D. A. Vogel, P. A. Keenan, J. R. Howard, US 9371669 B2, **2016**.

[191] R. Keller, T. D. Burleigh, Hydock, D. M., US 5507926 A, **1996**.

[192] M. D. Gilbert, US 7968188 B2, **2011**.

[193] C. Anduix-Canto, D. Peral, V. Pérez-Padilla, A. M. Diaz-Rovira, A. Belmez Lledó, C. A. Orme, S. Petrash, T. Engels, K. W. Chou, *Adv Materials Inter* **2022**, *9*, 2101447.

[194] A. Lapprand, F. Boisson, F. Delolme, F. Méchin, J.-P. Pascault, *Polymer Degradation and Stability* **2005**, *90*, 363.

[195] Everad Adhesives, "Mechanische Eigenschaften (Festigkeit und Dehnung) der wichtigsten Klebesysteme", can be found under https://www.everad-adhesives.com/de/technologien%20/reaktivkleber/, **2023**.

[196] Most of the practical work in this section was performed by Andrea Hoffmann under the author's supervision.

[197] S. Peter Pappas, B. C. Pappas, L. R. Gatechair, J. H. Jilek, W. Schnabel, *Polymer Photochemistry* **1984**, *5*, 1.

[198] a) J. V. Crivello, J. H. W. Lam, *Journal of Polymer Science: Polymer Chemistry Edition* **1981**, *19*, 539; b) P.-E. Sundell, S. Jönsson, A. Hult, *Journal of Polymer Science Part A: Polymer Chemistry* **1991**, *29*, 1535.

[199] J. Comyn in *Handbook of Adhesion Technology*, Springer, Cham, **2017**, pp. 1–30.

[200] P. Murias, Ł. Byczyński, H. Maciejewski, H. Galina, *J Therm Anal Calorim* **2015**, *122*, 215.

[201] F. Wu, X. Zhou, X. Yu, *RSC advances* **2018**, *8*, 8248.

[202] K. Wang, J. Wu, L. Ye, H. Zeng, *Composites Part A: Applied Science and Manufacturing* **2003**, *34*, 1199.

[203] a) A. L. Daniel-da-Silva, J. C. M. Bordado, J. M. Martín-Martínez, *Journal of Applied Polymer Science* **2008**, *107*, 700; b) J. Comyn, F. Brady, R.A. Dust, M. Graham, A. Haward, *International Journal of Adhesion and Adhesives* **1998**, *18*, 51; c) B. S. Lepene, T. E. Long, A. Meyer, D. E. Kranbuehl, *The Journal of Adhesion* **2002**, *78*, 297.

[204] a) R. A. Ortiz, A. P. Urbina, L. V. C. Valdez, Duarte L. B., R. G. Santos, A. E. G. Valdez, M. D. Soucek, *J. Polym. Sci. A Polym. Chem.* **2007**, *2007*, 8788; b) H. Wei, Q. Li, M. Ojelade, S. Madbouly, J. U. Otaigbe, C. E. Hoyle, *Macromolecules* **2007**, *40*, 8788.

[205] D. P. N. Satchell, R. S. Satchell, *Chem. Soc. Rev.* **1990**, *19*, 55.

[206] P. Esfandiari, S. C. Ligon, J. J. Lagref, R. Frantz, Z. Cherkaoui, R. Liska, *J. Polym. Sci. A Polym. Chem.* **2013**, *51*, 4261.

[207] A. V. Krasnoslobodtsev, S. N. Smirnov, *Langmuir* **2002**, *18*, 3181.

[208] Y. Xie, C. A.S. Hill, Z. Xiao, H. Militz, C. Mai, *Composites Part A: Applied Science and Manufacturing* **2010**, *41*, 806.

[209] a) J. V. Crivello, J. H. W. Lam, *Journal of Polymer Science: Polymer Chemistry Edition* **1980**, *18*, 1021; b) C.-L. Zhang, L.-F. Feng, G.-H. Hu, *Journal of Applied Polymer Science* **2006**, *101*, 1972.

[210] F. C. Nachod, J. J. Zuckerman (Eds.) *Determination of organic structures by physical methods. Vol. 4*, Academic Press, New York, London (24 Oval Rd, N.W.1), **1971**.

[211] Chemical Book, "Cyclohexanecarboxylic acid", can be found under https://www.chemicalbook.com/ChemicalProductProperty_EN_CB0332732.htm.

[212] J. Heller, D. W. H. Penhale, R. F. Helwing, *Journal of Polymer Science: Polymer Letters Edition* **1980**, *1980*, 293.

[213] Parts of the pratical work in this section were performed by Andrea Hoffmann under the author's supervision.

[214] a) M. F. D. Serafim, A. M. A. Leal, J. Bauer, I. A. Gomes, K. G. K. Carneiro, *RGO, Rev. Gaúch. Odontol.* **2018**, *66*, 339; b) A. Sezinando, I. Luque-Martinez, M. A. Muñoz, A. Reis, A. D. Loguercio, J. Perdigão, *Dental materials : official publication of the Academy of Dental Materials* **2015**, *31*, e236-46.

[215] a) A. A. El-Bindary, A. F. Shoair, H. A. Kiwaan, A. M. Eessa, *Journal of Molecular Liquids* **2017**, *244*, 226; b) D. A. Ramrus, J. C. Berg, *Journal of Adhesion Science and Technology* **2006**, *20*, 1615.

[216] J. D. Holbery, R. K. Bordia, *Journal of Materials Science* **2001**, *36*, 5301.

[217] S. R. Nozawa, I. C. Rigoli, G. Thedei, A. Rossi, *Fungal Genetics Reports* **1995**, *42*, 56.

[218] a) T. Higashimura, K. Kojima, M. Sawamoto, *Makromol. Chem.* **1989**, *15*, 127; b) M. Kato, *J. Photopol. Sci. Technol.* **2008**, *21*, 711.

[219] B. Escaig, *Journal de Physique IV* **1993**, *1993*, 753.

[220] a) Y. Ye, Y. A. Elabd, *Polymer* **2011**, *52*, 1309; b) R. Marcilla, J. Alberto Blazquez, J. Rodriguez, J. A. Pomposo, D. Mecerreyes, *Journal of Polymer Science Part A: Polymer Chemistry* **2004**, *42*, 208.

[221] The described syntheses in this section were performed by the author based on preliminary works by Sarah Kirchhecker and Zahra Mazloomi.

[222] Q. T. Pham, *Proton and carbon NMR spectra of polymers*, CRC Press, Boca Raton, Florida, London, New York, **1991**.

[223] M. Hesse, H. Meier, B. Zeeh, *Spektroskopische Methoden in der organischen Chemie. 102 Tabellen*, Thieme, Stuttgart, **2005**.

[224] B. H. Stuart, *Infrared spectroscopy. Fundamentals and applications*, Wiley, Chichester, **2008**.

[225] a) M. Buback, C. Kowollik, C. Kurz, A. Wahl, *Macromolecular Chemistry and Physics* **2000**, *201*, 464; b) M. Buback, R. G. Gilbert, R. A. Hutchinson, B. Klumperman, F.-D. Kuchta, B. G. Manders, K. F. O'Driscoll, G. T. Russell, J. Schweer, *Macromolecular Chemistry and Physics* **1995**, *196*, 3267.

[226] a) C. H. Lin, J. S. Xiang, K. Matyjaszewski, *Macromolecules* **1993**, *26*, 2785; b) T. Kunitake, K. Takarabe, *Macromolecules* **1979**, *12*, 1061.

[227] a) K. F. O'Driscoll, A. V. Tobolsky, *J. Polym. Sci.* **1959**, *35*, 259; b) J. E. L. Roovers, S. Bywater, *Trans. Faraday Soc.* **1966**, *62*, 701.

[228] a) S. Qin, D. Qin, W. T. Ford, J. E. Herrera, D. E. Resasco, S. M. Bachilo, R. B. Weisman, *Macromolecules* **2004**, *37*, 3965; b) P. D. Iddon, K. L. Robinson, S. P. Armes, *Polymer* **2004**, *45*, 759.

[229] S. J. Whicher, J. L. Brash, *Journal of Polymer Science: Polymer Chemistry Edition* **1981**, *19*, 1995.

[230] a) K. Krüger, K. Tauer, Y. Yagci, N. Moszner, *Macromolecules* **2011**, *44*, 9539; b) M. Buback, F.-D. Kuchta, *Macromolecular Chemistry and Physics* **1997**, *198*, 1455.

[231] C. Plessis, G. Arzamendi, J. R. Leiza, H. A. S. Schoonbrood, D. Charmot, J. M. Asua, *Macromolecules* **2001**, *34*, 5147.

[232] Q. Jiang, D. Xia, C. Liu, Q. Jiang, J. Li, B. Han, B. Jiang, W. Huang, X. Xue, H. Yang et al., *Polymer* **2020**, *189*, 122184.

[233] I. Sakurada, N. Ise, Y. Hayashi, *Journal of Macromolecular Science: Part A - Chemistry* **1967**, *1*, 1039.

[234] J. P. Kennedy, S. C. Feinberg, *J. Polym. Sci. Polym. Chem. Ed.* **1978**, *16*, 2191.

[235] A. Eftekhari, T. Saito, *European Polymer Journal* **2017**, *90*, 245.

[236] Organic Chemistry department, Michigan State University, "Ionization constants of Inorganic Polyprotic Acids", can be found under https://www2.chemistry.msu.edu/faculty/reusch/VirtTxtJml/acidity.htm, **2023**.

[237] E. P. Serjeant, B. Dempsey (Eds.) *Ionisation constants of organic acids in aqueous solution*, Pergamon Press, Oxford, **1979**.

[238] C. S. Marvel, R. Gilkey, C. R. Morgan, J. F. Noth, R. D. Rands, C. H. Young, *J. Polym. Sci.* **1951**, *6*, 483.

[239] a) C. Gainaru, R. Kumar, I. Popov, M. A. Rahman, M. Lehmann, E. Stacy, V. Bocharova, B. G. Sumpter, T. Saito, K. S. Schweizer et al., *Macromolecules* **2023**, *56*, 6051; b) X. He, A. Ye, X. Fu, W. Yang, Y. Wang, *Macromolecules* **2022**, *55*, 7117.

[240] A. Han, R. H. Colby, *Macromolecules* **2021**, *54*, 1375.

[241] a) W. R. Krigbaum, P. J. Flory, *J. Polym. Sci.* **1953**, *11*, 37; b) R. H. Colby, L. J. Fetters, W. W. Graessley, *Macromolecules* **1987**, *20*, 2226.

[242] a) J. Cohen, Z. Priel, Y. Rabin, *The Journal of Chemical Physics* **1988**, *88*, 7111; b) S. Kawaguchi, Y. Nishikawa, T. Kitano, K. Ito, A. Minakata, *Macromolecules* **1990**, *23*, 2710.

[243] F. Brochard, P. G. de Gennes, *Macromolecules* **1977**, *10*, 1157.

[244] P. C. Moon, R. E. Barker, *J. Polym. Sci. A-2 Polym. Phys.* **1973**, *11*, 909.

[245] M. Potschka, *Analytical Biochemistry* **1987**, *162*, 47.

[246] R. W. Dyson, C. H. Bamford, G. C. Eastmond, *Polymer* **1969**, *1969*, 885.

[247] A. N. Nikitin, R. A. Hutchinson, M. Buback, P. Hesse, *Macromolecules* **2007**, *40*, 8631.

[248] X. Guo, E. Laryea, M. Wilhelm, B. Luy, H. Nirschl, G. Guthausen, *Macromol. Chem. Phys.* **2017**, *218*, 1600440.

[249] K. F. Morris, C. S. Johnson, *J. Am. Chem. Soc.* **1992**, *114*, 3139.

[250] J. Viéville, M. Tanty, M.-A. Delsuc, *Journal of magnetic resonance (San Diego, Calif. : 1997)* **2011**, *212*, 169.

[251] R. Huo, R. Wehrens, J.v. Duynhoven, L.M.C. Buydens, *Analytica Chimica Acta* **2003**, *490*, 231.

[252] P. Groves, *Polym. Chem.* **2017**, *8*, 6700.

[253] A. Arrowood, M. A. Ansari, M. Ciccotti, R. Huang, K. M. Liechti, G. E. Sanoja, *Soft Matter* **2023**, *19*, 6088.

[254] D.-C. Kong, M.-H. Yang, X.-S. Zhang, Z.-C. Du, Q. Fu, X.-Q. Gao, J.-W. Gong, *Macro Materials & Eng* **2021**, *306*, 2100536.

[255] B. Erman in *Encyclopedia of materials*. *Science and technology* (Eds.: K. J. Buschow, R. W. Cahn, M. C. Flemings, B. Ilschner, E. J. Kramer, S. Mahajan, P. Veyssière, K. H. J. Buschow), Elsevier, Amsterdam, New York, **2010**, pp. 8227–8237.

[256] M. Doi, S. F. Edwards, *The theory of polymer dynamics*, Clarendon Press, Oxford, **2013**.

[257] P. G. de Gennes, *The Journal of Chemical Physics* **1971**, *55*, 572.

[258] L. J. Fetters, D. J. Lohse, S. T. Milner, W. W. Graessley, *Macromolecules* **1999**, *32*, 6847.

[259] a) S. E. Harding, K. Jumel, *Current Protocols in Protein Science* **2001**, *Chapter 7*, Unit 7.8; b) M. Shibayama, T. Karino, S. Okabe, *Polymer* **2006**, *47*, 6446.

[260] C. S. Johnson, *Prog. NMR Spectrosc.* **1999**, *34*, 203.

[261] C. Schick, *Analytical and bioanalytical chemistry* **2009**, *395*, 1589.

[262] H. F. Brinson, L. C. Brinson, *Polymer Engineering Science and Viscoelasticity*. *An Introduction*, Springer US, Boston, MA, s.l., **2015**.

[263] T. Mezger, *Das Rheologie-Handbuch*. *Für Anwender von Rotations- und Oszillations-Rheometern*, Vincentz Network, Hannover, **2012**.